INTERNATIONAL DOCTORAL
SCHOOL OF THE USC

Rubén
Prieto Díaz

PhD Thesis

A_{2B} Adenosine Receptor as a novel target in cancer immunotherapy: Validation and optimization of new ligands

Santiago de Compostela, 2023

Doctoral Programme in Drug Research and Development

DOCTORAL THESIS

A_{2B} ADENOSINE RECEPTOR AS A NOVEL TARGET IN CANCER IMMUNOTHERAPY: VALIDATION AND OPTIMIZATION OF NEW LIGANDS

Rubén Prieto Díaz

INTERNATIONAL PHD SCHOOL OF THE UNIVERSITY OF SANTIAGO DE COMPOSTELA
PHD PROGRAMME IN DRUG RESEARCH AND DEVELOPMENT

SANTIAGO DE COMPOSTELA
2023

DECLARACIÓN DO AUTOR DA TESE

D. **Rubén Prieto Díaz**

Título da tese: **A_{2B} Adenosine Receptor as a novel target for cancer immunotherapy: Validation and optimization of new ligands**

Presento a miña tese, seguindo o procedemento axeitado ao Regulamento, e declaro que:

1) A tese abarca os resultados da elaboración do meu traballo
2) De ser o caso, na tese faise referencia ás colaboracións que tivo este traballo.
3) Confirmo que a tese non incorre en ningún tipo de plaxio doutros autores nin de traballos presentados por min para a obtención doutros títulos.
4) A tese é a versión definitiva presentada para a súa defensa e coincide a versión impresa coa presentada en formato electrónico.

E comprométome a presentar o Compromiso Documental de Supervisión no caso de que o orixinal non estea na Escola.

En **Santiago de Compostela**, 21 de Xullo de 2023

AUTORIZACIÓN DO DIRECTOR

A_{2B} Adenosine Receptor as a novel target for cancer immunotherapy: Validation and optimization of new ligands

D. Eddy Sotelo Pérez

INFORMA:

Que a presente tese, correspóndese co traballo realizado por D. Rubén Prieto Díaz, baixo a miña dirección, e autorizo a súa presentación, considerando que reúne os requisitos esixidos no Regulamento de Estudos de Doutoramento da USC, e que como director desta non incorre nas causas de abstención establecidas na Lei 40/2015.

De acordo co indicado no Regulamento de Estudos de Doutoramento, declara tamén que a presente tese de doutoramento é idónea para ser defendida en base á modalidade de Monográfica con reproducción de publicaciones, nos que a participación do doutorando foi decisiva para a súa elaboración e as publicacións se axustan ao Plan de Investigación.

En Santiago de Compostela 21 de Xullo de 2023

Acknowledgments

En primer lugar, quiero expresar mi sincero agradecimiento al director de esta Tesis Doctoral, el Prof. **Eddy Sotelo**, tanto a nivel profesional como personal, por su inestimable orientación y apoyo a lo largo de los más de 7 años que he pasado en su laboratorio. Su dedicación, compromiso y entusiasmo han sido una fuente constante de motivación para mí. Sus comentarios, correcciones y sugerencias han sido fundamentales para el éxito de este proyecto, así como de gran ayuda para mejorar la calidad de la tesis.

Al Dr. **Jhonny Azuaje** por ser la persona que me introdujo al trabajo experimental. Desde los conceptos más básicos hasta las técnicas más avanzadas, él me enseñó todo lo necesario para desenvolverme en el laboratorio, además de darme soluciones efectivas a los problemas sintéticos que surgieron durante la tesis.

A la Dra. **Maria Majellaro** por su invaluable ayuda en la implementación de técnicas de purificación y caracterización. Su experiencia y conocimiento en estas áreas han sido fundamentales para el avance de mi investigación. Además, quiero destacar su contagiosa alegría y motivación en el laboratorio, que han creado un ambiente de trabajo divertido y estimulante.

Al Prof. **Hugo Gutiérrez de Terán**, de la Universidad de Uppsala, por su guía y motivación para profundizar mis conocimientos en química computacional. A todo el grupo de investigación, en especial a **Alejandro Díaz**, **Lucien Koenekoop** y **Florian van der Ent**, fantásticos investigadores, por hacerme sentir parte del grupo nada más llegar y por su ayuda constante en el trabajo diario.

Quiero expresar mi más sincero agradecimiento al Prof. **Xerardo García** y a la Prof. **Rita Paleo** por su invaluable experiencia, cuyo aporte ha elevado significativamente el nivel científico de las publicaciones y de esta tesis doctoral.

A todo el laboratorio del Dr. **Miguel Abal** del IDIS por su cálida acogida durante el último año y medio. En especial me gustaría agradecer al Dr. **Jorge Barbazán**, por enseñarme a trabajar en un laboratorio biológico. Sus propuestas innovadoras y apoyo incondicional en experimentos y escritura han sido de gran valor.

Durante el desarrollo de esta tesis han sido cruciales las colaboraciones con los grupos de farmacología de la Universidad de Santiago de Compostela, dirigido por la Prof. **María Isabel Loza** y de la Universidad de Barcelona, dirigido por el Prof. **Francisco Ciruela** y los grupos de inmunología de la Universidad de Santiago de Compostela, dirigido por la Prof. **Iria Gómez** y del Instituto Karolinska, dirigido por el Prof. **Andreas Lundqvist**.

Al personal técnico y administrativo de la Universidad de Santiago de Compostela, en especial a **Xosé González**, técnico del Laboratorio de Química Orgánica de la Facultad de Farmacia por facilitarnos el trabajo del día a día, y a los técnicos de **Unidad de Rayos X**, **Espectrometría** y **Resonancia Magnética Nuclear**. En esta misma línea, me gustaría volver a agradecer a la Prof. **Rita Paleo** por ayudarme con la caracterización estructural de los regioisómeros generados en la misma reacción de los capítulos I y III de esta tesis y de los tautómeros del capítulo II.

Quiero dedicar un especial agradecimiento a **Claudia Gioe** y **Carlos Rodríguez**, mis compañeros de tesis desde el inicio hasta el final. Ha sido genial tener su compañía durante todo este proceso, compartiendo tanto los malos como los buenos momentos. Gracias a los dos por enseñarme también que, sin duda, lo mejor es vivir solo.

No me olvido de mis compañeros de ComBioMed: Dr. **Rodrigo Bernárdez**, **Darío Miranda**, **Hugo Fojo**, **Lucía González**, **Lucía Campos**, **Aitor García**, **Sandra Ortigueira**, **Antonio Andújar** e **Iván Rodríguez**

Me gustaría agradecer también a la Prof. **Loli Torres** y a **Sagrario García** por la ayuda en los trámites burocráticos durante el doctorado.

Finalmente, agradecer a la **Xunta de Galicia** (Referencia: ED481A-2020/060) por la financiación de mi Tesis Doctoral, y a las acciones de COST ERNEST (CA 18133) e IMMUNO-model (CA 21135) por la financiación de una *Short-Term Scientific Mission* y asistencia a congresos.

A los tres pilares fundamentales en mi vida:
mi madre, mi hermana y Ana

INDEX

GLOSSARY ..... **I**

RESUMO ..... **IX**

1 INTRODUCTION **1**

1.1 CONVENTIONAL CANCER THERAPIES 2

1.2 TARGETED THERAPIES. HALLMARKS OF CANCER AND IMMUNE CHECKPOINTS 3

1.2.1 Sustaining proliferative signaling *4*

1.2.2 Evading growth suppressors *5*

1.2.3 Evading programmed cell death *6*

1.2.4 Enabling replicative immortality *6*

1.2.5 Sustained angiogenesis *6*

1.2.6 Activating tissue invasion and metastasis *6*

1.2.7 Deregulating cellular metabolism *7*

1.2.8 Avoiding immune system attack *7*

1.2.9 Unlocking phenotypic plasticity *9*

1.2.10 Senescent cells *9*

1.2.11 Enabling characteristics *9*

1.2.12 Immune checkpoints *10*

1.3 PURINERGIC SIGNALING IN CANCER 13

1.3.1 Adenosine roles in cell growth, survival, metastasis, and angiogenesis *18*

1.3.2 Adenosine roles in the immune system *20*

1.4 STRUCTURE AND PHARMACOLOGY OF ADENOSINE RECEPTORS 23

1.4.1 Expression and signaling pathways in the context of cancer *26*

1.4.2 Oligomerization of Adenosine Receptors *27*

1.5 MEDICINAL CHEMISTRY OF ADENOSINE RECEPTORS 28

1.5.1 Adenosine Receptor agonists *29*

1.5.2 Adenosine Receptors antagonists *33*

2 OBJECTIVES **55**

3 RESULTS AND DISCUSSION **63**

3.1 CHAPTER I: EXPLORING THE EFFECT OF HALOGENATION IN A SERIES OF POTENT AND SELECTIVE A_{2B} ADENOSINE RECEPTOR ANTAGONISTS 63
3.1.1 Design *66*
3.1.2 Chemistry *67*
3.1.3 Biological Evaluation *72*
3.1.4 Functional activity assays *79*
3.1.5 Structure-Activity Relationships and Molecular Modeling *82*
3.1.6 Enantiospecific binding to the A_{2B}AR *86*
3.1.7 FEP simulations on the eutomers *91*
3.1.8 Preliminary ADMET exploration *94*
3.2 CHAPTER II: SCAFFOLD HOPPING STRATEGIES OF THE 3,4-DIHYDROPYRIMIDIN-2(1*H*)-ONE CHEMOTYPE PROVIDE NOVEL POTENT A_{2B} ADENOSINE RECEPTOR ANTAGONISTS 101
3.2.1 Design *102*
3.2.2 Chemistry *106*
3.2.3 Biological Evaluation *108*
3.2.4 Analysis of the Structure-Activity Relationship and Molecular Modeling *120*
3.2.5 Enantiospecific binding to the A_{2A} and A_{2B}AR *135*
3.3 CHAPTER III: *N*-SUBSTITUTION OF A_{2B}AR ANTAGONISTS WITHIN THE PYRIMIDINONE CHEMOTYPES: DISCOVERY AND OPTIMIZATION OF A_{2B} AND DUAL A_{2A}/A_{2B} LIGANDS 141
3.3.1 Design *144*
3.3.2 Chemistry *147*
3.3.3 Biological Evaluation *150*
3.3.4 Structure-Activity Relationship and Molecular Modeling *158*
3.3.5 Enantiospecific binding to the A_{2A} and A_{2B}AR *172*
3.4 CHAPTER IV: OPTIMIZATION AND ADVANCED CHARACTERIZATION OF A_{2B}AR ANTAGONISTS AS DRUGS FOR CANCER (IMMUNO)THERAPY 179
3.4.1 In vitro and ex vivo validation of antiproliferative effects in tumor cells *179*
3.4.2 In vitro and ex vivo evaluation of immunostimulatory effects *191*
4 CONCLUSIONS 207
5 EXPERIMENTAL SECTION 213
5.1 GENERAL CONSIDERATIONS 213

5.1.1 Synthesis and purification *213*
5.1.2 Structural characterization *213*
5.1.3 Pharmacological evaluation and preliminary pharmacokinetic characterization *215*
5.1.4 Computational studies: docking and molecular dynamics simulations *219*
5.2 EXPLORING THE EFFECT OF HALOGENATION IN A SERIES OF POTENT AND SELECTIVE A_{2B} ADENOSINE RECEPTOR ANTAGONISTS 223
5.2.1 Synthesis of halogenated derivatives (1-80) *223*
5.2.2 Spectroscopic and analytical data for all compounds described *225*
5.2.3 Chiral HPLC separation of enantiomers and circular dichroism of ISAM-140, 50, 58, 60, 66, 67 and 79 ..... *246*
5.2.4 X-ray crystallography of ISAM-140 and of the 67 enantiomers *276*
5.2.5 Free Energy Perturbation data and calculations *278*
5.3 SCAFFOLD HOPPING STRATEGIES OF THE 3,4-DIHYDROPYRIMIDIN-2(1*H*)-ONE CHEMOTYPE PROVIDE NOVEL POTENT A_{2B} ADENOSINE RECEPTOR ANTAGONISTS 281
5.3.1 Synthesis of monocyclic derivatives (81-136) *281*
5.3.2 Synthesis of bicyclic derivatives (137-224 & 233-240) *284*
5.3.3 Synthesis of tricyclic derivatives (209-216 & 225-248) *287*
5.3.4 Spectroscopic and analytical data for all compounds described *288*
5.3.5 Chiral HPLC separation of enantiomers and characterization of 226, 228, and 243 ..... *332*
5.4 *N*-SUBSTITUTION OF A_{2B}AR ANTAGONISTS WITH PYRIMIDINONE CHEMOTYPE 347
5.4.1 Synthesis of mono-, bi-, and tricyclic Biginelli derivatives for alkylation (D1-D4) *347*
5.4.2 Synthesis of alkylated and benzylated derivatives (249-310) *349*
5.4.3 Spectroscopic and analytical data for all compounds described *351*
5.4.4 Chiral HPLC separation of enantiomers and characterization of 257, 266a, 269a, and 284a *387*
5.5 OPTIMIZATION AND PRE-CLINICAL VALIDATION OF A_{2B}AR ANTAGONISTS AS DRUGS FOR CANCER (IMMUNO)THERAPY 405
5.5.1 In vitro and ex vivo validation of antiproliferative effects *405*
5.5.2 In vitro and ex vivo evaluation of immunostimulatory effects *408*

6 REFERENCES 415

7 SUPPLEMENTARY RESULTS 441

7.1 *IN SILICO* STUDY OF THE PHYSICOCHEMICAL PROPERTIES OF THE MOLECULES OBTAINED 441

8 APPENDICES 447

APPENDIX 1. PHD PUBLICATION LIST AND AUTHOR CONTRIBUTION 449

APPENDIX 2. PUBLISHER'S PERMISSION FOR USE OF THE PUBLICATIONS 451

APPENDIX 3. PERMISSION TO PUBLISH IMAGES AND FIGURES 453

APPENDIX 4. CONFLICT OF INTEREST 455

GLOSSARY

7-BFC	7-benzyloxy-4-trifluoromethyl-coumarin
A_1AR	A_1 Adenosine Receptor
A_{2A}AR	A_{2A} Adenosine Receptor
A_{2B}AR	A_{2B} Adenosine Receptor
A_3AR	A_3 Adenosine Receptor
ABFE	Absolute Binding Free Energy
ACC	Acetyl-CoA Carboxylase
ACTB	Beta-Actin
AcOEt	Ethyl Acetate
ADA	Adenosine Deaminase
ADMET	Absorption, Distribution, Metabolism, Excretion, Toxicity
ADO	Adenosine
ADORA	Adenosine Receptor (gene)
ADP	Adenosine Diphosphate
AK	Adenosine Kinase
AMP	Adenosine Monophosphate
ANOVA	Analysis of Variance
AR	Androgen Receptor
ATP	Adenosine Triphosphate
AUC	Area Under the Curve
BBB	Blood-Brain Barrier
BLCA	Bladder Urothelial Carcinoma
Bn	Benzyl
BOILED-Egg	Brain Or IntestinaL EstimateD permeation method
BRCA	Breast Invasive Carcinoma
BRET	Bioluminescence Resonance Energy Transfer
BSA	Bovine Serum Albumin

c-RAF	Cellular Raf Kinase
CAFs	Cancer-Associated Fibroblasts
CC3	Caspase-3 Cleavage
CCDC	Cambridge Crystallographic Data Centre
CD	Circular Dichroism
CD39	Cluster of Differentiation 39, also known as NTPDase1 (Nucleoside Triphosphate Diphosphohydrolase 1), an ectonucleotidase enzyme involved in the hydrolysis of extracellular nucleotides.
CD4	Cluster of Differentiation 4, characteristic of Th lymphocytes
CD73	Cluster of Differentiation 73, also known as 5'-Nucleotidase, is an ectoenzyme that catalyzes the conversion of extracellular AMP (Adenosine Monophosphate) to Adenosine.
CD8	Cluster of Differentiation 8, characteristic of cytotoxic T cells
CD80	Cluster of Differentiation 80
CESC	Cervical Squamous Cell Carcinoma and Endocervical Adenocarcinoma
CFSE	Carboxyfluorescein Succinimidyl Ester
CHO	Chinese Hamster Ovary
CHOL	Cholangiocarcinoma
CI	Chemical Ionization
CNS	Central Nervous System
COAD	Colon Adenocarcinoma
COS	Chrondoblastic Osteosarcoma
COSY	Correlation Spectroscopy
CS G1	Chondrosarcoma G1
CSC	8-(3 chlorostyryl)caffeine
CTL	Cytotoxic T Lymphocyte
CTLA-4	Cytotoxic T-Lymphocyte-Associated Protein 4
CYP	Cytochrome P450
DAG	Diacylglycerol
DAPI	4',6-Diamidino-2-Phenylindole

DBF	Dibenzylfluorescein
DCM	Dichloromethane
DHP	Dihydropyridine
DLBC	Lymphoid Neoplasm Diffuse Large B-cell Lymphoma
DMEM	Dulbecco's Modified Eagle Medium
DMF	Dimethylformamide
DMSO	Dimethyl Sulfoxide
DNA	Deoxyribonucleic Acid
DPCPX	8-Cyclopentyl-1,3-dipropylxanthine
DR3	Death Receptor 3
ECM	Extracellular Matrix
EdU	5-Ethynyl-2'-deoxyuridine
EGF	Epidermal Growth Factor
EGFR	Epidermal Growth Factor Receptor
EI	Electron impact
ERK	Extracellular Signal-Regulated Kinase
ESCA	Esophageal Carcinoma
ESI	Electrospray Ionization
Et	Ethyl
FDA	Food and Drug Administration
FEP	Free Energy Perturbation
FGF	Fibroblast Growth Factor
FRET	Fluorescence Resonance Energy Transfer
GBM	Glioblastoma Multiforme
GC	Gas Chromatography
GADPH	Glyceraldehyde-3-Phosphate Dehydrogenase
GC/MSD	Gas Chromatography/Mass Spectrometry Detector
GDP	Guanosine Diphosphate
GF	Growth Factor

GLOBOCAN	Global Cancer Observatory
GPCRs	G-Protein Coupled Receptors
GTP	Guanosine Triphosphate
GUSB	Beta-Glucuronidase
HAC	Heavy Atom Count
HBD	Hydrogen Bond Donor
HCS	High-Content Screening
HEK	Human Embryonic Kidney
Hex	Hexane
HMBC	Heteronuclear Multiple Bond Coherence
HNSC	Head and Neck Squamous Cell Carcinoma
HPLC	High-Performance Liquid Chromatography
HRMS	High-Resolution Mass Spectrometry
HSQC	Heteronuclear Single Quantum Coherence
HTS	High-Throughput Screening
i-Pr	Isopropyl
IARC	International Agency for Research on Cancer
IC50	Half-Maximal Inhibitory Concentration
IFN	Interferon
IL	Interleukin
INO	Inosine
IPA	Isopropyl Alcohol
ITS	Insulin Transferrin Selenium
JNK	c-Jun N-terminal Kinase
K_i	Inhibition Constant
KICH	Kidney Chromophobe
KIRC	Kidney Renal Clear Cell Carcinoma
KIRP	Kidney Renal Papillary Cell Carcinoma
KO	Knockout

LAML	Acute Myeloid Leukemia
LC	Liquid Chromatography
LE	Ligand Efficiency
LGG	Brain Lower Grade Glioma
LIHC	Liver Hepatocellular Carcinoma
logD	Logarithm of the Distribution Coefficient
LogP	Logarithm of the Partition Coefficient
LRMS	Low Resolution Mass Spectrometry
LS	Leiomyosarcoma
LUAD	Lung Adenocarcinoma
LUSC	Lung Squamous Cell Carcinoma
mAb	Monoclonal Antibody
MAPK	Mitogen-Activated Protein Kinase
MCR	Multicomponent Reaction
MD	Molecular Dynamics
MDSC	Myeloid-Derived Suppressor Cells
Me	Methyl
MEK	Mitogen-Activated Protein Kinase
MeOH	Methanol
MESO	Mesothelioma
MFI	Mean Fluorescence Intensity
MFS G3	Myxofibrosarcoma G3
MHC I/II	Major Histocompatibility Complex Class I/II
Mp	Melting Point
MPNST	Malignant Peripheral Nerve Sheath Tumor
MPO	Multi-Parameter Optimization
ms	Milliseconds
MS	Mass Spectrometry
MUE	Mean Unassigned Error

MW	Molecular Weight
NAD+	Nicotinamide Adenine Dinucleotide
NADP	Nicotinamide Adenine Dinucleotide Phosphate
NECA	5'-N-Ethylcarboxamidoadenosine
NF-κβ	Nuclear Factor kappa B
NIH	National Institutes of Health
NK	Natural Killer
NMP	N-Methylpiperidine
NMR	Nuclear Magnetic Resonance
NOE/NOESY	Nuclear Overhauser Effect Spectroscopy
OV	Ovarian Serous Cystadenocarcinoma
P1	Purinergic Receptor P1
P2	Purinergic Receptor P2
P2X	Purinergic Receptor P2X
P2Y	Purinergic Receptor P2Y
PAAD	Pancreatic Adenocarcinoma
PAINS	Pan Assay Interference Compounds
PBMCs	Peripheral Blood Mononuclear Cells
PBS	Phosphate-Buffered Saline
PCPG	Pheochromocytoma and Paraganglioma
PD-1	Programmed Cell Death Protein 1
PD-L1/L2	Programmed Death-Ligand 1/2
PDB	Protein Data Bank
PET	Positron Emission Tomography
PKA	Protein Kinase A
PKC	Protein Kinase C
PLA	Proximity Ligation Assay
Pr	Propyl
PRAD	Prostate Adenocarcinoma

PS	Penicillin-streptomycin
RBFE	Relative Binding Free Energy
READ	Rectum Adenocarcinoma
ROESY	Rotating Frame Overhauser Enhancement Spectroscopy
rt	Retention Time
RT	Room Temperature
RTCA	Real-Time Cell Analysis
SAR	Structure-Activity Relationship
SARC	Sarcoma
SASP	Senescence-Associated Secretory Phenotype
SBC	Structure-Based Classification
SCAAS	Surface-Constrained All-Atom Solvent
SCS	Spindle cell sarcoma
SD	Standard Deviation
SEM	Standard Error of the Mean
SKCM	Skin Cutaneous Melanoma
SMH	Short Membrane-Associated Helix
SNAP	Self-labeling protein tag for specific and covalent tagging with fluorescent dyes
SSR	Structure-Selectivity Relationship
STAD	Stomach Adenocarcinoma
TAM	Tumor-Associated Macrophages
TGCT	Testicular Germ Cell Tumors
TGF	Transforming Growth Factor
Th	T Helper
THCA	Thyroid Carcinoma
THF	Tetrahydrofuran
THYM	Thymoma
TILs	Tumor-Infiltrating Lymphocytes

TLC	Thin-Layer Chromatography
TM	Transmembrane
TME	Tumor Microenvironment
TMZ	Temozolomide
TNF	Tumor Necrosis Factor
TNFR	Tumor Necrosis Factor Receptor
TPSA	Topological Polar Surface Area
TR-FRET	Time-Resolved Fluorescence Resonance Energy Transfer
U2OS	Human Osteosarcoma Cell Line
UCEC	Uterine Corpus Endometrial Carcinoma
UCS	Uterine Carcinosarcoma
UDP	Uridine Diphosphate
UMP	Uridine Monophosphate
UPS	Undifferentiated pleomorphic sarcoma
UTP	Uridine Triphosphate
UV	Ultraviolet
UVM	Uveal Melanoma
VEGF	Vascular Endothelial Growth Factor
VEGFR	Vascular Endothelial Growth Factor Receptor

RESUMO

O cancro é unha enfermidade complexa e dinámica na que as células medran e se reproducen descontroladamente, invadindo tecidos saudables e órganos circundantes. Con máis de 100 tipos diferentes, a súa alta heteroxeneidade convérteo nun desafío. Estímase que aproximadamente o 25% dos homes e o 20% das mulleres desenvolverán cancro ao longo da súa vida, e a metade deles morrerá debido á enfermidade. O tratamento do cancro experimentou unha notable evolución, pasando de terapias invasivas e pouco efectivas a enfoques máis selectivos con menos efectos adversos. No pasado, a cirurxía era a única opción de tratamento, que posteriormente se complementou coa radioterapia no século XX. Co descubrimento de fármacos sintéticos, introduciuse a quimioterapia, utilizando axentes como antimetabolitos e mostazas nitroxenadas, aínda que con efectos adversos significativos. Co aumento da esperanza de vida e o incremento da investigación, producíronse avances importantes na inmunoloxía, especialmente no uso de anticorpos para o tratamento de enfermidades. Isto deu lugar ao xurdimento de terapias selectivas, cuxo obxectivo principal era dirixirse especificamente ás células tumorais, evitando danar os tecidos saudables, o que mellorou tanto a seguridade como a eficacia dos tratamentos antitumorais. A partir da década de 2010, a inmunoterapia posicionouse como un enfoque selectivo que non se centraba unicamente no tumor ou nas células tumorais, senón que consideraba o importante papel do microambiente tumoral e as células do sistema inmunitario. Este microambiente promove o desenvolvemento do cancro ao proporcionar oxíxeno e nutrientes, limitar a acción do sistema inmunitario e favorecer a proliferación celular tumoral. A inmunoterapia busca reactivar o sistema inmunitario para que seleccione e ataque especificamente ás células tumorais, revertendo así o proceso e destruíndo o cancro dun xeito máis fisiolóxico.

A inmunoterapia, como enfoque terapéutico selectivo no tratamento do cancro, baséase nos Puntos de Control Inmunitario, que regulan a resposta inmune e evitan unha activación excesiva do sistema inmunitario. Entre os principais Puntos de Control Inmunitario atópanse as moléculas CTLA-4 (antíxeno asociado ao linfocito citotóxico 4) e PD-1 (proteína de morte celular programada 1), cuxa función é manter un equilibrio entre a activación e a supresión inmunolóxica (Figura 1). No contexto do cancro, as células tumorais poden explotar estas vías de control inmunolóxico para evadir a resposta inmunitaria e promover a súa supervivencia. Polo tanto, o bloqueo dos Puntos de Control Inmunitario converteuse nunha estratexia fundamental na inmunoterapia antitumoral. Utilízanse anticorpos monoclonais para bloquear a

interacción destas moléculas cos seus ligandos, desencadeando así unha resposta inmunitaria potente e específica contra as células tumorais. Exemplos notables inclúen o uso de Ipilimumab, que bloquea CTLA-4, Nivolumab e Pembrolizumab, que bloquean PD-1, e Atezolizumab, que bloquea PD-L1 (ligando de PD-1), todos eles empregados en diferentes tipos de cancro e demostrando resultados prometedores na mellora da supervivencia dos pacientes.

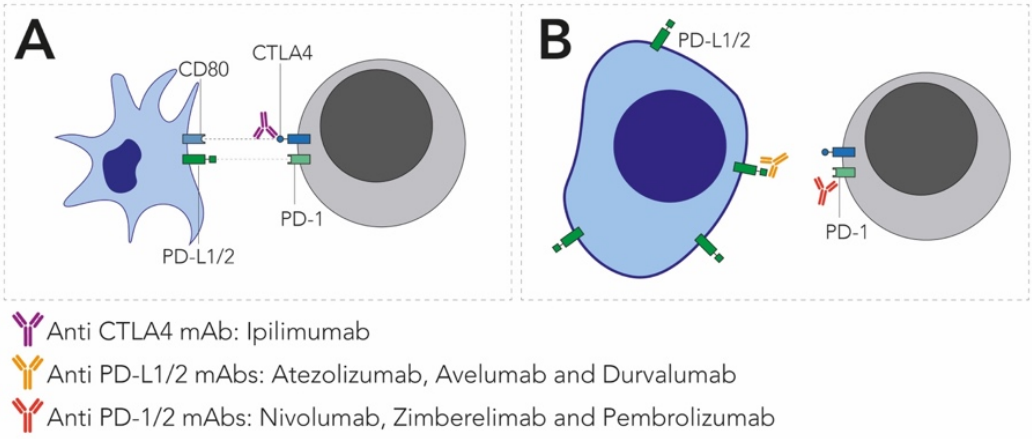

Figura 1. A) Regulación fisiolóxica da activación do sistema inmunitario a través das células dendríticas (azul) e dos linfocitos T (gris). B) Efecto oncoprotector do sistema PD1-PDL1 en células cancerosas (azul).

Aínda que os anticorpos monoclonais demostraron ser eficaces no bloqueo dos puntos de control inmunolóxico, presentan algunhas desvantaxes en comparación coas terapias baseadas en moléculas pequenas. A produción de anticorpos monoclonais require modelos de produción biolóxica complexos, como os hibridomas, o que resulta custoso e limita a súa dispoñibilidade. En contraste, as terapias baseadas en moléculas pequenas poden obterse de forma máis sinxela e económica, aproveitando a experiencia acumulada na industria farmacéutica. Estas moléculas tamén permiten a introdución de modificacións estruturais para mellorar as súas propiedades farmacocinéticas e farmacodinámicas, facilitando así o desenvolvemento de fármacos máis efectivos e seguros. Ademais, a administración oral das terapias baseadas en moléculas pequenas simplifica o proceso en comparación cos anticorpos monoclonais, que frecuentemente requiren inxeccións. En resumo, as terapias baseadas en moléculas pequenas presentan vantaxes significativas sobre os anticorpos monoclonais en termos de produción, desenvolvemento de fármacos e administración, o que as converte nunha alternativa prometedora na terapia do cancro.

Neste contexto, o sistema purinérxico está a adquirir un papel fundamental no desenvolvemento de terapias contra o cancro baseadas en moléculas pequenas. Como un dos

primeiros puntos de control inmunolóxico validados, o receptor A_{2A} de Adenosina (A_{2A}AR) despertou un gran interese no papel do sistema purinérxico no microambiente tumoral. Evidencias recentes tamén destacan o posible papel do receptor de Adenosina A_{2B}AR no control da proliferación celular e metástase en células tumorais, e a anxioxénese (xeración de novos vasos sanguíneos) no endotelio vascular, ademais da súa función no sistema inmunitario. Isto resalta aínda máis a importancia do sistema purinérxico como obxectivo terapéutico no tratamento do cancro baseado en moléculas pequenas.

A presente Tese de Doutoramento describe o deseño, síntese, caracterización estrutural, estudos de relación estrutura-actividade, modelización molecular, avaliación farmacolóxica e validación mediante ensaios biolóxicos a nivel antiproliferativo e inmunitario de novos ligandos potentes e selectivos para os receptores A_{2A} e A_{2B} de Adenosina para a inmunoterapia do cancro. O traballo realizado, organizado en catro grandes áreas (**Capítulos I-IV**, Seccións 3.1-3.4), preséntase en forma de tese monográfica con reprodución total ou parcial de publicacións, abordando de maneira exhaustiva temas relevantes e conceptos avanzados no campo da Química Médica e Biolóxica, especificamente enfocados na familia de receptores de Adenosina. Os resultados presentados nesta tese non só contribúen ao descubrimento de novos ligandos e ferramentas farmacolóxicas, senón que tamén forman parte dun proxecto metodolóxico deseñado para demostrar as vantaxes competitivas das reaccións multicompoñente no ámbito da Química Médica.

O primeiro capítulo da tese de doutoramento (Sección 3.1), cuxos resultados están publicados nas revistas Scientific Reports (*Sci. Rep.* **2021**, 11, 1–10) e Journal of Medicinal Chemistry (*J. Med. Chem.* **2023**, 66, 890–912), describe a optimización e exploración do efecto da haloxenación de antagonistas potentes e selectivos do receptor A_{2B} de Adenosina. O interese no desenvolvemento de fármacos metabolicamente estables estivo presente desde os primeiros tempos da medicina. Durante a primeira metade do século XX, produciuse un avance significativo no campo da Química Farmacéutica, co desenvolvemento da bioisostería e unha mellor comprensión dos principios científicos que rexen a estabilidade metabólica dos fármacos.

O metabolismo dos fármacos é un proceso de vital importancia na farmacocinética, e un dos factores determinantes na súa eficacia e seguridade. Entre as diversas vías metabólicas implicadas, destaca a degradación de fragmentos da molécula que presentan unha notable facilidade para a oxidación. Esta transformación química, mediada principalmente por enzimas

hepáticas, resulta na xeración de metabolitos oxidados que posúen unha estrutura modificada con respecto ao composto orixinal. A presenza de grupos funcionais susceptibles á oxidación dentro da molécula do fármaco (por exemplo, aneis aromáticos) confire un alto grao de influencia sobre a súa biodispoñibilidade, actividade farmacolóxica e vida media.

A substitución de átomos de hidróxeno por flúor en aneis aromáticos de compoñentes activos pode exercer un efecto significativo sobre diversos parámetros estruturais, farmacodinámicos e farmacocinéticos. Os átomos de flúor e hidróxeno son moi semellantes en tamaño (radio atómico do H = 0.50 Å, F = 0.57 Å), pero moi diferentes na súa configuración electrónica. Esta modificación, xeralmente, tradúcese nunha maior estabilidade metabólica, ao reducir a posibilidade de oxidación debido á súa elevada electronegatividade. Ademais, a substitución por outros halóxenos, como poden ser o cloro (0.97 Å) e o bromo (1.12 Å), evitan a oxidación tamén por impedir a entrada do anel aromático no sitio activo das enzimas do metabolismo oxidativo, pero poden alterar tamén a unión co receptor A_{2B} de Adenosina.

Tendo en conta os aspectos anteriormente mencionados, investigamos o efecto da introdución dun ou dous átomos de flúor, cloro e bromo na afinidade A_{2B} e en ensaios preliminares de estabilidade metabólica e solubilidade de antagonistas tricíclicos desenvolvidos anteriormente no grupo ComBioMed. Para iso, eliximos como ligandos modelo aqueles con esqueleto central de 4-heteroaril-2-metil-1,4-dihidrobenzo[4,5]imidazo[1,2-a]pirimidina-3-carboxilato de alquilo, substituídos na posición 3 con etilo ou isopropilo e na posición 4 con 2-furilo, 3-furilo, 2-tienilo, 3-tienilo e 4-oxazolilo. A metodoloxía sintética está baseada na reacción de Biginelli, obténdose nun paso sintético un (serie dihaloxenada) ou dous (series monohaloxenadas) ligandos por cada reacción, facendo a exploración altamente eficiente. Esta exploración supón un total de 80 novas moléculas sintetizadas e avaliadas. A caracterización estrutural dos ligandos que se obtiveron na mesma reacción fíxose empregando unha combinación de Resonancia Magnética Nuclear de protón (^{1}H), carbono (^{13}C), técnicas bidimensionais e cristalografía que raios X. O deseño dos compostos e a interpretación da relación estrutura-actividade resultante foron apoiados por ferramentas computacionais que incluíron os resultados do estudo de simulacións de perturbación da enerxía libre (FEP) máis grande realizado ata hoxe para este tipo de moléculas. Posteriormente, os seis mellores antagonistas haloxenados identificados separáronse nos seus enantiómeros para a súa avaliación por separado.

É importante resaltar que, do mesmo xeito que os ligandos de referencia, todos os ligandos obtidos neste capítulo conteñen un estereocentro na posición catro do núcleo heterocíclico. Todos os compostos illáronse e avaliáronse farmacolóxicamente como mesturas racémicas. Neste capítulo documentamos novos exemplos de antagonistas do receptor A_{2B} de Adenosina haloxenados que combinan unha excelente afinidade A_{2B} (K_i < 10 nM) e unha notable selectividade fronte aos outros receptores de Adenosina (A_1, A_{2A} e A_3). A haloxenación dos ligandos tricíclicos xera ligandos de alta afinidade, con tres tendencias en función do patrón de substitución: 1) a afinidade dos derivados dihaloxenados é alta nos derivados difluorados, pero baixa nos derivados diclorados e dibromados; 2) a afinidade dos derivados monohaloxenados en posición 7 é inversamente proporcional ao tamaño do halóxeno; e 3) a afinidade dos derivados monohaloxenados en posición 8 é excelente e independente do tamaño do halóxeno (Figura 2).

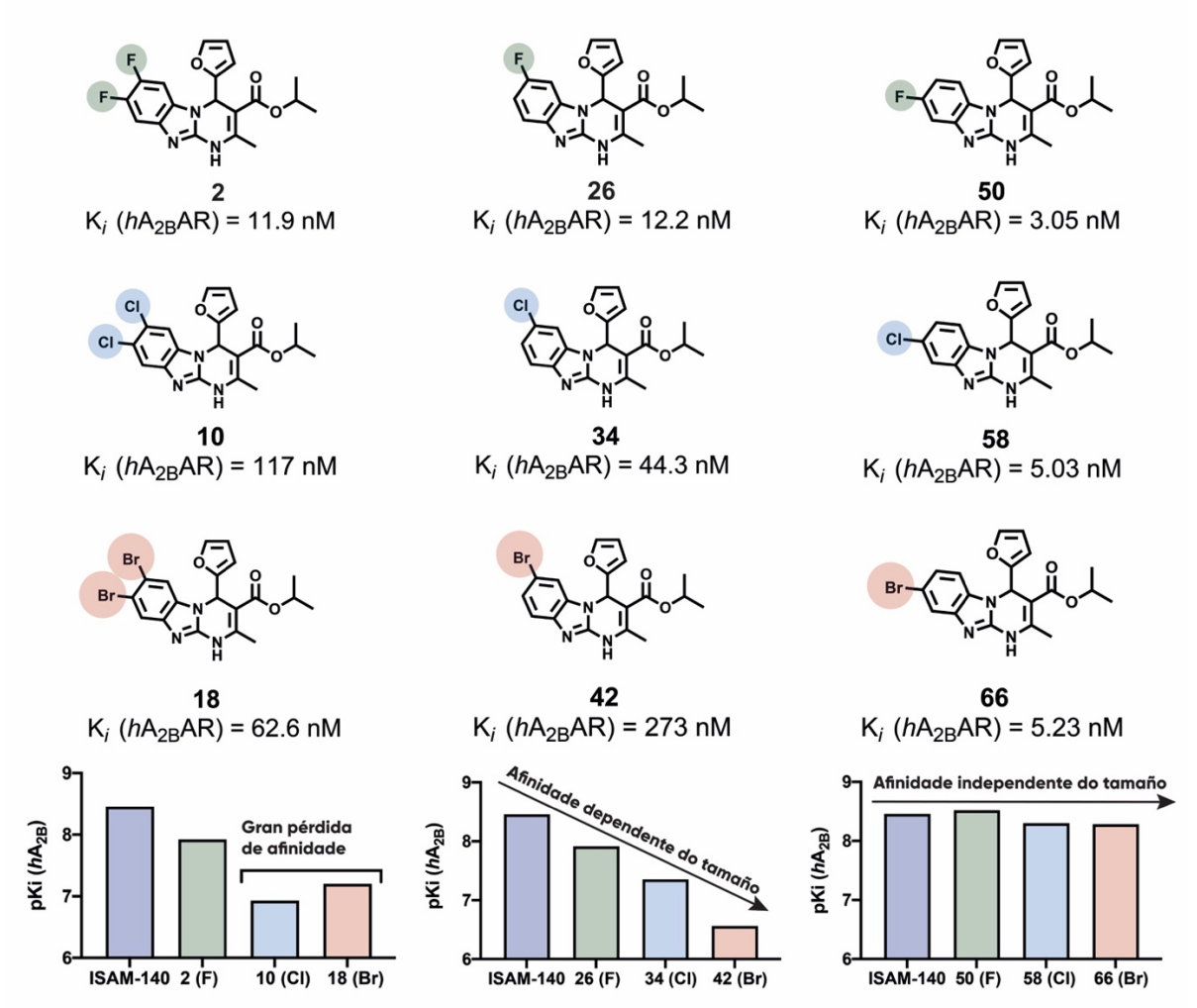

Figura 2. Tendencias na afinidade en función do patrón de haloxenación do sistema tricíclico.

Unha vez realizada a avaliación farmacolóxica, e debido á prometedora afinidade (do rango de nanomolar baixo) amosada pola mestura dos dous enantiómeros, realizouse a separación por HPLC quiral semipreparativo. A avaliación conxunta dos datos estruturais e de afinidade (K_i), así como os estudos de modelaxe molecular, proporcionan unha evidencia sólida da interacción estereoespecífica dos ligandos documentados neste capítulo co receptor A_{2B} de Adenosina. O uso combinado de HPLC quiral, dicroísmo circular e cristalografía de raios X permitiu obter evidencias experimentais inequívocas da interacción estereoespecífica dos nosos enantiómeros haloxenados co receptor A_{2B}. Ademais, neste capítulo documentamos por primeira vez a separación dun antagonista dual A_{2A}/A_{2B} (**60**) obtendo tamén evidencias da interacción enantioespecífica dos nosos ligandos duais tamén no receptor A_{2A} (Figura 3).

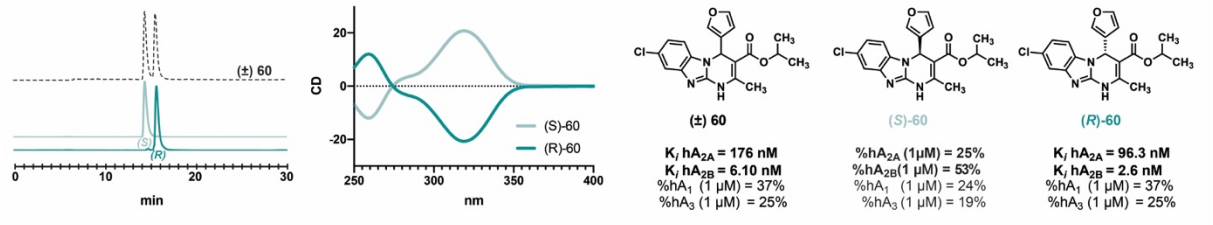

Figura 3. HPLC quiral, dicroísmo circular e datos farmacolóxicos do primeiro ligando dual descuberto nesta tese, **60**.

A análise do impacto da haloxenación no perfil farmacocinético dos novos ligandos avaliouse mediante a selección de 7 significativos – tanto a nivel estrutural como pola súa afinidade farmacolóxica – e mediuse a solubilidade, a estabilidade microsomal e a inhibición do citocromo P450. A solubilidade e a estabilidade microsomal aumentan a medida que se incrementa o tamaño do halóxeno (Br > Cl > F), mentres que a inhibición de citocromos aumenta ao aumentar o tamaño do halóxeno (F > Cl > Br), identificándose, pois, o Cloro como o mellor halóxeno para a 8-substitución. A combinación da estabilización do anel de benceno a través de halóxenos cos traballos previos de estabilización do anel heterocíclico pentagonal mediante bioisostería (*J. Med. Chem.* **2020**, 63, 14, 7721–7739) deu lugar a **78** (R^4 = 4-oxazolyl, R^3 = *i*-Pr, R^8 = F) que combina afinidade (K_i = 6.10 nM), selectividade (> 1000 veces nos receptores A_1, A_{2A} e A_3) e un excelente perfil farmacocinético.

O segundo capítulo desta tese de doutoramento (Sección 3.2) aborda o desenvolvemento de novos antagonistas A_{2B} (e duais A_{2A}/A_{2B}) mediante estratexias de "*Scaffold-Hopping"* empregando **SY1K-024** (monociclo), **ISAM-148** (biciclo) e **ISAM-140** (triciclo) como moléculas modelo. Baseándonos nos nosos logros anteriores, empregamos estratexias de salto de esqueleto para explorar a farmacocinética e, o máis importante, a farmacodinamia dos ligandos do A_{2B}AR. Este enfoque permítenos investigar modificacións estruturais e identificar novos esqueletos que poden mellorar a interacción coa parte máis profunda do sitio de unión ortostérico (Figura 3.19). Afondando nas complexidades das interaccións ligando-receptor, buscamos obter unha comprensión máis profunda dos mecanismos moleculares subxacentes da vía do A_{2B}AR e das súas posibles implicacións na terapia do cancro. Para alcanzar este obxectivo, empregamos a reacción de Biginelli como parte da nosa plataforma de síntese multicompoñente para desenvolver un número substancial de ligandos sinteticamente accesibles con estruturas diversas. Este enfoque permítenos explorar rapidamente o espazo químico e sintetizar conxuntos de compostos altamente diversos, acelerando así o descubrimento e desenvolvemento de novas terapias dirixidas para o tratamento do cancro.

Deseñáronse tres subconxuntos de compostos, explorando vinte e un aneis centrais (Figura 4): 1) 2-aminopirimidinas N^2-substituidas, 2) 4,7-dihidro-[1,2,4]triazolo[1,5-*a*]pirimidinas 2-substituidas, e 3) substitucións bioisostéricas na estrutura central de biciclos (4,7-dihidro-[1,2,4]triazolo[1,5-*a*]pirimidinas) e triciclos (1,4-dihidrobenzo[4,5]imidazo[1,2-*a*]pirimidinas). Esta exploración supón un total de 168 novas moléculas sintetizadas e avaliadas. A pesar da enorme diversidade estrutural, todas os compostos obtivéronse empregando a reacción de Biginelli como principal ferramenta sintética, con pequenos cambios nas condicións de reacción en función da estrutura a sintetizar. O primeiro subconxunto de moléculas permitiunos obter, mediante a substitución do grupo amino libre, diferentes tautómeros maioritarios na estrutura monocíclica, estudando como isto afecta ao modo de unión destes derivados no sitio ortostérico do receptor A_{2B}. Mentres que os compostos de tipo monocíclico e tricíclico foron amplamente estudadas no antagonismo A_{2B}, a estrutura central bicíclica non tanto. O obxectivo do subconxunto 2 é incrementar a exploración ao redor da estrutura bicíclica mediante a substitución en posición 2, explorando a interacción profunda co sitio ortostérico do receptor A_{2B}. Por último, o subconxunto 3 sintetizouse mediante a estratexia de *Scaffold-Hopping*, empregando substitucións bioisostéricas (por exemplo, CH-N e NH-S). Tras a avaliación farmacolóxica dos 168 ligandos, observáronse certas tendencias claras no

comportamento. Os mellores compostos sintetizados foron os de estrutura tricíclica e, a pesar de perder a interacción por dobre ponte de hidróxeno, os derivados 4H-benzo[4,5]tiazolo[3,2-a]pirimidínicos (bioisostería NH-S) mantiveron e incluso melloraron a afinidade con respecto á serie modelo. Por outra banda, a perda da interacción por dobre ponte de hidróxeno dos derivados monocíclicos fixo perder totalmente a afinidade farmacolóxica polo receptor A_{2B}. Isto indica claramente a superioridade da estrutura tricíclica con respecto á monocíclica e bicíclica para a unión co receptor A_{2B}.

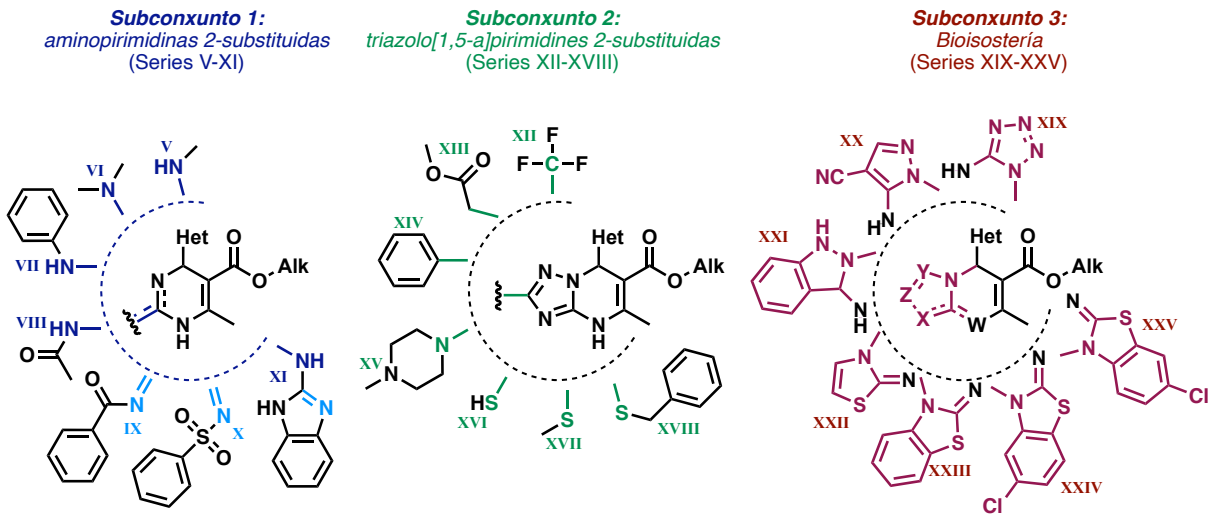

Figura 4. Estratexias de deseño empregadas no capítulo II.

Debido aos bos datos de afinidade obtidos nas mesturas racémicas dos compostos tricíclicos, separáronse enantiómeros dos 2 antagonistas selectivos A_{2B} e un dual A_{2A}/A_{2B} e avaliáronse por separado. Para iso, utilizouse unha mestura de HPLC quiral e dicroísmo circular. Os datos farmacolóxicos obtidos foron reveladores. Os resultados previos do grupo mostraban unha total enantioselectividade, onde un dos enantiómeros acumulaba toda a afinidade farmacolóxica, mentres que o outro era totalmente inactivo. Neste caso, ambos enantiómeros mostran afinidade, sempre en maior medida aquel co anel pentagonal cara atrás no plano (Figura 5). Este cambio pódese atribuír á ausencia do dobre ponte de hidróxeno, o que diminúe a rixidez da interacción co sitio ortostérico, permitindo que o distómero tamén se acomode. Ademais, grazas á avaliación por separado de cada enantiómero no ligando dual **243**, observamos que, ao igual que no capítulo anterior, o efecto enantioespecífico mantense no receptor A_{2A}.

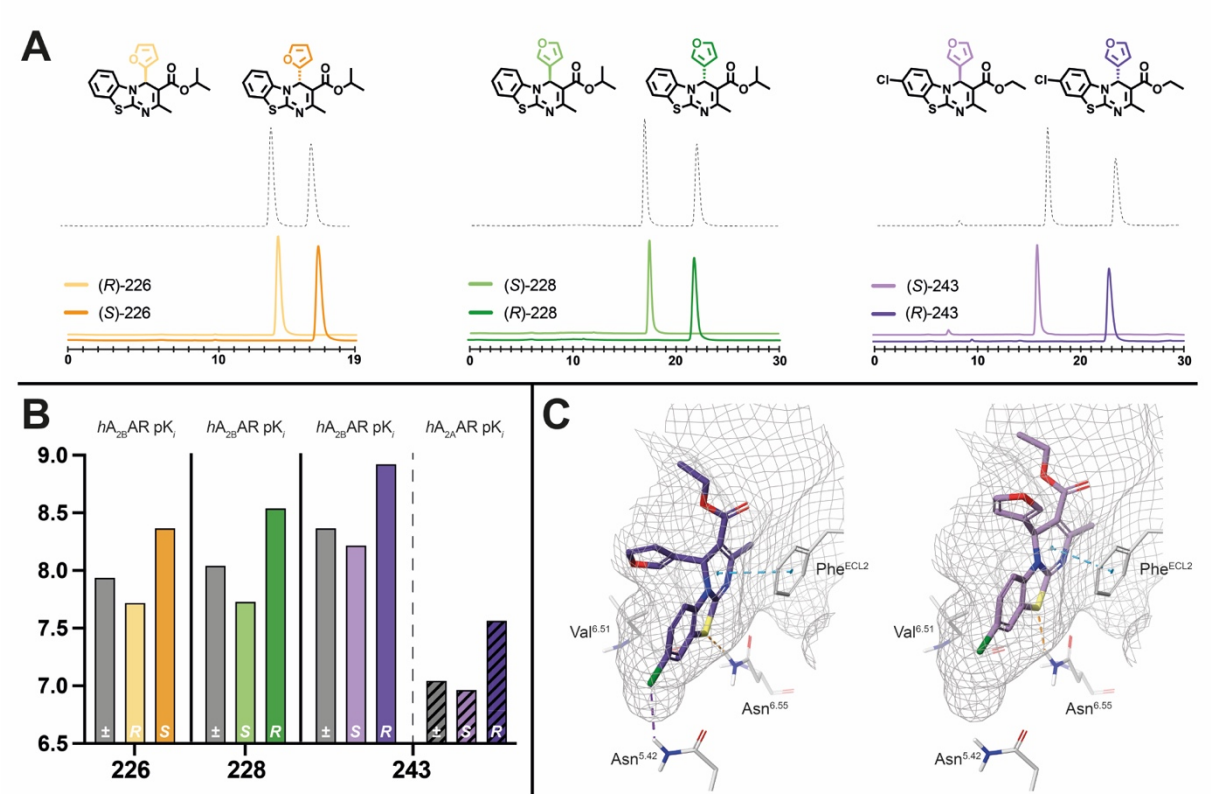

Figura 5. A) HPLC quiral dos compostos do capítulo II. B) Representación gráfica da afinidade dos enantiómeros en receptores A_{2A} e A_{2B}. C) Modo de unión do eutómero (esquerda) e o distómero (dereita).

O terceiro capítulo da tese (Sección 3.3) documenta o descubrimento racional de antagonistas duais A_{2A}/A_{2B}. Realizamos unha exhaustiva avaliación do impacto da substitución de nitróxeno(s) por residuos alquílicos e bencílicos. As nosas descubertas anteriores, presentadas no capítulo anterior, demostraron que o doador de ponte de hidróxeno non era esencial para manter a afinidade farmacolóxica co A_{2B}AR. Ademais, en publicacións anteriores descubrimos que os aneis aromáticos podían estabilizar a conformación aberta do A_{2A}AR. Estas observacións levaron ao desenvolvemento dunha nova serie de compostos que exploraban a parte extracelular do sitio de unión ortostérico (Figura 6).

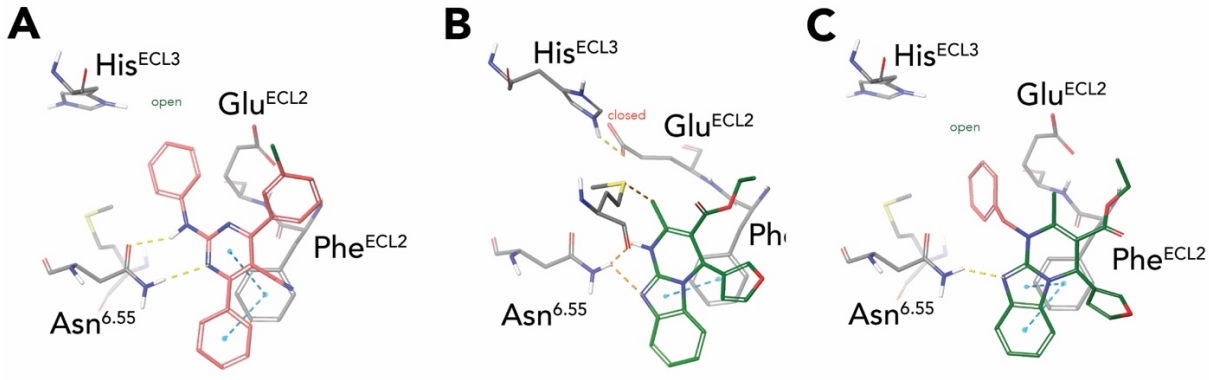

Figura 6. Estratexia de deseño empregada no capítulo III.

O obxectivo principal desta investigación era crear compoñentes híbridos que superpuxeran os antagonistas selectivos do $A_{2A}AR$ publicados polo noso grupo de investigación en 2022 (*J. Med. Chem.* **2022**, 65, 3, 2091–2106) co noso esqueleto selectivo do $A_{2B}AR$, obtendo así ligandos duais. Para este capítulo, sintetizamos e caracterizamos 12 novos ligandos monocíclicos e 62 novos ligandos tricíclicos (Figura 7). O deseño destes compostos está apoiado por *modeling* e *docking* de ligandos. Os nosos resultados demostran que a *N*-substitución ten un efecto significativo no aumento da afinidade de unión aos receptores A_{2A} e A_{2B}. Os nosos descubrimentos presentan grande promesa para o desenvolvemento en curso de novos antagonistas duais do $A_{2A}AR/A_{2B}AR$, destacando o potencial desta clase innovadora de compostos no tratamento de diversas enfermidades. Este traballo está a ser perseguido activamente e os nosos resultados ofrecen información valiosa no campo, abrindo o camiño para futuros avances no deseño e síntese de antagonistas duais.

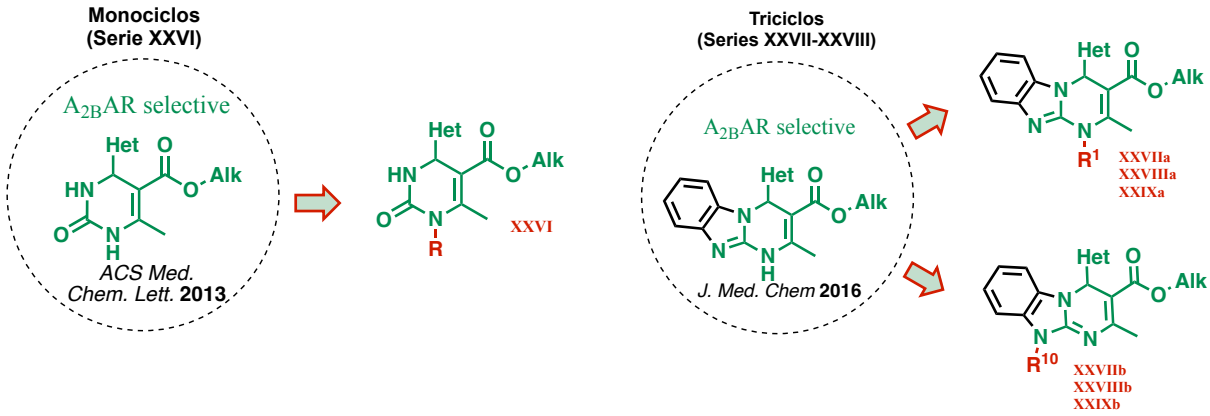

Figura 7. Series sintetizadas no capítulo III.

A síntese dos derivados fíxose mediante alquilación directa das moléculas modelo, obtendo un isómero no caso dos monociclos e dous rexioisómeros no caso dos triciclos. A avaliación farmacolóxica dos 74 novos ligandos amosou resultados prometedores no desenvolvemento de ligandos duais, sendo identificados vinte e seis antagonistas duais dos receptores A_{2A} e A_{2B}, quince dos cales combinan alta afinidade para ambos os receptores e destacada selectividade (K_i < 100 nM para A_{2A}AR e A_{2B}AR e > 1000 nM para outros dous subtipos). O estudo de *docking* apoia as nosas pesquisas iniciais, demostrando que os derivados bencílicos son capaces tanto de estabilizar a unión co receptor A_{2B} – a pesar da ausencia do dobre ponte de hidróxeno, como de facilitar a unión ao receptor A_{2A}, ao establecer novas interaccións ca parte extracelular do sitio ortostérico.

De igual forma que nos capítulos anteriores, todas as moléculas avaliáronse como mesturas racémicas, das cales catro (unha selectiva A_{2B} e tres duais A_{2A}/A_{2B}) foron seleccionadas para a súa separación mediante HPLC quiral, amosando as mesmas tendencias que as xa mencionadas. Con esta separación, obtivemos **(*S*)-266a**, o antagonista non xantínico máis potente (K_i = 0.52 nM) e selectivo para o receptor A_{2B} de Adenosina ata a data de hoxe.

O cuarto e último capítulo da tese (Sección 3.4) foi publicado na revista *Journal for Immunotherapy of Cancer* (*J. ImmunoTher. Cancer*, **2022**, 10, e004592). Neste traballo abordamos a validación dos novos antagonistas, tanto selectivos A_{2B} como duais A_{2A}/A_{2B} na inmunoterapia do cancro. Para isto, empregamos tres tipos e tumores, con características moi distintas: mama, colorrectal e glioblastoma. Co obxectivo de seleccionar as mellores moléculas para cada tipo tumoral, avaliamos *in silico* as propiedades fisicoquímicas de todos os compostos sintetizados. Os compostos foron avaliados a dous niveis: 1) immunoestimulador e 2) antiproliferativo. Ca publicación do noso artigo validouse por primeira vez ao receptor A_{2B} como punto de control inmunitario, xunto co receptor A_{2A} previamente validado. O bloqueo do receptor A_{2B} (e de A_{2A} no caso dos fármacos duais) demostrou reactivar ao sistema inmune contra as células tumorais, incrementando a cantidade de células inmunitarias, aumentando a liberación de citocinas pro-inflamatorias e a infiltración de células citotóxicas en esferoides de células tumorais. A avaliación a nivel antiproliferativo amosou tamén resultados excelentes, ao demostrarse unha inhibición do crecemento tumoral nos tres tipos de cancro avaliados, aumentando a apoptose e diminuíndo a entrada na fase celular, sen afectar as células sas.

En conxunto, os resultados aquí documentados destacan o potencial das reaccións multicompoñente, especificamente a reacción de Biginelli, para acelerar o descubrimento, a optimización de novas entidades farmacolóxicas, ademais de validar o papel dos antagonistas A_{2B} e duais A_{2A}/A_{2B} non xantínicos na inmunoterapia do cancro.

1 INTRODUCTION

Cancer is traditionally viewed as a condition in which cells in a specific part of the organism grow and reproduce uncontrollably, invading and destroying surrounding healthy tissue and organs. Its high heterogeneity, with more than 100 distinct types, makes the disease complex and dynamic. It is estimated that 25% of men and 20% of women will develop cancer in their lifetime (Figure 1.1), and of those, 50% and 45%, respectively, will die from it.[1] In view of the evidence provided, cancer is humanity's greatest pandemic. The incidence of cancer during the year 2020 in Spain was 276,239. The number of deaths for the same year was 113,054 for Spain and almost 10 million worldwide, being the leading cause of death in men and the third one in women, only behind circulatory and infectious diseases.[2]

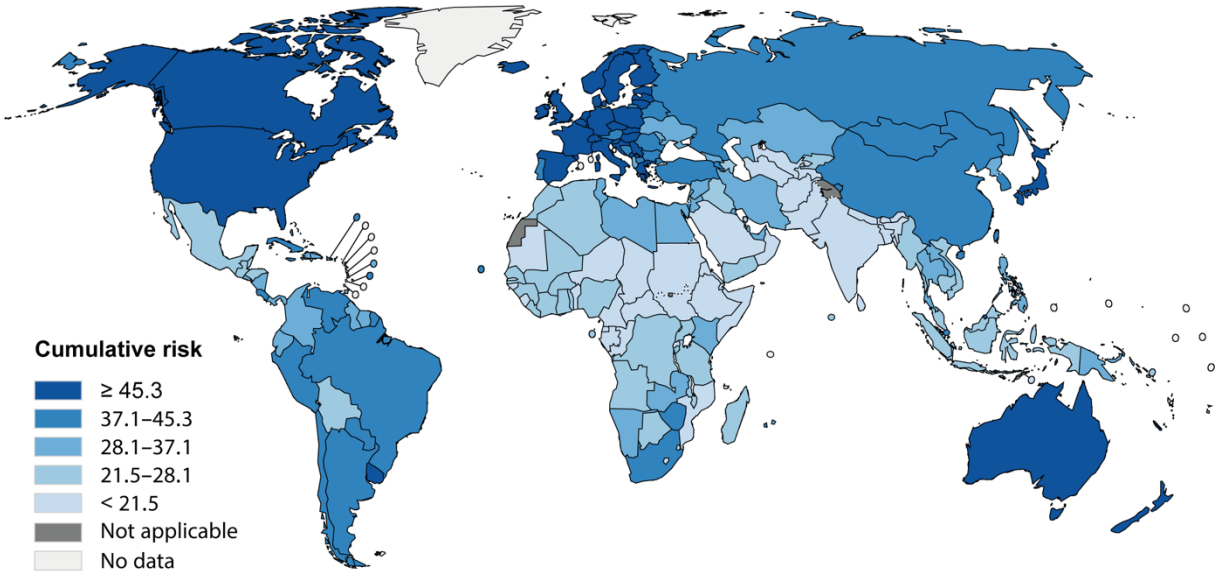

Figure 1.1. Cumulative risk of cancer incidence (probability for developing cancer of a person free of disease) in 2020, all cancer types, both sexes, all ages. Data source: GLOBOCAN 2020. Graph production: IARC (http://www.iarc.fr/), World Health Organization.[1]

Considering both sexes and all ages, the four most common cancer types are breast (11.7%,), lung (11.4%), colorectum (10%) and prostate (7.3%); lung (18%) and colorectum (9.4%) having a higher mortality rate. Race, sex, habits, and other factors are fundamental in the development and survival of cancer. Obesity, infections, UV radiation, and alcohol and tobacco consumption are the most important lifestyle and environmental risk factors

worldwide. To highlight, 6% of cancer cases in Spain are attributed to obesity, 14.6% to infections (*Helicobacter pylori*, Human papillomavirus, and Hepatitis virus), 2% to UV radiations (76% of all melanomas) and 14% to alcohol and tobacco (causing 90% of all lung cancer).[1] This, coupled with the longer life expectancy of more developed countries, means that they are at greater risk of developing and dying from cancer.

1.1 CONVENTIONAL CANCER THERAPIES

Cancer treatment has considerably evolved since the beginning of the 20th century.[3] The first and most obvious solution to treat a solid tumor was surgery, with the elimination of the malignant cell mass being the overall goal of this antitumor treatment. Therapy evolved into non-surgical less invasive treatments based on ionizing radiation (radiotherapy). With the scientific advances from the 1940s to the 1980s (e.g., first synthetic anticancer drugs, hybridoma technology), new therapeutic opportunities emerged (Figure 1.2).

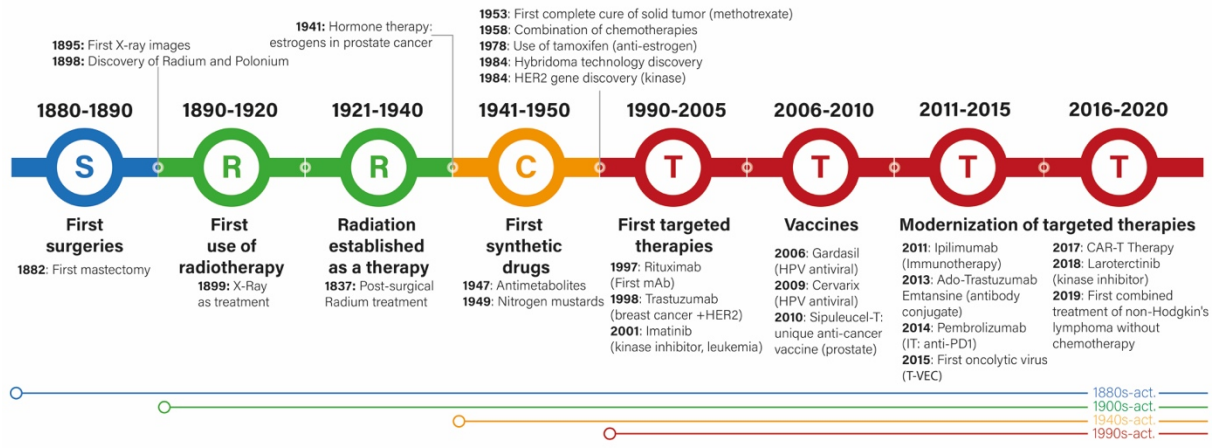

Figure 1.2. Milestones in cancer research and discovery over the last 250 years. Data taken from NIH (National Institutes of Health). S = Surgery, R = Radiotherapy, C = Chemotherapy, and T = Targeted therapies.

Chemotherapy involves of the use of chemical agents to attack and destroy cells that divide rapidly, such as tumor cells, by preventing mitosis or inducing DNA damage. While surgery and radiotherapy allow a "targeted" attack of the tumor mass, chemotherapy constitutes the first type of systemic therapy. Four major groups of chemotherapeutic agents can be distinguished: alkylating agents, antimetabolites, intercalating agents, and mitotic inhibitors. Alkylating agents (e.g., nitrogen mustards: Chlorambucil; nitrosoureas: Carmustine; and alkyl sulfonates: Busulfan), are highly electrophilic species, that react with DNA molecules, affecting cell division. Antimetabolites (e.g., Methotrexate, 5-Fluorouracil), on the other hand, replace purine

and pyrimidine bases in DNA synthesis, generating aberrant genetic material and resulting in cell death. Intercalating agents (e.g., Doxorubicin) are polyaromatic chemical compounds that can insert themselves between the base pairs of DNA, distorting its structure and interfering with its normal function. The latter, antimitotics (e.g., Paclitaxel and vinca alkaloids), generally derived from natural substances, are capable of blocking the formation of microtubules, thus preventing cell mitosis. Despite targeting non-specific mechanisms, treatments are generally dependent on the type of tumor, complicating antineoplastic therapy. Moreover, these cytotoxic mechanisms (affecting cell division) of chemotherapeutic agents cause damage to healthy cells, especially those that physiologically divide rapidly. This produces the most common side effects of chemotherapy: immune and myelosuppression, alopecia, and gastrointestinal distress. In addition to the above, we must add the possibility of drug resistance occurring, caused primarily by upregulated reparatory DNA enzymes, excretory pumps (p-glycoprotein) or modified apoptosis routes in tumor cells. For all these reasons, in the last decade of the 20th century, research and development of new antitumor treatments has focused on targeted therapies.

1.2 TARGETED THERAPIES. HALLMARKS OF CANCER AND IMMUNE CHECKPOINTS

Cancer research in recent years has opened a wide range of insights into how the disease works. Whereas in the past cancer was simplified as a "disease where cells divide uncontrollably", we now know that it is a complex and multifactorial disease. To organize and rationalize the complexities of cancer, Douglas Hanahan and Robert Weinberg proposed in 2000 six **Hallmarks of Cancer** (Figure 1.3).[4] These hallmarks included a) Self-sufficiency in growth signals, b) Insensivity to anti-growth signals, c) Unlimited replicative potential, d) Evading programmed cell death, e) Uninterrupted angiogenesis, and f) Tissue invasion and metastasis. In two updates published in 2011 and 2022,[5,6] Weinberg and Hanahan proposed four new hallmarks: g) Abnormal metabolic pathways, h) Avoiding the immune system attack, i) Unlocking phenotypic plasticity and j) Senescent cells. In the 2011 and 2022 publications,[5,6] four enabling characteristics have been added to the Hallmarks: a) genome instability and mutation, b) nonmutational epigenetic reprogramming, c) polymorphic microbiomes, and d) tumor-promoting inflammation.

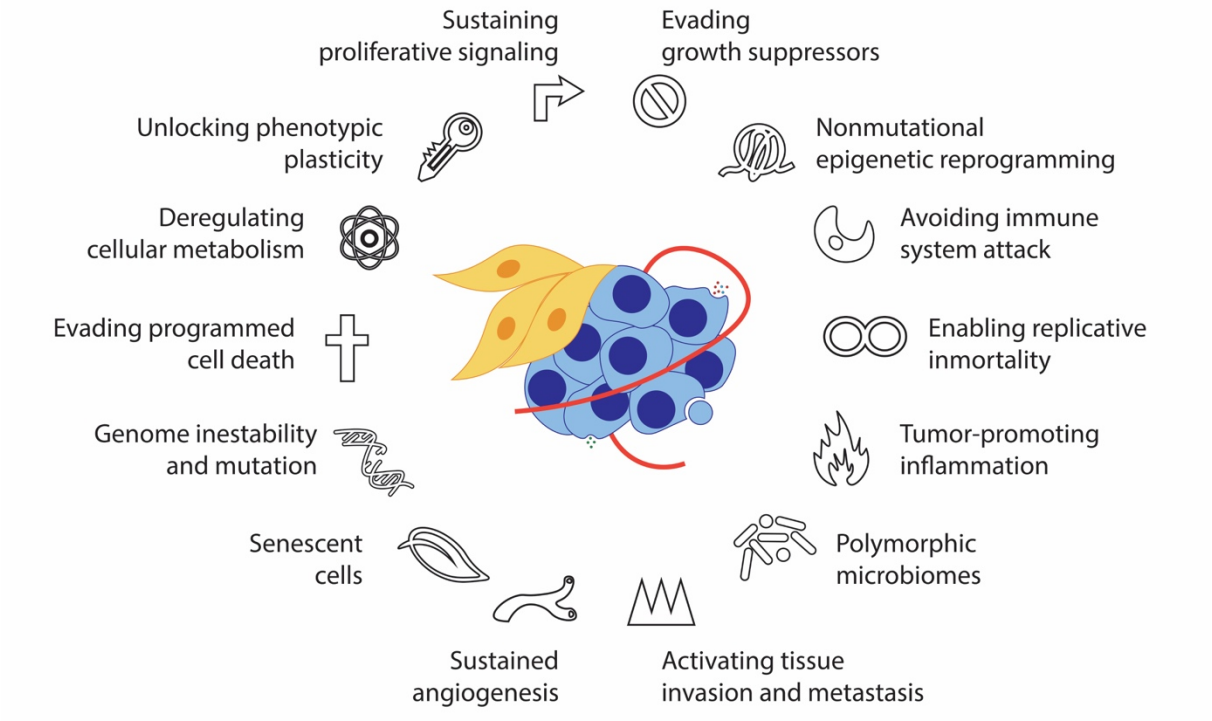

Figure 1.3. Hallmarks of cancer.

1.2.1 Sustaining proliferative signaling

Normal Cells require growth factors (GF) to enter a proliferative state. The GF signals interact with their receptors in a diffusible manner: endocrine, where the GF is synthesized by specific body cells or glands; paracrine, where the GF is produced by adjacent cells; juxtracrine, where the GF remains attached to the membrane and activates adjacent cells; and autocrine, where the GF is produced by the cell itself. There are more than 30 classes of GF,[7] being particularly relevant within the immune-based therapy of cancer:

- Interleukins (IL):
  - IL-1: activates T cells.
  - IL-2: T-cell GF. Stimulates IL-1 synthesis and activates B and NK-cells.
  - IL-4: GF for activated B cells.
  - IL-6: stimulates Ig synthesis. GF for plasma cells. Decreases cell adhesion.
  - IL-10: inhibits synthesis of pro-inflammatory cytokines such as IFN-γ, IL-2, TNF-α and decreases antigen presentation capacity.
- Transforming growth factors (TGF):
  - TGF-α: activates signaling pathway for cell proliferation, differentiation, and development.

- TGF-β: stops the cell cycle, inhibiting proliferation, inducing differentiation or apoptosis. In some cancer cells, parts of the TGF-β are mutated, increasing proliferation versus differentiation.

— Fibroblast growth factors (FGF): generated by macrophages and cancer-associated fibroblasts (CAFs), they are involved in an extensive diversity of growth processes.

— Epidermal growth factor (EGF): activation of its receptor (EGFR) results in cellular proliferation, differentiation, and survival.

— Tumor necrosis factor alpha (TNF-α): activation of his receptors (TNFR1 and TNFR2) allows the initiation of two signaling pathways:

- Activation of nuclear factor kappa-light-chain enhancer of activated B cells (NF-κB), which mediates the transcription of proteins involved in cell survival and proliferation, inflammatory response, and anti-apoptotic factors.
- Activation of the mitogen-activated protein kinase pathway (MAPK), involved in cell differentiation, proliferation, and apoptosis.

— Vascular endothelial growth factor (VEGF): stimulates the formation of blood vessels by activation of VEGF receptor (VEGFR).

The GF signals are transmitted to the cell by transmembrane receptors that bind distinctive classes of signaling molecules. This behavior contrasts strongly with cancer cells, which invariably show an independence on exogenous growth stimulation. While most GF act via paracrine or endocrine mechanisms, many cancer cells acquire the ability to synthesize GF for themselves, creating a positive feedback loop (autocrine stimulation).[4,7] Furthermore, juxtracrine signaling may be affected. Cancer cells promote the expression of integrins that transmit progrowth signals (enhancing resistance to apoptosis and entrance into the active cell cycle).

1.2.2 Evading growth suppressors

Antigrowth signals are mostly encoded by tumor suppressor genes. Generally, tumor suppressor genes inhibit the same pathways that are stimulated by oncogenes.[8] The proteins transcribed from these genes mostly inhibit cell proliferation, highlighting:

— Receptors or signal transducers for hormone inhibitors of cell proliferation (*e.g.,* TGF-β).

— Checkpoint controllers of cell cycle (e.g., pRb, BRCA-1).

— Proteins that induce apoptosis (*e.g.,* p53).
— Proteins involved in cell adhesion, suppressors of metastasis.
— Proteins involved in repairing mistakes in DNA.

In cancer these proteins are altered or inhibited, and they do not prevent cell division, even if the cell has serious irregularities.

1.2.3 Evading programmed cell death

Neoplastic cells expand in number not only due to their faster growth rate, but also thanks to their ability to evade death. Apoptosis is a highly regulated form of programmed cell death triggered by cellular stress (intrinsic pathway, e.g., Bcl-2 family) or ligand binding to cell-surface death receptors (extrinsic pathway, e.g., TNFR, DR3, PD-1). Cancer cells are characteristically able to avoid these mechanisms.

1.2.4 Enabling replicative immortality

The three previous features lead to an environment-independent cell growth. However, this does not ensure expansive tumor growth. Normal cells are programmed to limit their replication regardless of the characteristics explained above (senescence).[4,5] This is due to the telomeric DNA progressive shortening during each cell cycle. Cancer cells bypass this, mostly by upregulating telomerase to extend their telomeres.[9,10]

1.2.5 Sustained angiogenesis

For survival, any cell must reside within 100 μm of a capillary blood vessel, ensuring the arrival of nutrients and oxygen.[5] During normal organogenesis, this is guaranteed by coordinated growth of vessels and tissues. When oxygen and nutrient requirements are physiologically increased, the growth of new blood vessels (angiogenesis) is tightly regulated, with a perfect balance of pro- and anti-angiogenic signals. Tumors overproduce various pro-angiogenic factors (VEGF being ubiquitous), breaking that balance, causing the generation of novel vascular networks.[11]

1.2.6 Activating tissue invasion and metastasis

Metastasis involves several processes in which cancer cells migrate to other parts of the body through the circulatory or lymphatic system. To do this, malignant cells leave the primary tumor by degrading the proteins that make up the extracellular matrix (ECM) and are released

into circulation. Increased vascularization (angiogenesis), as well as the stromal invasiveness of the malignant cells, are two key points in the success of metastasis.[12]

1.2.7 Deregulating cellular metabolism

The uncontrolled growth and overactivity of cells causes a marked increase in tissue needs for nutrients and oxygen. Therefore, cancer cells must adjust their metabolism to continue their growth rate. Under aerobic conditions normal cells process glucose first to pyruvate (via glycolysis) and finally to carbon dioxide in the mitochondria. Under anaerobic conditions, glycolysis is promoted, and relatively little pyruvate is delivered to the mitochondria. To compensate the deficiency in the use of the anaerobic pathway in the generation of ATP (~ 18-fold lower), the production of glucose transporters is upregulated, increasing the entry of glucose into the cytoplasm. In addition to glucose metabolism, a plethora of metabolic pathways are affected, including the synthesis and degradation of extracellular adenosine (ADO).[13,14]

1.2.8 Avoiding immune system attack

Under physiological conditions, tissues and cells are constantly monitored by an ever-alert immune system capable of eradicating formation and progression of incipient tumors and metastasis. Solid tumors that survive have somehow managed to avoid detection and attack by the immune system.[5,6] The complexity of cancer advice new approaches that go beyond the tumor cell, taking into consideration the importance of surrounding environment. This environment, known as tumor microenvironment (TME), includes the surrounding blood vessels, immune cells, signaling molecules and the extracellular matrix. The TME is a determinant of tumor progression and treatment success rate, not only for immunotherapy but also for chemotherapy and radiotherapy.[15] Cancer cells are the starting point for the formation of TME, but the amount of the cancer cells in a tumor represents only a small portion of the total number of tumor cells and an even smaller part of the whole tumor mass.[16]

The principal non-cancer tumor component in the TME is constituted by immune cells and CAFs. Tumor associated immune cells derive from myeloid and lymphoid lineages (Figure 1.4). Myeloid lineages include tumor-associated macrophages (TAM), monocytes, granulocytes, myeloid-derived suppressor cells (MDSC) and dendritic cells (DCs). TAM can differentiate to two types of macrophages: M1, with antitumor activity; and M2, with oncoprotective functions. TME can also regulate the differentiation of circulating myeloid progenitors and monocytes from DCs to MDSCs, reducing antigen presentation and improving

immunosuppressive functions.[17] TME lymphoid component, the tumor infiltrating lymphocytes (TILs), include T and B lymphocytes together with natural killer (NK) cells. Tumor infiltrating T cells involve the $CD4^+$ T cells, also called helper T lymphocytes (Th) and majority of $CD8^+$ T cells, also known as cytotoxic T lymphocytes (CTLs). Type-1 $CD4^+$ T cells (T helper-1 or Th1 cells) produce and secrete effector cell activation cytokines (IL-2, TNF-α and IFN-γ), contributing to antitumor CTLs and TAM (via enhancement of M1 differentiation) immune response. T regulator lymphocytes (Treg), another type of Th, produce and secrete effector cell inhibition cytokines (TGF-β and IL-10), suppressing CTL and TAM functions (via enhancement of M2 differentiation) and activating MDSCs. Another subgroup of $CD4^+$ T cells, Th2 and Th17 cells, are considered to have tumor-assisting functions.[15,17]

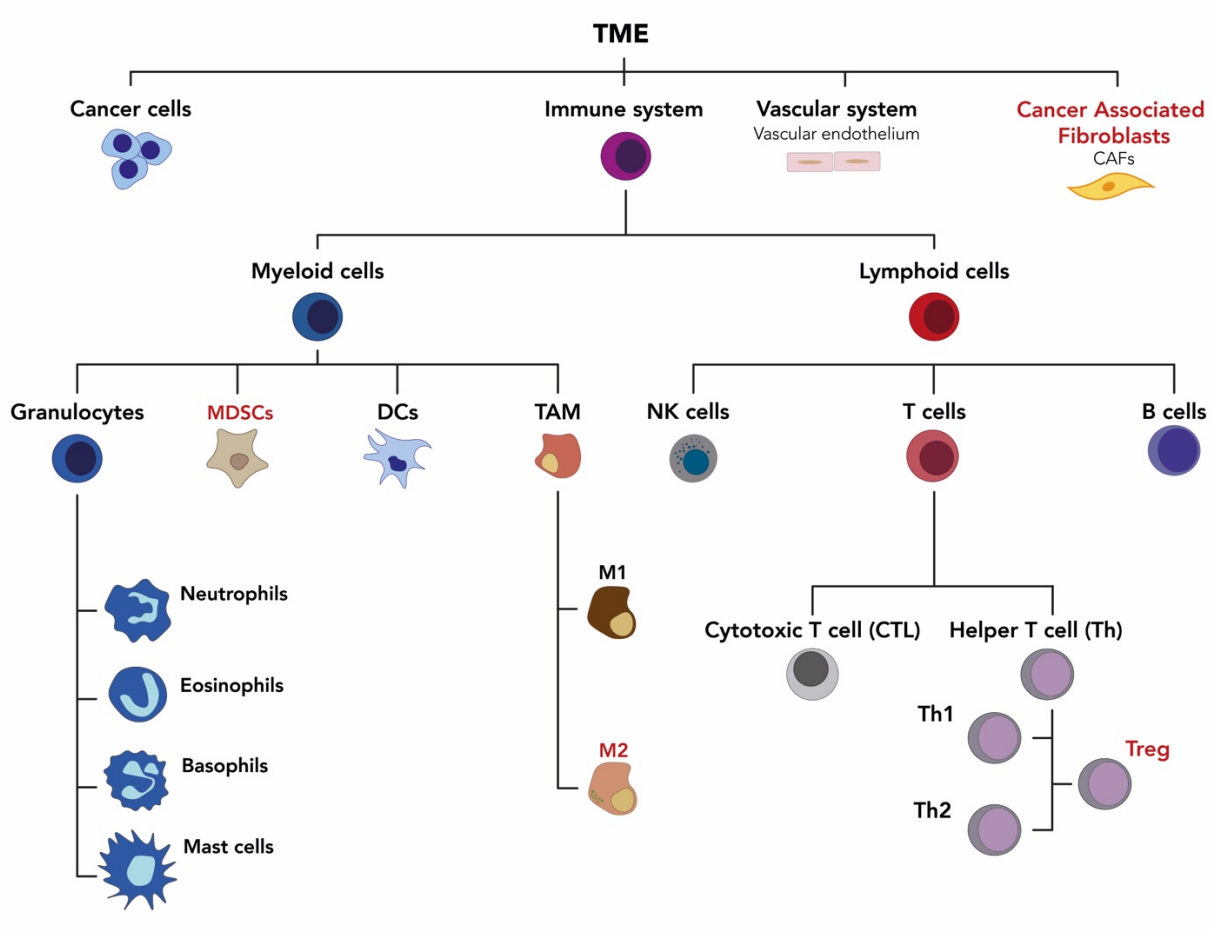

Figure 1.4. Cellular components in the tumor microenvironment. In red: pro-tumoral cell types (anti-inflammatory and pro-angiogenic functions).

1.2.9 Unlocking phenotypic plasticity

Phenotypic plasticity refers to some changes in cell behavior and physiology in response to a unique environment. During organogenesis, the cells differentiate from progenitor cells (normal differentiation). The end of this differentiation is in most cases antiproliferative and constitutes a barrier to the proliferation necessary for neoplasia. In the last few years, Cancer Stem Cell (CSC) theory has gained relevance. CSC is a hypothetical cancer cell with stem cell characteristics (self-renewal and multiple cell differentiation) that persists in tumors and is not affected by conventional therapy, causing relapses and metastasis.[18] It remains to be elucidated whether stem cells initiate the tumor or whether it is cell plasticity, through dedifferentiation, that transforms normal tumor cells into CSCs that contribute to the development and maintenance of the disease.[6]

1.2.10 Senescent cells

Cellular senescence is characterized by the cessation of cell division due to DNA damage (caused by telomere shortening or oncogenes). Senescence can be seen as a protective mechanism against neoplasia that prevents aging or damaged cells from continuing cell division; but increased evidence reveals the opposite: senescent cells stimulate tumor development and malignant progression.[6] Tumor progression relies primarily on the senescence associated secretory phenotype (SASP) of senescent cells, which leads to the release of paracrine pro-tumor factors. For example, SASP CAFs provide paracrine support for local invasion and metastasis of cancer developing in proximity,[19] recruit immunosuppressive immune cells and stimulate tumor growth.[20]

1.2.11 Enabling characteristics

While the four enabling characteristics of cancer - tumor-promoting inflammation, gene instability and mutation, non-mutational epigenetic reprogramming, and polymorphic microbiomes - are not sufficient on their own to cause cancer, they can create an environment that assists cells in transitioning from a normal state to an oncogenic state.

Genome instability and mutation refers to genetic changes that occur in cells, including mutations, chromosomal rearrangements, and DNA damage. These changes can disrupt normal cellular functions and contribute to the development of cancer. Causes of genome instability and mutation include exposure to environmental mutagens such as UV radiation, as well as errors that occur during DNA replication or repair. Highly related to the previous one, non-

mutational epigenetic reprogramming involves alterations in gene expression patterns without changes in the underlying DNA sequence (epigenetic changes). These changes can contribute to the development of cancer by promoting changes in cell behavior, such as increased proliferation and decreased apoptosis. Non-mutational epigenetic changes can be caused by a variety of factors, including exposure to environmental toxins, aging, and lifestyle factors such as diet and exercise. The role of polymorphic microbiome is important since the human body is inhabited by more than 100 billion bacteria. These microorganisms can play a role in cancer development by altering the immune system's response, promoting chronic inflammation, and producing metabolites that can influence cell behavior. The composition of the microbiome can vary between individuals and can be influenced by factors such as diet, lifestyle, and antibiotic use.

The last one, highly related with the context of this Thesis, is chronic inflammation.[21] This enabling characteristic can promote the development of cancer by causing DNA damage, promoting cell proliferation,[21] and suppressing immune responses[15] that would normally target cancer cells. Inflammation can be triggered by a variety of factors, including infections, exposure to environmental toxins, and lifestyle factors such as diet and obesity. Tumor-promoting inflammation can create an environment that supports cancer development and progression by creating conditions that allow mutated cells to survive and proliferate.

1.2.12 Immune checkpoints

The improved understanding of cancer, the availability of specific targets and the development of monoclonal antibodies, has given way to a new type of treatment, known as targeted or selective therapies. Targeted therapies are based in drugs that block the growth and spread of cancer by interfering with molecular targets involved in tumor progression (Hallmarks). These new therapies have three principal differences with conventional chemotherapy. First, and the most obvious difference, selective therapies concentrate on cells or systems highly involved in cancer, while in chemotherapy targets are the high-speed division cells. Second, selective therapies are designed with a specific target in mind, whereas many classical chemotherapies were discovered because of their cytotoxicity. The third and final difference is that targeted therapies aim to block cell proliferation, whereas conventional chemotherapy focuses on eliminating cells that grow irregularly.

Many different targeted therapies have been approved for use in cancer treatment: hormone-based therapy (for hormone-sensitive tumors, *e.g.*, breast and prostate), signal

transduction inhibitors, epigenetic modulators, gene expression modulators, apoptosis inducers, angiogenesis inhibitors, and immunotherapies. Particularly effective is the latter (immunotherapy), in which the immune system cells are stimulated to selectively attack the tumor through immune system modulators (immune checkpoints).[22]

Immune checkpoints are the cornerstones of cancer immunotherapy; they are inhibitory proteins responsible for tumor oncoprotection at the immune level. Currently, the most studied immune checkpoints are the CTLA-4, PD-1 and PD-L1 proteins, which facilitate tumor evasion by avoiding the immune system's attacks. Two families of immune checkpoint inhibitors drugs [with biologic origin, monoclonal antibodies (mAbs)] have been developed and introduced in clinical practice (which differ in their mechanism and site of action): anti-CTLA-4 and anti-PD/PD-L 1/2. CTLA-4 is a protein expressed on T cells during the early stages of their activation. CTLA-4 interacts with CD80, expressed on the antigen presenting cell, to prevent an excessive immune response (unwanted autoimmunity). CTLA-4 inhibitors (e.g., the monoclonal antibody Ipilimumab), block the CTLA-4/CD80 interaction which deactivates the inhibitory signal, thus increasing the T-cell immune response against the tumor. On physiological conditions T lymphocyte stimulated against an antigen expresses (on its surface) the PD (programmed death receptor) which prevents overactivation of the immune system (Figure 1.5A). The deactivation of this process occurs upon binding of the receptor to its ligand (PDL1 or PDL2) which is usually expressed by dendritic cells or macrophages. This mechanism is employed by multiple tumors, which express large amounts of PD-L1 or PD-L2 on their surface, thus escaping the immune system and facilitating their proliferation (Figure 1.5B). PD-1/2 antibodies (e.g., the mAbs Nivolumab, Zimberelimab and Pembrolizumab) or PD-L1/2 blockers (e.g., the mAbs Atezolizumab, Avelumab and Durvalumab) act on T cells and can stimulate the immune response against tumor cells.

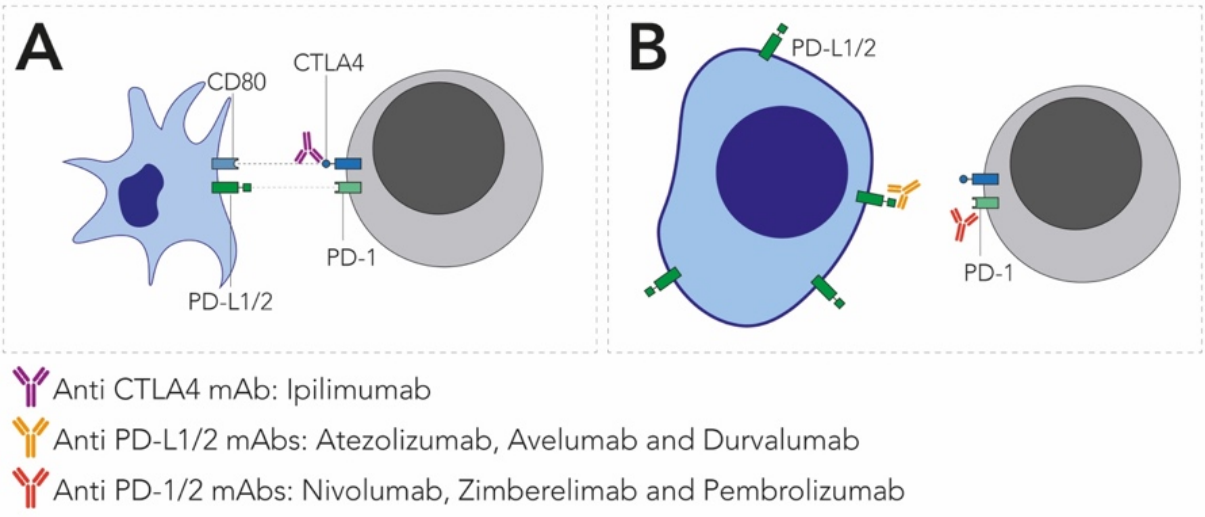

Figure 1.5. A) Physiological regulation of immune system activation through dendritic cells (blue) and T lymphocytes (grey) B) Oncoprotective effect of PD1-PDL1 system in cancer cells (blue).

All of the immune checkpoint inhibitors currently in clinical use are drugs of biological origin, primarily monoclonal antibodies.[22] With very satisfactory response and survival rates in patients who respond to treatment, their study, production and approval by regulatory agencies has grown considerably in the last 10 years.[23,24] Despite their specificity, and success in advanced malignancies, the structural uniqueness and their mechanism of action impose new challenges in cancer therapy. Their systematic study is identifying limitations that mark new lines of research and highlight the fact that monoclonal antibodies are far from being the ideal drug. Among their main limitations we can point out the lack of response to treatment found in around 50%[25] of patients and the appearance of severe allergic reactions, adverse effects (myocarditis, vasculitis, heart failure, etc.) and episodes of resistance (due to increased activity of the immune system), all of which are relatively frequent. In addition, their complex pharmacokinetics generate permeability problems and they are very expensive to manufacture (limiting the sustainability of healthcare systems and making them inaccessible to many patients). Finally, they require parenteral administrations (every 3 weeks) at high doses and, due to their long half-life, it is not possible to withdraw them rapidly from the body if adverse events occur (e.g., allergic reactions, myocarditis, etc.). These limitations suggest that the full potential of immune checkpoint blockade has not yet been realized and raises the need to explore new, safer, and more effective modalities.

Small molecules (classically bellow 500 $g \cdot mol^{-1}$ and more recently up to 750 $g \cdot mol^{-1}$) are emerging as viable, logical, and effective alternative for the replacement of monoclonal antibodies in the blockade of immune checkpoints. While obtaining monoclonal antibodies requires the development of complex biological production models (hybridomas), small molecules can be obtained in a relatively simple and inexpensive manner (with more than 100 years of experience in pharmaceutical industry). The way these molecules are produced facilitates the introduction of small structural modifications that, without altering their function, enable to improve their pharmacokinetic and pharmacodynamic properties, allowing the development of better and safer drugs. Furthermore, small molecules are usually administrated in a simple way, orally, without the complications associated with the high half-life and immunological reactions of monoclonal antibodies. As a proof of concept, some small molecule checkpoint blockers targeting PD-1 are being developed. However, the effectivity of these small molecule inhibitors is still far from that observed with monoclonal antibodies.[26] In any case, experimental data support the potential of this approach which is still in its infancy. The complexity of cancer forces the combination of different therapeutic approaches to achieve treatment success, so drugs (mAbs and small molecules) capable simultaneously and synergistically blocking cancer cell proliferation, angiogenesis, metastasis while also reactivating the immune system function are the future of modern oncology.

In this context, the purinergic system is becoming a key player for the development of small molecule-based cancer therapy. As one of the earliest validated immune checkpoints,[27,28] the A_{2A} adenosine receptor ($A_{2A}AR$) has early sparked an interest in the role of the purinergic system in the TME. Further studies have recognized the modulation of the purinergic system as a very innovative and promising strategy for cancer treatment.[13,14,29]

1.3 PURINERGIC SIGNALING IN CANCER

The recognition of the important role of TME for cancer progression has opened new avenues in the exploration of anticancer therapies. The study of the TME has allowed the identification of metabolic pathways that are indispensable for cancer cell survival and tumor progression. Tumor hypoxia causes important immunological and metabolic changes that enhances tumor proliferation.[13] As explained above, oxygen deprivation limits the availability of energy sources, inducing the accumulation of extracellular adenosine triphosphate (ATP) and, to a lesser extent, NAD^+.[30] Extracellular ATP signals through type 2 purinergic (P2) receptors, consisting of eight P2Y G-protein coupled receptors (GPCRs) and seven P2X cation selective

channel receptors (ionotropic receptors). While P2X receptors selectively recognize ATP, P2Y receptors can also be activated by UTP, ADP, NADP/NAD^+ and UDP. In immune cells, $P2Y_2$ and $P2Y_6$ activation enhances myeloid cell chemotaxis. On the other hand, $P2Y_{12}$ activation promotes antigen presentation by DCs and $P2Y_{11}$ activation increases M1 macrophage differentiation, regulates IL-10 release and enhances chemotaxis.[31]

The absence of oxygen results in nutrient deprivation, forcing both tumor and immune cells to compete for essential nutrients. During this process, cancer cells may hinder the proliferation and effector functions of lymphocytes by competing for glucose,[13,31] evading immune attack. Hypoxia-inducible factor 1α (HIF1α), released by cancer cells, is a strong inducer of ectonucleotidases and A_{2B} adenosine receptor (A_{2B}AR) expression (Figure 1.6).[14,32,33] Ectonucleotidases: ectonucleoside triphosphate diphosphohydrolase-1 (NTPDase 1, also known as CD39) and ecto-5′-nucleotidase (CD73) are fundamental hypoxia-upregulated enzymes responsible of ADO accumulation by ATP degradation in the TME. CD39 hydrolyzes P2 receptor ligands (ATP, UTP, ADP and UDP) to monophosphate compounds (AMP and UMP), while CD73 preferentially converts AMP into ADO, increasing its concentration, from nanomolar (nM) in physiological conditions, to the micromolar (μM) range in the TME (Figure 1.6).[34–36] ADO concentration is further increased due to downregulation of its metabolization to inosine (INO) by reuptake of adenosine deaminase (ADA) in tumor cells.[14,37,38] In addition to these metabolic pathways, ADO levels can be increased by the action of alkaline phosphatase (AP)[39] or the CD38/CD203a system[40] from ATP and NAD^+ respectively. The extracellular accumulation of ADO facilitates its regulatory functions by binding to P1 purinergic receptors (adenosine receptors, ARs). It is important to note that the action of this well-orchestrated enzymatic system not only increases the concentration of adenosine, but also notably decreases the ligands for the P2 receptors. The immune processes activated by ATP are restricted by extracellular ADO, promoting a self-limited immune response that aims to facilitate healing processes. However, the continued high concentration of ADO induces critical effects in TME such as angiogenesis, cell growth and immunosuppression.[13,41] Therefore, a negative feedback regulation between ADO and ATP is hence crucial to maintain immune homeostasis. Figure 1.6 shows ADO metabolism and catabolism in physiological and pathological conditions.

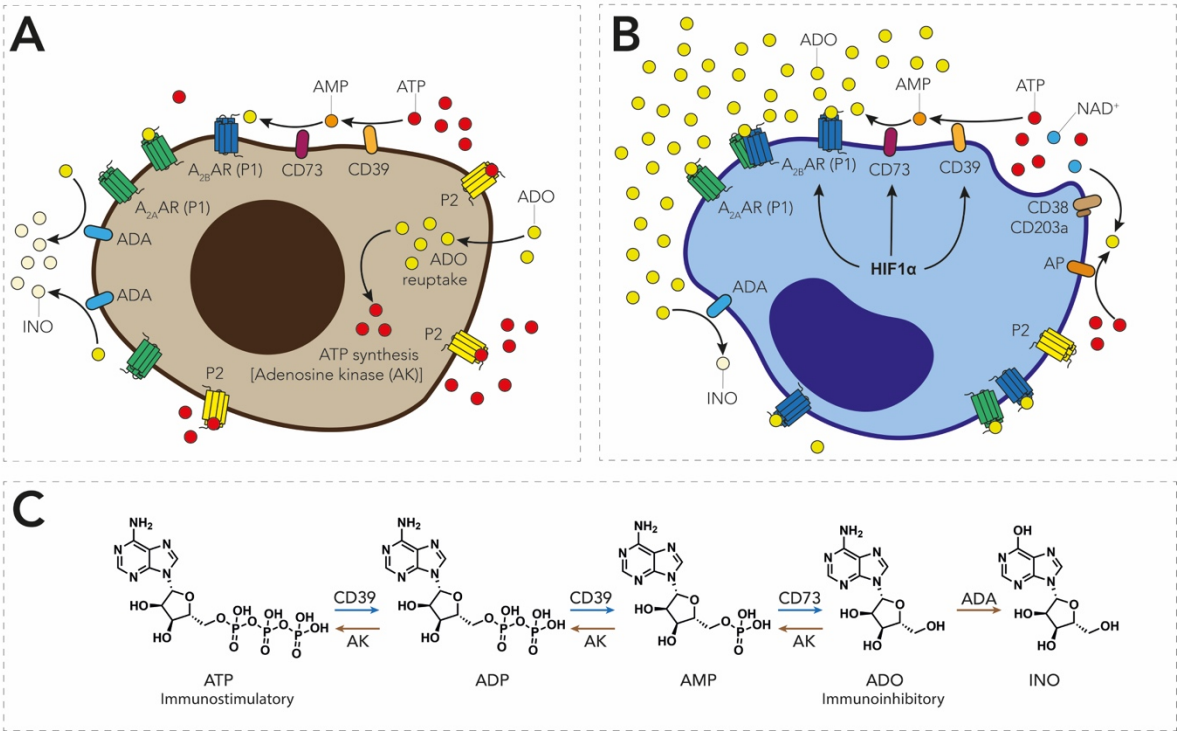

Figure 1.6. A) Purinergic metabolism and catabolism in normal tissues. ADO/ATP ratio is balanced in physiological conditions. B) Purinergic metabolism and catabolism in cancer cells. ADO/ATP ratio is highly increased in pathological conditions. C) Schematic representation of principal pathway of ADO synthesis and catabolism.

Extracellular ADO binds to purinergic type-1 (P1) receptors (that belong to the GPCR family), named adenosine receptors (AR) - A_1AR, $A_{2A}AR$, $A_{2B}AR$ and A_3AR.[13,42] Three of these receptor subtypes (A_1AR, $A_{2A}AR$ and A_3AR) bind ADO with high affinity (K_i: 100-300 nM), while the $A_{2B}AR$ exhibits a low affinity profile (K_i: 10-15 µM). Thus, $A_{2B}AR$ will only be activated by high (micromolar) ADO concentrations,[25,43] which usually take place under extreme environmental cues like inflammation, injury, hypoxia, or cellular stress (which are characteristic of TME). Emerging evidence demonstrate that $A_{2A}AR$ and $A_{2B}AR$ are the most prominent and influential in the TME. $A_{2A}AR$ is highly expressed in most immune cells, with evidence supporting that its activation in the TME suppresses anti-tumor immune responses (*e.g.*, suppression of cytotoxic $CD8^+$ T cell activity,[44,45] enhancement of regulatory T cells immune suppressive activity[46] and inhibition of dendritic cells' antigen presentation[47]). The immunosuppressive effect of ADO is predominantly mediated by A_{2A} and $A_{2B}AR$ (A_2AR) resulting in increased cAMP-PKA (protein kinase A) signaling with activation of downstream hypoxia-HIF1a. These reports set the foundation for inhibiting A_2AR in hypoxic tumors to improve anti-tumor immune responses. Consequently, $A_{2A}AR$ antagonism has emerged as a

prototypical approach of small molecule immunotherapeutics, with recent encouraging clinical outcomes in the treatment of refractory cancers.[28,48] Three A_{2A}AR antagonists are currently in or have completed clinical trials:, Ciforadenant, Inupadenant and Taminadenant (PBF-509).[49] Due to its lower ADO affinity, A_{2B}AR subtype has been traditionally considered of less relevance compared to A_{2A}AR.[50] Although A_{2A}AR genetical deletion or antagonism liberates CD8+ T cells from immunosuppression[45], recent evidences strongly suggest specific A_{2B}AR roles in cancer[14,51], with early studies highlighting that its activation is essential for tumor proliferation[14,30], angiogenesis[52], cell invasion and metastasis.[14]

The expression and signaling of each component of the purinergic system (Figure 1.7) is highly dependent of the pathological conditions.[14,43,53] In summary, CD39 and CD73 are expressed in cancer cells, fibroblasts, endothelial cells, MDSC, DCs, granulocytes, naïve $CD4^+$, Treg, NK, TAM and exosomes (cancer extracellular vesicles); CD38/CD203a is expressed in cancer cells, NK, T and B lymphocytes;[40,54] and P2 are expressed in granulocytes, TAM, DCs, Treg, NK, T and B lymphocytes.[55] The two A_2AR subtypes are also highly affected by pathological conditions, with the A_{2B}AR/A_{2A}AR expression ratio rapidly increasing under hypoxic conditions. In this context, a recent study demonstrated extensive heteromeric complex formation in tissues where A_{2B} and A_{2A} ARs were co-expressed.[43] Moreover, a dramatically altered pharmacology of the A_{2A}AR was observed when co-expressed with the A_{2B}AR, in both recombinant and native cells, with selective A_{2A}AR antagonists losing their binding affinity for A_{2A}AR. These data would have major implications for the clinical use of A_{2A}AR antagonists, as they would fail to modulate the receptor in an A_{2A}AR-A_{2B}AR heteromer context. Instead, the A_{2B}AR and the A_{2A}AR-A_{2B}AR heteromer are now considered as promising pharmacological targets for cancer immunotherapy.

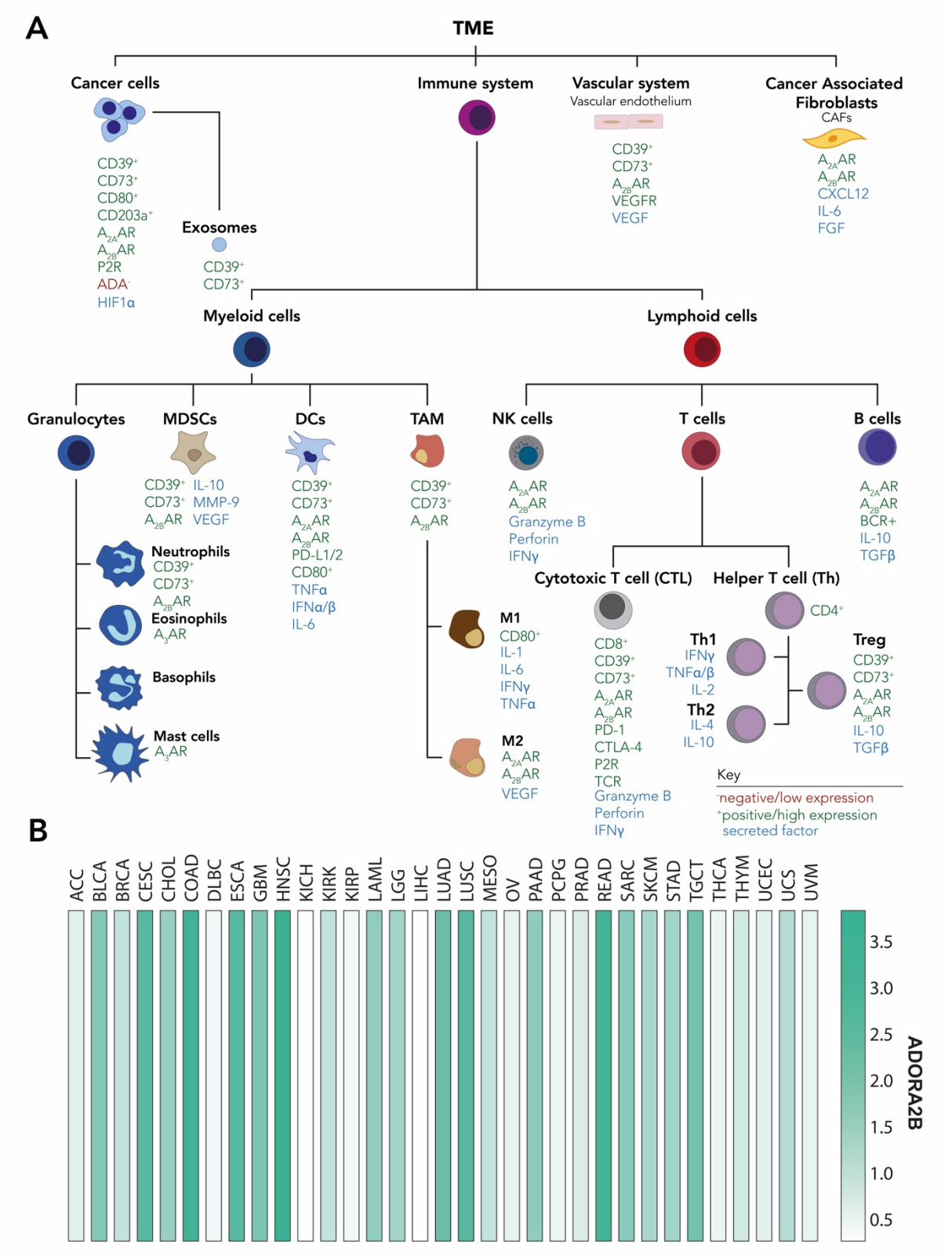

Figure 1.7. A) Tumor microenvironment cells, surface molecules and adenosine-related secreted factors. B) TCGA – Pan cancer analysis across 33 tumor types expressing $A_{2B}AR$ (ADORA2B). Abbreviations can be found in the glossary.

1.3.1 Adenosine roles in cell growth, survival, metastasis, and angiogenesis

Hypoxia-induced synthesis of ADO has an important role in tumor cell growth and migration in the TME.[13] ADO accumulation facilitates tumor growth and metastasis through its effects on tumor cells and stroma. A_{2B}AR activation can boost proliferation of multiple types of cancer cells and growth of solid tumors. A_{2B}AR blockade (with antagonists or genetic knock out of the A_{2B}AR) in various animal models of solid tumors confirm its decisive role in cell growth and cancer proliferation.[56,57] For example, stimulating with **BAY 60-6583** (A_{2B}AR agonist, see section 1.5) produces an increasing in both proliferation and migration of triple negative breast cancer cells, while **GS-6201** (A_{2B}AR antagonist, see section see section 1.5) blocked these effects.

The intrinsic mechanisms behind A_{2B}AR-mediated proliferation are unclear but they are believed to be linked to the activation of MAPKs and extracellular-signal regulated kinases (ERK). Other components of the purinergic system, such as CD73 and A_{2A}AR (in CAFs), also have an interesting role on cell growth.[13,15]

In CAFs (and senescent CAFs), A_{2B}AR promotes FGF expression, therefore increasing the number of activated fibroblasts. These A_{2B}AR activated fibroblasts release CXCL12, thus recruiting endothelial progenitor cells (EPC), leading to angiogenesis; and IL-6, which reduces tumor cell adhesion and leads to metastasis. Activation of CD73 in these cells may help tumor growth (Figure 1.8A),[15] and, in tumor cells inhibits tumor apoptosis and releases matrix metalloproteinases (MMPs) that induce breakdown of ECM. This facilitates tumor cell migration and invasion of remote organs (Figure 1.8B).[58] Exosome production by tumor cells is clearly regulated by A_{2A}AR, but the A_{2B}AR role during this process is not clear yet.[59] Regardless of this, tumor exosomes are capable of regulating adenosine production by presenting the ectonucleotidases CD39 and CD73 on their surface (Figure 1.8C).[13,60] Thus, exosomes strongly contribute to all ADO-dependent mechanisms in cancer progression, acting as small pro-tumor nodes. This is not only important for established tumors, but also for the generation of new cancer nuclei. Exosomes migrate to normal tissues, generating high-ADO pro-tumor microenvironment.

In vascular endothelial cells, activation of A_{2B}AR boost angiogenesis mainly through an increase in VEGF release, but also via other angiogenic factors such as nitric oxide (Figure 1.8D).[61,62] Furthermore, activation of A_{2B}AR also allows the release of VEGF by tumor cells, MDSC, and M2 macrophages (Figure 1.8E).[13]

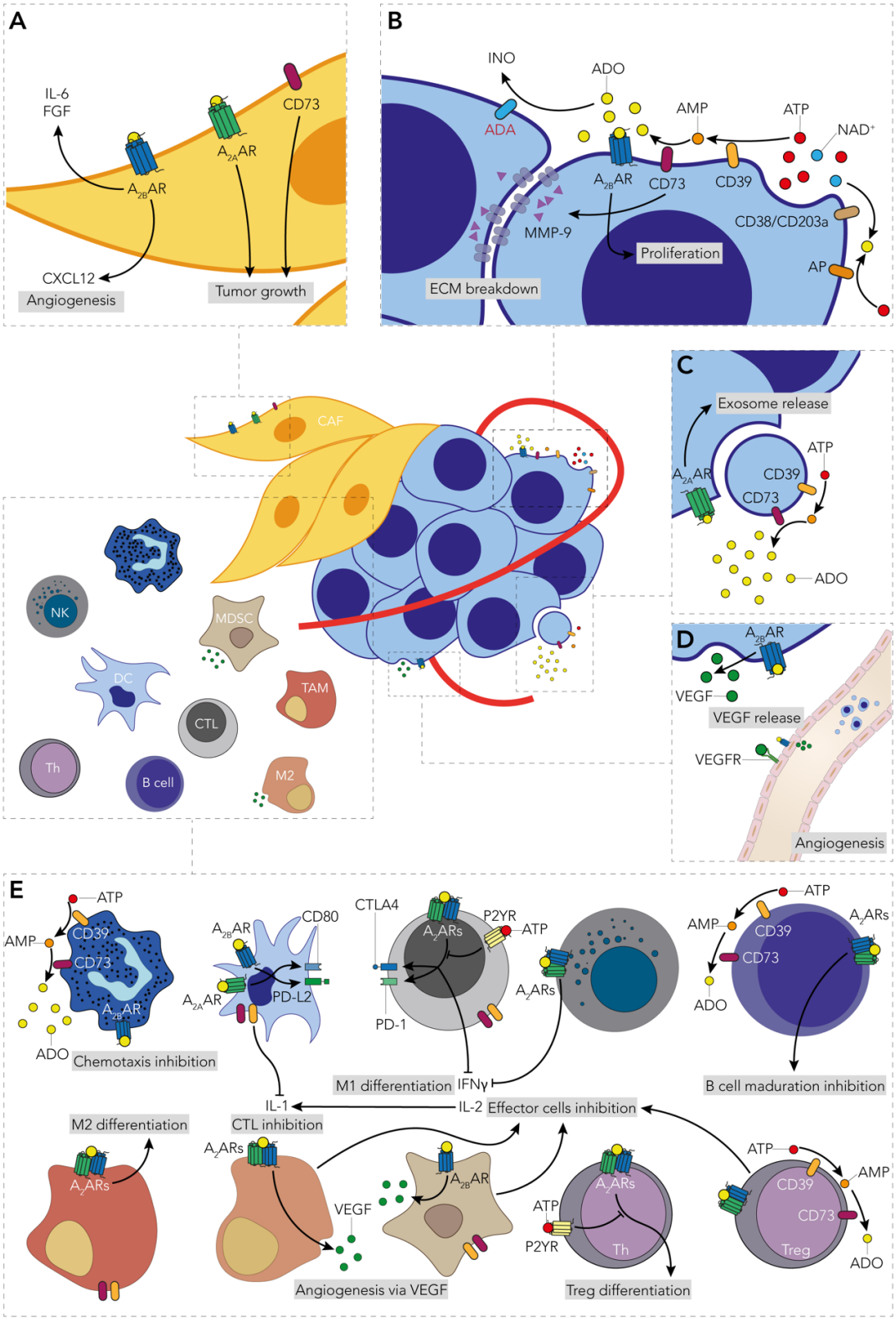

Figure 1.8. Role of the purinergic system in TME. A) ADO promotes tumor growth and angiogenesis in CAFs. B) Upregulated adenosine metabolic pathway and effects on metastasis. C) Nucleotidases-expressing exosome release. D) Pro-angiogenic effects of ADO in vascular endothelium. E) Immunosuppressive effects of ADO in immune system.

1.3.2 Adenosine roles in the immune system

ADO suppresses tumor immunity, mostly by restricting immune cell infiltration, cytotoxicity, stimulating the production of anti-inflammatory cytokines and promoting the proliferation and infiltration of immunosuppressive cells [like Treg, MDSC and TAM (M2 type)]. Genetic deletion or antagonist treatment of CD73 or A_{2A}AR helps the CTL functions and reduces tumor growth. The role of other actors of the purinergic system, is still unclear.[30,62–65] Notwithstanding, the dimerization of the A_{2A} and A_{2B} in the TME;[43] and the abundance of A_{2B}AR in MDSC, neutrophils, DCs, TAM, and lymphocytes;[13,21,66] demonstrate that A_{2B}AR is a key player within the immune suppressive TME (Figure 1.8E).

A brief description of the roles of ADO in different immune cells is presented below.

Granulocytes

Neutrophils, the most abundant granulocyte (and leucocyte) type, are phagocytes. They are important in the pathogenesis of many inflammatory diseases (such as cancer).[67] Neutrophil functions are affected by ADO, which they can also produce (through ectonucleotidases) thus, keeping a regulated neutrophil-behavior. A_1, A_{2B}, and A_3AR seems to be implicated in neutrophil chemotaxis, with a clear role of A_{2B}AR in neutrophil migration.[68]

In eosinophils and mast cells, ADO has anti-inflammatory effects (degranulation inhibition, downregulation of free radical generation, and migration blockade) mediated by A_{2A}AR activation.[69–71]

Myeloid-Derived Suppressor Cells (MDSCs)

MDSCs are a group of immune cells from the myeloid lineage. MDSCs increase in number (10-fold) in pathological situations such as cancer and inflammation.[72] These cells interact with T lymphocytes, DCs, TAM and NK cells in the TME, regulating their function. Their inhibitory capacity is so relevant that the number of MDSCs is considered an important parameter to evaluate the progression of cancer immunotherapy.

In addition to the effect (explained above) on the release of VEGF,[13,72] adenosine plays a key role in the regulation of MDSCs. Expression profile shows the presence of ectonucleotidases CD39 and CD73 in the cell membrane of MDSCs, whose surfacing is induced by the release of inhibitory cytokines such as TGF-β (produced by Treg).[73] *In vitro* studies demonstrated that A_{2B}AR stimulation induces the differentiation of hematopoietic progenitors to MDSCs and, in addition, the activation of these receptors in the cells themselves produces the release of IL-10 and MMP9, with immunosuppressive and pro-metastatic effects,

respectively.[74] These effects can be counteracted by adding an antagonist to the medium, showing a great reduction in the number of MDSCs, inhibiting angiogenesis, and enhancing T-lymphocyte-mediated immunity.

Dendritic Cells (DCs)

DCs are the most potent antigen-presenting cells that manage the activation and differentiation of T cells. After exposure to antigens, DCs migrate to lymph nodes and express major histocompatibility complex (MHC) class II and regulatory molecules on their membrane (CD39 and CD73) and secrete pro-inflammatory cytokines (TNF-α).[75] ADO is an important modulator of DCs functions via activation of A_{2A}AR predominantly, decreasing IL-6 and TNF-α production and increasing IL-10 release, leading to the accumulation of inhibitory Tregs.[51,75] ADO signaling increases the expression of PD-L2, ligand for T cell inhibitory receptor PD-1. The interaction between CD80 and PD-1 with CTLA-4 and PD-L2 causes inhibition and apoptosis, respectively, of T cells. The role of A_{2B}AR in DCs regulation is less clear than that of A_{2A}AR, but several studies[75,76] which use knock-out (KO) A_{2B}AR, selective agonists and antagonists, have revealed a new role for A_{2B}AR receptors in regulating DCs function. Human monocytes differentiated toward dendritic cells in the presence of adenosine transform into a cell type that resembles dendritic cells but is functionally different. These "adenosine-differentiated" cells represent an intermediate step between monocytes and dendritic cells and have an impaired capacity to induce T-cell proliferation and IFN production. However, these intermediate cells secrete VEGF, and are also anti-inflammatory due to their strong production of IL-10 and TGF-β.[77] In conclusion, ADO, through the A_2ARs, can induce a defective functional differentiation of DCs toward a phenotype with pro-angiogenic and anti-inflammatory features, which allows tumor survival.

Tumor-Associated Macrophages (TAM)

Macrophages (denominated TAM in TME) are an essential component of innate immunity, with high differentiation capacity. Depending on the TAM phenotype, it will have pro- or anti-inflammatory functions. As explained above, TAMs differentiate predominantly in two major phenotypes known as M1 and M2, with pro- and anti-inflammatory functions respectively. Undifferentiated TAMs contribute to ADO synthesis by expressing ectonucleotidases in their cell membrane. The purinergic system exerts an important effect on macrophage differentiation, maturation, and activation, mostly by inhibition of M1

differentiation (via $A_{2A}AR$), stimulation of M2 differentiation (via $A_{2B}AR$) and angiogenesis promotion (via VEGF release).

Natural Killer (NK) cells

Natural Killer (NK) cells, also known as large granular lymphocytes, are a type of innate immune system cell with cytotoxic functions. $A_{2A}AR$ signaling in NK cells impede maturation and decreases IFN-γ and perforin release, greatly affecting cytotoxicity in TME.[71] Recent studies have demonstrated a central role of $A_{2A}AR$ in the inhibitory effect of adenosine on the cytotoxic activity of NK cells.[21] The role of $A_{2B}AR$ is unclear, but the expression of this receptor [23]on NK cells suggest a contribution to the immunosuppressive effect.[32]

T lymphocytes (T cells)

T cells are adaptative (and to a lesser extent, innate) immune system cells with heterogeneous functions. T cells are produced by the lymphoid cell line, and maturated in thymus, presenting TCR (T-cell receptor) on their cell surface. T cells are grouped into subsets based on their function, categorized by the expression of CD8 or CD4 in their cell membrane.

Cytotoxic T lymphocytes (CTL) or $CD8^+$ T lymphocytes, are a type of T cell with cytotoxic functions, releasing perforin (that breaks cell membrane) and granzyme (that breaks DNA and induces apoptosis). Its function is so specific that it can damage malignant cells without affecting the surrounding healthy tissue. Purinergic signaling plays a key role in the regulation of CTL, due to the presence of ectonucleotidases, P1 and P2 receptors in their surface. Activation of A_2AR, specially $A_{2A}AR$, causes an enhanced expression of CTLA-4 and PD-1,[78] with immunoinhibitory functions, and the downregulation of IFN-γ release.[77] In contrast, activation of P2 receptors is accompanied by an increase in cytotoxic activity.[55] Activation of $A_{2A}AR$ inhibits the release of granules containing perforin and granzyme.[13]

Helper T lymphocytes (Th) or $CD4^+$ T lymphocytes, are a heterogeneous subset of cells with assisting functions. Six different types of Th are known, and all of them share a similar function: to secrete cytokines and other small protein mediators which stimulate CTL, NK, and B cells (Th1: IFN-γ, TNF-α/β, IL-2; Th2: IL-4, IL-10). In addition to IL-2 release inhibition, purinergic signaling stimulates $CD4^+$ cells differentiation to Treg. While most of Th have no ectonucleotidases in their membranes, Treg contributes to increase the immunosuppressive potential of other cells by increasing TME ADO concentration. Also, activation of $A_{2A}AR$ eventually decreases effector cell functions, by releasing IL-10 and TGF-β, among other

effects. As explained above, it has been shown that TGF-β contributes to an increased expression of CD39 and CD73 in MDSCs, but also in CTL and Treg (autocrine signaling).

B cells

B lymphocytes are a type of adaptative immune system cells with humoral functions. B cells are produced by the lymphoid cell line, and maturated in the bone marrow, presenting BCR (B-cell receptor) on their cell surface. The basic B cell function is to bind to an antigen, stimulate chemotaxis of Th and differentiate to plasma cell that secretes large amounts of antibodies against this antigen. In B lymphocytes, A_{2A}AR activation lessens B-cell receptor signaling by suppressing nuclear transcription factor-κB, which impairs the activation, maturation (to plasma cells), and cell survival. Also, B cells express ectonucleotidases in their cellular membrane, contributing to the increase of adenosine in the TME.[13,71]

The synergistic functions explained above, as well as the fact that these are receptors (and enzymes), make the purinergic system, specifically the A_{2B}AR, an obvious target for the development of small molecules for cancer therapy.

1.4 STRUCTURE AND PHARMACOLOGY OF ADENOSINE RECEPTORS

As explained above, ADO exerts its extracellular functions by activation of four receptor subtypes (ARs) that belong to the GPCR family. All four P1 subtypes differ in expression, effector coupling, affinity, and molecular structure (Table 1.1).[36] All ARs are well-known and have been pharmacology studied, presenting a common structure: seven transmembrane α-helices (7-TM), followed by one short membrane-associated helix (SMH), an extracellular amino-terminus (N-terminus), a cytosolic carboxy terminus (C-terminus), three extracellular loops (ECL1-3) and three intracellular loops (ICL1-3). Figure 1.9 shows 2D structure for A_{2A}AR.

The three-dimensional structure of GPCRs fluctuates between two main conformational states: active and inactive. The predominance of one or the other depends on the presence of different ligands in the biological medium. Thus, agonists stabilize the active conformations (which can interact with the second messenger systems) and antagonists stabilize the inactive conformations (at rest, without response). However, a plethora of intermediate conformational states, especially at the binding site, generate different active and inactive states. Specifically, for ARs, the 3D structure was elucidated with different biophysical methods (e.g., X-ray diffraction, cryogenic electron microscopy) for inactive states of A_1[79,80] and A_{2A}AR[79,81,82]; and active states of A_{2A}AR[83] and A_{2B}AR[84].

Table 1.1. Classification, structural data, signaling pathways and sequence of ARs.[36]

	hA_1AR	*h*A_{2A}AR	*h*A_{2B}AR	*h*A_3AR
Amino acids	326	412	332	318
G protein coupling	$G_{i/o}$	G_s	G_s G_q	G_i G_q
Signaling pathway(s)	↓ Adenylyl cyclase ↑ Phospholipase C	↑ Adenylyl cyclase ↑ MAPK/ERK	↑ Adenylyl cyclase ↑ MAPK/ERK ↑ Phospholipase C	↓ Adenylyl cyclase ↑ MAPK/ERK ↑ Phospholipase C
ADO affinity	1-10 nM	30 nM	1,000 nM	100 nM
Sequence identity vs. *h*A_1AR	100%	38.3%	44.0%	46.5%
Sequence identity vs. *h*A_{2A}AR	38.3%	100%	46.6%	31%
Sequence identity vs. *h*A_{2B}AR	44.0%	46.6%	100%	35.7%
3D structure	*AlphaFold:* P30542 *PDB (X-ray):* 5N2S,[79] 5UEN[80]	*AlphaFold:* P29274 *PDB (X-ray):* 5N2R,[79] 3EML,[82] 4EIY[85]	*AlphaFold:* P29275 PDB (*Cryo-EM):* 7XY7[84] Homology Model	*AlphaFold:* P0DMS8 Homology Model

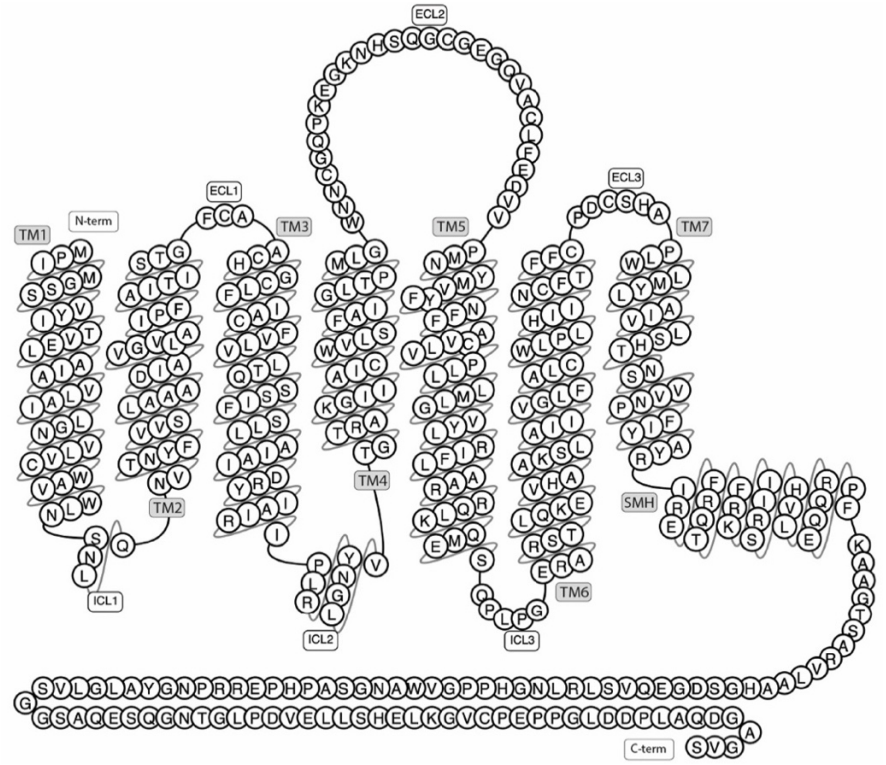

Figure 1.9. 2D schematic structure of A_{2A}AR (up: extracellular, bottom: intracellular). Residues are represented in a 1-letter code (https://gpcrdb.org/protein/aa2ar_human/).

With high sequence identity, particularly within the orthosteric binding site, $A_{2A}AR$ and $A_{2B}AR$ are quite similar. The main difference surrounding the orthosteric binding site is the presence of a salt bridge between extracellular loops 2 and 3 (His^{EL3} and Glu^{EL2}) in $A_{2A}AR$, generating two possible inactive conformations: open (Figure 1.10A, grey) and closed (Figure 1.10A, red). A new hypothesis, confirmed by molecular dynamics (MD) simulations,[86] is that bulky substituents in the ligand, like phenyl or benzyl groups, can stabilize the open conformation of $A_{2A}AR$. In the case of $A_{2B}AR$ this salt bridge does not exist, due the presence of Lysine (K265) instead of Histidine in ECL3. Focusing on the orthosteric binding site (3Å surrounding ligand), A_{2A} and $A_{2B}AR$ have a 93% of identity, sharing 14 of 15 aminoacids (Figure 1.10C), only differing in $Val^{6.51}$ (V250) in $A_{2B}AR$, being $Leu^{6.51}$ (L249) in $A_{2A}AR$. Two conserved residues play an important role in the binding of both ADO and antagonists to both receptors: $Phe^{5.29}$ (F168 in $A_{2A}AR$, F173 in $A_{2B}AR$), with a π-π interaction; and $Asn^{6.55}$ (N253 in $A_{2A}AR$, N254 in $A_{2B}AR$), with a double hydrogen bond.

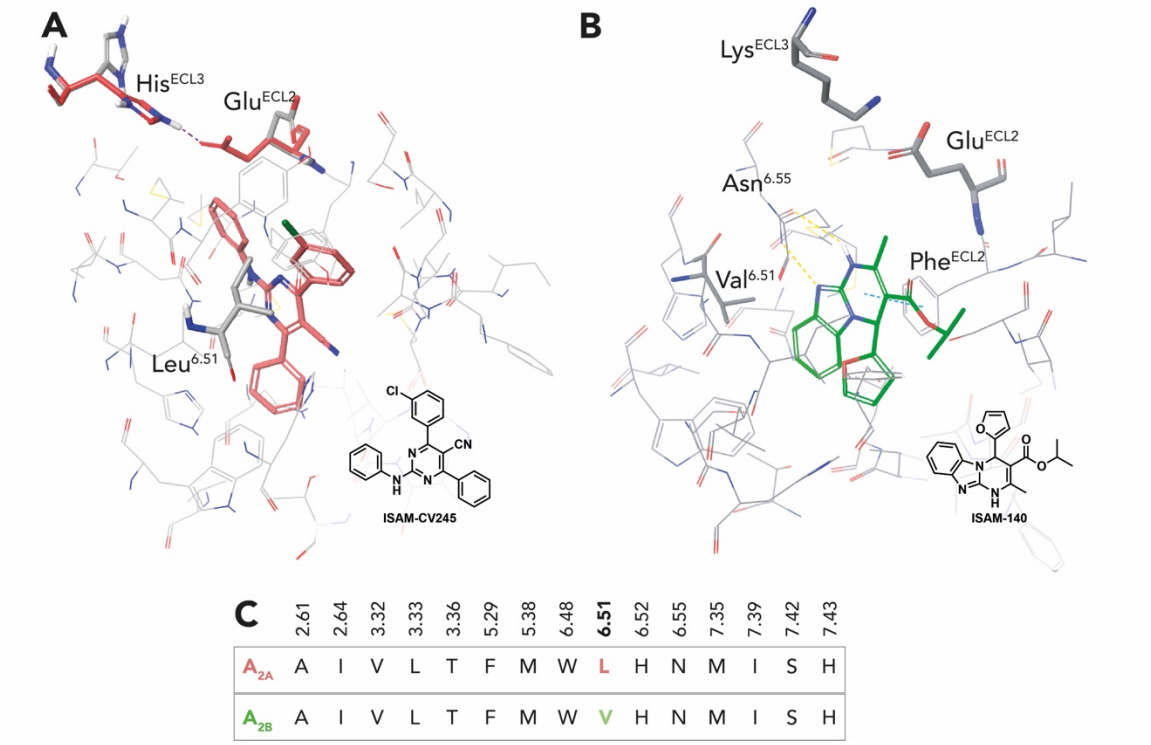

Figure 1.10. A) Binding mode of ISAM-CV245 (selective $A_{2A}AR$ antagonist) to $A_{2A}AR$[86] (PDB: 4EIY with closed conformation, red; PDB: 3UZC with open conformation, grey). Purple dashed line represent salt bridge between Histidine and Glutamine. B) Binding mode of (*S*)-ISAM-140 (selective $A_{2B}AR$ antagonist) to $A_{2B}AR$ ($A_{2A}AR$-based homology model).[87] Yellow dashed lines represent H-Bonds; Blue dashed line represents π-π interaction. C) Pseudo-sequence alignment of the residues within 3Å of any atom of ISAM-CV245 with $A_{2A}AR$ and (S)-ISAM-140 with $A_{2B}AR$ as predicted by docking.

1.4.1 Expression and signaling pathways in the context of cancer

G proteins are coupled to three different subunits: α, β and γ. When GDP is bound to the α-subunit, the protein is inactive (neither bound to the receptor nor to the effector). When the ligand binds to the receptor, the latter associates with the α-subunit, causing the exchange of GDP for GTP. In this way, the protein is activated and the βγ dimer unbinds. The α-subunit is then detached from the receptor and binds to different effector systems (activating them), which originates second messengers and, subsequently, the physiological response is triggered.

There are many reports describing high expression of all the ARs in tumor cells.[77] However, in tumor cells, A_{2B} and A_3ARs have been the most studied.[13] In some studies, A_3AR activation *in vitro* has been shown to induce apoptosis, but on the other hand, activation of A_3AR has been suggested to increase tumor cell migration and invasion.[77] These contradictory effects may be due to biased signaling,[88] but also the expression of A_3AR in different cell types. Activation of A_3AR with cAMP-PKA downregulation would be the responsible of anti-tumoral effects, while activation of A_3AR with upregulation of MEK/ERK pathway would be the responsible of pro-tumoral effects. As explained above, A_{2B}AR is highly overexpressed in different tumor types.[32] Several studies have shown that A_{2B}AR enhance tumor growth and metastasis mainly through G_s coupling, but MAPK/ERK and JunB N-terminal kinase (JNK) routes also contribute to migration and VEGF production, respectively.[32,77] To simplify, the downstream signaling pathways of ARs are summarized in Figure 1.11.

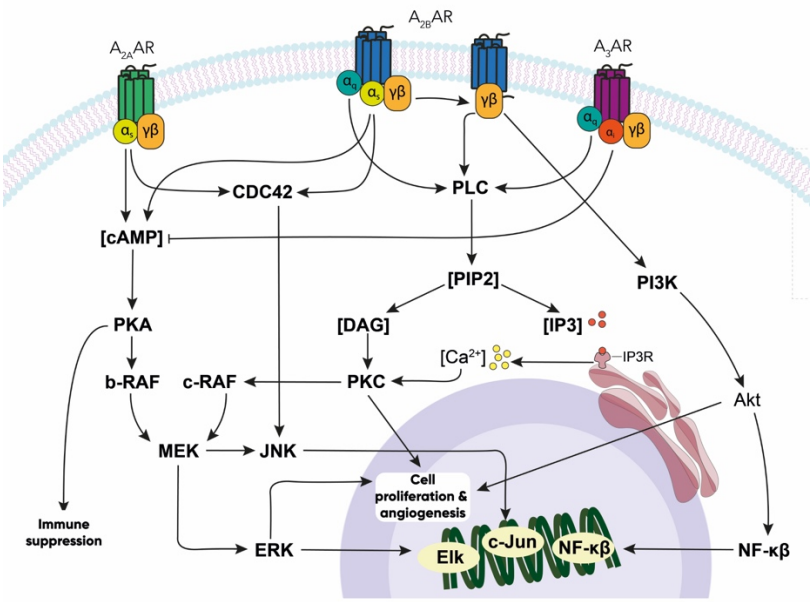

Figure 1.11. Principal signaling pathways for ARs, ending with transcription modulation by Elk, c-Jun and NF-κβ.

A_{2B}AR expression has been studied in various tumor cell lines, being particularly important in comparison to other ARs in prostate, colon and breast cancer.[32] While A_{2A}AR is only coupled to G_s protein; A_{2B}AR can promote various signaling pathways, depending on the subtype of G protein to which it is coupled: G_s or G_q (Figure 1.11). The activation of adenyl cyclase (AC) by α_s G protein subunit produces an increment in cAMP (second messenger) that activates protein kinase A (PKA), which activates MAPK pathway by b-RAF kinase activation. Both receptors, via α_s may also activate cell division control protein 42 (CDC42) and consequentially the JNK pathway. On the other hand, A_{2B}ARs coupled to α_q subunit activate phospholipase C, breaking the plasmatic membrane component phosphatidyl inositol biphosphate (PIP2) into diacylglycerol (DAG) and inositol triphosphate (IP3). IP3 binds to IP3 receptors (IP3R) ubicated in endoplasmic reticulum (stimulating calcium release) and calcium channels, increasing its intracellular concentration. This increase in calcium, jointly with DAG, activates protein kinase C (PKC), which phosphorylate c-RAF, activating MAPK pathway.

The βγ dimer released from G protein can also activate PKC-MAPK route in a lesser extent, but also Phosphoinositide 3-kinases (PI3K) route, increasing NF-κβ. All these mechanisms triggered by A_2ARs activation ends with a modification of transcription, changing cell behavior and configuring the TME with its three fundamental axes: 1) resistant tumor cells, 2) sustained angiogenesis, and 3) weakened immune system.

1.4.2 Oligomerization of Adenosine Receptors

Recent evidence documents the fact that most GPCRs, not only ARs, can form stable and functional oligomer and/or heteromer complexes. In theory, four homomeric pairs can be obtained for ARs: A_1AR-A_1AR, A_{2A}AR-A_{2A}AR, A_{2B}AR-A_{2B}AR and A_3AR-A_3AR, but only the first two have been unequivocally validated.[50] GPCR heteromers appear to be new signaling entities characterized by different functional properties in comparison with homomers.[36] The first relevant heterodimer identified formed by two ARs was A_1AR-A_{2A}AR. A_1AR and A_{2A}AR are coupled to G_i and G_s respectively, therefore the heterodimer has two opposite signaling pathways which can be activated in different contexts.[89] At low ADO concentration, the preferent signaling pathway is that of the higher affinity receptor, A_1AR (1-10 nM), decreasing cyclic adenosine monophosphate (cAMP), but at high ADO concentration, the preferent pathway is that of the lower affinity receptor, A_{2A}AR, increasing cAMP. Another heterodimer of great interest, but in this case involving dopamine receptors, is the A_{2A}AR-D_2.[90] A_{2A}AR negatively modulate D_2, which couples to G_i protein, opening the door to the treatment of

dopamine deficiency-related diseases (e.g. Parkinson) with $A_{2A}AR$ antagonists (e.g., the recently approved drug Istradefylline).[90,91] The latest to be characterized and most interesting AR heterodimer in cancer context is the one formed by $A_{2A}AR$-$A_{2B}AR$.[43] By employing different advances experimental techniques [Föster resonance energy transfer (FRET), bioluminescence resonance energy transfer (BRET), bimolecular fluorescence complementation (BiFC) and proximity ligation assays (PLA)], Hinz et al.[43] demonstrated not only the heterodimer complex formation, but also the altered pharmacology signaling of $A_{2A}AR$ in presence of $A_{2B}AR$. When co-expressed, potent selective $A_{2A}AR$ ligands lost their binding affinity and functional activity. These results would have major implications since both receptors' co-expression is increased in pathological conditions. With both receptors overexpressed in the TME, with the critical role of $A_{2A}AR$ in immune system control and $A_{2B}AR$ being critical for angiogenesis and tumor progression, blockade of this new entity is a promising strategy for future cancer treatment. This has greatly increased the interest of academy and industry by $A_{2B}AR$ antagonists and dual $A_{2A}AR/A_{2B}AR$ antagonists for the treatment of cancer.

1.5 MEDICINAL CHEMISTRY OF ADENOSINE RECEPTORS

Diverse medicinal chemistry approaches have been applied in the las two decades to develop selective agonists and antagonists for the four receptor subtypes. To facilitate the analysis of ligands for adenosine receptors, they are separated into agonists and antagonists. The criteria for the classification of the two families is based on chemical structure (Figure 1.12). Agonists are organized according to the presence or absence of the ribose moiety: nucleosidic and non-nucleosidic compounds, respectively. Antagonists, all lacking the ribose moiety, are classified according to the scaffold of the molecule, separating them into xanthine, adenine, or pyrimidine derivatives.

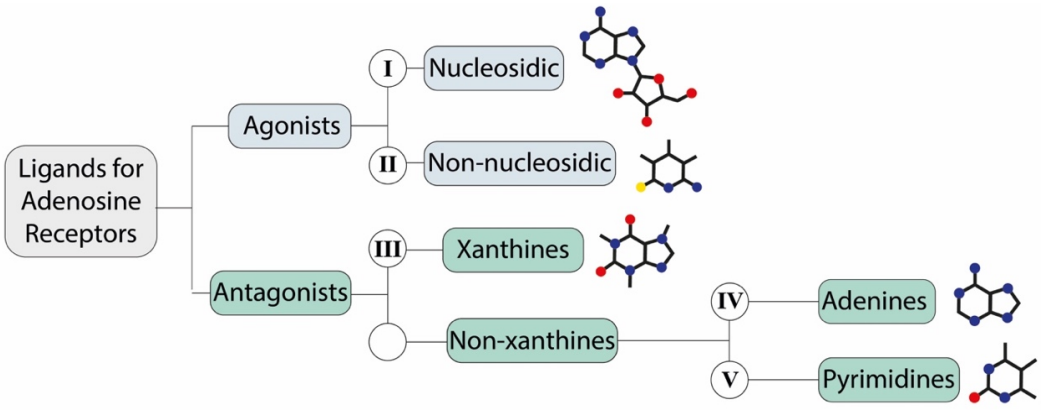

Figure 1.12. Classification of ARs ligands.

1.5.1 Adenosine Receptor agonists

Intensive efforts were being carried out in the development of improved ARs agonists, but most of them maintain the ADO (**Ia**) scaffold (nucleoside structure). The three main problems of nucleoside analogues as drugs are: 1) their low selectivity, 2) poor metabolic stability, and 3) low water solubility. For these reasons, the design of new ligands has taken into consideration improvements in bioavailability and metabolic stability in addition to receptor subtype selectivity.[92,93] Affinity data and structures of representative ARs agonists are shown below.

The half-life of adenosine in circulation is very short (approximately 1 second), due to the action of enzymes that convert it to inosine (ADA) or phosphorylate it to AMP [Adenosine Kinase (AK)], or due to the uptake through nucleoside transporters (Figure 1.13).

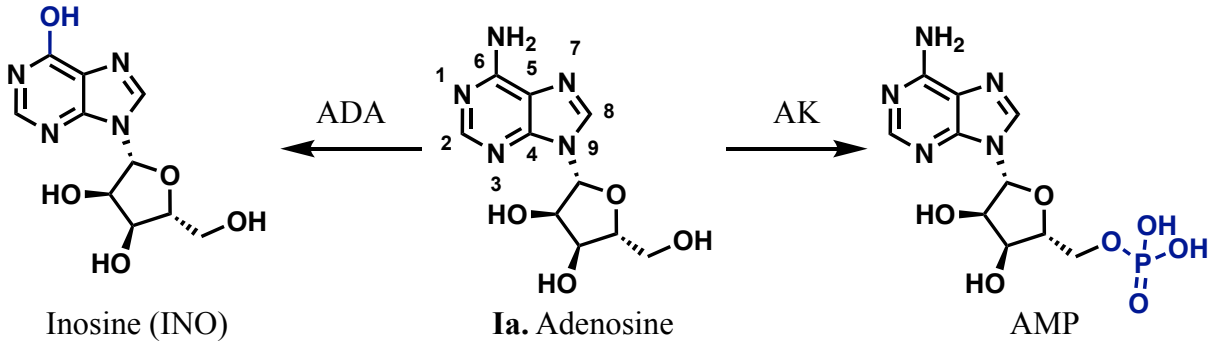

Figure 1.13. ADO and main metabolites.

ADO synthetic analogs were conceived (Figure 1.14) to prevent these processes, thus extending the half-life.[92] The substitutions made on the ADO scaffold, aimed at increasing its metabolic stability in the extracellular environment, can be simplified into three main categories:[94–96] 1) substitution at position 2, 2) modification of the ribose ring, and 3) amino group substitutions at position 6. By introducing substitutions at position 2 of the scaffold, the deamination of ADO is prevented, hindering the recognition and binding of ADA to the molecule. In fact, the first modification of ADO structure with the purpose of increasing metabolic stability was to introduce a chlorine atom at position 2 of the purine ring. 2-chloro-adenosine (**Ib**) demonstrated to be more stable against hydrolysis than ADO.[97] By modifying the ribose ring, the metabolization of ADO to AMP (and subsequent metabolites) by AK is reduced. The first and most popular example was NECA (**Ic**), a non-selective AR agonist, obtained by replacing the hydroxymethyl substituent with and ethylcarboxyamide group.

The last popular modification to gain metabolic stability and selectivity is the substitution of the purine exocyclic amino group. Although so far only benefits at the pharmacokinetic level have been described, his change and the combination of the three modifications in ADO scaffold (Figure 1.14); substitution at position 2, modification of the ribose ring, and substitution of exocyclic amino group), have been used to obtain selective agonists for the A_1AR (**Id-f**), A_{2A}AR (**Ig-i**) and A_3AR (**Ij-l**). In general, substitutions of ADO at the N^6-position with alkyl, cycloalkyl and arylalkyl groups increases selectivity for A_1AR and strongly increase metabolic stability against ADA. Selective A_{2A}AR agonists have been achieved by substitution of ADO at 2-position with ethers, amines, or alkynes. On the other hand, substitution with an N^6-benzyl group or substituted (mostly halogenated) benzyl group increases selectivity for the A_3AR. A_{2B}AR selective nucleosidic agonist were discovered, but they had no significant activity, probably due to the low affinity of ADO for the A_{2B}AR itself (Table 1.2).

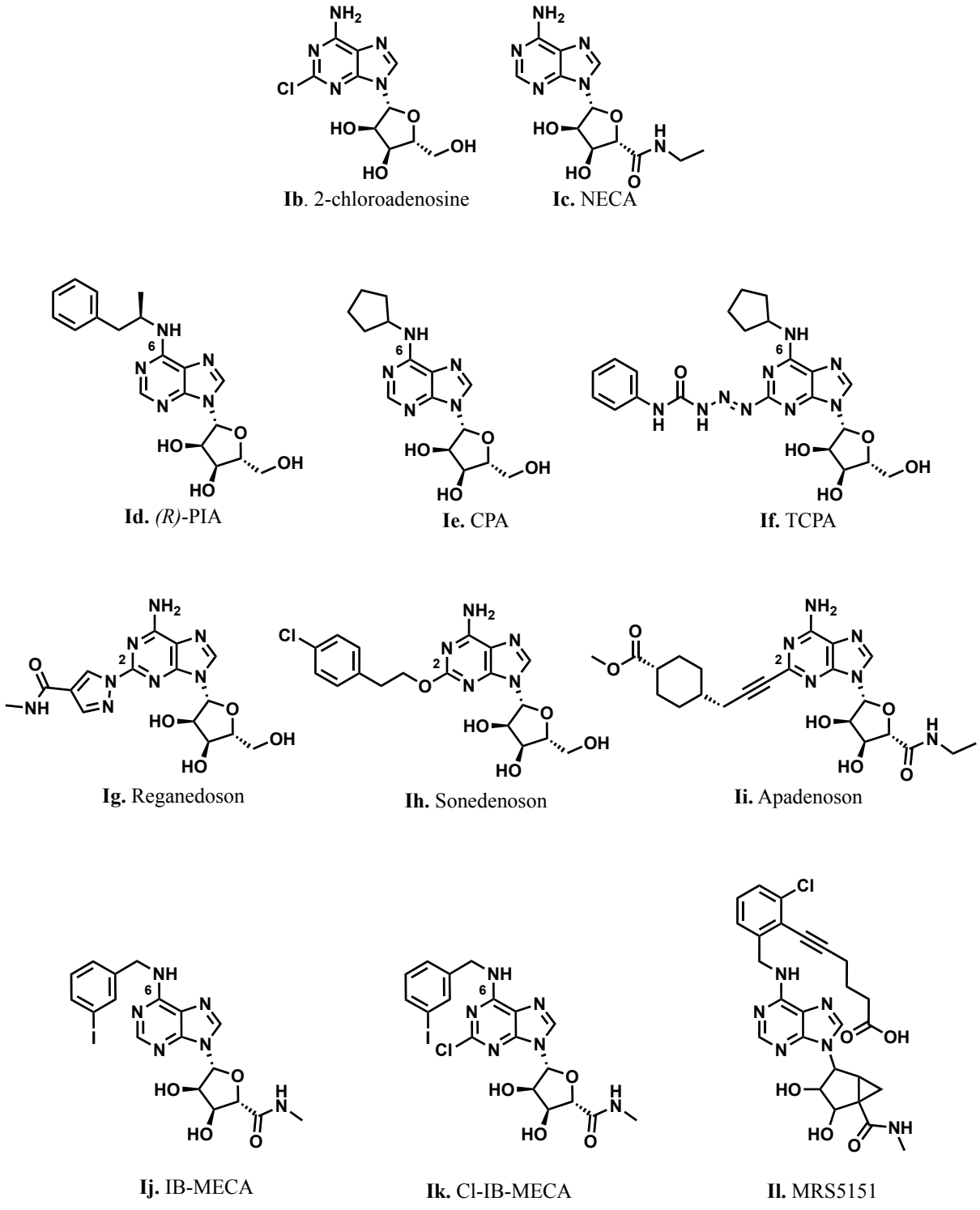

Figure 1.14. Structure of first two non-selective metabolic-stable nucleosidic agonists (first line), A_1AR (second line), A_{2A}AR (third line) and A_3AR (fourth line). The receptor affinities of the compounds are shown in Table 1.2.

To date, no nucleoside agonist of $A_{2B}AR$ has been described. As shown in the Table 1.2, ADO itself, an endogenous ligand, has a very low affinity (K_i = 1000 nM) for $A_{2B}AR$, whereas it has moderate to high affinity for the other subtypes ($K_i \leq 100$ nM). For this reason, structural modifications of ADO itself have not generated any agonist of analogous structure. Curiously, different 2-aminopyridine-3,5-dicarbonitrile derivatives (Figure 1.15) behave as selective agonists for different adenosine receptors, being **BAY60-6583** (**II**) the only potent and selective $A_{2B}AR$ agonist discovered to date.[98] Obtaining agonists for ARs, specifically for $A_{2B}AR$, is still a challenge today, due to the difficulty of obtaining metabolically stable analogues without a ribose ring that maintain the agonist behavior.[94]

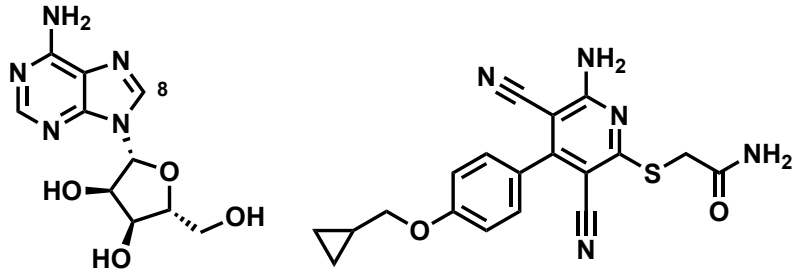

Ia. Adenosine **II.** BAY 60-6583

Figure 1.15. Structure for $A_{2B}AR$ selective non-nucleosidic agonist BAY 60-6583 compared with ADO. The receptor affinities of the compounds are shown in Table 1.2.

Table 1.2. AR affinities of representative agonists.

		K_i			
		***h*A$_1$AR**	***h*A$_{2A}$AR**	***h*A$_{2B}$AR**	***h*A$_3$AR**
	Nonselective agonists				
Ia	Adenosine (ADO)[50]	10.0 nM	30.0 nM	1,000 nM	100 nM
Ib	2-Chloro-ADO[99]	300 nM	80.0 nM	24,000 nM	1,900 nM
Ic	NECA[50]	14.0 nM	20.0 nM	2,400 nM	6.20 nM
	A_1AR selective agonists				
Id	*(R)*-PIA[50]	1.20 nM	>10,000 nM	>10,000 nM	79.0 nM
Ie	CPA[50]	2.30 nM	794 nM	>10,000 nM	33.0 nM
If	TCPA[50]	2.80 nM	210 nM	>10,000 nM	600 nM
	A_{2A}AR selective agonists				
Ig	Reganedoson[50]	>10,000 nM	290 nM	>10,000 nM	>10,000 nM
Ih	Sonedenoson[50*]	>10,000 nM	490 nM	>10,000 nM	>10,000 nM
Ii	Apadenoson[50]	77.0 nM	0.50 nM	N.D.	45.0 nM
	A_{2B}AR selective agonists				
Il	BAY 60-6583[100]	>10,000 nM	>10,000 nM	3.00 nM	>10,000 nM
	A_3AR selective agonists				
Ij	IB-MECA[63]	51.0 nM	2,900 nM	>10,000 nM	1.80 nM
Ik	Cl-IB-MECA[63]	220 nM	5,360 nM	>10,000 nM	1.25 nM
Il	MRS5151[101]	14,900 nM	>10,000 nM	N.D.	2.38 nM

N.D.: not determined

1.5.2 Adenosine Receptors antagonists

In ADO, the adenine core is the receptor binding part (Figure 1.16, **Ia**, in blue), while ribose is the receptor activation portion (Figure 1.16, **Ia**, in green).[94] Thus, adenines lacking the ribose fraction are often AR antagonists. Alkylxanthine derivatives are also the prototypical ARs antagonists (Figure 1.16). The stimulants caffeine [1,3,7-trimethylxhantine (**IIIa**)] and theophylline [1,3-dimethylxanthine (**IIIb**)] are natural alkaloids that behave as weak (micromolar) and nonselective AR antagonists.[92] The structure-activity relationship (SAR) of

xanthine derivatives as AR antagonists has been profoundly evaluated.[95] The influence of the substituents at positions 1, 3, 7 and 8 on receptor subtype selectivity have been studied in detail.[93] The first synthetic AR antagonist discovered was **CGS15943** (**IIIc**),[102–104] which, although it has almost no structural relationship to natural antagonists, the new triazolo[1,5-*c*]pyrimidine scaffold exhibits submicromolar affinity data for AR subtypes, thus becoming one of the firsts examples of synthetic non-xanthine-based antagonists.

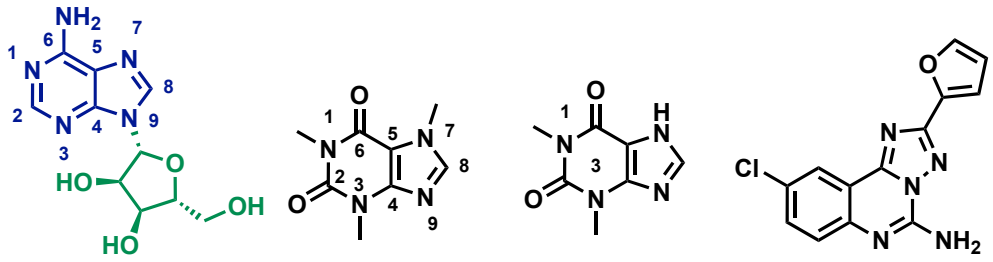

Ia. Adenosine **IIIa.** Caffeine **IIIb.** Theophylline **IIIc.** CGS15943

Figure 1.16. Xanthinic (IIIa-IIIb) and non-xanthinic (IIIc) non-selective AR antagonists compared with ADO structure (Ia). The receptor affinities of the compounds are shown in Table 1.3 and Table 1.4.

1.5.2.1 Xanthine-based antagonists

Those with a structure directly derived from natural [low affinity (μM)] antagonists such as caffeine and theophylline, called xanthine-based antagonists, constitute the largest subset of adenosine antagonists published to date. By thoroughly exploring positions 1, 3 and 8 of the xanthine scaffolds,[50,105–109] a large number of selective antagonists for the ARs have been obtained. The presence of a bulky carbon-based residue at positions 8 of the xanthine scaffold provided antagonists selective for the A_1AR. Discovered in 1987,[105] dipropylcyclopentylxanthine (**DPCPX**, **IIId**) represent the first example of a selective A_1AR antagonist. The 8-cycloalkyl group could be bridged to enhance the A_1AR affinity as with rolofylline (**IIIe**)[110], **PSB-36** (**IIIf**),[92,106] and toponafylline (**IIIg**)[111] an A_1AR subnanomolar antagonist discovered in 2006. It was discovered that introduction of a styryl fragment at position 8 of the xanthine core provides selective A_{2A}AR antagonists. First developed was 8-(3-chlorostyryl)caffeine (**CSC**, **IIIh**)[107] but the main ligand of this family is Istradefylline (**IIIi**)[112], which has been recently approved as a drug for Parkinson's disease treatment currently commercialized in Japan (from 2013) and USA (from 2019) under Nourianz® brand name, being the only adenosine antagonist used in therapeutic to date.

8-phenylxanthines, identified as A_1AR antagonists early on (**XAC, IIIj**)[113], were later found to have a higher affinity for the A_{2B}AR, for which the first selective antagonist was

MRS1754 (**IIIk**)[114]. Subsequently, several groups explored the pharmacokinetic profile, selectivity, and/or affinity of this class of compounds. Extensive modifications of the substituent at position 8 of the xanthine core structure have resulted in the identification of ligands with high selectivity and affinity for the A_{2B}AR. In addition to phenyl group, other heteroaromatic residues were directly connected to the position 8 of the xanthine scaffold, keeping position 7 unsubstituted, to provide a hydrogen bond donor (**IIIl-IIIm**)[115,116]. 9-Deazaxanthines (**IIIn**) were extensively explored by several groups, demonstrating that different modifications of the xanthine core still maintain the high A_{2B}AR affinity.[117–119] The best substituent for A_{2B}AR at position 1 of the xanthine is a propyl (or cyclopropyl) residue, while polar substituents are not well tolerated.[94] Ethyl or propyl are present at position 3 in many cases, but the xanthine scaffold showed a preference for hydrogen atom at position 3 since it increases the potency and selectivity of the xanthines for the A_{2B}AR. Sulfonamide derivatives (**IIIo-IIIq**)[108] show a particularly high affinity and selectivity.[108,120] This, coupled with subnanomolar potency in all species (human, rat, mouse) and commercial availability, has turned **PSB-603** (**IIIo**) one of the most widely used A_{2B}AR antagonists.[93] The main strategy to improve water solubility is the generation of salts of these compounds (sulfonates), but with the trade-off of being too polar to be orally bioavailable (e.g., **PSB-1115**, **IIIp**)[120]. Recently, playing with the role of halogens in **PSB-603**, Christa Müller's group discovered several compounds with picomolar potency, being **PSB-1901** (**IIIq**) the most potent A_{2B}AR antagonist found, with a K_i of 83.5 pM.[121] Finally, for the A_3AR antagonism, the cyclized phenylxanthines are the model structure, with **PSB-11** (**IIIr**)[109] as the best candidate.[94]

Just like the natural alkylxanthines, the antagonists described above, tend to be hydrophobic and poorly water-soluble, with low bioavailability. Researchers still are working on improving pharmacokinetic properties, but they themselves still claim that: "the solubility of the reported compounds should be improved for their use as therapeutics".[121] In addition to pharmacokinetic properties and affinity, synthetic accessibility is important for the development of potential drugs. The xanthine-derivatives synthesis process involves many stages, with the consequent expenditure of time and money and the generation of chemical toxic waste, mainly due to the high number of purifications required to obtain a final compound. For example, synthesis of **PSB-1901** involves at least 7 synthesis steps with a global average yield of 15% (Figure 1.18).

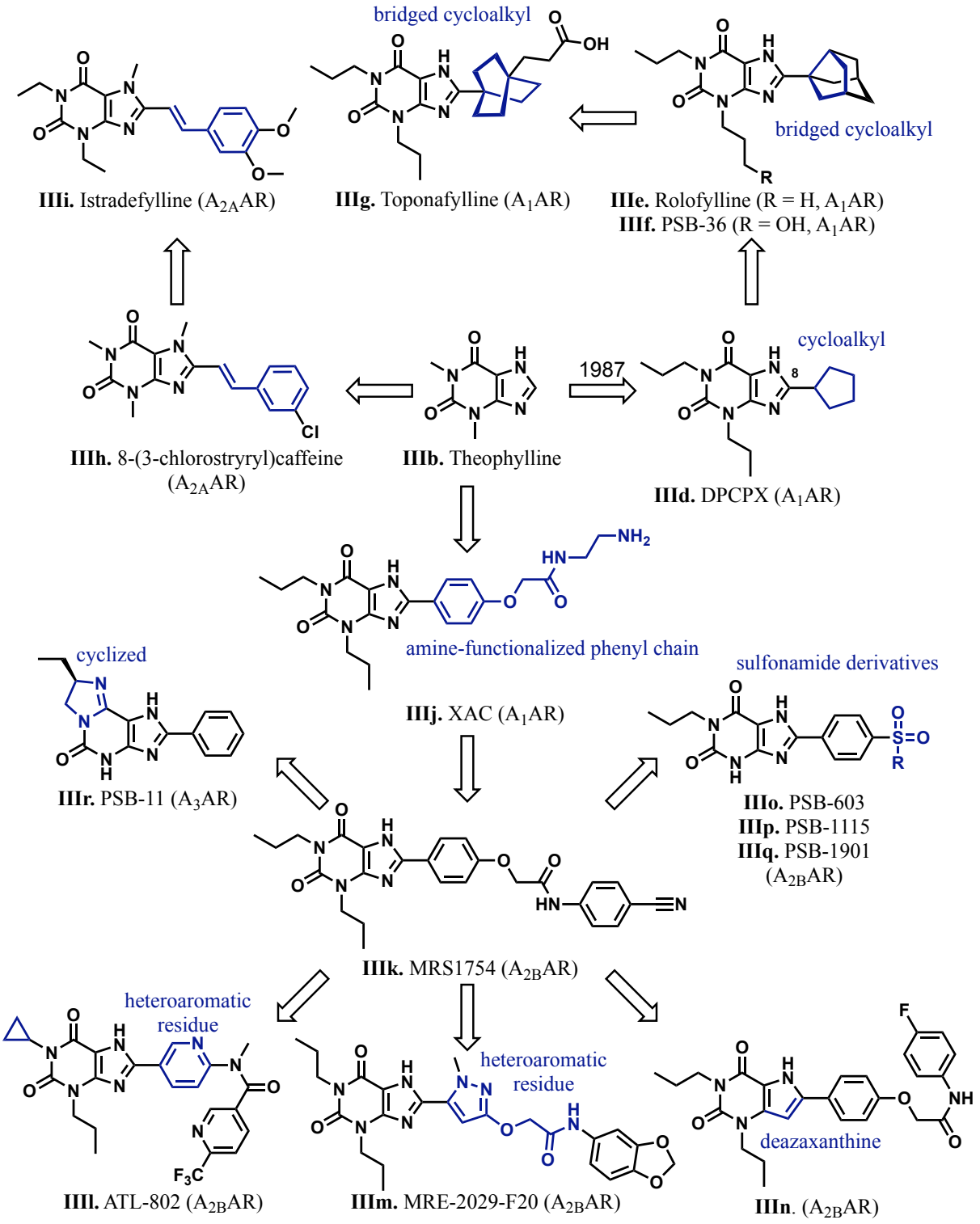

Figure 1.17. Adenosine receptor antagonists derived from xanthine scaffold. In blue, structural modifications that increase selectivity. The receptor affinities of the compounds are shown in Table 1.3. PSB-603 (R = 4-(4-chlorophenyl)piperazin-1-yl), PSB-1115 (R = OH), PSB-1901 (R = 4-(4-bromophenyl)piperazin-1-yl).

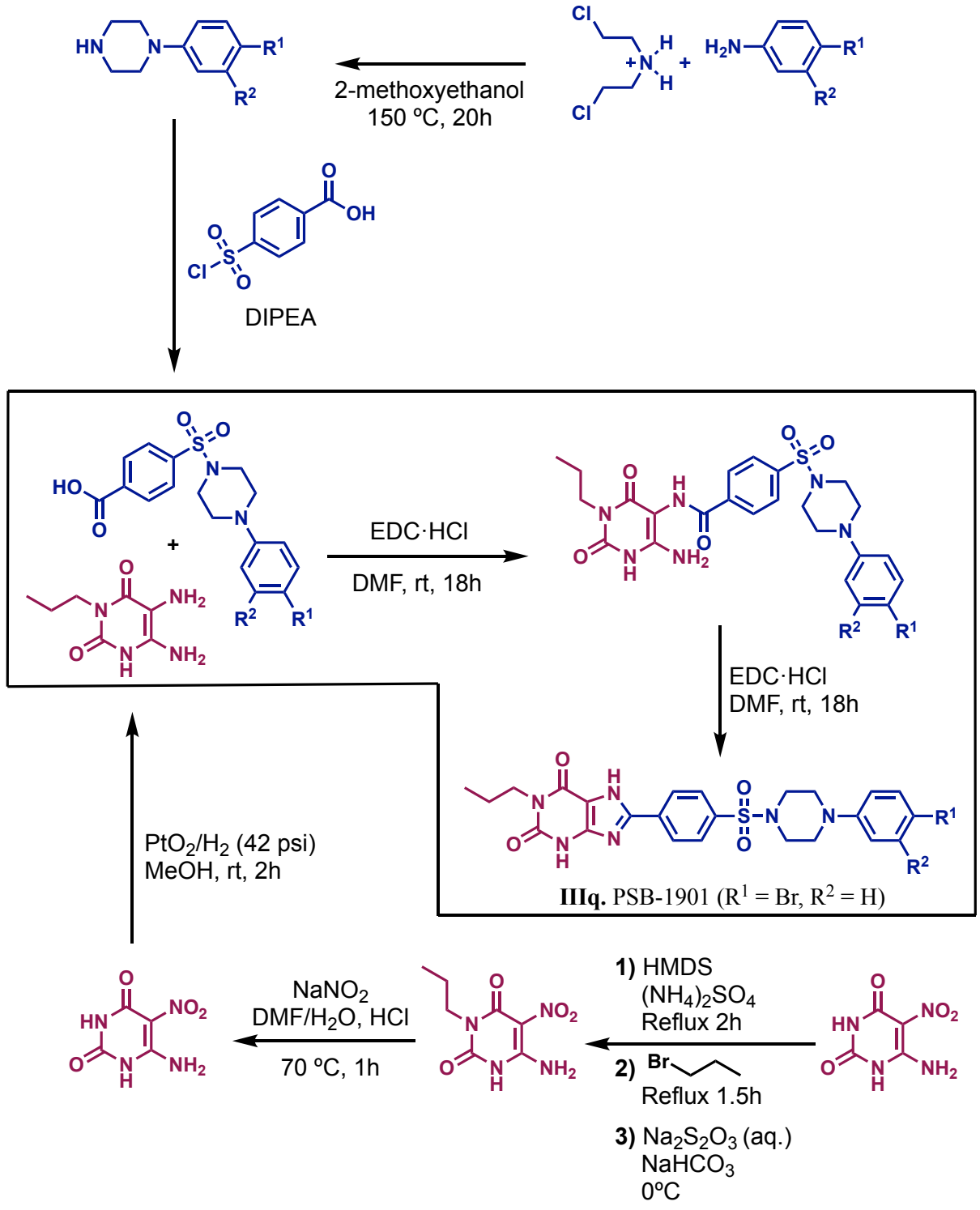

Figure 1.18. Representative example of xanthine-based sulfonamide derivatives.[121]

Table 1.3. Receptor binding data for AR xanthine-based antagonists.

		K_i			
	Xanthinic antagonists	***h*A$_1$AR**	***h*A$_{2A}$AR**	***h*A$_{2B}$AR**	***h*A$_3$AR**
	Nonselective antagonists				
IIIa	Caffeine[50]	10,700 nM	23,400 nM	33,800 nM	13,300 nM
IIIb	Theophylline[50]	6,700 nM	1,71 nM	9.07 nM	22,300 nM
IIIc	CGS15943[122]**	21 nM	3.3 nM	N.D.	13.8 nM
	A_1AR selective antagonists				
IIId	DPCPX[105]	2.20 nM	157 nM	73.2 nM	1,722 nM
IIIe	Rolofylline[123]	0.29 nM	108 nM	296 nM	4,390 nM
IIIf	PSB-36[106]	0.70 nM	980 nM	187 nM	2,300 nM
IIIg	Toponafylline[50]	7.4 nM	6,410 nM	90 nM	> 10,000 nM
IIIj	XAC[124]	6.82 nM	18.4 nM	12.3 nM	25.6 nM
	A_{2A}AR selective antagonists				
IIIh	CSC[107]	>1,000 nM	9.02 nM	>1,000 nM	>1,000 nM
IIIi	Istradefylline[50]	841 nM	12 nM	>10,000 nM	4,470 nM
	A_{2B}AR selective antagonists				
IIIk	MRS1754[93]	403 nM	503 nM	1.97 nM	570 nM
IIIl	ATL-802[93]	369 nM	654 nM	2.36 nM	>1,000 nM
IIIm	MRE-2029-F20[93]	200 nM	>1,000 nM	4.00 nM	>1,000 nM
IIIn	Deazaxanthine derivative[93]	76 nM	6,500 nM	2.90 nM	>1,000 nM
IIIo	PSB-603[108]*	>10,000 nM	>10,000 nM	0.40 nM	>10,000 nM
IIIp	PSB-1115[93]	>10,000 nM	3,790 nM	53.4 nM	>10,000 nM
IIIq	PSB-1901[121]	>1,000 nM	>1,000 nM	0.083 nM	>1,000 nM
	A_3AR selective antagonists				
IIIr	PSB-11[109]	1,640 nM	1.280 nM	2.100 nM	2.34 nM

* K_D values | ** IC_{50} values | N.D.: not determined

1.5.2.2 Non-xanthine-based antagonists

Adenine-based antagonists

Many adenine (**IVa)** derivatives, without the ribose substituent, have been reported as AR antagonists. The first indications that adenine derivatives act as AR antagonists was reported by Daly *et al*. with **N-0840** (**IVb**, A_1AR) and by Ukena *et al*. with **CGS15943** (**IVc**, A_{2A}AR).[102–104,125] Since this discovery, a plethora of heterocycles were explored mostly by removing the ribose and modifying the adenine scaffold (see Figure 1.19 and Table 1.4)
. In the same manner as in xanthinic antagonists, the introduction of cycloalkyl groups increased A_1AR selectivity (**SLV320**, **IVd**).[126]

Maintaining the unsubstituted exocyclic amino group and substituting position 2 of the adenine scaffold results in increased selectivity for the A_{2A}AR, obtaining **ST1535** (**IVe**) and **ATL-444** (**IVf**).[94] The combination of the 2'-substituted structure with the **CGS15943** (**IVc**) scaffold (8-furyl, cyclization at positions 2',3') lead to even better A_{2A}AR antagonists (**IVg-k**). Out of these ligands, it is important to highlight **Ciforadenant** (**IVh**) and Inupadenant (**IVk)**, currently in clinical trials for cancer; and **Preladenant** (**IVi**), which are in clinical trials for Parkinson's disease and is now being repurposed as cancer immunotherapy.

Detailed characterization of other ligands, such as **CGS15943** (**IVc**) and **ZM241385** (**IVg**) initially developed as A_{2A}AR antagonists, showed significant affinity for A_{2B}AR (Table 1.4).

Accordingly, they have been used as starting points for optimization towards A_{2B}AR-selective antagonists with little success.[93,94] Due to the low affinity of adenosine and adenine for the A_{2B}AR, almost no A_{2B}AR selective antagonist were discovered from this scaffold. The only exception to this trend is **OSIP-339391** (**IVl**), a 7-deaza-adenine, that shows a strong A_{2B}AR antagonistic profile.[93]

Also, starting with the **CGS15943** scaffold, keeping cyclization at positions 2',3' and furane ring at position 8'; but in this case with substituted exocyclic amines (carboxiamides), highly potent A_3AR antagonists were developed (**IVm-n**). Figure 1.19 summarizes the structural changes from the adenine scaffold to each selective antagonist.

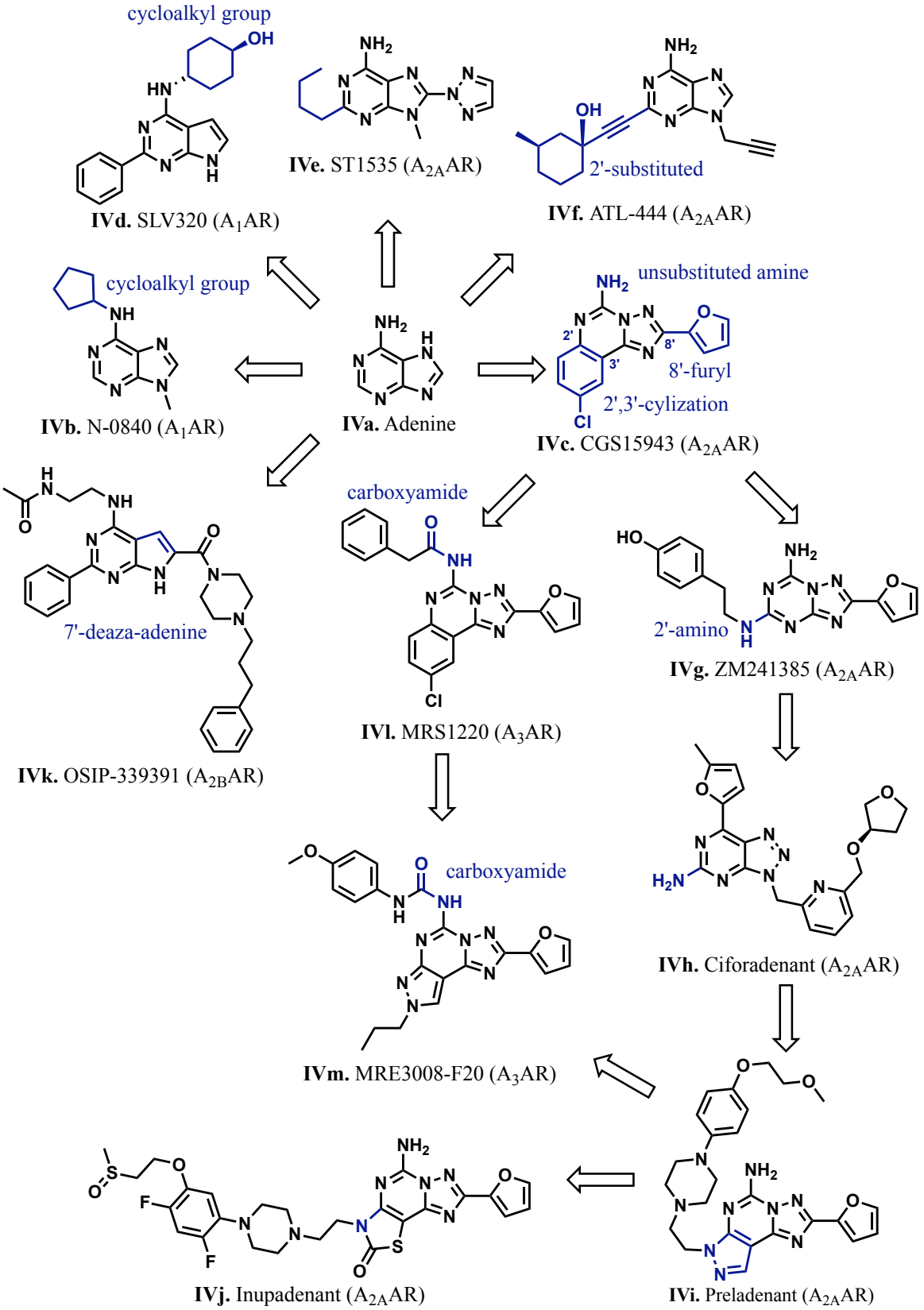

Figure 1.19. Adenine-derived AR antagonists. The receptor affinities of the compounds are shown in Table 1.4.

Pyridine- and pyrimidine-based antagonists

1,4-Dihydropyridines (DHP) have been used for a long time as calcium channel blockers (e.g., Nifedipine, **Va**). Several groups[96,127] identified that some known DHPs are able to interact with ARs. Van Veldhoven *at al*.[128] laid the initial groundwork for the development of A_1AR, A_{2A}AR and A_3AR pyrimidine antagonists (Figure 1.20). In A_3AR antagonism, work was done to separate calcium channel blockade from DHP structures, leading to the discovery of potent and selective antagonists (e.g., **MRS1334**, **Vb**).[96] These findings lead to the discovery of novel families of ARs antagonists based on library screening hits was developed in the last twenty years. 2- or 4-aminodiarylpyrimidine derivatives demonstrate an intrinsic nonselective antagonistic profile (**LUF-5740, Vc**). Pharmacomodulation of the pyrimidine central core made it possible to obtain A_1AR (**Vd**), A_{2A}AR (**Ve**) A_{2B}AR (**Vf**) and A_3AR (**Vg**) selective antagonists.[86,128–131] Two other pyrimidine-related structures, both of which are A_{2A}AR antagonists, **Tamidenant** (also known as **PBF-509**, **Vh**) and **AZD-4635** (**Vi**), were developed by PaloBioFarma and AstraZeneca respectively, and have reached clinical trials for cancer immunotherapy.[27]

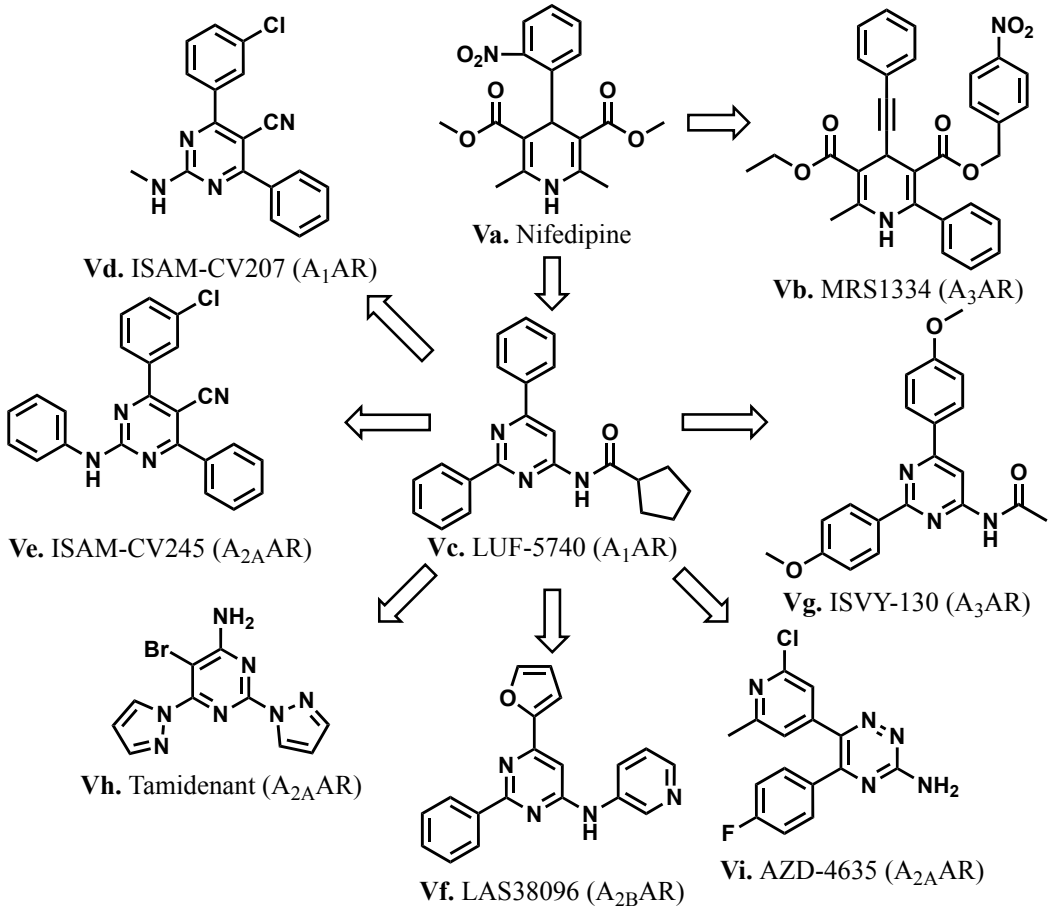

Figure 1.20. Pyridine and pyrimidine derived A_1AR, A_{2A}AR and A_3AR antagonists.

Table 1.4. Receptor binding data for non-xanthinic AR antagonists. IV: adenine-based antagonists, V: pyridine and pyrimidine-based antagonists.

		K_i			
	Non-xanthinic antagonists	***h*A$_1$AR**	***h*A$_{2A}$AR**	***h*A$_{2B}$AR**	***h*A$_3$AR**
	Nonselective antagonists				
IVa	Adenine[125]	> 100 μM	N.D.	N.D.	N.D.
Va	Nifedipine[127,132]	>4,000 nM	>4,000 nM	886 nM	>8,000 nM
Vc	LUF-5740[133]	2.14 nM	196 nM	>1,000 nM	170 nM
	A_1AR selective antagonists				
IVb	N-0840[125]	1.20 nM	N.D.	N.D.	N.D.
IVd	SLV320[134]	1.00 nM	398 nM	3,980 nM	200 nM
Vd	ISAM-CV207[86]	15.7 nM	>1,000 nM	>1,000 nM	>1,000 nM
	A_{2A}AR selective antagonists				
IVc	CGS15943[102,103]	3.50 nM	1.20 nM	32.4 nM	35.0 nM
IVe	ST1535[135]	100 nM	10.7 nM	103 nM	N.D.
IVf	ATL-444[136,137]	7.00 nM	2.50 nM	61.8 nM	>1,000 nM
IVg	ZM241385[50]	774 nM	1.60 nM	75.0 nM	743 nM
IVh	Ciforadenant[27]	192 nM	3.40 nM	3,975 nM	2,498 nM
IVi	Preladenant[50]	>1,000 nM	0.9 nM	>1,000 nM	>1,000 nM
IVj	Inupadenant[27]	500 nM*	1.83 nM*	2,200 nM*	>10,000 nM*
Ve	ISAM-CV245[86]	>1,000 nM	46.3 nM	>1,000 nM	>1,000 nM
Vh	Tamidenant (PBF-509)[27]	2,500 nM	12.0 nM	1,000 nM	5,000 nM
Vi	AZD-4635[28,49]	160 nM	1.70 nM	64.0 nM	>10,000 nM
	A_{2B}AR selective antagonists				
IVk	OSIP-339391[93]	37 nM	328 nM	0.41 nM	450 nM
Vf	LAS38096[138]	>1,000 nM	>2,500 nM	17.0 nM	>1,000 nM
	A_3AR selective antagonists				
IVl	MRS1220[122]	310* nM	52.0* nM	N.D.	0.65 nM
IVm	MRE3008-F20[50]	1,200 nM	141 nM	2,100 nM	0.82 nM
Vb	MRS1334[139]	>1,000* nM	>1,000* nM	N.D.	2.69 nM
Vg	ISVY-130[131]	>1,000 nM	>1,000 nM	>1,000 nM	3.60 nM

*: IC50 values | N.D.: Not determined

In this thesis, 3,4-dihydropyrimidin-2(1*H*)-one based A_{2B}AR selective antagonists, and A_{2A}/A_{2B}AR dual antagonists have been discovered. Therefore, we will focus on these compounds below. Our research group has contributed to the development of potent and selective A_{2B}AR antagonists with pyrimidine structure. This was done within the framework of a joint Multicomponent-assisted and High Throughput Screening (HTS) program aimed at discovering of ligands that target ARs. Employing the ComBioMed screening library (a collection of heterocyclic compounds assembled by multicomponent reaction-assisted methods that contains near 10,000 compounds), in 2013[140] we documented the discovery of the pyrimidine-derivative **V-Ia** (Figure 1.21) exhibiting submicromolar affinity (K_i = 585.5 nM) toward A_{2B}AR and high selectivity profile. This compound served as model to start an optimization study based on the 3,4-dihydropyrimidin-2(1*H*)-one scaffold. In several works[140,141] we studied diverse substitution patterns at positions 1, 2, 4, 5 and 6 of the pyrimidine ring (Figure 1.21, R^1 = NMe, NH; R^2 = carbonyl, thiocarbonyl, ketones, thioesters; R^4 = 2/3-furyl, 2/3-thienyl, phenyl; R^5 = ketones, amides, phosphonates, esters, and thioesters; R^6 = Me, Et, Pr, Ph). The best substitutions were an NH at position 1 and 3, carbonyl or thiocarbonyl at position 2, ethyl and isopropyl esters at position 5, furyl or thienyl rings at position 4 and a methyl group at position 6.[140,141] The most attractive ligands in this series are **SY1AF30** (**Vk**) and **SY1AF80** (**V-Ig**). From this point on, the project has focused on hit compound optimization. Starting from the previously discovered monocycles, the 2-cyanoimino-4-substituted-6-methyl-1,2,3,4-tetrahydro-pyrimidine-5-carboxylate scaffold was explored, **SY1K-024** (**V-Ij**) being the most attractive ligand obtained.[142] From these preliminary studies it was concluded that a pentagonal aromatic heterocycle at position 4 and an ester at position 5 are needed.

As part of the pharmacomodulation of the 3,4-dihydropyrimidine-2-one prototype, El Maatougui *et al*. identified novel A_{2B}AR antagonists,[87] mostly by cyclization in different positions. Cyclization through the 5,6 positions of the pyrimidine core leads to total loss of A_{2B}AR affinity, while fusion of heterocycles at positions 2 and 3 greatly increases it (**Figure 1.22**). In the latter case, bicyclic and tricyclic substitution patterns have been tested, with the tricycles having the best affinity for the A_{2B}AR, identifying **ISAM-140** (**V-IIIb**) as Lead compound from this exploratory project (K_i = 3.49 nM).

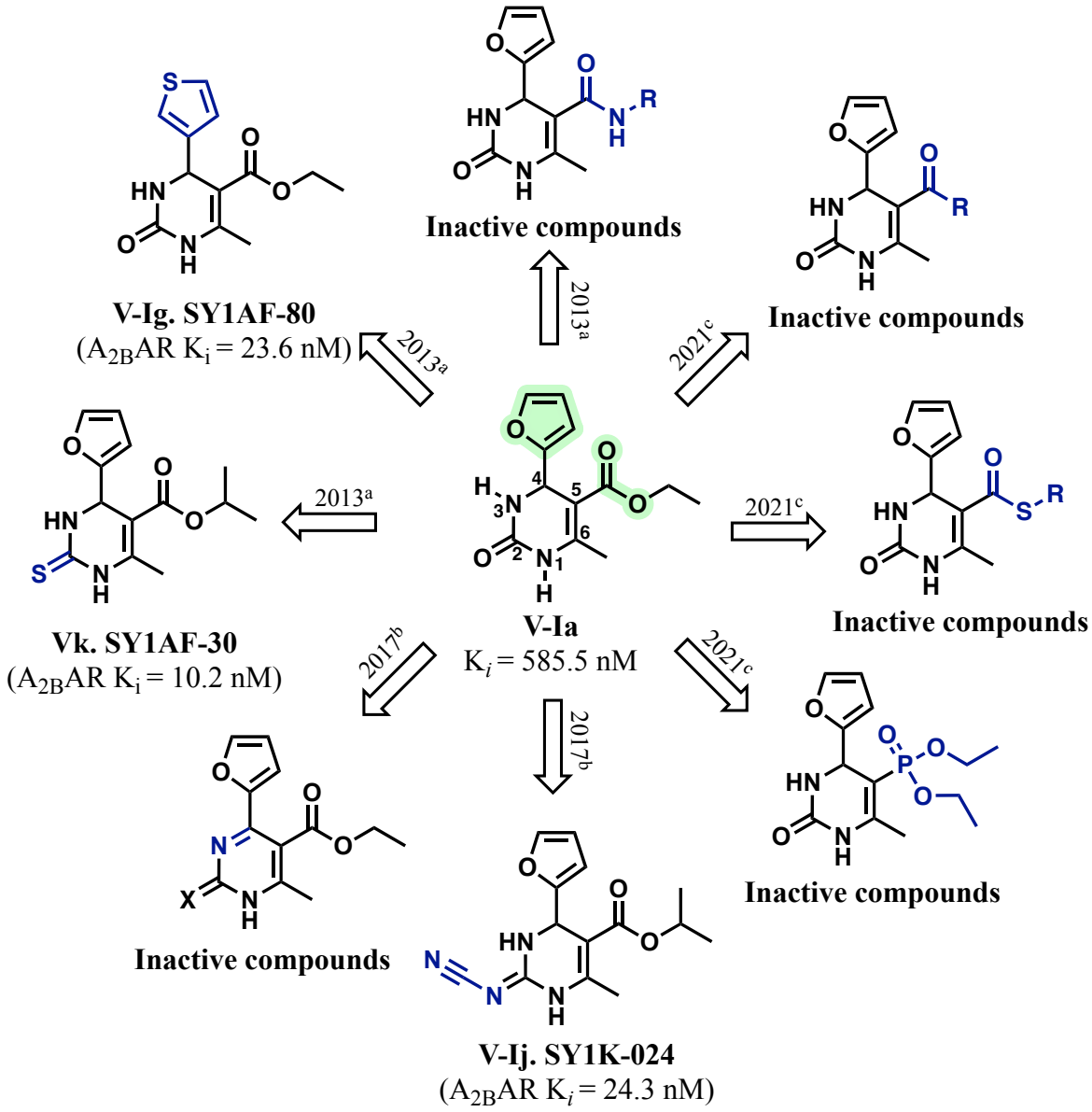

Figure 1.21. Preliminary exploration around Hit compound **V-Ia** and binding data for representative compounds. In light green, substituents essential for $A_{2B}AR$ affinity. In dark blue, substitutions explored. [a] *ACS Medicinal Chemistry Letters* **2013**, [b] *Journal of Medicinal Chemistry* **2017**, [c] *Journal of Medicinal Chemistry* **2021**.

Focused on the improvement of the compounds at the pharmacokinetic level and the exploration of the binding to $A_{2B}AR$ without altering the affinity, further studies were carried out aided by computational simulations of metabolism. First, fluorine atoms were introduced into the aliphatic zone of tricyclic scaffold (Figure 1.22, **Vm-n**). Replacement of hydrogen atoms with fluorine can improve pharmacodynamic, and pharmacokinetic parameters, leading to improved metabolic stability or optimized ligand efficiency.[143] In further work, also with the

aim of increasing the metabolic stability of tricyclic compounds, bioisosteric substitutions were made to the exocyclic pentagonal ring, due to the predicted low metabolic stability of the furan ring. The exploration of different pentacyclic rings allowed the discovery of **ISAM-C032** (Figure 1.22, **V-IIIi**), a metabolically stable **ISAM-140** analog with high potency and selectivity for the A_{2B}AR.[144] Table 1.5 shows binding affinity data for representative A_{2B}AR antagonists discovered by ComBioMed research group.

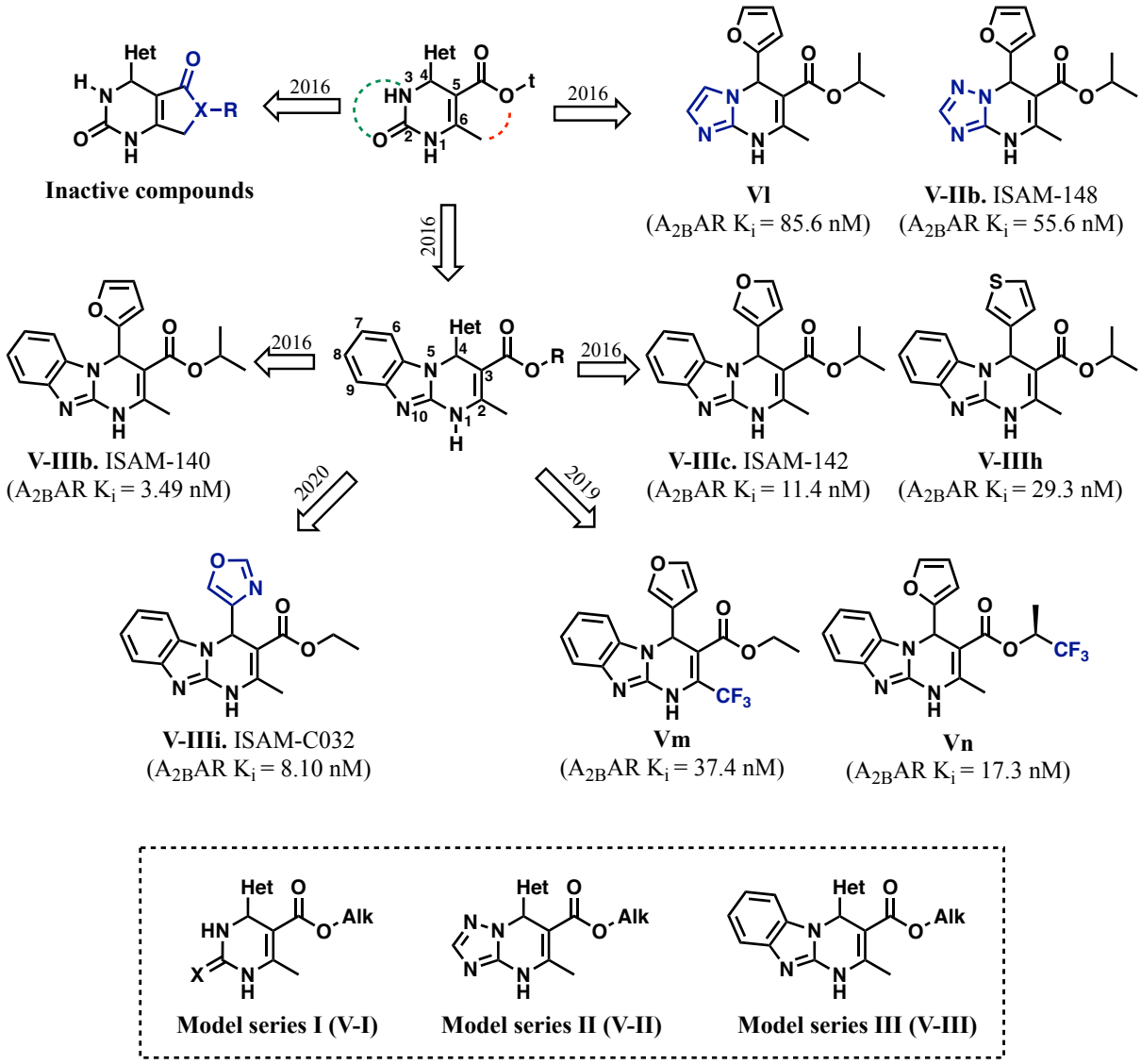

Figure 1.22. Evolution from monocyclic to bi- and tricyclic scaffold, Lead compound optimization, and model series for A_{2B}AR antagonists.

Table 1.5. Receptor binding data for ComBioMed's A_{2B}AR model series antagonists. The numbering I-III will be used in the experimental chapters for the model series represented here.

					K_i (nM)			
		Het	**Alk**	**X**	***h*A$_1$**[a)]	***h*A$_{2A}$**[b)]	***h*A$_{2B}$**[c)]	***h*A$_3$**[d)]
Monocycles (Model series **I**)								
V-Ia / D1	Hit compound[140]	2-furyl	Et	O	>1,000 nM	>1,000 nM	585 ± 89	>1,000 nM
V-Ib / D2	SY1AF-014[140]	2-furyl	*i*-Pr	O	>1,000 nM	>1,000 nM	40.8 ± 2.3	>1,000 nM
V-Ic / D3	SY1AF-101[140]	3-furyl	Et	O	>1,000 nM	>1,000 nM	39.6 ± 1.1	>1,000 nM
V-Id / D4	[140]	3-furyl	*i*-Pr	O	>1,000 nM	>1,000 nM	1486 ± 62	>1,000 nM
V-Ie	[140]	2-thienyl	Et	O	>1,000 nM	>1,000 nM	>1,000 nM	>1,000 nM
V-If	[140]	2-thienyl	*i*-Pr	O	>1,000 nM	>1,000 nM	>1,000 nM	>1,000 nM
V-Ig	SY1AF-080[140]	3-thienyl	Et	O	>1,000 nM	>1,000 nM	23.6 ± 1.0	>1,000 nM
V-Ih	SY1AF-020[140]	3-thienyl	*i*-Pr	O	>1,000 nM	>1,000 nM	56.6 ± 1.3	>1,000 nM
V-Ii	[142]	2-furyl	Et	NCN	>1,000 nM	>1,000 nM	900 ± 6	>1,000 nM
V-Ij	SY1K-024[142]	2-furyl	*i*-Pr	NCN	>1,000 nM	>1,000 nM	24.3 ± 0.9	>1,000 nM
V-Ik	[142]	3-furyl	Et	NCN	>1,000 nM	>1,000 nM	102 ± 3	>1,000 nM
V-Il	[142]	3-furyl	*i*-Pr	NCN	>1,000 nM	>1,000 nM	59.4 ± 1.8	>1,000 nM
V-Im	[142]	2-thienyl	Et	NCN	>1,000 nM	>1,000 nM	51.0 ± 2.1	>1,000 nM
V-In	[142]	2-thienyl	*i*-Pr	NCN	>1,000 nM	>1,000 nM	349 ± 3	>1,000 nM
V-Io	[142]	3-thienyl	Et	NCN	>1,000 nM	>1,000 nM	461 ± 2	>1,000 nM
V-Ip	[142]	3-thienyl	*i*-Pr	NCN	>1,000 nM	>1,000 nM	657 ± 4	>1,000 nM
Bicycles (Model series **II**)								
V-IIa	[87]	2-furyl	Et	-	>1,000 nM	>1,000 nM	>1,000 nM	>1,000 nM
V-IIb	ISAM-148[87]	2-furyl	*i*-Pr	-	>1,000 nM	>1,000 nM	55.6 ± 4	>1,000 nM
V-IIc	[87]	3-furyl	Et	-	>1,000 nM	>1,000 nM	602 ± 10	>1,000 nM
V-IId	[87]	3-furyl	*i*-Pr	-	>1,000 nM	>1,000 nM	350 ± 8	>1,000 nM
V-IIe	[87]	2-thienyl	Et	-	>1,000 nM	>1,000 nM	>1,000 nM	>1,000 nM
V-IIf	[87]	2-thienyl	*i*-Pr	-	>1,000 nM	>1,000 nM	>1,000 nM	>1,000 nM
V-IIg	[87]	3-thienyl	Et	-	>1,000 nM	>1,000 nM	699 ± 5	>1,000 nM
V-IIh	[87]	3-thienyl	*i*-Pr	-	>1,000 nM	>1,000 nM	816 ± 7	>1,000 nM
Tricycles (Model series **III**)								
V-IIIa / D5	ISAM-134[87]	2-furyl	Et	-	>1,000 nM	>1,000 nM	12.0 ± 0.7	>1,000 nM
V-IIIb / D6	ISAM-140[87]	2-furyl	*i*-Pr	-	>1,000 nM	>1,000 nM	3.49 ± 0.2	>1,000 nM
V-IIIc / D7	ISAM-141[87]	3-furyl	Et	-	>1,000 nM	>1,000 nM	20.6 ± 1.1	>1,000 nM
V-IIId / D8	ISAM-142[87]	3-furyl	*i*-Pr	-	>1,000 nM	>1,000 nM	11.40 ± 0.5	>1,000 nM
V-IIIe	[87]	2-thienyl	Et	-	>1,000 nM	>1,000 nM	484 ± 3	>1,000 nM
V-IIIf	[87]	2-thienyl	*i*-Pr	-	>1,000 nM	>1,000 nM	371 ± 5	>1,000 nM
V-IIIg	[87]	3-thienyl	Et	-	>1,000 nM	>1,000 nM	29.7 ± 1.2	>1,000 nM
V-IIIh	[87]	3-thienyl	*i*-Pr	-	>1,000 nM	>1,000 nM	29.3 ± 1.1	>1,000 nM
V-IIIi	ISAM-C032[144]	4-oxazolyl	Et	-	>1,000 nM	>1,000 nM	8.10 ± 0.5	>1,000 nM
V-IIIj	[144]	4-oxazolyl	*i*-Pr	-	>1,000 nM	>1,000 nM	43.4 ± 1.3	>1,000 nM

In contrast to the long and complicated synthesis of xanthine derivatives, pyrimidinone derivatives can be synthesized through an experimentally simple multicomponent reactions (MCR). MCRs are convergent synthetic reactions in which three or more reactants are combined in one step to obtain one (or more) products that contains most of the atoms from the starting materials. Specifically, for the synthesis of 3,4-dihydropyrimidin-2(1*H*)-ones (DHP), the essential MCR is the **Biginelli reaction** (Figure 1.23A).[145] This acid-catalyzed three-component reaction between an aldehyde, a 1,3-dinucleophile, and a β-ketoester, constitutes a very interesting chemical tool for the development of non-xanthinic A_{2B}AR antagonists. Most of the compounds shown in this thesis were synthesized through this reaction, although in some cases a second reaction is needed to generate new diversity.

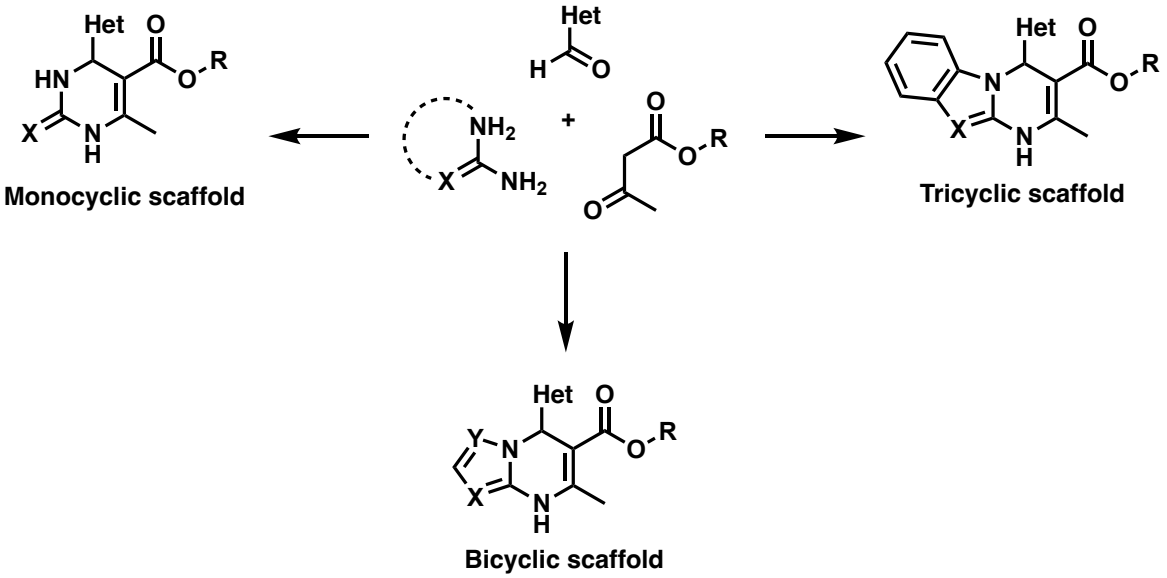

Figure 1.23. General Biginelli Reaction Scheme. Dotted lines represent cycles fusion position.

A peculiarity of the dihydropyrimidinone antagonists herein described is that they are the first examples of non-planar A_{2B}AR antagonists, with an asymmetric carbon at position 4 of heterocyclic core (Figure 1.20). The remarkable loss of affinity observed after aromatization of the dihydropyrimidin-2-one scaffold,[140] early suggested a critical role for stereochemistry at C4 and lead us to perform computational studies and to evaluate the biological activity of each enantiomer. As predicted by molecular modelling (Figure 1.24A), only the enantiomer showing the pentagonal exocyclic ring backwards has affinity for A_{2B}AR (Figure 1.24B, eutomer), the other being completely inactive (Figure 1.25). Furthermore, trifluorinated compounds demonstrated that the configuration at the ester moiety is not important for A_{2B}AR affinity [**(3*R*, 4*S*)-Vn** (K_i = 6.91 nM) vs **(3*S*, 4*S*)-Vn** (K_i = 8.37 nM), Figure 1.25].[143]

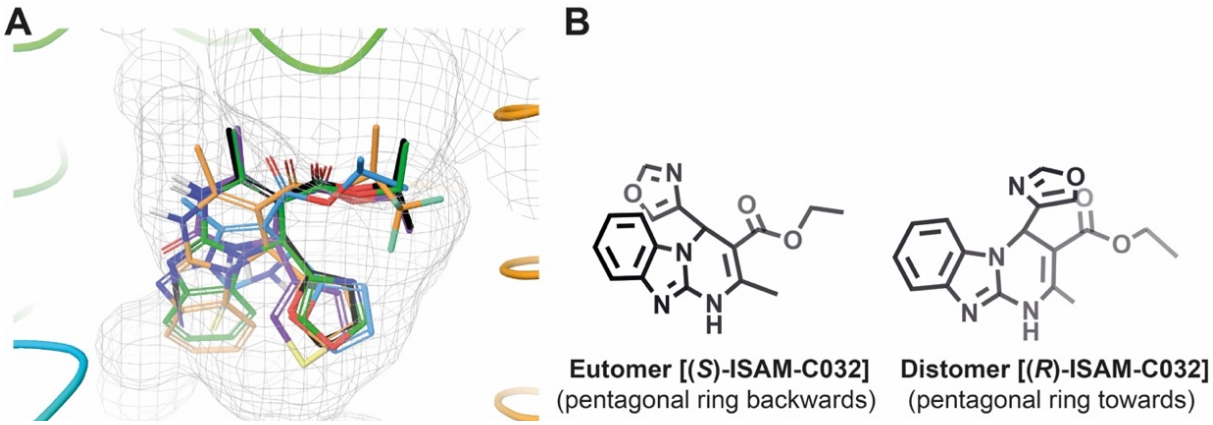

Figure 1.24. A) Alignment of ***(S)*-SY1K-024** (black), ***(3S,4S)*-16i** (orange), ***(S)*-ISAM-C032** (green), ***(S)*-SY1AF-30** (blue) and ***(S)*-SY1AF-80** (purple) predicted by docking in $A_{2B}AR$ homology model. Mesh represent $A_{2B}AR$ orthosteric binding site surface.[141-144] B) 3D representation of pyrimidinone-derived eutomer and distomer for $A_{2B}AR$.

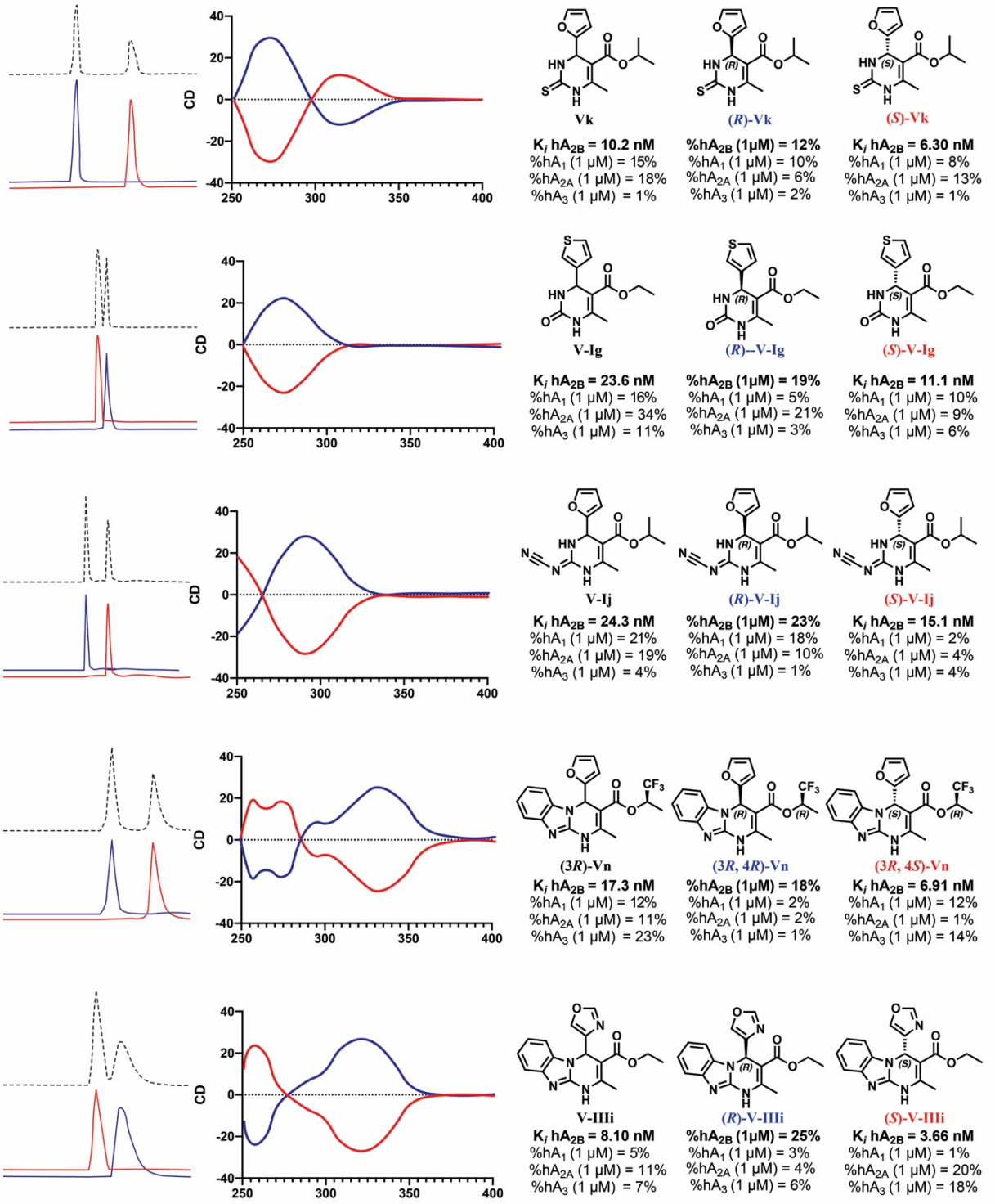

Figure 1.25. Chiral HPLC, circular dichroism spectra and binding data for resolved racemic A_{2B}AR antagonists. In blue: distomer (pentagonal ring forwards); in red: eutomer (pentagonal ring backwards).

$A_{2A}AR/A_{2B}AR$ dual antagonists

As explained at the beginning of this Thesis, the $A_{2A}AR$ and $A_{2B}AR$ are actors during tumor regulation (angiogenesis, cell growth, metastasis, and immune system), which coupled with the discovery of $A_{2A}AR/A_{2B}AR$ heterodimerization, make dual $A_{2A}AR/A_{2B}AR$ ligands promising candidates for cancer treatment. However, only a few dual $A_{2A}AR/A_{2B}AR$ antagonists are known. Therefore, industry (and academic) interest for this kind of molecules is growing. Recently, Gilead Sciences traded $725M for rights to a slate of cancer drugs, including **Etrumadenant** (**VIa**) from Arcus Biosciences.[146,147] A collaboration between Selvita and Ryvu Therapeutics led to the discovery of **SEL330-639**[148,149] (**VIb**) and **SEL330-584**[148] (**VIc**, structure not disclosed), which demonstrated antitumor effect in *in vitro* assays, restoring the cytotoxic potential of NK cells, believed to be essential in antitumor immune reactions.[149] The last disclosed $A_{2A}AR/A_{2B}AR$ antagonist is **M1069**[150] (**VId**, Merck), currently undergoing a phase 1 clinical trial in advanced solid tumors.[151] **M1069** showed superior suppression of protumorigenic cytokine secretion and rescue of IL12 secretion from adenosine-differentiated dendritic cells. These results were corroborated in *in vivo* experiments (murine $CD73^{hi}$/adenosine-rich 4T1 syngeneic breast tumor model). Dual $A_{2A}AR/A_{2B}AR$ blockade is expected to be superior to $A_{2A}AR$ or $A_{2B}AR$ blockade alone in the ADO rich TME, where one of the two may be complementary or compensatory to the other.

Academic research has not rationally found any dual $A_{2A}AR/A_{2B}AR$ antagonists; most of them have been obtained by serendipity in programs to obtain selective $A_{2A}AR$ or $A_{2B}AR$ antagonists. This is the case of **ISAM-CV247** (**VIe**) and **ISAM-CV248** (**VIf**), discovered in a program to increase $A_{2A}AR$ selectivity from non-selective antagonists for ARs.[86] Receptor affinities for the compounds mentioned are shown in Table 1.6.

To obtain better drugs, it is necessary to develop rational methods to design dual antagonists. This would allow us to not only study the SAR, but also to improve the pharmacokinetic properties of the designed drugs.

Another point to consider during the development of dual $A_{2A}AR/A_{2B}AR$ antagonists is that those shown in Table 1.6 have a planar structure. Considering that binding to the $A_{2B}AR$ for some scaffolds has been shown to be influenced by the stereochemistry,[141–144] the same role in $A_{2A}AR/A_{2B}AR$ ligands selectivity could be observed.

Table 1.6. Receptor affinities for selected dual $A_{2A}AR/A_{2B}AR$ antagonists.

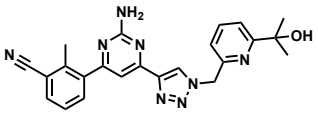

VIa. Etrumadenant

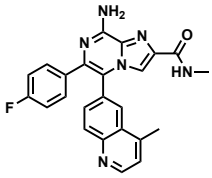

VIc. SEL330-639

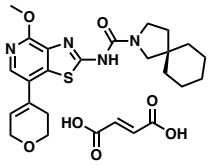

VId. M1069

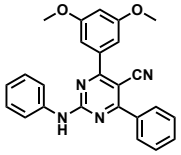

VIe. ISAM-CV247

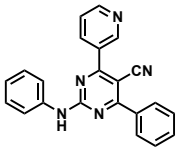

VIf. ISAM-CV248

		K_i			
		***h*A$_1$AR**	***h*A$_{2A}$AR**	***h*A$_{2B}$AR**	***h*A$_3$AR**
	$A_{2A}AR/A_{2B}AR$ dual antagonists				
VIa	Etrumadenant[152]*	N.P.	1.40 nM	1.90 nM	N.P.
VIb	SEL330-584[148]**	N.P.	0.26 nM	3.60 nM	N.P.
VIc	SEL330-639[148,149]**	N.P.	0.25 nM	6.40 nM	N.P.
VId	M1069[150]***	1200 nM	0.13 nM	9 nM	8800 nM
VIe	ISAM-CV247[86]	>1,000 nM	17.3 nM	64.0 nM	>1,000 nM
VIf	ISAM-CV248[86]	>1,000 nM	27.1 nM	29.4 nM	>1,000 nM

* K_D values. | **EC50 values determined by competition in presence of ADO (0.1 μM) | ***IC50 values.

N.P.: Data not published

2 OBJECTIVES

As indicated in the introduction of this thesis, $A_{2B}AR$ is a promising target for cancer immunotherapy. By selectively blocking it, many of the functions blocked in TME could be restored. ADO concentration is greatly increased under hypoxia and cancer-associated inflammation, activating the (low affinity) $A_{2B}AR$. This is understood as an alarm signal (of exacerbated tissue damage), resulting in increased cell proliferation, angiogenesis (to increase nutrient and oxygen delivery) and inhibition of the immune system (to prevent cell damage). In this situation a blockade (by antagonists) of $A_{2B}AR$ would reverse these effects, allowing to restore the immune system functions.

The classical antagonists of this receptor are xanthine derivatives (e.g., caffeine). Although the optimization of these ligands has advanced enormously, with highly potent and selective antagonists available, their sub-optimal pharmacokinetic profile (low solubility, low permeability and easily metabolizable compounds). For this reason, the development of $A_{2B}AR$ antagonists focusing not only on affinity, but also on its pharmacokinetic properties, is essential in the context of anticancer therapy.

The ComBioMed group has developed a multicomponent-assisted platform for the discovery and optimization of new drug candidates. During the last ten years, our group has greatly contributed to the discovery of novel drugs, pharmacological tools, and fluorescent ligands that target diverse GPCRs (e.g., A_1AR, $A_{2A}AR$, $A_{2B}AR$, A_3AR, dopamine D_2, cannabinoid CB_1 and CB_2, serotonin $5HT_{2A}$ and $5HT_{2B}$). These GPCRs are validated to face severe pathologies with ineffective treatments (Parkinson's disease, glaucoma, diabetes, schizophrenia, pain, inflammation, and cancer).

The present PhD Thesis focuses on the discovery and optimization of new potent and highly selective ligands and pharmacological tools targeting $A_{2B}AR$ to validate it as a new target for cancer immunotherapy. The herein described research is part of a long-term project aimed at the discovery of Adenosine Receptors antagonists. The project is divided into four main chapters, differentiated in the general structure of the compounds and in the specific aims. A summary of the main goals for each chapter is provided below.

Chapter I (Section 3.1) deals with the design, development, and optimization of $A_{2B}AR$ antagonists with improved pharmacokinetic properties. Using **ISAM-140** and **ISAM-C032** as model ligands, our objective was to identify the best halogenation patterns in the benzene ring of the tricyclic system to reduce its trend to oxidative metabolism, keeping or increasing binding affinity (Figure 2.1). In addition, by introducing halogens into the structure (along with the rest of the substitutions of the molecule), the objective was also to improve the solubility and permeability profiles of these series. The aim of the study included not only the characterization of the new ligands in terms of $A_{2B}AR$ potency and selectivity, but also a preliminary *in vitro* evaluation of solubility, microsomal stability and CYP3A4 inhibition. To validate the structural determinants that govern the stereospecific recognition of these series, it was decided to separate and evaluate the enantiomers of the most attractive ligands identified.

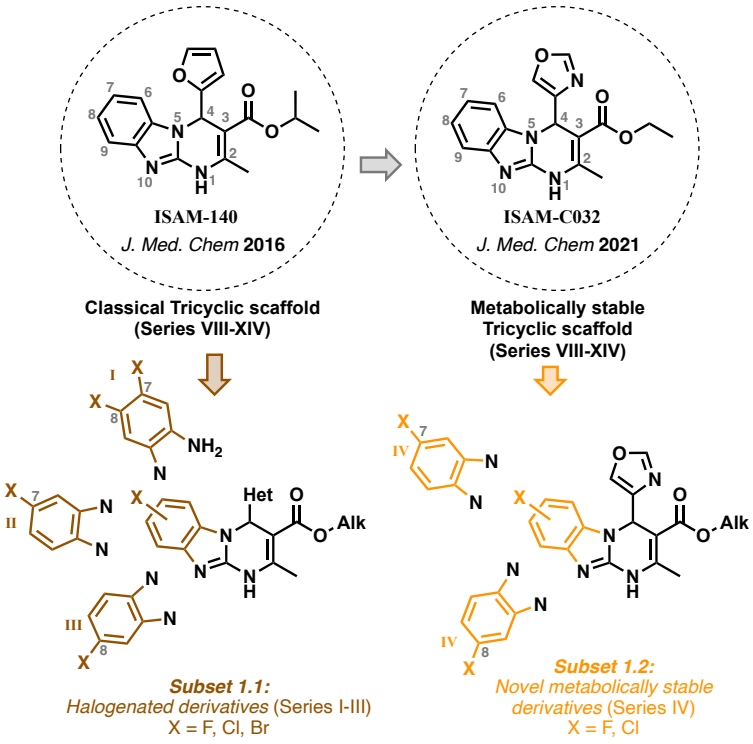

Figure 2.1.Design strategy and diversity elements studied in the first chapter of the thesis.

Chapter II (Section 3.2) deals with the exhaustive exploration of diverse heterocyclic cores (monocyclic, bicyclic, and tricyclic) through a multicomponent-assisted scaffold hopping strategy (Figure 2.2). The aim is to discover structurally novel compounds starting from well-known active compounds by transforming the central structure of the molecule. Three families of ligands have been designed from the Model Series **II** (bicyclic). The first, by ring opening generating monocycles (series **V-XI**), allows us to further explore the binding mode of this type

of compounds with $A_{2B}AR$. The second, by substitutions at position 2 of the bicyclic nucleus (series **XII-XVIII**), and the third, by bioisosteric replacements (series **XIX-XXV**), allows us to study comprehensively the binding modes and main interactions of bi- and tricyclic molecules with the $A_{2B}AR$. Furthermore, the most attractive ligands were separated into their enantiomers and evaluated.

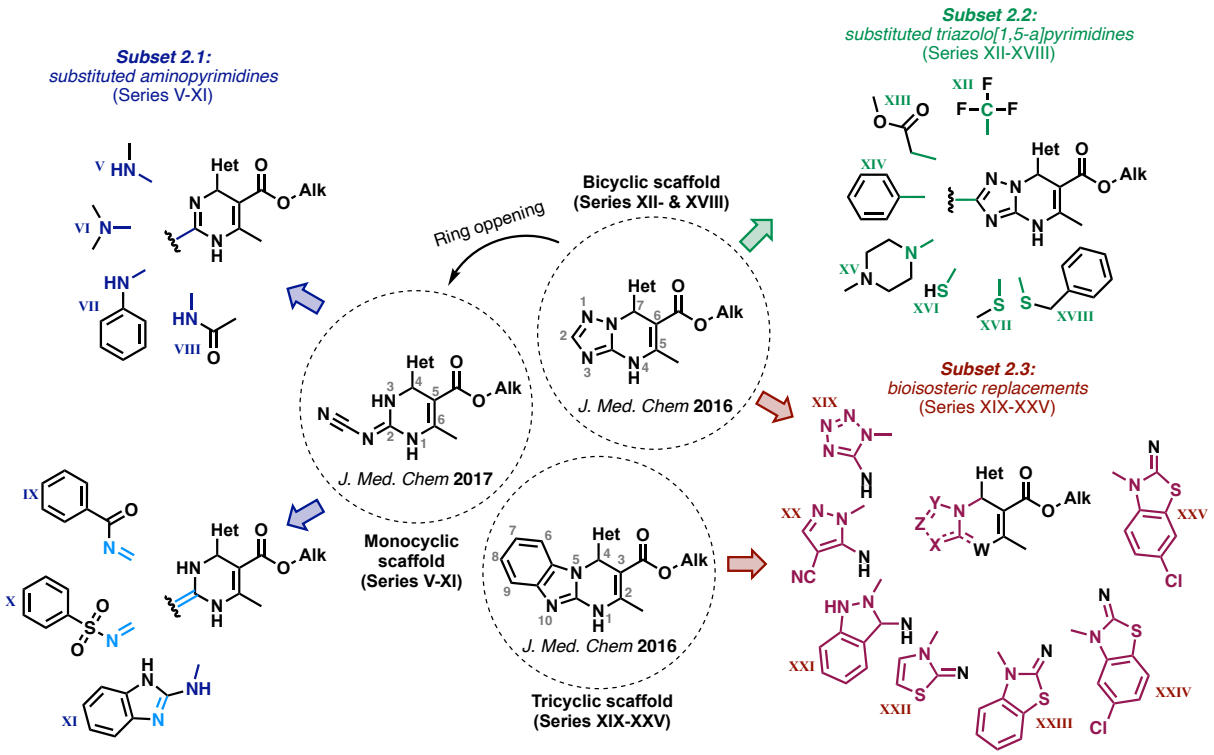

Figure 2.2. Scaffold-Hopping strategy for the design of novel $A_{2B}AR$ antagonists from bicyclic core. In blue (top), ring-opening series. In green (left), substitutions at position 2 series. In magenta (right), bioisosteric replacements series.

Chapter III (Section 3.3) deals with the discovery of novel anticancer drugs, with particular emphasis on novel $A_{2A}AR/A_{2B}AR$ dual antagonists. During the design of this chapter, we focused on a main goal: the identification of potent dual $A_{2A}AR/A_{2B}AR$ (and highly selective $A_{2B}AR$) antagonists (Figure 2.3). The rational design of *N*-substituted compounds as dual $A_{2A}AR/A_{2B}AR$ antagonists was based on **Chapter II** findings and previous published studies of our group with a 2-aminopyrimidine scaffold (non-selective $A_1AR/A_{2A}AR/A_{2B}AR$ antagonists).[86] The most attractive ligands, including $A_{2A}AR/A_{2B}AR$ dual antagonists, were separated and evaluated to study the role of configuration at C4 within $A_{2A}AR/A_{2B}AR$ recognition.

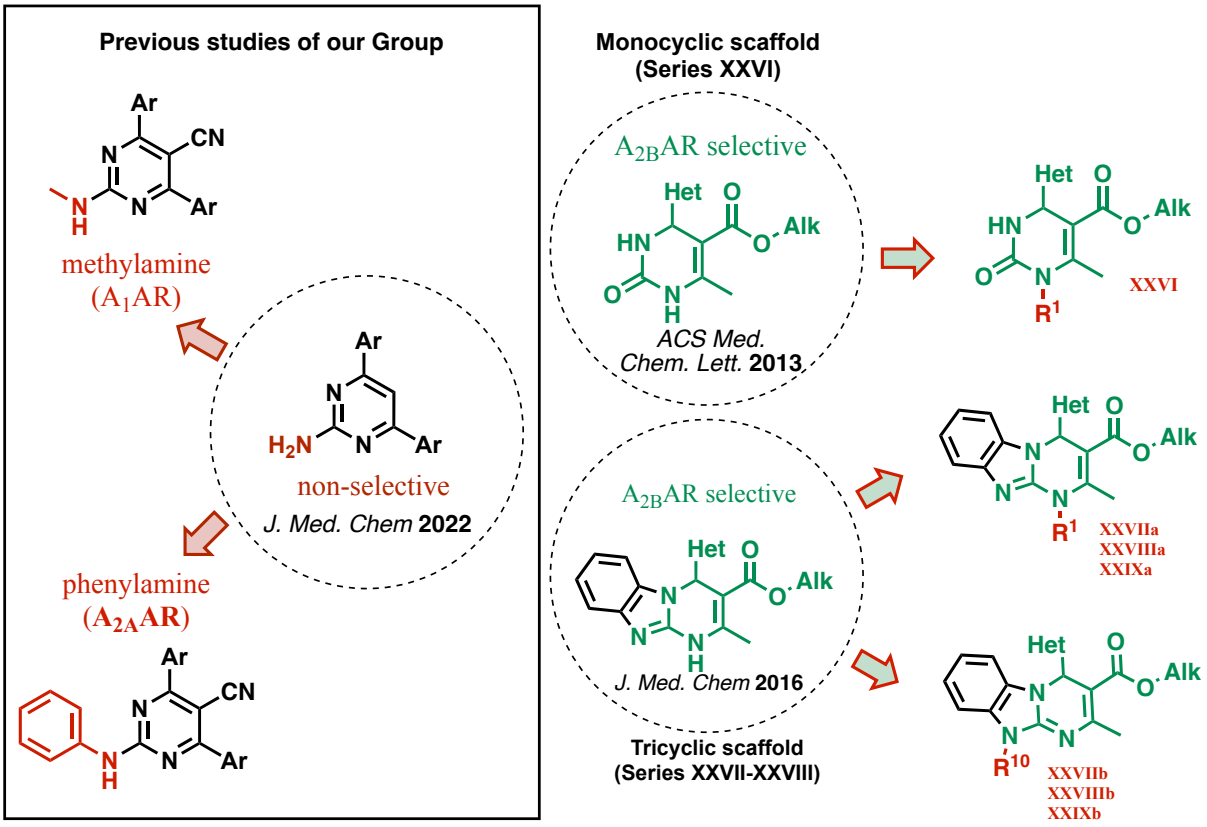

Figure 2.3. Rational design of $A_{2A}AR/A_{2B}AR$ dual (and $A_{2B}AR$) antagonists.

Chapter IV (Section 3.4) has a more translational aim, focused on providing evidences to validate $A_{2B}AR$ as an attractive target for cancer treatment. As explained above, purinergic system, specifically $A_{2B}AR$, is a promising target for cancer treatment due to its synergistic effects in the TME. With a well-validated role in angiogenesis, its effect on immunity and cell proliferation remains unexplored. Accordingly, the most attractive ligands discovered in this thesis were biologically evaluated in different *in vitro* and *ex vivo* assays. The compounds were assayed in the presence of adenosine (or with adenosine-producing tumor cells), with the aim to highlight their potential a) immunostimulatory effect (cell proliferation and activation, production of cytokines and other chemical mediators) and b) antiproliferative effect in three cancer models (breast, colorectal and glioblastoma).

CHAPTER I. EXPLORING THE EFFECT OF HALOGENATION IN A SERIES OF POTENT AND SELECTIVE A_{2B} ADENOSINE RECEPTOR ANTAGONISTS

The results of this chapter have been already published in:

Exploring the Effect of Halogenation in a Series of Potent and Selective A_{2B} Adenosine Receptor Antagonists. Prieto-Díaz, R.;[1,2,3] González-Gómez, M.;[1,2] Fojo-Carballo, H.;[1,2] Azuaje, J.;[1,2] El Maatougui, A.;[1,2] Majellaro, M.;[1,2] Loza, M. I.;[4,5] Brea, J.;[4,5]* Fernández-Dueñas, V.;[6,7] Paleo, M. R.;[1,2] Díaz-Holguín, A.;[3] Garcia-Pinel, B.;[4,8] Mallo-Abreu, A.;[1,2] Estévez, J. C.;[1,2] Andújar-Arias, A.;[1,2] García-Mera, X.;[2] Gomez-Tourino, I.;[4,8] Ciruela, F.;[6,7] Salas, C. O.;[9] Gutiérrez-de-Terán, H.;[3]* Sotelo, E.[1,2]*. *J. Med. Chem.* **2023**, *66*, 890–912.

[1]Center for Research in Biological Chemistry and Molecular Materials (CIQUS), University of Santiago de Compostela, 15782 Santiago de Compostela, Spain. [2]Department of Organic Chemistry, Faculty of Pharmacy, University of Santiago de Compostela, 15782 Santiago de Compostela, Spain. [3]Department of Cell and Molecular Biology, Uppsala University, Biomedical Center, 75124 Uppsala, Sweden. [4]Center for Research in Metabolic Diseases (CIMUS). University of Santiago de Compostela, 15782 Santiago de Compostela, Spain. [5]Department of Pharmacology, Pharmacy and Pharmaceutical Technology, Faculty of Pharmacy, University of Santiago de Compostela, 15782 Santiago de Compostela, Spain. [6]Pharmacology Unit, Department of Pathology and Experimental Therapeutics, Faculty of Medicine and Health Sciences, Institute of Neuroscience, University of Barcelona, 08907 L'Hospitalet de Llobregat, Spain. [7]Neuropharmacology and Pain Group, Neuroscience Program, Institut d'Investigació Biomèdica de Bellvitge, IDIBELL, 08907 L'Hospitalet de Llobregat, Spain. [8]Department of Biochemistry and Molecular Biology. Faculty of Pharmacy, University of Santiago de Compostela, 15782 Santiago de Compostela, Spain. [9]Department of Organic Chemistry, Faculty of Chemistry and Pharmacy, Pontificia Universidad Católica de Chile, Vicuña Mackenna 4860, Macul, Santiago 7820436, Chile.

Impact factor: 8.039 (N° 3/63 (D1) in the category of Medicinal Chemistry (JCR 2021)). ISSN: 0022-2623.

This article is an open access publication and may be used for authors in their own thesis in accordance with American Chemical Society policy (Creative Commons 4.0 License).

Contribution

Research conceptualization, synthesis, purification and structural characterization, separation and characterization of enantiomers, docking and molecular dynamics (FEP) studies, data analysis and manuscript writing.

3 RESULTS AND DISCUSSION

3.1 CHAPTER I: EXPLORING THE EFFECT OF HALOGENATION IN A SERIES OF POTENT AND SELECTIVE A_{2B} ADENOSINE RECEPTOR ANTAGONISTS

ADO is an essential signaling nucleoside that is either released from cells or extracellularly generated, by sequential hydrolysis of adenosine 5′-triphosphate and adenosine 5′-monophosphate by the ectonucleotidases CD39 and CD73.[36] Ado is ubiquitous in mammalian cells, being a key intermediate metabolite that modulates several biochemical processes,[153] ranging from energy transfer, signal transduction, sleep-wake cycle,[154] inflammation,[155] and immunity.[21,71] In healthy tissues the extracellular concentration of Ado is generally low, though it can increase rapidly from nanomolar to micromolar,[36] which contributes to the protection of tissues against damage caused by stress, injury, hypoxia, or inflammation.[50,156,157] Four rhodopsin-like G protein-coupled receptors (GPCRs) sense the extracellular Ado levels, constituting the class 1 purinergic receptors (P_1) A_1AR, A_{2A}AR, A_{2B}AR and A_3AR. Each adenosine receptor (AR) subtype has unique sequence homology, tissue distribution, second messenger coupling and pharmacology.[50] The physiology of Ado signaling through these receptors and its pathophysiological implications in human diseases has been recently reviewed.[36]

A_{2B}AR remains the most puzzling and poorest characterized AR subtype.[158] Ubiquitously expressed but usually at low levels (except at human cecum, large intestine, mast cells and hematopoietic cells), A_{2B}AR displays the lowest affinity for adenosine among all four subtypes (30-300 nM), remaining silent in healthy conditions.[36] Such a behavior, together with its high structural homology with the well characterized A_{2A}AR, led to the initial perception that A_{2B}AR would have only minor physiological relevance. However, it is now well documented that A_{2B}AR becomes activated under particular pathological conditions such as hypoxia, inflammation, infection, and cancer, where extracellular adenosine levels are increased up to micromolar concentrations, consequently increasing attention to the therapeutic potential of A_{2B}AR as a drug target.[159] A_{2B}AR antagonists have been recently proposed as potential drugs for the treatment of inflammation, diabetes, pain, asthma, and Alzheimer disease.[76,160–162] More recent is the identification of the A_{2B}AR as an important player to different facets of cancer

progression e.g., tumor growth, metastasis, and angiogenesis.[14,52] Advances in cancer immunotherapy highlight the importance of Ado as a key metabolite that suppresses anti-tumor immune response by T and NK cells in the tumor microenvironment,[41] being this immune role specifically mediated by A_{2A} and A_{2B} ARs.[29,32,39] Indeed, several A_{2A}AR antagonists are under clinical trials as immune checkpoint inhibitors for the treatment of different cancer types.[27] A_{2A}AR and A_{2B}AR exhibit high homology and are often co-expressed on cells.[163] Recent studies suggested formation of heteromeric A_{2A}AR–A_{2B}AR complexes and revealed that ligand recognition, signaling and pharmacology of A_{2A}AR is blocked by the A_{2B}AR.[43] According to all these evidence, A_{2B}AR antagonists and dual A_{2A}AR-A_{2B}AR antagonists are emerging as effective cancer (immuno)therapeutics, where the consequent reactivation of the immune system results in antiproliferative, antiangiogenic and antimetastatic effects.[141,164]

The therapeutic opportunities arising from A_{2B}AR modulation have driven the development of A_{2B}AR antagonists. The naturally occurring xanthine derivatives (e.g., caffeine and theophylline) early inspired the discovery and optimization of xanthine congeners and structurally related deaza-analogues and purine derivatives.[93] Xanthines have been intensively studied, allowing the identification of derivatives eliciting optimal affinity-selectivity profiles (Figure 3.1, first row), being so far the most widely explored A_{2B}AR antagonists.[121] However, their challenging physicochemical features and pharmacokinetic (PK) profiles remain as the major drawback of this chemotype to advance further on the drug discovery pipeline. Consequently, recent efforts have been focused on the development of non-xanthinic A_{2B}AR antagonists (Figure 3.1, second row).[87,140,144] In this context, we have reported novel series of pyrimidine-based ligands (Figure 3.1, **SY1AF30**, **ISAM-140**, **ISAM-134**, and **ISAM-C032**) which encompass structural novelty, exquisite affinity and selectivity and excellent synthetic feasibility.[87,140,144] A hybrid approach, combining scaffold hopping and thorough SAR investigation, have guided the expansion of these series. Importantly, these compounds contain a chiral center within the heterocyclic core (Figure 3.1, **SY1AF30**, **ISAM-140**, **ISAM-134**, and **ISAM-C032**), offering a novel structural element as compared to classical, planar A_{2B}AR antagonists. Consequent racemate separation provided the first examples of antagonists with enantiospecific A_{2B}AR recognition.[141–144,165]

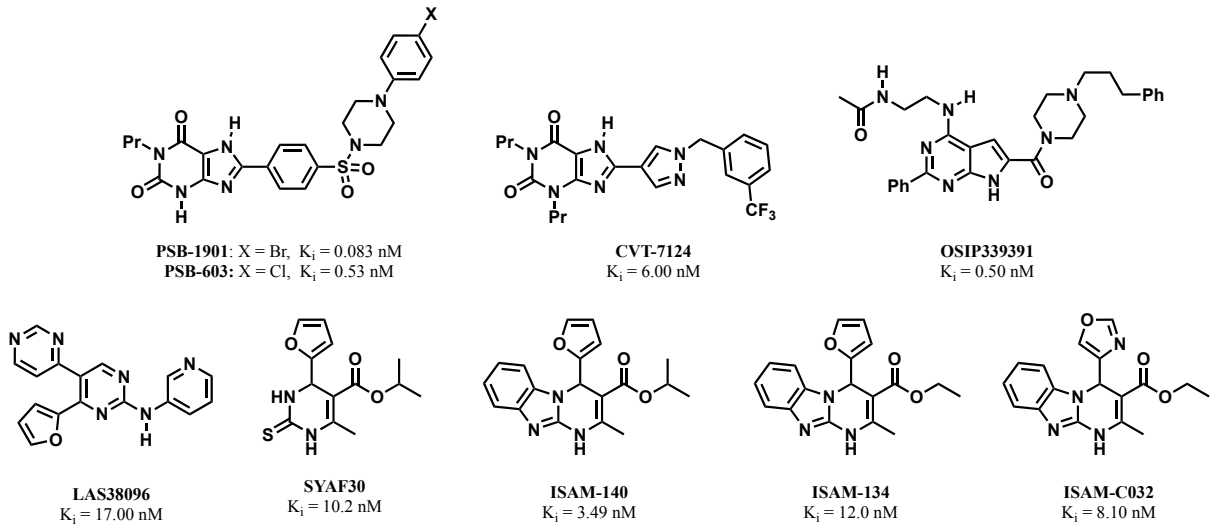

Figure 3.1. Structure of representative potent and selective A_{2B}AR antagonists.

In the frame of an optimization program of non-xanthine A_{2B}AR antagonists as promising cancer (immuno)therapeutics,[141] we determined to analyze the impact of di- and mono- halogenation at positions 7 and 8 of the tricyclic core of prototypical A_{2B}AR antagonists (Figure 3.1, **ISAM-140**, **ISAM-134**, and **ISAM-C032**).[87,144] The main goal was to improve the pharmacodynamic and pharmacokinetic profiles of this chemotype, while maintaining (or even improving) the affinity and selectivity profiles. The phenyl ring of the tricyclic system is the most easily metabolizable part, only after to the exocyclic pentagonal ring that was already optimized in a previous work,[144] and halogenation arises as a strategy to reduce the probability of intensive metabolization. At the same time, the size-variability of halogen substitution would allow a deeper exploration of the interactions proposed by earlier modeling studies in the internal cavity of the A_{2B}AR.[87,140,144] The synthesis and pharmacological characterization of a collection of 80 novel tricyclic ligands is here assessed by free energy perturbation (FEP) simulations, evidencing the superior profile of 8-halo derivatives by optimizing interactions with the modeled binding site. This study further confirms the previously modeled enantiospecific A_{2B}AR recognition of the pentagonal ring at position 4, and the antagonist profile of the most promising compounds. In addition, examination of the ADMET profile of representative antagonists confirmed that the introduction of a fluorine atom improves solubility and microsomal stability. Two of the ligands here optimized were selected to investigate the effect of A_{2B}AR antagonism on immune cell proliferation, demonstrating that the ligands reverse the reduction of adenosine-related proliferation in human primary immune cells.

3.1.1 Design

These novel series were conceived in the context of our ongoing projects to develop multi-target cancer (immuno)therapeutics for the A_{2B}AR, starting from the scaffold of **ISAM-140** (Figure 3.2, Model Series **I**, Het = 2-furyl, R = *i*-Pr) as a prototype ligand. Introduction of functional groups at positions 7 and 8 of the heterotricyclic core evidenced conspicuous effects on the affinity and selectivity profile, thus inspiring the design of the present series. It was anticipated that halogenation at positions 7 and 8 of the phenyl ring within the tricyclic core would result not only in compounds with improved pharmacodynamic and pharmacokinetic profiles but would also provide valuable data to understand the molecular basis behind the observed SAR trends.

Thus, we envisioned the development of the 80 new ligands (series **I**-**IV**) presented in Figure 3.2. Being aware that the impact of halogenation on binding affinity and selectivity might be position-dependent, and that it could heavily rely on the nature of the halogen, we systematically introduced F, Cl and Br atoms at positions 7 and 8 of the tricyclic scaffold (Figure 3.2). To preserve consistency from the early series and facilitate the comparative SAR, the herein obtained ligands (series **I**−**IV**) retained the structural elements that provided optimal A_{2B}AR affinity at positions 3 and 4 (Figure 3.2). Thus, for Het we initially considered a set of four pentagonal heteroaryl groups (2-furyl, 3-furyl, 2-thienyl, 3-thienyl), while the alkoxy residues of the ester moiety (Alk) consist of either ethyl or isopropyl groups. Three series were subsequently conceived, each consisting of 24 derivatives (Figure 3.2 and Table 3.2 to Table 3.4). Series **I** contain two identical halogen atoms at positions 7 and 8 (Compounds **1-24**), whereas in series **II** and **III** (mono-halogenated) the halogen atom is present at positions 7 or 8 respectively (Compounds **25-48** and **49-72**). Finally, a focused series consisted of eight 7-halo or 8-halo derivatives bearing a 4-oxazolyl group (Table 3.5), which we have recently identified as an optimal non-furan pentagonal nucleus for the position 4.[144] This limited series was obtained by prioritizing two halogens (F and Cl) and the substitution patterns that provided better affinity and selectivity profiles in series **I-III** (**73-80**).

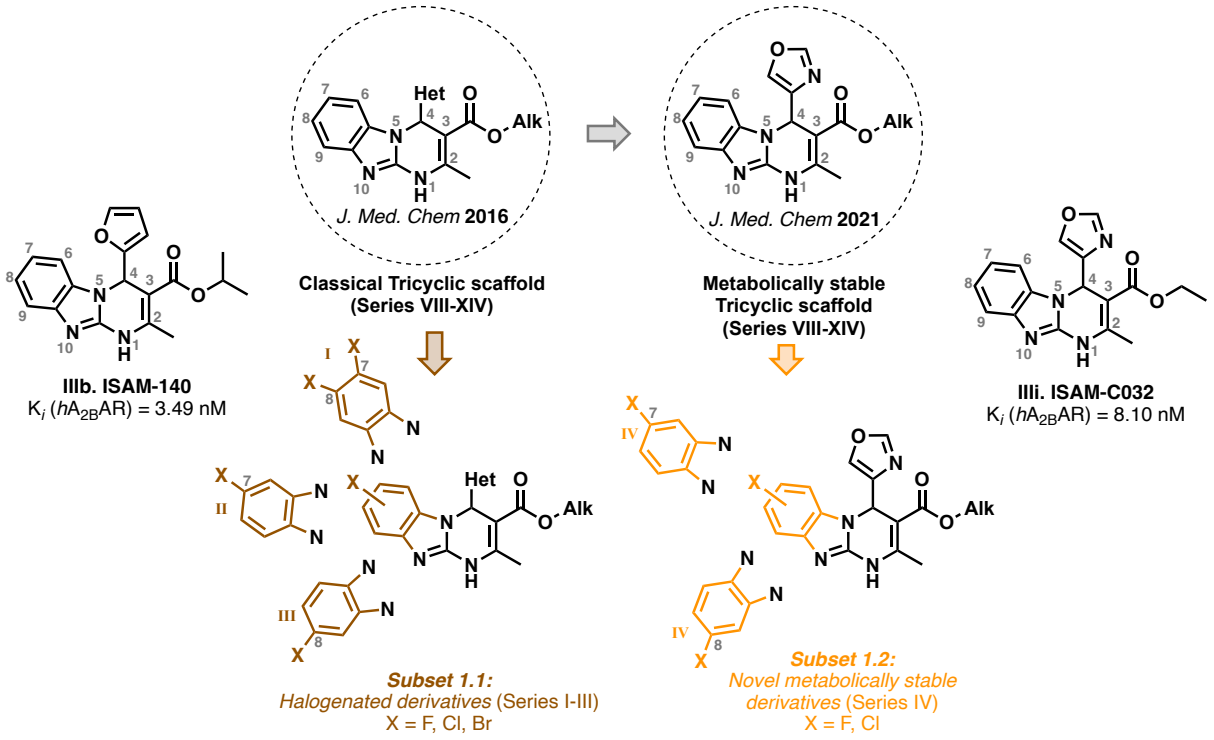

Figure 3.2 Model ligands and design strategy and diversity elements explored during the study.

3.1.2 Chemistry

The halogenated alkyl 4-heteroaryl-2-methyl-1,4-dihydrobenzo[4,5]-imidazo[1,2-*a*]pyrimidine-3-carboxylates (**1-80**) were obtained as depicted in Scheme 1. A three-component synthesis, based on the robust and efficient Biginelli reaction (i.e., the three-component reaction of an aldehyde, a β-ketoester and 1,3-dinucleophiles), enabled a time- and cost-effective assembly of the large collection obtained. A set of pentagonal carbaldehydes (**A1-5**) and β-ketoesters (**B1-2**) providing optimal substituents for positions 4 and 3 in combination with six halogenated 2-aminobenzimidazoles (**C1-6**) were employed as precursors. The starting materials, dissolved in THF and containing a catalytic amount of $ZnCl_2$ (or acetic acid), were submitted to orbital stirring at 90 ºC for 12 hours (Method A, series **I-III**) or microwave radiation at 80 ºC for 90 min (Method B, series **IV**). The targeted tricyclic derivatives were obtained in moderate to satisfactory yields (30-85%). For the synthesis of series of monohalogenated (7-halo or 8-halo) derivatives (Scheme 1, Cmpds **1-80**), the corresponding 2-amino-5-halobenzimidazoles (**C4-6**) were employed as precursors. The phenomenon of tautomerization enabled to directly obtain the targeted (7- or 8-)-halogenated alkyl 4-heteroaryl-2-methyl-1,4-dihydrobenzo-[4,5]imidazo[1,2-*a*]pyrimidine-3-carboxylates as regioisomeric

mixtures in a 1:1 ratio. Both regioisomers (Series **II-IV**) were isolated in pure forms after chromatographic separation. All reactions were monitored by thin-layer chromatography (TLC). After completion of the reaction, the solvent was evaporated to dryness and the isolated solid was purified by column chromatography on silica gel (Figure 3.3). A detailed description of the synthetic methods and the complete structural, spectroscopic, and analytical data for all compounds are provided in the Experimental Section.

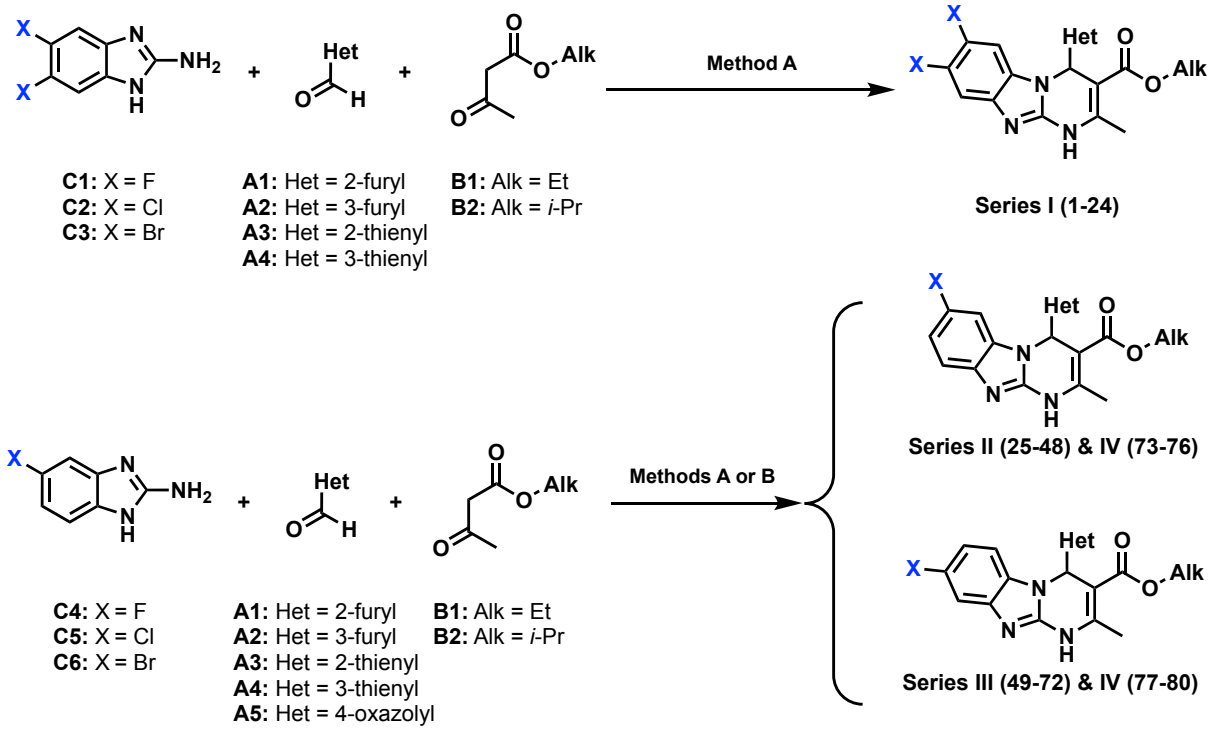

Figure 3.3. Biginelli-based synthesis, Method A) $ZnCl_2$, THF, 90 °C, 12 h. Method B) AcOH, THF/DMF (2:1), 80 °C, Mw, 90 min.

Unambiguous structural characterization of each regioisomer has been carried out with a combination of X-ray crystallography and 2D-NMR experiments (Figure 3.4). The monohalogenated compounds (Series **II-IV**) differ in the position of the halogen atom located either at C7 or C8. Both regioisomers present an ABX aromatic substitution pattern in the ^{1}H NMR (Figure 3.4). X-ray diffraction analysis of **67** (see Experimental Section) show that protons H-4 (hydrogen alpha to the 5-membered ring) and H-6 (aromatic proton) are 2.7Å apart, allowing us to perform NOE experiments (Figure 3.4). 2D-ROESY NMR spectrum of **67** (8-halo derivative, Figure 3.5) showed a correlation of H4 (singlet, δ 6.60 ppm) and the doublet (J = 8.4 Hz) at δ 7.41 ppm corresponding to H6. The coupling constant value is typical of ortho H-H coupling and indicates the presence of a hydrogen in C7 and therefore of the halogen at

C8. However, 2D-ROESY NMR spectrum of **43** (7-halo derivative, Figure 3.6) showed a correlation between H4 (singlet at δ 6.53 ppm) and H6 (doublet at δ 7.70 ppm). The coupling constant value, J = 1.9 Hz, indicates a H-H meta coupling, and thus the halogen is in ortho position (C7). Similar correlations were observed for other pairs of regioisomers (Figure 3.7). As in previous series[87,141–144] all ligands obtained in this study contain one stereocenter at position 4 of the heterocyclic core and were isolated and evaluated as racemic mixtures. Six ligands eliciting attractive A_{2B}AR affinity/selectivity profile were submitted to chiral resolution to isolate its corresponding enantiomer pairs.

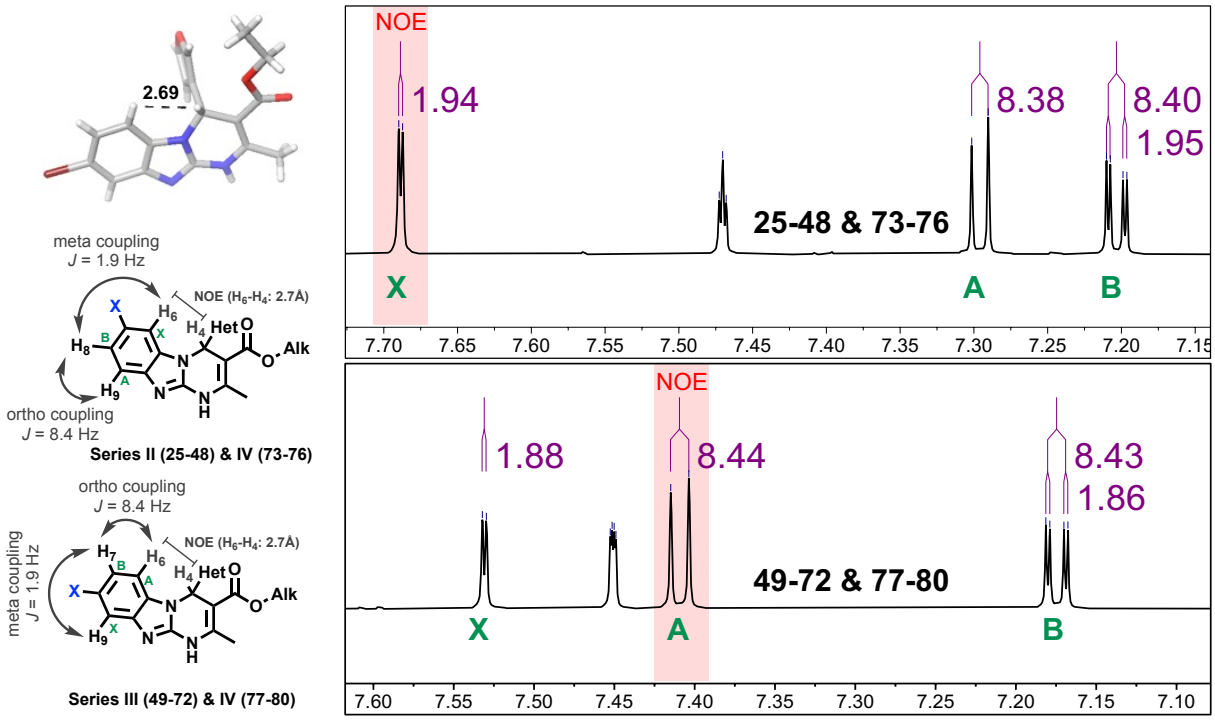

Figure 3.4. Regioisomer characterization strategy. In red: signal with NOE effect irradiating H-4; in purple: J (Hz) tree.

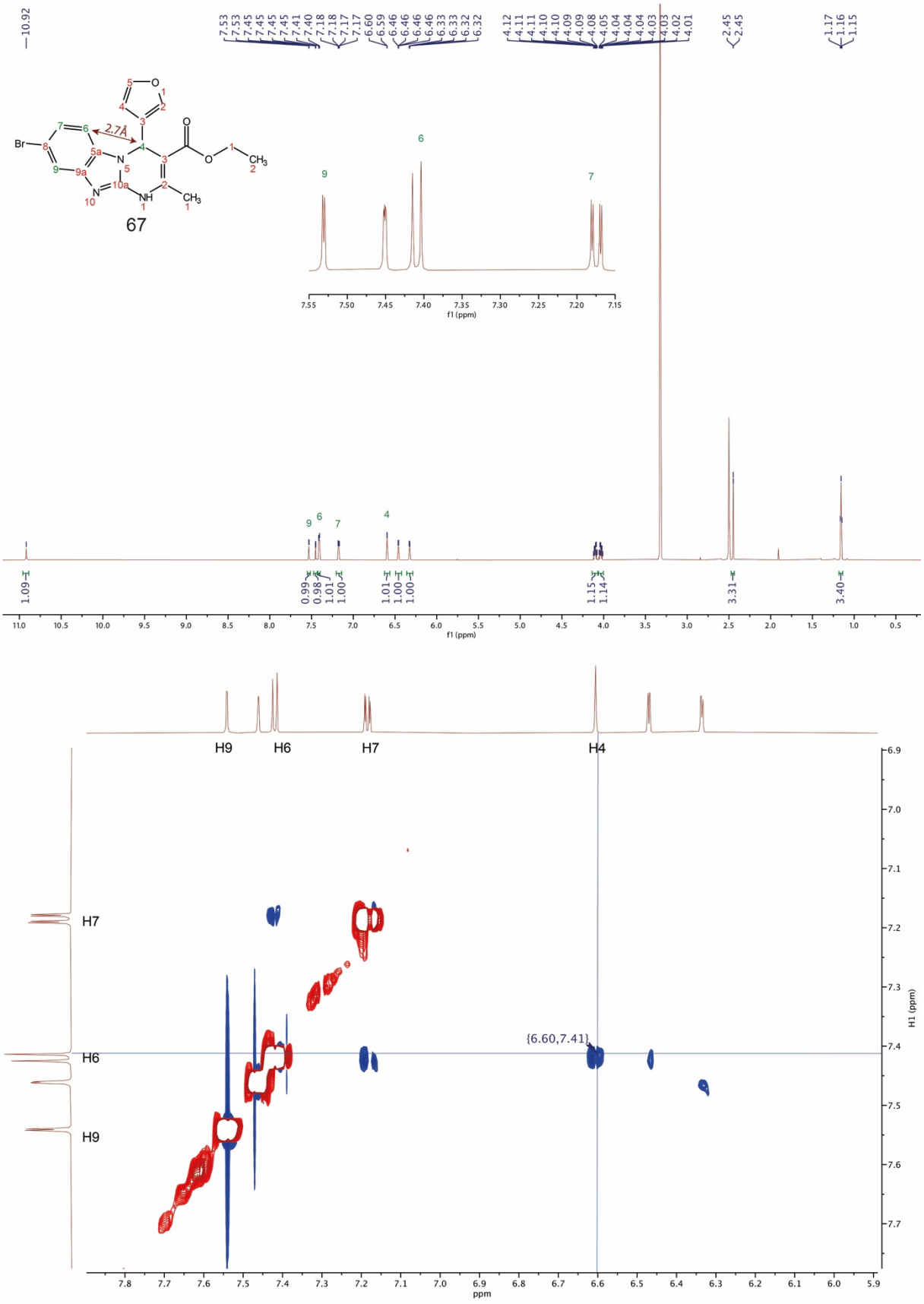

Figure 3.5. ^{1}H NMR and 2D-ROESY of **67**.

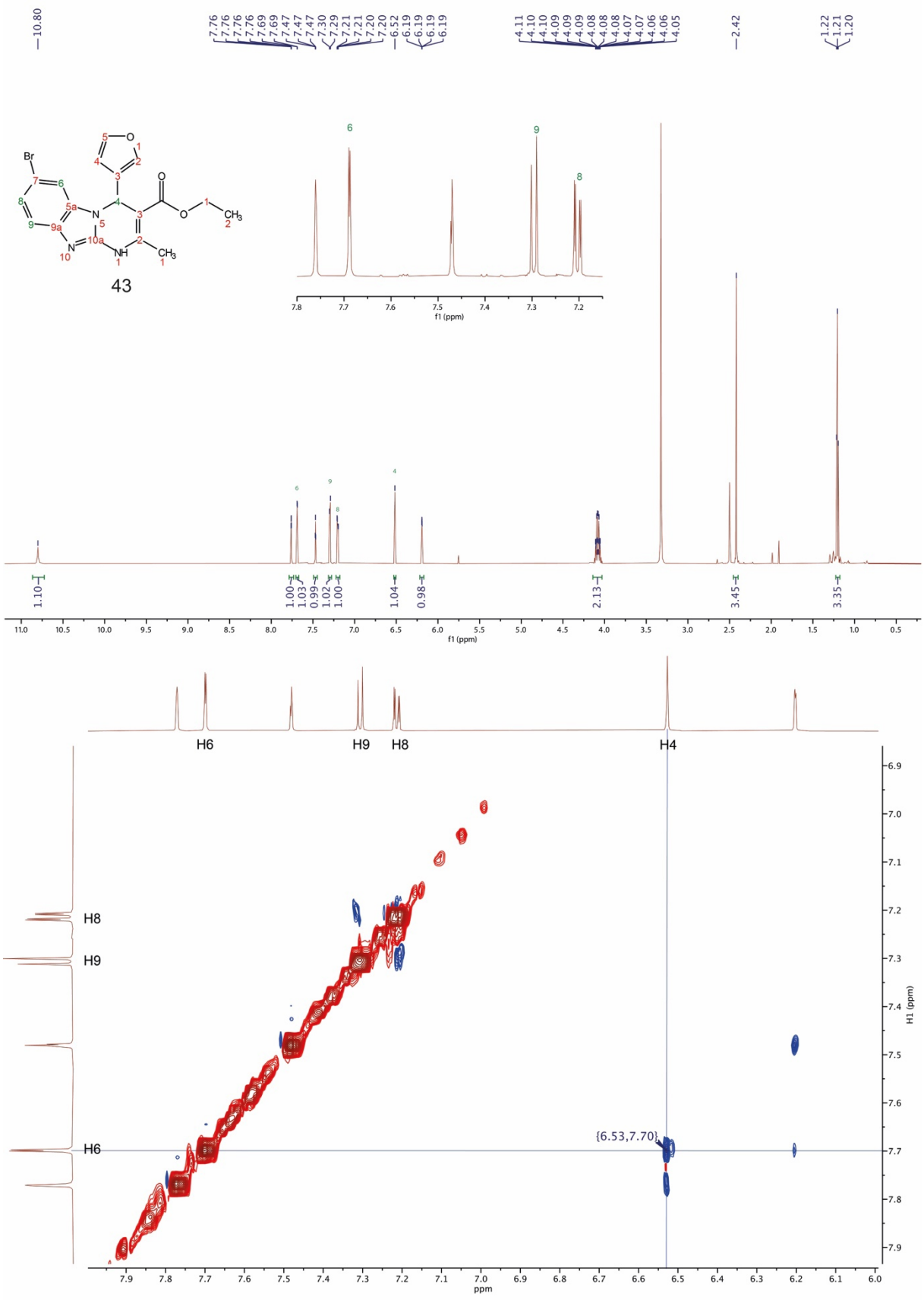

Figure 3.6. ^{1}H NMR and 2D-ROESY of **43**.

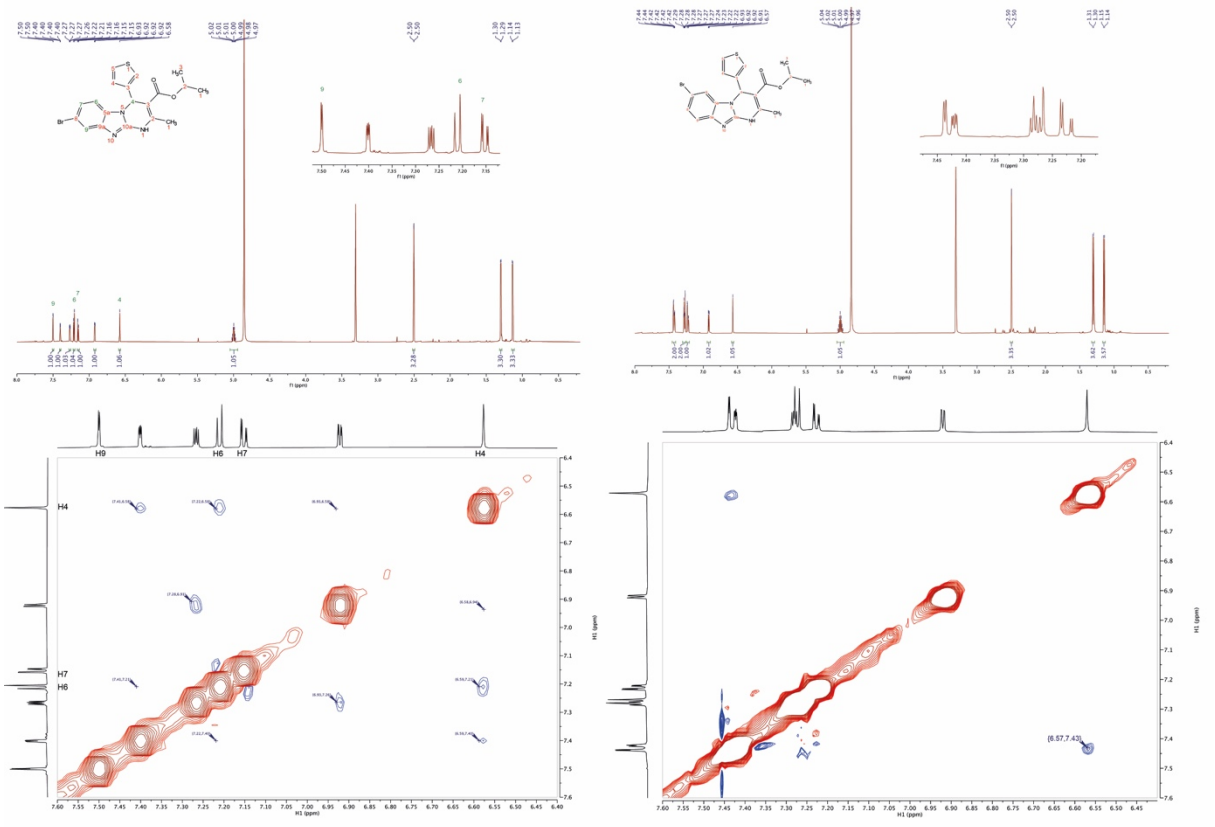

Figure 3.7. ^{1}H NMR (top) and 2D-NOESY (down) of **72** (left) and **48** (right)

3.1.3 Biological Evaluation

The adenosinergic profile (affinity and selectivity) of the 80 novel halogenated alkyl 1,4-dihydro-benzo[4,5]imidazo[1,2-*a*]pyrimidine-3-carboxy-lates was evaluated *in vitro* using radioligand binding assays at the four human AR subtypes.[87,142–144] Table 3.2 to Table 3.6 contain the binding data obtained while, to facilitate the comparative assessment, Table 3.1 shows the binding data for the tricyclic model series.[87] All ligands reported in Table 3.1 to Table 3.5 were obtained and tested as racemic mixtures. The whole set was evaluated *in silico* with a combination of RDKit[166] PAINS filter and InstantJChem from Chemaxon (https://www.chemaxon.com), to rule out the possibility that these ligands could be promiscuous pan-assay interference compounds (PAINS) and to assess their bioavailability, respectively. Human ARs were expressed in transfected cell lines [e.g., Chinese hamster ovary (CHO) cells (A_1AR), human epithelial carcinoma (HeLa) cells (A_{2A}AR and A_3AR) and human embryonic kidney (HEK-293) cells (A_{2B}AR)]. [^{3}H]DPCPX for A_1AR and A_{2B}AR, [^{3}H]NECA for A_3AR, and [^{3}H]ZM241385 for A_{2A}AR were employed as radioligands. The binding data is presented as K_i ± SEM (nM, n = 3) obtained by fitting the data by non-linear regression using

Prism 5.0 software (GraphPad, San Diego, CA), or as specific binding inhibition percentage at 1 μM (n = 2, average) for those compounds that did not completely displace the radioligand due to either little affinity or poor solubility. The binding affinity of reference AR ligands (**ISAM-140**, **DPCPX**, **NECA** and **ZM241385**) was assessed using our experimental protocols and reported in tables for comparison. The stereoisomers of selected compounds were obtained by chiral resolution and tested at the four human AR subtypes in their enantiopure forms (Table 3.6). This data was employed to complement the SAR study and to evaluate the importance of the configuration of the stereogenic center on the affinity.

Table 3.1. Structure and adenosine receptor affinity data of Alkyl 1,4-dihydrobenzo [4,5]imidazo[1,2-*a*]pyrimidine-3-carboxylates (Tricyclic Model Series).[87,144]

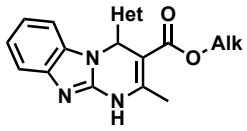

Compound	Het	Alk	K_i (nM) or % at 1 μM			
			hA_1[a)]	hA_{2A}[b)]	hA_{2B}[c)]	hA_3[d)]
IIIa (ISAM-134)	2-furyl	Et	5%	14%	12.0 ± 0.7	1%
IIIb (ISAM-140)	2-furyl	*i*-Pr	20%	28%	3.49 ± 0.2	2%
IIIc (ISAM-141)	3-furyl	Et	7%	11%	20.6 ± 1.1	1%
IIId (ISAM-142)	3-furyl	*i*-Pr	12%	23%	11.4 ± 0.5	2%
IIIe	2-thienyl	Et	8%	16%	484 ± 3	1%
IIIf	2-thienyl	*i*-Pr	1%	17%	371 ± 5	3%
IIIg	3-thienyl	Et	3%	10%	29.7 ± 1.2	2%
IIIh	3-thienyl	*i*-Pr	11%	3%	29.34± 1.1	21%
IIIi (ISAM-C032)	4-oxazolyl	Et	5%	11%	8.10 ± 0.5	7%
IIIj	4-oxazolyl	*i*-Pr	7%	19%	43.4 ± 1.3	16%
ISAM-140	-	-	20%	25%	3.49 ± 0.2	20%
DPCPX	-	-	2.20 ± 0.2	157 ± 3	73.2 ± 1.4	1722 ± 11
ZM241385	-	-	683 ± 4	1.9 ± 0.1	65.7 ± 1.1	863 ± 4
NECA	-	-	14.0 ± 1	20.0 ± 3	2400 ± 35	6.20 ± 0.9

[a)] Displacement of specific [^{3}H]DPCPX binding in human CHO cells expressed as K_i in nM (n = 3) or percentage displacement of specific binding at a concentration of 1 μM (n = 2). [b)] Displacement of specific [^{3}H]4-(2-[7-amino-2-(2-furyl)[1,2,4]triazolo[2,3-*a*][1,3,5]triazin-5-ylamino]ethyl)phenol binding in human HeLa cells expressed as K_i in nM (n = 3) or percentage displacement of specific binding at a concentration of 1 μM (n = 2). [c)] Displacement of specific [^{3}H]DPCPX binding in human HEK-293 cells expressed as K_i in nM (n = 3) or percentage displacement of specific binding at a concentration of 1 μM (n = 2). [d)] Displacement of specific [^{3}H]NECA binding in human HeLa cells expressed as K_i in nM (n = 3) or percentage displacement of specific binding at a concentration of 1 μM (n = 2).

Table 3.2. Structure and adenosine receptor affinity data of Series **I**: Alkyl 7,8-dihalo-1,4-dihydrobenzo[4,5]imidazo[1,2-*a*]pyrimidine-3-carboxylates (Cmpds **1-24**).

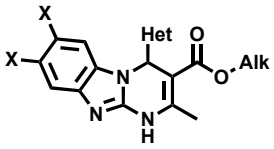

				K_i (nM) or % at 1 μM			
Compound	**Het**	**Alk**	**X**	**hA_1[a)]**	**hA_{2A}[b)]**	**hA_{2B}[c)]**	**hA_3[d)]**
1	2-furyl	Et	F	1%	2%	44.1 ± 1.7	2%
2	2-furyl	*i*-Pr	F	13%	22%	11.9 ± 1.1	14%
3	3-furyl	Et	F	22%	36%	28.2 ± 0.8	17%
4	3-furyl	*i*-Pr	F	17%	16%	52.9 ± 1.5	20%
5	2-thienyl	Et	F	2%	3%	25%	5%
6	2-thienyl	*i*-Pr	F	1%	1%	1%	10%
7	3-thienyl	Et	F	1%	1%	519 ± 7	5%
8	3-thienyl	*i*-Pr	F	1%	3%	43%	4%
9	2-furyl	Et	Cl	2%	5%	9%	1%
10	2-furyl	*i*-Pr	Cl	43%	12%	117 ± 5	7%
11	3-furyl	Et	Cl	33%	34%	54.7 ± 3.2	6%
12	3-furyl	*i*-Pr	Cl	4%	31%	36%	8%
13	2-thienyl	Et	Cl	2%	1%	9%	11%
14	2-thienyl	*i*-Pr	Cl	1%	4%	1%	9%
15	3-thienyl	Et	Cl	5%	1%	9%	1%
16	3-thienyl	*i*-Pr	Cl	2%	1%	359 ± 4	6%
17	2-furyl	Et	Br	1%	17%	37%	2%
18	2-furyl	*i*-Pr	Br	11%	28%	62.6 ± 1.9	21%
19	3-furyl	Et	Br	2%	2%	7%	10%
20	3-furyl	*i*-Pr	Br	1%	1%	32%	9%
21	2-thienyl	Et	Br	2%	7%	12%	5%
22	2-thienyl	*i*-Pr	Br	1%	1%	9%	3%
23	3-thienyl	Et	Br	2%	7%	47%	4%
24	3-thienyl	*i*-Pr	Br	4%	1%	9%	8%
ISAM-140	2-furyl	*i*-Pr	H	20%	25%	3.49 ± 0.2	20%
DPCPX	-	-	-	2.20 ± 0.2	157 ± 3	73.2 ± 1.4	1722 ± 11
ZM241385	-	-	-	683 ± 4	1.9 ± 0.1	65.7 ± 1.1	863 ± 4
NECA	-	-	-	14.0 ± 1	20.0 ± 3	2400 ± 35	6.20 ± 0.9

[a)]Displacement of specific [^{3}H]DPCPX binding in human CHO cells expressed as K_i in nM (n = 3) or percentage displacement of specific binding at a concentration of 1 μM (n = 2). [b)] Displacement of specific [^{3}H]4-(2-[7-amino-2-(2-furyl)[1,2,4]triazolo[2,3-*a*][1,3,5]triazin-5-ylamino]ethyl)phenol binding in human HeLa cells expressed as K_i in nM (n = 3) or percentage displacement of specific binding at a concentration of 1 μM (n = 2). [c)] Displacement of specific [^{3}H]DPCPX binding in human HEK-293 cells expressed as K_i in nM (n = 3) or percentage displacement of specific binding at a concentration of 1 μM (n = 2). [d)] Displacement of specific [^{3}H]NECA binding in human HeLa cells expressed as K_i in nM (n = 3) or percentage displacement of specific binding at a concentration of 1 μM (n = 2).

Table 3.3. Structure and adenosine receptor affinity data of Series **II**: Alkyl 7-halo-1,4-dihydrobenzo[4,5]imidazo[1,2-*a*]pyrimidine-3-carboxylates (Cmpds **25-48**).

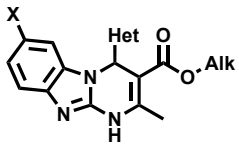

Compound	Het	Alk	X	K_i (nM) or % at 1 μM			
				hA_1[a)]	hA_{2A}[b)]	hA_{2B}[c)]	hA_3[d)]
25	2-furyl	Et	F	16%	2%	67.5 ± 3.1	10%
26	2-furyl	*i*-Pr	F	32%	3%	12.2 ± 1.2	5%
27	3-furyl	Et	F	26%	21%	25.0 ± 1.5	5%
28	3-furyl	*i*-Pr	F	25%	11%	136 ± 7	6%
29	2-thienyl	Et	F	25%	1%	37%	11%
30	2-thienyl	*i*-Pr	F	11%	2%	23%	6%
31	3-thienyl	Et	F	7%	1%	1031 ± 95	3%
32	3-thienyl	*i*-Pr	F	1%	1%	764 ± 11	1%
33	2-furyl	Et	Cl	26%	2%	18%	4%
34	2-furyl	*i*-Pr	Cl	667 ± 12	17%	44.3 ± 1.4	5%
35	3-furyl	Et	Cl	22%	30%	47.3 ± 1.9	3%
36	3-furyl	*i*-Pr	Cl	6%	4%	50%	3%
37	2-thienyl	Et	Cl	2%	3%	1%	1%
38	2-thienyl	*i*-Pr	Cl	1%	3%	7%	1%
39	3-thienyl	Et	Cl	4%	2%	50%	3%
40	3-thienyl	*i*-Pr	Cl	7%	9%	48%	3%
41	2-furyl	Et	Br	22%	21%	48%	5%
42	2-furyl	*i*-Pr	Br	46%	1%	273 ± 4	6%
43	3-furyl	Et	Br	10%	1%	318 ± 6	19%
44	3-furyl	*i*-Pr	Br	11%	3%	26%	12%
45	2-thienyl	Et	Br	1%	5%	1%	4%
46	2-thienyl	*i*-Pr	Br	1%	6%	11%	8%
47	3-thienyl	Et	Br	4%	3%	43%	3%
48	3-thienyl	*i*-Pr	Br	1%	1%	10%	1%
ISAM-140	2-furyl	*i*-Pr	H	20%	25%	3.49 ± 0.2	20%
DPCPX	-	-	-	2.20 ± 0.2	157 ± 3	73.2 ± 1.4	1722 ± 11
ZM241385	-	-	-	683 ± 4	1.9 ± 0.1	65.7 ± 1.1	863 ± 4
NECA	-	-	-	14.0 ± 1	20.0 ± 3	2400 ± 35	6.20 ± 0.9

[a)]Displacement of specific [^{3}H]DPCPX binding in human CHO cells expressed as K_i in nM (n = 3) or percentage displacement of specific binding at a concentration of 1 μM (n = 2). [b)] Displacement of specific [^{3}H]4-(2-[7-amino-2-(2-furyl)[1,2,4]triazolo[2,3-*a*][1,3,5]triazin-5-ylamino]ethyl)phenol binding in human HeLa cells expressed as K_i in nM (n = 3) or percentage displacement of specific binding at a concentration of 1 μM (n = 2). [c)] Displacement of specific [^{3}H]DPCPX binding in human HEK-293 cells expressed as K_i in nM (n = 3) or percentage displacement of specific binding at a concentration of 1 μM (n = 2). [d)] Displacement of specific [^{3}H]NECA binding in human HeLa cells expressed as K_i in nM (n = 3) or percentage displacement of specific binding at a concentration of 1 μM (n = 2).

Table 3.4. Structure and adenosine receptor affinity data of Series **III**: Alkyl 8-halo-1,4-dihydrobenzo[4,5]imidazo[1,2-*a*]pyrimidine-3-carboxylates (Cmpds **49-72**).

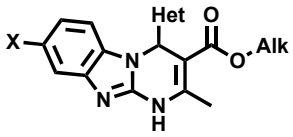

				K_i (nM) or % at 1 µM			
Compound	**Het**	**Alk**	**X**	**hA$_1$**[a)]	**hA$_{2A}$**[b)]	**hA$_{2B}$**[c)]	**hA$_3$**[d)]
49	2-furyl	Et	F	10%	29%	6.60 ± 1.0	2%
50	2-furyl	*i*-Pr	F	11%	2%	3.05 ± 0.7	3%
51	3-furyl	Et	F	29%	21%	13.7 ± 0.9	2%
52	3-furyl	*i*-Pr	F	14%	31%	8.60 ± 0.5	4%
53	2-thienyl	Et	F	1%	3%	724 ± 8	3%
54	2-thienyl	*i*-Pr	F	2%	1%	668 ± 6	7%
55	3-thienyl	Et	F	1%	1%	187 ± 2	3%
56	3-thienyl	*i*-Pr	F	2%	1%	75.5 ± 3.2	5%
57	2-furyl	Et	Cl	23%	10%	8.42 ± 1.4	4%
58	2-furyl	*i*-Pr	Cl	35%	24%	5.03 ± 0.3	2%
59	3-furyl	Et	Cl	31%	43%	7.21 ± 0.4	4%
60	3-furyl	*i*-Pr	Cl	27%	176 ± 4	6.10 ± 0.7	1%
61	2-thienyl	Et	Cl	3%	2%	41%	1%
62	2-thienyl	*i*-Pr	Cl	2%	2%	837 ± 11	1%
63	3-thienyl	Et	Cl	2%	7%	911 ± 14	8%
64	3-thienyl	*i*-Pr	Cl	7%	7%	165 ± 9	4%
65	2-furyl	Et	Br	18%	29%	26.9 ± 0.8	33%
66	2-furyl	*i*-Pr	Br	25%	2%	5.23 ± 0.4	10%
67	3-furyl	Et	Br	1%	37%	3.32 ± 0.4	25%
68	3-furyl	*i*-Pr	Br	2%	509 ± 6	8.20 ± 1.1	2%
69	2-thienyl	Et	Br	6%	3%	55%	6%
70	2-thienyl	*i*-Pr	Br	1%	1%	115 ± 3	1%
71	3-thienyl	Et	Br	1%	9%	537 ± 8	1%
72	3-thienyl	*i*-Pr	Br	2%	1%	61.1 ± 1.8	4%
ISAM-140	2-furyl	*i*-Pr	H	20%	25%	3.49 ± 0.2	20%
DPCPX	-	-	-	2.20 ± 0.2	157 ± 3	73.2 ± 1.4	1722 ± 11
ZM241385	-	-	-	683 ± 4	1.9 ± 0.1	65.7 ± 1.1	863 ± 4
NECA	-	-	-	14.0 ± 1	20.0 ± 3	2400 ± 35	6.20 ± 0.9

[a)]Displacement of specific [^{3}H]DPCPX binding in human CHO cells expressed as K_i in nM (n = 3) or percentage displacement of specific binding at a concentration of 1 μM (n = 2). [b)] Displacement of specific [^{3}H]4-(2-[7-amino-2-(2-furyl)[1,2,4]triazolo[2,3-*a*][1,3,5]triazin-5-ylamino]ethyl)phenol binding in human HeLa cells expressed as K_i in nM (n = 3) or percentage displacement of specific binding at a concentration of 1 μM (n = 2). [c)] Displacement of specific [^{3}H]DPCPX binding in human HEK-293 cells expressed as K_i in nM (n = 3) or percentage displacement of specific binding at a concentration of 1 μM (n = 2). [d)] Displacement of specific [^{3}H]NECA binding in human HeLa cells expressed as K_i in nM (n = 3) or percentage displacement of specific binding at a concentration of 1 μM (n = 2).

Table 3.5. Structure and adenosine receptor affinity data of Series **IV**: Alkyl 7/8-halo 4-(oxazol-4-yl)-1,4-dihydrobenzo[4,5]imidazo[1,2-*a*]pyrimidine-3-carboxylates (Cmpds **73-80**).

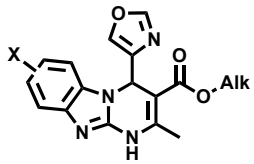

			K_i (nM) or % at 1 μM			
Compound	**Alk**	**X**	**hA_1[a)]**	**hA_{2A}[b)]**	**hA_{2B}[c)]**	**hA_3[d)]**
73	Et	7-F	43%	4%	44.7 ± 1.4	26%
74	*i*-Pr	7-F	34%	19%	7.60 ± 0.6	22%
75	Et	7-Cl	227 nM	14%	25.6 ± 1.2	11%
76	*i*-Pr	7-Cl	27%	1%	102 ± 7	20%
77	Et	8-F	25%	16%	14.7 ± 1.1	16%
78	*i*-Pr	8-F	29%	20%	6.10 ± 0.3	20%
79	Et	8-Cl	30%	13%	8.60 ± 0.4	15%
80	*i*-Pr	8-Cl	23%	35%	6.40 ± 0.7	23%
ISAM-140	-	-	20%	25%	3.49 ± 0.2	20%
DPCPX	-	-	2.20 ± 0.2	157 ± 3	73.2 ± 1.4	1722 ± 11
ZM241385	-	-	683 ± 4	1.9 ± 0.1	65.7 ± 1.1	863 ± 4
NECA	-	-	14.0 ± 1	20.0 ± 3	2400 ± 35	6.20 ± 0.9

[a)]Displacement of specific [^{3}H]DPCPX binding in human CHO cells expressed as K_i in nM (n = 3) or percentage displacement of specific binding at a concentration of 1 μM (n = 2). [b)] Displacement of specific [^{3}H]4-(2-[7-amino-2-(2-furyl)[1,2,4]triazolo[2,3-*a*][1,3,5]triazin-5-ylamino]ethyl)phenol binding in human HeLa cells expressed as K_i in nM (n = 3) or percentage displacement of specific binding at a concentration of 1 μM (n = 2). [c)] Displacement of specific [^{3}H]DPCPX binding in human HEK-293 cells expressed as K_i in nM (n = 3) or percentage displacement of specific binding at a concentration of 1 μM (n = 2). [d)] Displacement of specific [^{3}H]NECA binding in human HeLa cells expressed as K_i in nM (n = 3) or percentage displacement of specific binding at a concentration of 1 μM (n = 2).

Table 3.6. Structure and adenosine receptor affinity data of Racemic and Enantiomers of Selected Ligands.

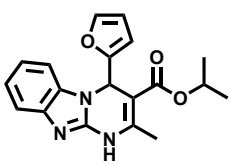

(±)-ISAM-140

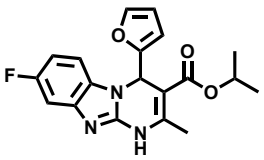

(±)-50

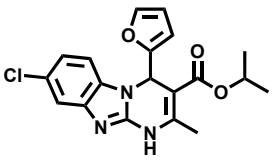

(±)-58

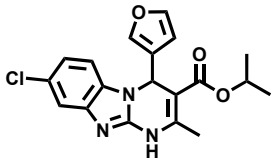

(±)-60

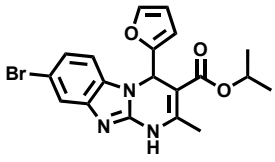

(±)-66

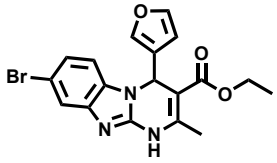

(±)-67

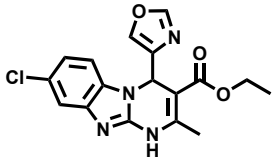

(±)-79

				K_i (nM) or % at 1 μM			
Compound	**Het**	**Alk**	**X**	**hA$_1$**[a)]	**hA$_{2A}$**[b)]	**hA$_{2B}$**[c)]	**hA$_3$**[d)]
(±)-ISAM-140	2-furyl	*i*-Pr	H	20%	28%	3.49 ± 0.2	2%
(*R*)-ISAM-140	2-furyl	*i*-Pr	H	14%	7%	17%	3%
(*S*)-ISAM-140	2-furyl	*i*-Pr	H	2%	12%	0.89 ± 0.2	4%
(±)-50	2-furyl	*i*-Pr	F	21%	2%	3.05 ± 0.7	3%
(*R*)-50	2-furyl	*i*-Pr	F	15%	5%	41%	19%
(*S*)-50	2-furyl	*i*-Pr	F	26%	11%	0.94 ± 0.1	12%
(±)-58	2-furyl	*i*-Pr	Cl	35%	24%	5.03 ± 0.3	2%
(*R*)-58	2-furyl	*i*-Pr	Cl	7%	37%	51%	5%
(*S*)-58	2-furyl	*i*-Pr	Cl	48%	19%	2.04 ± 0.2	6%
(±)-60	3-furyl	*i*-Pr	Cl	27%	176 ± 4	6.10 ± 0.7	1%
(*S*)-60	3-furyl	*i*-Pr	Cl	24%	25%	53%	19%
(*R*)-60	3-furyl	*i*-Pr	Cl	37%	96.3 ± 6	2.6 ± 0.3	24%
(±)-66	2-furyl	*i*-Pr	Br	25%	2%	5.23 ± 0.4	10%
(*R*)-66	2-furyl	*i*-Pr	Br	12%	7%	35%	2%
(*S*)-66	2-furyl	*i*-Pr	Br	32%	14%	2.97 ± 0.4	6%
(±)-67	3-furyl	Et	Br	1%	37%	3.32 ± 0.4	25%
(*R*)-67	3-furyl	Et	Br	10%	12%	1.17 ± 0.1	14%
(*S*)-67	3-furyl	Et	Br	11%	16%	34%	10%
(±)-79	4-oxazolyl	Et	Cl	30%	13%	8.60 ± 0.4	15%
(*R*)-79	4-oxazolyl	Et	Cl	9%	32%	26%	15%
(*S*)-79	4-oxazolyl	Et	Cl	22%	17%	3.39 ± 0.2	6%
ISAM-140	2-furyl	*i*-Pr	H	20%	25%	3.49 ± 0.2	20%
DPCPX	-	-	-	2.20 ± 0.2	157 ± 3	73.2 ± 1.4	1722 ± 11
ZM241385	-	-	-	683 ± 4	1.9 ± 0.1	65.7 ± 1.1	863 ± 4
NECA	-	-	-	14.0 ± 1	20.0 ± 3	2400 ± 35	6.20 ±9

[a)] Displacement of specific [^{3}H]DPCPX binding in human CHO cells expressed as K_i in nM (n = 3) or percentage displacement of specific binding at a concentration of 1 μM (n = 2). [b)] Displacement of specific [^{3}H]4-(2-[7-amino-2-(2-furyl)[1,2,4]triazolo[2,3-*a*][1,3,5]triazin-5-ylamino]ethyl)phenol binding in human HeLa cells expressed as K_i in nM (n = 3) or percentage displacement of specific binding at a concentration of 1 μM (n = 2). [c)] Displacement of specific [^{3}H]DPCPX binding in human HEK-293 cells expressed as K_i in nM (n = 3) or percentage displacement of specific binding at a concentration of 1 μM (n = 2). [d)] Displacement of specific [^{3}H]NECA binding in human HeLa cells expressed as K_i in nM (n = 3) or percentage displacement of specific binding at a concentration of 1 μM (n = 2). Enantiomers were separated by preparative chiral HPLC (IE-3 Chiralpack) and configuration at the stereocenter established by circular dichroism.

3.1.4 Functional activity assays

Four representative ligands (**50**, **58**, **66** and **67**) were selected to gain insight into the functional effect of the obtained series. To assess their ability to block $A_{2B}AR$ agonist intrinsic activity, the effect on $A_{2B}AR$-mediated cAMP accumulation and cellular impedance was evaluated. To this end, we used HEK-293 cells permanently expressing the $A_{2B}AR^{SNAP}$ construct, which could be visualized upon staining the cells with a SNAP-fluorescent substrate. As shown in Figure 3.8A, $A_{2B}AR^{SNAP}$ nicely decorated the cell surface of $A_{2B}AR^{SNAP}$ cells, indicating that the receptor was readily expressed at the plasma membrane. Subsequently, we evaluated the effect of **50**, **58**, **66** and **67** in $A_{2B}AR$ signaling by monitoring cAMP accumulation in $A_{2B}AR^{SNAP}$ cells treated with NECA, a non-selective adenosine receptor agonist. NECA induced a concentration-dependent cAMP accumulation in $A_{2B}AR^{SNAP}$ cells with an EC_{50} of 257 ± 94 nM (Figure 3.8B). Subsequently, $A_{2B}AR^{SNAP}$ cells were evaluated with a fixed concentration of NECA (1 μM) in the absence or presence of increasing concentrations of **50**, **58**, **66** and **67** and the K_B value for each compound was calculated, namely 0.8 ± 0.2 nM, 0.6 ± 0.2 nM, 1.7 ± 0.6 nM, and 1.5 ± 0.5 nM, respectively (Figure 3.8C). Overall, **50**, **58**, **66** and **67** displayed low nanomolar potency while blocking $A_{2B}AR$-mediated cAMP accumulation in $A_{2B}AR^{SNAP}$ cells, thus indicating an antagonist intrinsic activity nature. Comparative K_B and K_i data for selected compounds is shown in Table 3.7. It should be noticed that two these selective $A_{2B}AR$ antagonists exhibit sub-nanomolar K_B data.

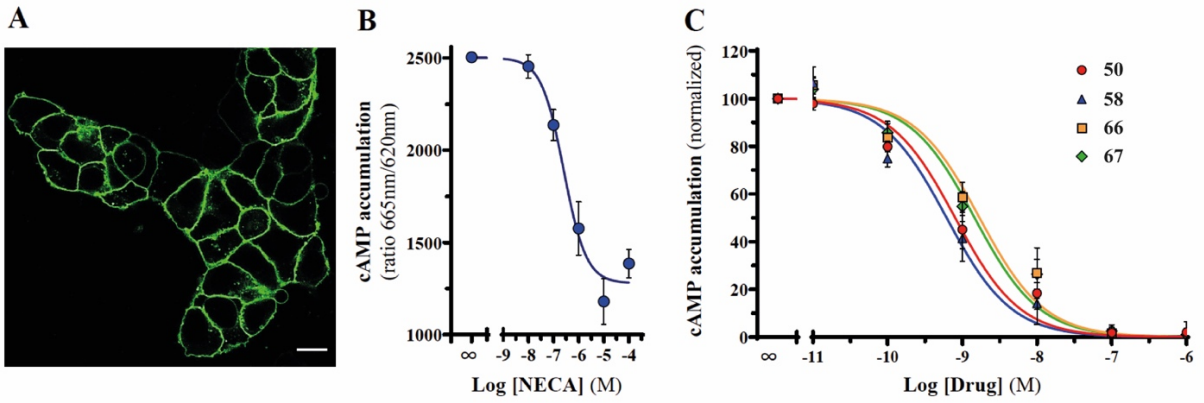

Figure 3.8. Blockade of $A_{2B}AR$-mediated cAMP accumulation. A) HEK-293 cells permanently expressing the $A_{2B}AR^{SNAP}$ construct were stained with the fluorescent SNAP-488 substrate and visualized using a confocal microscope.[167] Scale bar: 10 μM. B) Determination of NECA-mediated cAMP accumulation in $A_{2B}AR^{SNAP}$ cells. Cells were incubated in the absence or presence of increasing concentrations of NECA, and the cAMP accumulation determined as described in Experimental Section. The straight TR-FRET signal (ratio 665 nm/620 nm) of the assay is shown. **C)** cAMP accumulation in $A_{2B}AR^{SNAP}$ cells stimulated with NECA (1 μM) in the absence or presence of increasing concentrations of the **50**, **58**, **66** and **67**. Data are expressed as mean ± SEM (n=4).

Table 3.7. Functional data of the compounds **50**, **58**, **66** and **67**.

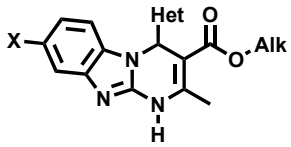

Compound	Het	Alk	X	K_i (hA_{2B})	K_B (hA_{2B})
(±)-50	2-furyl	*i*-Pr	F	3.05 ± 0.7	0.80 ± 0.2
(±)-58	2-furyl	*i*-Pr	Cl	5.03 ± 0.3	0.60 ± 0.2
(±)-66	2-furyl	*i*-Pr	Br	5.23 ± 0.4	1.70 ± 0.6
(±)-67	3-furyl	Et	Br	3.32 ± 0.4	1.50 ± 0.5

To further evaluate the ability of **50**, **58**, **66** and **67** to preclude A_{2B}AR function in living cells we took advantage of the cellular impedance label-free method, a widely accepted morphological and functional biosensor of cell status.[168] Accordingly, whole-cell NECA-mediated impedance responses of $A_{2B}AR^{SNAP}$ cells were monitored in real-time in the absence or presence of **50**, **58**, **66** and **67**. Indeed, NECA (1 μM) induced a significant increase in $A_{2B}AR^{SNAP}$ cells impedance recordings, thus reflecting changes in cell morphology upon agonist challenge (Figure 3.9A). Importantly, **50**, **58**, **66** and **67** partially blocked NECA-induced impedance increase in $A_{2B}AR^{SNAP}$ cells (Figure 3.9A). When calculating the area under the curve (AUC) for the different experimental conditions, we could observe that **50**, **58**, **66** and **67** significantly blocked NECA-induced changes in cellular impedance (Figure 3.9B). These results from an alternative cellular functional assay further confirmed that **50**, **58**, **66** and **67** were able to block A_{2B}AR agonist-mediated intrinsic activity.

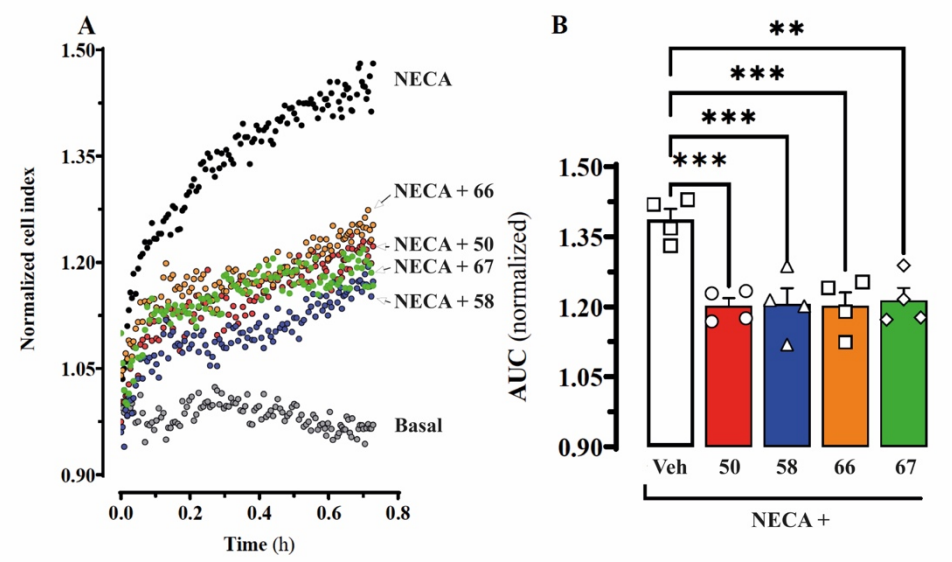

Figure 3.9. Blockade of A_{2B}AR-mediated whole cell label-free responses. A) Representative example of the impedance signal obtained over the time upon incubation with A_{2B}AR ligands. Cells were stimulated with vehicle or NECA (1 μM) in the absence or presence of **50**, **58**, **66** and **67** (1 μM), 18 h after seeding, and the impedance signal recorded in real-time during 45 min. B) The area under the curve (AUC) derived from the normalized cell index (NCI) shown in (A) was calculated for each condition. Data are expressed as mean ± SEM (n=4). *** $P < 0.001$ and ** $P < 0.01$, one-way ANOVA with a Dunnett's multiple comparison test when compared to vehicle (Veh).

Interestingly, the absolute **50**, **58**, **66** and **67** antagonist potencies in the cAMP accumulation assay were greater (~10-fold) than those determined in the radioligand binding assays, a fact that has been previously reported in HEK-293 cells stably overexpressing A_{2B}AR.[169] Indeed, this notion could be supported by the spare receptor theory defining that under some circumstances the potency of a named agonist in functional assays is proportional to the receptor density, thus producing a discontinuity between drug occupancy and cell response.[170] Our label-free experiments revealed a significant, but partial, blockade of NECA-induced impedance increase in $A_{2B}AR^{SNAP}$ cells. Indeed, HEK-293 cells express endogenous adenosine receptors as revealed by microarray analysis.[171] Thus, while the A_3AR was not detected, the remaining A_{2B}AR, A_{2A}AR and A_1AR were identified in HEK-293 cells.[171] Since NECA is a non-selective adenosine receptor agonist showing high affinity for A_{2A}AR and A_1AR (K_i values of 20 nM and 14 nM, respectively),[103] it can be speculated that the remaining impedance increase in NECA treated $A_{2B}AR^{SNAP}$ cells in the presence of **50**, **58**, **66** and **67** could be mediated by endogenous A_{2A} and A_1 ARs. These results might be interpreted as indirect evidence of selectivity for the A_{2B}AR for compounds **50**, **58**, **66** and **67**.

3.1.5 Structure-Activity Relationships and Molecular Modeling

In this section we examine the pharmacological data obtained for the newly synthesized series (Tables 3.2-6) and analyze the effect of halogenation in the structure-affinity (SAR) and structure-selectivity (SSR) relationships. All ligands were evaluated as racemic mixtures and comparative studies used as a reference the parent series (Table 3.1). The SAR here outlined is then further assessed by free energy perturbation (FEP) calculations in the context of a refined computational 3D model of the $hA_{2B}AR$.

The adenosinergic affinity profiles of the 80 alkyl 7/8-halo-4-heteroaryl-1,4-dihydro-benzo[4,5]imidazo[1,2-*a*]pyrimidine-3-carboxylates are presented in Tables 2–6. Up to 25 ligands combine attractive $A_{2B}AR$ affinity (K_i < 50 nM) and exquisite subtype selectivity (> 1000-fold), from which 14 ligands exhibit outstanding $A_{2B}AR$ affinity (K_i < 10 nM) [e.g., compounds **49**, **50**, **52**, **57**, **58**, **59**, **60**, **66, 67**, **68** (Table 3.4), **74**, **78**, **79** and **80** (Table 3.5)]. The available data reveal interesting and previously unexplored SAR trends, with derivatives bearing a halogen atom at position 8 of the heterotricyclic core collectively emerging as the most appealing $A_{2B}AR$ antagonists in these series (Series **III** and **IV**, Table 3.4 and Table 3.5). Compared to their congeners of the parent series (Table 1), ten of the ligands here identified present improved pharmacodynamic and pharmacokinetic profiles, with ligands **50**, **58**, **66** and **67** deserving particular attention, as they exhibit one digit K_i values (3-5 nM) and excellent subtype selectivity, thus justifying the selection of these compounds for further intrinsic activity assays (see previous section).

Comparative analysis of the binding data obtained for the parent series (Table 3.1) and ligands of series **I** (Table 3.2) evidence that simultaneous introduction of halogens at positions 7 and 8 have deleterious impact on $A_{2B}AR$ affinity. Moreover, it can be observed that this reduction in affinity is halogen dependent, with better affinity profiles observed for some 7,8-difluoro derivatives (Table 3.2, Cmpds **1**–**4**), and the affinity decay being proportional to atomic radius of the halogen (Table 3.2 and Figure 3.10). Ligands bearing a thienyl ring at position 4 of the heterotricyclic scaffold are inactive with the only exception of the low affinity **7** and **16**. For the case of ligands containing a furyl group at Het, the $A_{2B}AR$ affinity seems to be highly dependent of the halogens present (Table 3.2). Thus, all ligands containing a furyl group of the 7,8-difluorinated scaffold (Cmpds **1**-**4**) elicit potent $A_{2B}AR$ affinity (K_i = 11.9–52.9 nM) irrespective of the substitution pattern at the furan ring (2-furyl or 3-furyl) or the alkoxy residue in the ester moiety (Alk). Although potent, the difluorinated derivatives **1**-**4** show lower affinity

(3-fold) than their parent series analogues (Table 3.1). Similarly, in the subsets bearing chlorine atoms (Table 3.2, Cmpds **9-16**) only the derivatives incorporating an optimal substituent at Het and Alk (**10** and **11**) show moderate affinity. Following this trend, the only derivative eliciting A_{2B}AR affinity in the 7,8-dibromo subset is **18** (K_i = 62.6 nM), contains at Het and Alk the same substitution pattern of the lead compound **ISAM-140**, although with a 20-fold decay in affinity.

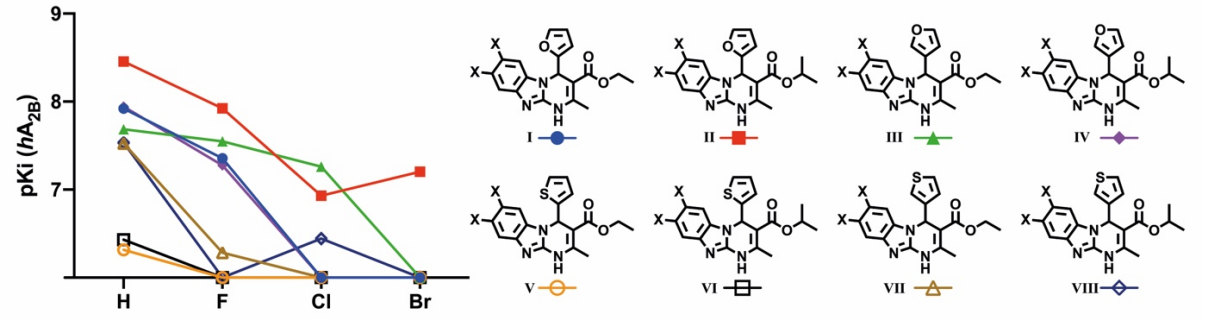

Figure 3.10. pK_i (*h*A_{2B}AR) versus halogen in 7,8-halogenated derivatives (Series **I**). Filled and unfilled shapes represent, respectively, ligands containing furyl and thienyl group at position 4.

The adenosinergic profile obtained for series **II** is presented in Table 3.3. Here, introduction of a halogen at position 7 reproduce some of the SAR trends detected in series **I** (Table 3.2). While some attractive ligands can be identified (e.g., **26** and **27**, K_i = 12.2 and 25.0 nM respectively), a comparison with the parent series (Table 3.1) reveal that halogenation at position 7 is deleterious. As for series **I**, the effect of halogenation relay on the nature of the halogen, being fluor the best tolerated (Table 3.3, Cmpds **25**-**28**). Similarly, most derivatives bearing thienyl groups remain inactive. For series bearing choro and bromo atoms at position 7, only optimal pair combinations at Het and Alk (e.g., 2-furyl and isopropyl, 3-furyl and ethyl respectively) produced ligands with moderate (K_i ~ 45 nM) affinity (Table 3, Cmpds **34**, **35**, **42** and **43**). This trend is also observed for 7-fluoro derivatives (Table 3, Cmpds **25**-**28**), while in this subset all furyl-containing derivatives exhibited attractive A_{2B}AR affinity (K_i = 12.2 – 136 nM).

Evaluation of series **III** (Table 3.4) enabled the identification of the most potent (K_i < 10 nM) A_{2B}AR antagonists in this study. It also allowed to envision the significant effect of halogen substitution at position 8 and its rationalization from a molecular modeling perspective. In contrast to previous series, halogenation at position 8 systematically improve the A_{2B}AR

affinity irrespective of the nature of the halogen atom (Table 3.4 and Figure 3.11). Indeed, most 8-halo derivatives have measurable $A_{2B}AR$ affinity values (Table 3.4). All 8-halogenated derivatives bearing a furan ring at position 4 exhibit excellent $A_{2B}AR$ affinity (K_i = 3.05–26.9 nM), indeed generally superior by 4-10-fold to their analogues in the parent series (Figure 3.11). A similar trend, but with attenuated affinity, is observed for thiophene-based analogues (K_i = 61.1–911 nM). It should also be noticed that for thienyl derivatives, the introduction of a halogen at position 8 does not improve $A_{2B}AR$ affinities as compared to the non-halogenated parent compounds (Table 3.1). A direct comparison of the $A_{2B}AR$ affinity profile (pK_i) of selected derivatives of different series is presented in Figure 3.11.

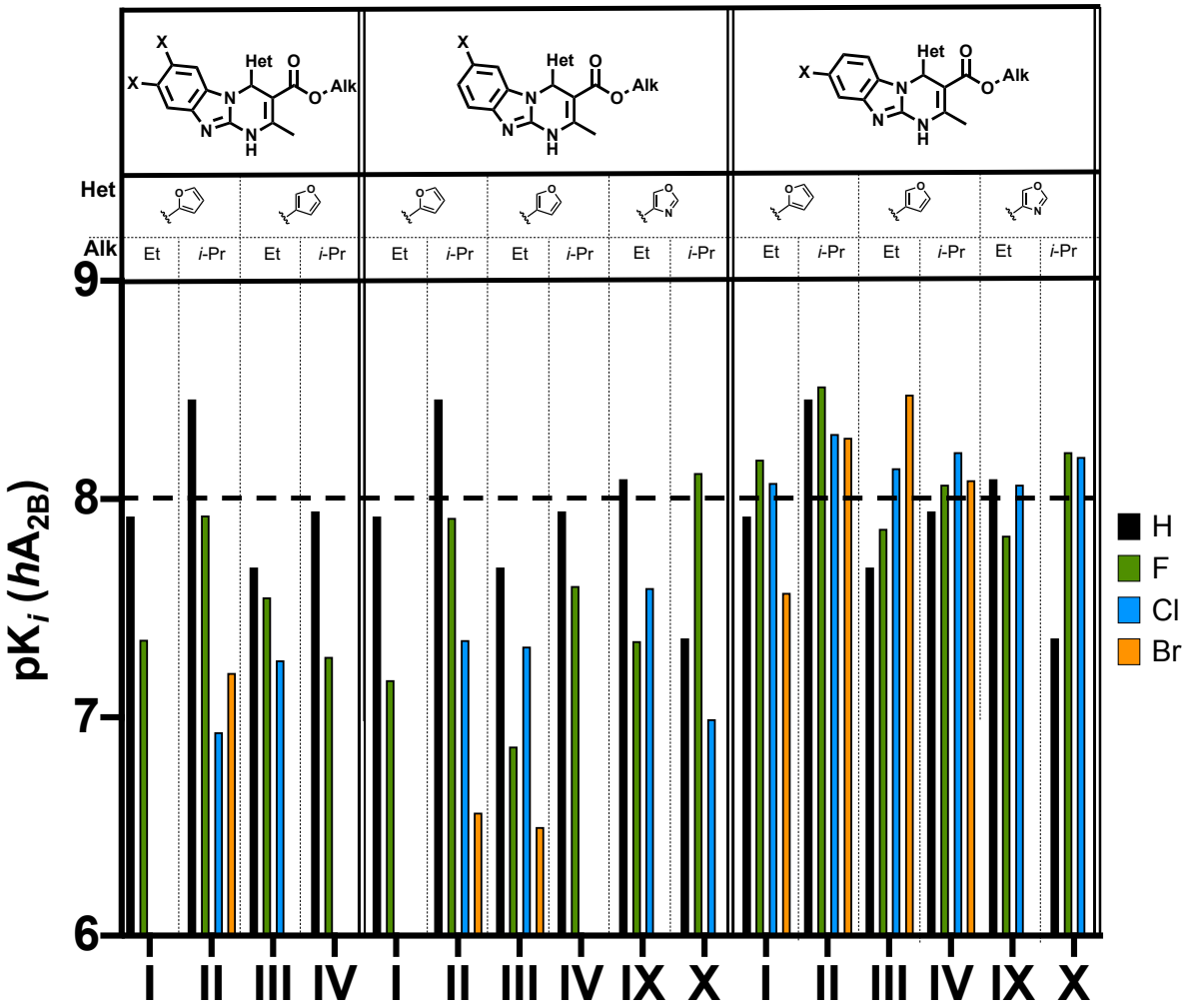

Figure 3.11. Interleaved bars chart showing $A_{2B}AR$ pK_i [-log(K_i)] for the halogenation of furyl and oxazolyl scaffolds (represented at x-axis as **I**-**IV** and **IX**-**X**). Black: non-halogenated, green: fluorinated, cyan: chlorinated, and orange: brominated compounds.

The pharmacological data obtained for the exploratory derivatives bearing a 4-oxazolyl residue at position 4 of the tricyclic core (Series **IV**, Table 3.5) introduced new SAR perspectives. Although in general this series reproduced the most prominent SAR trends discussed for the previous series, the effect of halogenation seems to be less marked if compared to their parent compounds (Table 3.1, Cmpds **IX** and **X**). Collectively, 8-halo derivatives in this series (Table 3.5, Cmpds **77**-**80**) exhibit excellent A_{2B}AR affinity (K_i 6.10–14.7 nM). A comparative analysis reveals that the affinity data in this series is lightly superior to the 7-halo analogues (Table 3.5, Cmpds **73**-**76**) or the parent compounds in the prototype series (Table 1, Cmpds **IX** and **X**). These data highlight the interest of the 4-oxazolyl moiety as a privileged non-furane core at A_{2B}AR, that in addition to a superior metabolic stability profile, can capture the two productive interactions predicted for 2-furyl and 3-furyl rings within the A_{2B}AR orthosteric binding site. This allows for better accommodation of the compounds at the A_{2B}AR (Figure 3.12), even allowing a successful fitting of the 7-halo derivatives (Table 3.5).

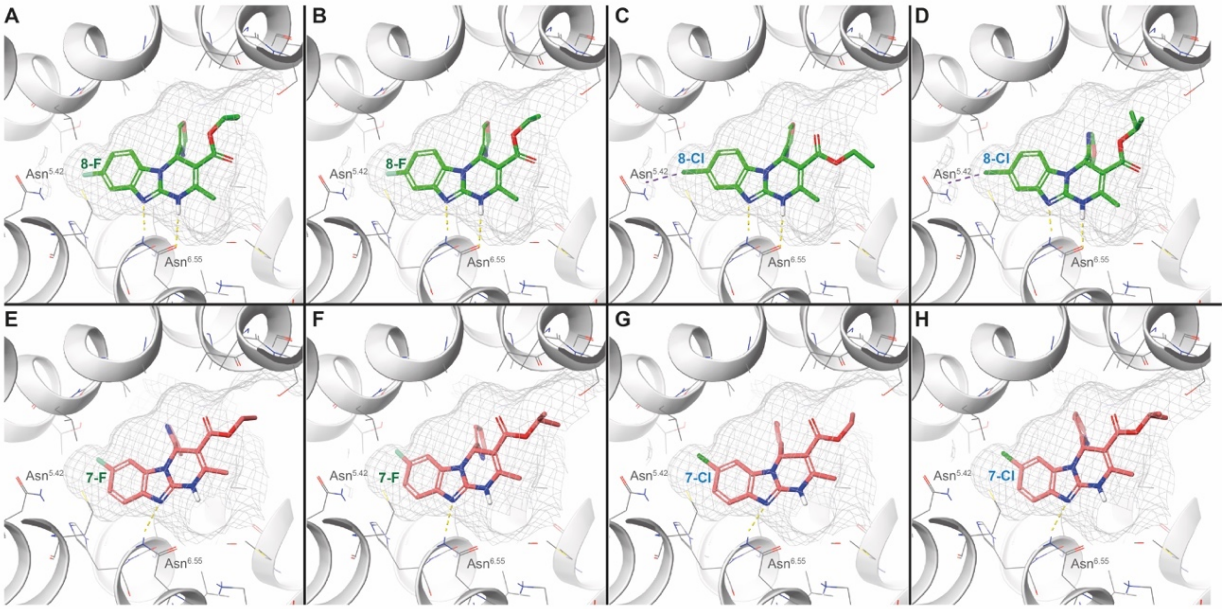

Figure 3.12. Docking poses for Series IV. A) **77**, B) **78**, C) **79**, D) **80**, E) **73**, F) **74**, G) **75** and H) **76**. Grey mesh represents A_{2B}AR binding site surface. Note the loss of a hydrogen bond with $Asn^{6.55}$ in 7-halo derivatives (E-H), and the formation of a halogen bond with $Asn^{5.42}$ on 8-chlorine compounds (C-D).

Due to their unique dual A_{2A}/A_{2B}AR profile, two ligands (Table 3.4, Cmpds **60** and **68**) caught our interest during the analysis of SAR trends within the series of 8-halo derivatives. Both ligands combine the typical high A_{2B}AR affinity of this subset (K_i = 6.10 and 8.20 nM respectively), with an incipient affinity by the A_{2A}AR (K_i = 176 and 509 nM respectively).

While sharing a common structural pattern (e.g., a 3-furyl ring at Het and isopropyl group in the alkoxy residue of the ester function at Alk), they differ in the halogen atom at position 8 (Cl vs. Br). Despite being equipotent at the A_{2B}AR, the important differences in A_{2A}AR affinity (3-fold) suggest that the chlorine atom is better tolerated for the binding at the A_{2A}AR. With further studies currently in progress to explore in depth the structural requirements for dual A_{2A}AR/A_{2B}AR antagonism, substitution at position 8 appears to be a key structural requirement for dual blockade of both receptors. It should be noticed a dual A_{2A}AR/A_{2B}AR profile like that showed by **60** is interesting in the context of cancer (immuno)therapy, with two compounds showing similar profiles in clinical trials.[172] Indeed, this dual profile allowed us to include compound **60** in a recent study with *ex vivo* assays to study the potential of the A_{2B}AR antagonism in the context of cancer immunotherapy (*results shown in Chapter IV*).

3.1.6 Enantiospecific binding to the A_{2B}AR

The four series of A_{2B}AR antagonists herein documented were initially obtained and tested as racemates. The stereocenter within the heterocyclic core is a signature element of our ligands,[141–144,165] which plays an important role for the recognition within the A_{2B}AR binding pocket, providing structural singularity respect to known planar A_{2B}AR ligands (e.g., Xanthines). Early molecular models and FEP calculations, supported by experimental data, predicted that only one enantiomer should bind to the orthosteric site of A_{2B}AR. To further elucidate the molecular basis underlying enantioselective recognition in these series and to expand the repertoire of stereoselective A_{2B}AR antagonists, we proceeded with enantiomeric separation, assignment, and biological evaluation (Table 3.6) of a representative subset of A_{2B}AR antagonists. A validated approach using chiral HPLC, circular dichroism (CD) spectroscopy (Figure 3.13) and X-ray crystallography (Figure 3.14),[141–144,165] was employed to separate and assign the configuration of six representative A_{2B}AR antagonists [(±)-**50**, (±)-**58**, (±)-**60**, (±)-**66**, (±)-**67** and (±)-**79**] and the prototype ligand of the parent series [(±)-**ISAM-140**]. Semipreparative HPLC separation of the selected racemic ligands on a chiral stationary phase (Figure 3.13 and Experimental Section) afforded each enantiomer with excellent stereochemical purity (e.e. > 97%). As documented for different Biginelli-based scaffolds,[173] the sign of the distinctive CD activity of the enamide group (around 300 nm) allow the unequivocal assignment of the absolute configuration of each enantiomer (Figure 3.13). At that wavelength, enantiomers showing negative Cotton effect (intense line) contain the pentagonal heterocycle (furan or oxazole) backward while the stereoisomers giving positive Cotton effect

(clear line) contain the heterocyclic core forward. As a complement of these studies, structural analysis of monocrystals of **(*S*)-67** and **(*R*)-67** and the prototype ligand enantiomers of the parent series [**(*S*)-ISAM-140** and **(*R*)-ISAM-140**] through X-ray crystallography (Figure 3.14A-B) provided additional experimental evidence corroborating the CD-assisted stereochemical configuration.

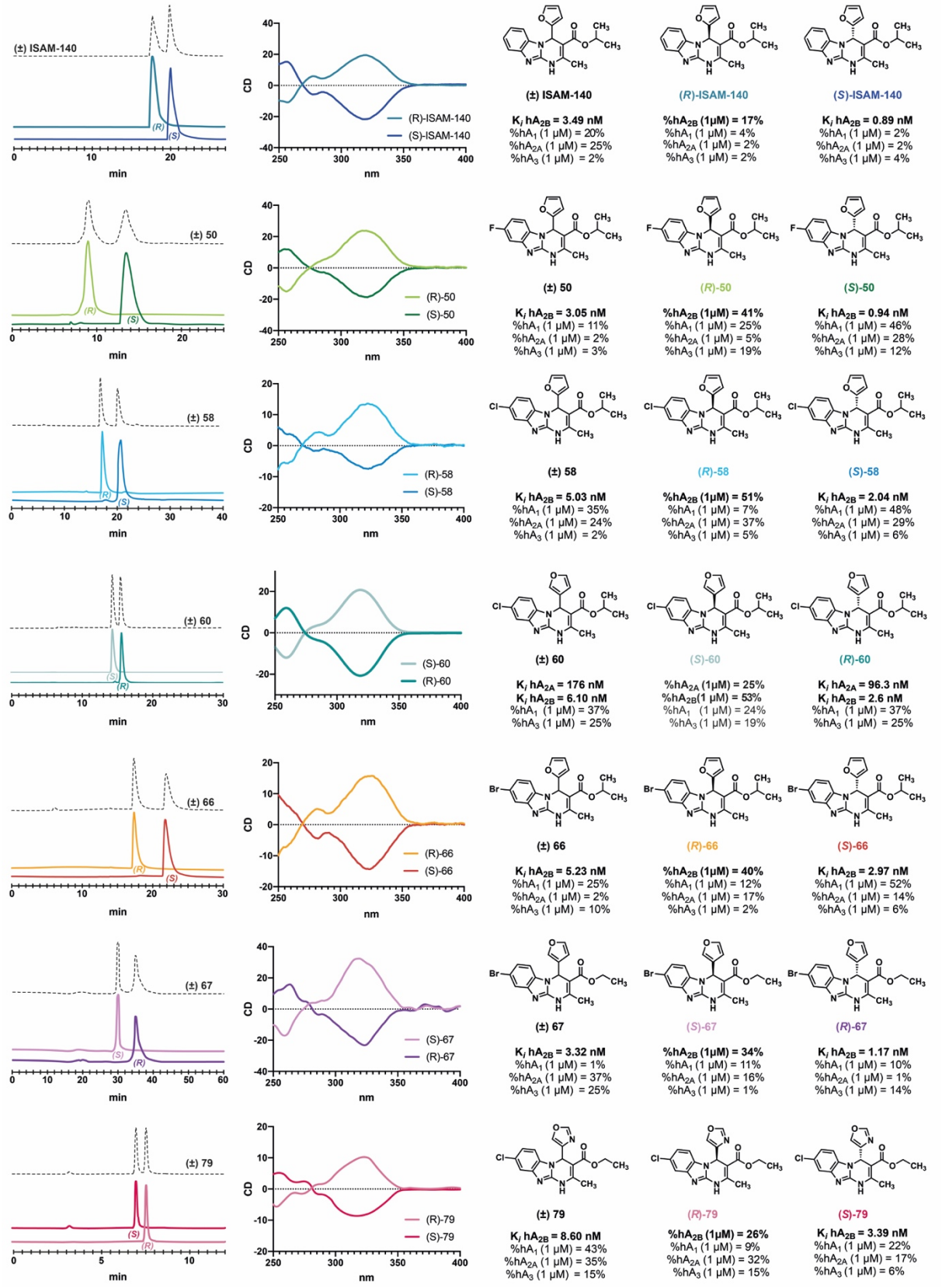

Figure 3.13. Chiral HPLC traces, circular dichroism spectra and binding data of selected racemic ligands (**ISAM-140**, **50**, **58**, **60**, **66**, **67** and **79**) and their enantiomers.

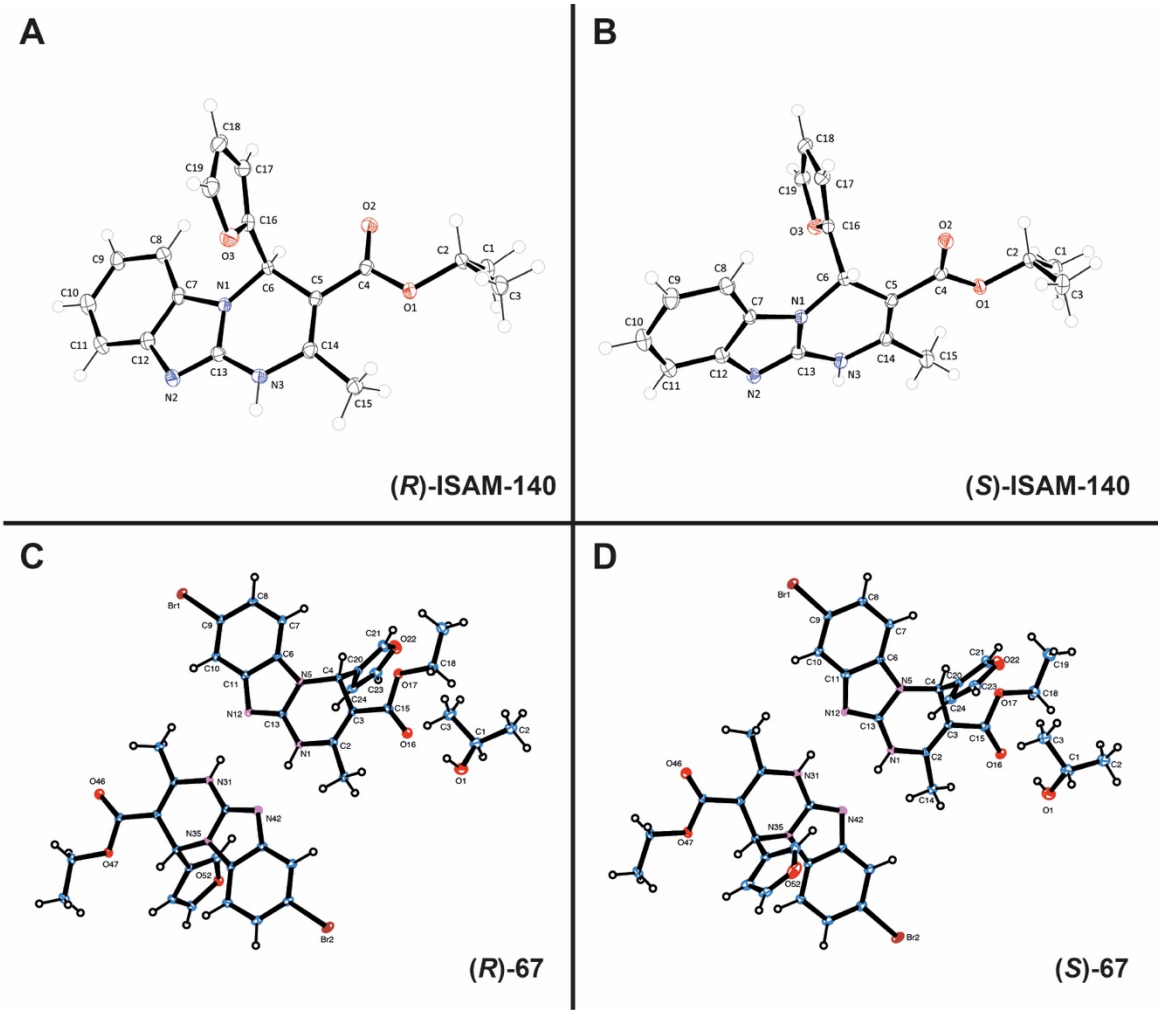

Figure 3.14. A) X-ray crystal structure of **(*R*)-ISAM-140** (CCDC: **1966312**) B) **(*S*)-ISAM-140** (CCDC: **1966450**) C) **(*R*)-67** (CCDC: **2048281**). D) **(*S*)-67** (CCDC: **2047365**).

The affinity profile of the obtained enantiomers at the four human ARs, together with the corresponding racemic ligands, is collected in Table 3.6. Inspection of the obtained data confirm that the observed A_{2B}AR affinity within the racemic ligands is exclusively due to one of the stereoisomers, in line with the A_{2B}AR enantiospecific recognition model documented for structurally analogous series.[141–144] In all cases, the eutomers (which contain the pentagonal core backward) are nearly two-fold more potent than their corresponding racemate, whereas the other stereoisomer is devoid in all cases of any affinity at the four ARs (Table 3.6 and Figure 3.13). Particularly noticeable are the two eutomers [**(*S*)-50** and **(*S*)-ISAM-140**] with sub-nanomolar A_{2B}AR affinities. The eutomer **(*R*)-60**, containing the pentagonal core backward (Figure 3.15A), emerges as the first example of a dual A_{2A}/A_{2B}AR ligand exhibiting

enantiospecific recognition at both receptors, since its enantiomer (which contain the pentagonal core forward, Figure 3.15B) is completely inactive. The enantioselective recognition reported here for **(*R*)-60** has inspired the design of new series of non-planar dual antagonists that will be reported in the following chapters of this thesis.

To provide a further structural rationale, we calculated the relative binding free energy difference between each pair of enantiomers for compounds **ISAM-140**, **50**, **58**, **60** and **79**. The corresponding FEP simulations were run taking as starting point the binding model proposed earlier for this scaffold,[141] illustrated in Figure 3.15. The binding mode of the eutomers (Figure 3.15A) has been largely explored with FEP simulations on previous series, allowing a rationalization of the observed SAR.[143,144] In the present computational analysis, we assumed an analogous binding orientation for the distomer (Figure 3.15B), although there could be other possibilities, which is difficult to assess given the inactive profile of these enantiomers. Nevertheless, the qualitative agreement with the experimental profile is remarkable, as the simulations indicate a clear binding preference for the eutomer in all five cases (Figure 3.16). These data confirm our previous computational models for enantiospecific recognition of structurally-related Biginelli-based scaffolds,[174] which was used to assess the growth of these scaffolds.

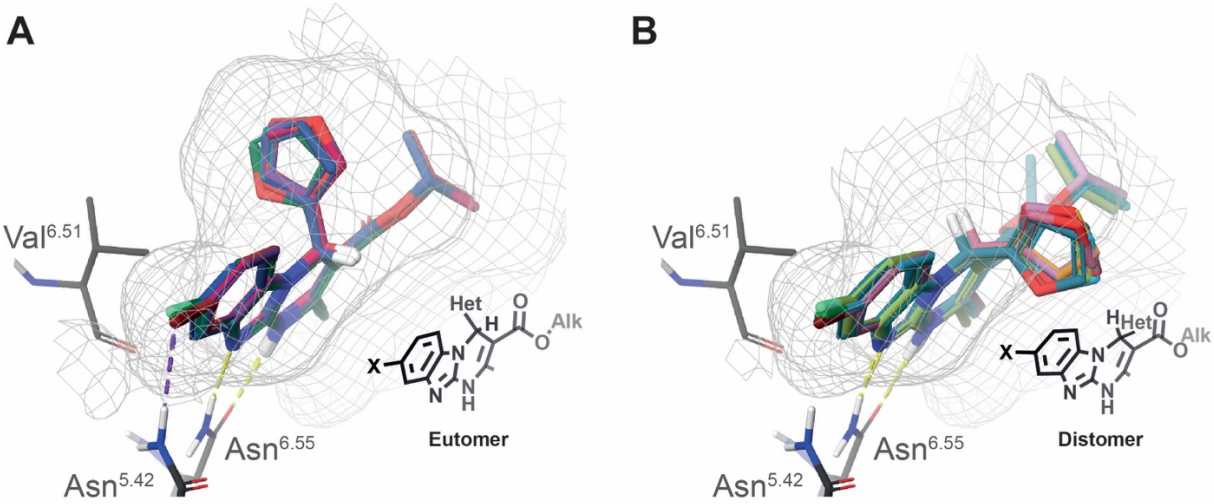

Figure 3.15. A) Docking superposition for eutomers (***S***)-**ISAM-140**, (***S***)-**50** (***S***)-**58**, (***R***)-**60**, (***S***)-**66**, (***R***)-**67,** and (***S***)-**79** (A_{2B}AR Homology Model from A_{2A}AR, PDB: 3EML). Note the formation of a halogen bridge with 8-chlorine and 8-bromine compounds ($Asn^{5.42}$). B) Docking superposition for distomers (***(R)***-**ISAM-140**, (***R***)-**50**, (***R***)-**58**, (***S***)-**60** (***R***)-**66**, (***S***)-**67,** and **(*R*)-79** (A_{2B}AR Homology Model from A_{2A}AR, PDB: 3EML). Grey mesh represents A_{2B}AR binding site surface.

3.1.7 FEP simulations on the eutomers

Using the stereospecific binding mode established in the previous stage, we setup a systematic scheme of FEP simulations aimed to provide structural understanding to the observed SAR. To this end, we selected all 56 compounds with measured experimental affinity for the *h*A_{2B}AR (K_i (< 1000 nM) and run a series of alchemical transformations to obtain relative binding free energies (RBFE), by FEP transformation of the substituents at positions 7 and 8, while retaining the same substituents on Alk and Het. Within each congeneric series (as defined in Table 1 for reference compounds), the compound pairs for the FEP simulations were defined by our mapping algorithm, and the absolute binding free energies (ABFE) were estimated following a cycle closure correction, taking the experimental affinity value of one compound as a reference (see Experimental Section). With this approach, we maintained simplicity within the alchemical transformations, ensuring a good convergence (average SEM = 0.44 kcal/mol). The pulled results obtained for all congeneric series are summarized on Figure 3.17. The correlation between calculated and experimental binding free energies is very good, according to the low value for the mean unassigned error (MUE = 1.08 kcal/mol). A closer look into the data revealed that most of this unassigned error is caused by the group of brominated compounds (red symbols, Figure 3.16B) which show a tendency to overprediction. The binding model proposed is thus reinforced by these calculations, which correctly reproduce the global SAR outlined in the previous section. Experimentally, we observed that 7-halogenated substitutions show halogen size-dependent A_{2B}AR affinity. The pattern observed for the 7,8-dihalogenated compounds seems to confirm this tendency, while 8-halogenated compounds show a halogen-size independent A_{2B}AR affinity (Figure 3.18). According to our binding model, the bulkier Cl and Br substituents on the last position can make a halogen-bond interaction with $Asn^{5.42}$, counterbalancing the excess of volume at position 8, something that is not possible when the halogen is at position 7, resulting in a decrease in affinity proportional to the volume of the buried halogen atom (Figure 3.12).

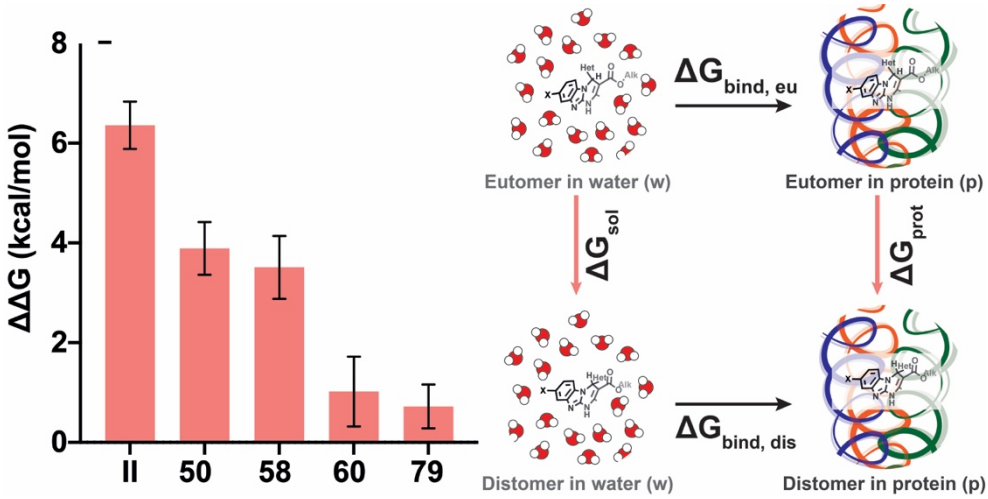

Figure 3.16. ΔΔG data for eutomer to distomer transition (positive ΔΔG). Data can be found in Table 5.3.

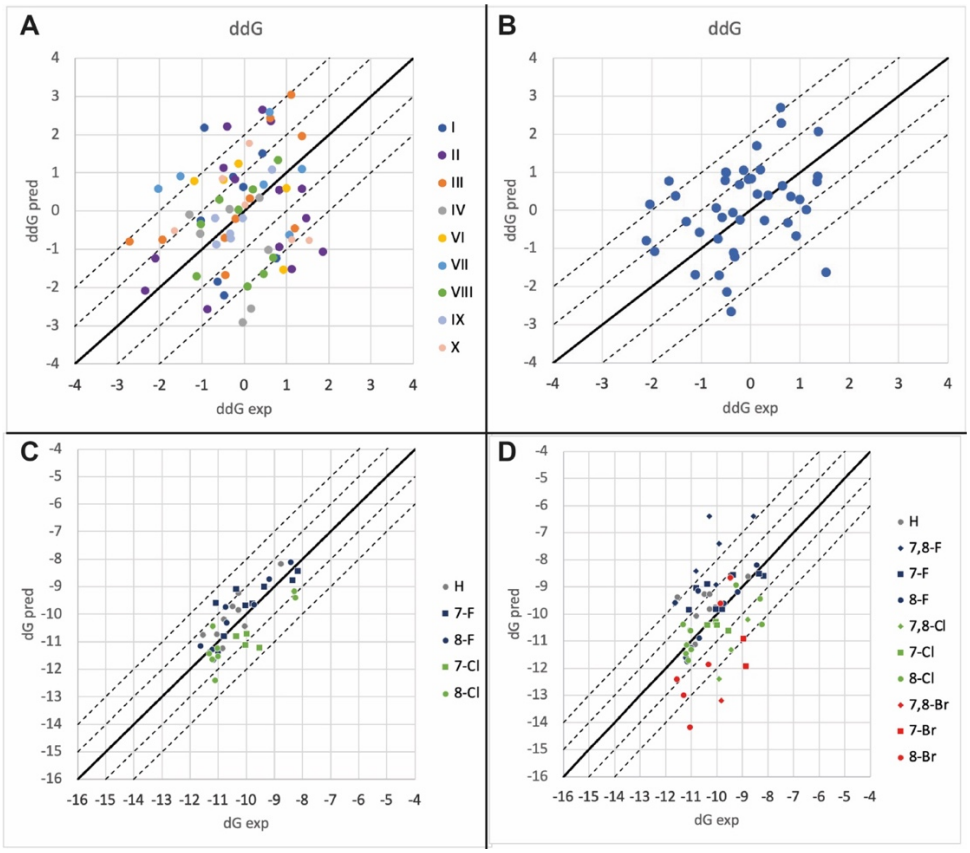

Figure 3.17. A), ΔΔG FEP correlation between all compounds showing K_i in pharmacology experimental assays, grouped by scaffold I-X. B), ΔΔG FEP correlation between all compounds showing K_i in pharmacology experimental assays, removing brominated and dihalogenated compounds. C), ΔG FEP correlation between compounds showing K_i in pharmacology experimental assays, removing brominated and dihalogenated compounds, grouped by position and halogen. D), ΔG FEP correlation between all compounds showing K_i in pharmacology experimental assays, including brominated and dihalogenated compounds, grouped by position and halogen. Data can be found in Table 5.4 and Table 5.5.

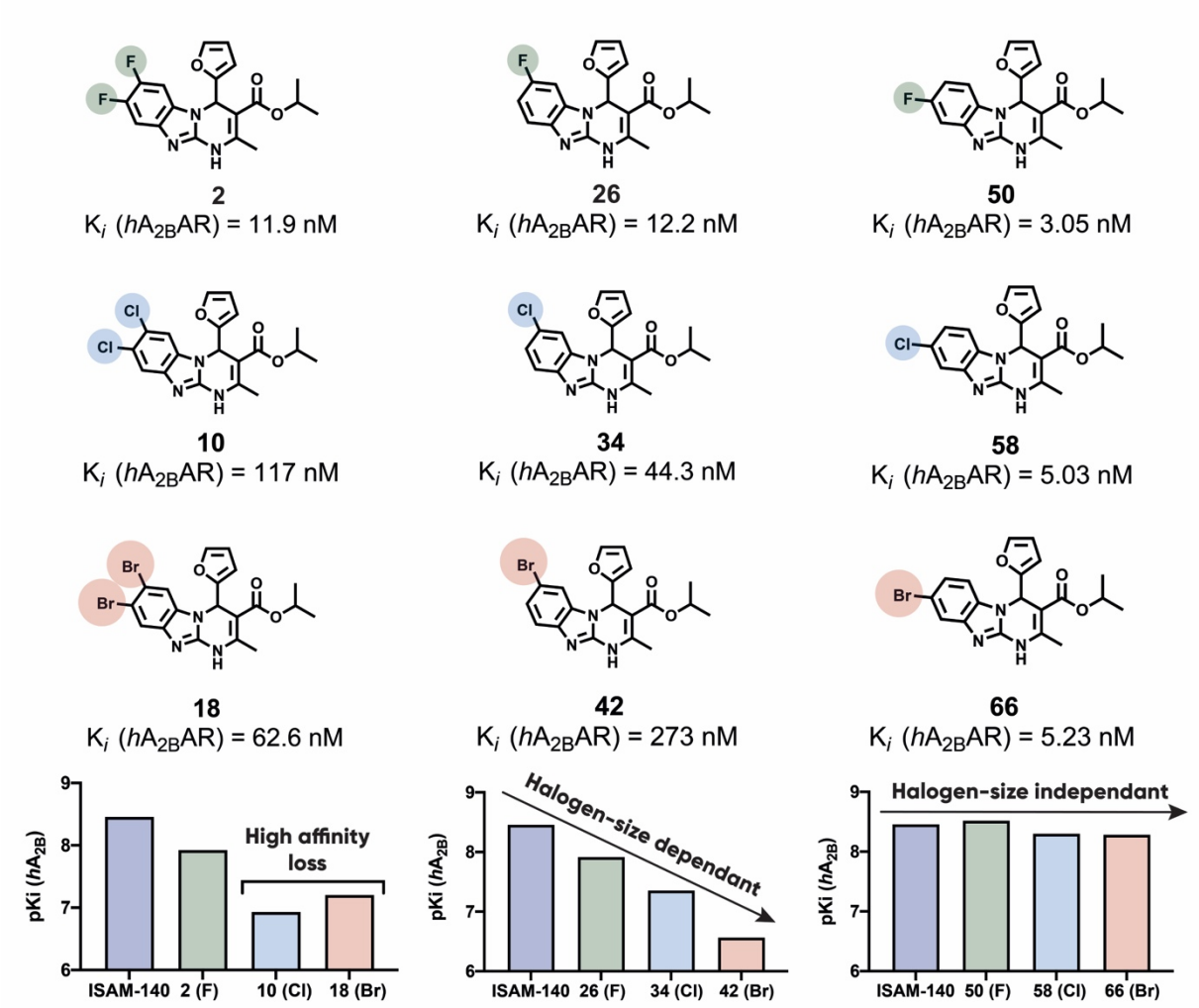

Figure 3.18. Docking pose for Series **I** (7,8-dihalo derivatives, left), Series **II** (7-halo derivatives, center) and **III** (8-halo derivatives, right), shown for the subset of derivatives with Het = 2-furyl and Alk = *i*-Pr, together with their affinity profile at $A_{2B}AR$ (Homology Model from $A_{2A}AR$, PDB: 3EML).

3.1.8 Preliminary ADMET exploration

An early understanding of the ADMET (absorption, distribution, metabolism, excretion and toxicity) profile of prototypical new lead compounds is crucial to reduce attrition and accelerate upstream drug discovery programs.[175,176] As reported in the bibliography, halogenation, and particularly fluorination usually enhances metabolic stability of chemical scaffolds.[177,178] To preliminarily explore the *in vitro* ADMET profile of the series documented here, seven representative A_{2B}AR antagonists (**2, 34, 50, 58, 60, 66** and **78**) were selected to evaluate their solubility, liver microsome stability, and inhibitory profile toward a prototypic cytochrome enzyme (CYP3A4). The selected compounds allow not only a preliminary evaluation of the impact of mono- or di-halogenation (positions 7, 8 or 7,8), but also to analyze the effect of different atoms (F, Cl, Br) on the pharmacokinetic parameters evaluated, while the inclusion of ligand **78** allowed us to assess the effect of fluorination on a representative non-furan A_{2B}AR antagonist. Table 3.8 shows the pharmacokinetic data obtained for the selected compounds; for comparison, the pharmacokinetic data available for the non-halogenated reference compounds (Cmpds **II**, and **X**) is included in Table 3.8, together with the adenosinergic data (hA$_{2B}$ K_i in nM, and hA$_{2A}$ K_i for **60**) in order to facilitate an integrated analysis for these compounds.

All ligands evaluated exhibit excellent solubility (21-70 μM) in PBS at pH 7, especially if compared to the solubility reported for a highly potent xanthine-based antagonist (PSB-603, Table 3.8).[121] The introduction of fluorine atoms (7,8-difluoro, 7-fluoro and 8-fluoro) improves up to 2-fold the solubility measured for the non-halogenated parent compounds. This trend also holds for the compound bearing an oxazole ring at position 4 (**78**). Chlorination at position 8 does not improve or slightly decreases solubility (see data for **58** and **60**), whereas bromination greatly increases solubility [e.g., **66** (70.7 μM) vs. **ISAM-140** (25.2 μM)]. Liver microsome assay data (Table 3.8) revealed that the selected A_{2B}AR antagonists showed moderate stability, with 16-41% of the compound remaining after 60 min of exposure to human microsomes and half-life ranging from 21-45 minutes. These data suggest that microsomal stability directly correlates with halogen size [e.g., **50** (F), **58** (Cl), **67** (Br) with 19.83, 22.75 and 32.13% remanent at 60 min respectively]. These findings are currently guiding an ongoing study to improve the microsomal stability of these promising A_{2B}AR antagonists.

To identify potential metabolic liabilities within the series here documented, the selected A_{2B}AR antagonists were tested *in vitro* for CYP3A4 inhibitory activity. CYP3A isoforms are

ubiquitous in the liver, have a broad substrate specificity[176] and are essential for the clearance of xenobiotics in humans (e.g., being involved in the metabolization of more than 50% of prescribed drugs). All experiments were performed in duplicate using fluorescence detection, employing ketoconazole as reference compound (Table 3.8). The results of this study reveal IC_{50} values lower than 10 μM for all fluorinated compounds towards CYP3A4 (with inhibitory activity ranging from 31-40% at 10 μM), improving in all cases the measured CYP3A4 activity as compared to their non-halogenated congeners. A comparative analysis suggests that for 8-halo derivatives (Table 3.8, Cmpds **50**, **58** and **66**) increasing the size of the halogen increases the interaction with CYP3A4 (Table 3.8). Although the preliminary CYP3A4 data for three ligands seem to be suboptimal, we should keep in mind that the differences between the *h*A_{2B}AR K_i of all compounds and the CYP3A4 IC_{50} (more than 200-fold in the worst case), makes CYP3A4 blockade not substantially important at the expected therapeutic doses. A more systematic study (e.g., including other relevant CYP subfamilies) would be required to draw definitive conclusions. In summary, an integrated analysis of pharmacodynamic studies and ADMET data allowed the identification of several new halogenated A_{2B}AR antagonists that combine excellent affinity and selectivity and improved ADMET profile.

Table 3.8. Preliminary ADME and binding data of novel and previously reported A_{2B}AR Antagonists.

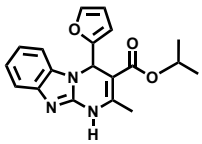

(±)-ISAM-140
(±)-IIIb

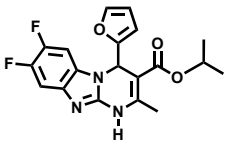

(±)-2

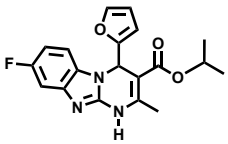

(±)-ISAM-163
(±)-50

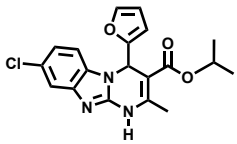

(±)-ISAM-161
(±)-58

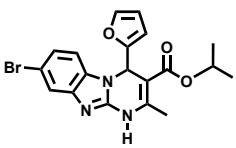

(±)-ISAM-157
(±)-66

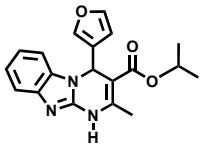

(±)-ISAM-142
(±)-IIId

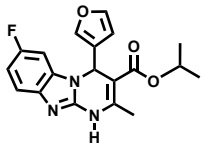

(±)-34

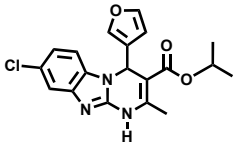

(±)-ISAM-M89A
(±)-60

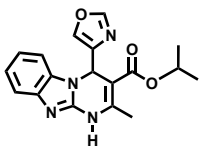

(±)-X

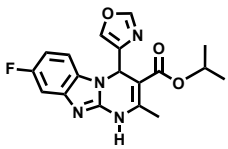

(±)-ISAM-R324A
(±)-78

Compound	Solubility (μM)[a]	Microsomal Stability			CYP3A4 IC_{50} (μM)[e] or % inh. at 10 μM[f]		hA_{2B} K_i (nM)
		%[b]	$t_{1/2}$[c]	Cl_{int}[d]	DBF	7-BFC	
IIIb (ISAM-140)[87]	**25.2**	**-**	**-**	**-**	**2.90 ± 0.37**	**-**	**3.49 ± 0.2**
2	62.0	20.97	28.93	21.65	> 10 (39%)	> 10 (58%)	11.9 ± 1.1
50	47.5	19.83	27.40	20.07	> 10 (40%)	> 10 (63%)	3.05 ± 0.7
58	23.7	22.75	28.14	18.60	3.68 ± 0.47	> 10 (54%)	5.03 ± 0.3
66	70.7	32.13	36.79	14.23	2.26 ± 0.30	> 10 (52%)	5.23 ± 0.4
IIId (ISAM-142)[87]	**26.1**	**-**	**-**	**-**	**2.68 ± 0.53**	**-**	**11.4 ± 0.5**
34	58.2	16.83	21.13	26.44	> 10 (47%)	> 10 (11%)	44.3 ± 1.4
60	21.9	41.02	44.80	11.68	6.36 ± 1.02	> 10 (44%)	6.10 ± 0.7 (A_{2B}) 176 ± 4 (A_{2A})
X[144]	**39.7**	**-**	**-**	**-**	**5.92 ± 0.68**	**-**	**43.4 ± 1.3**
78	64.6	35.15	40.8	12.83	> 10 (31%)	> 10 (52%)	6.10 ± 0.3
PSB-603[121]	0.2	-	-	-	-	-	0.553
Progesterone	6.7	-	-	-	-	-	-
Prazosin	31.3	-	-	-	-	-	-
Testosterone	-	7.11	16.13	32.44	-	-	-
Ketoconazole	-	-	-	-	0.008 μM	0.027 μM	-
Quinidine	-	-	-	-	-	-	-

[a] Solubility in 1:99 DMSO/PSB buffer. [b] Percentage remanent (sampling time 60 min). [c] $t_{1/2}$ in min. [d] Intrinsic clearance in $\mu l \cdot min^{-1} \cdot mg_{prot}^{-1}$. [e] IC_{50} value obtained by extrapolation with analysis software. [f] Due the low activity showed at CYP3A4, the percentage of inhibition at 10 μM is reported.

A large collection of pyrimidine-based A_{2B}AR antagonists was obtained and evaluated as part of our program aimed at uncovering the therapeutic potential of blocking A_{2B}AR in the context of cancer (immuno)therapy. During the assessment of the impact of (di- and mono-) halogenation at positions 7 and 8 on A_{2B}AR affinity in a series of alkyl 7/8-halo-4-heteroaryl-1,4-dihydro-benzo[4,5]-imidazo[1,2-a]pyrimidine-3-carboxylates, eight new A_{2B}AR antagonists with notable affinity (K_i < 10 nM) and attractive subtype selectivity were identified. The study revealed that the introduction of two halogen atoms (at positions 7 and 8) and halogenation at position 7 led to a halogen-size dependent decrease in A_{2B}AR affinity. Conversely, halogenation at position 8 resulted in highly potent A_{2B}AR ligands regardless of the halogen's nature. These observed trends in structure-activity relationships (SAR) were further supported by a structure-based molecular modeling study incorporating FEP simulations.

Additionally, this chapter provided further evidence supporting the significance of the stereodisposition of the pentagonal ring at position 4 on A_{2B}AR affinity. Some eutomers demonstrated sub-nanomolar A_{2B}AR affinity and maintained remarkable subtype selectivity. Notably, the study identified the first example of a dual A_{2A}AR/A_{2B}AR antagonist that exhibited stereoselective recognition at A_{2A}AR and A_{2B}AR. The functional profile of representative ligands as A_{2B}AR antagonists was confirmed through cAMP-based assays. Evaluation of various ADMET parameters helped verify the benefits of halogenation while identifying lead compounds that combined improved affinity, selectivity, and favorable pharmacokinetic profiles.

3.2 Chapter II: Scaffold hopping strategies of the 3,4-dihydropyrimidin-2(1*H*)-one chemotype provide novel potent A_{2B} adenosine receptor antagonists

As previously discussed in the introduction, the A_{2B}AR presents itself as a promising target for cancer treatment due to its validated antiproliferative and antimetastatic effects and its capacity for immunomodulation. Our research group has been at the forefront of ligand development for all four subtypes of adenosine receptors (A_1,[86] A_{2A},[86,179] A_{2B},[87,140–144] and A_3ARs[130,131,180]) over the past years. Specifically focusing on the A_{2B}AR, our group has undertaken a comprehensive Hit to Lead optimization project since 2013,[140] leading us to the discovery of **ISAM-140**[87] as a highly potent and selective non-xanthine-based A_{2B}AR antagonist. Furthermore, our investigations into the receptor have yielded significant insights, including the discovery of enantioselective modulation of the A_{2B}AR.[141–144]

Building upon our previous achievements, we herein propose to employ scaffold hopping strategies to further explore the pharmacokinetics and, most importantly, the pharmacodynamics optimization of A_{2B}AR ligand series. This approach allows us to investigate novel structural modifications and identify new scaffolds that can enhance the interaction with the orthosteric binding site (Figure 3.19). By delving into the intricacies of ligand-receptor interactions, we aim to gain a deeper understanding of the molecular mechanisms underlying the A_{2B}AR-mediated pathways and their potential implications in cancer therapy. In order to achieve this goal, we selected different variants of the Biginelli reaction as part of our multicomponent synthesis platform to develop a substantial number of synthetically accessible ligands with diverse structures. This approach enables us to explore the chemical space and synthesize collections of highly diverse compounds, thus driving the discovery and development of novel targeted therapies for cancer treatment.

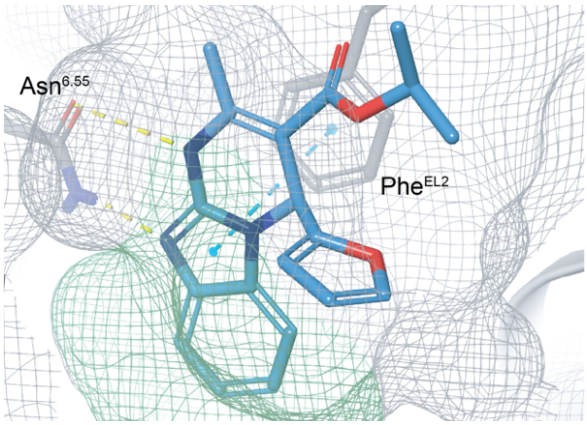

Figure 3.19. Binding mode of prototypical tricyclic A_{2B}AR antagonists. Grey mesh represents A_{2B}AR binding site (in green: internal cavity explored in this chapter).

3.2.1 Design

The novel series herein described were conceived in the context of our ongoing projects to develop $A_{2B}AR$ selective antagonists and multi-target agents using three series of propotypic (monocyclic, bicyclic and tricyclic) dihidropyrimidinone derivatives (Figure 3.20) as model ligands. Our recent reports document the $A_{2B}AR$ antagonistic effect of dihydropyrimidinone derivatives, exploring different SAR trends, the proposed binding mode for these heterocyclic core, and studying the different points of diversity around the scaffold: optimal diversity for aldehyde and ester precursors, better positions of fusion,[87] the impact of bioisosteric replacements,[144] and the introduction of halogens at aromatic[87] and/or aliphatic (ester and methyl moieties)[143] positions of the scaffold. The SAR data from previous studies was rationalized on the basis of binding mode originally proposed by us[87,140] and constituted the foundation to guide the design of 168 new dihydropyrimidinone derivatives. Herein synthesized and characterized ligands have been divided into twenty one series (Figure 3.20). To preserve consistency from the early series, and facilitate the comparative SAR, the herein obtained ligands (series **V**−**XXV**) retained the structural elements that provided optimal $A_{2B}AR$ affinity at ester group and the stereogenic centre. Thus, aldehyde moiety bears a set of pentagonal heteroaryl groups (2-furyl, 3-furyl, 2-thienyl, and 3-thienyl), while the alkoxy residues of the ester consist of ethyl or isopropyl groups. The integrated synthesis, binding data, SAR, and computational studies of the complete ligand library are described in this chapter.

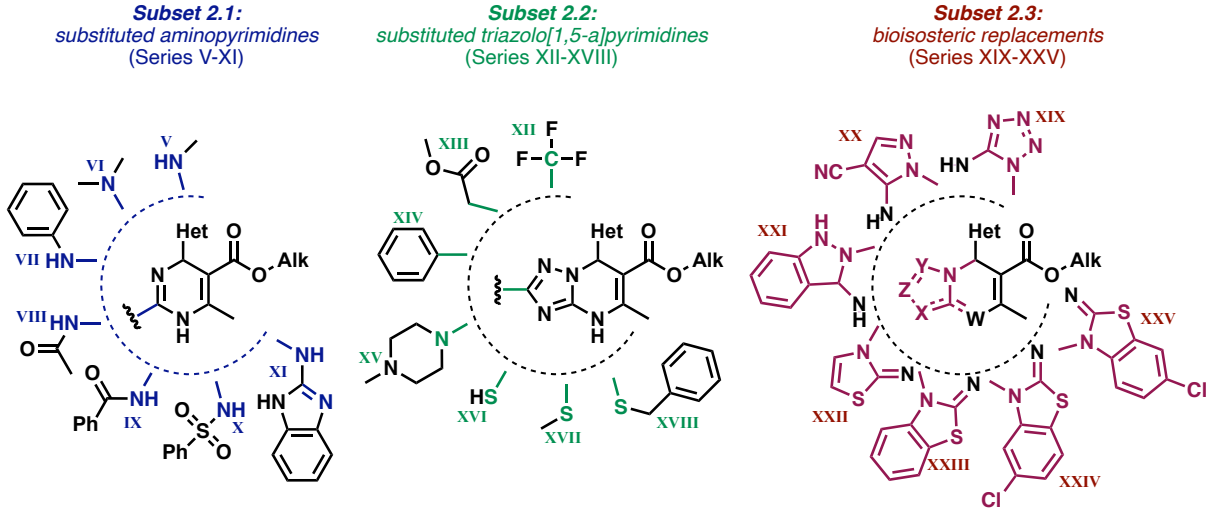

Figure 3.20. Scaffold-hopping strategy for the design of novel $A_{2B}AR$ antagonists from mono-, bi-, and tricyclic cores from model series **I-III**.

First subset [Series **V–XI** (Table 3.10, Table 3.11 and Table 3.12)] contains monocyclic compounds (2-aminopyrimidines) with different substituents at position 2 (Figure 3.21). These series were inspired by combination of previously published monocyclic scaffolds (Model series **I**)[140,142] and conceived as ring oppening strategies from bicyclic compounds (Model series **II**),[87] taking into account the potential co-existence of different tautomers. Series **V**, **VI** and **VII** are composed by 2-methylamino, 2,2-dimethylamino, and 2-phenylaminopyrimidines respectively (Cmpds **81–104**), whereas series **VIII**, **IX** and **X** are constituted by 2-acetamido, 2-benzamido and 2-phenylsulfonamido derivatives (Cmpds **105–128**). The design of Series **XI** (Cmpds **129–136**) differs from the others in being based on the tricyclic compounds ring opening (Figure 3.21). The approach would allow the formation of an intramolecular hydrogen bond that stabilize the structure similarity to in the previously proposed binding mode.[87]

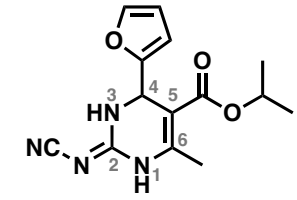

Monocyclic model ligand
SY1K-024
K_i ($hA_{2B}AR$) = 24.3 nM

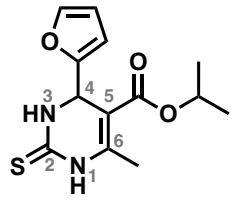

Monocyclic model ligand
SY1AF-30
K_i ($hA_{2B}AR$) = 10.2 nM

Subset 2.1: *substituted aminopyrimidines* (Series V-XI)

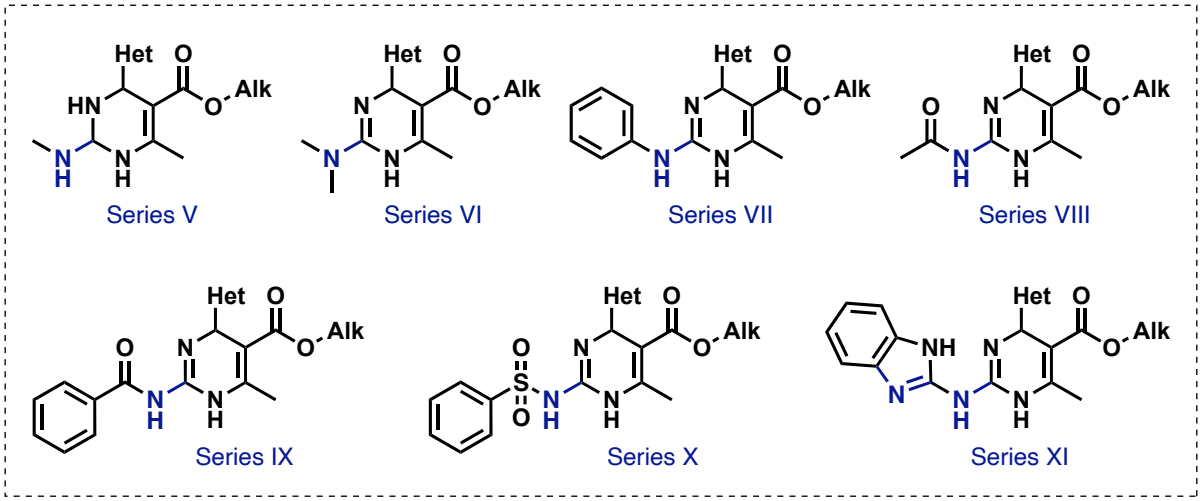

Figure 3.21. Monocyclic model ligands and Subset 2.1 general structures. Dark blue corresponds to the tautomeric forms of diamine type, and light blue corresponds to the tautomeric forms of enamine type. Het = Heteroaryl (2-furyl, 3-furyl, 2-thienyl or 3-thienyl), Alk = Alkyl (ethyl or isopropyl).

Second subset [Series **XII–XVIII** (Table 3.13 and Table 3.14)] includes compounds derived from **ISAM-148 (**Figure 3.22) substituted at position 2. Series **XII**, **XIII**, **XIV**, and **XV** (Table 3.13) explore carbon-based residues (trifluoromethyl, methoxycarbonyl, phenyl) and *N*-methylpiperazine (NMP), respetively; while series **XVI**, **XVII**, and **XVIII** (Table 3.14) focused into sulfur-based functional group (thiol, methyltio and benzylthio, respectively).

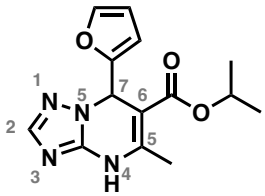

Bicyclic model ligand
ISAM-148
K_i ($hA_{2B}AR$) = 55.6 nM

Subset 2.2: *substituted triazolo[1,5-a]pyrimidines* (Series XII-XVIII)

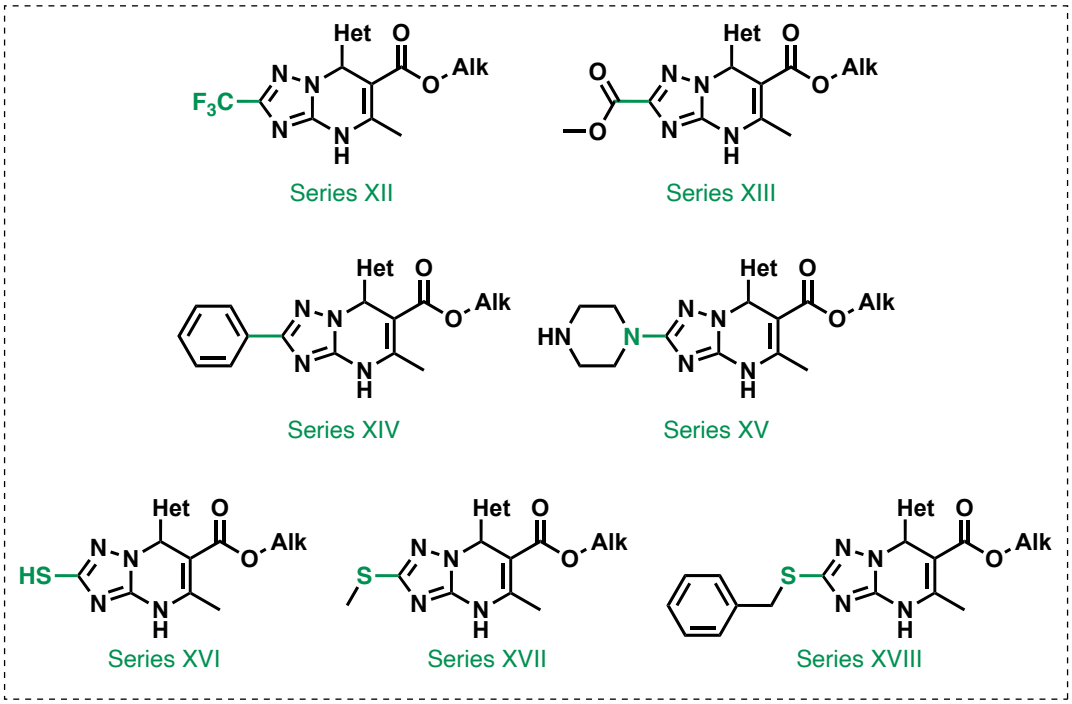

Figure 3.22. Bicyclic model ligand and Subset 2.2 series. Het = Heteroaryl (2-furyl, 3-furyl, 2-thienyl or 3-thienyl), Alk = Alkyl (ethyl or isopropyl).

The last subset, consisting of series **XIX–XXV** (Table 3.15 and Table 3.16), is based in bioisosteric replacement strategies around bi- and tricyclic model compounds (Figure 3.23). Series **XIX** explores the CH/N bioisosterism within **ISAM-148** structure (Figure 3.23), obtaining tetrazole derivatives. Series **XX** explores the replacement of the imine-type nitrogen at position 3 of the bicycle (**ISAM-148**) by a cyano group; and Series **XXI** was conceived with the inversion of the classical tricyclic system of **ISAM-140** (Figure 3.23), using the central structure of dihydropyrimido[1,2-*b*]indazole (Figure 3.23, Table 3.15). The last four series of this subset (**XXII–XXV**, Cmpds **217-248**) have been designed by NH/S replacement during the Biginelli reaction (employing either 2-aminothiazole or 2-aminobenzimidazoles) in the pentacyclic ring. This structural modification is critical to verify the importance of the double hydrogen bond interaction with the $A_{2B}AR$, we have proposed in previous works.[87]

Thus, series **XXII** and **XXIII** replace the imidazole ring with the thiazole core, generating new heterocyclic systems (bicyclic and tricyclic) lacking the NH group. Finally, a focused series consisting of benzo[4,5]thiazolo[3,2-*a*]pyrimidines bearing a chlorine atom at positions 7 (Series **XXIV**) or 8 (Series **XXV**), that we identified as optimal halogenation for tricyclic derivatives in chapter I (Figure 3.23**)**, was obtained to further explore the in-depth interaction with the $A_{2B}AR$ and potential dual $A_{2A}AR/A_{2B}AR$ binding behaviour (Table 3.16).

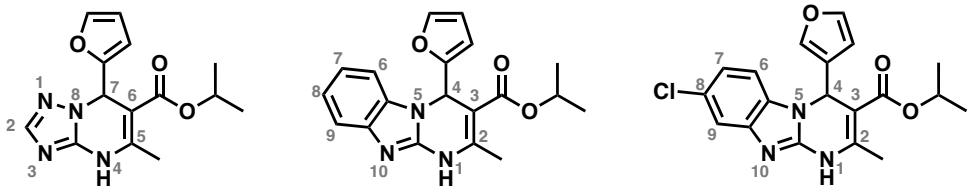

Bicyclic model ligand
ISAM-148
K_i ($hA_{2B}AR$) = 55.6 nM

Tricyclic model ligand
ISAM-140
K_i ($hA_{2B}AR$) = 3.49 nM

Tricyclic model ligand
60
K_i ($hA_{2A}AR$) = 176 nM
K_i ($hA_{2B}AR$) = 6.10 nM

Subset 2.3: *bioisosteric replacements* (Series XIX-XXV)

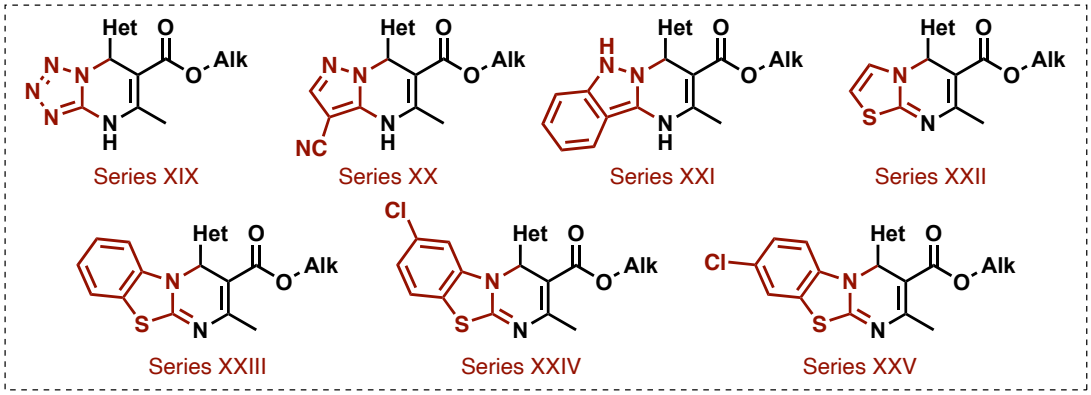

Figure 3.23. Tricyclic model ligands and Subset 2.3 series. Het = Heteroaryl (2-furyl, 3-furyl, 2-thienyl or 3-thienyl), Alk = Alkyl (ethyl or isopropyl).

3.2.2 Chemistry

Different, but conceptually homogeneous, three-component synthetic approaches, based on the robust and efficient Biginelli reaction (i.e., the three-component reaction of an aldehyde, a β-ketoester and 1,3-dinucleophiles), enabled a time- and cost-effective assembly of the large collection obtained. A set of pentagonal carbaldehydes (**A1–4**) and β-ketoesters (**B1–2**), providing optimal substituents for Het and Alk positions, in combination with different 1,3-dinucleophiles (**C7–27**) were employed as precursors.

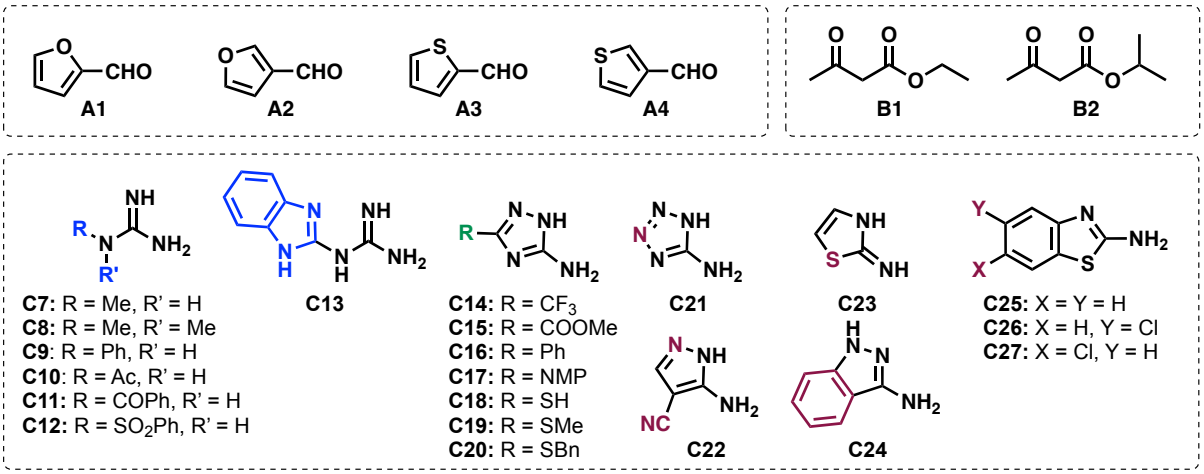

Figure 3.24. Synthetic precursors for the Biginelli-based synthesis of compounds **81-248**. A: pentagonal carbaldehydes, B: ß-ketoesters, and C: 1,3-dinucleophiles.

All the compounds (**81–248**) were obtained as depicted in Figure 3.25. The reaction conditions, highly dependent on the nature of the 1,3-dinucleophile, vary for the different series, with seven different methods for the synthesis of all the series (Figure 3.25). A detailed explanation of the synthetic methods can be found in the Experimental Section. Briefly, the three precursors were disolved in the appropiate solvent (THF, DMF, acetic acid or mixtures thereof) and the corresponding catalysts was added (Na_2CO_3, $ZnCl_2$, acetic acid, chloroacetic acid or *L*-proline). The reaction mixture was then heated (70 ºC, 90 ºC or 170 ºC) and 1) orbitallically stirred in Kimble vials on a PLS, or 2) irradiated in a microwave reactor (Anton Paar), or 3) stirred in a sealed tube for the required time (Figure 3.25). All reactions were monitored by thin-layer chromatography (TLC). After completion of the reaction, the solvent was evaporated to dryness and the obtained residue was purified by either column or preparative chromatography on silica gel. The targeted compounds were isolated in variable (10 – 60%) yields.

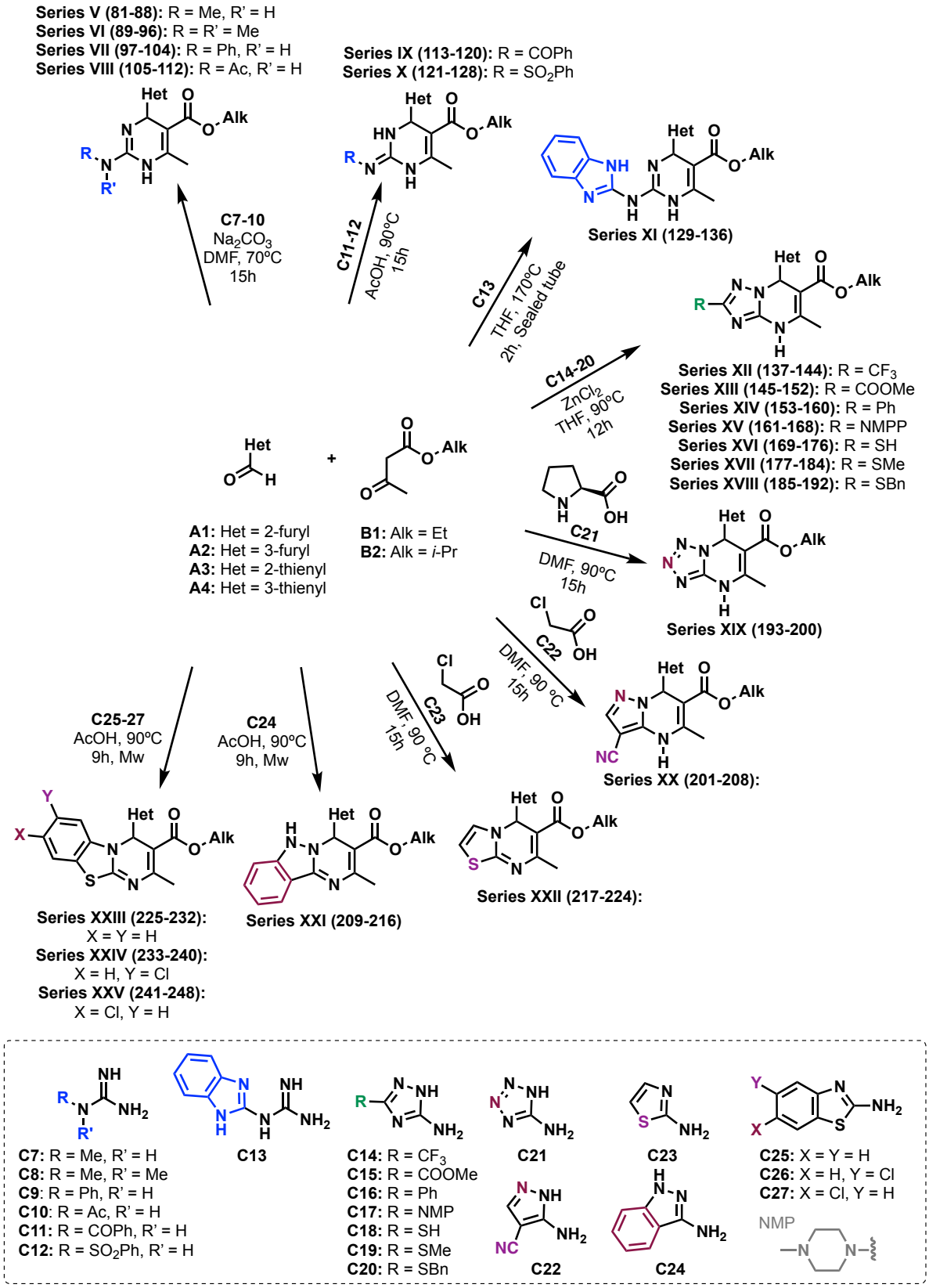

Figure 3.25. Biginelli-based synthesis of novel mono-, bi-, and tricyclic pyrimidinone derivatives. NMP: *N*-methylpiperidine.

A detailed description of the synthetic methods and the complete structural, spectroscopic, and analytical data for all compounds are provided in the Experimental Section. As in previous chapter, all ligands obtained in this study contain a stereocenter and were isolated and evaluated as racemic mixtures. Three ligands eliciting attractive A_{2B}AR affinity/selectivity profile and one dual A_{2A}AR/A_{2B}AR ligand were submitted to semipreparative chiral HPLC resolution to isolate their corresponding enantiomer pairs. The unequivocal assignation of the configuration of the different enantiomers was performed employing circular dichroism (CD) as described in previous chapter.

3.2.3 Biological Evaluation

The adenosinergic profile (affinity and selectivity) of the 168 novel compounds was evaluated *in vitro* using radioligand binding assays at the four human AR subtypes using previously described protocols.[87,140,142,143] Table 3.9 contains the binding data of model series (mono-, bi-, and tricyclic), while Tables 3.10-16 contain the binding data obtained for novel compounds. All ligands reported were obtained and tested as racemic mixtures. The whole set was in silico evaluated, using the PAINS filter in RDKit,[166] to rule out these ligands being promiscuous pan-assay interference compounds (PAINS). Human ARs were expressed in transfected cell lines [e.g. chinese hamster ovary (CHO) cells (A_1AR), human epithelial carcinoma (HeLa) cells (A_{2A}AR and A_3AR) and human embryonic kidney (HEK-293) cells (A_{2B}AR)]. [^{3}H]DPCPX for A_1AR and A_{2B}AR, [^{3}H]NECA for A_3AR, and [^{3}H]ZM241385 for A_{2A}AR were employed as radioligands. The binding data is presented as $K_i \pm$ SEM (nM, n = 3) or as specific binding inhibition percentage at 1 μM (n = 2, average) for those compounds that did not completely displace the radioligand. Using Prism 5.0 software (GraphPad, San Diego, CA) K_i values were acquired by fitting the data by non-linear regression. A specific binding inhibition percentage is reported for those compounds that exhibited either little affinity or poor solubility. Data reported are the average of three experiments, each performed in duplicate. For the sake of comparison, a set of well-known AR antagonists (**ISAM-140, DPCPX**, **NECA** and **ZM241385**) were assessed using our experimental protocols, their binding data is reported in tables. The stereoisomers obtained by semipreparative chiral resolution were tested at the four human AR subtypes in its enantiopure forms (Table 3.17) and, to facilitate the rational study, the structurally related enantiomers evaluated in Chapter I have been added. This data was employed to complement the SAR study and to evaluate the importance of the configuration of the stereogenic center on the affinity in the novel series.

As a part of the pharmacological characterization, **114**, **146** and **226** were tested in cAMP production assays. These experiments revealed that pyrimidinone-derived ligands targeting A_{2B}AR, with diverse scaffolds, effectively inhibit cAMP accumulation, unequivocally validating the antagonistic behavior if these compounds at A_{2B}AR. A comparison of K_i and K_B values reveals a good correlation between data obtained from binding and functional assays in both receptors (Table 3.18).

Table 3.9. Structure and adenosine receptor affinity data of model Series **I**-III.[87,142]

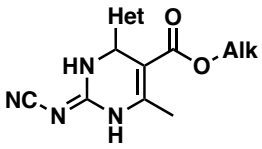

Model series I

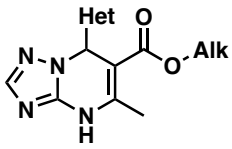

Model series II

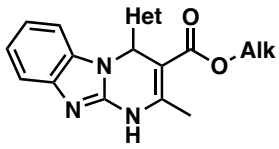

Model series III

			K_i (nM) or % at 1 μM			
	Het	**Alk**	***h*A$_1$**[a)]	***h*A$_{2A}$**[b)]	***h*A$_{2B}$**[c)]	***h*A$_3$**[d)]
Model series I						
Ii[142]	2-furyl	Et	27%	20%	900 ± 6	20%
Ij (SY1K-024)[142]	2-furyl	*i*-Pr	21%	19%	24.3 ± 0.9	4%
Ik[142]	3-furyl	Et	28%	31%	102 ± 3	14%
Il[142]	3-furyl	*i*-Pr	34%	25%	59.4 ± 1.8	41%
Im[142]	2-thienyl	Et	26%	33%	51.0 ± 2.1	3%
In[142]	2-thienyl	*i*-Pr	31%	16%	349 ± 3	27%
Io[142]	3-thienyl	Et	29%	30%	461 ± 2	23%
Ip[142]	3-thienyl	*i*-Pr	11%	18%	657 ± 4	13%
Model series II						
IIa[87]	2-furyl	Et	15%	20%	3%	4%
IIb (ISAM-148)[87]	2-furyl	*i*-Pr	2%	5%	55.6 ± 4	2%
IIc[87]	3-furyl	Et	2%	1%	602 ± 10	4%
IId[87]	3-furyl	*i*-Pr	2%	2%	350 ± 8	20%
IIe[87]	2-thienyl	Et	1%	2%	15%	15%
IIf[87]	2-thienyl	*i*-Pr	1%	1%	1%	3%
IIg[87]	3-thienyl	Et	3%	21%	699 ± 5	2%
IIh[87]	3-thienyl	*i*-Pr	3%	2%	816 ± 7	5%
Model series III						
IIIa (ISAM-134)[87]	2-furyl	Et	5%	14%	12.0 ± 0.7	1%
IIIb (ISAM-140)[87]	2-furyl	*i*-Pr	20%	25%	3.49 ± 0.2	2%
IIIc (ISAM-141)[87]	3-furyl	Et	7%	11%	20.6 ± 1.1	1%
IIId (ISAM-142)[87]	3-furyl	*i*-Pr	12%	22%	11.40 ± 0.5	2%
IIIe[87]	2-thienyl	Et	8%	16%	484 ± 3	1%
IIIf[87]	2-thienyl	*i*-Pr	1%	17%	371 ± 5	3%
IIIg[87]	3-thienyl	Et	3%	10%	29.7 ± 1.2	2%
IIIh[87]	3-thienyl	*i*-Pr	11%	3%	29.3 ± 1.1	21%
IIIi (ISAM-C032)[87]	4-oxazolyl	Et	5%	11%	8.10 ± 0.5	7%
IIIj[87]	4-oxazolyl	*i*-Pr	7%	19%	43.4 ± 1.3	16%
ISAM-140	2-furyl	*i*-Pr	20%	25%	3.49 ± 0.2	20%
DPCPX	-	-	2.20 ± 0.2	157 ± 3	73.24 ± 1.4	1722 ± 11
ZM241385	-	-	683 ± 4	1.9 ± 0.1	65.7 ± 1.1	863 ± 4
NECA	-	-	14.0 ± 1	20.0 ± 3	2400 ± 35	6.20 ± 9

[a)] Displacement of specific [^{3}H]DPCPX binding in human CHO cells expressed as K_i in nM (n = 3) or percentage displacement of specific binding at a concentration of 1 μM (n = 2). [b)] Displacement of specific [^{3}H]4-(2-[7-amino-2-(2-furyl)[1,2,4]triazolo[2,3-a][1,3,5]triazin-5-ylamino]ethyl)phenol binding in human HeLa cells expressed as K_i in nM (n = 3) or percentage displacement of specific binding at a concentration of 1 μM (n = 2). [c)] Displacement of specific [^{3}H]DPCPX binding in human HEK-293 cells expressed as K_i in nM (n = 3) or percentage displacement of specific binding at a concentration of 1 μM (n = 2). [d)] Displacement of specific [^{3}H]NECA binding in human HeLa cells expressed as K_i in nM (n = 3) or percentage displacement of specific binding at a concentration of 1 μM (n = 2).

Table 3.10. Structure and adenosine receptor affinity data of series **V-VIII**.

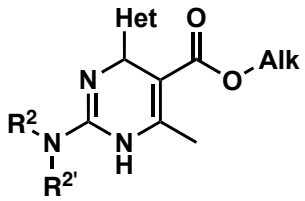

						K_i (nM) or % at 1 µM			
Compound	**Series**	**R^2**	**$R^{2'}$**	**Het**	**Alk**	***h*A$_1$**[a)]	***h*A$_{2A}$**[b)]	***h*A$_{2B}$**[c)]	***h*A$_3$**[d)]
81	V	Me	H	2-furyl	Et	4%	8%	26%	2%
82	V	Me	H	2-furyl	*i*-Pr	18%	3%	21%	10%
83	V	Me	H	3-furyl	Et	22%	15%	33%	22%
84	V	Me	H	3-furyl	*i*-Pr	4%	6%	20%	18%
85	V	Me	H	2-thienyl	Et	27%	2%	7%	25%
86	V	Me	H	2-thienyl	*i*-Pr	10%	7%	20%	13%
87	V	Me	H	3-thienyl	Et	16%	16%	16%	21%
88	V	Me	H	3-thienyl	*i*-Pr	2%	12%	53%	7%
89	VI	Me	Me	2-furyl	Et	16%	45%	19%	3%
90	VI	Me	Me	2-furyl	*i*-Pr	15%	1%	1%	13%
91	VI	Me	Me	3-furyl	Et	3%	9%	20%	11%
92	VI	Me	Me	3-furyl	*i*-Pr	4%	17%	11%	5%
93	VI	Me	Me	2-thienyl	Et	29%	27%	3%	15%
94	VI	Me	Me	2-thienyl	*i*-Pr	8%	21%	1%	3%
95	VI	Me	Me	3-thienyl	Et	11%	13%	8%	12%
96	VI	Me	Me	3-thienyl	*i*-Pr	22%	12%	10%	5%
97	VII	Ph	H	2-furyl	Et	13%	3%	13%	15%
98	VII	Ph	H	2-furyl	*i*-Pr	18%	8%	56%	27%
99	VII	Ph	H	3-furyl	Et	4%	20%	15%	18%
100	VII	Ph	H	3-furyl	*i*-Pr	15%	17%	34%	5%
101	VII	Ph	H	2-thienyl	Et	21%	6%	41%	20%
102	VII	Ph	H	2-thienyl	*i*-Pr	9%	12%	1%	11%
103	VII	Ph	H	3-thienyl	Et	23%	22%	28%	24%
104	VII	Ph	H	3-thienyl	*i*-Pr	1%	9%	37%	17%
ISAM-140	-	-	-	-	-	20%	25%	3.49 ± 0.2	20%
DPCPX	-	-	-	-	-	2.20 ± 0.2	157 ± 3	73.2 ± 1.4	1722 ± 11
ZM241385	-	-	-	-	-	683 ± 4	1.9 ± 0.1	65.7 ± 1.1	863 ± 4
NECA	-	-	-	-	-	14.0 ± 1	20.0 ± 3	2400 ± 35	6.20 ± 0.9

[a)] Displacement of specific [^{3}H]DPCPX binding in human CHO cells expressed as K_i in nM (n = 3) or percentage displacement of specific binding at a concentration of 1 μM (n = 2). [b)] Displacement of specific [^{3}H]4-(2-[7-amino-2-(2-furyl)[1,2,4]triazolo[2,3-*a*][1,3,5]triazin-5-ylamino]ethyl)phenol binding in human HeLa cells expressed as K_i in nM (n = 3) or percentage displacement of specific binding at a concentration of 1 μM (n = 2). [c)] Displacement of specific [^{3}H]DPCPX binding in human HEK-293 cells expressed as K_i in nM (n = 3) or percentage displacement of specific binding at a concentration of 1 μM (n = 2). [d)] Displacement of specific [^{3}H]NECA binding in human HeLa cells expressed as K_i in nM (n = 3) or percentage displacement of specific binding at a concentration of 1 μM (n = 2).

Table 3.11. Structure and adenosine receptor affinity data of series **IX-X.**

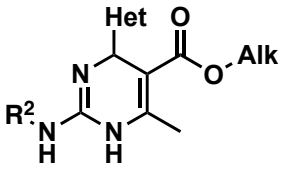

105-112

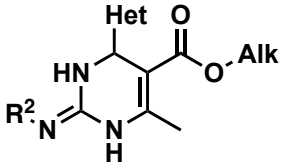

113-128

					K_i (nM) or % at 1 μM			
Compound	**Series**	**R^2**	**Het**	**Alk**	**hA_1[a)]**	**hA_{2A}[b)]**	**hA_{2B}[c)]**	**hA_3[d)]**
105	VIII	-COMe	2-furyl	Et	4%	9%	3%	1%
106	VIII	-COMe	2-furyl	*i*-Pr	12%	5%	35%	14%
107	VIII	-COMe	3-furyl	Et	3%	11%	15%	6%
108	VIII	-COMe	3-furyl	*i*-Pr	7%	3%	31%	3%
109	VIII	-COMe	2-thienyl	Et	3%	6%	3%	14%
110	VIII	-COMe	2-thienyl	*i*-Pr	1%	4%	2%	4%
111	VIII	-COMe	3-thienyl	Et	15%	6%	1%	7%
112	VIII	-COMe	3-thienyl	*i*-Pr	6%	3%	8%	21%
113	IX	-COPh	2-furyl	Et	13%	17%	126 ± 2	9%
114	IX	-COPh	2-furyl	*i*-Pr	5%	8%	83.5 ± 0.8	4%
115	IX	-COPh	3-furyl	Et	2%	6%	148 ± 1.1	11%
116	IX	-COPh	3-furyl	*i*-Pr	3%	2%	227 ± 2.2	7%
117	IX	-COPh	2-thienyl	Et	4%	12%	3%	4%
118	IX	-COPh	2-thienyl	*i*-Pr	11%	5%	18%	8%
119	IX	-COPh	3-thienyl	Et	4%	3%	39%	16%
120	IX	-COPh	3-thienyl	*i*-Pr	5%	9%	50%	31%
121	X	$-SO_2Ph$	2-furyl	Et	7%	1%	459 ± 4	5%
122	X	$-SO_2Ph$	2-furyl	*i*-Pr	2%	4%	375 ± 3	21%
123	X	$-SO_2Ph$	3-furyl	Et	6%	5%	15%	10%
124	X	$-SO_2Ph$	3-furyl	*i*-Pr	1%	4%	25%	2%
125	X	$-SO_2Ph$	2-thienyl	Et	2%	3%	7%	4%
126	X	$-SO_2Ph$	2-thienyl	*i*-Pr	4%	1%	7%	3%
127	X	$-SO_2Ph$	3-thienyl	Et	5%	2%	11%	15%
128	X	$-SO_2Ph$	3-thienyl	*i*-Pr	3%	7%	16%	4%
ISAM-140		-	-	-	20%	25%	3.49 ± 0.2	20%
DPCPX		-	-	-	2.20 ± 0.2	157 ± 3	73.2 ± 1.4	1722 ± 11
ZM241385		-	-	-	683 ± 4	1.9 ± 0.1	65.7 ± 1.1	863 ± 4
NECA		-	-	-	14.0 ± 1	20.0 ± 3	2400 ± 35	6.20 ± 0.9

[a)] Displacement of specific [^{3}H]DPCPX binding in human CHO cells expressed as K_i in nM (n = 3) or percentage displacement of specific binding at a concentration of 1 μM (n = 2). [b)] Displacement of specific [^{3}H]4-(2-[7-amino-2-(2-furyl)[1,2,4]triazolo[2,3-*a*][1,3,5]triazin-5-ylamino]ethyl)phenol binding in human HeLa cells expressed as K_i in nM (n = 3) or percentage displacement of specific binding at a concentration of 1 μM (n = 2). [c)] Displacement of specific [^{3}H]DPCPX binding in human HEK-293 cells expressed as K_i in nM (n = 3) or percentage displacement of specific binding at a concentration of 1 μM (n = 2). [d)] Displacement of specific [^{3}H]NECA binding in human HeLa cells expressed as K_i in nM (n = 3) or percentage displacement of specific binding at a concentration of 1 μM (n = 2).

Table 3.12. Structure and adenosine receptor affinity data of series **XI.**

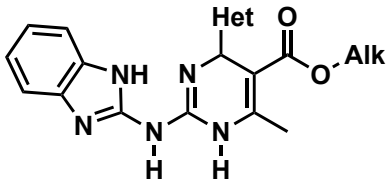

				K_i (nM) or % at 1 µM			
Compound	**Series**	**Het**	**Alk**	***h*A$_1$**[a)]	***h*A$_{2A}$**[b)]	***h*A$_{2B}$**[c)]	***h*A$_3$**[d)]
129	XI	2-furyl	Et	23%	13%	429 ± 2	26%
130	XI	2-furyl	*i*-Pr	13%	8%	127 ± 1.3	21%
131	XI	3-furyl	Et	3%	3%	40%	15%
132	XI	3-furyl	*i*-Pr	28%	12%	480 ± 4	23%
133	XI	2-thienyl	Et	23%	9%	32%	42%
134	XI	2-thienyl	*i*-Pr	6%	6%	11%	13%
135	XI	3-thienyl	Et	18%	10%	34%	7%
136	XI	3-thienyl	*i*-Pr	11%	6%	45%	17%
ISAM-140		-	-	20%	25%	3.49 ± 0.2	20%
DPCPX		-	-	2.20 ± 0.2	157 ± 3	73.2 ± 1.4	1722 ± 11
ZM241385		-	-	683 ± 4	1.9 ± 0.1	65.7 ± 1.1	863 ± 4
NECA		-	-	14.0 ± 1	20.0 ± 3	2400 ± 35	6.20 ± 0.9

[a)] Displacement of specific [^{3}H]DPCPX binding in human CHO cells expressed as K_i in nM (n = 3) or percentage displacement of specific binding at a concentration of 1 µM (n = 2). [b)] Displacement of specific [^{3}H]4-(2-[7-amino-2-(2-furyl)[1,2,4]triazolo[2,3-*a*][1,3,5]triazin-5-ylamino]ethyl)phenol binding in human HeLa cells expressed as K_i in nM (n = 3) or percentage displacement of specific binding at a concentration of 1 µM (n = 2). [c)] Displacement of specific [^{3}H]DPCPX binding in human HEK-293 cells expressed as K_i in nM (n = 3) or percentage displacement of specific binding at a concentration of 1 µM (n = 2). [d)] Displacement of specific [^{3}H]NECA binding in human HeLa cells expressed as K_i in nM (n = 3) or percentage displacement of specific binding at a concentration of 1 µM (n = 2).

Table 3.13. Structure and adenosine receptor affinity data of series **XII-XV.**

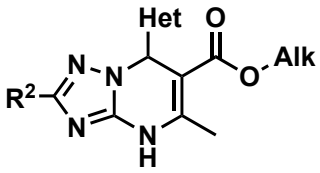

					K_i (nM) or % at 1 µM			
Compound	**Series**	**R^2**	**Het**	**Alk**	***h*A$_1$**[a)]	***h*A$_{2A}$**[b)]	***h*A$_{2B}$**[c)]	***h*A$_3$**[d)]
137	XII	CF_3	2-furyl	Et	22%	7%	839 ± 4	2%
138	XII	CF_3	2-furyl	*i*-Pr	30%	14%	589 ± 3	1%
139	XII	CF_3	3-furyl	Et	20%	25%	1219 ± 8	1%
140	XII	CF_3	3-furyl	*i*-Pr	8%	23%	1032 ± 5	1%
141	XII	CF_3	2-thienyl	Et	18%	17%	1%	3%
142	XII	CF_3	2-thienyl	*i*-Pr	16%	1%	54%	1%
143	XII	CF_3	3-thienyl	Et	1%	1%	840 ± 3.2	16%
144	XII	CF_3	3-thienyl	*i*-Pr	1%	2%	52%	7%
145	XIII	-COOMe	2-furyl	Et	27%	36%	429 ± 2	2%
146	XIII	-COOMe	2-furyl	*i*-Pr	7%	1%	41.4 ± 0.8	2%
147	XIII	-COOMe	3-furyl	Et	4%	8%	22%	3%
148	XIII	-COOMe	3-furyl	*i*-Pr	2%	19%	126 ± 2.2	11%
149	XIII	-COOMe	2-thienyl	Et	8%	5%	6%	1%
150	XIII	-COOMe	2-thienyl	*i*-Pr	17%	3%	1%	4%
151	XIII	-COOMe	3-thienyl	Et	18%	10%	5%	1%
152	XIII	-COOMe	3-thienyl	*i*-Pr	12%	4%	25%	3%
153	XIV	Ph	2-furyl	Et	47%	33%	52.1 ± 1.1	22%
154	XIV	Ph	2-furyl	*i*-Pr	39%	27%	25.3 ± 0.5	39%
155	XIV	Ph	3-furyl	Et	24%	19%	60.4 ± 1.6	10%
156	XIV	Ph	3-furyl	*i*-Pr	33%	42%	58.2 ± 2.1	22%
157	XIV	Ph	2-thienyl	Et	3%	1%	2%	15%
158	XIV	Ph	2-thienyl	*i*-Pr	41%	2%	31%	2%
159	XIV	Ph	3-thienyl	Et	9%	8%	25%	1%
160	XIV	Ph	3-thienyl	*i*-Pr	3%	4%	1%	2%
161	XV	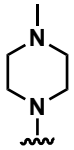	2-furyl	Et	32%	7%	3%	4%
162	XV		2-furyl	*i*-Pr	46%	5%	3630 ± 12	1%
163	XV		3-furyl	Et	1%	2%	4%	8%
164	XV		3-furyl	*i*-Pr	2%	6%	43%	13%
165	XV		2-thienyl	Et	4%	5%	3%	25%
166	XV		2-thienyl	*i*-Pr	1%	1%	25%	16%
167	XV		3-thienyl	Et	1%	2%	33%	18%
168	XV		3-thienyl	*i*-Pr	1%	1%	51%	21%
ISAM-140	-	-	-	-	20%	25%	3.49 ± 0.2	20%
DPCPX	-	-	-	-	2.20 ± 0.2	157 ± 3	73.2 ± 1.4	1722 ± 11
ZM241385	-	-	-	-	683 ± 4	1.9 ± 0.1	65.7 ± 1.1	863 ± 4
NECA	-	-	-	-	14.0 ± 1	20.0 ± 3	2400 ± 35	6.20 ± 0.9

[a)] Displacement of specific [^{3}H]DPCPX binding in human CHO cells expressed as K_i in nM (n = 3) or percentage displacement of specific binding at a concentration of 1 µM (n = 2). [b)] Displacement of specific [^{3}H]4-(2-[7-amino-2-(2-furyl)[1,2,4]triazolo[2,3-*a*][1,3,5]triazin-5-ylamino]ethyl)phenol binding in human HeLa cells expressed as K_i in nM (n = 3) or percentage displacement of specific binding at a concentration of 1 µM (n = 2). [c)] Displacement of specific [^{3}H]DPCPX binding in human HEK-293 cells expressed as K_i in nM (n = 3) or percentage displacement of specific binding at a concentration of 1 µM (n = 2). [d)] Displacement of specific [^{3}H]NECA binding in human HeLa cells expressed as K_i in nM (n = 3) or percentage displacement of specific binding at a concentration of 1 µM (n = 2).

Table 3.14. Structure and adenosine receptor affinity data of series **XVI-XVIII.** There is only a possibility of tautomerism when R^2 = H

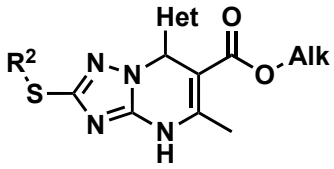

					K_i (nM) or % at 1 μM			
Compound	**Series**	**R^2**	**Het**	**Alk**	***h*A$_1$**[a)]	***h*A$_{2A}$**[b)]	***h*A$_{2B}$**[c)]	***h*A$_3$**[d)]
169	XVI	H	2-furyl	Et	1%	2%	9%	3%
170	XVI	H	2-furyl	*i*-Pr	2%	2%	17%	3%
171	XVI	H	3-furyl	Et	2%	10%	2%	6%
172	XVI	H	3-furyl	*i*-Pr	2%	2%	3%	1%
173	XVI	H	2-thienyl	Et	28%	19%	9%	1%
174	XVI	H	2-thienyl	*i*-Pr	2%	4%	2%	11%
175	XVI	H	3-thienyl	Et	9%	2%	3%	13%
176	XVI	H	3-thienyl	*i*-Pr	2%	3%	7%	4%
177	XVII	Me	2-furyl	Et	10%	13%	49.2 ± 1.6	9%
178	XVII	Me	2-furyl	*i*-Pr	8%	6%	17.3 ± 0.6	18%
179	XVII	Me	3-furyl	Et	2%	24%	123 ± 2	1%
180	XVII	Me	3-furyl	*i*-Pr	1%	3%	29.2 ± 1.1	6%
181	XVII	Me	2-thienyl	Et	2%	9%	15%	9%
182	XVII	Me	2-thienyl	*i*-Pr	6%	6%	22%	15%
183	XVII	Me	3-thienyl	Et	3%	4%	722 ± 4	23%
184	XVII	Me	3-thienyl	*i*-Pr	5%	1%	17%	2%
185	XVIII	Bn	2-furyl	Et	20%	4%	4%	15%
186	XVIII	Bn	2-furyl	*i*-Pr	1%	2%	9%	3%
187	XVIII	Bn	3-furyl	Et	6%	5%	19%	12%
188	XVIII	Bn	3-furyl	*i*-Pr	16%	21%	6%	20%
189	XVIII	Bn	2-thienyl	Et	3%	4%	4%	2%
190	XVIII	Bn	2-thienyl	*i*-Pr	1%	3%	2%	5%
191	XVIII	Bn	3-thienyl	Et	10%	11%	8%	3%
192	XVIII	Bn	3-thienyl	*i*-Pr	5%	3%	14%	10%
ISAM-140		-	-	-	20%	25%	3.49 ± 0.2	20%
DPCPX		-	-	-	2.20 ± 0.2	157 ± 3	73.2 ± 1.4	1722 ± 11
ZM241385		-	-	-	683 ± 4	1.9 ± 0.1	65.7 ± 1.1	863 ± 4
NECA		-	-	-	14.0 ± 1	20.0 ± 3	2400 ± 35	6.20 ± 0.9

[a)] Displacement of specific [^{3}H]DPCPX binding in human CHO cells expressed as K_i in nM (n = 3) or percentage displacement of specific binding at a concentration of 1 μM (n = 2). [b)] Displacement of specific [^{3}H]4-(2-[7-amino-2-(2-furyl)[1,2,4]triazolo[2,3-*a*][1,3,5]triazin-5-ylamino]ethyl)phenol binding in human HeLa cells expressed as K_i in nM (n = 3) or percentage displacement of specific binding at a concentration of 1 μM (n = 2). [c)] Displacement of specific [^{3}H]DPCPX binding in human HEK-293 cells expressed as K_i in nM (n = 3) or percentage displacement of specific binding at a concentration of 1 μM (n = 2). [d)] Displacement of specific [^{3}H]NECA binding in human HeLa cells expressed as K_i in nM (n = 3) or percentage displacement of specific binding at a concentration of 1 μM (n = 2).

Table 3.15. Structure and adenosine receptor affinity data of series **XIX-XXI.**

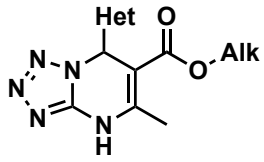

193-200

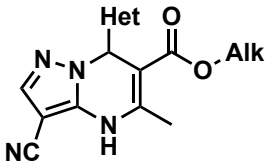

201-208

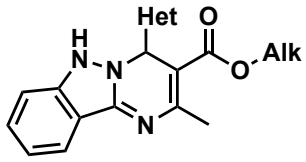

209-216

				K_i (nM) or % at 1 μM			
Compound	**Series**	**Het**	**Alk**	***h*A$_1$**[a)]	***h*A$_{2A}$**[b)]	***h*A$_{2B}$**[c)]	***h*A$_3$**[d)]
193	XIX	2-furyl	Et	4%	3%	511 ± 8	2%
194	XIX	2-furyl	*i*-Pr	6%	4%	257 ± 3	5%
195	XIX	3-furyl	Et	6%	5%	23%	13%
196	XIX	3-furyl	*i*-Pr	11%	2%	102 ± 8	13%
197	XIX	2-thienyl	Et	16%	6%	7%	16%
198	XIX	2-thienyl	*i*-Pr	3%	2%	12%	8%
199	XIX	3-thienyl	Et	2%	5%	29%	9%
200	XIX	3-thienyl	*i*-Pr	1%	2%	482 ± 6	11%
201	XX	2-furyl	Et	13%	3%	6%	3%
202	XX	2-furyl	*i*-Pr	12%	3%	9%	9%
203	XX	3-furyl	Et	20%	2%	1%	1%
204	XX	3-furyl	*i*-Pr	11%	6%	1%	2%
205	XX	2-thienyl	Et	1%	5%	7%	1%
206	XX	2-thienyl	*i*-Pr	3%	5%	1%	11%
207	XX	3-thienyl	Et	12%	4%	5%	3%
208	XX	3-thienyl	*i*-Pr	16%	3%	1%	4%
209	XXI	2-furyl	Et	5%	2%	9%	15%
210	XXI	2-furyl	*i*-Pr	10%	9%	3%	1%
211	XXI	3-furyl	Et	32%	22%	13%	22%
212	XXI	3-furyl	*i*-Pr	8%	3%	14%	11%
213	XXI	2-thienyl	Et	2%	1%	7%	16%
214	XXI	2-thienyl	*i*-Pr	3%	9%	6%	11%
215	XXI	3-thienyl	Et	18%	6%	17%	8%
216	XXI	3-thienyl	*i*-Pr	19%	9%	19%	1%
ISAM-140	-	-	-	20%	25%	3.49 ± 0.2	20%
DPCPX	-	-	-	2.20 ± 0.2	157 ± 3	73.2 ± 1.4	1722 ± 11
ZM241385	-	-	-	683 ± 4	1.9 ± 0.1	65.7 ± 1.1	863 ± 4
NECA	-	-	-	14.0 ± 1	20.0 ± 3	2400 ± 35	6.20 ± 0.9

[a)] Displacement of specific [^{3}H]DPCPX binding in human CHO cells expressed as K_i in nM (n = 3) or percentage displacement of specific binding at a concentration of 1 μM (n = 2). [b)] Displacement of specific [^{3}H]4-(2-[7-amino-2-(2-furyl)[1,2,4]triazolo[2,3-*a*][1,3,5]triazin-5-ylamino]ethyl)phenol binding in human HeLa cells expressed as K_i in nM (n = 3) or percentage displacement of specific binding at a concentration of 1 μM (n = 2). [c)] Displacement of specific [^{3}H]DPCPX binding in human HEK-293 cells expressed as K_i in nM (n = 3) or percentage displacement of specific binding at a concentration of 1 μM (n = 2). [d)] Displacement of specific [^{3}H]NECA binding in human HeLa cells expressed as K_i in nM (n = 3) or percentage displacement of specific binding at a concentration of 1 μM (n = 2).

Table 3.16. Structure and adenosine receptor affinity data of series **XXII-XXV**.

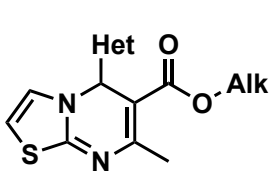

217-224

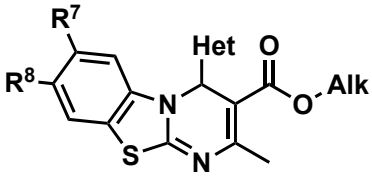

225-248

						K_i (nM) or % at 1 µM			
Compound	**Series**	**R^7**	**R^8**	**Het**	**Alk**	***h*A$_1$**[a)]	***h*A$_{2A}$**[b)]	***h*A$_{2B}$**[c)]	***h*A$_3$**[d)]
217	XXII	-	-	2-furyl	Et	24%	7%	15%	1%
218	XXII	-	-	2-furyl	*i*-Pr	1%	1%	15%	4%
219	XXII	-	-	3-furyl	Et	20%	2%	27%	12%
220	XXII	-	-	3-furyl	*i*-Pr	2%	3%	43%	4%
221	XXII	-	-	2-thienyl	Et	14%	4%	3%	5%
222	XXII	-	-	2-thienyl	*i*-Pr	7%	3%	10%	3%
223	XXII	-	-	3-thienyl	Et	16%	2%	17%	4%
224	XXII	-	-	3-thienyl	*i*-Pr	11%	8%	22%	3%
225	XXIII	H	H	2-furyl	Et	24%	29%	9.40 ± 0.4	4%
226	XXIII	H	H	2-furyl	*i*-Pr	1%	16%	11.6 ± 0.8	5%
227	XXIII	H	H	3-furyl	Et	17%	47%	8.60 ± 0.3	6%
228	XXIII	H	H	3-furyl	*i*-Pr	5%	33%	9.10 ± 0.4	1%
229	XXIII	H	H	2-thienyl	Et	6%	3%	138 ± 4	6%
230	XXIII	H	H	2-thienyl	*i*-Pr	3%	1%	214 ± 4	2%
231	XXIII	H	H	3-thienyl	Et	1%	4%	11.2 ± 0.8	3%
232	XXIII	H	H	3-thienyl	*i*-Pr	2%	8%	44.2 ± 0.4	1%
233	XXIV	Cl	H	2-furyl	Et	34%	36%	76.7 ± 1.2	2&
234	XXIV	Cl	H	2-furyl	*i*-Pr	1%	1%	48%	4%
235	XXIV	Cl	H	3-furyl	Et	2%	2%	65.4 ± 2.2	2%
236	XXIV	Cl	H	3-furyl	*i*-Pr	3%	23%	99.2 ± 1.2	12%
237	XXIV	Cl	H	2-thienyl	Et	13%	11%	14%	27%
238	XXIV	Cl	H	2-thienyl	*i*-Pr	14%	12%	8%	6%
239	XXIV	Cl	H	3-thienyl	Et	8%	10%	37.1 ± 2.1	11%
240	XXIV	Cl	H	3-thienyl	*i*-Pr	8%	2%	12%	1%
241	XXVI	H	Cl	2-furyl	Et	13%	43%	14.5 ± 0.6	17%
242	XXVI	H	Cl	2-furyl	*i*-Pr	2%	15%	30.8 ± 0.5	1%
243	XXVI	H	Cl	3-furyl	Et	20%	90.7 ± 4	4.30 ± 0.2	3%
244	XXVI	H	Cl	3-furyl	*i*-Pr	8%	49%	10.2 ± 0.9	5%
245	XXVI	H	Cl	2-thienyl	Et	18%	29%	61.4 ± 2.1	10%
246	XXVI	H	Cl	2-thienyl	*i*-Pr	5%	21%	165 ± 4	8%
247	XXVI	H	Cl	3-thienyl	Et	1%	5%	77.2 ± 1.6	5%
248	XXVI	H	Cl	3-thienyl	*i*-Pr	4%	20%	52.8 ± 1.3	1%
ISAM-140	-	-	-	-	-	20%	25%	3.49 ± 0.2	20%
DPCPX	-	-	-	-	-	2.20 ± 0.2	157 ± 3	73.2 ± 1.4	1722 ± 11
ZM241385	-	-	-	-	-	683 ± 4	1.9 ± 0.1	65.7 ± 1.1	863 ± 4
NECA	-	-	-	-	-	14.0 ± 1	20.0 ± 3	2400 ± 35	6.20 ± 0.9

[a)] Displacement of specific [^{3}H]DPCPX binding in human CHO cells expressed as K_i in nM (n = 3) or percentage displacement of specific binding at a concentration of 1 μM (n = 2). [b)] Displacement of specific [^{3}H]4-(2-[7-amino-2-(2-furyl)[1,2,4]triazolo[2,3-*a*][1,3,5]triazin-5-ylamino]ethyl)phenol binding in human HeLa cells expressed as K_i in nM (n = 3) or percentage displacement of specific binding at a concentration of 1 μM (n = 2). [c)] Displacement of specific [^{3}H]DPCPX binding in human HEK-293 cells expressed as K_i in nM (n = 3) or percentage displacement of specific binding at a concentration of 1 μM (n = 2). [d)] Displacement of specific [^{3}H]NECA binding in human HeLa cells expressed as K_i in nM (n = 3) or percentage displacement of specific binding at a concentration of 1 μM (n = 2).

Table 3.17. Structure and adenosine receptor affinity data of racemic and enantiomers of selected ligands and previous reported derivatives.

Selective A_{2B}AR antagonists

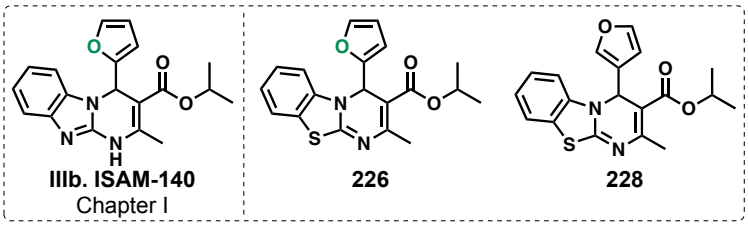

IIIb. ISAM-140
Chapter I

226

228

Dual A_{2A}AR/A_{2B}AR antagonists

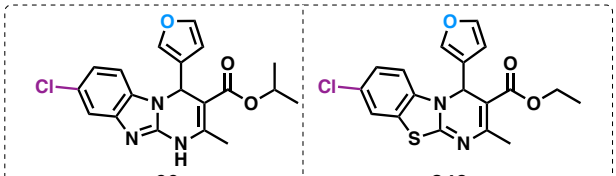

60
Chapter I

243

Compound	K_i (nM) or % at 1 μM			
	hA_1[a)]	hA_{2A}[b)]	hA_{2B}[c)]	hA_3[d)]
(±)-ISAM-140 (Chapter I)	20%	25%	3.49 ± 0.2	2%
(*R*)-ISAM-140 (Chapter I)	4%	2%	17%	2%
(*S*)-ISAM-140 (Chapter I)	2%	2%	0.89 ± 0.2	4%
(±)-226	1%	16%	11.6 ± 0.8	5%
(*R*)-226	26%	10%	19.2 ± 1.2	12%
(*S*)-226	24%	4%	4.30 ± 0.6	1%
(±)-228	5%	33%	9.10 ± 0.4	1%
(*S*)-228	18%	8%	18.7 ± 3	3%
(*R*)-228	6%	44%	2.90 ± 0.4	20%
(±)-60(Chapter I)	37%	176 ± 4	6.10 ± 0.7	25%
(*S*)-60 (Chapter I)	24%	25%	53%	19%
(*R*)-60 (Chapter I)	37%	96.3 ± 6	2.60 ± 0.3	25%
(±)-243	20%	90.7 ± 4	4.30 ± 0.2	3%
(*S*)-243	5%	109 ± 6	6.10 ± 0.6	20%
(*R*)-243	1%	27.3 ± 1.8	1.20 ± 0.2	1%
ISAM-140	20%	25%	3.49 ± 0.2	20%
DPCPX	2.20 ± 0.2	157 ± 3	73.24 ± 1.4	1722 ± 11
ZM241385	683 ± 4	1.9 ± 0.1	65.7 ± 1.1	863 ± 4
NECA	14.0 ± 1	20.0 ± 3	2400 ± 35	6.20 ± 9

[a)] Displacement of specific [^{3}H]DPCPX binding in human CHO cells expressed as K_i in nM (n = 3) or percentage displacement of specific binding at a concentration of 1 μM (n = 2). [b)] Displacement of specific [^{3}H]4-(2-[7-amino-2-(2-furyl)[1,2,4]triazolo[2,3-*a*][1,3,5]triazin-5-ylamino]ethyl)phenol binding in human HeLa cells expressed as K_i in nM (n = 3) or percentage displacement of specific binding at a concentration of 1 μM (n = 2). [c)] Displacement of specific [^{3}H]DPCPX binding in human HEK-293 cells expressed as K_i in nM (n = 3) or percentage displacement of specific binding at a concentration of 1 μM (n = 2). [d)] Displacement of specific [^{3}H]NECA binding in human HeLa cells expressed as K_i in nM (n = 3) or percentage displacement of specific binding at a concentration of 1 μM (n = 2). Enantiomers were separated by preparative chiral HPLC (IE-3 Chiralpack) and configuration at the stereocenter established by circular dichroism.

Table 3.18. Functional data of compounds **114**, **146**, **226**, and **243** in $A_{2A}AR$ and $A_{2B}AR$.

	hA_{2A}		*h*A_{2B}	
Compound	**K_i**	**K_B**[a)]	**K_i**	**K_B**[b)]
114	-	-	83.5 ± 0.8	**72.9 ± 3.2**
146	-	-	41.4 ± 0.8	29.6 ± 2.0
226	-	-	11.6 ± 0.8	7.20 ± 1.1
243	90.7 ± 4	45.2 ± 2	4.30 ± 0.2	2.40 ± 1.4

[a)] Inhibition of cAMP production in HeLa-A_{2A} cells [b)] Inhibition of cAMP production in HEK-293-A_{2B} cells.

3.2.4 Analysis of the Structure-Activity Relationship and Molecular Modeling

We initially explored the impact of the scaffold-hopping strategy as structure affinity (SAR) and structure-selectivity (SSR) relationships, arising from comparison of pharmacological data obtained for the recently synthesized series (Tables 3.10-16) and the model series (Table 3.9), in all cases evaluated as racemic mixtures. The defined SAR is accompanied and advised by docking and free energy perturbation (FEP) calculations using our refined computational 3D model of the *h*A_{2B}AR. The biological evaluation of the 168 compounds revealed 25 ligands (Figure 3.26) with attractive A_{2B}AR affinity (K_i < 100 nM) and selectivity (> 1000-fold), from which 9 ligands exhibit remarkable A_{2B}AR affinity (K_i < 25 nM) [e.g. compounds **178** (Table 3.14), **225**, **226**, **227**, **228**, **231**, **241**, **243**, **244** (Table 3.16)]. The available data show clear SAR trends, being the benzo[4,5]thiazolo[3,2-*a*]pyrimidines (and their 8-chlorine derivatives) the most potent ligands obtained for A_{2B}AR antagonism and relevant compounds from structural points of view [Series **XXIII** and **XXV** (Table 3.16)].

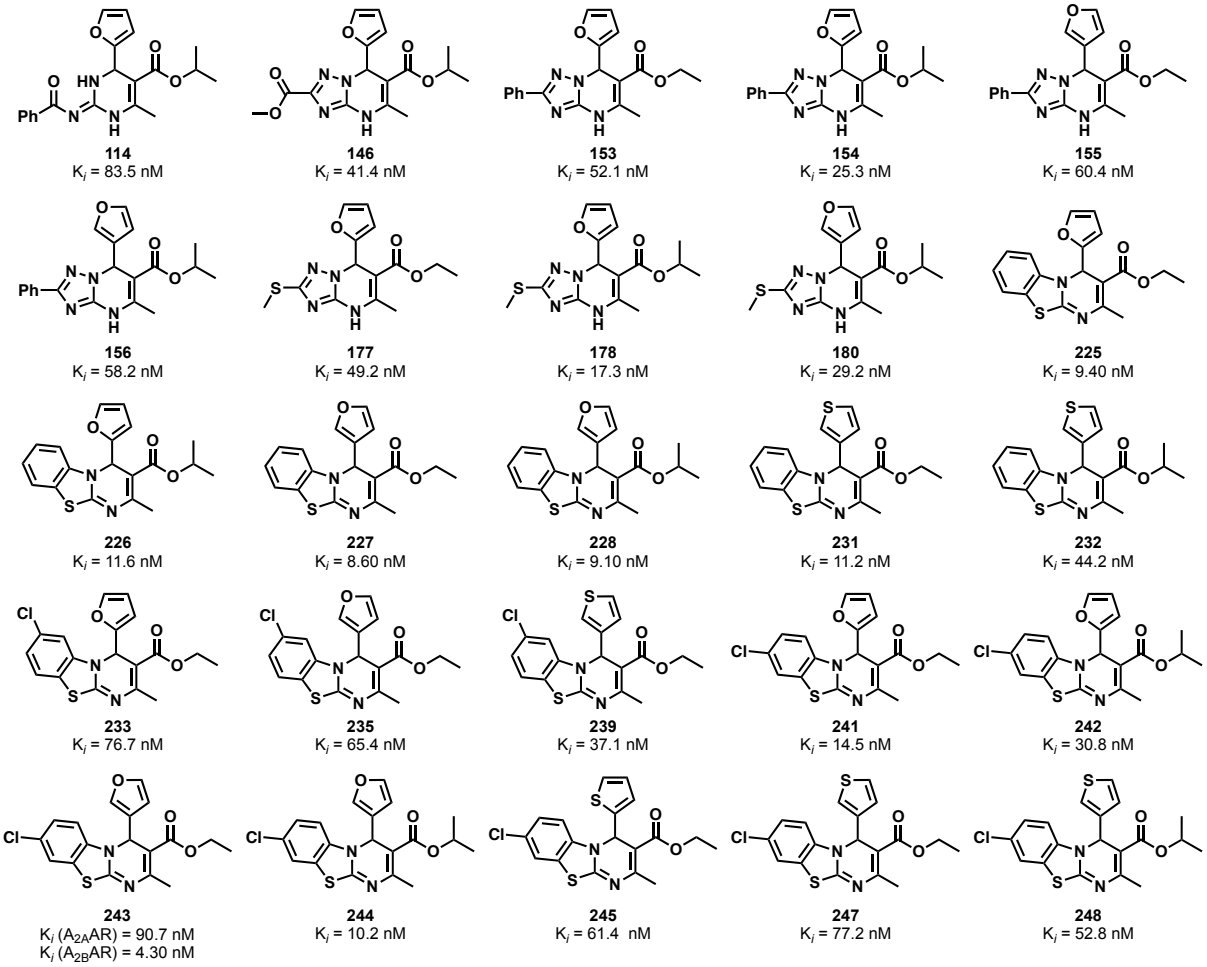

Figure 3.26. Ligands with better A_{2B}AR affinity (K_i < 100 nM) obtained in this chapter.

Comparative analysis of the binding data obtained for model series and ligands of monocyclic family (Series **V–XI**) prove that the bicyclic ring opening, leaving different mono- (or di-) substituted amine residues at position 2 of the monocyclic ring, has a negative impact on the $A_{2B}AR$ affinity. These results were not anticipated by early docking studies, that suggested the obtained compounds could bind the $A_{2B}AR$ with moderate affinity.[141] 2-Methylamino, 2,2-dimethylamino, 2-phenylamino and 2-acetamido monocyclic derivatives (Series **V–VIII**) are totally inactive. Interestingly, monocyclic derivatives bearing a benzyl or sulfonyl groups at the exocyclic amino exhibit moderate $A_{2B}AR$ affinity. Only 9 over 56 ligands in this subset of compounds show $A_{2B}AR$ binding affinity (K_i = 83.5 – 480 nM), containing all of them a 2- or 3-furyl group at position 4 of the monocyclic core (Series **IX–XI**). Ligands bearing a thienyl ring at position 4 of the monocyclic scaffold are all inactive. The best substitution pattern is 2-furyl as heteroaromatic ring (Het) and isopropyl as alcoxy residue at the ester moiety (Alk) [e.g compounds **114** (Series **IX**, Table 3.11), **122** (Series **X**, Table 3.11) and **130** (Series **XI**,Table 3.12)] as is already the case in the model series **I–III** (Table 3.10).

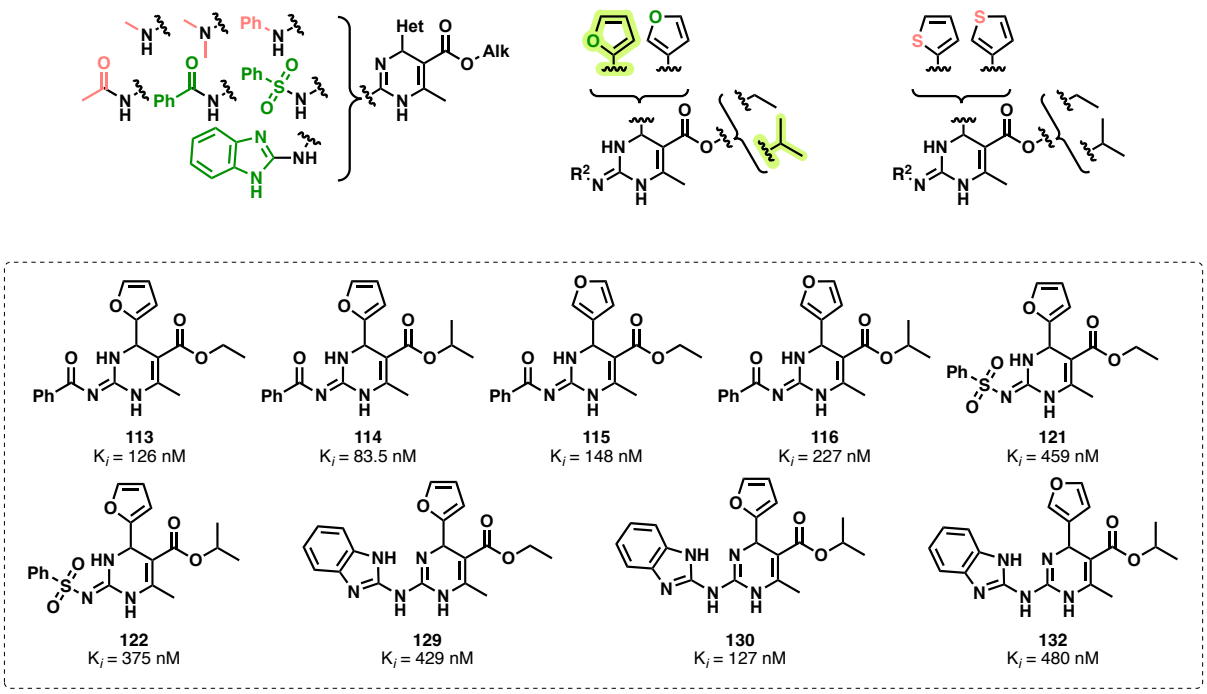

Figure 3.27. SAR of subset 2.1 and active compounds obtained. In red or green: substitutions generating inactive and active compounds, respectively. Highlighted in green: best substitution pattern.

The comparative analysis of the binding data and structure of the 2-aminosubstituted monocyclic series (**V**-**XI**) inspired a structural study to better understand the molecular clue of the observed affinity differences among series. This analysis suggested that, while highly similar, the different series could be grouped attending the predominant tautomer in each subset, and that the main contributor to tautomer stability is the substitution pattern at the amino group at position 2 of the pyrimidine core. Figure 3.28A contains a representation of the three most likely stable (predominant) tautomers for these series. As observed, the main differences among the tautomers is the position of the imino group, that can be exocyclic (tautomer 3) or endocyclic (tautomers 1 and 2). The fact that substitution pattern at the amino group govern the predominant tautomers can be easily comprobed for the 2-dimethylaminoderivatives (series **VI**) which do not favour the exocyclic tautomer.

Using a combination of NMR techniques, the predominant tautomer in DMSO of each monocyclic series (**V–XI**) has been established. It was observed that for all the inactive series [series **V** (R = Me, R' = H), series **VI**, (R = R' = Me), series **VII** (R = Ph, R' = H) and series **VIII** (R = COMe, R' = H) tautomer 1 (wich contain the imino group endocyclic, between C2 and N3) thus bearing hydrogen atoms at N1 and N2) seems to be the predominant tautomer (Figure 3.28, Tautomer 1). Interestingly, NMR studies also revealed that monocyclic series eliciting some noticeable A_{2B}AR affinity [series **IX** (R = COPh, R' = H) and **X** (R = SO_2Ph, R' = H)], on the contrary, predominantly exist in the tautomeric form 3 (Figure 3.28, Tautomer 3).

A joint rationalization of predominant tautomers and the proposed binding modes of these series (that highlight the importance of the double hydrogen bond established in our compounds with $Asn^{6.55}$) would enable to understand the observes differences. Thus, series that predominantly exist in tautomer 3 could enable to stablish the favorable double interaction with $Asn^{6.55}$. To corroborate these observations, we selected a representative ligand of each series (bearing 2-furyl as exocyclic heterocycle and an isopropyl residue as the ester moiety) and performed in deep docking studies.

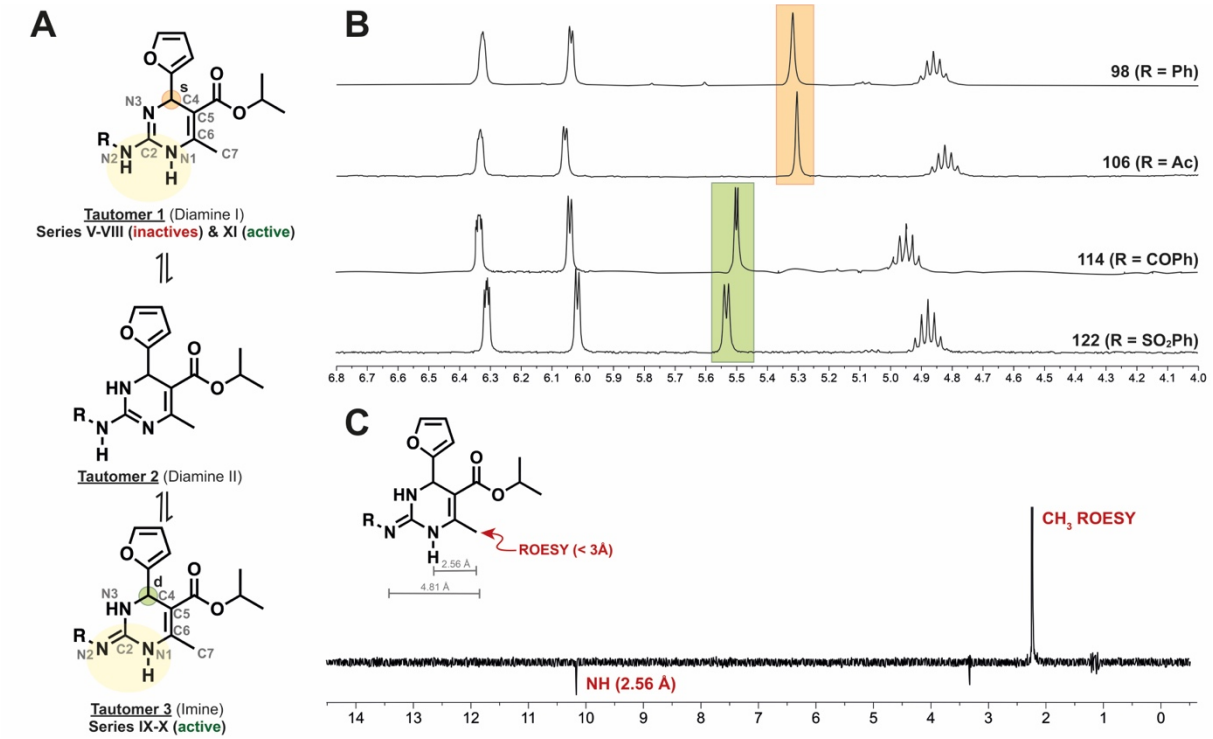

Figure 3.28. A) Different possible tautomers for the monocyclic series in DMSO-d_6. In yellow: zone of double hydrogen bond interaction with Asn$^{6.55}$ B) ^{1}H NMR peaks (4.0 – 6.8 ppm) for inactive compounds **98** and **106**; and active compounds **114** and **122**. Singlet at ~5.3 ppm (orange) confirms C2-N3 double bond (diamine form), while doublet at ~5.5 ppm (green) could be a C2-N2 (Tautomer 1) or C2-N1 (Tautomer 2) double bond. **C)** ROESY example of CH_3 (C7) irradiation. It is only possible to see the ROESY effect (< 3Å) if the protonated nitrogen is N1, confirming C2-N2 imine tautomeric state (Tautomer 3).

Interestingly, NMR analysis of the series **XI** shows diamine I (Tautomer 1) as the predominant tautomer, but pharmacology assays show moderate affinity (e.g., **130**, K_i = 127 nM). This may be due to the presence of the benzimidazole ring as a substituent (Figure 3.29), being able to form double (and triple) hydrogen bonds with Asn$^{6.55}$ (Figure 3.30).

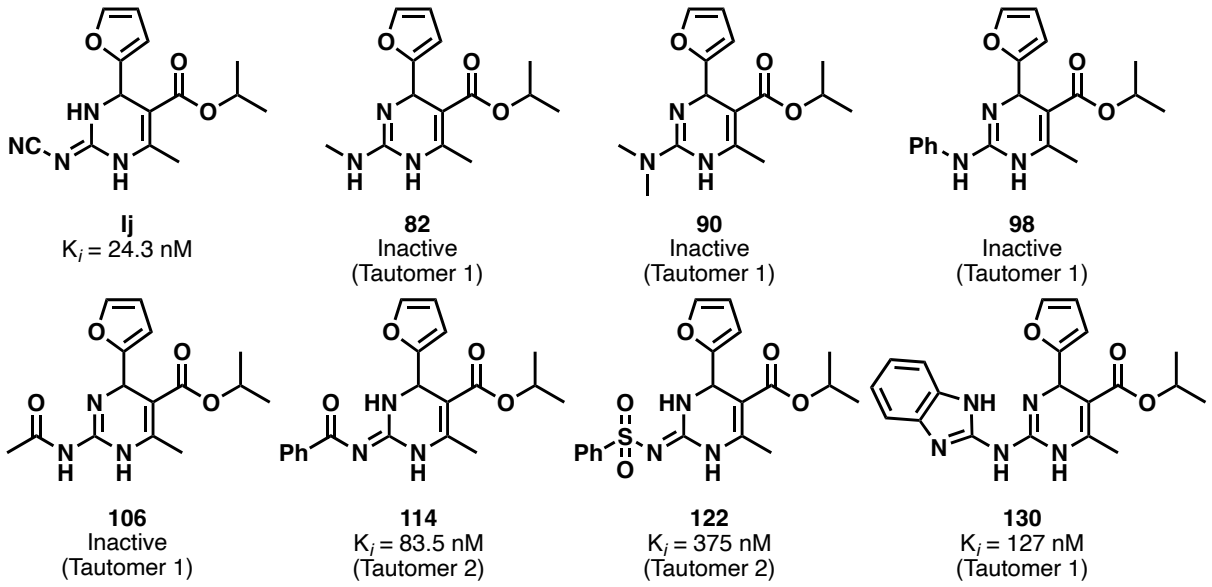

Figure 3.29. $A_{2B}AR$ binding affinity of monocyclic compounds for docking analysis.

In comparison with binding orientation of model Series **I**[142] (Figure 3.30A) with two hydrogen bonds with $Asn^{6.55}$, the series with tautomer I as the predominant form are only able to establish one hydrogen bond with $Asn^{6.55}$ (Figure 3.30B-D**)**, being the substituents of these structures (methyl, dimethyl and phenyl) deleterious for the $A_{2B}AR$ affinity. In the series with carbonyl or sulfonyl substituents (series **VIII–X**) a differentiated behavior is observed. NMR studies reveal that 2-acetamido derivatives (**105–112**) mostly exists as the tautomer I, preventing the formation of the double hydrogen bond with $Asn^{6.55}$, thus resulting in compounds with no affinity for $A_{2B}AR$ (Figure 3.30E). In clear contrast, the compounds of series **IX** (**113-120**, K_i = 83.5 – 227 nM) and **X** (**121–122**, K_i = 375 – 459 nM) are capable of forming hydrogen bond with $Asn^{6.55}$. Differences between series **IX** and **X** can be rationalized considering the interaction between aromatic phenyl substituent with $Trp^{6.48}$ (Figure 3.30F-G). While series **IX** have the possibility of forming a double hydrogen bond with $Asn^{6.55}$, for series **X** it is not observed in docking studies.

Compounds with the most possible tautomeric forms are those of the series **XI**. As shown in Figure 3.30H, four hydrogen bonds are observed, one intramolecular (stabilizing the structure) and three with $Asn^{6.55}$. The binding data for this series are not as expected based on its binding mode (**129**, **130** and **132**, K_i = 127 – 480 nM), probably due to the size of the benzimidazole substituent. In summary, none of the compounds synthesized with this structure shows better affinity than the previous compounds (model series **I**), clarifying the role of the substituent at position 2 for the monocyclic series.

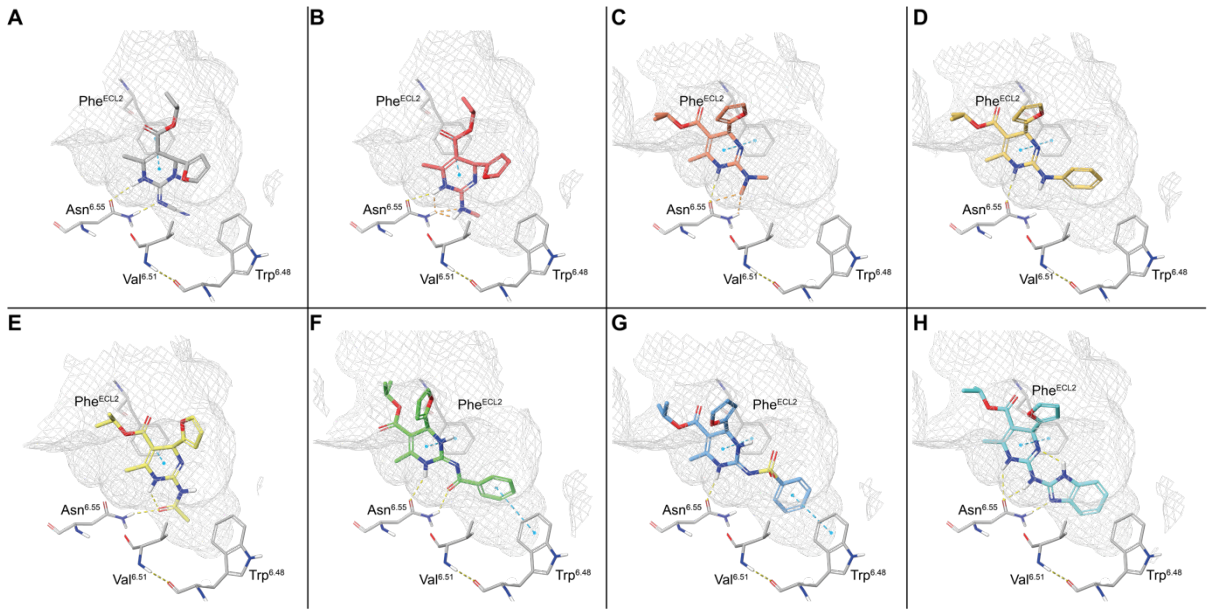

Figure 3.30. Docking poses for monocyclic Series. **A) Ij** (model Series **I**), **B) 82** (Series **V**), **C) 90** (Series **VI**), **D) 98** (Series **VII**), **E) 106** (Series **VIII**), **F) 114** (Series **IX**), **G) 122** (Series **X**) and **H) 130** (Series **XI**). Receptor is $A_{2B}AR$ homology model from $A_{2A}AR$ (PDB: 3EML), and grey mesh represent $A_{2B}AR$ binding site. Note the effect of the tautomerization on hydrogen bonds with Asn$^{6.55}$. Yellow dashed lines: hydrogen bonds, blue dashed lines: π-π interactions, orange dashed lines: bad contacts.

The next series of ligands to be analyzed are the bicyclic derivatives **137**–**208** The adenosinergic profile obtained for bicyclic compounds for 2-substituted family (Series **XII**–**XVIII**) and bioisosteric replacements (series **XIX-XXIII**) is summarized in Figure 3.33. As in previous series, independently of the scaffold, only compounds containing furyl group on the stereogenic center maintain affinity for the $A_{2B}AR$ (K_i = 17.3 – 3630 nM), except for the low affinity observed for thienyl derivatives **183** (series **XVII**, K_i = 722 nM) and **200** (series **XIX**, K_i = 482 nM).

Substitution of position 2 of model series **II** (Alkyl 7-heteroaryl-5-methyl-4,7-dihydro-[1,2,4]triazolo[1,5-a]pyrimidine-6-carboxylates) explored in series **XII**–**XVIII** (trifluoromethyl, methoxycarbonyl, phenyl, *N*-methylpiperazine, thiol, methyltio and benzylthio) appears to be a good strategy, with several representative molecules with K_i below 100 nM (Figure 3.31).

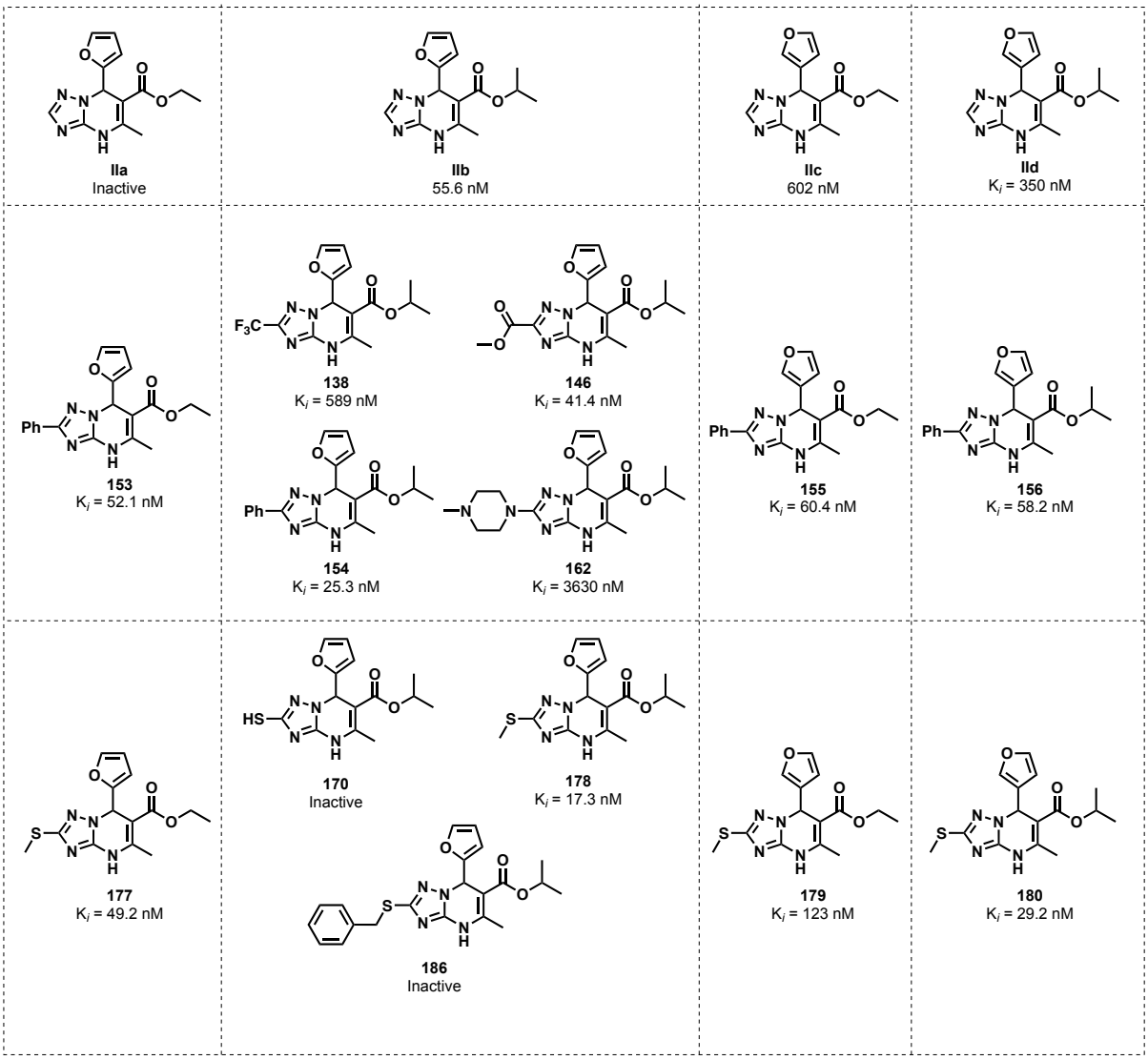

Figure 3.31. Model series II and representative ligands for subset 2.2 (2-substituted bicycles).

Series **XII**, trifluoromethyl derivatives (Figure 3.33, Table 3.13), exhibits only low affinity with three derivatives being submicromolar, none of the compounds surpassed the affinity of the model series **II** (Figure 3.33). However, compounds of the series **XIII** (**145-152**) and particularly **XIV** (**153-160**) showed high affinity at the A_{2B}AR, improving in many cases the affinity shown in the model series **II** (Figure 3.33). As in monocycles series, best substitution pattern is 2-furyl as heteroaromatic ring (Het) and isopropyl as alkoxy residue in the ester moiety (Alk), being always the best compounds of these series [e.g., **138**, **146**, **154**].

Substitution with heteroatom-based groups (*N*-methylpiperazine, thiol, methylthio and benzylthio) was explored [series **XV-XVIII** (Figure 3.33)]. Only one compound within the methylpiperazinyl derivatives (series XV) has measurable (but very low) affinity (**162**, K_i =

3630 nM), probably because the non-aromatic bulky substituent prevents the formation of the hydrogen double bond (Figure 3.34E). Among the sulfur-based groups, series **XVI** shows a significant affinity. Considering series **XVI**; in addition to their different tautomers, we should considerate that contain an ionizable -SH group, there is a possibility that in the solution these compounds exist as anions and for this reason do not bind within the hydrophobic binding site. This was confirmed by quantum chemical pKa calculations performed at the m062x/6-311+g(d,p) level of theory with thiophenol as the reference base. The calculated pKa of the thiol group in the model compound is 3.54, which suggest that these compounds are anions under physiological conditions. On the other hand, due to the introduction of a methyl group, series **XVII** remains in a neutral form and binds perfectly as such within the binding site (Figure 3.34F-G). In fact, the series **XVII** contains some of the best compounds obtained in this exploration, far surpassing the affinity of the model series **II** [e.g., **177** (K_i = 49.2 nM) vs **IIa** (inactive), **178** (K_i = 17.3 nM) vs **IIb** (K_i = 55.6 nM), **179** (K_i = 123 nM) vs **IIc** (K_i = 602 nM) and **180** (K_i = 29.2 nM) vs **IId** (K_i = 350 nM)]. The predicted binding mode of series **XII–XVIII**, in comparison with model series **II**, is shown in Figure 3.34A-J. The adenosinergic profile correlates very well with the binding mode showed. Methoxycarbonyl, phenyl and methylthio- substituents allows the formation of double hydrogen bond with $Asn^{6.55}$, enabling π-π interactions with Phe^{ECL2} and $Trp^{6.48}$, stabilizing receptor binding (Figure 3.34B-H). Focusing on compounds with sulfur-based groups, while thiol (series **XVI**) and methylthio (series **XVII**) have very similar sizes (Figure 3.34F-G), the possible ionization of the thiol group obstructs binding to the receptor, whereas the methylated derivatives fit perfectly. On the other hand, benzylthio substituent (series **XVIII**) seems to be too bulky to fit at A_{2B}AR (Figure 3.34H).

Structure modification of model series **II** and **III** was studied in series **XIX-XXIII** (Figure 3.32). Series **XIX** is based on the bioisosteric replacements of the CH of the triazole by N, using classical isostery, while series **XX** contain compounds in which one of the nitrogen of the triazole falls outside the aromatic ring as a cyano group. Whereas the presence of tetrazole as the pentagonal ring of the bicycle maintains [or improves (e.g. **196**: Het = 3-furyl, Alk = *i*-Pr, K_i = 102 nM, Figure 3.33)] the affinity compared to model series **II** (e.g. **IId**: Het = 3-furyl, Alk = *i*-Pr, K_i = 350 nM, Figure 3.33), the introduction of a cyano group (series **XX**) is deleterious for the A_{2B}AR affinity with complete abolition of the affinity. Series **XXI**, based on the inversion of tricyclic structure generate totally inactive compounds at all four ARs subtypes

by preventing the formation of the double hydrogen bond with Asn$^{6.55}$ and π-π stabilization with Phe^{EL2} (Figure 3.34K). Series **XXII-XXIII** were designed to explore the effect of the loss of the double hydrogen bond in bicyclic and tricyclic scaffolds.

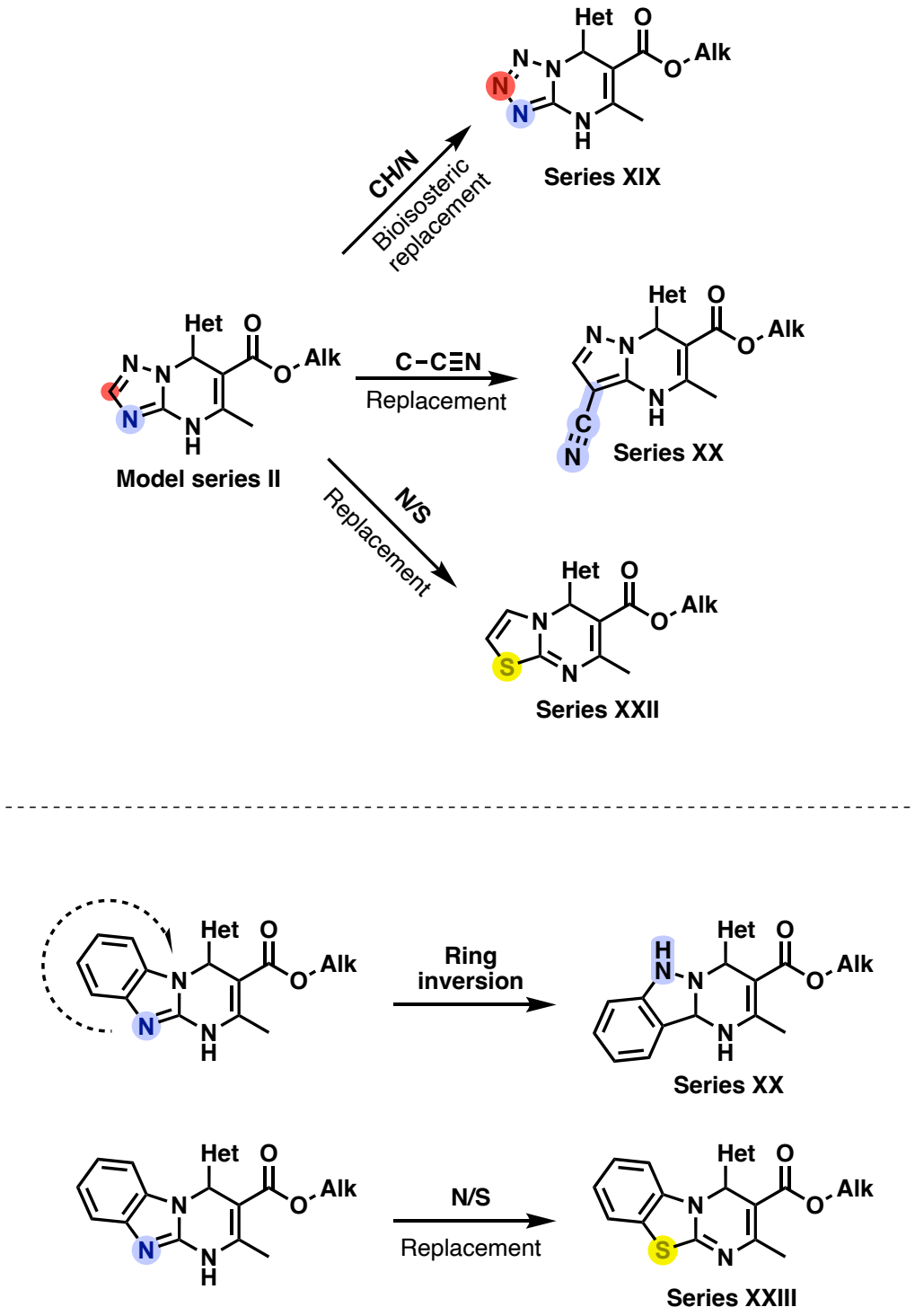

Figure 3.32. Structure modifications of model series **II** and **III**.

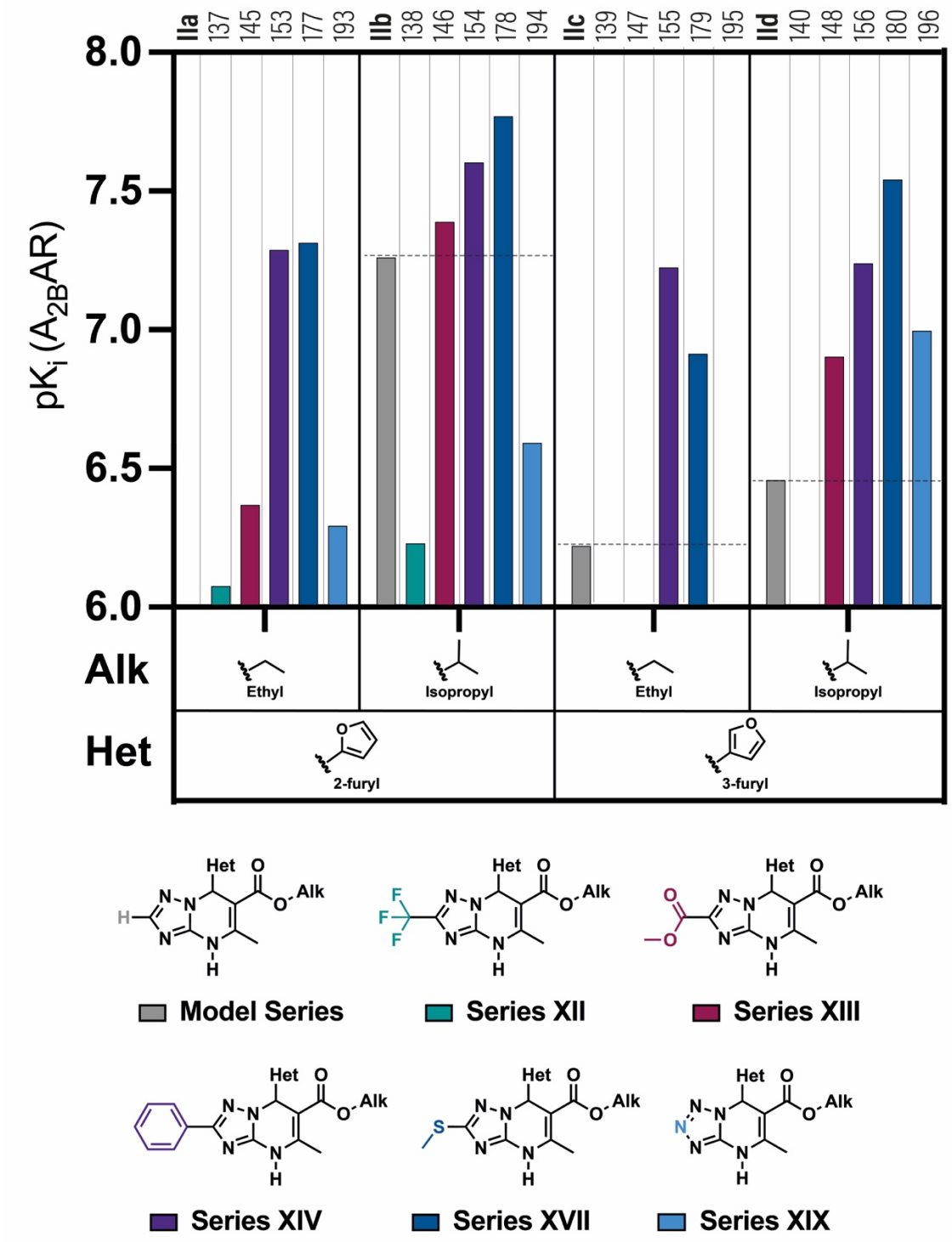

Figure 3.33. Interleaved bars chart showing $A_{2B}AR$ pK_i [-log(K_i)] for bicyclic series showing $A_{2B}AR$ binding affinity (**XII-XIV, XVII** and **XIX**) compared with model series II. Compounds with thienyl as a heterocyclic residue are not shown in this graphic as they have no relevant affinity.

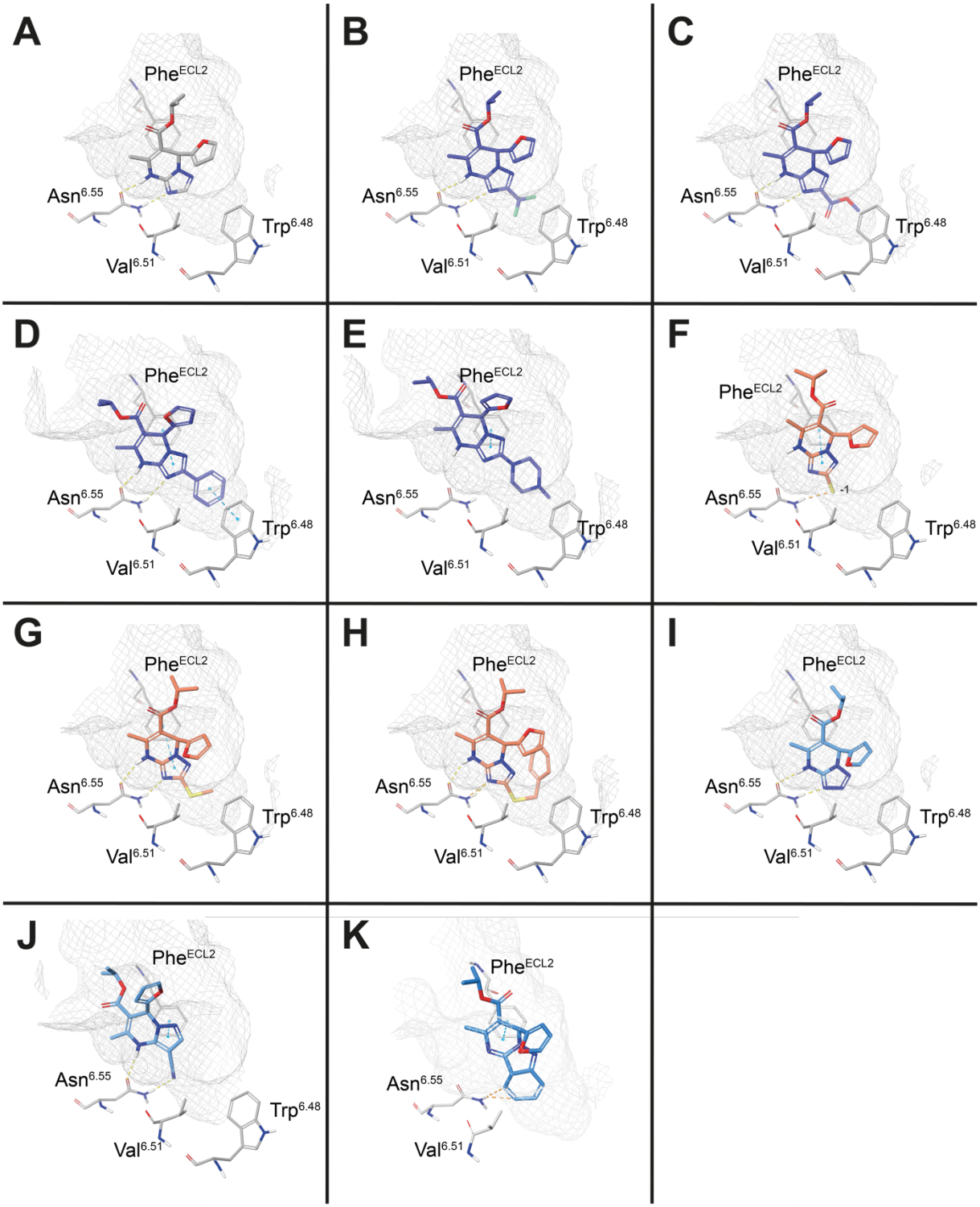

Figure 3.34. Binding mode for series **XII-XX**. **A) IIb** (model Series **II**), **B) 138** (Series **XII**), **C) 146** (Series **XIII**), **D) 154** (Series **XIV**), **E) 162** (Series **XV**), **F) 170** (Series **XVI**), **G) 178** (Series **XVII**), **H) 186** (Series **XVIII**), **I) 194** (Series **XIX**), **J) 202** (Series **XX**), and **K) 210** (Series **XXI**). Receptor is $A_{2B}AR$ homology model from $A_{2A}AR$ (PDB: 3EML), and grey mesh represent $A_{2B}AR$ binding site. Note the effect of the tautomerization on hydrogen bonds with $Asn^{6.55}$. Yellow dashed lines: hydrogen bonds, blue dashed lines: π-π interactions, orange dashed lines: bad contacts.

Interestingly, compared with thiazolopyrimidines (series **XXII, 217–224** (Table 3.16) that not showed any measurable affinity, benzothiazolopyrimidines (series **XXIII-XXV)** show an excellent A_{2B}AR affinity and selectivity profile, with very good affinity data (Figure 3.35, Table 3.16). Despite the absence of a double hydrogen bond formation ability in both bicyclic (thiazolopyrimidines) and tricyclic (benzothiazolopyrimidines) compounds, the tricyclic system demonstrates enhanced binding stabilization compared to thiazole derivatives (series **XXII**). This could be attributed to the better fit of the tricyclic system to the receptor, which allows the loss of a critical interaction required by all adenosine receptors without losing remarkable affinity.

Inspired by the favorable outcomes in terms of affinity and selectivity observed in series **XXIII** and guided by the findings from Chapter I, we have developed two new series through chlorination at positions 7 and 8 of the novel benzothiazolopyrimidine scaffold (Figure 3.35). The main objective was to introduce the halogen bonding interaction discovered between the chlorine atom in the 8-halo benzoimidazopyrimidines (Chapter I, series **III–IV**) and $Asn^{5.42}$ into the novel scaffold.

As was the case in Chapter I, some compounds with chlorine at position 7 (series **XXIV**) maintain the binding affinity, but always lower than chlorinated at position 8 compounds (series **XXV**). As proposed, 8-chlorinated compounds (series **XXV**), also stabilize the binding through the formation of a halogen bond between $Asn^{5.42}$ and the chlorine atom at position 8.

Comparative analysis of the binding data obtained for series **XXIII** and model series **III** prove that the imidazole-thiazole bioisosterism has a positive impact on the A_{2B}AR affinity. In 2- and 3-furyl derivatives (**225–228**, K_i = 8.60 – 11.6 nM) no major differences are observed with the model series **III** (**IIIa–IIId**, K_i = 3.49 – 20.6 nM). The new compounds show higher affinity than the predecessors, apart from compound **226** (K_i = 11.6 nM), with lower affinity than **IIIb** (**ISAM-140**, K_i = 3.49 nM). The effect of NH-S bioisosterism on compounds with thiophene derivatives is much higher (**229–232**, K_i = 11.2 - 214 nM), increasing the affinity by at least 2-fold compared to model series **III** (**IIIe-IIIf**, K_i = 29.34 - 484.6 nM).

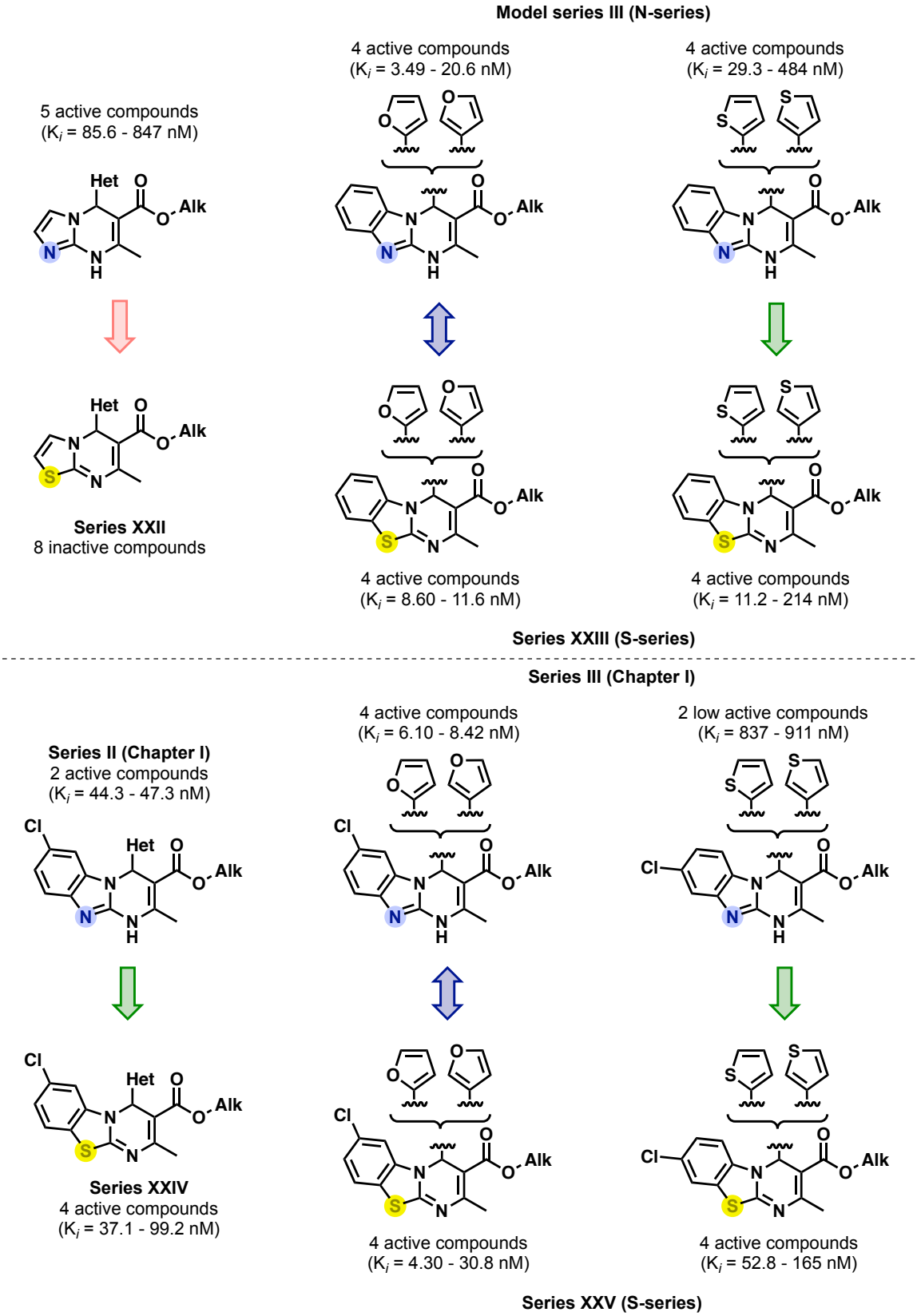

Figure 3.35. SAR of N/S replacements. In red, blue and green modifications that modifications that reduce, maintain and increase A_{2B}AR binding affinity, respectively.

Cross-analysis between the chlorinated series with benzimidazole and benzothiazole scaffolds (series **XXIV–XXV**) shows a behavior that is similar to that previously described in previous Chapter. Figure 3.36 shows a comparison of the affinity data and binding mode of thiazole and benzothiazole derivatives herein described and previously published imidazole and benzimidazole derivatives.[87] Chlorination at position 7 (series **XXIV**) worsens the affinity with respect to the non-halogenated series (series **XXV**) in all cases, obtaining moderate affinities (K_i = 37.1 – 99.2 nM) for the A_{2B}AR for those compounds with a high percentage of radioligand displacement (**233**, **235**, **236** and **239**). However, if this series is compared with its benzimidazole analogues[87] (with only two compounds showing moderate affinity), the results are equal or better, obtaining in this case a ligand with 3-thiophene in Het and ethyl in Alk with high affinity for the A_{2B}AR (**239**, K_i = 37.1 nM).

Position 8 remains the preferred position for halogenation, with the chlorinated benzothiazole having high affinity values for the A_{2B}AR (K_i = 4.30 – 165 nM). As in previous chapter (Figure 3.36C), chlorine atom at position 8 appears to perform an halogen interaction with Asn$^{5.42}$, stabilizing the compound at the receptor. This, in the context of the loss of the double hydrogen bridge by the benzothiazole derivatives, becomes a very important interaction for binding to A_{2B}AR. The effect of NH-S bioisostery on chlorinated compounds at position 8 is even greater than that shown by non-halogenated compounds (series **XXIII**), especially in derivatives with thiophene at R^4. The effect of NH-S bioisostery on chlorinated compounds at position 8 is even greater than that shown by non-halogenated compounds (series **XXIII**), especially in derivatives with thiophene at R^4 (Het). As shown in Figure 3.36, the benzimidazole derivatives with thiophene have little or no affinity for A_{2B}AR, whereas the benzothiazole derivatives with thiophene show acceptable affinity values (K_i = 52.8 - 165 nM). This effect in series **XXIII**–**XXV** may be due to the absence of the double hydrogen bond (Asn$^{6.55}$), allowing greater flexibility of compound binding to the A_{2B}AR, more easily accommodating traditionally worse groups such as 3-furan or thiophenes.

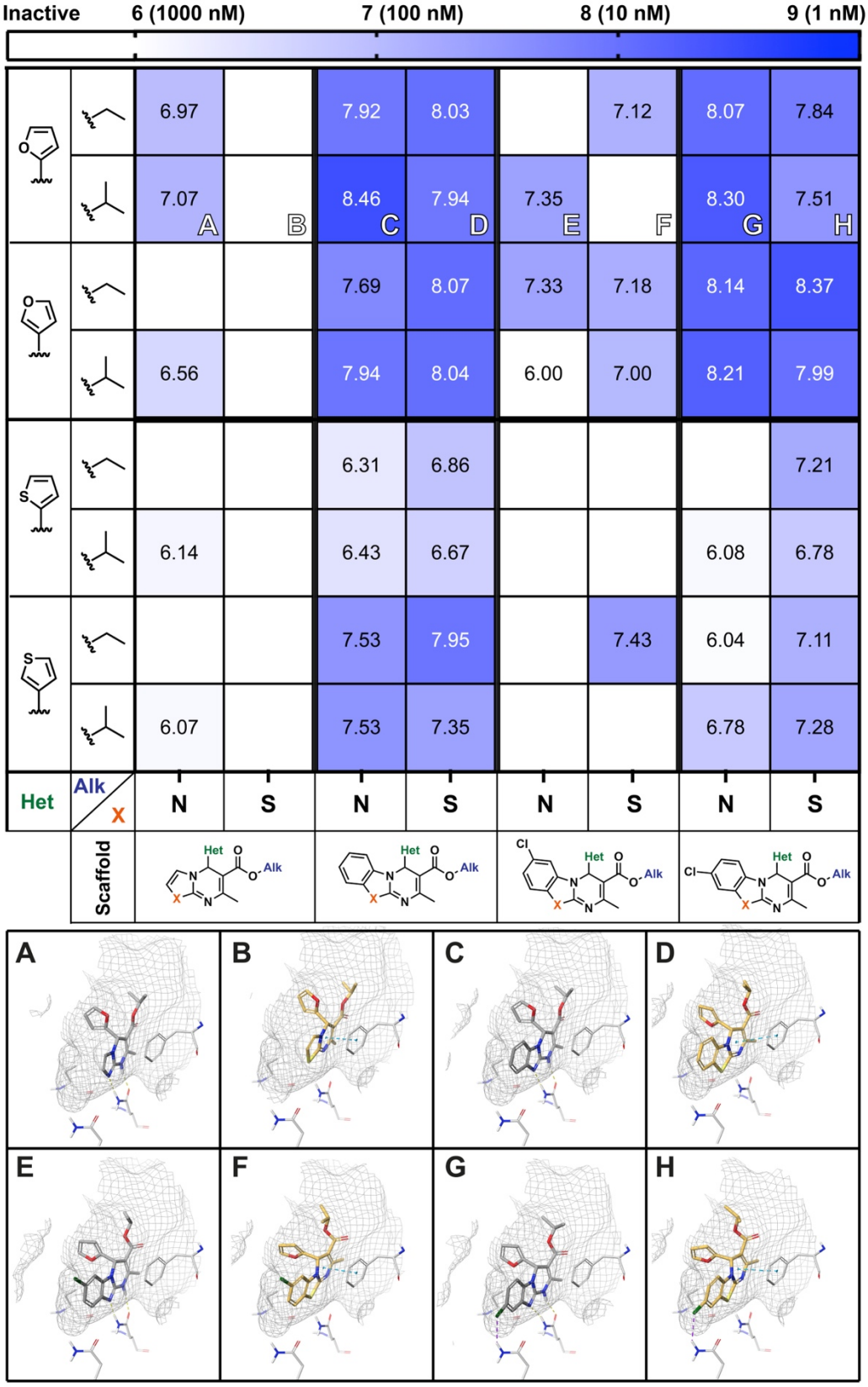

Figure 3.36. Heatmap chart showing $A_{2B}AR$ pK_i [-log(K_i)] for series **XXII-XXV** (S columns) compared with Chapter I compounds (N columns).

Interestingly, the compound **243** has dual $A_{2A}AR/A_{2B}AR$ behavior (K_i = 90.7 and 4.30 nM respectively) in the same way as **60** (Table 3.17, K_i = 176 and 6.10 nM respectively), described in chapter I,[87] also a 3-furyl derivative chlorinated at position 8 (Figure 3.37), making the 8-chlorine and 3-furan ring as pentagonal ring substitutions important in the rational discovery of dual $A_{2A}AR/A_{2B}AR$ compounds.

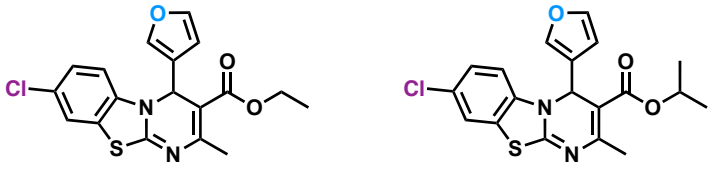

243
K_i ($A_{2A}AR$) = 90.7 nM
K_i ($A_{2B}AR$) = 4.30 nM

60
K_i ($A_{2A}AR$) = 176 nM
K_i ($A_{2B}AR$) = 6.10 nM

Figure 3.37. Structure and binding data of **243** and **60**, two dual $A_{2A}AR/A_{2B}AR$ compounds.

Four representative compounds with different structures (monocyclic: **114**, bicyclic: **146**, and tricyclics: **226** and **243**) were selected to perform functional evaluation through cAMP accumulation assays. The results (Table 3.18) exhibit a high correlation between K_i and K_B values, indicating a selective $A_{2B}AR$ antagonist profile for **114**, **146**, and **226**, while compound **243** demonstrates a dual $A_{2A}AR/A_{2B}AR$ antagonist profile.

3.2.5 Enantiospecific binding to the A_{2A} and $A_{2B}AR$

To determine the role of stereoselectivity on the synthesized compounds, three representative ligands were resolved into its enantiopure forms and evaluated at the four human adenosine receptor subtypes (Table 3.17). The selected derivatives were **226** and **228** (from series **XXIII**, two selective $A_{2B}AR$ antagonists); and **243** (from series **XXV**, dual $A_{2A}AR/A_{2B}AR$ antagonist). These compounds presented a promising affinity and selectivity profiles when evaluated as racemic mixture, while they cover the stereochemical diversity within tricyclic collection. Determining the affinities of the purified enantiomers would provide structural insights about the role of double hydrogen bond (with $Asn^{6.55}$) in enantiospecific binding to $A_{2B}AR$ (and $A_{2A}AR$).

A combination of chiral HPLC and circular dichroism (CD) spectroscopy was employed to separate and unequivocally assign the configuration of the stereocenter in each stereoisomer (Figure 3.38A). Semipreparative HPLC separation of **(±)-226**, **(±)-228** and **(±)-243** on a chiral stationary phase (see Experimental Section) provided the expected six enantiomers with

excellent stereochemical purity (>99%). As previously described for structurally related 3,4-dihydropirimidin-2-ones,[141–144,165] the characteristic CD activity of the enamide chromophore (300-370 nm)[173] allowed the unequivocal assignment of the absolute configuration of each enantiomer (Figure 3.38A), by comparison with the reported CD data for enantiopure 3,4-dihydropyrimidin-2(1*H*)-ones of known configuration. At that wavelength, enantiomers showing a negative Cotton effect (dark line) contain the furan ring backward (and correspond to **(*S*)-226**, **(*R*)-228** and **(*R*)-243**), while the stereoisomers giving positive Cotton effect (light line) contain the pentagonal heterocycle forward (and correspond to **(*R*)-226**, **(*S*)-228** and **(*S*)-243**). The affinity of the enantiomers of **226**, **228** and **243** was evaluated at the four human adenosine receptors. The results, summarized in Table 3.17 and Figure 3.38 for the four ARs, allow the identification of stereoisomers with excellent A_{2B}AR affinity and selectivity. The structural interpretation for this binding data is in accordance with our stereospecific binding model to the *h*A_{2B}AR (Figure 3.38B) where only the enantiomer with pentagonal heterocycle backward shows affinity for the receptor. In benzothiazole derivatives both enantiomers bind to the receptor but with different affinity.[141–144,165] The enantiomer with pentagonal heterocycle backward shows 2-fold higher affinity, while the other enantiomer shows 2-fold decreased affinity than racemic mixture (Table 3.17). This behavior can be explained by the absence of the double hydrogen bond with Asn$^{6.55}$ facilitating the distomer binding (Figure 3.38B-C), maintaining some affinity for the A_{2B}AR. This trend is also observed in the case of the dual A_{2A}AR/A_{2B}AR ligand (**243**). Furthermore, as reported in previous chapter,[87] the enantiospecific binding occurs in both A_{2A}AR and A_{2B}AR, exhibiting higher affinity the enantiomer with the pentagonal ring backward. The resolution of the racemates has allowed us to obtain two very potent (K_i < 5 nM) and selective (> 1000 fold) ligands for A_{2B}AR [**(*S*)-226** and **(*R*)-228**] and a new ligand with an excellent A_{2A}AR/A_{2B}AR dual profile [**(*R*)-243**; K_i = 27.3 and 1.20 nM for A_{2A}AR and A_{2B}AR, respectively).

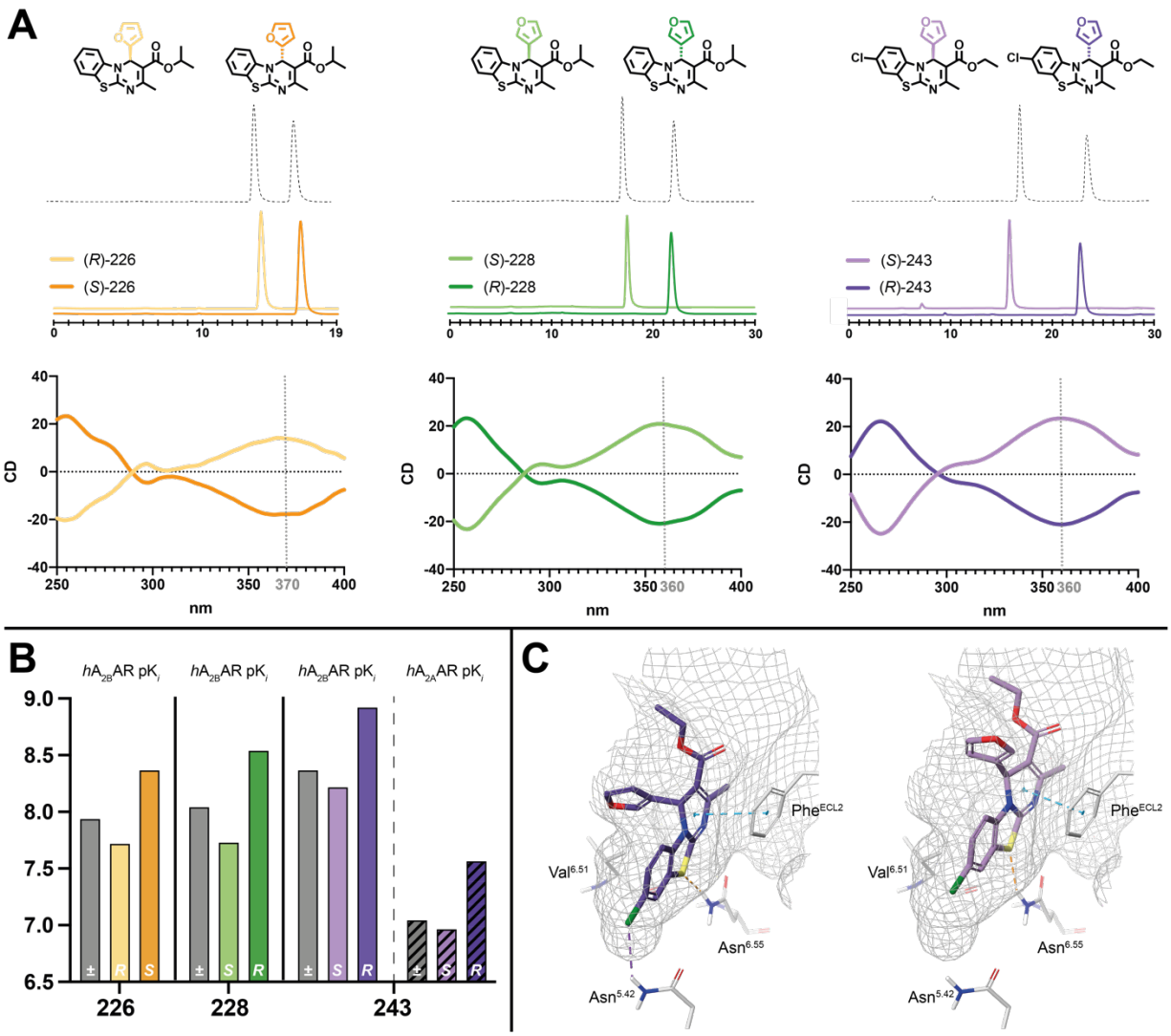

Figure 3.38. Enantiospecific binding to A_{2B} and A_{2A}AR. **A)** Chiral HPLC traces and circular dichroism spectra of selected racemic ligands (**226, 228, 243**) and their enantiomers. **B**) Interleaved bar chart showing A_{2A} (pattern fill) and A_{2B}AR (solid fill) pK_i for racemic mixtures (grey), distomers (light colored) and eutomers (dark colored). **C)** Binding mode of (*R*)-**243** (eutomer, left) and (*S*)-**243** (distomer, right). Receptor is A_{2B}AR homology model from A_{2A}AR (PDB: 3EML), and grey mesh represent A_{2B}AR binding site. Note that the eutomer fits better in the receptor, forming a halogen bond with $Asn^{5.42}$, not present in the distomer.

3.3 CHAPTER III: *N*-SUBSTITUTION OF A_{2B}AR ANTAGONISTS WITHIN THE PYRIMIDINONE CHEMOTYPES: DISCOVERY AND OPTIMIZATION OF A_{2B} AND DUAL A_{2A}/A_{2B} LIGANDS

There is increasing evidence that the development of multi-target drugs (drugs that simultaneously modulate several targets) is the most appropriate strategy for the treatment of multifactorial diseases, whose onset and progression involve multiple receptors and/or signaling pathways. Due to the synergistic roles of A_{2A} and A_{2B}AR in the tumor microenvironment, simultaneous blockade of both receptors appears to be the most promising strategy in purinergic-based anticancer therapy. Multi-target treatment can be carried out through three main approaches, ordered from the least to the most technically difficult in development:

- **Medication combination** (polypharmacology): administration of two different preparations simultaneously. The main advantage of this strategy is the ease of development and dose adjustment, but it involves two different medications, which can lead to adherence problems or administration incompatibilities.
- **Combination of drugs**: similar to the previous one, but both drugs are in the same pharmaceutical form, reducing problems of adherence to treatment. It is only possible if both drugs are compatible (in terms of mode of administration and administration times).
- **Dual drugs**: in this case treatment is carried out with only one drug capable of interacting with two (or more) therapeutic targets. The main advantage of this is that we do not have different metabolic or administration profiles or compatibility problems.

The development of dual drugs in a rational manner is a complex and challenging process that involves several different strategies. Among these strategies, three main approaches have been identified (as illustrated in Figure 3.39).[181,182] The first approach is the "*linked*" type, which involves the joining of two chemical structures through a linker or spacer to form a new molecule with pharmacological activity against two targets. Depending on the length of the linker and the proximity of the targets, this molecule may even act simultaneously on both targets. The second approach is the "*fused*" type, which is similar to the linked type, but instead of using a linker, the two chemical entities are fused at one point. This strategy is frequently used to combine acids and amines to form amides. However, both the linked and fused strategies generate compounds of high molecular weight, which may significantly impact the pharmacokinetic profile of these compounds. The last strategy, the "*merged*" type, is an

alternative approach that does not generate molecules with significantly higher molecular weight than their predecessors. This strategy involves merging the two chemical entities into a new molecule that maintains the necessary structural requirements for recognition by both targets.

It should be noted that developing dual drugs using any of these approaches requires a deep understanding of the chemical and pharmacological properties of both targets and the potential interactions between them. Additionally, it is essential to carefully consider the potential impact of the selected strategy on the pharmacokinetic profile of the resulting compound, as this can have a significant effect on the drug's efficacy and safety. Therefore, the development of dual drugs requires a rational and systematic approach that considers various factors, including the chemical properties of the targets, the pharmacokinetic profile of the resulting compound, and the desired therapeutic outcomes.

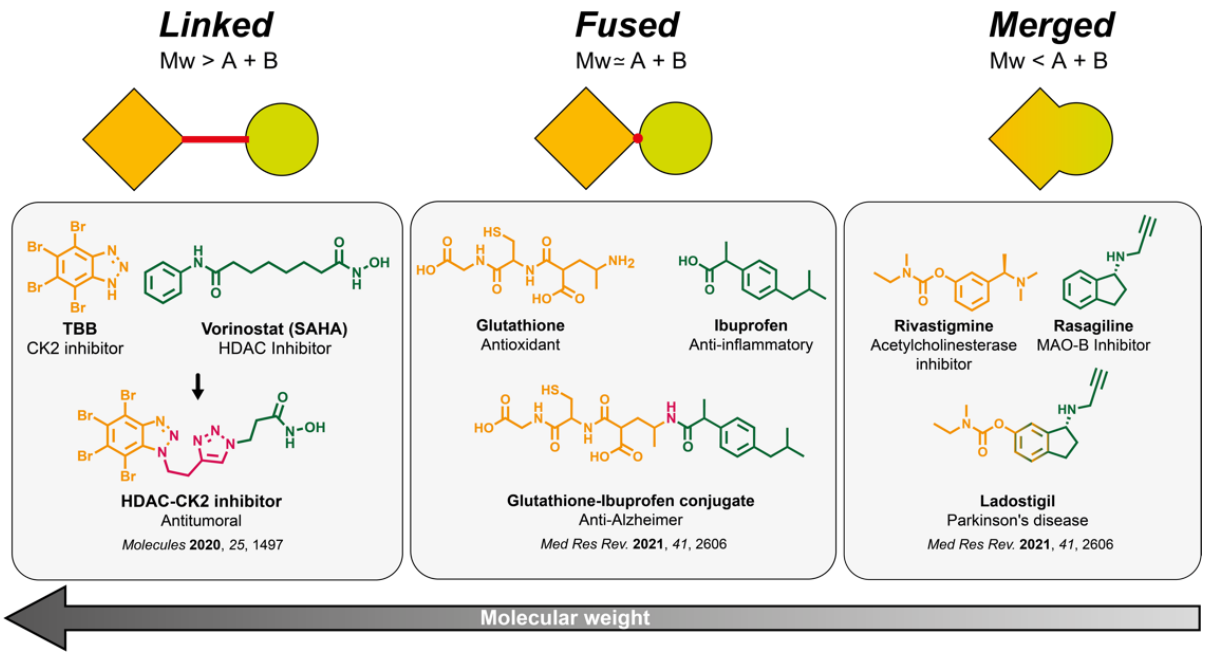

Figure 3.39. Strategies and examples for dual target drug design.

As a part of our ongoing $A_{2A}AR/A_{2B}AR$ dual antagonist discovery program, we have conducted a thorough evaluation of the impact of substituting nitrogen(s) with alkyl and benzylic residues. Our previous findings, presented in the previous chapter, demonstrated that the hydrogen bond donor was not essential for maintaining pharmacological affinity for the

A_{2B}AR. Additionally, we discovered that aromatic rings could stabilize the open conformation of the A_{2A}AR.[86] These observations led to the development of a novel series of compounds exploring the extracellular part of the orthosteric binding site (Figure 3.40). The primary objective of this research was to create hybrid compounds by overlapping the selective A_{2A}AR antagonists discovered by our research group in 2022 and our selective A_{2B}AR scaffold, thereby obtaining dual ligands. Furthermore, we sought to investigate the impact of *N*-substitution on our best A_{2B}AR antagonism scaffolds, including monocyclic and tricyclic dihydropyrimidinone derivatives.

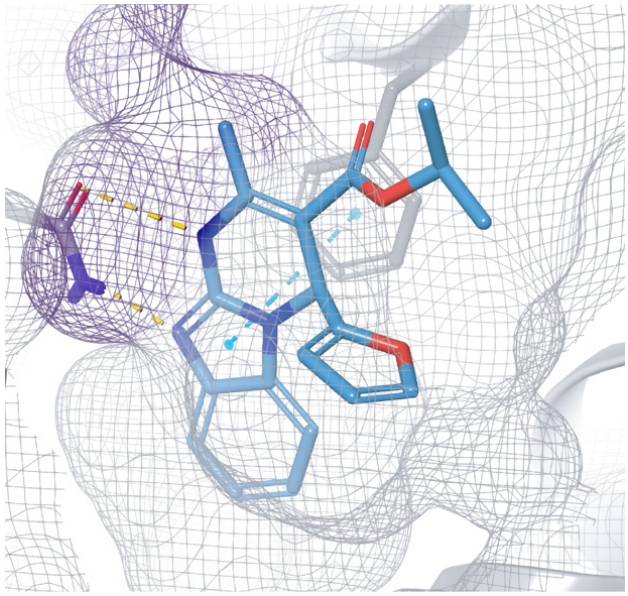

Figure 3.40. Binding mode of prototypical tricyclic A_{2B}AR antagonists. Grey mesh represents A_{2B}AR binding site (in purple: external cavity explored in this chapter).

For this chapter, we have synthesized and characterized 12 new monocyclic and 62 new tricyclic ligands. The design of these compounds is supported by modeling and ligand docking. Our results demonstrate that *N*-substitution has a significant effect on enhancing the A_{2A} and A_{2B}AR binding affinity. Our findings hold great promise for the ongoing development of new A_{2A}AR/A_{2B}AR dual antagonists, underscoring the potential of this innovative class of compounds in the treatment of various diseases. This work is actively being pursued, and our results provide valuable insights in the field, paving the way for further advancements in the design and synthesis of dual antagonists.

3.3.1 Design

Four novel series were conceived in the context of the development of multi-target cancer (immuno)therapeutics and tracers for the A_{2B}AR, starting from the monocyclic and tricyclic scaffolds. To obtain dual ligands, a *merging* strategy was employed in the design of the new series. Specifically, the monocyclic and tricyclic dihydropyrimidine-type scaffolds, known for their potency and selectivity on A_{2B}AR, were superimposed with the aminopyrimidine structure of the A_{2A}AR antagonists that had been previously discovered by our research group. As shown in Figure 3.41, neither **ISAM-140** nor **ISAM-CV245** bind well to A_{2A}AR (Figure 3.41B) and A_{2B}AR (Figure 3.41D), respectively. However, the designed ligands, fit both receptors, combining the shown binding modes of their predecessors.

Thus, we have carried out the development of 112 new ligands (series **XXVI-XXIX**) presented in Figure 3.42. Being aware that this type of substitution may have a high impact on the pharmacodynamic profile, we have designed two exploratory series (series **XXVI** and **XXVII**) in which the effect of substitution with propyl, benzyl and 2-fluorobenzyl on monocyclic and tricyclic scaffolds, respectively, is evaluated. The main reason for introducing these substituents in the exploratory series is to study the effect of different substituent sizes (propyl and benzyl) and the effect on the interaction with the receptor on electronic level changes of the substituents (propyl; nonaromatic, benzyl; aromatic, 2-fluorobenzyl; aromatic substituted with fluorine). To maintain consistency with previous chapters and to facilitate comparative SAR, the ligands obtained here (series **XXVI-XXIX**) retained the structural elements that provided optimal A_{2B}AR affinity at positions 3 (Alk) and 4 (Het). Thus, for Het we considered only the set of pentagonal furyl-derived heteroaryl (2-furyl, 3-furyl) while the alkoxy residues of the ester moiety (Alk) consist of ethyl or isopropyl groups.

Based on these results, series **XXVIII** and **XXIX** have been designed, in which the best scaffolds (tricyclic, Het = 2-furyl, Alk = isopropyl, and Het = 3-furyl, Alk = ethyl, respectively, Figure 3.42) has been combined with different types of alkyl (R = methyl, ethyl, propyl, and propargyl) and benzyl *N*-substituents (R = benzyl, phenethyl, 2-fluorobenzyl, 2-fluorophenethyl, 4-cyano-2-fluorobenzyl, 3-fluorobenzyl, 4-fluorobenzyl, 2,3-difluorobenzyl, 2,4-difluorobenzyl, 2,5-difluorobenzyl, 2,6-difluorobenzyl, 2,6-difluorobenzyl, 3,5-difluorobenzyl, 2,4,6-trifluorobenzyl, 2-chlorobencyl, 3-chlorobenzyl, 4-chlorobenzyl, 3-chloro-2-fluorobenzyl, and 2-chloro-6-fluorobenzyl). The integrated synthesis, binding data, SAR, and computational studies of the complete ligand library are described in this chapter.

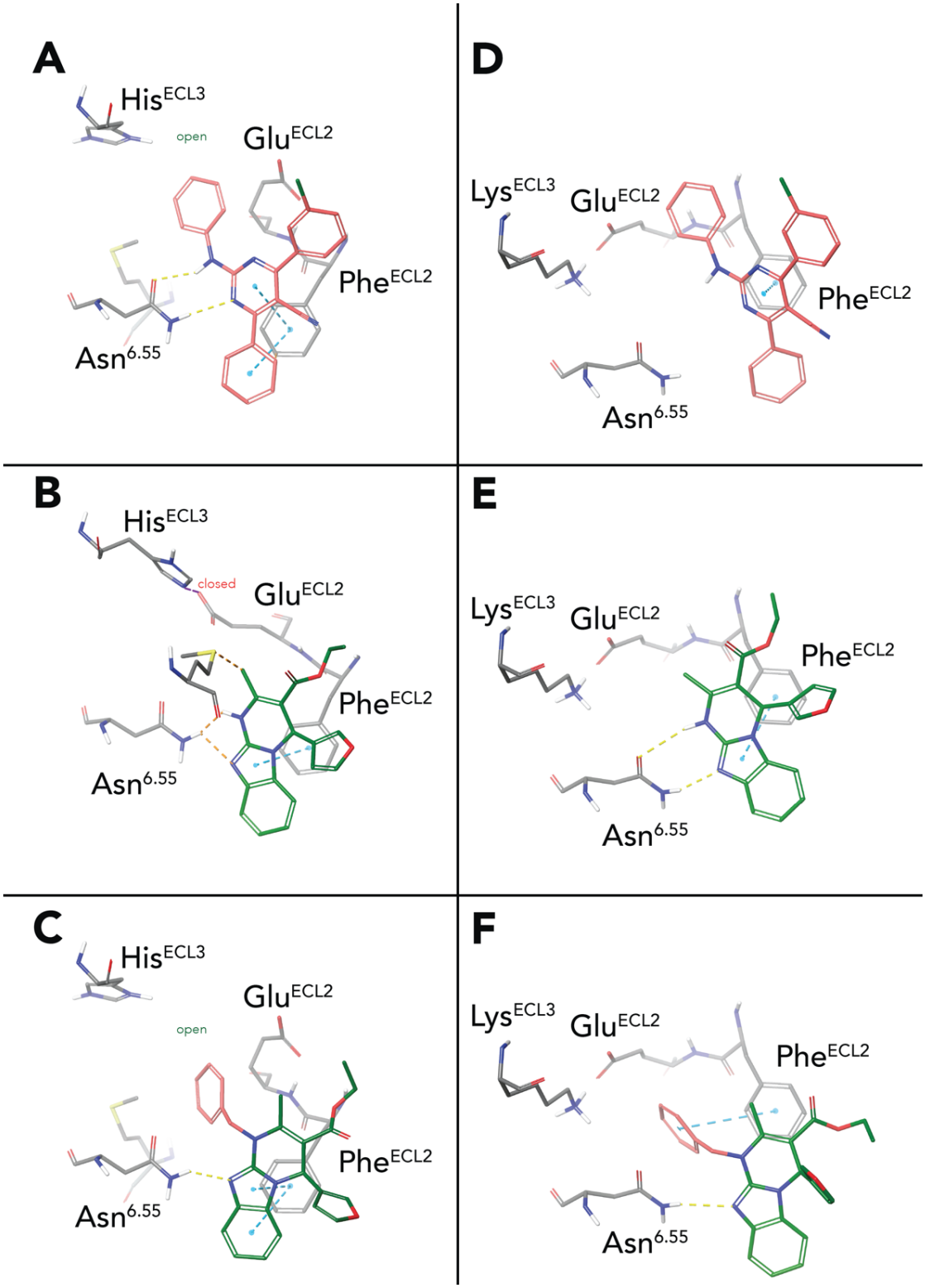

Figure 3.41. Structure of A) **ISAM-CV245** (selective A_{2A}AR antagonist), B) **ISAM-140** (selective A_{2B}AR antagonist) and C) novel ligands designed in this chapter (potential A_{2A}AR/A_{2B}AR dual antagonist) in A_{2A}AR. Structure of D) **ISAM-CV245** (selective A_{2A}AR antagonist), E) **ISAM-140** (selective A_{2B}AR antagonist) and F) novel ligands designed in this chapter (potential A_{2A}AR/A_{2B}AR dual antagonist) in A_{2A}AR. A_{2A}AR PDB structures: 4EIY with closed conformation; PDB: 3UZC with open conformation. A_{2B}AR PDB structure: Homology Model from A_{2A}AR, PDB: 3EML.

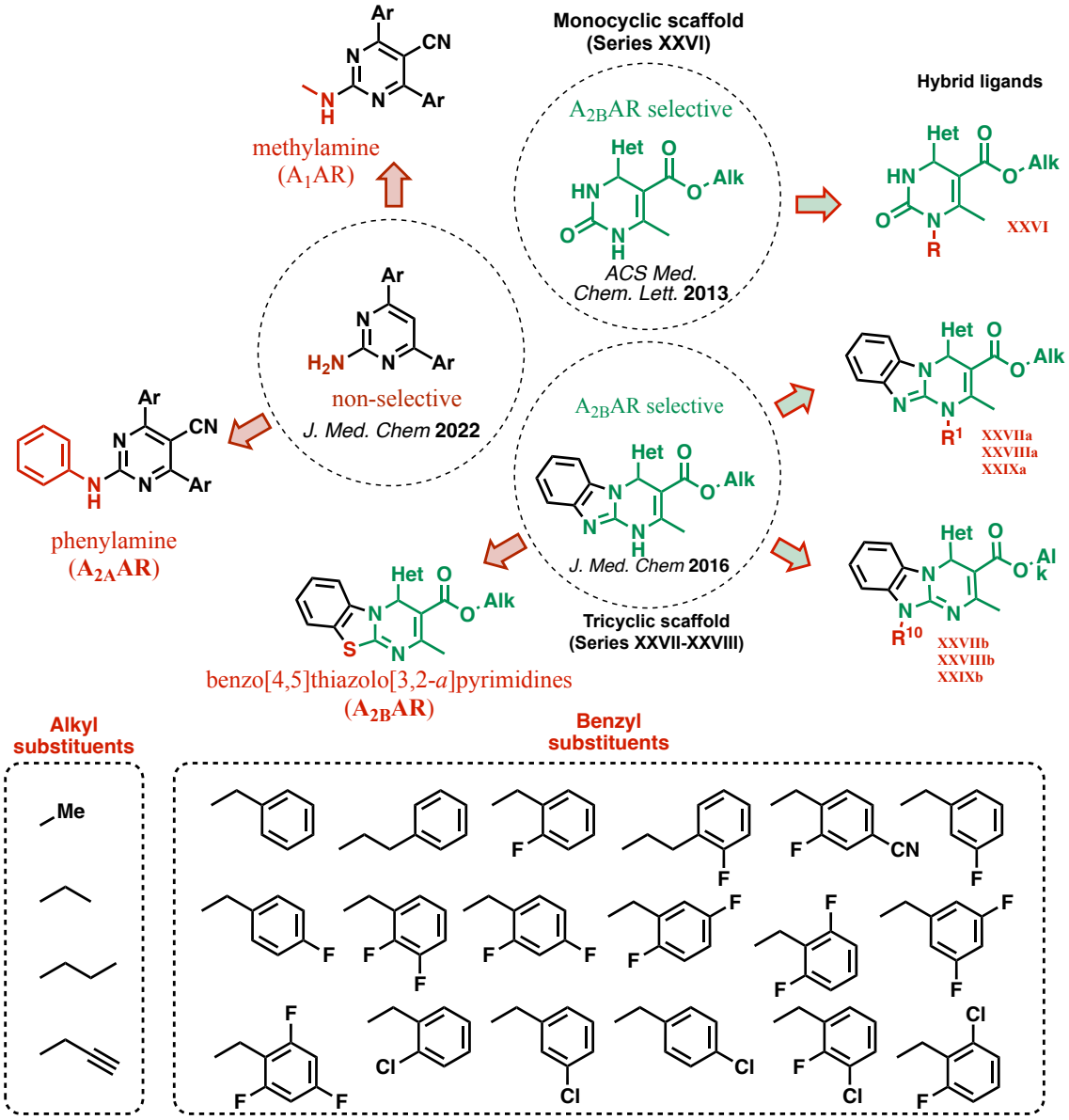

Figure 3.42. Rational design of $A_{2A}AR/A_{2B}AR$ dual antagonists. In red, previous discoveries made by our research group that led to the design of this type of compounds. In green, classic scaffold of $A_{2B}AR$ selective antagonists.

In this chapter, in addition to the development of new dual ligands, the substitutions introduced on the monocyclic and tricyclic structures will make it possible to obtain labeled molecules. The series have been designed to contain fluorine or hydrogen atoms easily substituted by ^{18}F and ^{3}H, considered as "cold ligands" for radioligand binding assays and PET. In addition, the design has been made in such a way that the substituents are oriented towards the extracellular region of the receptor, providing the basis for fluorescent labeling or dual targeting by *linking* strategies.

3.3.2 Chemistry

The synthesis of all compounds (**249–260**, **261a–310a**, and **261b–310b**) was achieved following the methodology outlined in Figure 3.43. The procedure involved a Biginelli reaction, combining different aldehyde, β-ketoesters, and 1,3-dinucleophiles, to reach model series **I** and **III** lead compounds. Subsequently, an alkylation under basic conditions was performed to assemble the library of compounds in an efficient manner. Notably, in the case of tricyclic derivatives, the alkylation step produced two regioisomers, enabling an exploration of the SAR of N^1- and N^{10}-alkylation. This aspect is particularly relevant as it allows for a more detailed investigation into the impact of these modifications on the biological activity of the compounds. A set of pentagonal carbaldehydes (**A1–2**) and β-ketoesters (**B1–2**) providing optimal substituents for positions 4 and 3 in combination with different 1,3-dinucleophiles (**C28–29**) were employed as precursors of the Biginelli Reaction. The starting materials, dissolved in THF and containing catalytic amount of $ZnCl_2$, were submitted to orbital stirring at 90 ºC for 12 h. in This approach resulted in the production of four monocyclic (**D1–4**, model series **I**) and four tricyclic precursors (**D5–8**, model series **III**) in satisfactory yields (60-75%) which were then subjected to alkylation. For the synthesis of the series **XXVI-XXIX**, alkylation (or benzylation) was carried out using different alkyl and benzyl halides (**E1–21**) through orbital stirring in DMF with potassium carbonate at 80 ºC for 15 hours. All reactions were monitored by thin-layer chromatography (TLC). After completion of the reaction, the solvent was evaporated to dryness and the oily residue was purified by column chromatography on silica gel (Figure 3.43). For monocyclic compounds (**249–260**), single spot revealing green in *p*-anisaldehyde was found in TLC with a yield of 36–50%. For tricyclic compounds, two well-resolved spots revealing green in *p*-anisaldehyde were found in TLC (**261a–310a**, and **261b–310b**), with the N^{10}-substituted compound clearly being the major regioisomer. A detailed description of the synthetic methods and the complete structural, spectroscopic, and analytical data for all compounds are provided in the Experimental Section.

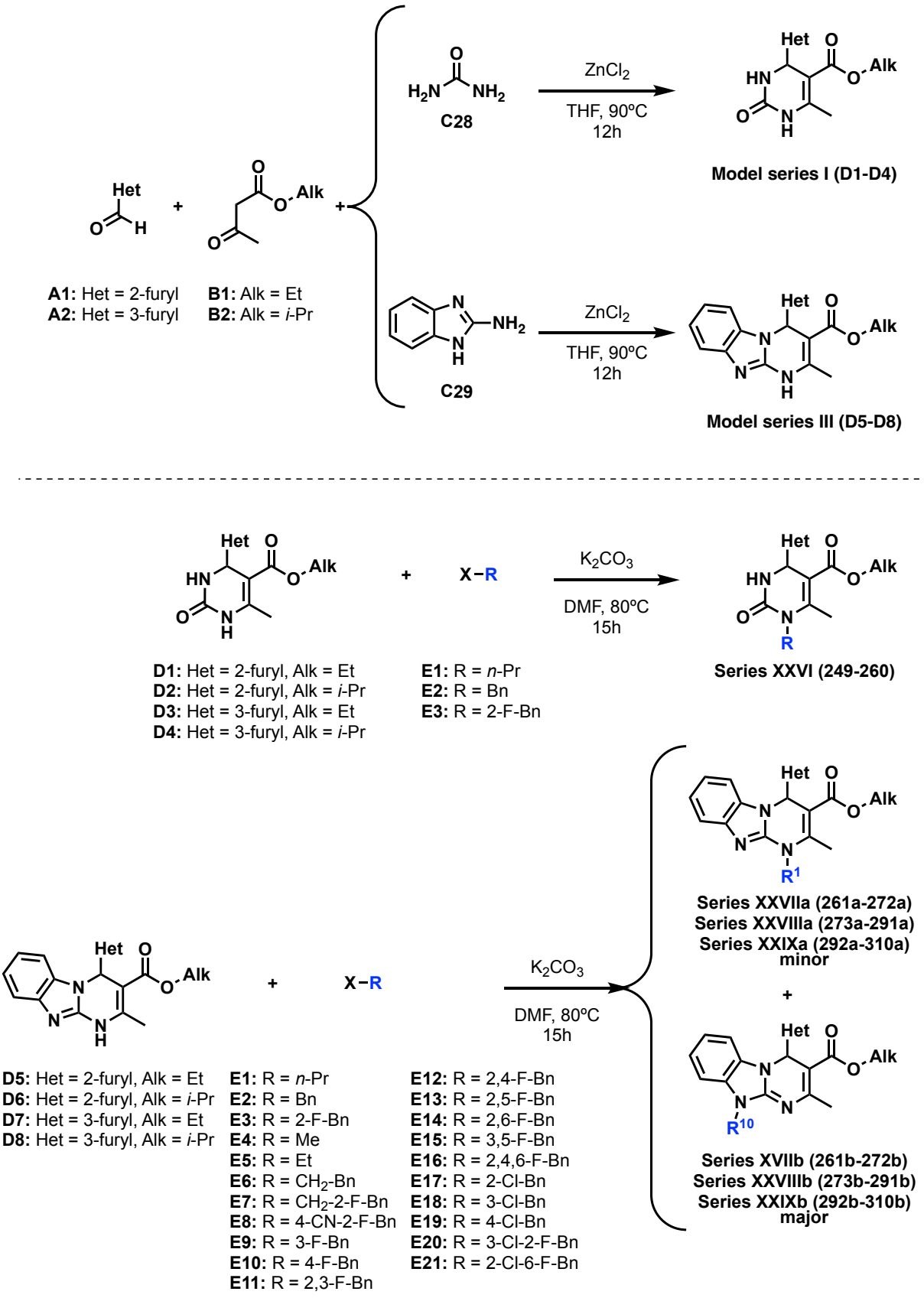

Figure 3.43. Biginelli-based synthesis (top) and alkylation (bottom) of model ligands.

Unequivocal structural characterization of each regioisomer has been carried out with NMR experiments (Figure 3.44). The tricyclic derivatives (series **XXVII-XXIX**) differ in the position of the substituent located either at N^1 or N^{10}. In cases where the alkylation occurs on N^1, a NOESY correlation can be observed between CH_3 and N-CH_2 of the substituent, as illustrated in Figure 3.44, due to the proximity (1.93Å). Conversely, in N^{10} derivatives, the correlation cannot be established owing to the significant distance between these entities (4.35Å). With this results it has been possible to make a correlation between the substitution position and the ^{1}H NMR ($CDCl_3$), observing that in all cases the N^1-substituted compounds two doublets can be observed (N-CH_2-R) at 5.3 – 5.8 ppm, while all the N^{10}-substituted compounds present a quartet at 5.2 – 5.5 ppm. In all cases, the N^1-substituted compounds were found to be the most apolar under the purification conditions utilized (Experimental Section).

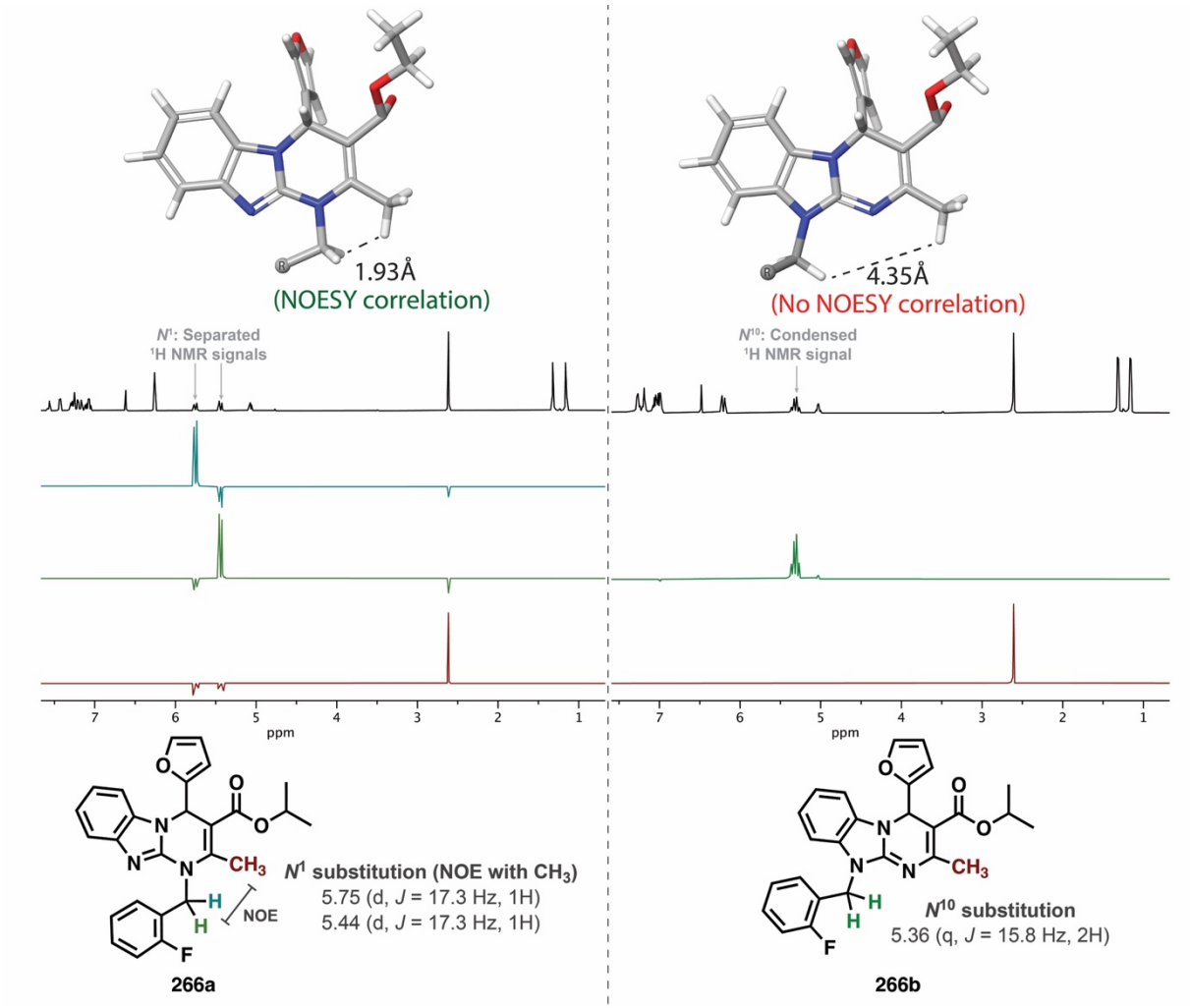

Figure 3.44. Regioisomer characterization strategy through ^{1}H NMR experiments. Positive signals correspond to irradiated protons in NOESY experiments.

As in previous chapters, all ligands obtained in this study contain one stereocenter at position 4 of the heterocyclic core and were isolated and evaluated as racemic mixtures. Four ligands eliciting attractive A_{2B}AR affinity/selectivity profile (one very potent and selective and three potent dual antagonists) were submitted to chiral resolution to isolate its corresponding enantiomer pairs. The unequivocal assignation of the configuration of the different enantiomers was performed employing circular dichroism (CD) as described in previous chapters.

3.3.3 Biological Evaluation

The adenosinergic profile (affinity and selectivity) of the 74 novel halogenated alkyl 1,4-dihydro-benzo[4,5]imidazo[1,2-*a*]pyrimidine-3-carboxy-lates was evaluated *in vitro* using radioligand binding assays at the four human AR subtypes.[87,142–144] Table 3.19 to Table 3.24 contain the binding data obtained and for the model ligands to facilitate the comparative assessment.[87] All ligands reported were obtained and tested as racemic mixtures. The whole set was evaluated *in silico* with a combination of RDKit[166] PAINS filter and InstantJChem from Chemaxon (https://www.chemaxon.com), to rule out the possibility that these ligands could be promiscuous pan-assay interference compounds (PAINS) and to assess their bioavailability, respectively. Human ARs were expressed in transfected cell lines [e.g., Chinese hamster ovary (CHO) cells (A_1AR), human epithelial carcinoma (HeLa) cells (A_{2A}AR and A_3AR) and human embryonic kidney (HEK-293) cells (A_{2B}AR)]. [^{3}H]DPCPX for A_1AR and A_{2B}AR, [^{3}H]NECA for A_3AR, and [^{3}H]ZM241385 for A_{2A}AR were employed as radioligands. The binding data is presented as $K_i \pm$ SEM (nM, n = 3) obtained by fitting the data by non-linear regression using Prism 5.0 software (GraphPad, San Diego, CA), or as specific binding inhibition percentage at 1 μM (n = 2, average) for those compounds that did not completely displace the radioligand due to either little affinity or poor solubility. The binding affinity of reference AR ligands (**ISAM-140**, **DPCPX**, **NECA** and **ZM241385**) was assessed using our experimental protocols and reported in tables for comparison. The stereoisomers of selected compounds were obtained by chiral resolution and tested at the four human AR subtypes in their enantiopure forms (Table 3.25). This data was employed to complement the SAR study and to evaluate the importance of the configuration of the stereogenic center on the affinity. For comparative purposes, the biological data of structurally related enantiomer pairs discovered in this thesis is also shown in Table 3.25. As a part of the pharmacological characterization, **257**, **266a** and **269a** were tested in cAMP production. These experiments demonstrated that *N*-substituted A_{2B}AR pyrimidinone-derived antagonists inhibits cAMP accumulation, unequivocally validating the

antagonistic behavior if these compounds at A_{2A} and A_{2B}ARs. A comparison of K_i and K_B values reveals a good correlation between data obtained from binding and functional assays in both receptors (Table 3.26).

Table 3.19.Structure and adenosine receptor affinity data of Series **XXVI**: Alkyl *N*-substituted 4-heteroaryl-6-methyl-2-oxo-1,2,3,4-tetrahydropyrimidine-5-carboxylates (**249-260**).

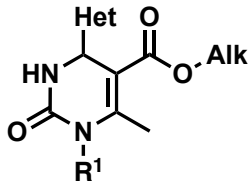

				K_i (nM) or % at 1 μM			
Compound	**Het**	**Alk**	**R^1**	**hA_1[a)]**	**hA_{2A}[b)]**	**hA_{2B}[c)]**	**hA_3[d)]**
Ia[140]	**2-furyl**	**Et**	**H**	**15%**	**31%**	**585 ± 89**	**2%**
249	2-furyl	Et	Pr	5%	23%	37%	19%
250	2-furyl	Et	Bn	14%	56.8 ± 2.1	53.6 ± 1.9	29%
251	2-furyl	Et	2-F-Bn	18%	97.8 ± 3.2	40.1 ± 2.0	5%
Ib[140]	**2-furyl**	***i*-Pr**	**H**	**18%**	**23%**	**40.8 ± 2.3**	**4%**
252	2-furyl	*i*-Pr	Pr	5%	24%	39%	3%
253	2-furyl	*i*-Pr	Bn	13%	29%	688 ± 6	25%
254	2-furyl	*i*-Pr	2-F-Bn	19%	315 ± 4	80.4 ± 2.2	23%
Ic[140]	**3-furyl**	**Et**	**H**	**21%**	**24%**	**39.6 ± 1.1**	**1%**
255	3-furyl	Et	Pr	25%	6%	17%	17%
256	3-furyl	Et	Bn	1%	10%	1%	1%
257	3-furyl	Et	2-F-Bn	13%	39.0 ± 1.1	50.0 ± 1.0	9%
Id[140]	**3-furyl**	***i*-Pr**	**H**	**25%**	**26%**	**1486 ± 62**	**3%**
258	3-furyl	*i*-Pr	Pr	34%	6%	502 ± 42	3%
259	3-furyl	*i*-Pr	Bn	18%	65.7 ± 2.2	33.7 ± 2.0	18%
260	3-furyl	*i*-Pr	2-F-Bn	7%	131 ± 4	43.6 ± 2.0	13%
ISAM-140	-	-	-	20%	28%	3.49 ± 0.2	2%
DPCPX	-	-	-	2.20 ± 0.2	157 ± 3	73.2 ± 1.4	1722 ± 11
ZM241385	-	-	-	683 ± 4	1.9 ± 0.1	65.7 ± 1.1	863 ± 4
NECA	-	-	-	14.0 ± 1	20.0 ± 3	2400 ± 35	6.20 ± 0.9

[a)] Displacement of specific [^{3}H]DPCPX binding in human CHO cells expressed as K_i in nM (n = 3) or percentage displacement of specific binding at a concentration of 1 μM (n = 2). [b)] Displacement of specific [^{3}H]4-(2-[7-amino-2-(2-furyl)[1,2,4]triazolo[2,3-*a*][1,3,5]triazin-5-ylamino]ethyl)phenol binding in human HeLa cells expressed as K_i in nM (n = 3) or percentage displacement of specific binding at a concentration of 1 μM (n = 2). [c)] Displacement of specific [^{3}H]DPCPX binding in human HEK-293 cells expressed as K_i in nM (n = 3) or percentage displacement of specific binding at a concentration of 1 μM (n = 2). [d)] Displacement of specific [^{3}H]NECA binding in human HeLa cells expressed as K_i in nM (n = 3) or percentage displacement of specific binding at a concentration of 1 μM (n = 2).

Table 3.20.Structure and adenosine receptor affinity data of Series **XXVII**: Alkyl 1- and 10-substituted-4-heteroaryl-2-methyl-1,4-dihydrobenzo[4,5]imidazo[1,2-*a*]pyrimidine-3-carboxylates (**261a-272a & 261b-272b**).

Series XVIIa

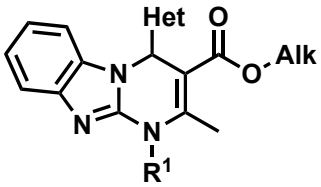

Series XVIIb

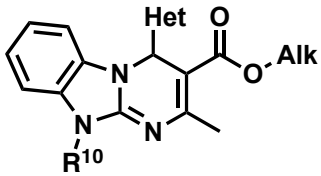

					K_i (nM) or % at 1 μM			
Compound	**Het**	**Alk**	**R^1**	**R^{10}**	**hA_1[a)]**	**hA_{2A}[b)]**	**hA_{2B}[c)]**	**hA_3[d)]**
IIIa[87]	**2-furyl**	**Et**	**H**	**-**	**5%**	**14%**	**12.03 ± 0.7**	**1%**
261a	2-furyl	Et	Pr	-	3%	23%	322 ± 6	2%
261b	2-furyl	Et	-	Pr	11%	14%	12%	4%
262a	2-furyl	Et	Bn	-	8%	16%	412 ± 8	6%
262b	2-furyl	Et	-	Bn	1%	15%	17%	5%
263a	2-furyl	Et	2-F-Bn	-	26%	32%	183 ± 3	14%
263b	2-furyl	Et	-	2-F-Bn	1%	41%	37%	13%
IIIb[87]	**2-furyl**	***i*-Pr**	**H**	**-**	**20%**	**28%**	**3.49 ± 0.2**	**2%**
264a	2-furyl	*i*-Pr	Pr	-	3%	25%	31.9 ± 2.1	5%
264b	2-furyl	*i*-Pr	-	Pr	11%	24%	37%	8%
265a	2-furyl	*i*-Pr	Bn	-	1%	5%	25.7 ± 1.2	7%
265b	2-furyl	*i*-Pr	-	Bn	5%	6%	55%	3%
266a	2-furyl	*i*-Pr	2-F-Bn	-	19%	24%	1.50 ± 0.4	40%
266b	2-furyl	*i*-Pr	-	2-F-Bn	1%	1%	43%	2%
IIIc[87]	**3-furyl**	**Et**	**H**	**-**	**7%**	**11%**	**20.6 ± 1.1**	**1%**
267a	3-furyl	Et	Pr	-	22%	35%	64.0 ± 3	12%
267b	3-furyl	Et	-	Pr	1%	252 ± 4	29%	7%
268a	3-furyl	Et	Bn	-	17%	57%	14.4 ± 2.1	14%
268b	3-furyl	Et	-	Bn	14%	1%	41%	33%
269a	3-furyl	Et	2-F-Bn	-	4%	28.9 ± 2.1	10.2 ± 1.6	33%
269b	3-furyl	Et	-	2-F-Bn	8%	5%	2%	25%
IIId[87]	**3-furyl**	***i*-Pr**	**H**	**-**	**12%**	**22%**	**11.4 ± 0.5**	**2%**
270a	3-furyl	*i*-Pr	Pr	-	28%	22%	54.2 ± 2.2	1%
270b	3-furyl	*i*-Pr	-	Pr	24%	2%	22%	1%
271a	3-furyl	*i*-Pr	Bn	-	17%	49%	33.9 ± 2.4	20%
271b	3-furyl	*i*-Pr	-	Bn	2%	1%	44%	2%
272a	3-furyl	*i*-Pr	2-F-Bn	-	3%	193 ± 2	59.2 ± 2.2	3%
272b	3-furyl	*i*-Pr	-	2-F-Bn	2%	24%	44%	7%
DPCPX	-	-	-	-	2.20 ± 0.2	157 ± 3	73.2 ± 1.4	1722 ± 11
ISAM-140	-	-	-	-	20%	28%	3.49 ± 0.2	2%
ZM241385	-	-	-	-	683 ± 4	1.9 ± 0.1	65.7 ± 1.1	863 ± 4
NECA	-	-	-	-	14.0 ± 1	20.0 ± 3	2400 ± 35	6.20 ± 0.9

[a)] Displacement of specific [^{3}H]DPCPX binding in human CHO cells expressed as K_i in nM (n = 3) or percentage displacement of specific binding at a concentration of 1 μM (n = 2). [b)] Displacement of specific [^{3}H]4-(2-[7-amino-2-(2-furyl)[1,2,4]triazolo[2,3-*a*][1,3,5]triazin-5-ylamino]ethyl)phenol binding in human HeLa cells expressed as K_i in nM (n = 3) or percentage displacement of specific binding at a concentration of 1 μM (n = 2). [c)] Displacement of specific [^{3}H]DPCPX binding in human HEK-293 cells expressed as K_i in nM (n = 3) or percentage displacement of specific binding at a concentration of 1 μM (n = 2). [d)] Displacement of specific [^{3}H]NECA binding in human HeLa cells expressed as K_i in nM (n = 3) or percentage displacement of specific binding at a concentration of 1 μM (n = 2).

Table 3.21. Structure and adenosine receptor affinity data of Series **XXVIIIa**: Isopropyl 1-substituted-4-(furan-2-yl)-2-methyl-1,4-dihydrobenzo[4,5]imidazo[1,2-*a*]pyrimidine-3-carboxylates (**273a-291a**).

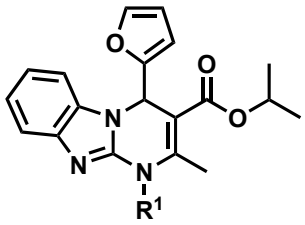

		K_i (nM) or % at 1 μM			
Compound	**R^1**	**hA_1[a)]**	**hA_{2A}[b)]**	**hA_{2B}[c)]**	**hA_3[d)]**
IIIb (ISAM-140)[87]	**H**	**20%**	**28%**	**3.49 ± 0.2**	**2%**
273a	Me	2%	3%	78.3 ± 2.1	5%
274a	Et	23%	8%	37.1 ± 1.5	9%
264a	**Pr**	**3%**	**25%**	**31.9 ± 2.1**	**5%**
275a	Propargyl	47%	13%	22.7 ± 0.9	6%
265a	**Bn**	**1%**	**5%**	**25.7 ± 1.2**	**7%**
276a	CH_2-Bn	1%	16%	10%	11%
266a	**2-F-Bn**	**19%**	**24%**	**1.50 ± 0.4**	**40%**
277a	CH_2-2-F-Bn	1%	17%	11%	9%
278a	4-CN-2-F-Bn	4%	5%	21%	2%
279a	3-F-Bn	7%	322 ± 6	41.3 ± 2.2	4%
280a	4-F-Bn	6%	5%	24%	3%
281a	2,3-F-Bn	1%	283 ± 4	65.2 ± 3.1	24%
282a	2,4-F-Bn	1%	45%	104 ± 5	19%
283a	2,5-F-Bn	3%	3%	51%	11%
284a	2,6-F-Bn	8%	52.9 ± 2.3	8.5 ± 1.1	23%
285a	3,5-F-Bn	5%	2%	542 ± 6	5%
286a	2,4,6-F-Bn	1%	44%	25.1 ± 2.2	3%
287a	2-Cl-Bn	4%	32%	75.9 ± 2.1	3%
288a	3-Cl-Bn	2%	442 ± 8	182 ± 4	7%
289a	4-Cl-Bn	2%	3%	109 ± 3	5%
290a	3-Cl-2-F-Bn	10%	40%	115 ± 3	4%
291a	2-Cl-6-F-Bn	6%	792 ± 12	432 ± 8	1%
ISAM-140	-	20%	28%	3.49 ± 0.2	2%
DPCPX	-	2.20 ± 0.2	157 ± 3	73.2 ± 1.4	1722 ± 11
ZM241385	-	683 ± 4	1.9 ± 0.1	65.7 ± 1.1	863 ± 4
NECA	-	14.0 ± 1	20.0 ± 3	2400 ± 35	6.20 ± 0.9

[a)] Displacement of specific [^{3}H]DPCPX binding in human CHO cells expressed as K_i in nM (n = 3) or percentage displacement of specific binding at a concentration of 1 μM (n = 2). [b)] Displacement of specific [^{3}H]4-(2-[7-amino-2-(2-furyl)[1,2,4]triazolo[2,3-*a*][1,3,5]triazin-5-ylamino]ethyl)phenol binding in human HeLa cells expressed as K_i in nM (n = 3) or percentage displacement of specific binding at a concentration of 1 μM (n = 2). [c)] Displacement of specific [^{3}H]DPCPX binding in human HEK-293 cells expressed as K_i in nM (n = 3) or percentage displacement of specific binding at a concentration of 1 μM (n = 2). [d)] Displacement of specific [^{3}H]NECA binding in human HeLa cells expressed as K_i in nM (n = 3) or percentage displacement of specific binding at a concentration of 1 μM (n = 2).

Table 3.22. Structure and adenosine receptor affinity data of Series **XXVIIIb**: Isopropyl 10-substituted-4-(furan-2-yl)-2-methyl-1,4-dihydrobenzo[4,5]imidazo[1,2-*a*]pyrimidine-3-carboxylates (**273b-291b**).

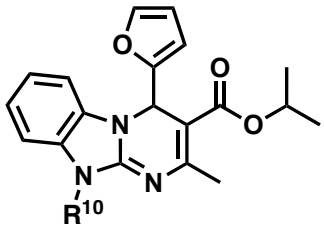

		K_i (nM) or % at 1 μM			
Compound	**R^{10}**	**hA_1[a)]**	**hA_{2A}[b)]**	**hA_{2B}[c)]**	**hA_3[d)]**
IIIb (ISAM-140)[87]	**H**	**20%**	**28%**	**3.49 ± 0.2**	**2%**
273b	CH_3	3%	4%	147 ± 3.3	4%
274b	Et	13%	17%	41.9 ± 1.3	10%
264b	**Pr**	**11%**	**24%**	**37%**	**8%**
275b	Propargyl	12%	22%	30%	2%
265b	**Bn**	**5%**	**6%**	**55%**	**3%**
276b	CH_2-Bn	6%	18%	30%	17%
266b	**2-F-Bn**	**1%**	**1%**	**43%**	**2%**
277b	CH_2-2-F-Bn	8%	3%	8%	5%
278b	4-CN-2-F-Bn	5%	2%	22%	4%
279b	3-F-Bn	4%	1%	38%	7%
280b	4-F-Bn	3%	4%	32%	3%
281b	2,3-F-Bn	1%	12%	44%	1%
282b	2,4-F-Bn	1%	2%	41%	7%
283b	2,5-F-Bn	14%	10%	17%	9%
284b	2,6-F-Bn	10%	1%	43%	5%
285b	3,5-F-Bn	4%	5%	57%	1%
286b	2,4,6-F-Bn	9%	2%	40%	2%
287b	2-Cl-Bn	11%	4%	13%	7%
288b	3-Cl-Bn	6%	21%	35%	3%
289b	4-Cl-Bn	4%	5%	57%	1%
290b	3-Cl-2-F-Bn	1%	14%	42%	2%
291b	2-Cl-6-F-Bn	2%	10%	20%	4%
ISAM-140	-	20%	28%	3.49 ± 0.2	2%
DPCPX	-	2.20 ± 0.2	157 ± 3	73.2 ± 1.4	1722 ± 11
ZM241385	-	683 ± 4	1.9 ± 0.1	65.7 ± 1.1	863 ± 4
NECA	-	14.0 ± 1	20.0 ± 3	2400 ± 35	6.20 ± 0.9

[a)] Displacement of specific [^{3}H]DPCPX binding in human CHO cells expressed as K_i in nM (n = 3) or percentage displacement of specific binding at a concentration of 1 μM (n = 2). [b)] Displacement of specific [^{3}H]4-(2-[7-amino-2-(2-furyl)[1,2,4]triazolo[2,3-*a*][1,3,5]triazin-5-ylamino]ethyl)phenol binding in human HeLa cells expressed as K_i in nM (n = 3) or percentage displacement of specific binding at a concentration of 1 μM (n = 2). [c)] Displacement of specific [^{3}H]DPCPX binding in human HEK-293 cells expressed as K_i in nM (n = 3) or percentage displacement of specific binding at a concentration of 1 μM (n = 2). [d)] Displacement of specific [^{3}H]NECA binding in human HeLa cells expressed as K_i in nM (n = 3) or percentage displacement of specific binding at a concentration of 1 μM (n = 2).

Table 3.23. Structure and adenosine receptor affinity data of Series **XXIXa**: Ethyl 1-substituted-4-(furan-3-yl)-2-methyl-1,4-dihydrobenzo[4,5]imidazo[1,2-*a*]pyrimidine-3-carboxylates (**292a-310a**).

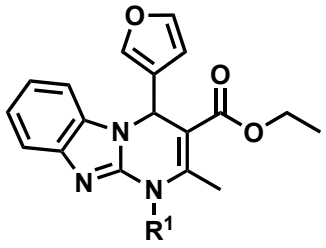

		K_i (nM) or % at 1 μM			
Compound	**R^1**	**hA_1[a)]**	**hA_{2A}[b)]**	**hA_{2B}[c)]**	**hA_3[d)]**
IIIc (ISAM-141)[84]	**H**	**7%**	**11%**	**20.60 ± 1.1**	**1%**
292a	Me	11%	7%	274 ± 8	8%
293a	Et	28%	12%	159 ± 6	3%
267a	**Pr**	**22%**	**35%**	**64.0 ± 3**	**12%**
294a	Propargyl	38%	22%	44.5 ± 1.6	23%
268a	**Bn**	**17%**	**57%**	**14.4 ± 2.1**	**14%**
295a	CH_2-Bn	16%	18%	52%	3%
269a	**2-F-Bn**	**4%**	**28.9 ± 1.1**	**10.2 ± 0.9**	**33%**
296a	CH_2-2-F-Bn	9%	13%	31%	2%
297a	4-CN-2-F-Bn	1%	5%	213 ± 2	1%
298a	3-F-Bn	4%	91.2 ± 3.1	6.4 ± 0.8	3%
299a	4-F-Bn	7%	121 ± 6	31.0 ± 2.1	12%
300a	2,3-F-Bn	14%	29.7 ± 2.1	10.9 ± 1.1	11%
301a	2,4-F-Bn	36%	95.1 ± 1.1	31.1 ± 1.3	12%
302a	2,5-F-Bn	10%	72.1 ± 1.6	9.6 ± 0.9	32%
303a	2,6-F-Bn	6%	51.0 ± 3	2.5 ± 0.5	1%
304a	3,5-F-Bn	4%	92.7 ± 1.3	142 ± 3	17%
305a	2,4,6-F-Bn	14%	42.0 ± 2.2	8.9 ± 1.3	28%
306a	2-Cl-Bn	1%	46%	34.8 ± 1.2	13%
307a	3-Cl-Bn	5%	18.4 ± 1.2	52.6 ± 3.2	9%
308a	4-Cl-Bn	2%	16%	137 ± 6	2%
309a	3-Cl-2-F-Bn	2%	23.7 ± 1.4	38.9 ± 2.1	21%
310a	2-Cl-6-F-Bn	5%	16.2 ± 1.2	7.6 ± 0.8	32%
ISAM-140	-	20%	28%	3.49 ± 0.2	2%
DPCPX	-	2.20 ± 0.2	157 ± 3	73.2 ± 1.4	1722 ± 11
ZM241385	-	683 ± 4	1.9 ± 0.1	65.7 ± 1.1	863 ± 4
NECA	-	14.0 ± 1	20.0 ± 3	2400 ± 35	6.20 ± 0.9

[a)] Displacement of specific [^{3}H]DPCPX binding in human CHO cells expressed as K_i in nM (n = 3) or percentage displacement of specific binding at a concentration of 1 μM (n = 2). [b)] Displacement of specific [^{3}H]4-(2-[7-amino-2-(2-furyl)[1,2,4]triazolo[2,3-*a*][1,3,5]triazin-5-ylamino]ethyl)phenol binding in human HeLa cells expressed as K_i in nM (n = 3) or percentage displacement of specific binding at a concentration of 1 μM (n = 2). [c)] Displacement of specific [^{3}H]DPCPX binding in human HEK-293 cells expressed as K_i in nM (n = 3) or percentage displacement of specific binding at a concentration of 1 μM (n = 2). [d)] Displacement of specific [^{3}H]NECA binding in human HeLa cells expressed as K_i in nM (n = 3) or percentage displacement of specific binding at a concentration of 1 μM (n = 2).

Table 3.24. Structure and adenosine receptor affinity data of Series **XXIXb**: Ethyl 10-substituted-4-(furan-3-yl)-2-methyl-1,4-dihydrobenzo[4,5]imidazo[1,2-*a*]pyrimidine-3-carboxylates (**292b-310b**).

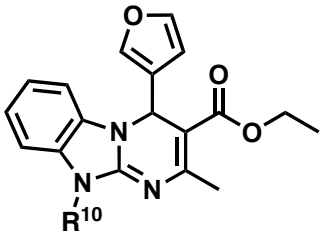

		K_i (nM) or % at 1 μM			
Compound	**R^{10}**	**hA_1[a)]**	**hA_{2A}[b)]**	**hA_{2B}[c)]**	**hA_3[d)]**
IIIc (ISAM-141)[84]	**H**	**7%**	**11%**	**20.60 ± 1.1**	**1%**
292b	CH_3	2%	10%	50%	2%
293b	Et	8%	46%	77.1 ± 2.7	1%
267b	**Pr**	**1%**	**252 ± 4**	**29%**	**7%**
294b	Propargyl	4%	137 ± 6	67.3 ± 4.1	3%
268b	**Bn**	**14%**	**1%**	**41%**	**33%**
295b	CH_2-Bn	6%	12%	16%	5%
269b	**2-F-Bn**	**8%**	**5%**	**2%**	**25%**
296b	CH_2-2-F-Bn	12%	1%	7%	1%
297b	4-CN-2-F-Bn	2%	1%	39%	3%
298b	3-F-Bn	7%	101 ± 3	324 ± 4	19%
299b	4-F-Bn	12%	47%	307 ± 6	33%
300b	2,3-F-Bn	3%	48%	243 ± 3	1%
301b	2,4-F-Bn	4%	21%	274 ± 9	1%
302b	2,5-F-Bn	4%	45%	42%	36%
303b	2,6-F-Bn	7%	17%	57%	2%
304b	3,5-F-Bn	2%	63.6 ± 2.6	46%	4%
305b	2,4,6-F-Bn	4%	16%	55%	1%
306b	2-Cl-Bn	8%	24%	30%	6%
307b	3-Cl-Bn	10%	35%	45%	4%
308b	4-Cl-Bn	8%	18%	31%	2%
309b	3-Cl-2-F-Bn	6%	6%	275 ± 8	2%
310b	2-Cl-6-F-Bn	4%	16%	27%	2%
ISAM-140	-	20%	28%	3.49 ± 0.2	2%
DPCPX	-	2.20 ± 0.2	157 ± 3	73.2 ± 1.4	1722 ± 11
ZM241385	-	683 ± 4	1.9 ± 0.1	65.7 ± 1.1	863 ± 4
NECA	-	14.0 ± 1	20.0 ± 3	2400 ± 35	6.20 ± 0.9

[a)] Displacement of specific [^{3}H]DPCPX binding in human CHO cells expressed as K_i in nM (n = 3) or percentage displacement of specific binding at a concentration of 1 μM (n = 2). [b)] Displacement of specific [^{3}H]4-(2-[7-amino-2-(2-furyl)[1,2,4]triazolo[2,3-*a*][1,3,5]triazin-5-ylamino]ethyl)phenol binding in human HeLa cells expressed as K_i in nM (n = 3) or percentage displacement of specific binding at a concentration of 1 μM (n = 2). [c)] Displacement of specific [^{3}H]DPCPX binding in human HEK-293 cells expressed as K_i in nM (n = 3) or percentage displacement of specific binding at a concentration of 1 μM (n = 2). [d)] Displacement of specific [^{3}H]NECA binding in human HeLa cells expressed as K_i in nM (n = 3) or percentage displacement of specific binding at a concentration of 1 μM (n = 2).

Table 3.25. Structure and adenosine receptor affinity data of Racemic and Enantiomers of Selected Ligands.

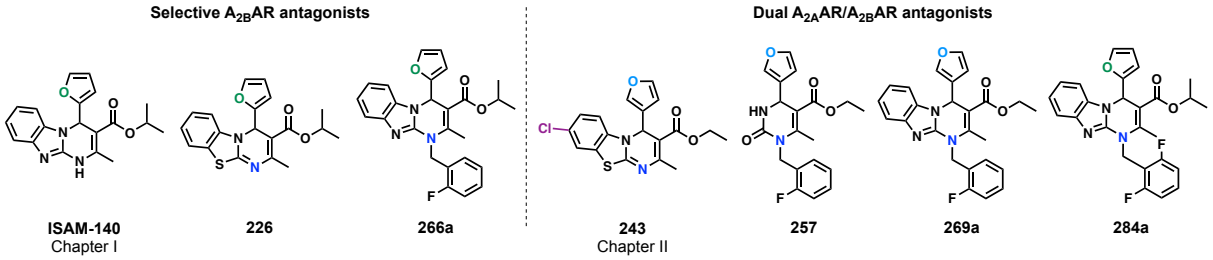

Compound	K_i (nM) or % at 1 µM			
	hA_1[a)]	hA_{2A}[b)]	hA_{2B}[c)]	hA_3[d)]
(±)-ISAM-140 (Chapter I)	**20%**	**25%**	**3.49 ± 0.2**	**2%**
(*R*)-ISAM-140 (Chapter I)	4%	2%	17%	2%
(*S*)-ISAM-140 (Chapter I)	2%	2%	0.89 ± 0.2	4%
(±)-226 (Chapter II)	**1%**	**16%**	**11.6 ± 0.8**	**5%**
(*R*)-226 (Chapter II)	26%	10%	19.2 ± 1.2	12%
(*S*)-226 (Chapter II)	24%	4%	4.30 ± 0.6	1%
(±)-266a	**19%**	**24%**	**1.50 ± 0.4**	**40%**
(*R*)-266a	7%	12%	65.9 ± 3.1	13%
(*S*)-266a	8%	44%	0.52 ± 0.1	6%
(±)-243 (Chapter II)	**20%**	**90.7 ± 4**	**4.30 ± 0.2**	**3%**
(*S*)-243 (Chapter II)	5%	109 ± 6	6.10 ± 0.6	20%
(*R*)-243 (Chapter II)	1%	27.3 ± 1.8	1.20 ± 0.2	1%
(±)-257	**13%**	**39.0 ± 1.1**	**50.0 ± 1.0**	**9%**
(*S*)-257	1%	4%	16%	4%
(*R*)-257	19%	20.2 ± 1.3	7.0 ± 0.5	41%
(±)-269a	**4%**	**28.9 ± 1.1**	**10.2 ± 0.9**	**33%**
(*S*)-269a	8%	8%	27%	20%
(*R*)-269a	6%	14.2 ± 0.9	5.2 ± 0.8	41%
(±)-284a	**8%**	**52.9 ± 2.3**	**8.5 ± 1.1**	**23%**
(*R*)-284a	13%	3%	1%	17%
(*S*)-284a	9%	23.9 ± 2.1	3.1 ± 0.9	20%
ISAM-140	20%	28%	3.49 ± 0.2	2%
DPCPX	2.20 ± 0.2	157 ± 3	73.2 ± 1.4	1722 ± 11
ZM241385	683 ± 4	1.9 ± 0.1	65.7 ± 1.1	863 ± 4
NECA	14.0 ± 1	20.0 ± 3	2400 ± 35	6.20 ± 0.9

[a)] Displacement of specific [^{3}H]DPCPX binding in human CHO cells expressed as K_i in nM (n = 3) or percentage displacement of specific binding at a concentration of 1 µM (n = 2). [b)] Displacement of specific [^{3}H]4-(2-[7-amino-2-(2-furyl)[1,2,4]triazolo[2,3-*a*][1,3,5]triazin-5-ylamino]ethyl)phenol binding in human HeLa cells expressed as K_i in nM (n = 3) or percentage displacement of specific binding at a concentration of 1 µM (n = 2). [c)] Displacement of specific [^{3}H]DPCPX binding in human HEK-293 cells expressed as K_i in nM (n = 3) or percentage displacement of specific binding at a concentration of 1 µM (n = 2). [d)] Displacement of specific [^{3}H]NECA binding in human HeLa cells expressed as K_i in nM (n = 3) or percentage displacement of specific binding at a concentration of 1 µM (n = 2).

Table 3.26. Functional data of compounds **257**, **266a** and **269a** in $A_{2A}AR$ and $A_{2B}AR$.

	hA_{2A}		*h*A_{2B}	
Compound	K_i	K_B[a)]	K_i	K_B[b)]
257	39.0 ± 1.1	**50.9 ± 2.1**	50.0 ± 1.0	**60.2 ± 3.0**
266a	-	-	1.50 ± 0.4	6.15 ± 1.2
269a	28.9 ± 2.1	52.3 ± 1.4	10.2 ± 1.6	15.0 ± 2.1

[a)] Inhibition of cAMP production in HeLa-A_{2A} cells [b)] Inhibition of cAMP production in HEK-293-A_{2B} cells.

3.3.4 Structure-Activity Relationship and Molecular Modeling

Examination of the binding data reveals the identification of twenty six $A_{2A}AR/A_{2B}AR$ dual antagonists, fifteen of which combining high affinity for both receptors and outstanding selectivity (K_i < 100 nM for $A_{2A}AR$ and $A_{2B}AR$ and > 1000 nM for other two subtypes, Table 3.19; **250**, **251**, **257** and **259**, Table 3.20; **269a**, Table 3.21; **284a**, Table 3.23; **298a**, **300a**, **301a**, **302a**, **303a**, **305a**, **307a**, **309a** and **310a**). Although this chapter emphasizes the identification of $A_{2A}AR/A_{2B}AR$ dual antagonists, during the pharmacological screening of the obtained library, we identified thirty-two ligands with high or moderate affinity for $A_{2B}AR$ (K_i < 100 nM) and, anecdotally, two ligands with moderate affinity for $A_{2A}AR$ (K_i < 300 nM, Table 3.20; **267b**, Table 3.24; **304b**).

After analyzing the exploratory series **XXVI-XXVII**, which are based on monocyclic and tricyclic scaffolds respectively, initial conclusions can be drawn. The first and clearest trend observed is that substitution with propyl, benzyl and 2-fluorobenzyl at position 10 of the tricyclic system (Table 3.20, compounds b) causes a total and absolute loss of affinity for $A_{2B}AR$. Anecdotally, only one compound substituted at position 10 shows moderate affinity, in this case for $A_{2A}AR$: **267b** (Table 3.20, Het = 3-furyl, Alk = Et, R = propyl, K_i ($A_{2A}AR$) = 252 nM). Comparative analysis of the binding data obtained for model ligands (**Ia-d** and **IIIa-d**) and ligands of exploratory series (**249–260** and **261a–272a**) prove that N^1-substitution either has no effect or a positive effect on the affinity for the $A_{2B}AR$. As we are already aware from earlier chapters, the best substitution pattern for model ligands is 2-furyl as heteroaromatic ring (Het) and isopropyl as alcoxy residue in the ester moiety (Alk), with the differences in affinity depending on the substitution pattern being much more notable in the monocyclic scaffold (Table 3.19, Figure 3.45, dark blue). On monocyclic compounds, *N*-substitution with propyl has a negative effect, resulting in compounds that are completely inactive across all four

adenosine receptor subtypes with the exception of **258** [K_i ($A_{2B}AR$) = 502 nM], that increases 3-fold the affinity in $A_{2B}AR$ in comparison with its model ligand **Id** [K_i ($A_{2B}AR$) = 1486 nM (Table 3.19, Figure 3.45)]. For scaffolds lacking an optimal substitution pattern, such as **Ia** (Het = 2-furyl, Alk = Et) and **Id** (Het = 3-furyl, Alk = *i*Pr), *N*-substitution with benzyl or 2-fluorobenzyl can substantially enhance the binding affinity for the $A_{2B}AR$ receptor, increasing it from 10 to 40-fold in the most favorable cases (e.g., **250**, **251**, **259**, **260**), generating in all cases highly balanced dual $A_{2A}AR/A_{2B}AR$ antagonists. When the substitution pattern of the scaffold is already optimal (**Ib-c**), using benzyl substitutions causes a substantial (15 to 25-fold) decrease [e.g., **253** (K_i = 688 nM) and **256** (no affinity)], whereas introducing 2-fluorobenzyl substitutions results in a minor reduction in $A_{2B}AR$ affinity (e.g., **254** and **257**). Despite this, their ability to function as dual $A_{2A}AR/A_{2B}AR$ antagonists compensates for this slight decrease in potency (Figure 3.45). The substituted tricyclic compounds exhibit comparable behavior, but because the unsubstituted model molecules have a higher affinity, most substitutions lead to a decrease in affinity for $A_{2B}AR$. In this case the propyl group is also the most deleterious substitution, causing the reduction in affinity compared with model ligands. Except for compounds derived from **IIIa** (Het = 2-furyl, Alk = Et), *N*-substitution of the tricyclic scaffold generates compounds with high affinity for $A_{2B}AR$ (K_i = 1.50 – 64.0 nM). The best substitution is 2-fluorobenzyl, being the only one able to increase the affinity of its model ligand (e.g. **266a** vs **IIb** and **269a** vs **IIIb,** Figure 3.45). These two molecules are special for different reasons. Compound **266a** is the best $A_{2B}AR$ antagonist with non-xanthine structure described to date, with very high affinity (K_i = 1.5 nM) and full selectivity for the $A_{2B}AR$, overtaking the predecessor **IIb** (**ISAM-140**, K_i = 3.49 nM). Compound **269a** stands out, not only for its high affinity for $A_{2B}AR$ (2 times higher than **ISAM-140**), but also for its dual $A_{2A}AR/A_{2B}AR$ profile, being the dual antagonist with the best affinity for both adenosine receptor subtypes (Figure 3.45 and Figure 3.46).

In terms of dual behavior, monocyclic compounds have a greater tendency to generate dual compounds. In this case, substitution with benzyl and 2-fluorobenzyl generates dual $A_{2A}AR/A_{2B}AR$ in those with measurable affinity for $A_{2B}AR$ (Figure 3.46, in blue). For tricyclic compounds, however, only those presenting 3-furyl scaffold with *N*-(2-fluorobenzyl)substituted exhibit dual behavior (Figure 3.46, in green). This perfectly fits with the findings of the previous chapters on the higher tendency to dual activity in those tricyclic compounds with 3-furyl as pentagonal heteroaromatic substituent (Het).

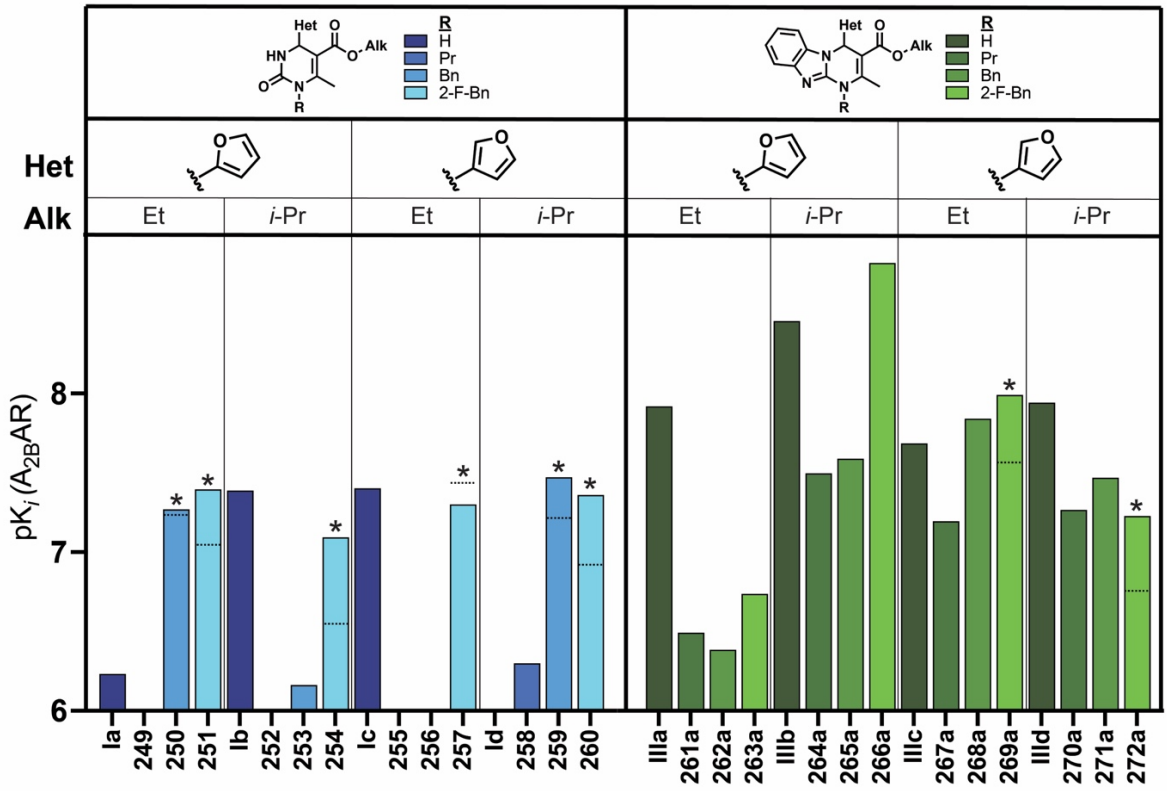

Figure 3.45. Interleaved bars chart showing $A_{2B}AR$ pK_i [-log(K_i)] for the *N*-substitution of monocyclic (blue) and tricyclic (green) scaffolds. The color shade indicates the substituent at N^1 position. The asterisk indicates molecules with dual $A_{2A}AR$/$A_{2B}AR$ behavior, and the pKi value for $A_{2A}AR$ is marked with a dotted line. N^{10}-substituted tricycles were not included in the chart as they do not show relevant affinity in $A_{2B}AR$.

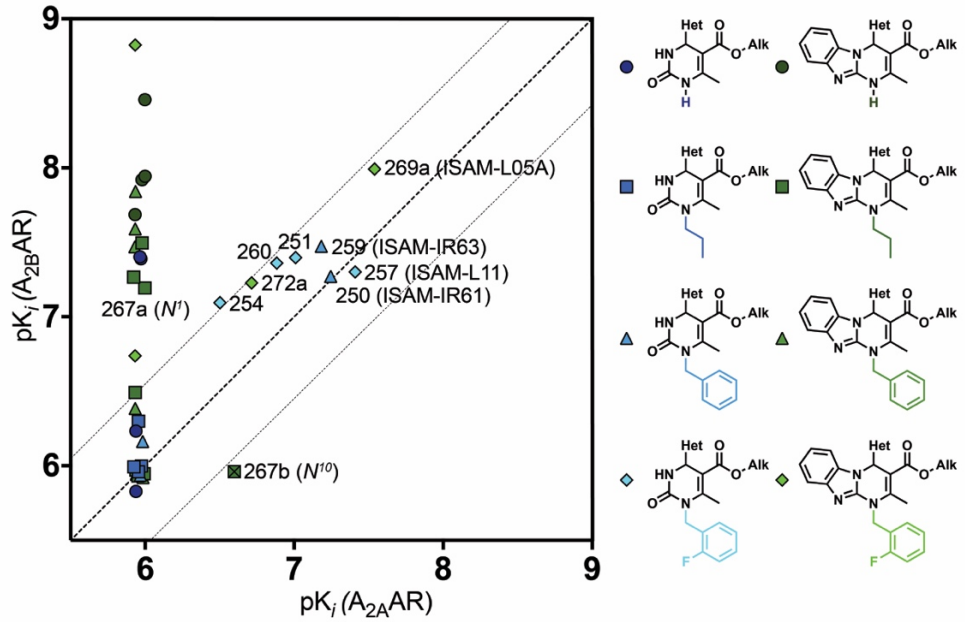

Figure 3.46. Affinity-selectivity plot of exploratory series **XXVI-XXVII**. Shape indicates the substituent, and the color indicates scaffold (blue: monocyclic, green: tricyclic).

The findings demonstrate that exploring *N*-substitution, particularly with benzyl derivatives, represents a novel point of diversity for the discovery of improved druglike properties in $A_{2B}AR$ (and dual $A_{2A}AR/A_{2B}AR$) antagonists. The significant alteration in the structure caused by these substitutions results in considerable changes in the physicochemical properties, especially for logP. The term "molecular obesity" describes how the biological activity of a molecule can be affected by an increase in size and lipophilicity (logP), which can lead to a greater preference for the molecule to be in the cell membrane rather than in the extracellular medium.[183] This can result in artificially inflated affinity values. In order to account for this effect, a linear regression analysis was performed between the pK_i ($A_{2B}AR$) and WlogP values of the molecules in the exploratory series. Figure 3.47 shows the results, which indicate no correlation ($R^2 = 0.2472$) between the predicted values of lipophilicity and affinity. This rules out the possibility that the observed increase in affinity is due to an increase in lipophilicity.

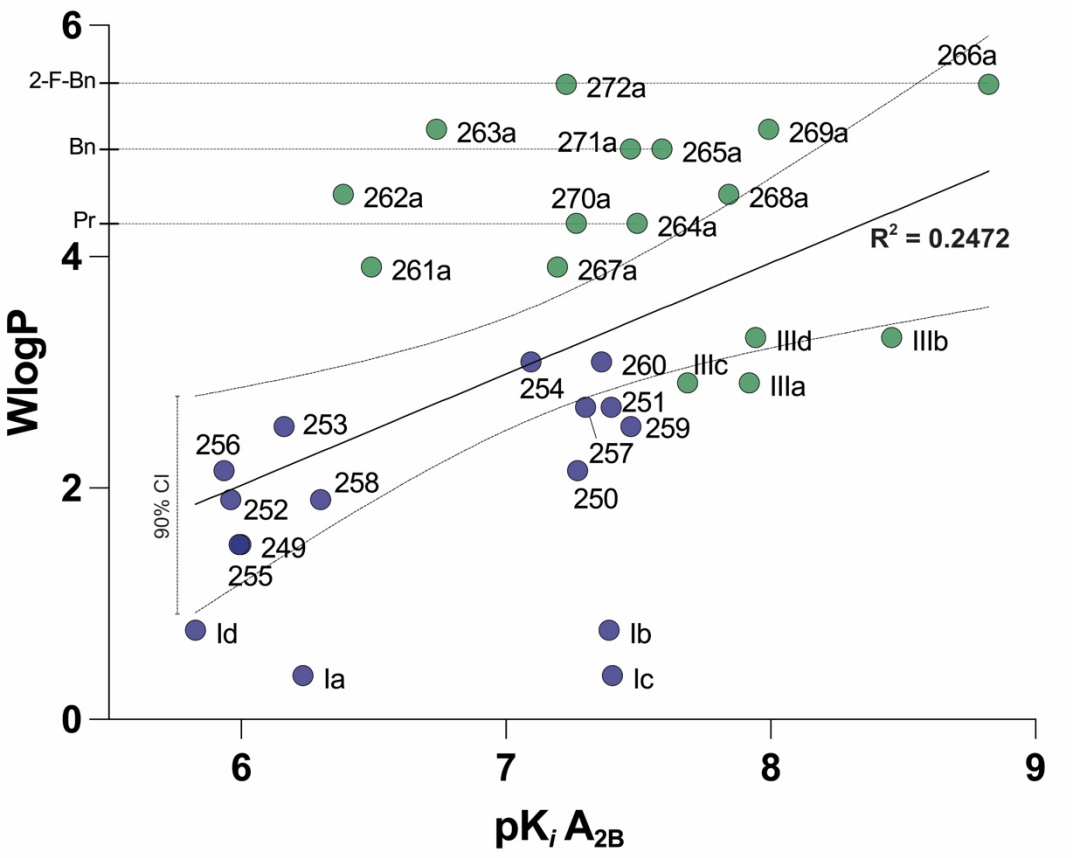

Figure 3.47. WlogP vs pK_i A_{2B} plot for exploratory series **XXVI-XXVII**. The graphic shows no correlation between lipophilicity and binding affinity, ruling out "molecular obesity". WlogP values were calculated with SwissADME (http://swissadme.ch). In blue, monocyclic compounds, less lipophilic than tricyclic compounds, in green.

Docking assays were conducted on representative monocyclic (series **XXVI**, Figure 3.48) and tricyclic compounds (series **XXVII**, Figure 3.49) on $A_{2A}AR$ (open conformation PDB: 3UZC, closed conformation PDB: 4EIY) and $A_{2B}AR$ ($A_{2A}AR$ homology model, PDB: 3EML) to elucidate the structure-activity relationship and complete the binding study of these compounds. The resultant binding mode is in good agreement with the pharmacological data. As explained in the introduction of this Thesis (1.4 Structure and Pharmacology of Adenosine Receptors), one of the main differences surrounding the of $A_{2A}AR$ and $A_{2B}AR$ orthosteric binding site is the presence of a salt bridge between extracellular loops 2 and 3 (His^{EL3} and Glu^{EL2}) in $A_{2A}AR$, generating two possible inactive conformations: open and closed (Figure 3.48).[86]

Model series **I** exhibits a favorable binding mode in the $A_{2B}AR$, as depicted for **Ic** (K_i = 39.6 nM) in Figure 3.48A. However, due to steric hindrance and the inability to stabilize an open conformation, it does not fit well in the $A_{2A}AR$. All *N*-propyl derivatives, including **255** (series **XXVI**, Figure 3.48B), are low affinity or inactive compounds in both $A_{2A}AR$ and $A_{2B}AR$. For $A_{2B}AR$, the loss of affinity may be due to the loss of a hydrogen bridge with Asn6.55 without adding any new interaction with the binding site. The decrease in affinity observed in the $A_{2B}AR$ receptor could be linked to the loss of one hydrogen bond with $Asn^{6.55}$, without the presence of any alternative interactions being established within the binding site. *N*-propyl derivatives are also unable to stabilize the open conformation of the $A_{2A}AR$ receptor. Propyl appears to clash with the salt bridge that forms between His^{ECL3} and Glu^{ECL2}, which hinders proper receptor binding (Figure 3.48B, left). For substitution with benzyl, the possibility of stabilization of the $A_{2A}AR$ open conformation is observed, allowing us to obtain two dual N-benzylated antagonists. For $A_{2B}AR$, being *N*-benzyl an aromatic substituent, the possibility of interaction with Lys^{ECL3} through a π-cation bond appears. However, the free turn of the benzyl substituent may or may not generate this interaction, depending on the way the molecule is positioned (Figure 3.48C). Regardless of the scaffold, dual ligands have consistently been obtained for compounds that have been 2-fluorobenzylated (Figure 3.48D). In the case of $A_{2A}AR$, the open conformation of the receptor is also stabilized, allowing the accommodation of the molecule at the binding site. For $A_{2B}AR$, the aforementioned π-cation interaction is forced due to steric hindrance of the fluor at position 2 (Figure 3.48E).

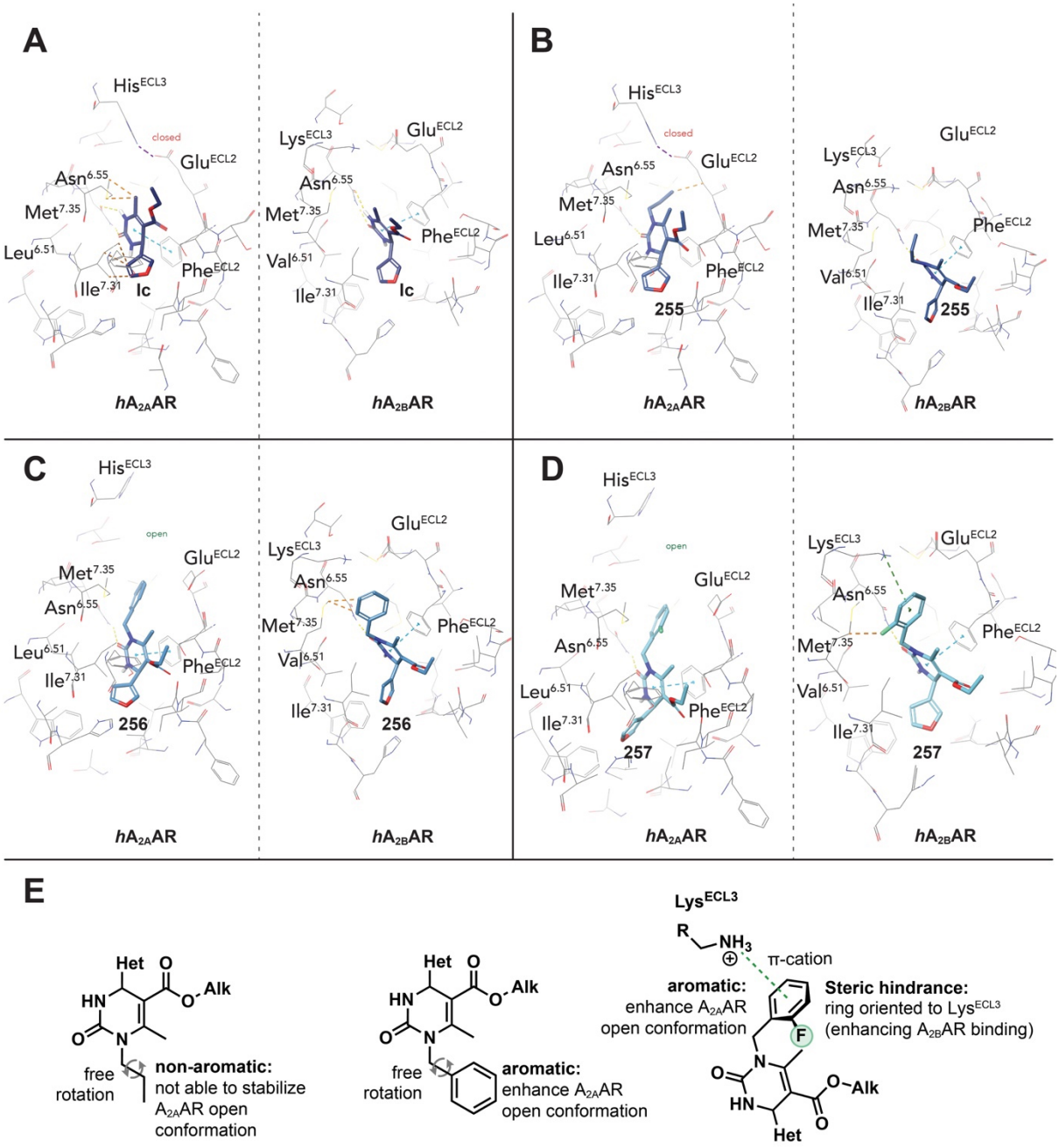

Figure 3.48. Docking-predicted binding modes in $A_{2A}AR$ (open conformation PDB: 3UZC, closed conformation PDB: 4EIY) and $A_{2B}AR$ ($A_{2A}AR$ homology model, PDB: 3EML) for A) **Ic** (R = H), B) 255 (R = Pr), C) 256 (R = Bn), and D) 257 (R = 2-F-Bn). E) SAR scheme for monocyclic *N*-substituted compounds. Note that while compounds **255** and **256** do not fit well in $A_{2A}AR$ and $A_{2B}AR$ (orange clashes), compound **257** fits perfectly despite the loss of one hydrogen bond (yellow dashed lines) with $Asn^{6.55}$. This could be attributed to the formation of a π-cation interaction (green dashed line) with Lys^{ECL3}.

The behavior demonstrated by the monocyclic compounds is preserved in the tricyclic compounds, albeit with some variations. Since the tricyclic model compounds exhibit superior affinity compared to monocyclic compounds, a majority of the *N*-substituted tricyclic derivatives demonstrate higher affinity than their monocyclic equivalents. In contrast to the monocyclic series, this series produces *N*-propyl derivatives that exhibit favorable pharmacological affinity values. This is likely due to its more consistent binding mode in A_{2B}AR [Figure 3.49A (monocyclic model ligand) vs Figure 3.49B (tricyclic model ligand)]. Also, a significant differentiation between the two regioisomers generated in the Biginelli reaction is shown. As presented in Table 3.20 and explained above, in all cases the N^1-derivatives shown moderate or high affinity while N^{10}-substitution generates totally inactive compounds in both A_{2A}AR and A_{2B}AR. Figure 3.49C-F illustrates the binding mode of different derivatives at A_{2B}AR, revealing a reduction in crucial receptor interactions – hydrogen-bond with $Asn^{6.55}$ and π-π stacking with Phe^{ECL2} – and an increase in binding site clashes for N^{10}-substituted compounds (Figure 3.49D and F), whereas N^1-derivatives maintain a both interactions in A_{2B}AR binding site (Figure 3.49C and E).

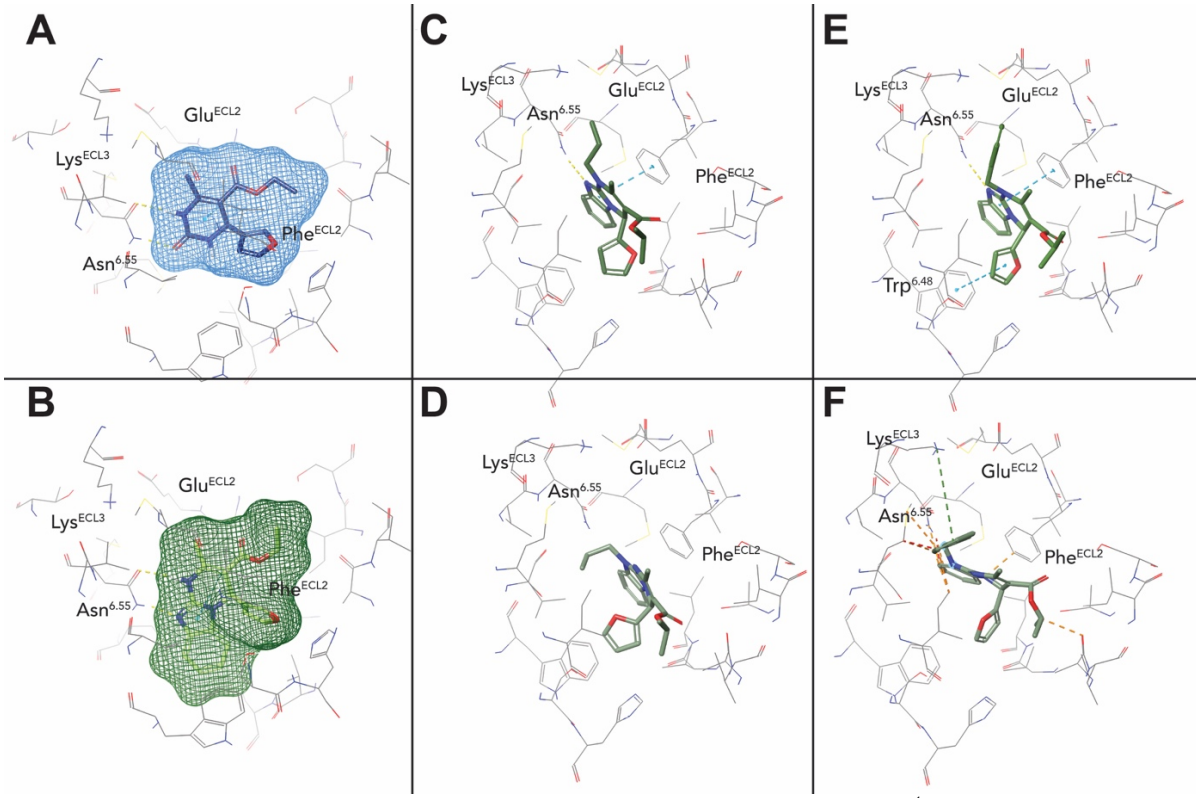

Figure 3.49. Mesh surfaces of A) **Ic** vs B) **IIIc** at A_{2B}AR binding site. Docking poses of C) N^1-propyl tricyclic derivative (**267a**), D) N^{10}-propyl tricyclic derivative (**267b**), E) N^1-benzyl tricyclic derivative (**268a**), and F) N^{10}-benzyl tricyclic derivative (**268b**). Yellow dashed lines represent H-Bonds; blue dashed line represents π-π interaction; green dashed line represent π-cation interactions; orange and red dashed lines represent clashes.

To comprehensively investigate the potential for substitution, the most effective scaffolds in the exploratory series (**IIIb** and **IIIc**) was chosen, and nineteen different substituents were incorporated, including alkyl residues ranging in size, as well as benzyl residues with varying substitution patterns.

When compared to the model ligand **ISAM-140** (**IIIb**), N^1-alkyl derivatives showed a considerable decrease in affinity for $A_{2B}AR$, similar to the *N*-propyl derivatives previously explored. Despite this decrease, it is noteworthy that the affinities obtained for the different alkyl substitutions were consistently similar, ranging from 22.7 to 78.3 nM (Table 3.21). Interestingly, there was a slight increase in affinity observed as the size of the substituent increased (Figure 3.50), with propargyl (**275a**) showing the highest affinity, followed by propyl (**255a**), ethyl (**274a**), and methyl (**273a**). For N^{10}-alkyl derivatives, the size of the substituent plays an important role. Among the compounds tested, only two N^{10}-substituted derivatives – with smaller alkyl substituents – exhibited measurable affinity for $A_{2B}AR$ (Figure 3.50): **273b** (R = Me, K_i = 147 nM) and **274b** (R = Et, with a K_i value of 41.9 nM).

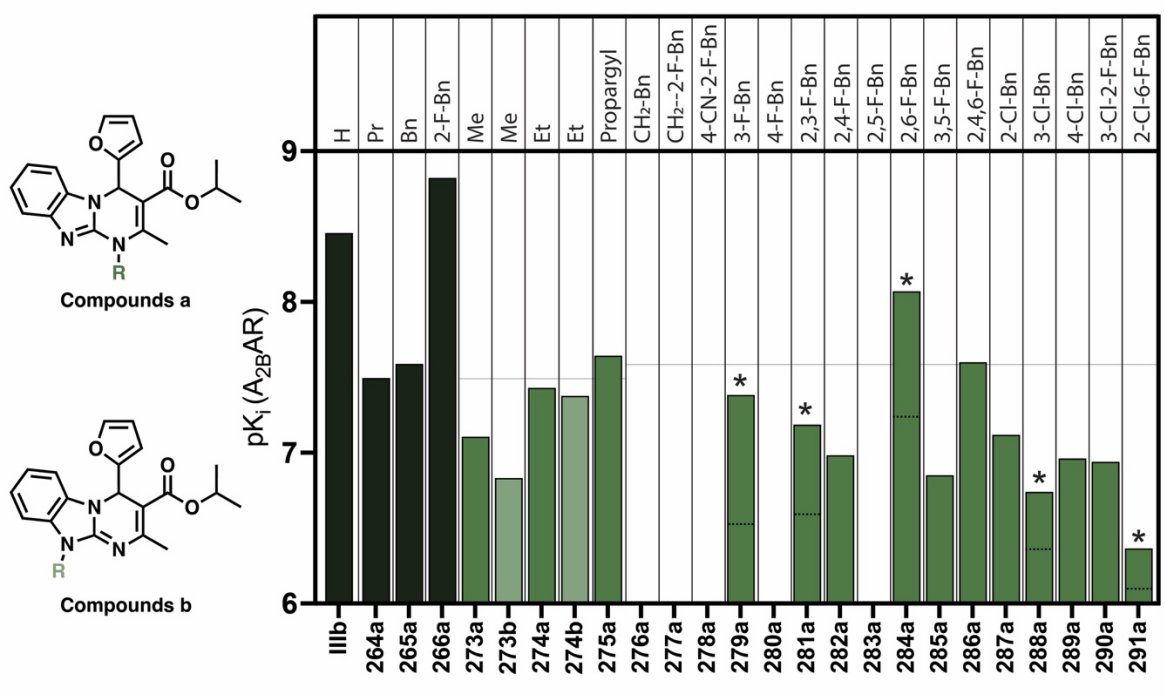

Figure 3.50. Interleaved bars chart showing $A_{2B}AR$ pK_i [-log(K_i)] for the exhaustive exploration of *N*-substitution of **IIIb**. The asterisk indicates molecules with dual $A_{2A}AR/A_{2B}AR$ behavior, and the pKi value for $A_{2A}AR$ is marked with a dotted line. Not all N^{10}-substituted tricycles were included in the chart as they do not show relevant affinity in $A_{2B}AR$.

When larger residues such as phenethyl (**276a**) and 2-fluorophenethyl (**277a**) were used in *N*-substitution, the resulting ligands were found to be completely inactive, unlike the benzyl (**256a**, K_i = 25.7 nM) and 2-fluorobenzyl derivatives (**266a**, K_i = 1.5 nM). Among the different benzyl halogenation patterns, fluorine was found to be superior to chlorine in most cases. However, there was one exception where the introduction of chlorine at position 4 of benzyl (**289a**, K_i = 109 nM) was found to be at least 10 times more effective than the introduction of fluorine at the same position (**280a**, K_i > 1000 nM).

Most of the N^1-benzylations explored have led to selective ligands for $A_{2B}AR$ (Figure 3.50), similar to what occurred in the preliminary series. However, five dual ligands with moderate potency were also obtained: **279a** [K_i ($A_{2A}AR$) = 322 nM, K_i ($A_{2B}AR$) = 41.3 nM], **281a** [K_i ($A_{2A}AR$) = 283 nM, K_i ($A_{2B}AR$) = 65.2 nM], **284a** [K_i ($A_{2A}AR$) = 52.9 nM, K_i ($A_{2B}AR$) = 8.5 nM], **288a** [K_i ($A_{2A}AR$) = 442 nM, K_i ($A_{2B}AR$) = 182 nM], and **291a** [K_i ($A_{2A}AR$) = 792 nM, K_i ($A_{2B}AR$) = 432 nM]. These compounds share common structural features: **279a** and **288a** are 3-halogenated benzyl derivatives (with fluorine and chlorine substitutions, respectively), **281a** is a 2,3-difluorobenzyl derivative, while **284a** and **291a** are 2,6-dihalogenated benzyl derivatives (with 2,6-difluoro and 2-chloro-6-fluoro substitutions, respectively). After comparing different benzyl substitution positions, some preliminary conclusions can be drawn. Position 2 seems to be the best substitution site, although the affinity decreases as the size of the halogen increases (e.g., **266a** vs **287a**, Table 3.21 and Figure 3.50). The remaining positions with fluoro- and chloro-substitutions are not as effective, but they still maintain a significant amount of affinity compared to **265a** (**ISAM-140** N^1-benzyl derivative), particularly the fluoroderivatives. Comparing the monohalogenation of benzyl with fluorine and chlorine, clearly the fluorobenzyl derivatives are superior to chlorobenzyl, except in the case of position 4, where only 4-chlorobenzyl (**289a**) was able to keep $A_{2B}AR$ binding affinity. Regarding the pharmacological data of the poly-halogenated derivatives (**281a–286a** and **290a–291a**), we observed that simultaneous substitutions of position 2 and 3, 4 and/or 6 result in antagonists with a good affinity profile for $A_{2B}AR$ (e.g., **281a**, **282a**, **284a**, **286a**). On the other hand, simultaneous substitutions of position 2 and 5 (**283a**) or 3 and 5 (**285a**) led to compounds with low affinity for $A_{2B}AR$.

The differences on $A_{2B}AR$ binding mode of these compounds provides a consistent explanation for the varying affinities observed in different substitution patterns (Figure 3.51). Regarding alkyl substituents, those shorter than propyl (R = Me and Et) seem to fit in both

positions (with better affinity at N^1), by not exerting such a large steric hindrance at the binding site (Figure 3.49D and F). Concerning benzyl substituents, as already highlighted, there are significant differences depending on the substitution pattern, also in binding mode. To facilitate the analysis, the compounds were categorized into three groups: fluoroderivatives (depicted in green in Figure 3.51), chloroderivatives (depicted in blue in Figure 3.51), and chlorofluoroderivatives (depicted in cyan in Figure 3.51). All the fluoroderivatives with good affinity data shows a similar binding mode, characterized by the π-cation interaction stablished between benzyl aromatic ring and Lys^{ECL3} (Figure 3.51A-B,D-E,G,I), with a decrease in the affinity of the difluorinated compounds due to possible steric hindrance at the binding site. The same behavior observed in the exploratory series with the substituent at position 2 is also observed here, expanded to the substitution at position 3, both stabilizing the benzyl in the correct angle for interaction with Lys^{ECL3}. The only difference lies with the 4-fluoroderivative which allows for free rotation of the benzyl group without directly orienting it towards lysine, in addition to generating steric hindrance with Glu^{ECL2} (Figure 3.51C). For this reason, 2,3-difluorobenzyl derivative also keep $A_{2B}AR$ affinity (Figure 3.51D), while 2,4- and 2,5-difluorobenzyl substitution generate moderate and inactive compounds, respectively (Figure 3.51E-F). The 2,6-difluorobenzyl derivative **284a** exhibits a significantly high affinity for $A_{2B}AR$ (K_i = 8.5 nM), similar to the 2-fluorobenzyl derivative **266a** (K_i = 1.5 nM), due to the stabilization of the benzyl ring towards Lys^{ECL3} on both sides (Figure 3.51G). Conversely, the 3,5-difluorobenzyl derivative **285a** shows a lower affinity for $A_{2B}AR$ (K_i = 542 nM) than the 3-fluorobenzyl derivative **279a** (K_i = 41.3 nM), confirming 5 as a deleterious position for dual fluorination (Figure 3.51H). Interestingly, although the substitution at position 4 is not favorable, the 2,4,6-trifluorobenzyl derivative (**286a**) shows a very good affinity data (K_i = 25.1 nM), improving 4 times the affinity of the 2,4-difluorobenzyl derivative (**282a**, K_i = 104 nM). This could be attributed to the strong stabilization effect resulting from the simultaneous substitution at positions 2 and 6 (Figure 3.51I), countering the deleterious effect of fluorination at position 4.

As a result of the significant increase in substituent size when using chlorine instead of fluorine, there is a noticeable decrease in affinity. Consequently, the chlorobenzyl derivatives were unable to establish a π-cation interaction. However, in the case of the derivatives substituted at positions 2 and 3 (Figure 3.51A-B), the formation of a halogen bond with Lys^{ECL3} is allowed, maintaining a moderate affinity in $A_{2B}AR$. As a result of the good results in the

difluorination at positions 2,3 and 2,6, the obtaining of ligands combining fluorine and chlorine in these positions was also tested. The decrease in affinity compared to the difluorinated derivatives is quite significant (7 to 15-fold), primarily due to the steric hindrance caused by chlorine at the binding site (Figure 3.51D and Figure 3.51G), which prevents the establishment of π-cation interaction but allows for halogen bonding.

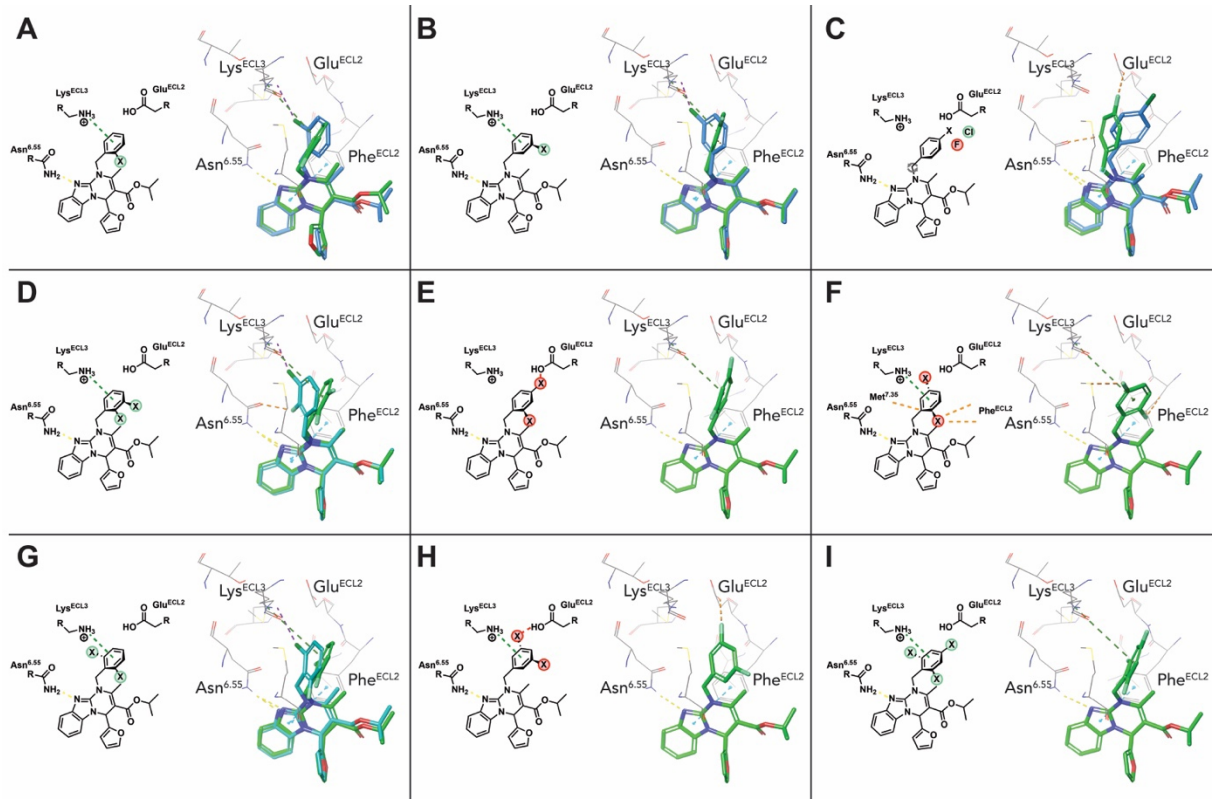

Figure 3.51. Schematic 2D and docking-predicted binding modes in A_{2B}AR (A_{2A}AR homology model, PDB: 3EML) for A) **266a** (X = 2-F) and **287a** (X = 2-Cl), B) **279a** (X = 3-F) and **288a** (X = 3-Cl), C) **280a** (X = 4-F) and **289a** (X = 4-Cl), D) **281a** (X = 2,3-F) and **290a** (X = 3-Cl-2-F), E) **282a** (X = 2,4-F), F) **283a** (X = 2,5-F), G) **284a** (X = 2,6-F) and **291a** (X = 6-Cl-2-F), H) **285a** (X = 3,5-F), and I) **286a** (X = 2,4,6-F). The compounds are colored based on their halogen (green: fluorine, blue: chlorine, cyan: fluorine and chlorine). Yellow dashed lines represent H-Bonds; blue dashed line represents π-π interaction; green dashed line represent π-cation interactions; purple dashed line represent π-cation interaction; orange and red dashed lines represent clashes.

As seen so far, the replacement of **ISAM-140** (Het = 2-furyl, Alk = isopropyl) produces very few dual A_{2A}AR/A_{2B}AR antagonists with moderate affinity. This behavior makes sense when considering the results in the exploratory series (series **XXVII**), where although there was a substantial increase in affinity for A_{2B}AR, none of the substitutions (R = Pr, Bn, and 2-F-Benzyl) generated any dual ligands. However, the substitution did result in the most potent dual antagonist in the exploratory series, **269a.** This evidence, combined with findings from

previous chapters, where the majority of obtained dual ligands contained a 3-furan as the exocyclic pentagonal ring [e.g., **60**, **243**], has led us to study the effect of alkylation and benzylation using **ISAM-141** (**IIIc**) as core structure.

When compared to the model ligand **ISAM-141** (**IIIc**), N^1-alkyl derivatives showed a considerable decrease in affinity for $A_{2B}AR$, with a similar behavior to that shown in previous series. Given the high structural similarity to the derivatives of **ISAM-140** (series **XXVIII**), the behavior of the alkyl derivatives is very similar. The affinity remains more or less constant in all N^1-alkyl derivatives. (Table 3.23) keeping the slight increase in affinity observed as the size of the substituent increased (Figure 3.52), with propyl (**268a**) showing the highest affinity, followed by propargyl (**294a**), ethyl (**293a**), and methyl (**292a**). For N^{10}-alkyl derivatives, the size of the substituent plays an important role. Among the compounds tested, two N^{10}-alkyl derivatives exhibited measurable affinity for $A_{2B}AR$ (Figure 3.52): **293b** (R = Et, K_i = 77.1 nM) and **294b** (R = Propargyl, with a K_i value 67.3 nM in $A_{2B}AR$ and 137 nM in $A_{2A}AR$). From these two compounds, we can draw two anecdotal conclusions: **293b** is the first and only case in the entire study where the N^{10} derivative has higher affinity than N^1, and **294b** is the first and only case in the entire study where the N^{10} derivative have dual $A_{2A}AR/A_{2B}AR$ behavior and the N^1 derivative exhibits selectivity for $A_{2B}AR$.

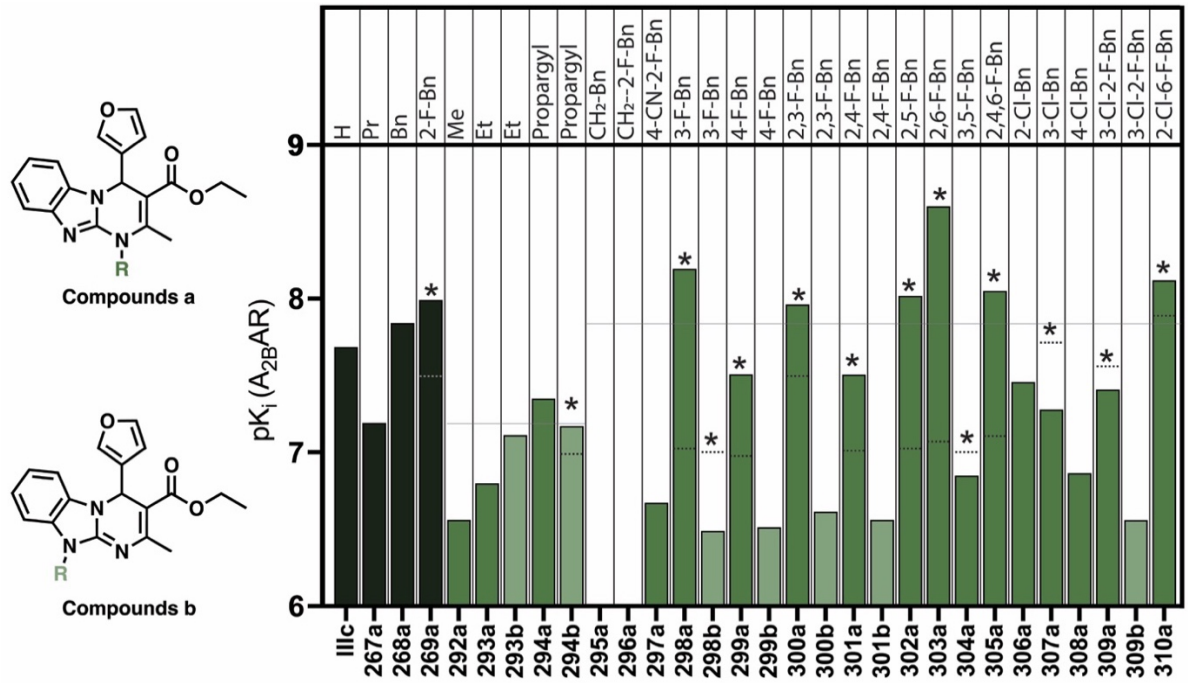

Figure 3.52. Interleaved bars chart showing $A_{2B}AR$ pK_i [-log(K_i)] for the exhaustive exploration of *N*-substitution of **IIIc**. The asterisk indicates molecules with dual $A_{2A}AR/A_{2B}AR$ behavior, and the pKi value for $A_{2A}AR$ is marked with a dotted line. Not all N^{10}-substituted tricycles were included in the chart as they do not show relevant affinity in $A_{2B}AR$.

When comparing series **XXVIII** and **XXIX** in terms of dual $A_{2A}AR/A_{2B}AR$ behavior, a clear difference can be observed (Figure 3.53 and Figure 3.54). The substitution of **ISAM-141** (Het = 3-furyl, Alk = ethyl, series **XXIX**) shows a higher tendency to generate dual ligands compared to the substitution of **ISAM-140** (Het = 2-furyl, Alk = isopropyl, series **XXVIII**). Out of the twenty tricyclic dual ligands, thirteen are derivatives of **ISAM-141** (eleven N^1 and two N^{10} substituted), while only seven are **ISAM-140** derivatives (all of them N^1). Regardless of the scaffold, all dual ligands in these series are benzyl derivatives (Figure 3.53, triangle), except for the previously mentioned propargylic derivative **294b** (substituted at N^{10}). If we are stricter, setting the K_i limit for both receptors at 100 nM, out of the 11 tricyclic dual ligands listed, 10 ligands were **ISAM-141** derivatives. This clearly highlights the significance of 3-furyl and ethyl as heteroaryl and alkyl substituents, respectively, for dual behavior.

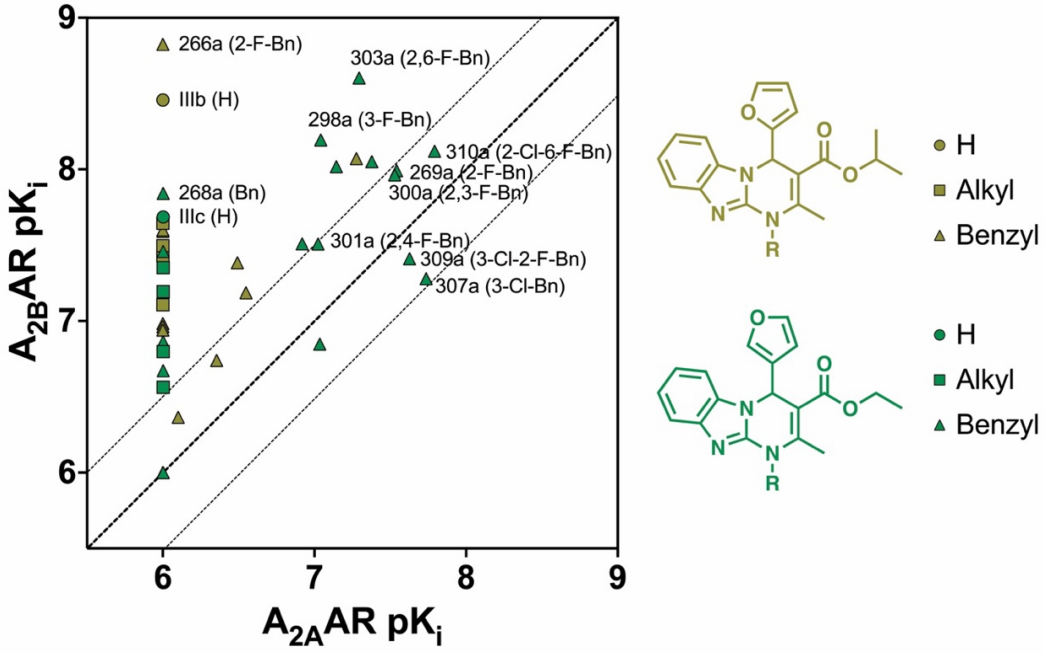

Figure 3.53. Affinity-selectivity plot of exploratory series **XXVIIIa-XXIXa**. Shape indicates the type of substituent, and the color indicates scaffold (olive: 2-furyl and isopropyl tricycle, green: 3-furyl and ethyl tricycle).

In terms of the benzyl substitution pattern, the observed behavior in terms of affinity for $A_{2B}AR$ differs from the previous series (**ISAM-140** derivatives). Most compounds in the current series exhibit good affinity for $A_{2B}AR$ regardless of the observed pattern. However, the observed trends in the previous series are (almost always) maintained in this series as well. In summary, for the derivatives of **ISAM-140**, the best substitution patterns were 2-F (**266a**), 2-Cl (**287a**), 3-F (**279a**), 3-Cl (**288a**), 4-Cl (**289a**), 2,3-F (**281a**), 3-Cl-2-F (**290a**), 2,6-F (**284a**),

and 2,4,6-F (**286a**), yielding compounds with either no affinity or low affinity (> 100 nM) in the remaining substitutions. For the N^1-benzylation of **ISAM-141**, these patterns continue to hold, with the addition of 4-CN-2-F-Bn, 2,5-F-Bn, and 2-Cl-6-F-Bn. As shown in Figure 3.54 the trend in affinity for different benzyl substitution patterns remains consistent in the majority of cases.

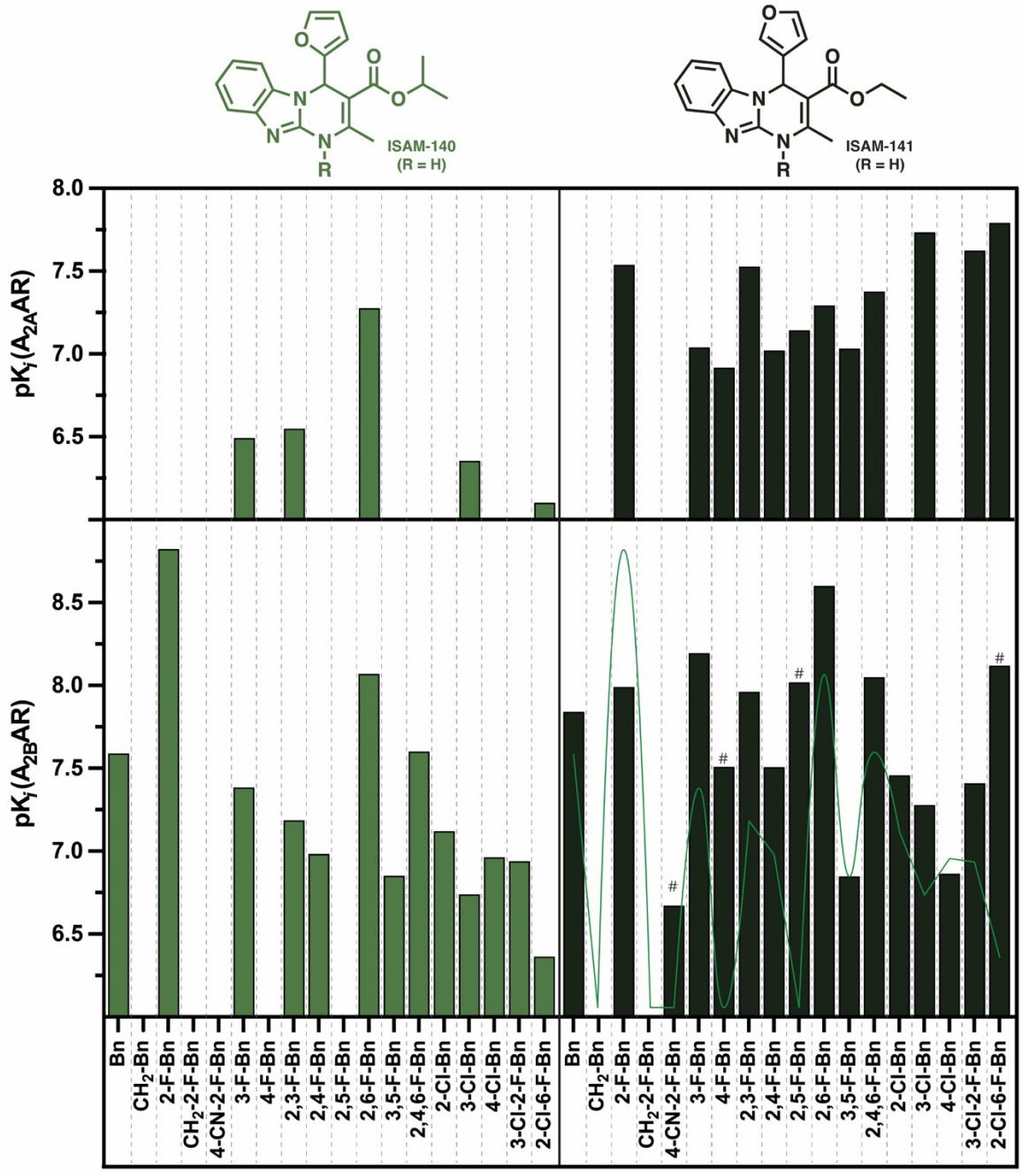

Figure 3.54. Interleaved bars chart showing $A_{2A}AR$ (top) and $A_{2B}AR$ (bottom) pK_i [-log(K_i)] for the N^1-benzylation of **ISAM-140** (green) and **ISAM-141** (black). The light green line represents the trend in the substitution of ISAM-140, correlating quite well with the trend observed in the substitution of **ISAM-141**. Those molecules that deviate from the trend are marked with a hash sign (#).

Given the minimal structural changes between series **XXVIII** and **XXIX**, the docking study of the binding mode reflects very similar results to those obtained for the previous series. To fully understand the differences in binding mode and the significant effect shown by the substitution of 2-furan to 3-furan, computational methods should be employed. Considering the possibility of water molecule interactions with the receptor, the interactions with the 3-furan ring may be promoted. This could lead to as yet unexplored binding modes that explain the formation of dual ligands and the ability of N^{10} isomers to bind with moderate affinity. This study is currently underway and will be published soon, but it goes beyond the scope of this doctoral thesis.

3.3.5 Enantiospecific binding to the A_{2A} and A_{2B}AR

In order to investigate the impact of stereoselectivity on synthesized compounds, four representative ligands were separated into their enantiopure forms and tested on the four human adenosine receptor subtypes (Table 3.25). The chosen derivatives were **266a** (a selective A_{2B}AR antagonist), **257**, **269a**, and **284a** (three dual A_{2A}AR/A_{2B}AR antagonists), all fluorobenzyl derivatives. These compounds showed promising affinity and selectivity profiles as a racemic mixture and provided stereochemical diversity within the N^1-(2-fluorobenzyl derivatives). As the compounds synthesized in this chapter involve a significant structural modification of the antagonists discussed in this Thesis, assessing the affinities of the purified enantiomers would yield valuable structural information about the impact of the new substituents on the enantiospecific interaction with A_{2A}AR and A_{2B}AR.

A combination of chiral HPLC and circular dichroism (CD) spectroscopy was employed to separate and unequivocally assign the configuration of the stereocenter in each stereoisomer (Figure 3.55). Semipreparative HPLC separation of **(±)-266a**, **(±)-257**, **(±)-269a** and **(±)-284a** on a chiral stationary phase (see Experimental Section) provided the expected eight enantiomers with excellent stereochemical purity (>99%). As previously described for structurally related 3,4-dihydropirimidin-2-ones,[137–140,157,164] the characteristic CD activity of the enamide chromophore (300-370 nm)[158] allowed the unequivocal assignment of the absolute configuration of each enantiomer (Figure 3.55), by comparison with the reported CD data for enantiopure 3,4-dihydropyrimidin-2(1*H*)-ones of known configuration. At that wavelength, enantiomers showing a negative Cotton effect (dark line) contain the furan ring backward (and correspond to **(*S*)-266a**, **(*R*)-257**, **(*R*)-269a** and **(*S*)-284a**, while the stereoisomers giving positive Cotton effect (light line) contain the pentagonal heterocycle forward (and correspond

to **(*R*)-266a**, **(*S*)-257**, **(*S*)-269a** and **(*R*)-284a**). The affinity of the enantiomers of **266a**, **257**, **269a** and **284a** was evaluated at the four human adenosine receptors. The results, summarized in Table 3.25 and Figure 3.55 for the four ARs, allowed the identification of stereoisomers with excellent A_{2A}AR and A_{2B}AR/A_{2B}AR dual affinity. The structural interpretation for this binding data is in accordance with our stereospecific binding model to the *h*A_{2B}AR. In contrast to the previous, chapter where the interaction with $Asn^{6.55}$ was completely eliminated with benzothiazopyrimidines, with this compounds, a hydrogen bond is retained, resulting in a more rigid binding of these compounds to A_{2A}AR and A_{2B}AR. Thus, the observed trend is similar to that of classical dihydropyrimidine antagonists, where one enantiomer (with pentagonal heterocycle backward, Figure 3.55) exhibits measurable affinity for both receptors,[137–140,157,164] whereas the other enantiomer is completely inactive. **266a** is an exception to this behavior as both enantiomers exhibit binding to A_{2B}AR (with a 120-fold difference), possibly owing to its exceptionally high affinity. Despite being more pronounced for A_{2B}AR (up to 7-fold), enantiospecific effects are also observed for A_{2A}AR in the case of dual antagonists, as seen in previous chapters, increasing the affinity by approximately 2-fold (Table 3.25 and Figure 3.55). The resolution of the racemates has allowed us to obtain one very potent (K_i < 1 nM) and selective (>1000 fold) ligand for A_{2B}AR [**(*S*)-266a**, K_i = 0.52 nM] and a three ligands with an excellent A_{2A}AR/A_{2B}AR dual profile [**(*R*)-257**; K_i = 20.2 and 7.0 nM; **(*R*)-269a**; K_i = 14.2 and 5.2 nM; and **(*S*)-266a**; K_i = 23.9 and 3.1 nM; for A_{2A}AR and A_{2B}AR respectively).

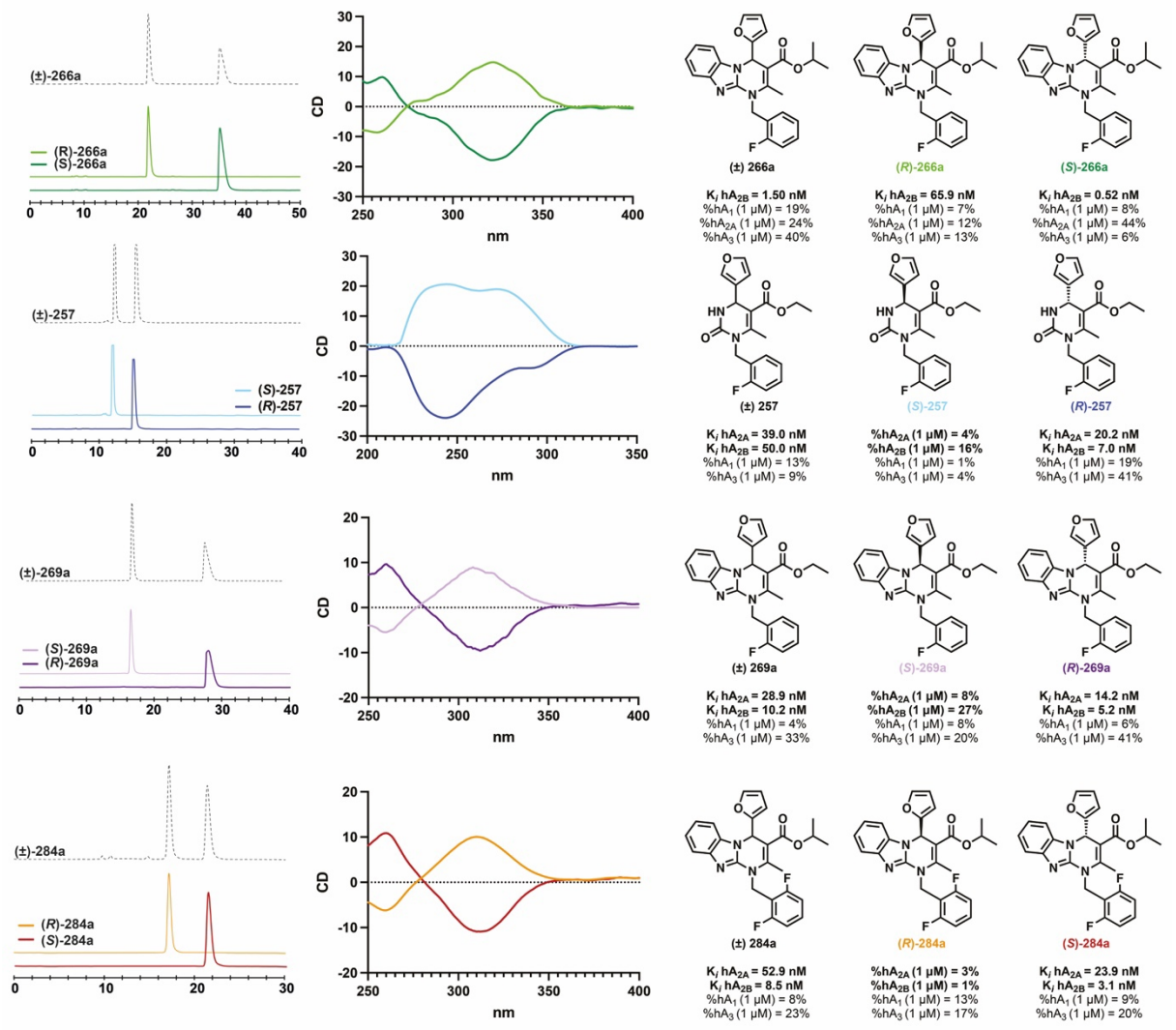

Figure 3.55. Chiral HPLC traces, circular dichroism spectra and binding data of selected racemic ligands (**266a**, **257**, **269a** and **284a**) and their enantiomers.

CHAPTER IV. OPTIMIZATION AND ADVANCED CHARACTERIZATION OF A_{2B}AR ANTAGONISTS AS DRUGS FOR CANCER (IMMUNO)THERAPY

The results of this chapter have been already published in:

(1) A_{2B} Adenosine Receptor Antagonists Rescue Lymphocyte Activity in Adenosine-Producing Patient-Derived Cancer Models. Tay A. H. M.;[1,2#] Prieto-Díaz, R.;[3,#] Neo, S.;[1] Tong, L.;[1] Chen, X.;[1] Carannante, V.;[4] Önfelt, B.;[4,5] Hartman, J.;[1] Haglund, F.;[1] Majellaro, M.;[3] Azuaje, J.;[2] Garcia-Mera, X.;[2] Brea, J. M.;[6] Loza, M. I.;[6] Jespers, W.;[7] Gutiérrez-De-Terán, H.;[7] Sotelo, E.;[3] Lundqvist, A. *J Immunother Cancer* **2022**, *10*, 4592–4592.

[#]Authors contributed equally. [1]Department of Oncology-Pathology, Karolinska Institute, Stockholm SE-17177, Sweden. [2]School of Biological Sciences, Nanyang Technological University, Singapore. [3]Center for Research in Biological Chemistry and Molecular Materials (CiQUS), University of Santiago de Compostela, Santiago de Compostela ES-15782, Spain. [4]Department of Microbiology, Tumor and Cell Biology, Science for Life Laboratory, Karolinska Institutet, Stockholm, Sweden. [5]Department of Applied Physics, Science for Life Laboratory, KTH Royal Institute of Technology, Stockholm SE-11419, Sweden. [6]Center for Research in Molecular Medicine and Chronic Diseases (CiMUS), University of Santiago de Compostela, Santiago de Compostela ES-15782, Spain. [7]Department of Cell and Molecular Biology, Uppsala University, Uppsala SE-75124, Sweden.

Impact factor: 8.039 (N° 3/63 (D1) in the category of Medicinal Chemistry (JCR 2021). ISSN: 2051-1426.

This article is an open access publication which permits unrestricted use, distribution, and reproduction in any medium in accordance with BMJ Publishing Group policy (Creative Commons 4.0 License).

Contribution

Synthesis, purification and characterization of ligands, data analysis and manuscript writing.

(2) Exploring the Effect of Halogenation in a Series of Potent and Selective A_{2B} Adenosine Receptor Antagonists. Prieto-Díaz, R.;[1,2,3] González-Gómez, M.;[1,2] Fojo-Carballo, H.;[1,2] Azuaje, J.;[1,2] El Maatougui, A.;[1,2] Majellaro, M.;[1,2] Loza, M. I.;[4,5] Brea, J.;[4,5]* Fernández-Dueñas, V.;[6,7] Paleo, M. R.;[1,2] Díaz-Holguín, A.;[3] Garcia-Pinel, B.;[4,8] Mallo-Abreu, A.;[1,2] Estévez, J. C.;[1,2] Andújar-Arias, A.;[1,2] García-Mera, X.;[2] Gomez-Tourino, I.;[4,8] Ciruela, F.;[6,7] Salas, C. O.;[9] Gutiérrez-de-Terán, H.;[3]* Sotelo, E.[1,2]*. *J. Med. Chem.* **2023**, *66*, 890–912.

[1]Center for Research in Biological Chemistry and Molecular Materials (CIQUS), University of Santiago de Compostela, 15782 Santiago de Compostela, Spain. [2]Department of Organic Chemistry, Faculty of Pharmacy, University of Santiago de Compostela, 15782 Santiago de Compostela, Spain. [3]Department of Cell and Molecular Biology, Uppsala University, Biomedical Center, 75124 Uppsala, Sweden. [4]Center for Research in Metabolic Diseases (CIMUS). University of Santiago de Compostela, 15782 Santiago de Compostela, Spain. [5]Department of Pharmacology, Pharmacy and Pharmaceutical Technology, Faculty of Pharmacy, University of Santiago de Compostela, 15782 Santiago de Compostela, Spain. [6]Pharmacology Unit, Department of Pathology and Experimental Therapeutics, Faculty of Medicine and Health Sciences, Institute of Neuroscience, University of Barcelona, 08907 L'Hospitalet de Llobregat, Spain. [7]Neuropharmacology and Pain Group, Neuroscience Program, Institut d'Investigació Biomèdica de Bellvitge, IDIBELL, 08907 L'Hospitalet de Llobregat, Spain. [8]Department of Biochemistry and Molecular Biology. Faculty of Pharmacy, University of Santiago de Compostela, 15782 Santiago de Compostela, Spain. [9]Department of Organic Chemistry, Faculty of Chemistry and Pharmacy, Pontificia Universidad Católica de Chile, Vicuña Mackenna 4860, Macul, Santiago 7820436, Chile.

Impact factor: 8.039 (N° 3/63 (D1) in the category of Medicinal Chemistry (JCR 2021)). ISSN: 0022-2623.

This article is an open access publication and may be used for authors in their own thesis in accordance with American Chemical Society policy (Creative Commons 4.0 License).

Contribution

Research conceptualization, synthesis, purification and structural characterization, separation and characterization of enantiomers, docking and molecular dynamics (FEP) studies, data analysis and manuscript writing.

3.4 CHAPTER IV: OPTIMIZATION AND ADVANCED CHARACTERIZATION OF $A_{2B}AR$ ANTAGONISTS AS DRUGS FOR CANCER (IMMUNO)THERAPY

In recent years, cancer immunotherapy has emerged as a promising approach for the treatment of various types of cancer. However, despite significant progress in this field, there is still a need for the development of novel and effective immunotherapeutic agents. In this final chapter, we will discuss how the novel drugs synthesized in this Thesis hold great potential as both immunostimulants and antiproliferative agents for cancer immunotherapy. Specifically, we will explore the unique mechanisms of action of these drugs, and how they enhance the immune response against cancer cells while also inhibiting tumor growth.

The findings of this doctoral thesis indicate that the Lead compounds identified possess promising profile as drug candidates, primarily attributed to their favorable physicochemical profiles, described in Section 7.1. However, it is crucial to note that further validation of these results is required through additional in vitro and *in vivo* studies to unequivocally confirm the simulated outcomes. Moreover, a variety of pharmacodynamic profiles have been optimized, spanning from selective compounds to dual-acting agents, showcasing the diverse functional attributes. The ligands presented in this thesis have been specifically designed as $A_{2B}AR$ antagonists or dual $A_{2A}AR/A_{2B}AR$ antagonists, intended to act as synergistic ligands that can target multiple levels in the treatment of cancer. By utilizing synergistic ligands, this work aims to provide effective and multifaceted approaches for combating cancer.

In this section, we assessed a range of small molecule $A_{2B}AR$ (and dual $A_{2A}AR/A_{2B}AR$) antagonists with diverse pharmacodynamic and pharmacokinetic profiles to examine their potential synergistic effects in both tumor cells and the TME. Our evaluation primarily focused on their impact on cancer cell proliferation and immune system activation, while also investigating their influence on other cells of the TME (e.g., CAFs), providing a comprehensive understanding of the compounds' efficacy and their broader implications in cancer treatment.

3.4.1 *In vitro* and *ex vivo* validation of antiproliferative effects in tumor cells

As explained in the introduction of this Thesis, adenosine have validated key roles in tumor cell growth, mainly due the interaction with $A_{2B}AR$. Here, a comprehensive evaluation was conducted to assess the antiproliferative effects of our compounds – including both $A_{2B}AR$ and dual $A_{2A}AR/A_{2B}AR$ antagonists – across a range of cancer types, including breast cancer, colon cancer, and glioblastoma. Our objective was to gain a holistic understanding of their efficacy as potential therapeutic interventions for diverse tumors. By assessing their impact in these

distinct cancer types, we aimed to provide valuable insights into the broad applicability of these compounds in the field of oncology.

Blockade of the adenosinergic pathway has been widely studied in breast cancer [38–47]. To preliminarily validate the effect of our antagonists at the tumor level, the effect of four selective A_{2B}AR antagonists (**Ig**, **Ij**, **IIIb**, **266a**) and the dual antagonist **60** on breast cancer spheroids has been evaluated (Figure 3.56A). Spheroids, unlike traditional 2D cell cultures, provide a more physiologically relevant and representative model of tumors due to their three-dimensional (3D) structure. This 3D organization allows for cell-cell interactions, nutrient and oxygen gradients, and the development of heterogeneous cell populations, mirroring the complexity of solid tumors *in vivo*. Therefore, studying the effect of our antagonists on breast cancer spheroids provides valuable insights into their potential efficacy and mechanism of action in a more realistic tumor microenvironment.. Upon exposure to **IIIb** (**ISAM–140**), **266a** and **60** for four days, the relative cell viability of breast cancer spheroids was significantly reduced (Figure 3.56B). To confirm this antagonist effects of the cell growth, the kinetics of the observed cytotoxic effect mediated by the antagonists at 12 μM was studied using real-time imaging within the same spheroid culture setting (Figure 3.56C). Treatment with model tricycle **IIIb** (**ISAM-140**), **60** and **266a** significantly affected the spheroid growth over time compared to untreated control (Figure 3.56D).

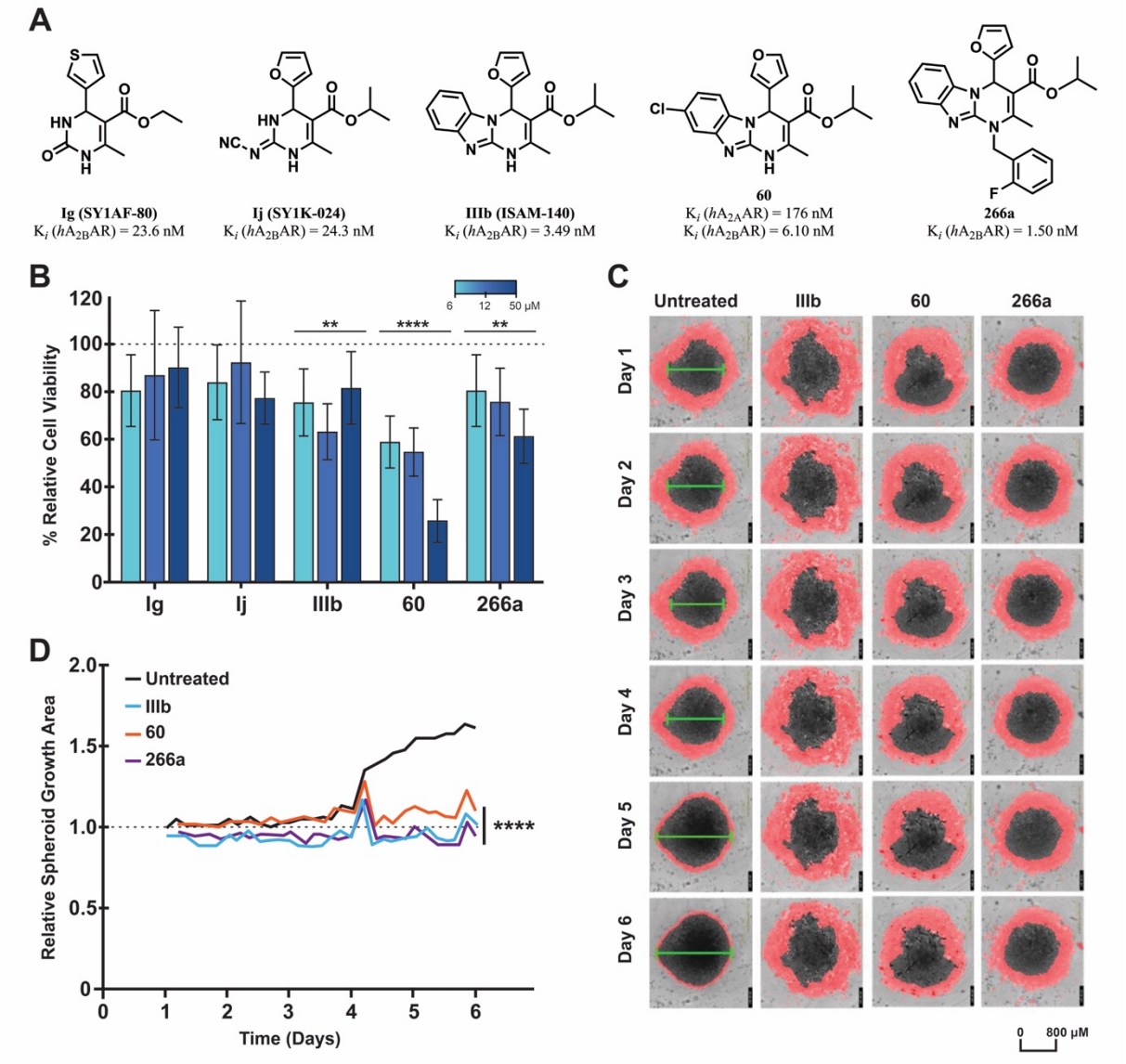

Figure 3.56. Anti-tumor effect of $A_{2B}AR$ antagonists on breast cancer patient-derived spheroid cultures. A) Structure of selected ligands and affinity data. B) Relative cell viability to untreated control spheroid cultures (n=3, mean ± SD) measured by Cell-Titer Glo assay. C) Representative real time imaging of spheroid cultures over six days under 4X objective, with untreated (first column) or added 12 µM concentration respective of $A_{2B}AR$ antagonists indicated. Red mask demarcates area surrounding the spheroid. Green line indicates estimated diameter of spheroid body. D) Relative area of the representative spheroid growth (as shown in B) normalized to day one. Statistical analysis – 2-way (B) and 1-way (D) ANOVA with Dunnett's multiple comparisons to untreated control was performed with * $p<0.05$, ** $p<0.01$, *** $p<0.001$ and **** $p<0.0001$.

In order to further validate the antiproliferative effect with other antagonists and based on the moderate antiproliferative results of **ISAM-140** published by Barbazán et al.,[184] three ligands (two selective $A_{2B}AR$, one dual $A_{2A}AR/A_{2B}AR$) were selected for evaluation of the effect on cell proliferation in colorectal cancer cultures. While our initial focus has been on

breast cancer, it is essential to broaden our scope to understand the impact of our molecules on other forms of cancer. Colorectal cancer represents a significant global cause of morbidity and mortality, making it crucial to investigate how our molecules may influence its development and progression. By expanding our research to include colorectal cancer, we can explore new therapeutic opportunities and uncover potential common mechanisms of action among different cancer types. This broadening of our focus will provide a more comprehensive understanding of the efficacy of our molecules and their potential application in multiple oncological contexts, contributing to a broader and more relevant field of research. To investigate the disparities between tumoral and non-tumoral cells within the tumor microenvironment (TME), the expression of $A_{2A}AR$ and $A_{2B}AR$ in the HCT116 colorectal cell line and human CAFs was assessed. As depicted in Figure 3.57A, the expression of $A_{2B}AR$ is higher in both cell types. Furthermore, the expression it is significantly higher for $A_{2A}AR$ in HCT116 cells compared to CAFs (Figure 3.57B). This could imply that blocking $A_{2B}AR$ in both cell types would lead to similar effects, with the blockade of $A_{2A}AR$ being an interesting addition to the inhibition of malignant cell proliferation.

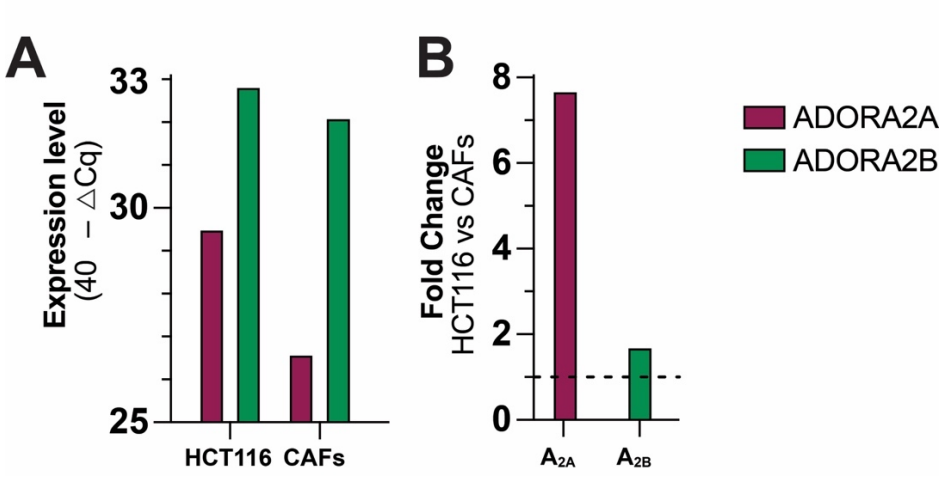

Figure 3.57. Expression of ADORA2A and ADORA2B genes between human and murine colorectal cancer cell lines (HCT116 and CT26 respectively) and human CAFs obtained by qPCR assay (n = 2) A) Absolute expression of ADORA2A and ADORA2B on HCT and CAFs using GAPDH as a reference gene. B) Fold change on expression in HCT116 vs CAFs.

The significant differences in the expression of the two subtypes of adenosine receptors have justified the selection of two specific $A_{2B}AR$ ligands and a dual $A_{2A}AR/A_{2B}AR$ antagonist for the cell proliferation studies, as shown in Figure 3.58A.

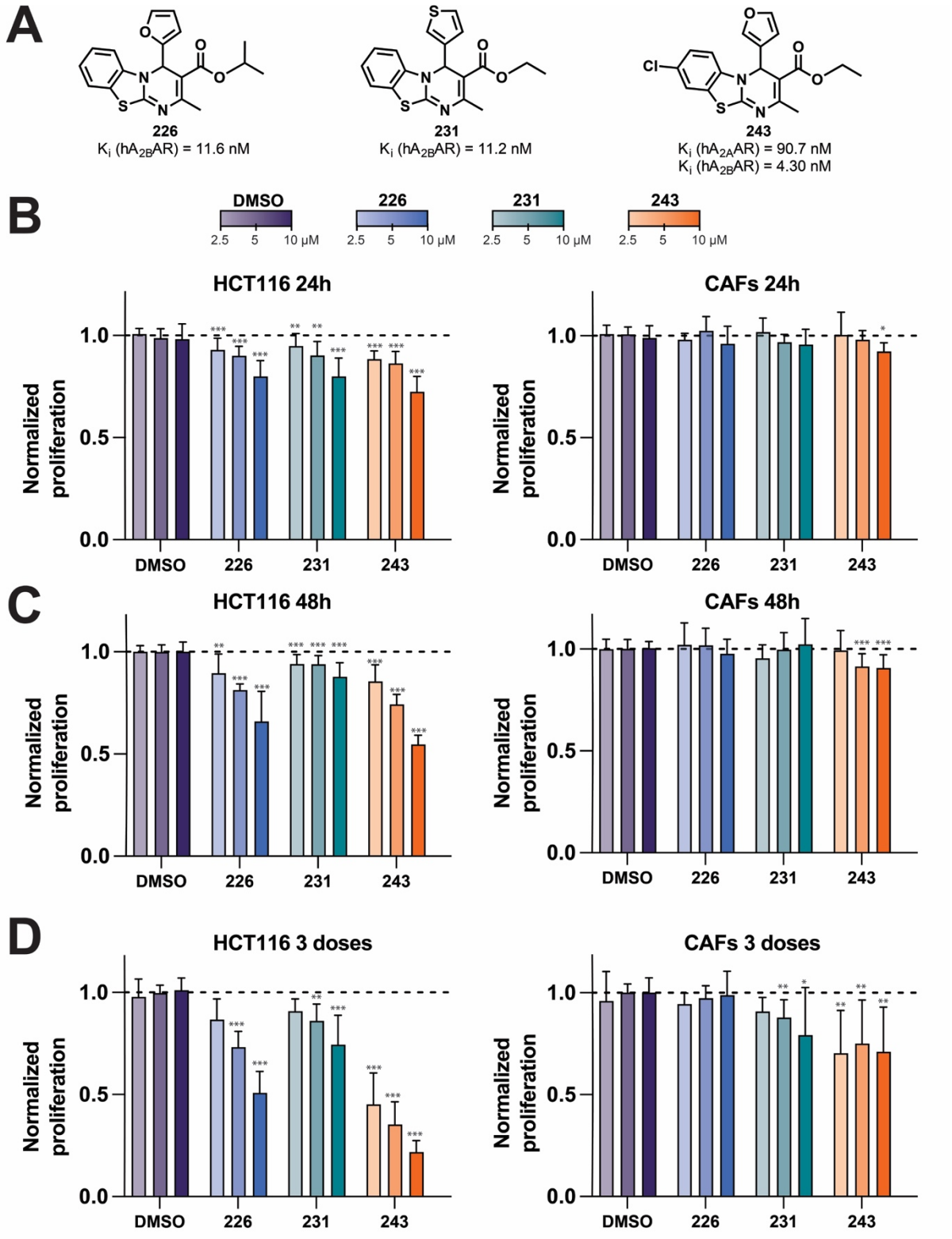

Figure 3.58. Antiproliferative effect of selected antagonists in human tumor (HCT116) and non-tumor (CAFs) cells. A) Structure of selected ligands and affinity data. B) Relative cell viability to untreated control HCT116 and CAFs (n = 12, mean ± SD) measured by AlamarBlue assay 24h after treatment, C) 48h after treatment, and D) after 24h of three consecutive doses, administered at 24-hour intervals. Statistical analysis ANOVA with Dunnett's multiple comparisons to untreated control was performed with * $p<0.05$, ** $p<0.01$, and *** $p<0.001$.

Treatment with the three antagonists results in a dose-dependent reduction in cell proliferation of the human cell line HCT116, both at 24 hours (Figure 3.58B) and 48 hours (Figure 3.58C) after administration of one single dose of concentrations ranging from 2.5 to 10 μM. Among the three evaluated ligands, **243** shows the highest reduction in cell proliferation, followed by **226**, with 45% and 34% cell proliferation reduction at 48 hours with the highest dose (10 μM) compared to the control. None of the selective A_{2B}AR antagonists affect CAFs at any of the concentrations tested, both at 24 and 48h. However, **243** slightly inhibits cell proliferation in CAFs at the two highest doses (9% of proliferation reduction), suggesting an effect on non-tumoral cells within the tumor microenvironment. The observed effect (and the big differences with cancer cells) can be attributed to the expression of both A_{2A}AR and A_{2B}AR in CAFs, albeit at lower levels. On the other hand, none of the selective A_{2B}AR antagonists affect CAFs at any of the concentrations tested, both at 24 and 48 hours. By examining the effects of treatment with the antagonists using multiple doses over a span of three consecutive days, we observe a significant enhancement in the overall effect. However, it is important to note that this enhanced effect is also observed in CAFs. In these conditions, we observe a notable reduction in cell proliferation. Specifically, compound **226** leads to a 50% reduction, while compound **226** demonstrates an even more substantial reduction of 78%. Although **243** appears to be the most effective treatment, the significant effect observed in **226** without causing a decrease in CAFs' cell proliferation makes **226** a promising molecule in the treatment of colorectal cancer. Upon closer examination, there is a significant difference between **226** and **231**, despite having the same scaffold and similar affinity values for A_{2B}AR. This difference may be attributed to the pentagonal substituent, which could alter the ligand's binding time to the receptor. Kinetic binding assays are currently being conducted in Prof. Laura Heitman laboratory (University of Leiden, the Netherlands) to understand these differences, and the results will be published soon.

To validate the displayed results, a primary colorectal cancer cell line was utilized, and the same experiments were conducted. The Figure 3.59 demonstrates a less pronounced decrease in proliferation compared to HCT116, with up to a 20% reduction in proliferation with **243**, but still with a more pronounced response in comparison to the impact on CAFs' proliferation (Figure 3.59). The relatively reduced effect observed in primary cancer cells compared to HCT116 may be attributed to their slower proliferation rate, necessitating the evaluation of longer treatment durations and potentially repeated dosing.

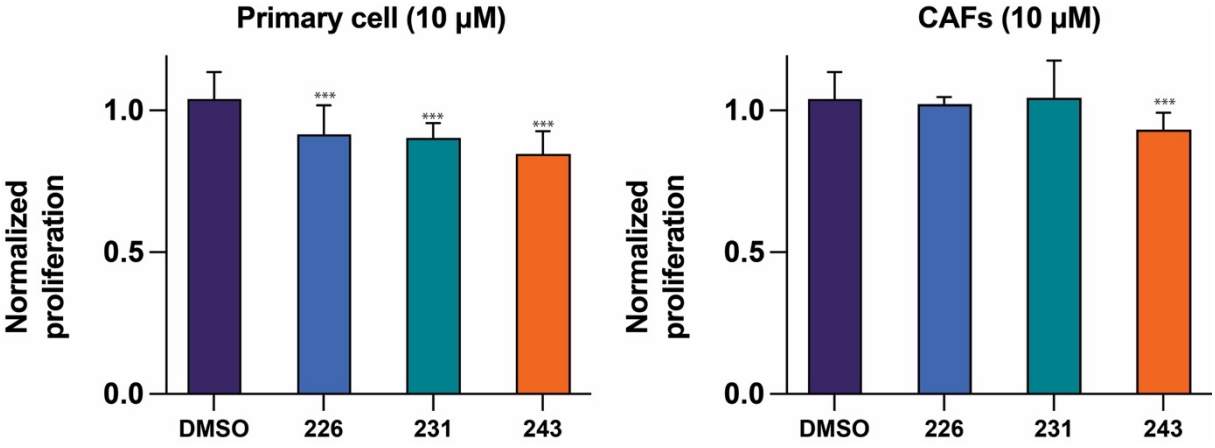

Figure 3.59. Relative cell viability to untreated control of colorectal cancer primary cell line and CAFs (n = 12, mean ± SD) measured by AlamarBlue assay 48h after treatment with 10 µM of antagonists.

So far, we have demonstrated that blocking adenosine receptors using a panel of antagonists specifically reduces tumor cell proliferation, but the exact mechanism by which this happens remains unknown. The reduced amount of cellularity observed upon treatment can be explained by a direct induction of apoptosis in cancer cells or through a slowdown of cell cycle dynamics, or both simultaneously. To deepen into this, we explored these mechanisms by checking apoptosis and cell cycle markers 48 hours after treatment with 10 µM of selected antagonists.

As a readout of cell cycle dynamics, we used the EdU incorporation assay, which measures the number of cells in S-phase. EdU is a thymidine analog, 5-ethynyl-2'-deoxyuridine, that is incorporated into newly synthesized DNA during the S-phase of the cell cycle and can be then detected by fluorescence using click chemistry (Figure 3.60A). Using this assay, we observed that the antagonists **226** and **243** exhibited a comparable reduction in cell division (Figure 3.60B), whereas antagonist **231** had the least effect, aligning with the findings from the proliferation assays. Importantly, none of the antagonists impacted the amount of CAFs in S-phase, with no differences between the antagonist-treated and the control.

On the other hand, to identify cells undergoing apoptosis after treatments, we stained cells for Cleaved caspase-3 (CC3), an activated form of caspase-3 (an apoptotic enzyme), involved in the proteolytic cleavage of various cellular substrates, leading to the dismantling of the cell's structural components and DNA fragmentation, and a well-established apoptotic marker. As observed in Figure 3.60C, there is a significant increase in the number of apoptotic HCT116 cells with treatment using antagonists **226** and **243**. Consistent with all previous assays,

compound **231** does not exhibit a significant difference compared to the control. These results correlate well with the experimental experience. For instance, in the assay involving three consecutive doses every 24 hours, by the third day, a significant number of dead cells were observed floating in the well treated with compounds **226** and **243**, likely due to induced apoptosis. Additionally, similar to the previous experiments, these effects are not observed in CAFs. A representative selection of the images taken with confocal microscopy is shown in Figure 3.60D, showing a decrease in the number of cell dividing and increasing apoptotic cells.

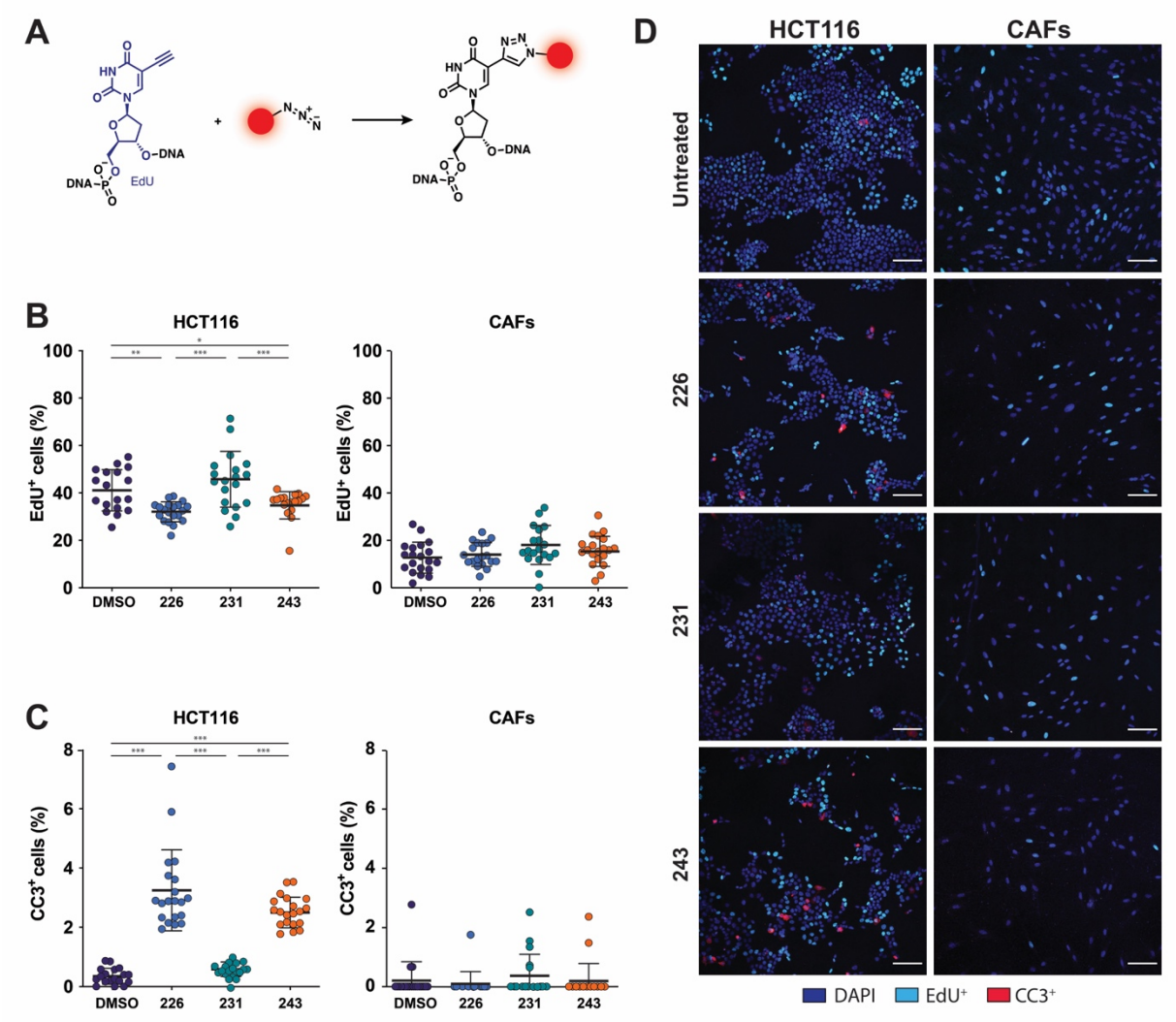

Figure 3.60. A) EdU Click Reaction for DNA labeling. B) EdU positive cells for HCT116 and CAFs (n = 20, mean ± SD). C) CC3 positive cells for HCT116 and CAFs (n = 20, mean ± SD) D) Representative imaging of labeled cells, with untreated (first row) or added 10 μM concentration respective of antagonists indicated. In blue: all nuclei (DAPI staining), in cyan: nuclei in division (phase S, staining with EdU), in red: apoptotic cells ($CC3^+$ staining). Statistical analysis Kruskal-Wallis was performed with * $p<0.05$, ** $p<0.01$, and *** $p<0.001$.

Although the effects shown may not appear to be large in absolute terms, they are significant compared to untreated cells. As explained, the antagonists result in a decrease in cell division entry and an increase in apoptosis in colon cancer cells, causing a cascade of small effects that ultimately lead to a considerable reduction in cell proliferation and/or viability. The effect observed in the AlamarBlue assays (inhibition of cell proliferation) could be attributed both to increase of apoptosis and decrease in cell cycle. As explained in the introduction, the effects induced by the activation of A_{2B}AR can be attributed to signaling through the ERK/MAPK pathway,[185] which regulates these processes. Activation of specific MAPK pathways, such as the ERK (Extracellular Signal-Regulated Kinase) pathway, can promote cell survival and proliferation, while inhibition of these pathways can lead to reduced cell proliferation and increased susceptibility to apoptosis.[185]

To approximate our findings to a future *in vivo* study, we have performed the same assays using mouse cell lines (CT26 and *m*CAFs). To investigate the disparities between human and murine tumoral (CT-26) and non-tumoral (*m*CAFs), the expression of A_{2A}AR and A_{2B}AR was assessed. As depicted in Figure 3.61A, human cell lines exhibit higher expression levels of A_{2A}AR and A_{2B}AR. Unlike human cells, mouse cells (CT26) exhibit lower expression of A_{2B}AR compared to *m*CAFs (Figure 3.61A, Fold Change < 1). The results of cell viability are shown in Figure 3.61B-C, demonstrating different trends to those previously described in humans, with a lower impact on reducing cell viability in CT26 compared to HCT116 cells and much stronger effect observed in *m*CAFs compared to *h*CAFs, both in 24 (Figure 3.61B) and 48 h (Figure 3.61C) after the treatment. These results align well with the measured expression of ADORA2A and ADORA2B in these cell types. Considering the conflicting results obtained, it is evident that a transition to a different *in vivo* model is crucial to comprehensively evaluate the efficacy of the compounds being studied. Therefore, it would be a good idea to explore the effects on alternative murine cell lines (MC38 or Colon-26) in order to gather additional insights and conducting experiments using patient-derived xenografts (PDX). PDX models involve the implantation of patient-derived tissues into immunodeficient mice (Nude or NOD-SCID), providing a more clinically relevant and reliable assessment of the compounds' therapeutic potential. This approach will allow for a thorough evaluation of their effectiveness and facilitate a more accurate translation of the findings to clinical applications.

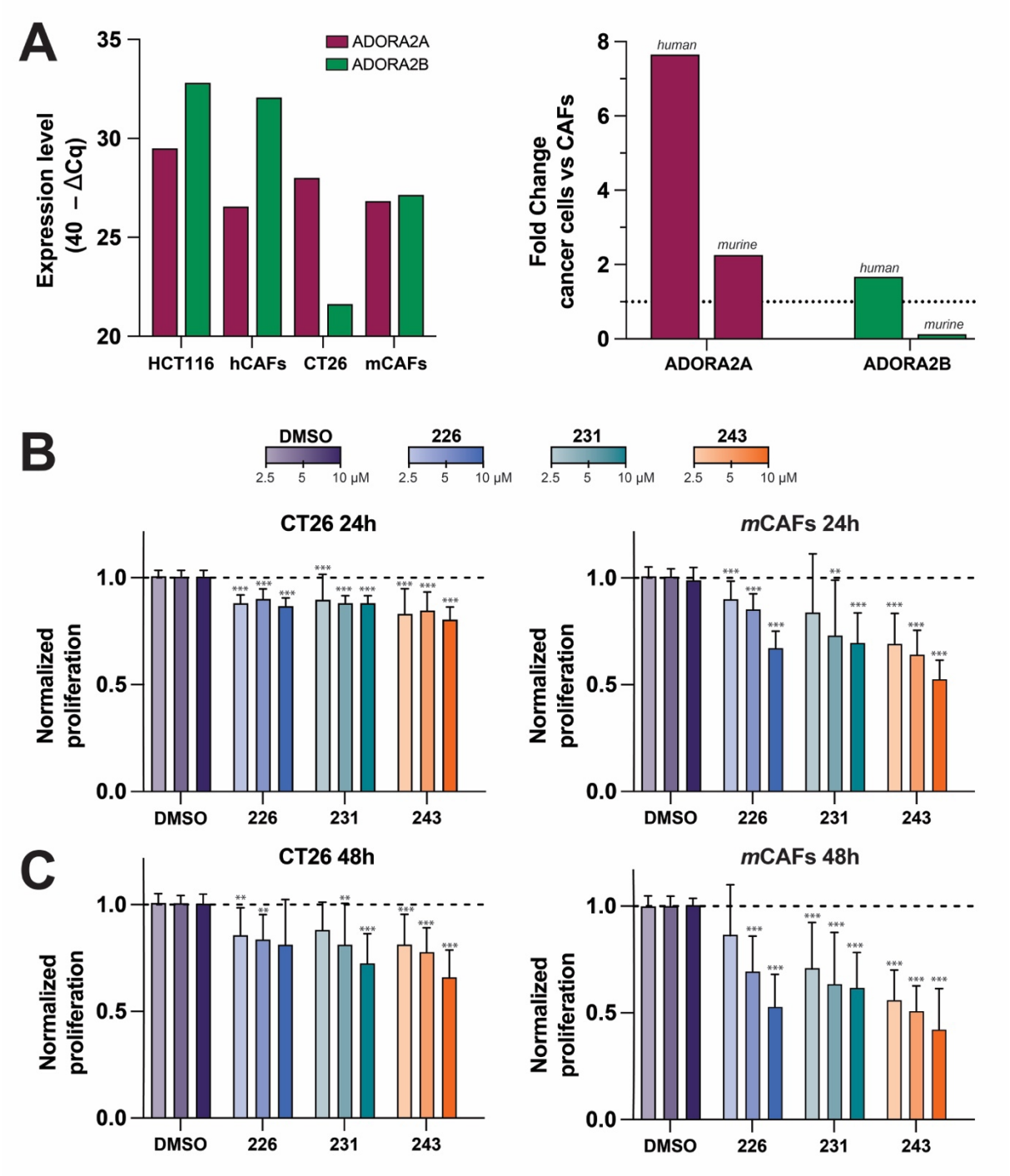

Figure 3.61. Antiproliferative effect of selected antagonists in murine cells. A) Ex B) Relative cell viability to untreated control CT26 and *m*CAFs (n = 12, mean ± SD) measured by AlamarBlue assay 24h after treatment, and C) 48h after treatment. Statistical analysis ANOVA with Dunnett's multiple comparisons to untreated control was performed with * $p<0.05$, ** $p<0.01$, and *** $p<0.001$.

To evaluate the antagonist treatment with A_{2B}AR antagonists in a third type of cancer, cell viability experiments have been conducted on two glioblastoma cell lines, U87 and U251. As observed in Figure 3.62A, the expression of A_{2A}AR and A_{2B}AR is very similar to that observed in HCT116, therefore similar results are expected. In this case, with the aim of determining the IC50, the assays were carried out identically to the previous ones in colorectal cancer with six different concentrations: 100 μM, 30 μM, 10 μM, 3 μM, 1 μM, and 300 nM. For this study were selected **243**, with very good results in colorectal cancer, **257**, one of the most balanced dual antagonists obtained (A_{2A}AR K_i = 39.0 nM, A_{2B}AR K_i = 50 nM) and **266a**, the best selective A_{2B}AR antagonist obtained in this thesis (K_i = 1.5 nM). The selection of ligands was due to the use of a ligand with known effect on another cell line (**243** in HCT116) in addition to two ligands with physicochemical properties suitable for crossing the BBB (Figure 3.62B).

The results, shown in Figure 3.62C-D, demonstrate a significant inhibition in the growth of both cell lines, with IC50 values calculated for the three compounds around 20 μM. These values are much lower than the IC_{50} value of Temozolomide (TMZ), being the reference drug used for glioblastoma treatment (in combination with radiotherapy), which is 841 μM for U87 and 404 μM for U251. These results are promising due to the urgent need to improve prognoses and treatment options for patients with glioblastoma. Despite the aggressiveness of this disease and its challenging survival statistics, advancements in research and the discovery of compounds with potent inhibition of cell growth offer hope for the development of more effective therapies.

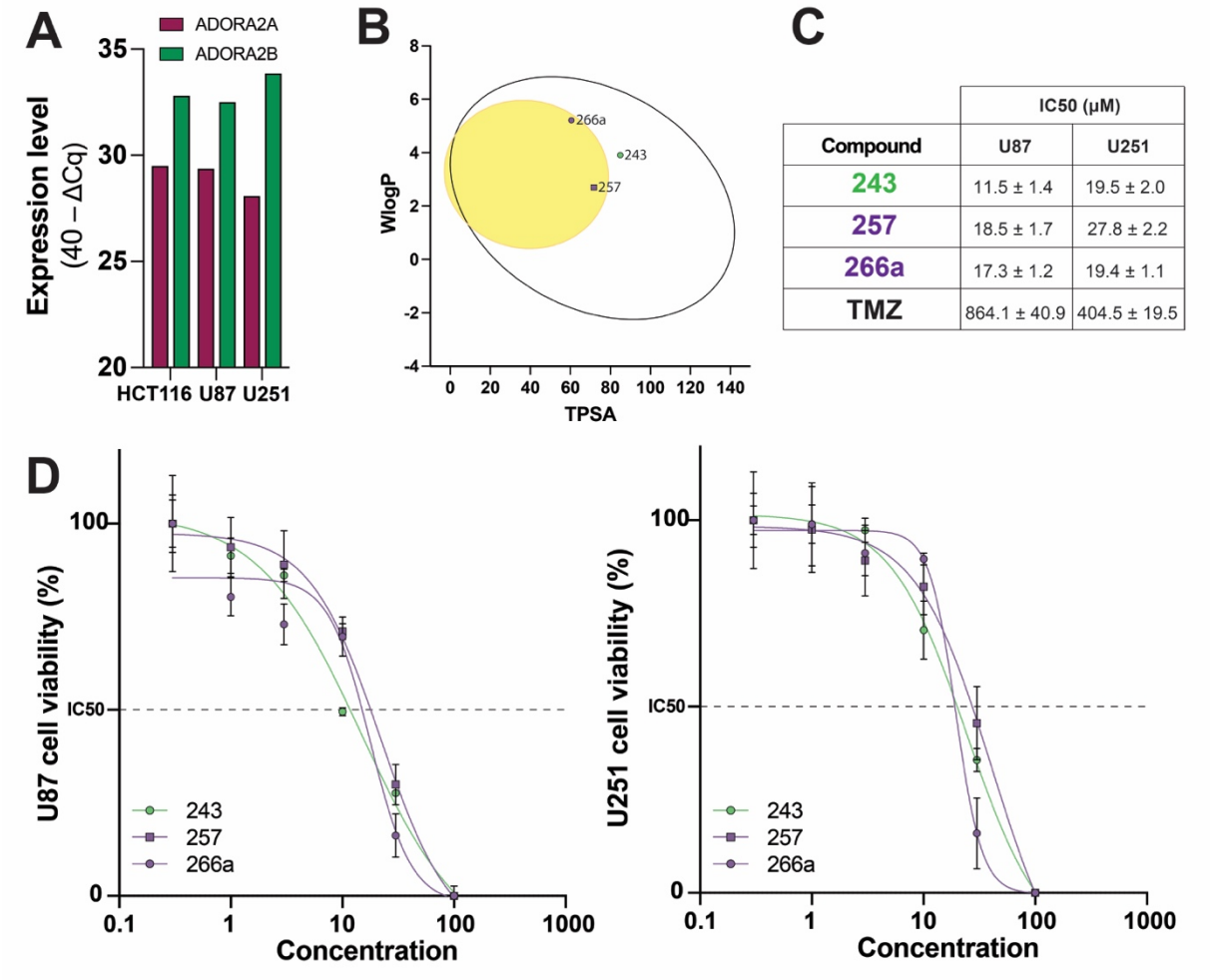

Figure 3.62. A) Absolute expression of ADORA2A and ADORA2B on U87 and U251 compared with HCT116 using GAPDH as a reference gene. B) Boiled egg representation of selected ligands tested in glioblastoma (see Supplementary Results). C) IC_{50} values of selected compounds on U87 and U251 cell lines. Temozolomide (TMZ) values were taken from bibliography.[186] D) Viability versus concentration curves to determine IC_{50} for U87 and U251 (non-linear regression with n = 2).

Indeed, it is important to consider that, so far, all these effects are observed in isolated cancer cells cultured *in vitro*, in the absence of important components of the tumor microenvironment like the immune system. Immune cells play a crucial role in modulating the response to cellular changes, including apoptosis and cell proliferation. In an *in vivo* setting with an intact immune system, the interaction between tumor cells, immune cells, and the other components of TME can significantly improve the outcomes observed. The presence of the immune system can lead to additional factors that can affect cell viability, proliferation, and apoptosis. Immune cells such as cytotoxic T cells and natural killer cells can directly target and

eliminate tumor cells. Additionally, immune cells can release cytokines and other signaling molecules that can further modulate cell behavior and the overall immune response.

Therefore, while the results obtained in cell culture experiments provide valuable insights into the potential effects of the antagonists on cell viability and proliferation, it is crucial to consider the dynamic interplay between tumor cells and the immune system in an *in vivo* setting to fully understand the broader implications and potential therapeutic applications of these findings.

3.4.2 *In vitro* and *ex vivo* evaluation of immunostimulatory effects

While the roles of adenosine in cell proliferation have been extensively studied and validated, its role in the immune system is still an area of ongoing research and exploration. Recently, the A_{2A}AR has been recognized as an immune checkpoint, demonstrating several valuable effects at this level. This has led to the repurposing of various drugs (previously proposed for Parkinson's disease) towards cancer immunotherapy, as mentioned earlier in the introduction (e.g., Tamidenant, and AZD-4635).[28,53] Furthermore, with the increasing interest in dual antagonists, some have been proposed for clinical trials, and one of the most promising ones is **M1069**.

Since A_{2A}AR and A_{2B}AR are commonly coexpressed and considering the recent hypothesis of dimer formation controlled by A_{2B}AR, we aimed to evaluate and validate A_{2B}AR as well for cancer immunotherapy. In this context, once the antiproliferative effects of our compounds have been validated in tumor cells, A_{2B}AR antagonists and A_{2A}AR/A_{2B}AR dual antagonists would not only serve as immunotherapeutic drugs but also provide a targeted therapy with multiple effects on the tumor microenvironment. To explore whether A_{2B}AR antagonists have any immunological effects, we decided to evaluate the effect of two representative compounds [**50** (K_i *h*A_{2B}AR = 3.05 nM) and **58** (K_i *h*A_{2B}AR = 5.03 nM)] in the proliferative activity of a prototypical immune cell. For this study, we used human peripheral blood mononuclear cells (PBMCs) were selected for the study, as they are critical components of the immune system and are involved in both humoral and cell-mediated immunity. Adenosine-mediated blockade of PBMC proliferation is well documented and characterized,[187,188] we therefore investigated whether our A_{2B}AR antagonists (**50** and **58**) could reverse the blockade of ADO-mediated proliferation in human peripheral blood mononuclear cells. PBMCs, isolated from a healthy donor, were labelled with carboxyfluorescein succinimidyl ester (CFSE) and then activated by adding Anti-CD3/CD28 antibodies and interleukin 2 (IL-2). CFSE is a cell dye that allows for

the determination of cell proliferation. CFSE gets transformed in cytoplasm and emits fluorescence, getting reduced by half every time a cell divides. We found that, as expected, the addition of adenosine caused a reduction in the frequency of PBMCs dividing cells (Figure 3.63A) and a corresponding increase of CFSE Median Fluorescence Intensity (MFI) (Figure 3.63B) compared to the stimulated PBMCs. Notably, compounds **50** and **58** unequivocally reversed the adenosine-induced blocking effect, resulting in an enhancement in the frequency of proliferative cells (Figure 3.63A, C-F) that correlates with a marked decrease in CFSE MFI (Figure 3.63B).

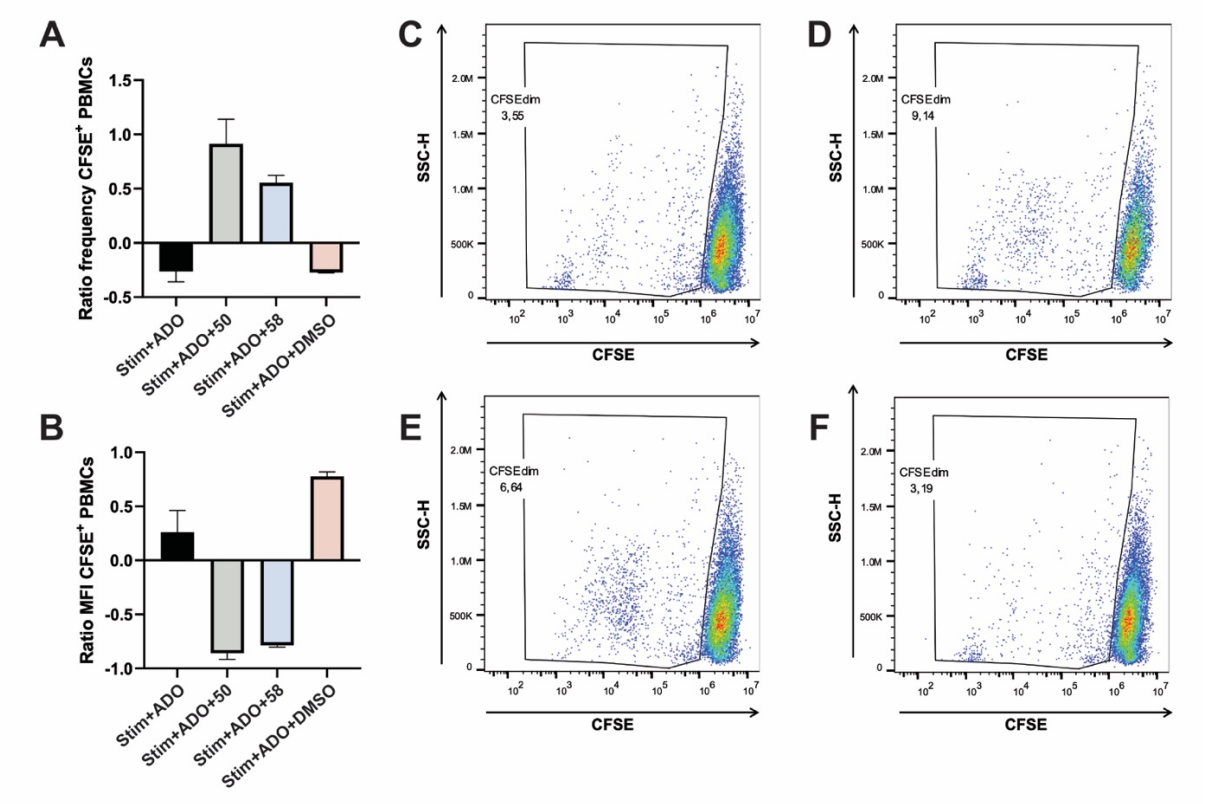

Figure 3.63. Effect of compounds **50** and **58** on the proliferation of PBMCs stimulated with AntiCD3/CD28 + IL-2 in the presence of adenosine (ADO) for 3 days. A) frequency of proliferating cells. B) MFI of proliferating cells. C) Representative dots plots of the proliferation of CFSE-stained PBMCs treated with Anti-CD3/CD28 + IL-2 + ADO, D) Anti-CD3/CD28 + IL-2 + ADO + 50, E) Anti-CD3/CD28 + IL-2 + ADO + 58, and F) Anti-CD3/CD28 + IL-2 + ADO + DMSO.

From a quantitative point of view, the effect measured for compound **50** (9.14%) is superior to that observed for **58** (6.54%) (Figure 3.63D-E). Control experiments verified that the vehicle used to dissolve the compounds (DMSO) has a similar profile to that shown by ADO, thereby demonstrating that it does not favor PBMC proliferation by itself (Figure **10A-C, F**). These

initial results confirm the effect of the A_{2B}AR antagonists optimized here at the immune system level and their potential in the context of cancer immunotherapy.

Having tested the overall effect of A_{2B}AR antagonism on the immune system, we set out to evaluate the mechanisms responsible for the observed effects. For this, we have selected a subset of compounds, including molecules developed before and during this thesis: **SY1AF-30** (**Vk**), **SY1AF-80** (**Ig**), **SY1K-024** (**Ij**), **ISAM-140** (**IIIb**), **60**, **266a**, all of them compared to the A_{2A}AR antagonist model **AZD-4635**.

The binding data obtained from the five A_{2B}AR antagonists, the dual A_{2B}AR/A_{2A}AR ligand and the A_{2A}AR clinical candidate (**AZD-4635**) are depicted in Table 3.27. The selected A_{2B}AR and A_{2B}AR/A_{2A}AR ligands were tested in cAMP assays to evaluate their ability to inhibit NECA-stimulated (100 nM) cAMP production. These experiments demonstrated that all of them inhibited cAMP accumulation, thus validating its A_{2B}AR antagonistic behavior (Table 3.27). A comparison of their K_i and K_B values revealed complete agreement (data within 1-7-fold) between the binding and functional assays. Ectonucleotidases, in particular CD73, play a key role in the context of adenosine-mediated tumor immune escape.[4] Consequently, we evaluated the effect of A_{2B}AR ligands on the blockade of *h*CD73 as part of the pharmacological characterization of the selected A_{2B}AR ligands (Table 3.27). These experiments revealed that none of the five A_{2B}AR antagonists, nor the A_{2A}/A_{2B} dual antagonist, showed any noticeable inhibitory effect on *h*CD73 (1 μM or 10 μM). This data excluded a dual A_{2B}AR-CD73 inhibition, allowing us to attribute the pharmacological effects described below to the specific A_{2B}AR antagonistic effect (or the dual A_{2A}/A_{2B} antagonism in the case of **60**) of these ligands.

Table 3.27. Adenosine receptors binding data, $A_{2B}AR$ functional data and *h*CD73 inhibitory data of the $A_{2B}AR$ antagonists employed in the study.

Compound	K_i (nM) or % at 1 μM					K_B (nM)
	hA_1[a)]	hA_{2A}[b)]	hA_{2B}[c)]	hA_3[d)]	*h*CD73[e)]	*h*A_{2B}[f)]
Vk (SY1AF-30)	15%	18%	10.2 ± 0.5	4%	2%	4.72 ± 0.9
Ig (SY1AF-80)	16%	34%	23.6 ± 1.0	11%	3%	25.2 ± 3.1
Ij (SY1K-024)	21%	19%	24.3 ± 0.9	4%	2%	115 ± 21
IIIb (ISAM-140)	20%	25%	3.49 ± 0.2	2%	1%	27.0 ± 4.1
60	27%	176 ± 4	6.10 ± 0.7	1%	5%	18.44 ± 2.2
266a	19%	24%	1.50 ± 0.4	40%	3%	6.15 ± 1.2
AZD-4635[28]	160	1.7	64	>1000	-	-

[a)] Displacement of specific [^{3}H]DPCPX binding in human CHO cells expressed as K_i in nM (n = 3) or percentage displacement of specific binding at a concentration of 1 μM (n = 2). [b)] Displacement of specific [^{3}H]4-(2-[7-amino-2-(2-furyl)[1,2,4]triazolo[2,3-*a*][1,3,5]triazin-5-ylamino]ethyl)phenol binding in human HeLa cells expressed as K_i in nM (n = 3) or percentage displacement of specific binding at a concentration of 1 μM (n = 2). [c)] Displacement of specific [^{3}H]DPCPX binding in human HEK-293 cells expressed as K_i in nM (n = 3) or percentage displacement of specific binding at a concentration of 1 μM (n = 2). [d)] Displacement of specific [^{3}H]NECA binding in human HeLa cells expressed as K_i in nM (n = 3) or percentage displacement of specific binding at a concentration of 1 μM (n = 2). [e)] Inhibition of *h*CD73 in presence of α-β-methylene adenosine, ATP and AMP (expressed as K_i in nM). [f)] cAMP production in HEK-293 cells in presence of NECA and test compound at a concentration of 10 μM expressed as K_B in nM (n = 3).

To elucidate if the anti-tumor effects observed by the $A_{2B}AR$ antagonists depended on increased lymphocyte activity, the different antagonists were added directly to T and NK cells in the presence of exogenous adenosine. While no statistical difference in viability at different adenosine concentrations was observed, a trend of decreasing viability with increasing adenosine concentration among CD8 T cell subsets was observed. Conversely, the viability of CD56 positive NK cells was not affected by adenosine (Figure 3.64A). However, a dose-dependent adenosine-mediated suppression of cell proliferation was observed across the different subtypes of T and NK cells with naïve CD8 T cells being the most affected (Figure 3.64A and C). Figure 3.64B shows a representative histogram that will be used as a model to determine the division or not in different cell types.

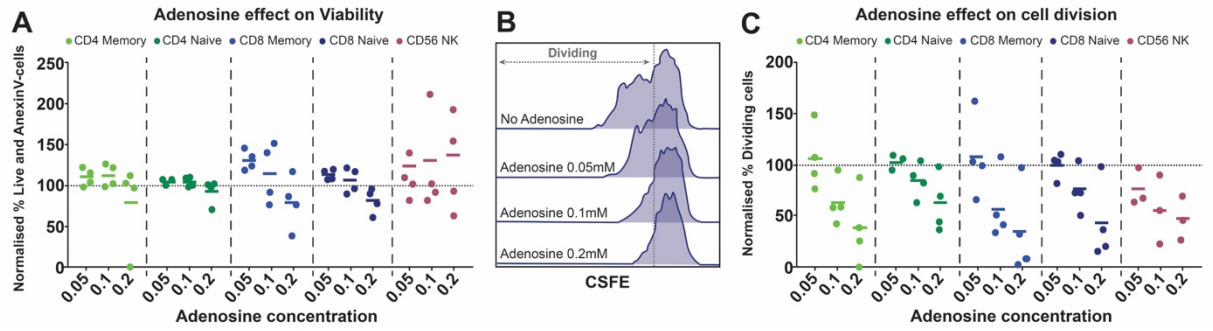

Figure 3.64. A) Adenosine effect on viability for CD3 T cell subsets and CD56 NK cells after 3-day and 6-day incubation respectively. B) Representative CSFE histogram on naïve CD8 T cells dividing cells. C) Adenosine effect on proliferation for CD3 T cell subsets and CD56 NK cells after 3-day and 6-day incubation respectively. Normalized percentage to no adenosine suppression. Mean from 4 different healthy donors are presented. Statistical analysis 1-way ANOVA (within each cell type) is performed with * $p<0.05$, ** $p<0.01$, *** $p<0.001$ and **** $p<0.0001$.

Due to its suppressive effect on cell proliferation without compromising viability, adenosine concentration at 0.1 mM was used to investigate the ability of the different A_{2B}AR antagonists in rescuing adenosine-mediated suppression of lymphocyte proliferation. A sub-apoptotic concentration of 12 μM A_{2B}AR antagonists was added to proliferating lymphocyte cultures, later analyzed with flow cytometry. The cellular types studied are characterized by different combinations of surface markers on T lymphocytes. CD4 CD45RA negative (CD4-CD45RA-) cells are memory cells that rapidly respond to previously encountered antigens. CD4 CD45RA positive (CD4-CD45RA+) cells are naïve T cells that have not yet encountered specific antigens. CD8 CD45RA negative (CD8-CD45RA-) cells are memory cells with the ability to kill virus-infected or abnormal cells. CD8 CD45RA positive (CD8-CD45RA+) cells are naïve T cells that have not been activated by specific antigens. **ISAM-140** rescued the proliferation of CD45RA+ (naïve and effector) CD8 T cells, CD45RA- (central and effector memory) and CD45RA+ CD4 T cells, and NK cells (Figure 3.65). While **266a** did not restore the proliferation of T cell subsets, NK cell proliferation was significantly rescued. None of the other A_{2B}AR antagonists (**SY1AF-30**, **SY1AF-80** and **SY1KO-24**) had any measurable impact on the rescue of lymphocyte proliferation (Figure 3.65). Similarly, the dual A_{2A}AR/A_{2B}AR antagonist **60** or the A_{2A}AR antagonist **AZD-4635** did not restore the proliferation of either T or NK cells.

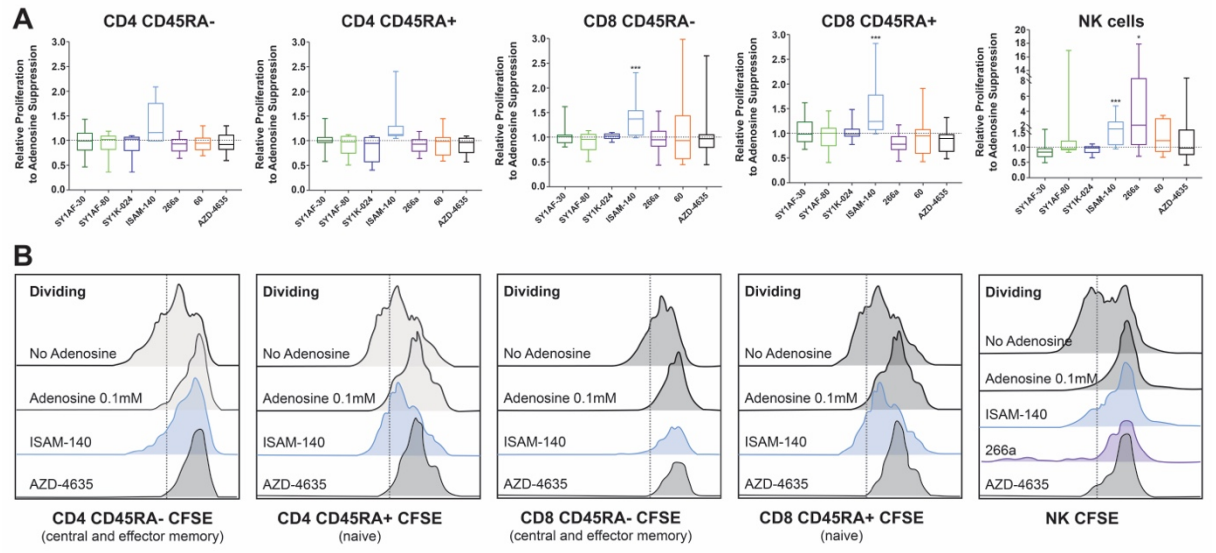

Figure 3.65. A) Rescue of lymphocyte proliferation by of A2BAR antagonism. Relative proliferation of: CD45RA- CD4 T cells, CD45RA+ CD4 T cells, CD45RA- CD8 T cells, CD45RA+ CD8 T cells, and NK cells, after incubation with exogenous adenosine 0.1 mM and A2BAR antagonist 12 µM for three (T cells) and six (NK cells) days. (n=10) CD45RA expression differentiates naïve and effector T cells from central and effector memory T cells. Box plots with minimum, first quartile, median, third quartile, and maximum are presented. Unpaired and non-parametric statistical analysis – Mann-Whitney test was performed against untreated control with * p<0.05, ** p<0.01, *** p<0.001 and **** p<0.0001. B) Representative CFSE histogram on the corresponding lymphocyte subset.

Given the different effects on proliferation across lymphocyte subsets, we hypothesized that the expression of $A_{2A}AR$ and $A_{2B}AR$ might differ accordingly. Flow cytometry analysis showed a highly donor-dependent variability of the expression intensity of $A_{2A}AR$ and $A_{2B}AR$, and no significant difference in their expression was observed between the different lymphocyte populations and was highly donor dependent (Figure 3.66).

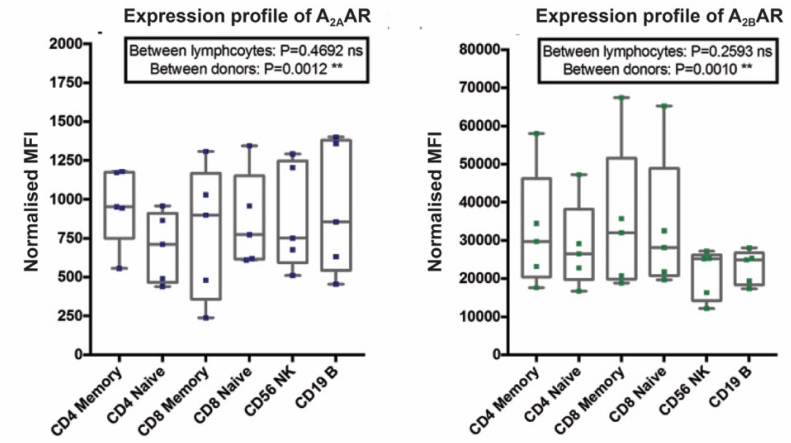

Figure 3.66. Expression of $A_{2A}AR$ and $A_{2B}AR$ from healthy donors (n=5). Box plots with minimum, first quartile, median, third quartile, and maximum are presented. Statistical analysis – 1-way ANOVA is performed with * p<0.05, ** p<0.01, *** p<0.001 and **** p<0.0001.

With the rescue of adenosine-mediated suppression of lymphocyte proliferation, effector function through pro-inflammatory cytokines – IFNγ and perforin, and the early activation marker – CD69 were successively examined. IFNγ production by CD4 and CD8 T cells was successfully rescued by several antagonists (Figure 3.67A-B). Similarly, perforin production by cytotoxic CD8 T cells was significantly upregulated upon A_{2B}AR antagonisms (Figure 3.67C). Of which, **SY1AF-30** and **266a** significantly improved both IFNγ and perforin production upon adenosine suppression. CD69 expression, associated with early lymphocyte activation, was also increased (Figure 3.67D-E) whereby **60** had positive effect on both CD4 and CD8 T cells.

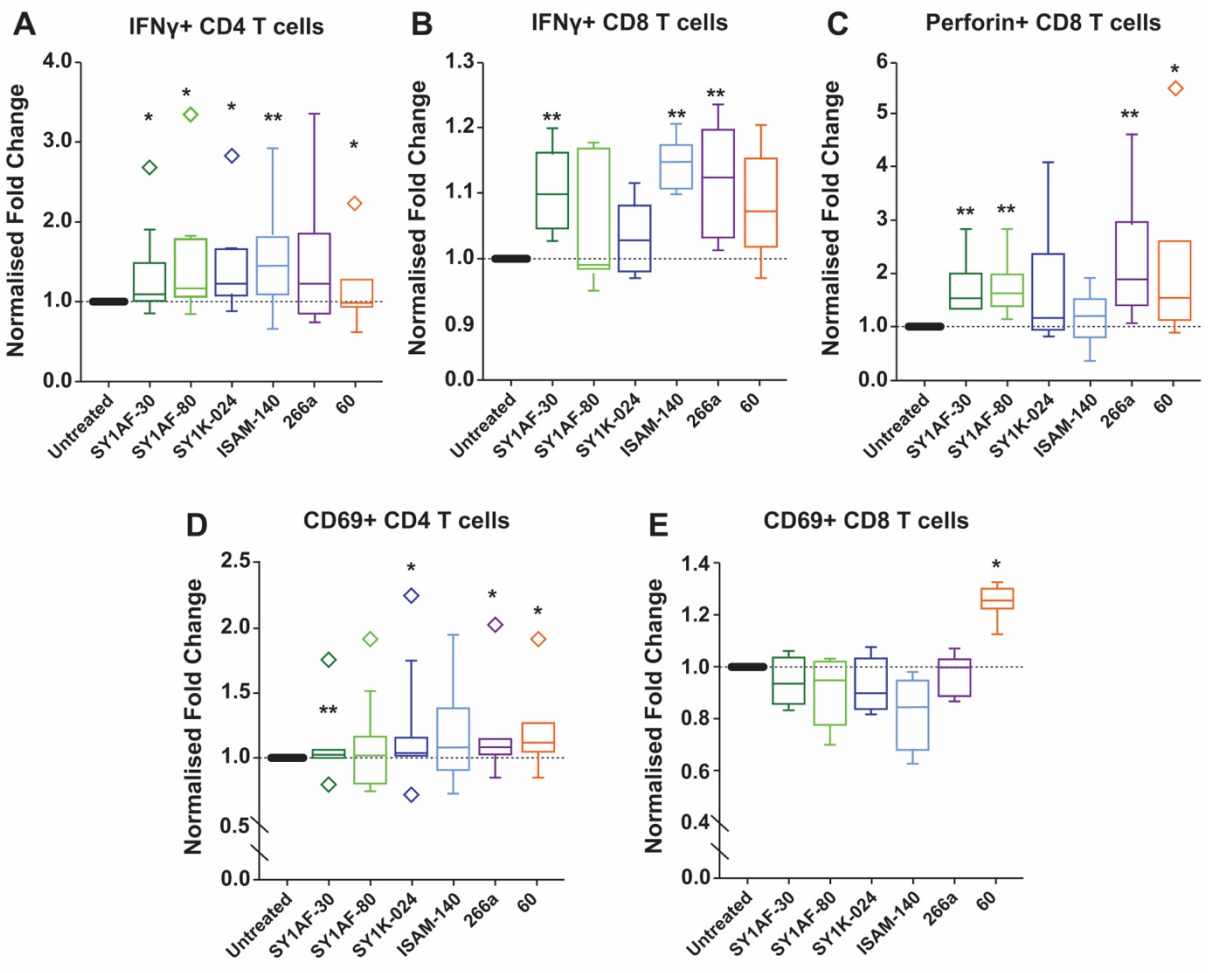

Figure 3.67. A-B) IFNγ and C) Perforin in CD4 (n=5) and CD8 (n=6) T cells. D) Expression of CD69 adhesion molecule in CD4 (n=7) and E) CD8 (n=4) T cells. A_{2B}AR antagonist 12 μM was added. Outlier is presented as diamond shape and defined by Tukey's rule, which is not included in statistical analysis. Box plots with minimum, first quartile, median, third quartile, and maximum are presented. Normalized Fold Change is based on percent values compared to untreated controls. Unpaired and non-parametric statistical analysis – Mann-Whitney test was performed against untreated control with * $p<0.05$, ** $p<0.01$, *** $p<0.001$ and **** $p<0.0001$.

To investigate the effect of $A_{2B}AR$ antagonism on lymphocyte proliferation in a more physiological relevant model, a sarcoma spheroid model that produce endogenous adenosine to better mimic the tumor microenvironment instead of using exogenous adenosine was developed. The relative production of adenosine was validated in spheroids including patient-derived tumors and the commercial U2OS cell line (Figure 3.68A). The expression of the ectonucleotidases CD39 and CD73 was highest in primary tumor spheroids from undifferentiated pleomorphic sarcoma, myxofibrosarcoma, and malignant peripheral nerve sheath tumors (MPNSTs, Figure 3.68B). Based on these results, lymphocyte proliferation was analyzed in MPNST-derived sarcoma spheroids. In contrast to the rescue of lymphocyte proliferation observed with exogenous adenosine, the $A_{2B}AR$ antagonists **SY1AF-30**, **SY1AF-80** and **266a** significantly rescued naïve CD8 T cell proliferation (Figure 3.68).

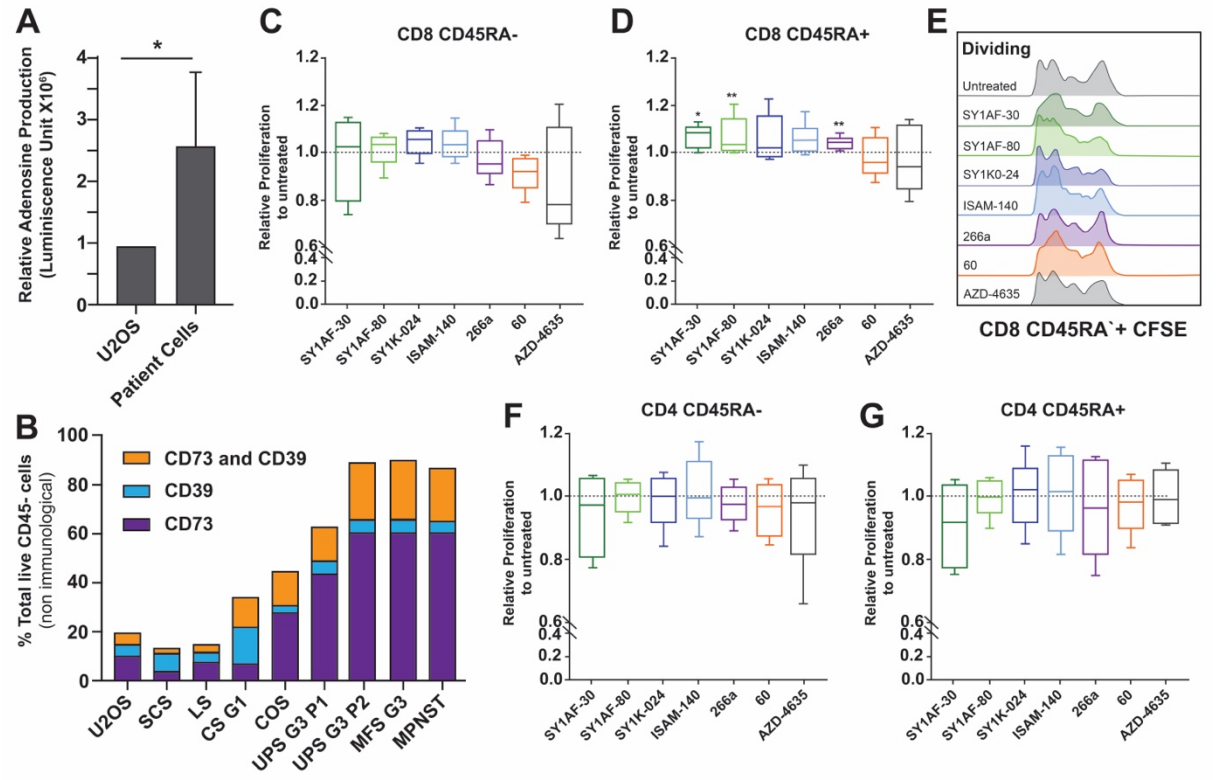

Figure 3.68. A) Relative adenosine production measured by ectonucleotidase CD73 assay and B) differential expression of CD73 and CD39 ectonucleotidases measured by flow cytometry of patient-derived sarcoma spheroids (n=8) and the commercial U2OS 3D culture. Abbreviations can be found in the glossary. Rescue of lymphocyte proliferation in sarcoma spheroids by $A_{2B}AR$ antagonism. Relative proliferation of: C) CD45RA- CD8 T cells; D) CD45RA+ CD8 T cells and E) representative CSFE dilution of CD45RA+ CD8 T cells; F) CD45RA- CD4 T cells; and G) CD45RA+ CD4 T cells after antagonist 12 μM treatment for three days in MPNST patient-derived sarcoma spheroid (n=5). Box plots with minimum, first quartile, median, third quartile, and maximum are presented. Unpaired and non-parametric statistical analysis – Mann-Whitney test was performed against untreated control with * $p<0.05$, ** $p<0.01$, *** $p<0.001$ and **** $p<0.0001$.

To increase the translational impact of the immunomodulatory effects of the A_{2B}AR antagonists, their ability in rescuing adenosine-mediated suppression was tested in patient-derived *ex vivo* expanded tumor-infiltrating lymphocytes (TILs) and autologous sarcoma spheroids. These expanded TILs were mainly composed of CD4 and CD8 effector memory cells (Figure 3.69A-C). Real-time imaging showed the blockade of A_{2B}AR, especially by **266a**, resulted in an overall improved TIL infiltration in comparison with untreated tumor spheroids (Figure 3.69D-E). Although not statistically significant, both **60** and **AZD-4635** treatments resulted in a median increased infiltration of 7% and 20% respectively, whereas **ISAM–140** did not have any effect on TIL infiltration (Figure 3.69D). To confirm the frequency of TIL infiltration, the spheroids were collected and analyzed for CSFE positive and CD73 negative TILs by flow cytometry. Despite a high variability, **266a** treatment showed significantly enhanced TIL infiltration into the spheroids (Figure 3.69E-F).

With the recruitment and retention of T cells within the tumor, expression of adhesion molecules is required. Thus, the expression of tissue resident T cells markers - CD11a (cell adhesion), CD49a (cell adhesion), CD69 (early cell activation) and CD103 (cell adhesion) was analyzed to gain insights into the phenotype of spheroid-infiltrated T cells. T-distributed stochastic neighboring embedding (tSNE) analysis revealed that the majority of infiltrating TILs are CD8 positive (cluster 1) and CD4 positive (cluster 9) T cells (Figure 3.69G). Among them, the infiltrated CD8 T cells were enriched with 2.5-fold higher CD49a and CD103 co-expression, while no significant difference was observed, the infiltrated CD4 T cells showed an enrichment of CD69 (Figure 3.69H), related with an early activation. Furthermore, the total CD3 T cells were 20% greater inside the spheroid (Figure 3.69I). To investigate the effect of A_{2B}AR antagonism in modulating the phenotype of infiltrated TILs, various antagonists were added to the TIL-tumor spheroids. All antagonists increased the CD8/CD4 T cell ratio though it was statistically significant only in the presence of **ISAM-140** (Figure 3.69J). In contrast, no significant change in the expression of the adhesion molecules CD11a, CD69, and CD49a/CD103 between untreated and A_{2B}AR antagonist-treated spheroid cultures was observed, suggesting that the impact of the A_{2B}AR antagonism on TIL infiltration is not mediated through alterations in the expression of these specific adhesion molecules (data not shown).

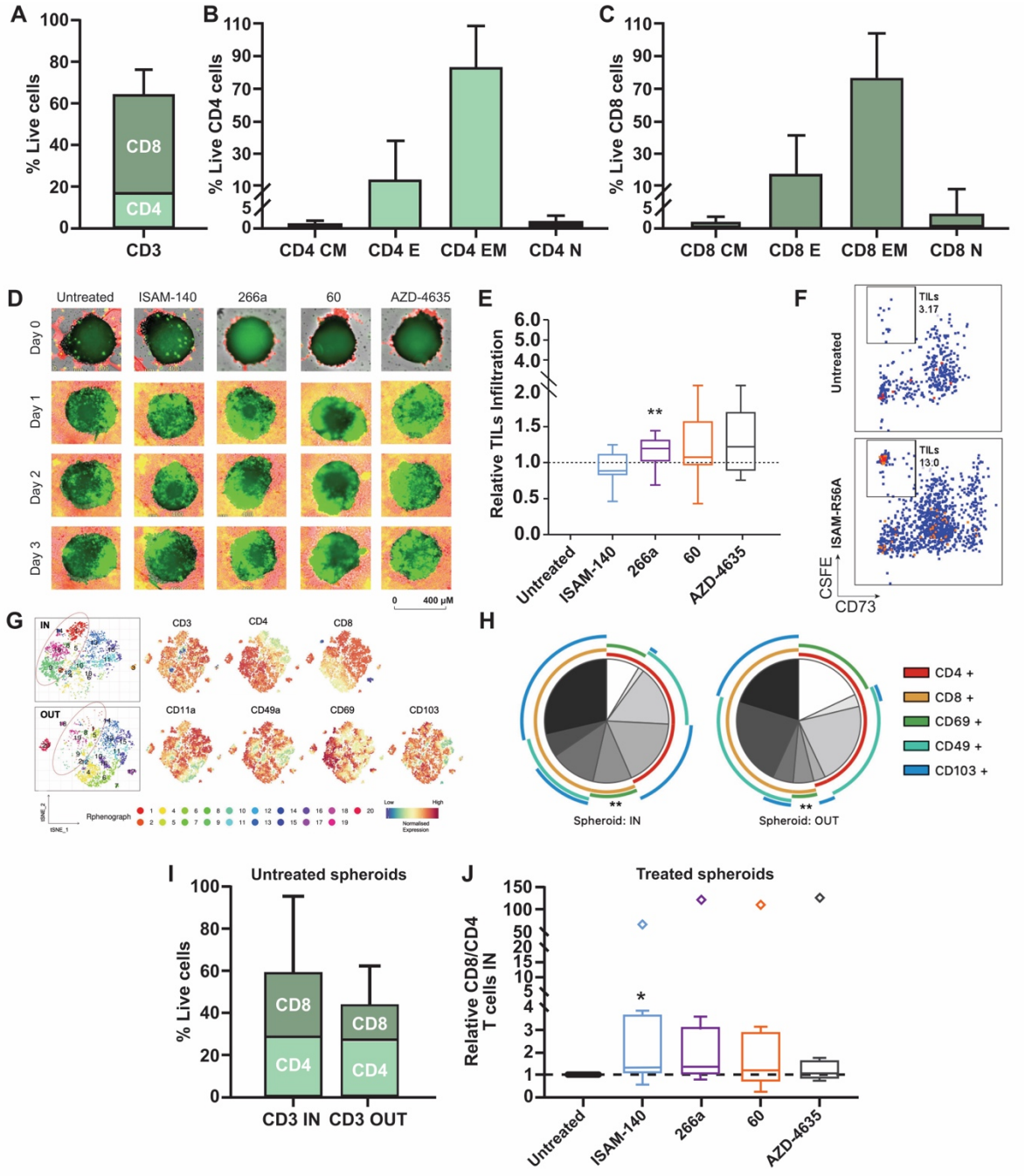

Figure 3.69. A) Expression of CD3, B) CD4 and C) CD8 **C** in expanded TILs (n=8). D) Representative real-time imaging of spheroid TIL infiltration over three days. Green areas demarcate CFSE-labelled TILs infiltrated into the red boundary tumor spheroid. E) Relative TIL infiltration into autologous spheroids (n=8) measured by flow cytometer. Antagonist 12 µM was added with CSFE-labelled TILs after spheroid formation. F) Representative flow cytometry plot of CFSE positive TILs in CD73+ tumor spheroid. G) T-distributed stochastic neighboring embedding (tSNE) analysis and H) Annotated pie chart of TILs within (IN) and outside of (OUT) the spheroids without treatment (n=8). Wilcoxon Rank Sum test was performed to compare the various IN vs OUT adhesion markers. I) Expression of CD3 T cells, CD49a+ CD103+ among CD8 T cells and CD69 MFI among CD4 T cells IN and OUT of the spheroids without treatment (n=8). J) Relative CD8/CD4 TIL ratio IN the spheroids. Outlier is presented as diamond shape and defined by Tukey's rule, which is not included in statistical analysis.

While blockade of $A_{2A}AR$ is well documented to rescue T and NK cell proliferation, the effect of targeting the $A_{2B}AR$ in lymphocytes remained almost unexplored.[35,45,48] Only recently, it was reported that $A_{2B}AR$ deficiency in tumor-bearing mice resulted in an increased infiltration of dendritic cells to promote cross-priming of adoptively transferred tumor antigen-specific T cells.[51] As commented in the introduction, $A_{2B}AR$ activation plays critical roles during tumor development including but not limited to proliferation, angiogenesis, invasion and metastasis, as well as immune suppression, which make the antagonists of this receptor hold great promise for the development of new polyvalent cancer therapeutics.[30,66]

Given the short half-life of endogenous adenosine,[189] exogenous adenosine is still commonly used to study adenosine-mediated immunosuppression in the TME. In general, lymphocyte assays are based on phenotypic analysis and often complemented with read-outs to analyze canonical functions such as cell viability, proliferation, and the ability to produce inflammatory cytokines as well as to recognize and kill target cells. Throughout these experiments, the $A_{2B}AR$ antagonists were evaluated in lymphocyte viability and proliferation assays. Since prognosis is often associated with the frequency of tumor-infiltrating lymphocytes,[190–192] we developed two models to study the blockage of $A_{2B}AR$ in recovery anti-tumor immune responses. An exogenous adenosine *in vitro* healthy donor model and endogenously produced adenosine *ex vivo* patient derived model were used to better study the dynamic crosstalk of adenosine in the TME as well as being clinically relevance. As a result, $A_{2B}AR$ antagonists successfully rescued anti-tumor immune response through cytotoxicity of patient-derived spheroid cultures, proliferation of lymphocytes and tumor spheroid immune cell infiltration accompanied with differences in phenotype.

The six ligands examined exhibited high $A_{2B}AR$ affinity and excellent selectivity profiles. Two of them (**266a** and **60**) were herein originally reported, by introduction of a 2-fluorobenzyl group or a chlorine atom at positions 1 and 8 of the tricyclic core respectively. Indeed, **266a** (K_i = 1.50 nM) is confirmed as one of the most potent $A_{2B}AR$ antagonist to date, while **60** exhibited a highly promising dual $A_{2B}AR/A_{2A}AR$ antagonistic profile (while devoid of affinity for the remaining AR subtypes). The selected ligands revealed negligible CD73 inhibitory action, thus allowing to attribute the herein observed effects to their specific $A_{2B}AR$ (and $A_{2A}AR$ in the case of **60**) antagonistic effect.

By exposure of these $A_{2B}AR$ antagonists to breast cancer patient-derived cells, their anti-tumor activity was first revealed through a reduced tumor spheroids growth rate. Additionally,

the immunomodulatory effect of A_{2B}AR antagonism was demonstrated with the successful rescue of T and NK cell proliferation under exogenous adenosine-mediated suppression, with CD8 naïve T cell being the most responsive of the T cell types examined. These findings correspond to an adenosine-producing human melanoma cell line, showing higher suppression of CD8 T cell proliferation than CD4 T cells.[193] A_{2B}AR antagonists were subsequently shown improved production of pro-inflammatory cytokines IFNγ and perforin along with the expression of the activation marker CD69.

Patient outcome in various sarcoma types is shown to correlate with the presence of TILs.[190–192] Patient-derived spheroids can retain the unique characteristic of the original tumor compared to 2D monoculture or patient-derived xenograft by enabling cell-cell and cell-extracellular interactions.[194,195] Using a patient-derived sarcoma spheroids model, we observed that treatment with A_{2B}AR antagonists improved autologous TIL infiltration into sarcoma spheroids. Tumor spheroid-infiltrating lymphocytes were enriched for the expression of the tissue resident markers CD49a and CD103 in CD8 T cells and CD69 in CD4 T cells.[56] A recent study identified a unique population of CD8 TILs co-expressing CD39 and CD103 that were reactive against both primary and metastatic tumors.[196] Another study defined CD8 tissue resident T cells in human epithelia with cytotoxic function to express CD49a and correlate with inflammatory skin diseases.[197] *In vivo* A_{2A}AR antagonism has also been reported to upregulate the expression of CD69 on TILs, while A_{2B}AR antagonism enhanced CXCR3-dependent TIL responses.[13,53] Notably, a recent study demonstrated that adenosine can mediate functional and metabolic suppression of tumor-infiltrating CD8+ T cells.[187] Thereby, A_{2B}AR antagonism not only potentially increase TIL infiltration into solid tumors but may also improve the overall metabolic fitness of tumor-infiltrating T cells.

Here we demonstrate that **ISAM-140** exerts biologically improved immune cell proliferation on T and NK cells in an A_{2B}AR expression independent manner in healthy donor PBMCs. This response was dose-dependent with a higher concentration further restoring proliferation (data not shown). This lymphocyte proliferation rescue was accompanied with upregulated IFNγ production in both CD4 and CD8 T cells. **ISAM-140** was also non-toxic and even improved cell viability (data not shown). In addition, our novel A_{2B}AR antagonist – **266a**, with K_i to the A_{2B}AR similar to the corresponding A_{2A}AR value of the preclinical A_{2A}AR antagonist – **AZD-4635** (1.50 nM vs 1.70 nM respectively), improved TILs infiltration into autologous patient-derived sarcoma spheroids. CD8 naïve T-cell proliferation response was

also observed in the adenosine-producing spheroid model, while a specific NK cell proliferation response was noted in the exogenous adenosine assay. CD8 T cell IFNγ and perforin production was also significantly rescued under exogenous adenosine suppression. Thereby, the potential of **266a** to induce tumoral TILs infiltration is highly promising. This induction of tumoral CD8 T cell infiltration was already observed from the clinical trial of a dual $A_{2A}AR/A_{2B}AR$ antagonist – Etrumadenant combined treatment with anti-PD1.[152]

4 CONCLUSIONS

- Pyrimidine-based A_{2B}AR antagonists were extensively evaluated, resulting in the discovery of eight new antagonists with high affinity (K_i < 10 nM) and desirable subtype selectivity toward the other three adenosine receptors. The FEP experiments have contributed to establishing a clear binding mode of this type of ligands.
- Halogenation has been shown to be a favorable substitution at the pharmacokinetic level as well, increasing solubility and microsomal stability while reducing binding to CYP3A4. Non-xanthine-based compounds exhibit a better physicochemical properties compared to those based on xanthines.
- The Scaffold-Hopping strategy (such as heterocycle substitution, ring opening) allowed the identification of new A_{2B}AR antagonists with monocyclic, bicyclic, and tricyclic structures. Several new ligands with attractive affinity (K_i < 100 nM) and exquisite selectivity (> 1000-fold) were identified by evaluation of 21 novel scaffolds. This exploration has also enabled the evaluation of the effect on binding to the orthosteric site by removing the classical interaction via a double hydrogen bond with $Asn^{6.55}$.
- The *N*-substitution through alkylation and benzylation of monocyclic and tricyclic ligands has generated numerous dual A_{2A}AR/A_{2B}AR antagonists with attractive affinity for both receptors (K_i < 100 nM for A_{2A}AR and A_{2B}AR) and outstanding selectivity (> 1000-fold for the other two receptors). A preliminary binding mode has been established for both A_{2A}AR and A_{2B}AR, but further studies are necessary for the complete understanding of dual compounds binding mode.
- The antagonistic behavior of the lead compounds was corroborated through functional cAMP and label-free experiments and joint analysis of the current and previous series allowed a comprehensive understanding of the binding mode and SARs within the series.
- In the frame of this project unequivocal evidence supporting the stereospecific interaction between the *h*A_{2B}AR and some has been obtained. For the first time, evidence of enantioselective effect has been demonstrated and also confirmed for *h*A_{2A}AR in dual antagonists. Previously stated evidence was established through the synergistic use of different experimental techniques (e.g., chiral HPLC, circular dichroism, and X-ray crystallography).

- The in silico evaluation of physicochemical properties (e.g., logP, TPSA, HBD, HBA, MW) of the synthesized compounds has led to the identification of different families, offering potential for the treatment of diverse tumor types.
- The immunomodulatory potential of the new drugs has been validated using patient-derived cells. For the first time, pyrimidine-derived A_{2B}AR antagonists have been validated as potent immunomodulators, effectively restoring immune system function inhibited by adenosine. This includes the restoration of pro-inflammatory cytokine production, increased proliferation, and lymphocyte infiltration in tumor cell spheroids.
- The potential of new drugs has been validated in terms of their antiproliferative effects on breast cancer, colorectal cancer, glioblastoma, including cancer-associated fibroblasts (CAFs), through *in vitro* cell lines and *ex vivo* cultures. Both selective A_{2B}AR antagonists and dual A_{2A}AR/A_{2B}AR antagonists demonstrated significant antiproliferative effects, effectively preventing excessive proliferation of breast cancer spheroids and reducing tumor cell proliferation up to 80% without affecting CAFs. However, these assays need to be confirmed in immunocompetent murine *in vivo* models, evaluating both effects simultaneously in an *in vivo* system.

5 EXPERIMENTAL SECTION

5.1 GENERAL CONSIDERATIONS

5.1.1 Synthesis and purification

Unless otherwise indicated, all starting materials, reagents and solvents were purchased and used without further purification. The Biginelli and alkylation reactions were performed in coated Kimble vials on a PLS (6×4) Organic Synthesizer with orbital stirring or Anton Paar Microwave Synthesis Reactor in the indicated reactions. The reactions were monitored by thin-layer chromatography (TLC) on 2.5 mm Merck silica gel GF 254 strips, and the purified compounds each showed a single spot; unless stated otherwise, UV light, iodine vapor and/or *p*-anisaldehyde were used to detect compounds. After extraction from aqueous phases, the organic solvents were dried over anhydrous magnesium or sodium sulfate. The purity and identity of all tested compounds were established by a combination of HPLC, mass spectrometry and NMR spectroscopy. Purification of isolated products was carried out by one of following methods: a) column chromatography (Kieselgel 0.040–0.063 mm, E. Merck), b) medium pressure liquid chromatography (MPLC) on a Combi Flash Companion (Teledyne ISCO) with RediSep pre-packed normal-phase silica gel (35–60 μm) columns or c) preparative chromatography (Uniplate^{TM} Techware 20x20 cm Silica G 1000mm Thick 15μm). The solvent mixtures used in the purification are shown in the section Spectroscopic and analytical data for all compounds described and their enantiomers for each chapter separately, using the following abbreviations for the solvents: Hex, Hexane; AcOEt, ethyl acetate; MeOH, methanol; DCM, dichloromethane; IPA, *i*-propanol.

5.1.2 Structural characterization

Melting points were determined on a Stuart Scientific melting point apparatus SMP3 and are uncorrected. Samples were dissolved in deuterated solvent ($CDCl_3$, DMSO-d_6 or MeOD) and the NMR spectra were recorded on Bruker AM300 and XM500 spectrometers. For regioisomer differentiation experiments (Chapters 1 & 3), HSQC, HMBC, COSY, NOESY and ROESY were recorded on AV NEO 750 MHz instrument. Chemical shifts are given as δ values

against tetramethylsilane as internal standard and *J* values are given in Hz. The signal multiplicity shown with the abbreviatures s, singlet; d, doublet; t, triplet; q, quartet; p, pentuplet; hept, heptuplet; dd, doublet of doublets; dt, doublet of triplets; td, triplet of doublets; brs, broad singlet; and m, multiplet, followed by number of protons (deduced by integration). The coupling constants (*J*) are deduced in Hertz (Hz). Low-resolution mass spectra (LRMS) were obtained on a Varian MAT-711 instrument (EI, 70 eV) or Agilent 8890 GC coupled to 5977B GC/MSD system (CI). High-resolution mass spectra (HRMS) were obtained on an Autospec Micromass spectrometer. Analytical HPLC was performed on a Water Breeze™ 2 system (binary pump 1525, detector UV/Visible 2489, 7725i Manual Injector Kit 1500 Series) using a Luna 5 µm Silica (2) 100 Å, LC Column 150 x 4.6 mm column with gradient elution using the mobile phases dichloromethane, isopropanol, and a flow rate of 1 ml/min. The purity of all tested compounds was determined to be >95%. The structural and spectroscopic data obtained for all compounds described is provided in can be found in Spectroscopic and Analytical Data, in the section corresponding to each chapter.

Taking into consideration the quantity of compounds obtained within the framework of this Doctoral Thesis and following the general criteria accepted by the scientific community for the characterization of chemotheques, the general guidelines indicated below have been followed in the structural characterization of the compounds:

1 All the described compounds have been routinely characterized including:
   a. ^{1}H-NMR.
   b. Mass spectrometry (LRMS).
   c. Melting point (Mp).
2 In each series, representative compounds have been chosen for determination of (in addition to the characterization indicated in the previous section):
   a. ^{13}C NMR.
   b. High Resolution Mass Spectrometry (HRMS).
3 For the differentiation of the regioisomers pairs obtained in the same reaction, COSY, NOESY (or ROESY), HSQC and HMBC techniques have been used.
4 The precursor compounds of the alkylation (**D1-D8**) have been described previously, so their characterization was carried out routinely. The analytical data shown for these compounds are those reported in the literature.

5.1.3 Pharmacological evaluation and preliminary pharmacokinetic characterization

5.1.3.1 Radioligand binding competition assays

Radioligand binding competition assays were performed *in vitro* by the group of the Professor Maria I. Loza (University of Santiago de Compostela, Spain) using human ARs expressed in transfected HeLa [hA$_{2A}$AR (9 pmol/mg protein) and hA$_3$AR (3 pmol/mg protein)], HEK-293 [hA$_{2B}$AR (1.5 pmol/mg protein)] and CHO [hA$_1$AR (1.5 pmol/mg protein)] cells as described in previously published works.[141,144] A brief description is given below. A$_1$AR competition binding experiments were carried out in membranes from CHO-A$_1$ cells labelled with 1 nM [^{3}H]DPCPX (K_D = 0.7 nM). Non-specific binding was determined in the presence of 10 µM R-PIA. The reaction mixture was incubated at 25 °C for 60 min. A$_{2A}$AR competition binding experiments were carried out in membranes from HeLa-A$_{2A}$ cells labelled with 3 nM [^{3}H]ZM241385 (K_D = 2 nM). Non-specific binding was determined in the presence of 50 µM NECA. The reaction mixture was incubated at 25 °C for 30 min. A$_{2B}$AR competition binding experiments were carried out in membranes from HEK-293-A$_{2B}$ cells (Euroscreen, Gosselies, Belgium) labelled with 25 nM [^{3}H]DPCPX (K_D = 21 nM). Non-specific binding was determined in the presence of 400 µM NECA. The reaction mixture was incubated at 25 °C for 30 min. A$_3$AR competition binding experiments were carried out in membranes from HeLa-A$_3$ cells labelled with 10 nM [^{3}H]NECA (K_D = 8.7 nM). Non-specific binding was determined in the presence of 100 µM R-PIA. The reaction mixture was incubated at 25 °C for 180 min. After the incubation time, membranes were washed and filtered, radioactivity was detected in a Microbeta Trilux reader (PerkinElmer).

5.1.3.2 Blockade of *h*CD73 assays

Blockade of *h*CD73 assays were performed *in vitro* by the group of the Professor Maria I. Loza (University of Santiago de Compostela, Spain). The selected AR antagonists were tested at 1 μM and 10 μM. Experiments (human CD73) were carried out in a white 384-Optiplate (Perkin Elmer 6007290). Test compounds and the standard (α-β-methylene adenosine, Sigma M3763), 0.5 μg/mL enzyme (Cayman RYD-5795-EN-010), 300 μM AMP (Sigma A2252) and 100 μM ATP (A2383) were added in a final volume of 25 μL/well, using 25 mM Tris-HCl, 5 mM $MgCl_2 \cdot 6H_2O$, pH = 7.4 as assay buffer. The reaction mixture was incubated at 37ºC for 15 min, after incubation 25 μL of Cell Titer-Glo Luminescent cell viability (Promega G7571) was added and shaken during two minutes before incubation at RT for 10 min. Luminescence at 100 ms was measured in the Perkin Elmer Enspire multimode plate reader.

5.1.3.3 Functional experiments

Functional experiments were performed by the group of Professor Francisco Ciruela (University of Barcelona, Spain). The following reagents were used: adenosine deaminase (ADA, Roche Diagnostics, Mannheim, Germany), 5'-N-Ethylcarboxamidoadenosine (NECA, Tocris, Brisltol, UK), zardaverin (Calbiochem, San Diego, CA, USA), SNAP-Surface Alexa Fluor 488 (New England BioLabs, Ipswich, MA, USA). *Cloning.* The cDNA encoding the human A_{2B}AR was amplified by polymerase chain reaction using the primers FA2BREcoRV (5'- tcgag**GATATC**CTGCTGGAGACACAGGACGC -3') and RA2BRHindIII (5'- cgag**AAGCTT**TCATAGGCCCACACCGAGAGC -3') and subcloned into the *Eco*RV/*Hind*III restriction sites of the pRK5-A_1R^{SNAP} vector (kindly provided by Dr. J. P. Pin, Université de Montpellier and Institut de Génomique Fonctionnelle, Montpellier, France) by replacing the adenosine A_1 receptor. The resulting construct encoded the human A_{2B}AR tagged with SNAP, a 20 kDa mutant of the DNA repair protein O^6-alkylguanine-DNA alkyltransferasthe (AGT), at its N-terminus (pRK5-$A_{2B}AR^{SNAP}$). *Cell culture and stable transfection.* Human embryonic kidney (HEK)-293T cells were grown in Dulbecco's modified Eagle's medium (DMEM) (Sigma-Aldrich, St. Louis, MO, USA) supplemented with 1 mM sodium pyruvate (Biowest, Nuaillé, France), 2 mM L-glutamine (Biowest), 100 U/ml streptomycin (Biowest), 100 mg/ml penicillin (Biowest) and 5% (v/v) fetal bovine serum (Invitrogen, Carlsbad, CA, U.S.A.) at 37°C and in an atmosphere of 5% CO_2. HEK-293 cells growing in 60 cm^2 plates were transfected with pRK5-$A_{2B}AR^{SNAP}$ using the polyethylenimine (PEI) method.[198] After 48 hours of transfection, cells were stained using SNAP-Surface Alexa Fluor 488.[167] Fluorescent cells were selected every 2 weeks for 2 months using a Cell sorter (MoFlo Astrios, Beckman Coulter) to enrich the percentage of cells that express the receptor, thus ensuring its permanent expression.[199]

5.1.3.4 cAMP accumulation assay.

cAMP accumulation was measured using the LANCE Ultra cAMP kit (PerkinElmer, Waltham, MA, USA) as previously described.[199] In brief, HEK-293T cells permanently expressing the $A_{2B}AR^{SNAP}$ construct ($A_{2B}AR^{SNAP}$ cells) were detached with accutase (Sigma-Aldrich) and incubated for 1 h at 22°C in Dulbecco's modified Eagle's medium (DMEM) (Sigma-Aldrich) supplemented with 0,1% BSA, ADA (0.5 U/ml) and zardaverin (100 µM). $A_{2B}AR^{SNAP}$ cells ($1x10^4$ cells/200µl) were incubated with NECA in the presence/absence of increasing concentrations, during 30 min at 22°C. Eu-cAMP tracer and ULight™-anti-cAMP

reagents were prepared and added to the sample following manufacturer's instructions. The 384-wells plate was incubated 1 h at 22°C in the dark and was then read on a CLARIOstar microplate reader (BMG Labtech, Durham, NC, USA). Measurements at 620 nm and 665 nm were used to detect the TR-FRET signal and the concomitant cAMP levels were calculated following manufacturer's instructions. Data were fitted by non-linear regression using GraphPad Prism 9 (San Diego, CA, USA). Data was expressed as K_B by following the formula reported by Leff and Dougall (Equation 5.1):[200]

$$K_B = \frac{IC_{50}}{\left(2 + \left(\frac{[A]}{[A_{50}]}\right)^n\right)^{\frac{1}{n}}}$$

Equation 5.1 K_B value calculation.

Where IC_{50} is the concentration of compound that inhibits NECA effect by a 50%; [A] is the concentration of NECA employed in the assay, $[A_{50}]$ is the NECA EC_{50} value and n is the Hill slope of the curve.

5.1.3.5 Cellular impedance label free experiments

Functional experiments were performed by the group of Professor Francisco Ciruela (University of Barcelona, Spain). The xCELLigence RTCA system (Roche) was employed to assess the impact of blocking A_{2B}AR-mediated effects in cellular impedance upon receptor activation, as previously described.[201–204] To this end, $A_{2B}AR^{SNAP}$ cells were growth in 16-wells E-plates (Roche), using DMEM supplemented with 1 mM sodium pyruvate, 2 mM L-glutamine, 100 U/ml streptomycin, 100 mg/ml penicillin and 1.5% (v/v) fetal bovine serum in the presence of 0.5 U/ml of ADA. Of note, wells were previously coated with 50 µl fibronectin (10 µg/ml; Sigma-Aldrich) and the background index for each well was determined with supplemented DMEM (90 µl) in the absence of cells. Subsequently, $A_{2B}AR^{SNAP}$ cells (90 µl) were plated at a cell density of 10,000 cells/well and grown for 18 hours in the RTCA SP device station (Roche) at 37° C in an atmosphere of 5% CO_2. Then, before ligands' addition, cell index values were normalized to the same time point using the RTCA software, providing the normalized cell index (NCI). After ligand stimulation, NCI was recorded every 15 seconds for a total time of at least 45 minutes. The area under the curve (AUC) for every condition was calculated using GraphPad Prism 9. Data are represented as mean ± standard error of mean

(SEM) with statistical significance set at $P < 0.05$. The number of samples (n) in each experimental condition is indicated in the corresponding figure legend. Outliers were assessed by the ROUT method,[205] thus any sample was excluded assuming a Q value of 1% in GraphPad Prism 9 (San Diego, CA, USA). Comparisons among experimental groups were performed by Student's t test or one-way analysis of variance (ANOVA) followed by Tukey's multiple comparisons post-hoc test using GraphPad Prism 9, as indicated.

5.1.3.6 Preliminary pharmacokinetic assays

All the assays contained in this section were performed by the group of the Professor Maria I. Loza (University of Santiago de Compostela, Spain).

CYP3A4 Inhibition

Incubations were conducted in a 200 µl volume in 96 well microtiter plates (COSTAR 3915). Addition of cofactor-buffer mixture (KH_2PO_4 buffer, 1.3 mM NADP, 3.3 mM $MgCl_2$, 3.3 mM glucose-6-phosphate and 0.4U/ml glucose-6-phosphate dehydrogenase), supersomes control, standard inhibitor (Ketoconazole from Sigma Aldrich) previously diluted and compounds to plates were carried out by a liquid handling station (Zephyr Caliper). The plate was then pre- incubated at 37 °C for 5 min, and the reaction initiated by the addition of pre-warmed enzyme/substrate (E/S) mix. The E/S mix contained buffer (KH_2PO_4), c-DNA-expressed P450 in insect cell microsomes, substrate (DBF: dibenzylfluorescein or 7-BFC: 7-benzyloxy-4-trifluoromethyl-coumarin) and other components to give the final assay concentrations in a reaction volume of 200 µl. Reactions were terminated after various times (a specific time for each cytochrome) by addition of STOP solution (ACN/TrisHCl 0.5M 80:20, and NaOH 2N for CYP3A4). Fluorescence per well was measured using a fluorescence plate reader (Tecan Infinite M1000 pro) and percentage of inhibition was calculated. *In silico* predictions were performed using free web-based models (FAME3, SmartCYP and Xenosite).[176,206,207]

Human Microsomal Stability

The human microsomes employed were purchased from Tebu-Xenotech. The compound was incubated with the microsomes at 37 ºC in a 50 mM phosphate buffer (pH=7.4) containing 3 mM $MgCl_2$, 1 mM NADP, 10 mM glucose-6-phosphate and 1 U/ml glucose-6-phosphate-dehydrogenase. Samples (75 µl) were taken from each well at 0, 10, 20, 40 and 60 minutes and transferred to a plate containing 4 ºC 75 µl acetonitrile and 30 µl of 0.5% formic acid in water were added for improving the chromatographic conditions. The plate was

centrifuged (46000 g, 30 min) and supernatants were taken and analyzed in an UPLC-MS/MS (Xevo-TQD, Waters) by employing a BEH C18 column and an isocratic gradient of 0.1% formic acid in water: 0.1% formic acid acetonitrile (60:40). The metabolic stability of the compounds was calculated from the logarithm of the remaining compounds at each of the time point studied.

Solubility determinations

A 10 mM stock solution of the compound was serially diluted in 100% DMSO and 2.5 µl of this solution was added to a 384-well UV-transparent plate (Greiner) containing 47.5 µl of PBS (pH=7). The plate was incubated at 37 ºC for 4 h and the light scattering was measured in a Nephelostar plus reader (BMG LABTECH). The data was fitted to a segmented linear regression for measuring the compound solubility.

5.1.4 Computational studies: docking and molecular dynamics simulations

5.1.4.1 Docking and molecular dynamics

Docking and molecular dynamics simulations were conducted with Professor Hugo Gutiérrez de Terán and his group at the University of Uppsala, both during a predoctoral stay and in subsequent studies. The structural model for A_{2A}AR was obtained from ProteinDataBank (PDB: 4EIY with closed conformation; PDB: 3UZC with open conformation) for A_{2B}AR derives from a homology model from A_{2A}AR (PDB: 4EIY) processed using the Protein Preparation Wizard pipeline in Maestro (Schrodinger ver. 2023-1). Subsequently, possible 3D tautomer and protomers at pH 7 ± 2 were generated for each compound using OPLS4 force field[208] and Epik, the lowest energy conformer was chosen for molecular docking. A receptor grid was generated with the default Van der Waals radius scaling settings, and it was positioned in the center of geometry of the binding site. Thereafter, Glide SP docking was performed leading to the protein-ligand complexes which were used as the starting point for the MD/FEP simulations carried out with the software package Q.[209] An FEP network was generated for each of chemical series using ECFP4 as a measure of the chemical similarity between ligand pairs, ensuring smooth alchemical transformations while covering the entire dataset. For each vertex comparing a pair of compounds part of the FEP network, the QligFEP[210] pipeline was used for generating the MD/FEP input files and its posterior analysis. The MD simulations were carried out under spherical boundary conditions (SBC) with a sphere size of 25 Å, with solvent atoms lying in the outer shell of the sphere (22-25 Å) subject to radial and polarization restrains using the surface-constrained all-atom solvent (SCAAS).[211,212] All titratable residues outside the

sphere were neutralized and histidine protonation states were set by the Protein Preparation Wizard. Atoms outside the simulation sphere were excluded from the calculation of the nonbonded interactions and tightly constrained (200 kcal/mol·Å²) to its position. Long-range electrostatic interactions beyond a 10 Å threshold were evaluated using the local reaction field method,[211] excluding the atoms undergoing the FEP transformation where no cutoff is applied. The OPLS-AA/M force field[213] was used for the protein and solvent (TIP3P) parameters, while OPLS2005 ligand parameters were generated using the ffld_server,[214] solvent bonds and angles were constrained using the SHAKE algorithm.[215] The MD/FEP simulations are preceded by a heating phase of the sphere from 0.1 to 298 K during a short 31 ps stage were a positional restraint of 10 kcal/mol·Å² is progressively released. This is followed by a 100 ps unbiased and unrestrained equilibration and subsequently, MD sampling is performed across a predefined sigmoidal λ schedule, consisting of 101 λ windows, each consisting of 10 ps sampling using a 2 fs timestep. To get initial relative binding free energy estimates (RBFE), the thermodynamic cycles are closed for each ligand pair defined in the FEP network by performing the corresponding MD/FEP simulation in a water sphere, and the free energies are calculated with the Bennett acceptance ratio (BAR) method.[216] The cycle closure correction framework[217] was utilized for assessing the convergence of the initial RBFE estimates and, additionally it yielded corrected RBFE values which eliminate the hysteresis along all the thermodynamic cycles encompassed by the FEP network. To get the ABFE for all the compounds of interest, the corrected RBFE values together with the FEP networks and the experimental binding free energy for a reference compound per network are used. The Bellman-Ford implementation from Networkx[218] was used for finding the shortest path connecting a reference with the remaining target compounds and, for each target compound, Equation 5.2 was used to get the ABFE estimates. Finally, a correction offset value for all the ABFE estimates was calculated as described by Wang, et al.[219] in order to minimize the experimental error introduced to the final estimates.

$$\Delta G_{pred}^{Targ.comp.} = \Delta G_{exp}^{Ref.comp.} + \sum_{i=1}^{N} \Delta\Delta G_{pred}^{FEP,i}$$

Equation 5.2 Correction offset value for all the ABFE estimates.[219]

5.1.4.2 Quantum Mechanical pK_a calculation.

Isodesmic method or relative pK a calculation[220] was used to calculate solution-phase pKa values in water, following the formula: $pKa = \frac{\Delta Gs}{RT} ln(10) + pKa(HREF)$, from the solution phase reaction free energy (ΔG_s) using the following proton transfer reaction: $HA + REF- \leftrightarrow A^- + HREF$, where HA and A^- represent examined acid and its conjugate base while REF and HREF represent reference base and its conjugate acid respectively. Reaction free energy is calculated as the difference between free energies of products and reactants according to the formula: $\Delta Gs = (G(A^-) + G(REF^-)) - (G(HA) + G(HREF))$. The reference base should be as chemically similar as possible to the group whose pK_a is to be determined, in this case the thiol group on the aromatic ring, thus thiophenol was selected as referent base.[221–223]

As a good compromise between accuracy and feasibility, all geometries optimizations and free energy calculations were carried out by the very efficient M06–2X/6–31+G(d) method. SMD continuum model[224] was considered to account solvent effects during both geometry optimization and energy calculation, with parameters corresponding to pure water. All calculations were performed using the Gaussian 16 software.[225]

5.2 EXPLORING THE EFFECT OF HALOGENATION IN A SERIES OF POTENT AND SELECTIVE A_{2B} ADENOSINE RECEPTOR ANTAGONISTS

5.2.1 Synthesis of halogenated derivatives (1-80)

METHOD A. General procedure for the synthesis of mono and dihalogenated 4-furyl or thienyl tricyclic derivatives (Series **I-III**)

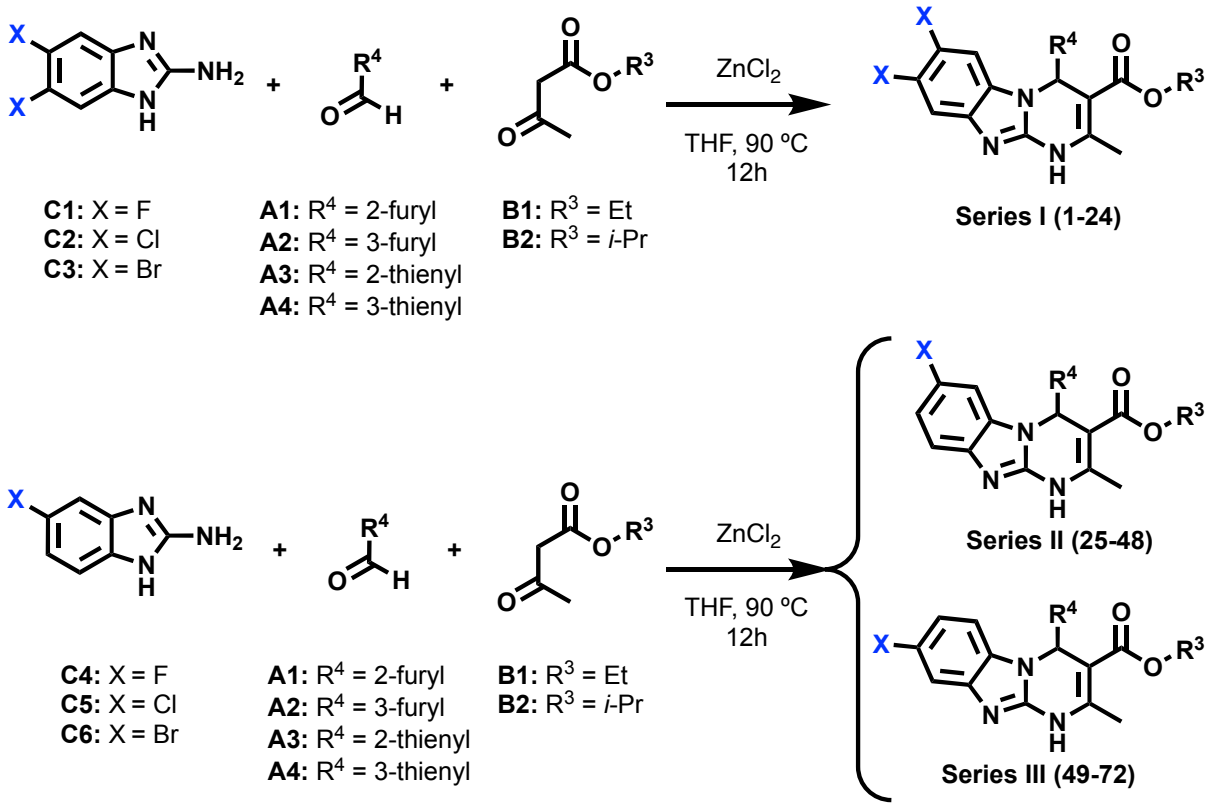

A mixture of halogenated 2-aminobenzoimidazole derivative (**C1-6**, 1.5 equiv.), pentagonal carbaldehyde (**A1-4**, 1 equiv.), alkyl acetoacetate (**B1-2**, 1 equiv.) and $ZnCl_2$ (0.1 equiv.) in THF was stirred with orbital stirring at 90 ºC for 12 hours. After completion of the reaction, as indicated by TLC (revealing green with *p*-anisaldehyde), the solvent was removed in vacuum and the obtained oily residue was purified with flash chromatography at using Hex:AcOEt mixtures as mobile phase.

METHOD B. General procedure for the synthesis of monohalogenated 4-oxazolyl tricyclic derivatives (Series **IV**)

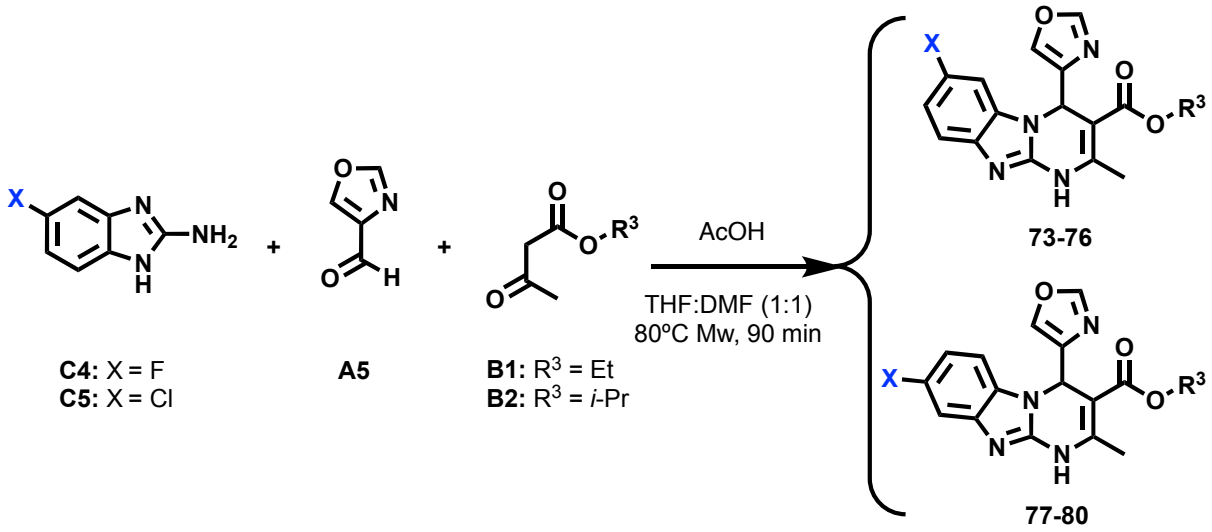

A mixture of halogenated 2-aminobenzoimidazole derivative (**C4-5**, 1.5 equiv.), oxazole-4-carbaldehyde (**A5**, 1 equiv.), alkyl acetoacetate (**B1-2**, 1 equiv.) and AcOH (0.1 equiv.) in THF:DMF (1:1) was stirred under microwave (Mw) radiation at 80 ºC for 90 minutes. After completion of the reaction, as indicated by TLC (revealing green with *p*-anisaldehyde), the solvent was removed in vacuum and the obtained oily residue was purified with flash chromatography at using Hex:AcOEt mixtures as mobile phase.

5.2.2 Spectroscopic and analytical data for all compounds described

(±) Ethyl 7,8-difluoro-4-(furan-2-yl)-2-methyl-1,4-dihydrobenzo[4,5]imidazo[1,2-*a*]pyrimidine-3-carboxylate (1). Purified by column chromatography (Hex–AcOEt 3:1 – 1:2). Yield: 31%. Mp: 268 – 269 ºC. ^{1}H NMR (300 MHz, DMSO-d_6), δ (ppm): 10.80 (brs, 1H, NH), 7.62 – 7.50 (m, 1H, Ar-H), 7.47 – 7.30 (m, 2H, Ar-H), 6.57 (s, 1H, CH), 6.47 (d, J = 3.1 Hz, 1H, Ar-H), 6.35-6.27 (m, 1H, Ar-H), 4.19 – 3.94 (m, 2H, OCH_2CH$_3$), 2.43 (s, 3H, CH$_3$) 1.15 (t, J = 7.1 Hz, 3H, OCH$_2$CH_3). ^{13}C NMR (75 MHz, DMSO-d_6), δ (ppm): 170.1, 157.3, 152.7 (d, J = 245.1 Hz), 150.3 (d, J = 245.0 Hz), 148.9, 143.1, 132.3, 115.6, 113.3, 109.9, 104.1, 103.8, 99.7, 70.1, 64.6, 54.4, 23.8, 19.3. HRMS (APCI) *m/z* calcd for $C_{18}H_{16}F_2N_3O_3$ $[M+H]^+$: 360.1081; found: 360.1155.

(±) Isopropyl 7,8-difluoro-4-(furan-2-yl)-2-methyl-1,4-dihydrobenzo[4,5]imidazo[1,2-*a*]pyrimidine-3-carboxylate (2). Purified by column chromatography (Hex–AcOEt 3:1 – 1:2). Yield: 38% Mp: 261 – 262 ºC. ^{1}H NMR (300 MHz, DMSO-d_6), δ (ppm): 10.90 (brs, 1H, NH), 7.61-7.55 (m, 1H, Ar-H), 7.44-7.37 (m, 2H, Ar-H), 6.54-6.51 (m, 2H, Ar-H), 6.32 (s, 1H, CH), 4.90-4.82 (m, 1H, OCH(CH$_3$)$_2$), 2.42 (s, 3H, CH$_3$), 1.21 (d, J = 6.5 Hz, 3H, OCH(CH_3)$_2$), 1,04 (d, J = 6.4 Hz, 3H, OCH(CH_3)$_2$). ^{13}C NMR (75 MHz, CDCl$_3$), δ (ppm): 165.0, 152.9 (d, J = 245.0), 147.5 (d, J = 245.0), 146.6, 142.3, 136.3, 127.1, 110.5, 108.0, 104.3, 104.1, 98.7, 98.4, 96.0, 67.6, 50.2, 22.1, 21.7, 19.2. HRMS (APCI) *m/z*: calcd for $C_{19}H_{18}F_2N_3O_3$ $[M+H]^+$: 374.1238; found: 374.1273.

(±) Ethyl 7,8-difluoro-4-(furan-3-yl)-2-methyl-1,4-dihydrobenzo[4,5]imidazo[1,2-*a*]pyrimidine-3-carboxylate (3). Purified by column chromatography (Hex–AcOEt 3:1 – 1:2). Yield: 27%. Mp: 275 – 277 ºC. ^{1}H NMR (300 MHz, DMSO-d_6), δ (ppm): 11.53 (brs, 1H, NH), 7.74 (s, 1H, Ar-H), 7.65 – 7.46 (m, 1H, Ar-H), 7.45 (s, 1H, Ar-H), 7.44 – 7.35 (m, 1H, Ar-H), 6.45 (s, 1H, CH), 6.19 (s, 1H, Ar-H), 4.14 – 3.98 (m, 2H), 2.40 (s, 3H, CH$_3$), 1.16 (t, J = 7.2, 3H, OCH$_2$CH_3). ^{13}C NMR (75 MHz, CDCl$_3$), δ (ppm): 165.6, 148.0, 146.3, 145.7, 143.7, 139.6, 136.5, 125.2, 108.6, 104.6, 104.3, 98.5, 98.4, 98.1, 60.4, 48.6, 19.4, 14.4. HRMS (APCI) *m/z* calcd for $C_{18}H_{16}F_2N_3O_3$ $[M+H]^+$: 360.1081; found: 360.1156.

(±) Isopropyl 7,8-difluoro-4-(furan-3-yl)-2-methyl-1,4-dihydrobenzo[4,5]imidazo[1,2-*a*]pyrimidine-3-carboxylate (4). Purified by column chromatography (Hex–AcOEt 3:1 – 1:2). Yield: 31%. Mp: 237 – 238 ºC. ^{1}H NMR (300 MHz, DMSO-d_6), δ (ppm): 10.75 (brs, 1H, NH), 7.76 (s, 1H, Ar-H), 7.66 – 7.59 (m, 1H, Ar-H), 7.45 (s, 1H, Ar-H), 7.40 – 7.33 (m, 1H, Ar-H), 6.43 (s, 1H, Ar-H), 6.21 (s, 1H, CH), 4.88 (m, 1H, OC*H*$(CH_3)_2$), 2.40 (s, 3H, CH_3), 1.22 (d, J = 6.1 Hz, 3H, OCH(CH_3)$_2$), 1,08 (d, J = 6.0 Hz, 3H, OCH(CH_3)$_2$). ^{13}C NMR (75 MHz, $CDCl_3$), δ (ppm): 165.2, 148.1, 146.3, 145.5, 143.7, 139.7, 136.6, 126.8, 125.2, 108.7, 104.6, 104.3, 98.7, 98.1, 67.9, 48.7, 22.2, 21.9, 19.4. LRMS (CI) *m/z* calcd for $C_{19}H_{18}F_2N_3O_3$ $[M+H]^+$: 374.4; found: 374.1.

(±) Ethyl 7,8-difluoro-2-methyl-4-(thiophen-2-yl)-1,4-dihydrobenzo[4,5]imidazo[1,2-*a*]pyrimidine-3-carboxylate (5). Purified by column chromatography (Hex–AcOEt 3:1 – 1:2). Yield: 29%. Mp: 272 – 273 ºC. ^{1}H NMR (300 MHz, DMSO-d_6), δ (ppm): 10.94 (brs, 1H, NH), 7.71 – 7.63 (m, 1H, Ar-H), 7.41 – 7.30 (m, 2H, Ar-H), 7.16 – 7.14 (m, 1H, Ar-H), 6.88 – 6.85 (m, 1H, Ar-H), 6.82 (s, 1H, CH), 4.12 – 4.00 (m, 2H, OCH_2CH$_3$), 2.42 (s, 3H, CH_3), 1.15 (t, J = 7.0, 3H, OCH$_2$CH_3). LRMS (CI) *m/z* calcd for $C_{18}H_{16}F_2N_3O_2S$ $[M+H]^+$: 376.4; found: 376.1.

(±) Isopropyl 7,8-difluoro-2-methyl-4-(thiophen-2-yl)-1,4-dihydrobenzo[4,5]imidazo [1,2-*a*]pyrimidine-3-carboxylate (6). Purified by column chromatography (Hex–AcOEt 3:1 – 1:2). Yield: 34%. Mp: 263 – 264 ºC. ^{1}H NMR (300 MHz, DMSO-d_6), δ (ppm): 10.9 (brs, 1H, NH), 7.76 – 7.72 (m, 1H, Ar-H), 7.41 – 7.35 (m, 1H, Ar-H), 7.32 (d, J = 5.5 Hz, 1H, Ar-H), 7.19 (d, J = 3.5 Hz, 1H, Ar-H), 6.92 – 6.77 (m, 1H, Ar-H), 6.79 (s, 1H, CH), 4.88 (m, 1H, OC*H*$(CH_3)_2$), 2.42 (s, 3H, CH_3), 1.22 (d, J = 6.3 Hz, 3H, OCH(CH_3)$_2$), 1.05 (d, J = 6.3 Hz, 3H, OCH(CH_3)$_2$). LRMS (CI) *m/z* calcd for $C_{19}H_{18}F_2N_3O_2S$ $[M+H]^+$: 390.4; found: 390.2.

(±) Ethyl 7,8-difluoro-2-methyl-4-(thiophen-3-yl)-1,4-dihydrobenzo[4,5]imidazo[1,2-*a*]pyrimidine-3-carboxylate (7). Purified by column chromatography (Hex–AcOEt 3:1 – 1:2). Yield: 29%. Mp: 278 – 280 ºC. ^{1}H NMR (300 MHz, DMSO-d_6), δ (ppm): 10.83 (brs, 1H, NH), 7.61 – 7.53 (m, 2H, Ar-H), 7.40 – 7.33 (m, 2H, Ar-H), 6.90 – 6.88 (m, 1H, Ar-H), 6.55 (s, 1H, CH), 4.10 – 3.98 (m, 2H, OCH_2CH$_3$), 2.48 (s, 3H, CH_3), 1.14 (t, J = 7.2, 3H, OCH$_2$CH_3). LRMS (CI) *m/z* calcd for $C_{18}H_{16}F_2N_3O_2S$ $[M+H]^+$: 376.4; found: 376.1.

(±) Isopropyl 7,8-difluoro-2-methyl-4-(thiophen-3-yl)-1,4-dihydrobenzo[4,5]imidazo-[1,2-*a*]pyrimidine-3-carboxylate (8). Purified by column chromatography (Hex–AcOEt 3:1 – 1:1). Yield: 28 %. Mp: 264 – 265 ºC. ^{1}H NMR (300 MHz, DMSO-d_6), δ (ppm): 10.82 (brs, 1H, NH), 7.63 – 7.57 (m, 2H, Ar-H), 7.40 – 7.33 (m, 2H, Ar-H), 6.91 – 6.89 (m, 1H, Ar-H), 6.52 (s, 1H, CH), 4.85 – 4.78 (m, 1H, OC*H*$(CH_3)_2$), 2.41 (s, 3H, CH_3), 1.21 (d, J = 6.1 Hz, 3H, OCH(C*H*$_3)_2$), 1.01 (d, J = 6.4 Hz, 3H, OCH(C*H*$_3)_2$). LRMS (CI) *m/z* calcd for $C_{19}H_{18}F_2N_3O_2S$ $[M+H]^+$: 390.4; found: 390.1.

(±) Ethyl 7,8-dichloro-4-(furan-2-yl)-2-methyl-1,4-dihydrobenzo[4,5]imidazo[1,2-*a*]pyrimidine-3-carboxylate (9). Purified by column chromatography (Hex–AcOEt 3:1 – 1:1). Yield: 48%. Mp: 285 – 286 ºC. ^{1}H NMR (300 MHz, DMSO-d_6), δ (ppm): 10.98 (s, 1H, NH), 7.76 (s, 1H, Ar-H), 7.58 (s, 1H, Ar-H), 7.49 – 7.42 (m, 1H, Ar-H), 6.64 (s, 1H, CH), 6.51 (d, J = 3.2 Hz, 1H, Ar-H), 6.32 (dd, J = 3.3, 1.8 Hz, 1H, Ar-H), 4.17 – 3.93 (m, 2H, OC*H*$_2$CH$_3$), 2.43 (s, 3H, CH_3), 1.15 (t, J = 7.1 Hz, 3H, OCH_2C*H*$_3$). LRMS (CI) *m/z* calcd for $C_{18}H_{16}Cl_2N_3O_3$[M+H]$^+$: 393.2; found: 393.0.

(±) Isopropyl 7,8-dichloro-4-(furan-2-yl)-2-methyl-1,4-dihydrobenzo[4,5]imidazo[1,2-*a*]pyrimidine-3-carboxylate (10). Purified by column chromatography (Hex–AcOEt 3:1 – 1:1). Yield: 39%. Mp: 299 – 300 ºC. ^{1}H NMR (300 MHz, DMSO-d_6), δ (ppm): 10.95 (brs, 1H, NH), 7.76 (s, 1H, Ar-H), 7.58 (s, 1H, Ar-H), 7.46 (s, 1H, Ar-H), 6.61 (s, 1H, Ar-H), 6.53 (s, 1H, CH), 6.34 – 6.32 (m, 1H, Ar-H), 4.92 – 4.83 (m, 1H, OC*H*$(CH_3)_2$), 2.43 (s, 3H, CH_3), 1.22 (d, J = 6.1 Hz, 3H, OCH(C*H*$_3)_2$), 1.05 (d, J = 6.4 Hz, 3H, OCH(C*H*$_3)_2$). ^{13}C NMR (75 MHz, DMSO-d_6), δ (ppm): 164.8, 152.5, 148.0, 147.5, 143.3, 142.7, 131.8, 124.9, 122.6, 118.2, 111.8, 110.9, 108.8, 95.7, 67.2, 49.8, 22.2, 21.9, 18.9. LRMS (CI) *m/z* calcd for $C_{19}H_{18}Cl_2N_3O_3$ $[M+H]^+$: 407.3; found: 406.1.

(±) Ethyl 7,8-dichloro-4-(furan-3-yl)-2-methyl-1,4-dihydrobenzo[4,5]imidazo[1,2-*a*]pyrimidine-3-carboxylate (11). Purified by column chromatography (Hex–AcOEt 3:1 – 1:1). Yield: 46%. Mp: 267 – 269 ºC. ^{1}H NMR (300 MHz, $CDCl_3$), δ (ppm): 10.89 (brs, 1H, NH), 7.78 (s, 1H, Ar-H), 7.76 (s, 1H, Ar-H), 7.76 (s, 1H, Ar-H), 7.57 (s, 1H, Ar-H), 7.46 (s, 1H, Ar-H), 6.51 (s, 1H, CH), 4.12 – 4.04 (m, 2H, OC*H*$_2$CH$_3$), 2.40 (s, 3H, CH_3), 1.18 (t, J = 7.0 Hz, 3H, OCH_2C*H*$_3$). ^{13}C NMR (75 MHz, DMSO-d_6), δ (ppm): 165.4, 155.5, 148.2, 145.5, 143.8, 139.7, 133.74, 130.8, 126.7, 124.9, 117.6, 110.9, 108.5, 99.1, 60.4, 48.6, 25.3, 14.3. LRMS (CI) *m/z* calcd for $C_{18}H_{16}Cl_2N_3O_3$ $[M+H]^+$: 392.1; found: 392.1.

(±) Isopropyl 7,8-dichloro-4-(furan-3-yl)-2-methyl-1,4-dihydrobenzo[4,5]imidazo[1,2-*a*]pyrimidine-3-carboxylate (12). Purified by column chromatography (Hex–AcOEt 3:1 – 1:1). Yield: 31%. Mp: 253 – 255 ºC. ^{1}H NMR (300 MHz, $CDCl_3$), δ (ppm): 11.18 (brs, 1H, NH), 7.56 (s, 1H, Ar-H), 7.25 – 7.18 (m, 3H, Ar-H), 6.43 (s, 1H, CH), 6.21 (s, 1H, Ar-H), 5.05 – 4.96 (m, 1H, OC*H*$(CH_3)_2$), 2.58 (s, 3H, CH_3), 1.28 (d, J = 6.0 Hz, 3H, OCH(C*H*$_3)_2$), 1,22 (d, J = 5.9 Hz, 3H, OCH(C*H*$_3)_2$). LRMS (CI) *m/z* calcd for $C_{19}H_{18}Cl_2N_3O_3$ $[M+H]^+$: 407.3; found: 407.3.

(±) Ethyl 7,8-dichloro-2-methyl-4-(thiophen-2-yl)-1,4-dihydrobenzo[4,5]imidazo[1,2-*a*]pyrimidine-3-carboxylate (13). Purified by column chromatography (Hex–AcOEt 3:1 – 1:1). Yield: 46%. Mp: 279 – 280 ºC. ^{1}H NMR (300 MHz, $CDCl_3$), δ (ppm): 10.9 (brs, 1H, NH), 7.76 – 7.72 (m, 1H, Ar-H), 7.38 (s, 1H, Ar-H), 7.25 (s, 1H, Ar-H), 6.96 – 6.90 (m, 1H, Ar-H), 6.93 – 6.85 (m, 1H, Ar-H), 6.70 (s, 1H, CH), 4.31 – 4.26 (m, 2H, OC*H*$_2$CH$_3$), 2.67 (s, 3H, CH_3), 1.29 (t, J = 7.1 Hz, 3H, OCH_2C*H*$_3$). LRMS (CI) *m/z* calcd for $C_{18}H_{16}Cl_2N_3O_2S$ $[M+H]^+$: 409.3; found: 409.3.

(±) Isopropyl 7,8-dichloro-2-methyl-4-(thiophen-2-yl)-1,4-dihydrobenzo[4,5]imidazo[1,2-*a*]pyrimidine-3-carboxylate (14). Purified by column chromatography (Hex–AcOEt 3:1 – 1:1). Yield: 28%. Mp: 281 – 283 ºC. ^{1}H NMR (300 MHz, $CDCl_3$), δ (ppm): 11.22 (brs, 1H, NH), 7.38 (s, 1H, Ar-H), 7.29 – 7.06 (m, 2H, Ar-H), 6.98 – 6.91 (m, 1H, Ar-H), 6.45 (s, 1H, CH), 5.12 – 4.98 (m, 1H, OC*H*$(CH_3)_2$), 2.65 (s, 3H, CH_3), 1.28 (d, J = 6.0 Hz, 3H, OCH(C*H*$_3)_2$), 1,21 (d, J = 5.9 Hz, 3H, OCH(C*H*$_3)_2$). LRMS (CI) *m/z* calcd for $C_{19}H_{18}Cl_2N_3O_2S$ $[M+H]^+$: 422.0; found: 422.0.

(±) Ethyl 7,8-dichloro-2-methyl-4-(thiophen-3-yl)-1,4-dihydrobenzo[4,5]imidazo[1,2-*a*]pyrimidine-3-carboxylate (15). Purified by column chromatography (Hex–AcOEt 3:1 – 1:1). Yield: 36%. Mp: 279 – 281 ºC. ^{1}H NMR (300 MHz, $CDCl_3$), δ (ppm): 11.19 (brs, 1H, NH), 7.38 (s, 1H, Ar-H), 7.29 (s, 1H, Ar-H), 7.21 – 7.16 (m, 1H, Ar-H), 6.95 – 6.92 (m, 1H, Ar-H), 6.92 – 6.84 (m, 1H, Ar-H), 6.70 (s, 1H, CH), 4.31 – 4.26 (m, 2H, OC*H*$_2$CH$_3$), 2.65 (s, 3H, CH_3), 1.25 (t, J = 7.0 Hz, 3H, OCH_2C*H*$_3$). LRMS (CI) *m/z* calcd for $C_{18}H_{16}Cl_2N_3O_2S$ $[M+H]^+$: 409.0; found: 409.0.

(±) Isopropyl 7,8-dichloro-2-methyl-4-(thiophen-3-yl)-1,4-dihydrobenzo[4,5]imidazo-[1,2-*a*]pyrimidine-3-carboxylate (16). Purified by column chromatography (Hex–AcOEt 3:1 – 1:1). Yield: 41%. Mp: 285 – 286 ºC. ^{1}H NMR (300 MHz, $CDCl_3$), δ (ppm): 11.05 (brs, 1H, NH), 7.49 (s, 1H, Ar-H), 7.18 – 7.13 (m, 3H, Ar-H), 6.92 – 6.83 (m, 1H, Ar-H), 6.55 (s, 1H, CH), 5.18 – 5.02 (m, 1H, OC*H*$(CH_3)_2$), 2.62 (s, 3H, CH_3), 1.30 (d, J = 6.0 Hz, 3H, OCH(C*H*$_3)_2$), 1.21 (d, J = 6.1 Hz, 3H, OCH(C*H*$_3)_2$). ^{13}C NMR (75 MHz, $CDCl_3$), δ (ppm): 165.0, 145.0, 141.1, 126.7, 125.9, 124.7, 122.9, 117.6, 110.9, 99.9, 67.9, 52.2, 22.2, 21.8, 19.4. LRMS (CI) *m/z* calcd for $C_{19}H_{18}Cl_2N_3O_2S$ $[M+H]^+$: 422.0; found: 422.0.

(±) Ethyl 7,8-dibromo-4-(furan-2-yl)-2-methyl-1,4-dihydrobenzo[4,5]imidazo[1,2-*a*]pyrimidine-3-carboxylate (17). Purified by column chromatography (Hex–AcOEt 2:1 – 1:2). Yield: 38%. Mp: ≥ 300 ºC dec. ^{1}H NMR (300 MHz, DMSO-d_6), δ (ppm): 10.98 (s, 1H, NH), 7.89 (s, 1H, Ar-H), 7.71 (d, J = 1.2 Hz, 1H, Ar-H), 7.45 (d, J = 1.6 Hz, 1H, Ar-H), 6.65 (s, 1H, CH), 6.50 (d, J = 3.3 Hz, 1H, Ar-H), 6.33 (dt, J = 3.2, 1.5 Hz, 1H, Ar-H), 4.14 – 3.94 (m, 2H, OC*H*$_2$CH$_3$), 2.42 (s, 3H, CH_3), 1.15 (t, J = 7.1, 3H, OCH_2C*H*$_3$). LRMS (CI) *m/z* calcd for $C_{18}H_{16}Br_2N_3O_3$ $[M+H]^+$: 479.9; found: 479.9.

(±) Isopropyl 7,8-dibromo-4-(furan-2-yl)-2-methyl-1,4-dihydrobenzo[4,5]imidazo[1,2-*a*]pyrimidine-3-carboxylate (18). Purified by column chromatography (Hex–AcOEt 2:1 – 1:2). Yield: 50 %. Mp: 273 – 275 ºC. ^{1}H NMR (300 MHz, DMSO-d_6), δ (ppm): 10.95 (s, 1H, NH), 7.89 (s, 1H, Ar-H), 7.71 (s, 1H, Ar-H), 7.50 – 7.42 (m, 1H, Ar-H), 6.62 (s, 1H, CH), 6.50 (t, J = 3.4 Hz, 1H, Ar-H), 6.33 (t, J = 2.5 Hz, 1H, Ar-H), 4.87 (p, J = 6.3 Hz, 1H, OC*H*$(CH_3)_2$), 2.42 (s, 3H, CH_3), 1.22 (d, J = 6.1 Hz, 3H, OCH(C*H*$_3)_2$), 1.05 (d, J = 6.0 Hz, 3H, OCH(C*H*$_3)_2$). ^{13}C NMR (75 MHz, $CDCl_3$), δ (ppm): 164.8, 152.4, 147.6, 146.4, 142.5, 141.4, 132.9, 120.6, 118.0, 115.9, 114.3, 110.5, 108.2, 96.7, 67.8, 50.2, 22.1, 21.8, 19.3. LRMS (CI) *m/z* calcd for $C_{19}H_{18}Br_2N_3O_3$ $[M+H]^+$: 493.9; found: 493.9.

(±) Ethyl 7,8-dibromo-4-(furan-3-yl)-2-methyl-1,4-dihydrobenzo[4,5]imidazo[1,2-*a*]pyrimidine-3-carboxylate (19). Purified by column chromatography (Hex–AcOEt 2:1 – 1:2). Yield: 47 %. Mp: 289 – 290 ºC. ^{1}H NMR (300 MHz, $CDCl_3$), δ (ppm): 11.17 (brs, 1H, NH), 7.68 (s, 1H, Ar-H), 7.42 (s, 1H, Ar-H), 7.37 (s, 1H, Ar-H), 7.28 – 7.22 (m, 1H, Ar-H), 6.38 (s, 1H, CH), 6.08 (s, 1H, Ar-H), 4.24 – 4.16 (m, 2H, OC*H*$_2$CH$_3$), 2.69 (s, 3H, CH_3), 1.28 – 1.18 (m, 3H, OCH_2C*H*$_3$). HRMS (APCI) *m/z* calcd for $C_{18}H_{16}Br_2N_3O_3$ $[M+H]^+$: 479.9553; found: 479.9552.

(±) Isopropyl 7,8-dibromo-4-(furan-3-yl)-2-methyl-1,4-dihydrobenzo[4,5]imidazo[1,2-*a*]pyrimidine-3-carboxylate (20). Purified by column chromatography (Hex–AcOEt 2:1 – 1:2). Yield: 49 %. Mp: 258 – 260 ºC. ^{1}H NMR (300 MHz, $CDCl_3$), δ (ppm): 11.38 (brs, 1H, NH), 7.69 (s, 1H, Ar-H), 7.44 – 7.39 (m, 1H, Ar-H), 7.33 (s, 1H, Ar-H), 7.31 – 7.26 (m, 1H, Ar-H), 6.41 (s, 1H, CH), 6.18 (s, 1H, Ar-H), 5.18 – 5.05 (m, 1H, OC*H*$(CH_3)_2$), 2.58 (s, 3H, CH_3), 1.37 (d, J = 6.1 Hz, 3H, OCH(C*H*$_3)_2$), 1.25 (d, J = 6.1 Hz, 3H, OCH(C*H*$_3)_2$). LRMS (CI) *m/z* calcd for $C_{19}H_{18}Br_2N_3O_3$ $[M+H]^+$: 494.0; found: 493.9.

(±) Ethyl 7,8-dibromo-2-methyl-4-(thiophen-2-yl)-1,4-dihydrobenzo[4,5]imidazo[1,2-*a*]pyrimidine-3-carboxylate (21). Purified by column chromatography (Hex–AcOEt 2:1 – 1:2). Yield: 48%. Mp: ≥ 300 ºC dec. ^{1}H NMR (300 MHz, $CDCl_3$), δ (ppm): 10.56 (brs, 1H, NH), 7.68 (s, 1H, Ar-H), 7.56 (s, 1H, Ar-H), 7.20 – 7.15 (m, 1H, Ar-H), 6.92 – 6.75 (m, 1H, Ar-H), 6.88 – 6.80 (m, 1H, Ar-H), 6.67 (s, 1H, CH), 4.24 – 4.00 (m, 2H, OC*H*$_2$$CH_3$), 2.64 (s, 3H, CH_3), 1.18 – 1.09 (m, 3H, OCH_2C*H*$_3$). LRMS (CI) *m/z* calcd for $C_{18}H_{16}Br_2N_3O_2S$ $[M+H]^+$: 495.9; found: 496.0.

(±) Isopropyl 7,8-dibromo-2-methyl-4-(thiophen-2-yl)-1,4-dihydrobenzo[4,5]imidazo-[1,2-*a*]pyrimidine-3-carboxylate (22). Purified by column chromatography (Hex–AcOEt 2:1 – 1:2). Yield: 41%. Mp: 280 – 282 ºC. ^{1}H NMR (300 MHz, $CDCl_3$), δ (ppm): 10.89 (brs, 1H, NH), 7.69 (s, 1H, Ar-H), 7.56 (s, 1H, Ar-H), 7.19 – 7.17 (m, 1H, Ar-H), 6,96 (s, 1H, Ar-H), 6.89 – 6.86 (m, 1H, Ar-H), 6.68 (s, 1H, CH), 5.14 – 5.05 (m, 1H, OC*H*$(CH_3)_2$), 2.65 (s, 3H, CH_3), 1.31 (d, J = 6.1 Hz, 3H, OCH(C*H*$_3)_2$), 1.20 (d, J = 6.2 Hz, 3H, OCH(C*H*$_3)_2$). LRMS (CI) *m/z* calcd for $C_{19}H_{18}Br_2N_3O_2S$ $[M+H]^+$: 509.9; found: 509.9.

(±) Ethyl 7,8-dibromo-2-methyl-4-(thiophen-3-yl)-1,4-dihydrobenzo[4,5]imidazo[1,2-*a*]pyrimidine-3-carboxylate (23). Purified by column chromatography (Hex–AcOEt 2:1 – 1:2). Yield: 34%. Mp: 288 – 290 ºC. ^{1}H NMR (300 MHz, DMSO-d_6), δ (ppm): 10.92 (brs, 1H, NH), 7.86 (s, 1H, Ar-H), 7.70 (s, 1H, Ar-H), 7.53 (dd, J = 3.0, 1.4 Hz, 1H, Ar-H), 7.37 (dd, J = 5.0, 3.0 Hz, 1H, Ar-H), 6.88 (d, J = 5.0 Hz, 1H, Ar-H), 6.62 (s, 1H, CH), 4.18 – 3.90 (m, 2H, OC*H*$_2$$CH_3$), 2.41 (s, 3H, CH_3), 1.16 (t, J = 7.0 Hz, 3H, OCH_2C*H*$_3$). LRMS (CI) *m/z* calcd for $C_{18}H_{16}Br_2N_3O_2S$ $[M+H]^+$: 495.9; found: 495.9.

(±) Isopropyl 7,8-dibromo-2-methyl-4-(thiophen-3-yl)-1,4-dihydrobenzo[4,5]imidazo-[1,2-*a*]pyrimidine-3-carboxylate (24). Purified by column chromatography (Hex–AcOEt 2:1 – 1:2). Yield: 51%. Mp: ≥300 dec. ^{1}H NMR (300 MHz, DMSO-d_6), δ (ppm): 10.65 (brs, 1H, NH), 7.78 (s, 1H, Ar-H), 7.40 (s, 1H, Ar-H), 7.32 – 7.15 (m, 2H, Ar-H), 6.92 – 6.85 (m, 1H, Ar-H), 6.49 (s, 1H, CH), 5.18 – 5.06 (m, 1H, OC*H*$(CH_3)_2$), 2.58 (s, 3H, CH_3), 1.32 (d, J = 6.0 Hz, 3H, OCH(CH_3)$_2$), 1.21 (d, J = 6.4 Hz, 3H, OCH(CH_3)$_2$). LRMS (CI) *m/z* calcd for $C_{19}H_{18}Br_2N_3O_2S$ $[M+H]^+$: 509.9; found: 509.9.

(±) Ethyl 7-fluoro-4-(furan-2-yl)-2-methyl-1,4-dihydrobenzo[4,5]imidazo[1,2-*a*]pyrimidine-3-carboxylate (25). Purified by column chromatography (Hex–AcOEt 3:1 – 1:2). Yield: 19%. Mp: 273 – 274 ºC. ^{1}H NMR (300 MHz, $CDCl_3$), δ (ppm): 7.45 – 7.35 (m, 1H, Ar-H), 7.32 – 7.28 (s, 2H, Ar-H), 7.27 – 7.10 (m, 1H, Ar-H), 6.51 (s, 1H, CH), 6.32 – 6.23 (m, 2H, Ar-H), 4.29 – 4.08 (m, 2H, OCH_2CH$_3$), 2.72 (s, 3H, CH_3), 1.28 (t, J = 7.1 Hz, 3H, OCH$_2$CH_3). LRMS (CI) *m/z* calcd for $C_{18}H_{17}FN_3O_3$ $[M+H]^+$: 342.1, found, 342.1.

(±) Isopropyl 7-fluoro-4-(furan-2-yl)-2-methyl-1,4-dihydrobenzo[4,5]imidazo[1,2-*a*]pyrimidine-3-carboxylate (26). Purified by column chromatography (Hex–AcOEt 3:1 – 1:2). Yield: 19%. Mp: 236 – 237 ºC. ^{1}H NMR (300 MHz, DMSO-d_6), δ (ppm): 10.84 (brs, 1H, NH), 7.43 – 7.38 (m, 2H, Ar-H), 7.16 – 7.12 (m, 1H, Ar-H), 6.89 – 6.82 (m, 1H, Ar-H), 6.54 (s, 1H, Ar-H), 6.49 (s, 1H, CH), 6.45 (s, 1H, Ar-H), 4.91 – 4.83 (m, 1H, OC*H*$(CH_3)_2$), 2.44 (s, 3H, CH_3), 1.21 (d, J = 6.1 Hz, 3H, OCH(CH_3)$_2$), 1.04 (d, J = 6.1 Hz, 3H, OCH(CH_3)$_2$). ^{13}C NMR (75 MHz, $CDCl_3$), δ (ppm): 165.2, 158.2, 153.2, 147.6, 146.8, 142.2, 141.8, 128.1, 110.0, 108.7, 107.8, 103.1, 102.7, 96.0, 67.5, 50.1, 22.1, 21.8, 19.3. HRMS (APCI) *m/z* calcd for $C_{19}H_{19}FN_3O_3$ $[M+H]^+$: 356.1332; found: 356.1369.

(±) Ethyl 7-fluoro-4-(furan-3-yl)-2-methyl-1,4-dihydrobenzo[4,5]imidazo[1,2-a]pyrimidine-3-carboxylate (27). Purified by column chromatography (Hex–AcOEt 3:1 – 1:2). Yield: 19%. Mp: 260 – 262 ºC. ^{1}H NMR (300 MHz, $CDCl_3$), δ (ppm): 7.45 – 7.17 (m, 3H, Ar-H), 6.91 – 6.80 (m, 1H, Ar-H), 6.51 (s, 1H, CH), 6.26 – 6.18 (m, 2H, Ar-H), 4.25 – 4.10 (m, 2H, OCH_2CH$_3$), 2.67 (s, 3H, CH_3), 1.32 (t, J = 7.1 Hz, 3H, OCH$_2$CH_3). LRMS (CI) *m/z* calcd for $C_{18}H_{17}FN_3O_3$ $[M+H]^+$: 342.1, found, 342.1.

(±) Isopropyl 7-fluoro-4-(furan-3-yl)-2-methyl-1,4-dihydrobenzo[4,5]imidazo[1,2-*a*]pyrimidine-3-carboxylate (28). Purified by column chromatography (Hex–AcOEt 3:1 – 1:2). Yield: 15%. Mp: 239 – 241 ºC. ^{1}H NMR (300 MHz, $CDCl_3$), δ (ppm): 7.41 – 7.35 (m, 1H, Ar-H), 7.25 – 7.05 (m, 2H, Ar-H), 6.98 – 6.68 (m, 2H, Ar-H), 6.48 (s, 1H, CH), 6.25 – 6.19 (m, 1H, Ar-H), 5.10 – 4.99 (m, 1H, OC*H*$(CH_3)_2$), 2.73 (s, 3H, CH_3), 1.32 (d, J = 6.1 Hz, 3H, OCH(C*H*$_3)_2$), 1.16 (d, J = 6.2 Hz, 3H, OCH(C*H*$_3)_2$). ^{13}C NMR (75 MHz, $CDCl_3$), δ (ppm): 165.1, 160.0, 156.9, 153.0, 146.9, 142.3, 137.1, 116.6, 116.5, 107.8, 97.6, 97.2, 95.7, 67.5, 50.1, 22.1, 21.8, 19.3. HRMS (APCI) *m/z*: calcd for $C_{19}H_{19}FN_3O_3$ $[M+H]^+$, 356.1332; found: 256.1362.

(±) Ethyl 7-fluoro-2-methyl-4-(thiophen-2-yl)-1,4-dihydrobenzo[4,5]imidazo[1,2-*a*]pyrimidine-3-carboxylate (29). Purified by column chromatography (Hex–AcOEt 3:1 – 1:2). Yield: 16%. Mp: 257 – 258 ºC. ^{1}H NMR (300 MHz, $CDCl_3$), δ (ppm): 7.41 – 7.36 (m, 1H, Ar-H), 7.18 – 7.12 (m, 1H, Ar-H), 7.02 – 6.84 (m, 4H, Ar-H), 6.72 (s, 1H, CH), 4.25 – 4.12 (m, 2H, OC*H*$_2$CH$_3$), 2.70 (s, 3H, CH_3), 1.28 (t, J = 6.9 Hz, 3H, OCH_2C*H*$_3$). LRMS (CI) *m/*z calcd for $C_{18}H_{17}FN_3O_2S$ $[M+H]^+$: 358.1; found: 358.1.

(±) Isopropyl 7-fluoro-2-methyl-4-(thiophen-2-yl)-1,4-dihydrobenzo[4,5]imidazo[1,2-*a*]pyrimidine-3-carboxylate (30). Purified by column chromatography (Hex–AcOEt 3:1 – 1:2). Yield: 13%. Mp: 257 – 258 ºC. ^{1}H NMR (300 MHz, $CDCl_3$), δ (ppm): 7.45 – 7.35 (m, 1H, Ar-H), 7.25 (d, J = 6.9 Hz, 1H, Ar-H), 7.14 – 7.09 (m, 1H, Ar-H), 7.02 – 6.95 (m, 3H, Ar-H), 6.68 (s, 1H, CH), 5.12 – 5.09 (m, 1H, OC*H*$(CH_3)_2$), 2.69 (s, 3H, CH_3), 1.33 (d, J = 6.2 Hz, 3H, OCH(C*H*$_3)_2$), 1.21 (d, J = 6.2 Hz, 3H, OCH(C*H*$_3)_2$). LRMS (CI) *m/z* calcd for $C_{19}H_{19}FN_3O_2S$ $[M+H]^+$: 372.1; found: 372.1.

(±) Ethyl 7-fluoro-2-methyl-4-(thiophen-3-yl)-1,4-dihydrobenzo[4,5]imidazo[1,2-*a*]pyrimidine-3-carboxylate (31). Purified by column chromatography (Hex–AcOEt 3:1 – 1:2). Yield: 17%. Mp: 271 – 273 ºC. ^{1}H NMR (300 MHz, $CDCl_3$), δ (ppm): 7.42 – 7.36 (m, 1H, Ar-H), 7.36 (s, 2H, Ar-H) 7.28 – 7.15 (m, 1H, Ar-H), 6.99 – 6.88 (m, 2H, Ar-H), 6.55 (s, 1H, CH), 4.26-4.05 (m, 2H, OC*H*$_2$CH$_3$), 2.45 (s, 3H, CH_3), 1.25 (t, J = 7.2 Hz, 3H, OCH_2C*H*$_3$). LRMS (CI) *m/*z calcd for $C_{18}H_{17}FN_3O_2S$ $[M+H]^+$: 358.1; found: 358.1.

(±) Isopropyl 7-fluoro-2-methyl-4-(thiophen-3-yl)-1,4-dihydrobenzo[4,5]imidazo[1,2-*a*]pyrimidine-3-carboxylate (32). Purified by column chromatography (Hex–AcOEt 3:1 – 1:2). Yield: 14%. Mp: 251 – 253 ºC. ^{1}H NMR (300 MHz, $CDCl_3$), δ (ppm): 11.85 (brs, 1H, NH), 7.39 – 7.05 (m, 4H, Ar-H), 6.85 – 6.72 (m, 2H, Ar-H), 6.59 – 6.49 (m, 1H, CH), 5.18 – 4.95 (m, 1H, OC*H*$(CH_3)_2$), 2.67 (s, 3H, CH_3), 1.30 (d, J = 5.8 Hz, 3H, OCH(C*H*$_3)_2$), 1.20 (d, J = 6.0 Hz, 3H, OCH(C*H*$_3)_2$). LRMS (CI) *m/z* calcd for $C_{19}H_{19}FN_3O_2S$ $[M+H]^+$: 372.1; found: 372.1.

(±) Ethyl 7-chloro-4-(furan-2-yl)-2-methyl-1,4-dihydrobenzo[4,5]imidazo[1,2-*a*]pyrimidine-3-carboxylate (33). Purified by column chromatography (Hex–AcOEt 3:1 – 1:1). Yield: 21%. Mp: 256 – 257 ºC. ^{1}H NMR (300 MHz, DMSO-d_6), δ (ppm): 7.41 – 7.36 (m, 1H, Ar-H), 7.29 – 7.26 (m, 2H, Ar-H), 7.19 – 7.11 (m, 1H, Ar-H), 6.53 – 6.47 (m, 1H, CH), 6.25 – 6.18 (m, 2H, Ar-H), 4.22 – 4.05 (m, 2H, OC*H*$_2$CH$_3$), 2.68 (s, 3H, CH_3), 1.22 (t, J = 7.0 Hz, 3H, OCH_2C*H*$_3$). ^{13}C NMR (75 MHz, DMSO-d_6), δ (ppm): 165.4, 152.8, 147.9, 147.3, 143.8, 143.2, 130.9, 126.8, 120.5, 116.8, 111.4, 110.9, 95.2, 59.9, 49.7, 40.6, 19.0, 14.6. LRMS (EI) m/z calcd for $C_{18}H_{16}ClN_3O_3$ $[M]^+$: 357.1; found: 357.1.

(±) Isopropyl 7-chloro-4-(furan-2-yl)-2-methyl-1,4-dihydrobenzo[4,5]imidazo[1,2-*a*]-pyrimidine-3-carboxylate (34). Purified by column chromatography (Hex–AcOEt 3:1 – 1:1). Yield: 21%. Mp: 232 – 234 ºC. ^{1}H NMR (300 MHz, $CDCl_3$), δ (ppm): 7.38 (s, 2H, Ar-H), 7.28 – 7.06 (m, 2H, Ar-H), 6.42 (s, 1H, CH), 6.13 (s, 2H, Ar-H), 5.09 – 4.98 (m, 1H, OC*H*$(CH_3)_2$), 2.65 (s, 3H, CH_3), 1.37 (d, J = 6.2 Hz, 3H, OCH(C*H*$_3)_2$), 1.26 (d, J = 6.2 Hz, 3H, OCH(C*H*$_3)_2$). ^{13}C NMR (75 MHz, $CDCl_3$), δ (ppm): 165.1, 153.0, 147.3, 146.8, 142.3, 141.8, 130.3, 128.3, 121.4, 116.2, 110.5, 110.4, 107.9, 96.3, 67.6, 50.1, 22.1, 21.8, 19.4. LRMS (EI) *m/z* calcd for $C_{19}H_{18}ClN_3O_3$ $[M]^+$: 371.1; found: 371.1.

(±) Ethyl 7-chloro-4-(furan-3-yl)-2-methyl-1,4-dihydrobenzo[4,5]imidazo[1,2-*a*]pyrimidine-3-carboxylate (35). Purified by column chromatography (Hex–AcOEt 3:1 – 1:1). Yield: 19%. Mp: 236 – 237 ºC. ^{1}H NMR (300 MHz, DMSO-d_6), δ (ppm): 10.80 (s, 1H, NH), 7.70 (s, 1H, Ar-H), 7.48 – 7.34 (m, 2H, Ar-H), 7.01 (dd, J = 8.5, 2.0 Hz, 1H, Ar-H), 6.47 (s, 1H, CH), 6.22 – 6.14 (m, 1H, Ar-H), 4.19 – 3.96 (m, 2H, OC*H*$_2$CH$_3$), 2.41 (s, 3H, CH_3), 1.17 (t, J = 7.1 Hz, 3H, OCH_2C*H*$_3$).^{13}C NMR (75 MHz, $CDCl_3$), δ (ppm): 165.7, 147.9, 146.1, 143.5, 142.2, 139.6, 130.1, 128.3, 125.4, 121.3, 116.4, 110.2, 108.7, 98.6, 60.3, 48.5, 19.5, 14.4. LRMS (EI) m/z calcd for $C_{18}H_{16}ClN_3O_3$ $[M]^+$: 357.1; found: 357.1.

(±) Isopropyl 7-chloro-4-(furan-3-yl)-2-methyl-1,4-dihydrobenzo[4,5]imidazo[1,2-*a*]pyrimidine-3-carboxylate (36). Purified by column chromatography (Hex–AcOEt 3:1 – 1:1). Yield: 17%. Mp: 241 – 243 ºC. ^{1}H NMR (300 MHz, $CDCl_3$), δ (ppm): 7.38 – 7.29 (m, 2H, Ar-H), 7.28 – 7.06 (m, 3H, Ar-H), 6.42 (s, 1H, CH), 6.15 – 6.09 (m, 1H, Ar-H), 5.14 – 4.99 (m, 1H, OC*H*$(CH_3)_2$), 2.65 (s, 3H, CH_3), 1.37 (d, *J* = 6.2 Hz, 3H, OCH(C*H*$_3)_2$), 1.26 (d, *J* = 6.2 Hz, 3H, OCH(C*H*$_3)_2$). ^{13}C NMR (75 MHz, $CDCl_3$), δ (ppm): 165.1, 147.6, 146.0, 143.6, 139.8, 139.7, 132.1, 126.6, 125.3, 123.1, 117.0, 109.7, 108.7, 98.8, 67.8, 48.4, 22.2, 21.9, 19.3. HRMS (APCI) *m/z* calcd. for $C_{19}H_{19}ClN_3O_3$ $[M+H]^+$: 372.1109; found: 372.1111.

(±) Ethyl 7-chloro-2-methyl-4-(thiophen-2-yl)-1,4-dihydrobenzo[4,5]imidazo[1,2-*a*]pyrimidine-3-carboxylate (37). Purified by column chromatography (Hex–AcOEt 3:1 – 1:1). Yield: 22%. Mp: 259 – 260 ºC. ^{1}H NMR (300 MHz, $CDCl_3$), *δ* (ppm): 7.44 – 7.38 (m, 1H, Ar-H), 7.30 – 7.22 (m, 1H, Ar-H), 7.21 – 7.16 (m, 1H, Ar-H), 6.96 – 6.91 (m, 1H, Ar-H), 6.99 – 6.86 (m, 1H, Ar-H), 6.85 – 6.82 (m, 1H, Ar-H), 6.72 (s, 1H, CH), 4.22 – 4.10 (m, 2H, OC*H*$_2$$CH_3$), 2.68 (s, 3H, CH_3), 1.37 (t, *J* = 7.1 Hz, 3H, OCH_2C*H*$_3$). LRMS (EI) *m/z* calcd for $C_{18}H_{16}ClN_3O_2S$ $[M]^+$: 373.1; found: 372.9.

(±) Isopropyl 7-chloro-2-methyl-4-(thiophen-2-yl)-1,4-dihydrobenzo[4,5]imidazo[1,2-*a*]pyrimidine-3-carboxylate (38). Purified by column chromatography (Hex–AcOEt 3:1 – 1:1). Yield: 17%. Mp: 251 – 252 ºC. ^{1}H NMR (300 MHz, $CDCl_3$), *δ* (ppm): 11.79 (brs, 1H, NH), 7.38 – 7.08 (m, 3H, Ar-H), 6.99 – 6.93 (m, 1H, Ar-H), 6.90 – 6.84 (m, 1H, Ar-H), 6.75 (s, 1H, CH), 5.20 – 5.06 (m, 1H, OC*H*$(CH_3)_2$), 2.69 (s, 3H, CH_3), 1.36 (d, *J* = 6.0 Hz, 3H, OCH(C*H*$_3)_2$), 1.22 (d, *J* = 6.0 Hz, 3H, OCH(C*H*$_3)_2$). LRMS (EI) *m/z* calcd for $C_{19}H_{18}ClN_3O_2S$ $[M]^+$: 387.1; found: 386.9.

(±) Ethyl 7-chloro-2-methyl-4-(thiophen-3-yl)-1,4-dihydrobenzo[4,5]imidazo[1,2-*a*]pyrimidine-3-carboxylate (39). Purified by column chromatography (Hex–AcOEt 3:1 – 1:1). Yield: 15%. Mp: 267 – 268 ºC. ^{1}H NMR (300 MHz, $CDCl_3$), *δ* (ppm): 11,78 (brs, 1H, NH), 7.42 – 7.04 (m, 5H, Ar-H), 6.96 – 6.89 (m, 1H, Ar-H), 6.57 (s, 1H, CH), 4.22 – 4.04 (m, 2H, OC*H*$_2$$CH_3$), 2.68 (s, 3H, CH_3), 1.31 – 1.29 (m, 3H, OCH_2C*H*$_3$). LRMS (CI) *m/z* calcd for $C_{18}H_{17}ClN_3O_2S$ $[M+H]^+$: 374.1; found: 374.1.

(±) Isopropyl 7-chloro-2-methyl-4-(thiophen-3-yl)-1,4-dihydrobenzo[4,5]imidazo[1,2-*a*]pyrimidine-3-carboxylate (40). Purified by column chromatography (Hex–AcOEt 3:1 – 1:1). Yield: 16%. Mp: 279 – 281 ºC. ^{1}H NMR (300 MHz, $CDCl_3$), δ (ppm): 11.68 (brs, 1H, NH), 7.38 – 7.35 (m, 1H, Ar-H), 7.21 – 6.99 (m, 4H, Ar-H), 6.82 (s, 1H, Ar-H), 6.51 (s, 1H, CH), 5.18 – 5.02 (m, 1H, OC*H*$(CH_3)_2$), 2.68 (s, 3H, CH_3), 1.30 (d, J = 6.0 Hz, 3H, OCH(C*H*$_3)_2$), 1.20 (d, J = 6.0 Hz, 3H, OCH(C*H*$_3)_2$). LRMS (CI) *m/z* calcd for $C_{19}H_{19}ClN_3O_2S$ $[M+H]^+$: 388.1; found: 388.1.

(±) Ethyl 7-bromo-4-(furan-2-yl)-2-methyl-1,4-dihydrobenzo[4,5]imidazo[1,2-*a*]pyrimidine-3-carboxylate (41). Purified by column chromatography (Hex–AcOEt 2:1 – 1:2). Yield: 18%. Mp: 262 – 264 ºC. ^{1}H NMR (300 MHz, $CDCl_3$), δ (ppm): 7.45 (s, 1H, Ar-H), 7.30 – 7.25 (m, 3H, Ar-H), 6.54 (s, 1H, CH), 6.29 – 6.25 (m, 2H, Ar-H), 4.29 – 4.06 (m, 2H, OC*H*$_2$CH$_3$), 2.69 (s, 3H, CH_3), 1.29 – 1.12 (m, 3H, OCH_2C*H*$_3$). LRMS (CI) *m/z* calcd for $C_{18}H_{17}BrN_3O_3$ $[M+H]^+$: 402.0; found: 402.0.

(±) Isopropyl 7-bromo-4-(furan-2-yl)-2-methyl-1,4-dihydrobenzo[4,5]imidazo[1,2-*a*]pyrimidine-3-carboxylate (42). Purified by column chromatography (Hex–AcOEt 2:1 – 1:2). Yield: 22%. Mp: 237 – 238 ºC. ^{1}H NMR (300 MHz, $CDCl_3$), δ (ppm): 11.25 (brs, 1H, NH), 7.43 (s, 1H, Ar-H), 7.34 – 7.12 (m, 3H, Ar-H), 6.48 (s, 1H, CH), 6.11 – 6.08 (m, 2H, Ar-H), 5.10 – 4.98 (m, 1H, OC*H*$(CH_3)_2$), 2.70 (s, 3H, CH_3), 1.26 (d, J = 6.0 Hz, 3H, OCH(C*H*$_3)_2$), 1.18 (d, J = 6.1 Hz, 3H, OCH(C*H*$_3)_2$). ^{13}C NMR (75 MHz, $CDCl_3$), δ (ppm): 165.0, 153.0, 147.2, 146.8, 142.2, 130.7, 124.0, 119.1, 115.6, 111.0, 110.4, 107.9, 96.2, 67.6, 50.1, 22.1, 21.8, 19.4. LRMS (EI) *m/z* calcd for $C_{19}H_{18}BrN_3O_3$ $[M]^+$: 415.0; found: 414.9.

(±) Ethyl 7-bromo-4-(furan-3-yl)-2-methyl-1,4-dihydrobenzo[4,5]imidazo[1,2-*a*]pyrimidine-3-carboxylate (43). Purified by column chromatography (Hex–AcOEt 2:1 – 1:2). Yield: 21%. Mp: 261 – 263 ºC. ^{1}H NMR (750 MHz, DMSO-d_6), δ (ppm): 10.8 (s, 1H, NH), 7.76 (dd, J = 1.6, 0.9 Hz, 1H), 7.69 (d, J = 1.9 Hz, 1H, H-6), 7.47 (t, J = 1.8 Hz, 1H), 7.30 (d, J = 8.4 Hz, 1H, H-9), 7.20 (dd, J = 8.4, 1.9 Hz, 1H, H-8), 6.52 (s, 1H, CH), 6.19 (dd, J = 1.9, 0.9 Hz, 1H), 4.08 (m, 2H, OC*H*$_2$CH$_3$), 2.42 (s, 3H, CH_3), 1.21 (t, J = 7.1 Hz, 3H, OCH_2C*H*$_3$). ^{13}C NMR (126 MHz, $CDCl_3$), δ (ppm): 165.7, 147.2, 145.9, 143.8, 139.8, 132.7, 126.1, 125.4, 118.0, 114.0, 112.7, 108.8, 99.0, 60.5, 48.6, 19.7, 14.5. LRMS (CI) *m/z* calcd for $C_{18}H_{17}BrN_3O_3$ $[M+H]^+$: 402.0; found: 402.0.

(±) Isopropyl 7-bromo-4-(furan-3-yl)-2-methyl-1,4-dihydrobenzo[4,5]imidazo[1,2-*a*]pyrimidine-3-carboxylate (44). Purified by column chromatography (Hex–AcOEt 2:1 – 1:2). Yield: 22%. Mp: 235 – 236 ºC. ^{1}H NMR (300 MHz, $CDCl_3$), δ (ppm): 11.36 (brs, 1H, NH), 7.47 – 7.30 (m, 5H, Ar-H), 6.47 (s, 1H, CH), 6.20 (s, 1H, Ar-H), 5.29 – 5.05 (m, 1H, OC*H*$(CH_3)_2$), 2.64 (s, 3H, CH_3), 1.32 (d, J = 6.0 Hz, 3H, OCH(C*H*$_3)_2$), 1.26 (d, J = 6.0 Hz, 3H, OCH(C*H*$_3)_2$). ^{13}C NMR (75 MHz, $CDCl_3$), δ (ppm): 166.5, 147.4, 145.3, 144.1, 141.7, 141.0, 134.5, 128.2, 126.8, 118.9, 118.0, 116.1, 109.7, 101.8, 68.2, 53.5, 22.0, 19.2. LRMS (CI) *m/z* calcd for $C_{19}H_{19}BrN_3O_3$ $[M+H]^+$: 416.0; found: 416.0.

(±) Ethyl 7-bromo-2-methyl-4-(thiophen-2-yl)-1,4-dihydrobenzo[4,5]imidazo[1,2-*a*]pyrimidine-3-carboxylate (45). Purified by column chromatography (Hex–AcOEt 2:1 – 1:2). Yield: 23%. Mp: 256 – 258 ºC. ^{1}H NMR (300 MHz, $CDCl_3$), δ (ppm): 11.68 (brs, 1H, NH), 7.58 (s, 1H, Ar-H), 7.28 – 7.15 (m, 3H, Ar-H), 6.98 – 6.75 (m, 3H, Ar-H + CH), 4.31 – 4.15 (m, 2H, OC*H*$_2$CH$_3$), 2.63 (s, 3H, CH_3), 1.30 (t, J = 7.1 Hz, 3H, OCH_2C*H*$_3$). LRMS (CI) *m/z* calcd for $C_{18}H_{17}BrN_3O_2S$ $[M+H]^+$: 418.0; found: 418.0.

(±) Isopropyl 7-bromo-2-methyl-4-(thiophen-2-yl)-1,4-dihydrobenzo[4,5]imidazo[1,2-*a*]pyrimidine-3-carboxylate (46). Purified by column chromatography (Hex–AcOEt 2:1 – 1:2). Yield: 18%. Mp: 250 – 252 ºC. ^{1}H NMR (300 MHz, $CDCl_3$), δ (ppm): 11.68 (brs, 1H, NH), 7.45 (s, 1H, Ar-H), 7.38 – 7.09 (m, 3H, Ar-H), 6.91 (s, 1H, Ar-H), 6.79 – 6.86 (m, 1H, Ar-H), 6.72 (s, 1H, CH), 5.98 – 5.14 (m, 1H, OC*H*$(CH_3)_2$), 2.84 (s, 3H, CH_3), 1.29 (d, J = 6.0 Hz, 3H, OCH(C*H*$_3)_2$), 1.19 (d, J = 6.0 Hz, 3H, OCH(C*H*$_3)_2$). LRMS (CI) *m/z* calcd for $C_{19}H_{19}BrN_3O_2S$ $[M+H]^+$: 432.0; found: 432.0.

(±) Ethyl 7-bromo-2-methyl-4-(thiophen-3-yl)-1,4-dihydrobenzo[4,5]imidazo[1,2-*a*]pyrimidine-3-carboxylate (47). Purified by column chromatography (Hex–AcOEt 2:1 – 1:2). Yield: 18%. Mp: 268 – 270 ºC. ^{1}H NMR (300 MHz, $CDCl_3$), δ (ppm): 11.53 (brs, 1H, NH), 7.32 – 7.20 (m, 5H, Ar-H), 6.94 (s, 1H, Ar-H), 6.56 (s, 1H, CH), 4.23 – 4.02 (m, 2H, OC*H*$_2$CH$_3$), 2.65 (s, 3H, CH_3), 1.28 (t, J = 7.1 Hz, 3H, OCH_2C*H*$_3$). LRMS (CI) *m/z* calcd for $C_{18}H_{17}BrN_3O_2S$ $[M+H]^+$: 418.0; found: 418.0.

(±) Isopropyl 7-bromo-2-methyl-4-(thiophen-3-yl)-1,4-dihydrobenzo[4,5]imidazo[1,2-*a*]pyrimidine-3-carboxylate (48). Purified by column chromatography (Hex–AcOEt 2:1 – 1:2). Yield: 22%. Mp: 264 – 265 ºC. ^{1}H NMR (750 MHz, MeOD), δ (ppm): 7.44 (d, J = 1.9 Hz, 1H, H-6), 7.42 (dd, J = 2.9, 1.4 Hz, 1H), 7.28 (dd, J = 5.1, 2.9 Hz, 1H), 7.27 (d, J = 8.4 Hz, 1H, H-9), 7.23 (dd, J = 8.4, 1.9 Hz, 1H, H-8), 6.92 (dd, J = 5.1, 1.3 Hz, 1H, Ar-H), 6.57 (s, 1H, CH), 4.99 (hept, J = 6.2 Hz, 1H, OC*H*$(CH_3)_2$), 2.50 (d, J = 0.7 Hz, 3H, CH_3), 1.30 (d, J = 6.2 Hz, 3H, OCH(C*H*$_3)_2$), 1.15 (d, J = 6.2 Hz, 3H, OCH(C*H*$_3)_2$). LRMS (CI) *m/z* calcd for $C_{19}H_{19}BrN_3O_2S$ $[M+H]^+$: 432.0; found: 432.0.

(±) Ethyl 8-fluoro-4-(furan-2-yl)-2-methyl-1,4-dihydrobenzo[4,5]imidazo[1,2-*a*]pyrimidine-3-carboxylate (49). Purified by column chromatography (Hex–AcOEt 3:1 – 1:2). Yield: 19%. Mp: 236 – 238 ºC. ^{1}H NMR (300 MHz, $CDCl_3$), δ (ppm): 9.29 (brs, 1H, NH), 7.29 – 7.09 (m, 4H, Ar-H), 6.47 (s, 1H, Ar-H), 6.25 (d, J = 7.0 Hz, 1H, Ar-H), 6.23 – 6.18 (m, 1H, CH), 4.09 – 4.29 (m, 2H, OC*H*$_2$CH$_3$), 2.69 (s, 3H, CH_3), 1.28 (t, J = 7.1 Hz, 3H, OCH_2C*H*$_3$). ^{13}C NMR (75 MHz, $CDCl_3$), δ (ppm): 166.9, 158.6, 153.2, 147.9, 147.7, 142.7, 142.3, 132.1, 113.9, 113.2, 110.2, 109.5, 102.7, 97.6, 60.3, 54.7, 18.9, 14.3. HRMS (APCI) *m/z*: calcd for $C_{18}H_{17}FN_3O_3$ $[M+H]^+$, 342.1176; found: 342.1201.

(±) Isopropyl 8-fluoro-4-(furan-2-yl)-2-methyl-1,4-dihydrobenzo[4,5]imidazo[1,2-*a*]pyrimidine-3-carboxylate (50). Purified by column chromatography (Hex–AcOEt 3:1 – 1:2). Yield: 19%. Mp: 242 – 243 ºC. ^{1}H NMR (300 MHz, DMSO-d_6), δ (ppm): 10.77 (brs, 1H, NH), 7.44 (s, 1H, Ar-H), 7.34 – 7.28 (m, 2H, Ar-H), 6.93 – 6.86 (m, 1H, Ar-H), 6.53 – 6.49 (m, 1H, Ar-H), 6.35 – 6.32 (m, 1H, Ar-H), 6.20 (s, 1H, CH), 4.88 – 4.84 (m, 1H, OC*H*$(CH_3)_2$), 2.42 (s, 3H, CH_3), 1.20 (d, J = 6.0 Hz, 3H, OCH(C*H*$_3)_2$), 1.04 (d, J = 6.0 Hz, 3H, OCH(C*H*$_3)_2$). ^{13}C NMR (75 MHz, DMSO-d_6), δ (ppm): 166.6, 160.7, 159.0, 153.1, 148.7, 142.8, 142.6, 132.2, 114.2, 113.1, 110.2, 109.5, 102.7, 97.1, 68.3, 54.8, 21.9, 19.2. HRMS (APCI) *m/z*: calcd for $C_{19}H_{19}FN_3O_3$ $[M+H]^+$, 356.1332; found: 356.1343.

(±) Ethyl 8-fluoro-4-(furan-3-yl)-2-methyl-1,4-dihydrobenzo[4,5]imidazo[1,2-*a*]pyrimidine-3-carboxylate (51). Purified by column chromatography (Hex–AcOEt 3:1 – 1:2). Yield: 19%. Mp: 262 – 263 ºC. ^{1}H NMR (300 MHz, $CDCl_3$), δ (ppm): 7.39 – 7.14 (m, 3H, Ar-H), 6.94 – 6.82 (m, 1H, Ar-H), 6.49 (s, 1H, CH), 6.29 – 6.19 (m, 2H, Ar-H), 4.22 – 4.12 (m, 2H, OC*H*$_2$CH$_3$), 2.71 (s, 3H, CH_3), 1.35 (t, J = 7.2 Hz, 3H, OCH_2C*H*$_3$). HRMS (APCI) *m/z*: calcd for $C_{18}H_{17}FN_3O_3$ $[M+H]^+$, 342.1248; found: 342.1250.

(±) Isopropyl 8-fluoro-4-(furan-3-yl)-2-methyl-1,4-dihydrobenzo[4,5]imidazo[1,2-*a*]pyrimidine-3-carboxylate (52). Purified by column chromatography (Hex–AcOEt 3:1 – 1:2). Yield: 15%. Mp: 240 – 242 ºC. ^{1}H NMR (300 MHz, $CDCl_3$), δ (ppm): 7.28 – 7.02 (m, 3H, Ar-H), 6.84 – 6.78 (m, 1H, Ar-H), 6.53 (s, 1H, CH), 6.28 – 6.20 (m, 2H, Ar-H), 5.11 – 4.98 (m, 1H, OC*H*$(CH_3)_2$), 2.69 (s, 3H, CH_3), 1.30 (d, J = 6.0 Hz, 3H, OCH(C*H*$_3)_2$), 1.18 (d, J = 6.0 Hz, 3H, OCH(C*H*$_3)_2$). ^{13}C NMR (75 MHz, $CDCl_3$), δ (ppm): 165.2, 161.3, 158.1, 153.2, 146.8, 142.2, 141.7, 128.1, 110.4, 108.7, 107.8, 102.8, 96.1, 92.3, 76.0, 67.5, 50.1, 22.1, 19.3. HRMS (APCI) *m/z*: calcd for $C_{19}H_{19}FN_3O_3$ $[M+H]^+$, 356.1332; found: 356.1361.

(±) Ethyl 8-fluoro-2-methyl-4-(thiophen-2-yl)-1,4-dihydrobenzo[4,5]imidazo[1,2-*a*]pyrimidine-3-carboxylate (53). Purified by column chromatography (Hex–AcOEt 3:1 – 1:2). Yield: 16%. Mp: 253 – 255 ºC. ^{1}H NMR (300 MHz, $CDCl_3$), δ (ppm): 11.95 (brs, 1H, NH), 7.25 – 7.10 (m, 2H, Ar-H), 6.95 (s, 2H, Ar-H), 6.93 – 6.82 (m, 2H, Ar-H), 6.89 (s, 1H, CH), 4.25 – 4.09 (m, 2H, OC*H*$_2$CH$_3$), 2.70 (s, 3H, CH_3), 1.29 (t, J = 7.1 Hz, 3H, OCH_2C*H*$_3$). LRMS (CI) *m/*z calcd for $C_{18}H_{17}FN_3O_2S$ $[M+H]^+$: 358.1; found: 358.1.

(±) Isopropyl 8-fluoro-2-methyl-4-(thiophen-2-yl)-1,4-dihydrobenzo[4,5]imidazo[1,2-*a*]pyrimidine-3-carboxylate (54). Purified by column chromatography (Hex–AcOEt 3:1 – 1:2). Yield: 13%. Mp: 249 – 251 ºC. ^{1}H NMR (300 MHz, $CDCl_3$), δ (ppm): 12.02 (brs, 1H, NH), 7.45 – 7.15 (m, 3H, Ar-H), 6.95 (s, 1H, Ar-H), 6.83 – 6.78 (m, 2H, Ar-H), 6.71 (s, 1H, CH), 5.11 – 4.97 (m, 1H, OC*H*$(CH_3)_2$), 2.72 (s, 3H, CH_3), 1.31 (d, J = 6.1 Hz, 3H, OCH(C*H*$_3)_2$), 1.23 (d, J = 6.0 Hz, 3H, OCH(C*H*$_3)_2$). LRMS (CI) *m/z* calcd for $C_{19}H_{19}FN_3O_2S$ $[M+H]^+$: 372.1; found: 372.1.

(±) Ethyl 8-fluoro-2-methyl-4-(thiophen-3-yl)-1,4-dihydrobenzo[4,5]imidazo[1,2-*a*]pyrimidine-3-carboxylate (55). Purified by column chromatography (Hex–AcOEt 3:1 – 1:2). Yield: 17%. Mp: 260 – 261 ºC. ^{1}H NMR (300 MHz, $CDCl_3$), δ (ppm): 7.22 – 6.82 (m, 6H, Ar-H), 6.45 (s, 1H, CH), 4.22 – 4.02 (m, 2H, OC*H*$_2$CH$_3$), 2.65 (s, 3H, CH_3), 1.30 (t, J = 7.0 Hz, 3H, OCH_2C*H*$_3$). LRMS (CI) *m/*z calcd for $C_{18}H_{17}FN_3O_2S$ $[M+H]^+$: 358.1; found: 358.1.

(±) Isopropyl 8-fluoro-2-methyl-4-(thiophen-3-yl)-1,4-dihydrobenzo[4,5]imidazo[1,2-*a*]pyrimidine-3-carboxylate (56). Purified by column chromatography (Hex–AcOEt 3:1 – 1:1). Yield: 14%. Mp: 253 – 255 ºC. ^{1}H NMR (300 MHz, $CDCl_3$), δ (ppm): 11.95 (brs, 1H, NH), 7.42 – 7.16 (m, 4H, Ar-H), 6.98 – 6.89 (m, 2H, Ar-H), 6.62 – 6.54 (m, 1H, CH), 5.18 – 4.96 (m, 1H, OC*H*$(CH_3)_2$), 2.69 (s, 3H, CH_3), 1.32 (d, J = 6.4 Hz, 3H, OCH(C*H*$_3)_2$), 1.22 (d, J = 6.2 Hz, 3H, OCH(C*H*$_3)_2$). ^{13}C NMR (75 MHz, $CDCl_3$), δ (ppm): 166.5, 160.9, 158.9, 149.2, 147.3, 142.6, 140.8, 132.0, 126.9, 126.6, 123.2, 114.1, 113.5, 102,5, 101.6, 68.6, 56.8, 22.1, 19.3. LRMS (CI) *m/z* calcd for $C_{19}H_{19}FN_3O_2S$ $[M+H]^+$: 372.1; found: 372.1.

(±) Ethyl 8-chloro-4-(furan-2-yl)-2-methyl-1,4-dihydrobenzo[4,5]imidazo[1,2-*a*]pyrimidine-3-carboxylate (57). Purified by column chromatography (Hex–AcOEt 3:1 – 1:1). Yield: 21%. Mp: 232 – 234 ºC. ^{1}H NMR (300 MHz, DMSO-d_6), δ (ppm): 10.95 (brs, 1H, NH), 7.49 – 7.38 (m, 3H, Ar-H), 7.10 – 7.01 (m, 1H, Ar-H), 6.62 – 6.49 (m, 1H, Ar-H), 6.44 – 6.33 (m, 1H, Ar-H), 6.25 (s, 1H, CH), 4.18 – 3.96 (m, 2H, OC*H*$_2$CH$_3$), 2.46 (s, 3H, CH_3), 1.26 (t, J = 7.0 Hz, 3H, OCH_2C*H*$_3$). ^{13}C NMR (75 MHz, DMSO-d_6), δ (ppm): 165.4, 152.7, 147.9, 147.3, 143.8, 143.2, 130.9, 126.8, 120.5, 116.8, 111.4, 110.8, 108.4, 95.1, 59.9, 49.6, 19.1, 14.6. HRMS (APCI) *m/z* calcd for $C_{18}H_{17}ClN_3O_3$ $[M+H]^+$: 358.0880; found: 358.0911.

(±) Isopropyl 8-chloro-4-(furan-2-yl)-2-methyl-1,4-dihydrobenzo[4,5]imidazo[1,2-*a*]pyrimidine-3-carboxylate (58). Purified by column chromatography (Hex–AcOEt 3:1 – 1:1). Yield: 21%. Mp: 252 – 253 ºC. ^{1}H NMR (300 MHz, DMSO-d_6), δ (ppm): 10.90 (brs, 1H, NH), 7.45 – 7.32 (m, 2H, Ar-H), 7.06 – 7.02 (m, 1H, Ar-H), 6.55 (s, 1H, Ar-H), 6.45 (s, 1H, Ar-H), 6.33 (s, 1H, Ar-H), 5.74 (s, 1H, CH), 4.92 – 4.87 (m, 1H, OC*H*$(CH_3)_2$), 2.44 (s, 3H, CH_3), 1.21 (d, J = 6.3 Hz, 3H, OCH(C*H*$_3)_2$), 1.05 (d, J = 6.0 Hz, 3H, OCH(C*H*$_3)_2$). ^{13}C NMR (75 MHz, $CDCl_3$), δ (ppm): 165.0, 152.9, 147.0, 146.9, 142.3, 139.7, 132.3, 126.6, 123.1, 116.9, 110.4, 110.1, 107.9, 96.1, 67.5, 50.1, 22.1, 21.7, 19.2. HRMS (APCI) *m/z* calcd for $C_{19}H_{19}ClN_3O_3$ $[M+H]^+$: 372.1037; found: 372.1042.

(±) Ethyl 8-chloro-4-(furan-3-yl)-2-methyl-1,4-dihydrobenzo[4,5]imidazo[1,2-*a*]pyrimidine-3-carboxylate (59). Purified by column chromatography (Hex–AcOEt 3:1 – 1:1). Yield: 19%. Mp: 241 – 243 ºC. ^{1}H NMR (300 MHz, $CDCl_3$), δ (ppm): 7.38 (s, 1H, Ar-H), 7.28 – 7.18 (m, 2H, Ar-H), 7.10 – 7.04 (m, 1H, Ar-H), 6.48 (s, 1H, CH), 6.11 – 6.08 (m, 2H, Ar-H), 4.44 – 4.02 (m, 2H, OC*H*$_2$CH$_3$), 2.70 (s, 3H, CH_3), 1.18 (t, J = 7.1 Hz, 3H, OCH$_2$C*H*$_3$). ^{13}C NMR (75 MHz, $CDCl_3$), δ (ppm): 168.0, 149.0, 146.6, 143.2, 141.0, 140.6, 132.5, 130.9, 128.3, 122.9, 118.1, 113.5, 109.7, 101.3, 60.1, 53.5, 18.9, 14.4. HRMS (APCI) *m/z* calcd for $C_{18}H_{17}ClN_3O_3$ $[M+H]^+$: 358.0940; found: 358.0950.

(±) Isopropyl 8-chloro-4-(furan-3-yl)-2-methyl-1,4-dihydrobenzo[4,5]imidazo[1,2-*a*]pyrimidine-3-carboxylate (60). Purified by column chromatography (Hex–AcOEt 3:1 – 1:1). Yield: 17%. Mp: 256 – 258 ºC. ^{1}H NMR (300 MHz, $CDCl_3$), δ (ppm): 11.95 (brs, 1H, NH), 7.48 (s, 1H, Ar-H), 7.38 (s, 1H, Ar-H), 7.25 (s, 1H, Ar-H), 7.21 – 7.06 (m, 2H, Ar-H), 6.52 (s, 1H, CH), 6.11 (s, 1H, Ar-H), 5.11 – 5.05 (m, 1H, OC*H*$(CH_3)_2$), 2.70 (s, 3H, CH_3), 1.35 (d, J = 6.1 Hz, 3H, OCH(C*H*$_3)_2$), 1.31 (d, J = 6.0 Hz, 3H, OCH(C*H*$_3)_2$). ^{13}C NMR (75 MHz, $CDCl_3$), δ (ppm): 165.3, 147.8, 145.6, 142.3, 141.7, 130.3, 128.2, 126.4, 126.1, 122.7, 121.3, 116.3, 110.2, 99.4, 67.8, 52.1, 21.9, 19.5. HRMS (APCI) *m/z* calcd. for $C_{19}H_{19}ClN_3O_3$ $[M+H]^+$: 372.1109; found: 372.1111.

(±) Ethyl 8-chloro-2-methyl-4-(thiophen-2-yl)-1,4-dihydrobenzo[4,5]imidazo[1,2-*a*]pyrimidine-3-carboxylate (61). Purified by column chromatography (Hex–AcOEt 3:1 – 1:1). Yield: 22%. Mp: 247 – 249 ºC. ^{1}H NMR (300 MHz, $CDCl_3$), δ (ppm): 7.52 – 7.46 (m, 1H, Ar-H), 7.28 – 7.05 (m, 3H, Ar-H), 6.96 – 6.9 (m, 1H, Ar-H), 6.83 – 6.81 (m, 1H, Ar-H), 6.69 (s, 1H, CH), 4.25 – 4.10 (m, 2H, OC*H*$_2$CH$_3$), 2.72 (s, 3H, CH_3), 1.33 (t, J = 7.0 Hz, 3H, OCH$_2$C*H*$_3$). LRMS (EI) *m/z* calcd for $C_{18}H_{16}ClN_3O_2S$ $[M]^+$: 373.1; found: 372.9.

(±) Isopropyl 8-chloro-2-methyl-4-(thiophen-2-yl)-1,4-dihydrobenzo[4,5]imidazo[1,2-*a*]pyrimidine-3-carboxylate (62). Purified by column chromatography (Hex–AcOEt 3:1 – 1:1). Yield: 17%. Mp: 248 – 249 ºC. ^{1}H NMR (300 MHz, $CDCl_3$), δ (ppm): 7.42 (s, 2H, Ar-H), 7.26 – 7.08 (m, 3H, Ar-H), 6.90 – 6.84 (m, 1H, Ar-H), 6.78 (s, 1H, CH), 5.18 – 5.05 (m, 1H, OC*H*$(CH_3)_2$), 2.72 (s, 3H, CH_3), 1.34 (d, J = 6.2 Hz, 3H, OCH(C*H*$_3)_2$), 1.18 (d, J = 6.2 Hz, 3H, OCH(C*H*$_3)_2$). LRMS (EI) *m/z* calcd for $C_{19}H_{18}ClN_3O_2S$ $[M]^+$: 387.1; found: 386.9.

(±) Ethyl 8-chloro-2-methyl-4-(thiophen-3-yl)-1,4-dihydrobenzo[4,5]imidazo[1,2-*a*]pyrimidine-3-carboxylate (63). Purified by column chromatography (Hex–AcOEt 3:1 – 1:1). Yield: 15%. Mp: 255 – 256 ºC. ^{1}H NMR (300 MHz, $CDCl_3$), δ (ppm): 11,65 (brs, 1H, NH), 7,42 (s, 1H, Ar-H), 7.19 – 6.94 (m, 5H, Ar-H), 6.60 (s, 1H, CH), 4.25 – 4.02 (m, 2H, OC*H*$_2$CH$_3$), 2.68 (s, 3H, CH_3), 1.31 (t, J = 7.1 Hz, 3H, OCH$_2$C*H*$_3$). LRMS (CI) *m/z* calcd for $C_{18}H_{17}ClN_3O_2S$ $[M+H]^+$: 374.1; found: 374.1.

(±) Isopropyl 8-chloro-2-methyl-4-(thiophen-3-yl)-1,4-dihydrobenzo[4,5]imidazo[1,2-*a*]pyrimidine-3-carboxylate (64). Purified by column chromatography (Hex–AcOEt 3:1 – 1:1). Yield: 16%. Mp: 248 – 250 ºC. ^{1}H NMR (300 MHz, $CDCl_3$), δ (ppm): 12.02 (brs, 1H, NH), 7.39 (s, 1H, Ar-H), 7.22 – 6.98 (m, 5H, Ar-H), 6.76 (s, 1H, CH), 5.19 – 5.05 (m, 1H, OC*H*(CH$_3$)$_2$), 2.69 (s, 3H, CH_3), 1.31 (d, J = 6.1 Hz, 3H, OCH(C*H*$_3$)$_2$), 1.22 (d, J = 6.0 Hz, 3H, OCH(C*H*$_3$)$_2$). ^{13}C NMR (75 MHz, $CDCl_3$), δ (ppm): 165.3, 147.8, 145.6, 142.3, 141.7, 130.3, 128.2, 126.4 126.1, 122.7, 121.2, 116.3, 110.2, 99.5, 67.8, 52.1, 22.2, 21.9, 19.5. LRMS (CI) *m/z* calcd for $C_{19}H_{19}ClN_3O_2S$ $[M+H]^+$: 388.1; found: 388.1.

(±) Ethyl 8-bromo-4-(furan-2-yl)-2-methyl-1,4-dihydrobenzo[4,5]imidazo[1,2-*a*]pyrimidine-3-carboxylate (65). Purified by column chromatography (Hex–AcOEt 2:1 – 1:2). Yield: 18%. Mp: 242 – 243 ºC. ^{1}H NMR (300 MHz, $CDCl_3$), δ (ppm): 11,45 (brs, 1H, NH), 7.61 (s, 1H, Ar-H), 7.30 – 7.25 (m, 3H, Ar-H), 6.53 (s, 1H, CH), 6.28 – 6.24 (m, 2H, Ar-H), 4.26 – 4.12 (m, 2H, OC*H*$_2$CH$_3$), 2.71 (s, 3H, CH_3), 1.26 (t, J = 7.1 Hz, 3H, OCH$_2$C*H*$_3$). ^{13}C NMR (75 MHz, $CDCl_3$), δ (ppm): 167.1, 152.9, 146.7, 142.5, 141.8, 132.7, 124.3, 119.2, 118.5, 114.3, 111.0, 110.4, 97.3, 108.0, 60.3, 50.0, 19.5, 14.3. LRMS (CI) *m/z* calcd for $C_{18}H_{17}BrN_3O_3$ $[M+H]^+$: 402.0; found: 402.0.

(±) Isopropyl 8-bromo-4-(furan-2-yl)-2-methyl-1,4-dihydrobenzo[4,5]imidazo[1,2-*a*]pyrimidine-3-carboxylate (66). Purified by column chromatography (Hex–AcOEt 2:1 – 1:2). Yield: 22%. Mp: 245 – 247 ºC. ^{1}H NMR (300 MHz, $CDCl_3$), δ (ppm): 11.35 (brs, 1H, NH), 7.42 (s, 1H, Ar-H), 7.32 – 7.10 (m, 3H, Ar-H), 6.49 (s, 1H, CH), 6.13 – 6.08 (m, 2H, Ar-H), 5.11 – 4.98 (m, 1H, OC*H*(CH$_3$)$_2$), 2.69 (s, 3H, CH_3), 1.25 (d, J = 6.0 Hz, 3H, OCH(C*H*$_3$)$_2$), 1.12 (d, J = 6.1 Hz, 3H, OCH(C*H*$_3$)$_2$). ^{13}C NMR (75 MHz, $CDCl_3$), δ (ppm): 165.0, 152.8, 147.2, 146.9, 142.3, 140.0, 132.7, 125.9, 117.3, 113.8, 112.9, 110.4, 107.9, 96.1, 67.5, 50.1, 22.1, 21.7, 19.2. HRMS (APCI) *m/z* calcd for $C_{19}H_{19}BrN_3O_3$ $[M+H]^+$: 416,0618; found: 416.0605.

(±) Ethyl 8-bromo-4-(furan-3-yl)-2-methyl-1,4-dihydrobenzo[4,5]imidazo[1,2-*a*]pyrimidine-3-carboxylate (67). Purified by column chromatography (Hex–AcOEt 2:1 – 1:2). Yield: 21%. Mp: 228 – 230 ºC. ^{1}H NMR (750 MHz, DMSO-d_6), δ (ppm): 10.9 (s, 1H, NH), 7.53 (d, J = 1.9 Hz, 1H, H-9), 7.45 (dd, J = 1.8, 0.9 Hz, 1H), 7.41 (d, J = 8.4 Hz, 1H, H-6), 7.17 (dd, J = 8.4, 1.9 Hz, 1H, H-7), 6.60 (d, J = 0.8 Hz, 1H, CH), 6.46 (dd, J = 3.3, 0.9 Hz, 1H, Ar-H), 6.33 (dd, J = 3.3, 1.8 Hz, 1H, Ar-H), 4.10 (dq, J = 10.9, 7.1 Hz, 1H, OCH_2CH$_3$), 4.03 (dq, J = 10.9, 7.1 Hz, 1H, OCH_2CH$_3$), 2.45 (d, J = 0.7 Hz, 3H, CH$_3$), 1.16 (t, J = 7.1 Hz, 3H, OCH$_2$CH_3). ^{13}C NMR (126 MHz, CDCl$_3$), δ (ppm): 165.7, 147.4, 145.7, 143.8, 139.8, 131.7, 130.5, 125.4, 124.4, 119.6, 115.9, 110.8, 108.8, 99.2, 60.6, 48.6, 19.8, 14.5. HRMS (APCI) *m/z* calcd for $C_{18}H_{17}BrN_3O_3$ $[M+H]^+$: 402.0375; found: 402.0382.

(±) Isopropyl 8-bromo-4-(furan-3-yl)-2-methyl-1,4-dihydrobenzo[4,5]imidazo[1,2-*a*]pyrimidine-3-carboxylate (68). Purified by column chromatography (Hex–AcOEt 2:1). Yield: 22%. Mp: 248 – 249 ºC. ^{1}H NMR (300 MHz, CDCl$_3$), δ (ppm): 11.36 (brs, 1H, NH), 7.61 (s, 1H, Ar-H), 7.37 (s, 1H, Ar-H), 7.31 – 7.12 (m, 3H, Ar-H), 6.48 (s, 1H, CH), 6.19 (s, 1H, Ar-H), 5.19 – 5.08 (m, 1H, OCH(CH$_3$)$_2$), 2.66 (s, 3H, CH$_3$), 1.32 (d, J = 6.0 Hz, 3H, OCH(CH_3)$_2$), 1.27 (d, J = 6.0 Hz, 3H, OCH(CH_3)$_2$). ^{13}C NMR (75 MHz, CDCl$_3$), δ (ppm): 166.7, 148.7, 146.9, 143.2, 141.1, 140.73, 133.4, 128.3, 126.1, 118.9, 118.3, 114.1, 109.8, 101.8, 68.1, 53.5, 21.9, 20.9, 19.0. HRMS (APCI) *m/z* calcd for $C_{19}H_{17}BrN_3O_3$ $[M-1]^-$: 414.0459; found: 414.0457.

(±) Ethyl 8-bromo-2-methyl-4-(thiophen-2-yl)-1,4-dihydrobenzo[4,5]imidazo[1,2-*a*]pyrimidine-3-carboxylate (69). Purified by column chromatography (Hex–AcOEt 2:1 – 1:2). Yield: 23%. Mp: 236 – 238 ºC. ^{1}H NMR (300 MHz, CDCl$_3$), δ (ppm): 11.86 (brs, 1H, NH), 7.58 (s, 1H, Ar-H), 7.25 – 7.03 (m, 3H, Ar-H), 6.99 – 6.65 (m, 3H, Ar-H + CH), 4.28 – 4.16 (m, 2H, OCH_2CH$_3$), 2.65 (s, 3H, CH$_3$), 1.28 (t, J = 7.0 Hz, 3H, OCH$_2$CH_3). LRMS (CI) *m/z* calcd for $C_{18}H_{17}BrN_3O_2S$ $[M+H]^+$: 418.0; found: 418.0.

(±) Isopropyl 8-bromo-2-methyl-4-(thiophen-2-yl)-1,4-dihydrobenzo[4,5]imidazo[1,2-*a*]pyrimidine-3-carboxylate (70). Purified by column chromatography (Hex–AcOEt 2:1 – 1:2). Yield: 18%. Mp: 224 – 226 ºC. ^{1}H NMR (300 MHz, $CDCl_3$), δ (ppm): 11.89 (brs, 1H, NH), 7.60 (s, 1H, Ar-H), 7.30 – 7.05 (m, 3H, Ar-H), 6.89 (s, 1H, Ar-H), 6.85 – 6.75 (m, 1H, Ar-H), 6.70 (s, 1H, CH), 5.96 – 5.12 (m, 1H, OC*H*$(CH_3)_2$), 2.81 (s, 3H, CH_3), 1.32 (d, J = 6.1 Hz, 3H, OCH(C*H*$_3)_2$), 1.21 (d, J = 6.1 Hz, 3H, OCH(C*H*$_3)_2$). ^{13}C NMR (75 MHz, $CDCl_3$), δ (ppm): 165.1, 158.5, 147.4, 145.9, 144.0, 142.7, 126.5, 125.6, 125.4, 124.0, 119.4, 115.7, 110.9, 99.6, 67.9, 51.7, 22.2, 21.8, 19.5. LRMS (CI) *m/z* calcd for $C_{19}H_{19}BrN_3O_2S$ $[M+H]^+$: 432.0; found: 432.0.

(±) Ethyl 8-bromo-2-methyl-4-(thiophen-3-yl)-1,4-dihydrobenzo[4,5]imidazo[1,2-*a*]pyrimidine-3-carboxylate (71). Purified by column chromatography (Hex–AcOEt 2:1 – 1:2). Yield: 18%. Mp: 252 – 254 ºC. ^{1}H NMR (300 MHz, $CDCl_3$), δ (ppm): 11.53 (brs, 1H, NH), 7.31 (s, 2H, Ar-H), 7.18 – 7.15 (m, 3H, Ar-H), 6.96 (s, 1H, Ar-H), 6.58 (s, 1H, CH), 4.18 – 4.02 (m, 2H, OC*H*$_2$CH$_3$), 2.68 (s, 3H, CH_3), 1.27 (t, J = 7.0 Hz, 3H, OCH_2C*H*$_3$). LRMS (CI) *m/z* calcd for $C_{18}H_{17}BrN_3O_2S$ $[M+H]^+$: 418.0; found: 417.9.

(±) Isopropyl 8-bromo-2-methyl-4-(thiophen-3-yl)-1,4-dihydrobenzo[4,5]imidazo[1,2-*a*]pyrimidine-3-carboxylate (72). Purified by column chromatography (Hex–AcOEt 2:1 – 1:2). Yield: 22%. Mp: 248 – 249 ºC. ^{1}H NMR (750 MHz, MeOD), δ (ppm): 7.50 (d, J = 1.8 Hz, 1H, H-9), 7.40 (dd, J = 3.0, 1.3 Hz, 1H), 7.27 (dd, J = 5.1, 3.0 Hz, 1H), 7.21 (d, J = 8.5 Hz, 1H, H-6), 7.15 (dd, J = 8.5, 1.8 Hz, 1H, H-7), 6.92 (dd, J = 5.1, 1.3 Hz, 1H, Ar-H), 6.58 (s, 1H, CH), 5.00 (hept, J = 6.3 Hz, 1H, OC*H*$(CH_3)_2$), 2.50 (d, J = 0.7 Hz, 3H, CH_3), 1.30 (d, J = 6.3 Hz, 3H, OCH(C*H*$_3)_2$), 1.14 (d, J = 6.3 Hz, 3H, OCH(C*H*$_3)_2$). ^{13}C NMR (126 MHz, MeOD), δ (ppm): 166.8, 148.1, 147.0, 144.5, 143.1, 132.1, 127.5, 127.0, 124.8, 124.3, 120.3, 116.3, 112.3, 100.7, 69.0, 53.2, 22.3, 22.0, 18.9.LRMS (CI) *m/z* calcd for $C_{19}H_{19}BrN_3O_2S$ $[M+H]^+$: 432.0; found: 432.0.

(±) Ethyl 7-fluoro-2-methyl-4-(oxazol-4-yl)-1,4-dihydrobenzo[4,5]imidazo[1,2-*a*]pyrimidine-3-carboxylate (73). Purified by column chromatography (Hex–AcOEt 1:1). Yield: 12%. Mp: 253 – 254 ºC. ^{1}H NMR (300 MHz, $CDCl_3$), δ (ppm): 7.79 – 7.66 (m, 1H, Ar-H), 7.55 – 7.32 (m, 1H, Ar-H), 7.32 – 7.13 (m, 1H, Ar-H), 7.13 – 7.02 (m, 1H, Ar-H), 7.02 – 6.80 (m, 1H, Ar-H), 6.53 (s, 1H, CH), 4.36 – 4.04 (m, 2H, OC*H*$_2$CH$_3$), 2.73 (s, 3H, CH_3), 1.32 (t, J = 7.1 Hz, 3H, OCH$_2$C*H*$_3$). LRMS (CI) *m/z* calcd for $C_{17}H_{16}FN_4O_3$ $[M+H]^+$: 343.1; found: 343.2.

(±) Isopropyl 7-fluoro-2-methyl-4-(oxazol-4-yl)-1,4-dihydrobenzo[4,5]imidazo[1,2-*a*]pyrimidine-3-carboxylate (74). Purified by column chromatography (Hex–AcOEt 1:1). Yield: 25%. Mp: 240 – 241 ºC. ^{1}H NMR (300 MHz, $CDCl_3$), δ (ppm): 11.97 (s, 1H, NH), 7.77 – 7.68 (m, 1H, Ar-H), 7.41 (dd, J = 8.7, 4.5 Hz, 1H, Ar-H), 7.28 (s, 1H, Ar-H), 7.19 (dd, J = 9.5, 2.4 Hz, 1H, Ar-H), 7.02 – 6.83 (m, 1H, Ar-H), 6.57 – 6.49 (m, 1H, CH), 5.22 – 5.01 (m, 1H, OC*H*(CH$_3$)$_2$), 2.73 (s, 3H, CH_3), 1.33 (d, J = 6.3 Hz, 3H, OCH(C*H*$_3$)$_2$), 1.23 (d, J = 6.2 Hz, 3H, OCH(C*H*$_3$)$_2$). LRMS (CI) *m/z* calcd for $C_{18}H_{18}FN_4O_3$ $[M+H]^+$: 357.1; found: 357.4.

(±) Ethyl 7-chloro-2-methyl-4-(oxazol-4-yl)-1,4-dihydrobenzo[4,5]imidazo[1,2-*a*]pyrimidine-3-carboxylate (75). Purified by column chromatography (Hex–AcOEt 1:1). Yield: 12%. Mp: 256 – 258 ºC. ^{1}H NMR (300 MHz, $CDCl_3$), δ (ppm): 7.79 – 7.63 (m, 1H, Ar-H), 7.59 – 7.21 (m, 3H, Ar-H), 7.21 – 7.00 (m, 1H, Ar-H), 6.55 (s, 1H, CH), 4.23 (q, J = 7.2 Hz, 2H, OC*H*$_2$CH$_3$), 2.73 (s, 3H, CH_3), 1.32 (t, J = 7.2 Hz, 3H, OCH$_2$C*H*$_3$). LRMS (CI) *m/z* calcd for $C_{17}H_{16}ClN_4O_3$ $[M+H]^+$: 359.1; found: 359.1.

(±) Isopropyl 7-chloro-2-methyl-4-(oxazol-4-yl)-1,4-dihydrobenzo[4,5]imidazo[1,2-*a*]pyrimidine-3-carboxylate (76). Purified by column chromatography (Hex–AcOEt 1:1). Yield: 13%. Mp: 247 – 248 ºC. ^{1}H NMR (300 MHz, $CDCl_3$), δ (ppm): 8.00 – 7.60 (m, 2H, Ar-H), 7.47 – 7.23 (m, 2H, Ar-H), 7.19 – 7.05 (m, 1H, Ar-H), 6.55 (s, 1H, CH), 5.20 – 5.00 (m, 1H, OC*H*(CH$_3$)$_2$), 2.69 (s, 3H, CH_3), 1.34 (d, J = 6.1 Hz, 3H, OCH(C*H*$_3$)$_2$), 1.22 (d, J = 6.1 Hz, 3H, OCH(C*H*$_3$)$_2$). LRMS (CI) *m/z* calcd for $C_{18}H_{18}ClN_4O_3$ $[M+H]^+$: 373.1; found: 373.1.

(±) Ethyl 8-fluoro-2-methyl-4-(oxazol-4-yl)-1,4-dihydrobenzo[4,5]imidazo[1,2-*a*]pyrimidine-3-carboxylate (77). Purified by column chromatography (Hex–AcOEt 1:1). Yield: 12%. Mp: 247 – 249 ºC. ^{1}H NMR (300 MHz, $CDCl_3$), δ (ppm): 7.77 – 7.67 (m, 2H, Ar-H), 7.33 – 7.23 (m, 1H, Ar-H), 7.22 – 7.16 (m, 1H, Ar-H), 6.92 – 6.78 (m, 1H, Ar-H), 6.58 (s, 1H, CH), 4.24 (q, J = 7.1, 2H, OC*H*$_2$CH$_3$), 2.72 (s, 3H, CH$_3$), 1.31 (t, J = 7.1 Hz, 3H, OCH$_2$C*H*$_3$). LRMS (CI) *m/z* calcd for $C_{17}H_{16}FN_4O_3$ $[M+H]^+$: 343.1; found: 343.2.

(±) Isopropyl 8-fluoro-2-methyl-4-(oxazol-4-yl)-1,4-dihydrobenzo[4,5]imidazo[1,2-*a*]pyrimidine-3-carboxylate (78). Purified by column chromatography (Hex–AcOEt 1:1). Yield: 12%. Mp: 255 – 256 ºC. ^{1}H NMR (300 MHz, $CDCl_3$), δ (ppm): 7.86 – 7.65 (m, 2H, Ar-H), 7.49 – 7.05 (m, 2H, Ar-H), 7.05 – 6.77 (m, 1H, Ar-H), 6.54 (d, J = 12.3 Hz, 1H, CH), 5.11 (p, J = 6.3 Hz, 1H, OC*H*(CH$_3$)$_2$), 2.73 (s, 3H, CH$_3$), 1.33 (d, J = 6.3 Hz, 3H, OCH(C*H*$_3$)$_2$), 1.23 (d, J = 6.2 Hz, 3H, OCH(C*H*$_3$)$_2$). LRMS (CI) *m/z* calcd for $C_{18}H_{18}FN_4O_3$ $[M+H]^+$: 357.1; found: 357.4.

(±) Ethyl 8-chloro-2-methyl-4-(oxazol-4-yl)-1,4-dihydrobenzo[4,5]imidazo[1,2-*a*]pyrimidine-3-carboxylate (79). Purified by column chromatography (Hex–AcOEt 1:1). Yield: 11%. Mp: 250 – 252 ºC. ^{1}H NMR (300 MHz, $CDCl_3$), δ (ppm): 7.79 – 7.68 (m, 2H, Ar-H), 7.49 (d, J = 8.1 Hz, 1H, Ar-H), 7.44 – 7.23 (m, 1H, Ar-H), 7.12 (d, J = 8.1 Hz, 1H, Ar-H), 6.57 (s, 1H, CH), 4.24 (q, J = 7.1 Hz, 2H, OC*H*$_2$CH$_3$), 2.72 (s, 3H, CH$_3$), 1.33 (t, J = 7.1 Hz, 3H, OCH$_2$C*H*$_3$). HRMS (APCI) *m/z*: calcd for $C_{17}H_{15}ClN_4O_3$ $[M+H]^+$: 359.0833; found: 359.0833.

(±) Isopropyl 8-chloro-2-methyl-4-(oxazol-4-yl)-1,4-dihydrobenzo[4,5]imidazo[1,2-*a*]pyrimidine-3-carboxylate (80). Purified by column chromatography (Hex–AcOEt 1:1). Yield: 20%. Mp: 244 – 246 ºC. ^{1}H NMR (300 MHz, $CDCl_3$), δ (ppm): 8.00 – 7.60 (m, 2H, Ar-H), 7.47 (d, J = 1.8 Hz, 1H, Ar-H), 7.37 – 7.23 (m, 1H, Ar-H), 7.12 (dd, J = 8.5, 1.8 Hz, 1H, Ar-H), 6.55 (s, 1H, CH), 5.12 (p, J = 6.2 Hz, 1H, OC*H*(CH$_3$)$_2$), 2.70 (s, 3H, CH$_3$), 1.33 (d, J = 6.2 Hz, 3H, OCH(C*H*$_3$)$_2$), 1.24 (d, J = 6.2 Hz, 3H, OCH(C*H*$_3$)$_2$). LRMS (CI) *m/z* calcd for $C_{18}H_{18}ClN_4O_3$ $[M+H]^+$: 373.1; found: 373.1.

5.2.3 Chiral HPLC separation of enantiomers and circular dichroism of ISAM-140, 50, 58, 60, 66, 67 and 79

The chiral resolution was performed using a Water Breeze™ 2 (binary pump 1525, detector UV/Visible 2489, 7725i Manual Injector Kit 1500 Series). Compound **50** (**ISAM-163**) enantiomers were separated using a 250 mm x 10 mm Lux® 5 μm Amylose-2 (Phenomenex) while **ISAM-140**, **58**, **60**, **66**, **67** and **79** enantiomers were separated using a 250 mm x 20 mm Chiralpak® 5μm IE-3 (DAICEL). All the separations were performed at 25 ºC with *Hex* (or dichloromethane)/*i*-propanol mixture in different percentages as mobile phase (see above). The enantiomers **(*R*)-ISAM-140** (0.5 mg, t_R = 17.98 min), **(*S*)-ISAM-140** (0.5 mg, t_R = 20.31 min), **(*R*)-50** (0.5 mg, t_R = 9.08 min), **(*S*)-50** (0.5 mg, t_R = 13.64 min), **(*R*)-58** (0.5 mg, t_R = 16.96 min), **(*S*)-58** (0.5 mg, t_R = 20.32 min), **(*S*)-60** (0.5 mg, t_R = 14.43 min), **(*R*)-60** (0.5 mg, t_R = 15.67 min), **(*R*)-66** (0.5 mg, t_R = 17.44 min), **(*S*)-66** (0.5 mg, t_R = 20.04 min), **(*S*)-67** (0.5 mg, t_R = 31.02 min), **(*R*)-67** (0.5 mg, t_R = 36.61 min), **(*S*)-79** (0.5 mg, t_R = 6.99 min) and **(*R*)-79** (0.5 mg, t_R = 7.53 min) were isolated, their stereochemical purity analyzed by chiral HPLC (e.e.: 97-99% for each enantiomer, reports showed below, chromatogram at 254 nM) and then characterized by ^{1}H NMR and Circular dichroism (CD).

CD spectra were recorded on a Jasco-815 system equipped with a Peltier-type thermostatic accessory (CDF-426S, Jasco). Measurements were carried out at 20 °C using a 1 mm quartz cell in a volume of 600 μL. Compounds (0.5 mg) were dissolved in MeOH (1.0 mL) and then diluted 10-fold in MeOH. The instrument settings were bandwidth, 1.0 nm; data pitch, 1.0 nm; speed, 500 nm/min; accumulation, 10; wavelengths, 400−190 nm.

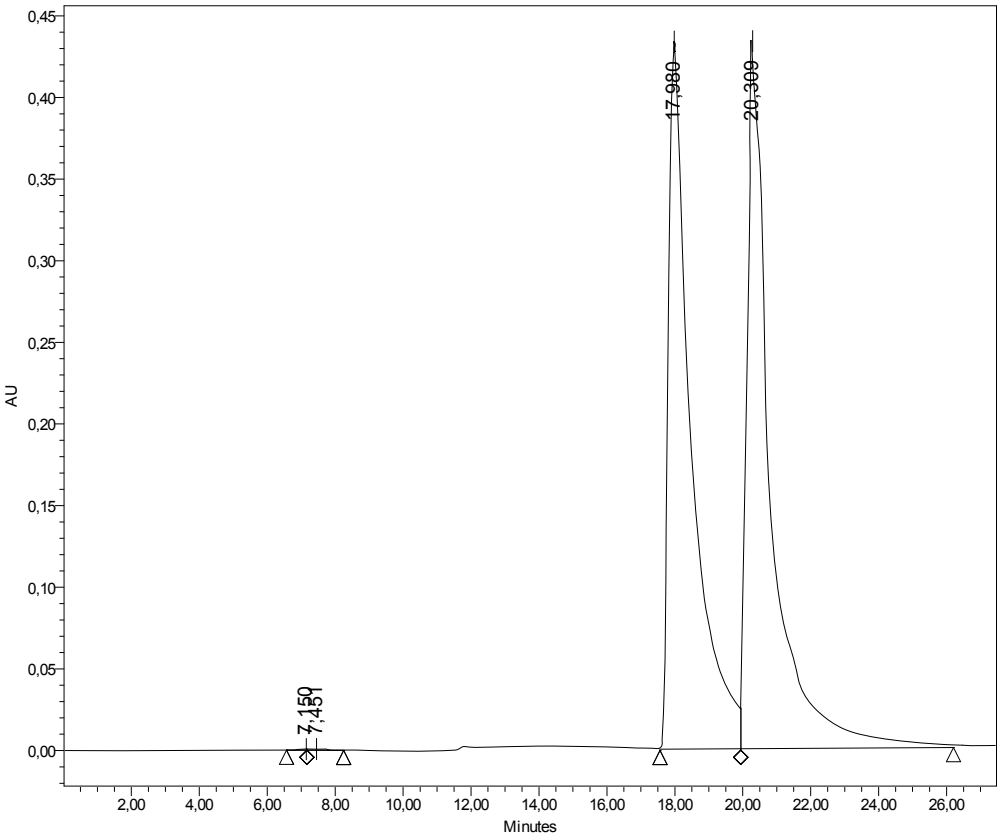

Sample Name: ISAM-140RAC; Date Acquired: 23/05/2019 11:24:09 CEST; Vial: 1; Injection: 2

Peak Summary with Statistics

Peak Name:

	Sample Name	Vial	Inj.	RT (min)	Area (µV*sec)	% Area	Height (µV)
1	ISAM-140	1	2	7,150	6012	0,06	616
2	ISAM-140	1	2	7,451	12411	0,13	770
3	ISAM-140	1	2	17,980	22957829	47,98	423618
4	ISAM-140	1	2	20,309	22742873	47,17	489245

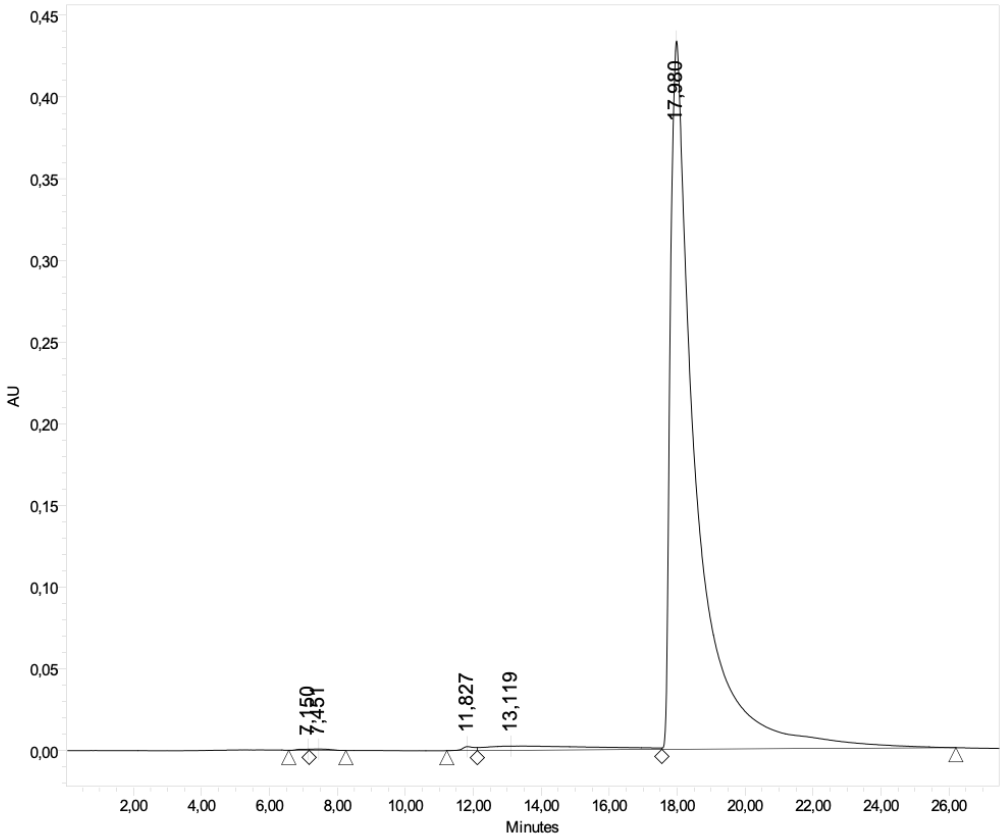

Sample Name: (R)-ISAM-140A; Date Acquired: 24/05/2019 12:53:09 CEST; Vial: 1; Injection: 2

Peak Summary with Statistics

Peak Name:

	Sample Name	Vial	Inj.	RT (min)	Area (µV*sec)	% Area	Height (µV)
1	(R)-ISAM-140A	1	2	7,150	13556	0,06	616
2	(R)-ISAM-140A	1	2	7,451	29911	0,13	770
3	(R)-ISAM-140A	1	2	17,980	22742873	96,99	433618
4	(R)-ISAM-140A	1	2	13,119	601581	2,57	2535
5	(R)-ISAM-140A	1	2	11,827	59911	0,26	2385

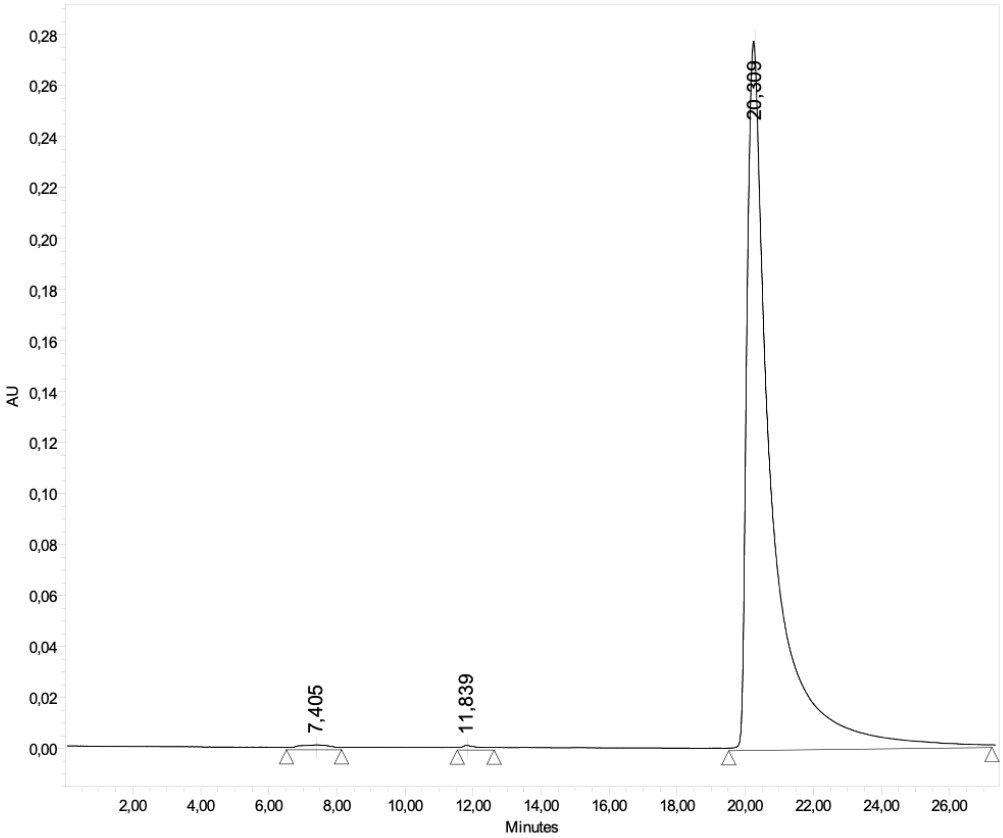

Sample Name: (S)-ISAM-140B ; Date Acquired: 24/05/2019 13:22:31 CEST; Vial: 1; Injection: 4

Peak Summary with Statistics
Peak Name:

	Sample Name	Vial	Inj.	RT (min)	Area (µV*sec)	% Area	Height (µV)
1	(S)-ISAM-140B	1	4	11,839	15880	0,11	850
2	(S)-ISAM-140B	1	4	7,405	45157	0,32	918
3	(S)-ISAM-140B	1	4	20,309	13845102	99,56	278538
Mean				13,184	4635379,763		93435,310
Std. Dev.				6,556	7975866,842		160303,31

SAMPLE INFORMATION

Sample Name:	50	Acquired By:	Breeze
Sample Type:	Racemate	Sample Set Name:	Halogenated
Vial:	1	Acq. Method:	10%HexiPAISOF25 set
Injection #:	1	Date Acquired:	05/11/2019 11:09:20 CET
Run Time:	25,00 Minutes	Injection Volume:	200,00 ul

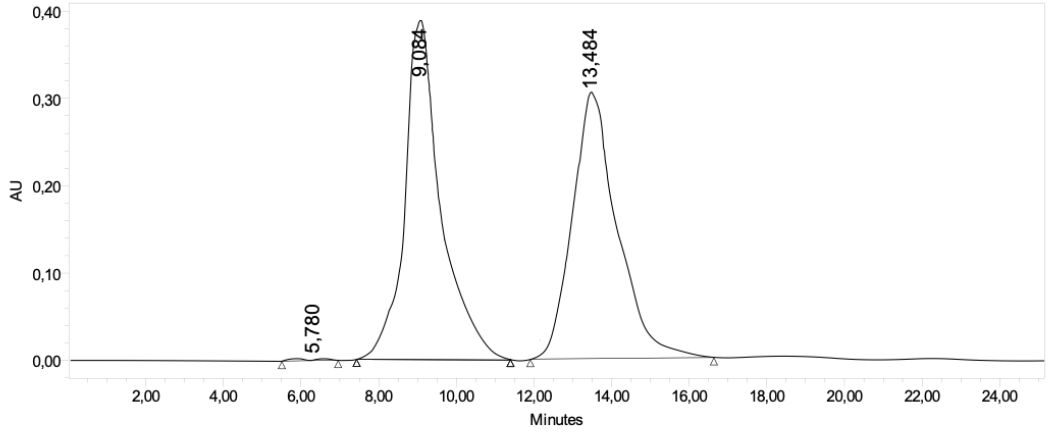

	RT (min)	Area (µV*sec)	% Area	Height (µV)
1	5,780	130009	0,22	2408
2	9,084	29905180	51,44	381108
3	13,484	28103184	48,34	287862

SAMPLE INFORMATION			
Sample Name:	50	Acquired By:	Breeze
Sample Type:	Enantiomer A	Sample Set Name:	Halogenated
Vial:	1	Acq. Method:	10%HexiPAISOF25 set
Injection #:	2	Date Acquired:	05/11/2019 11:35:31 CET
Run Time:	25,00 Minutes	Injection Volume:	200,00 ul

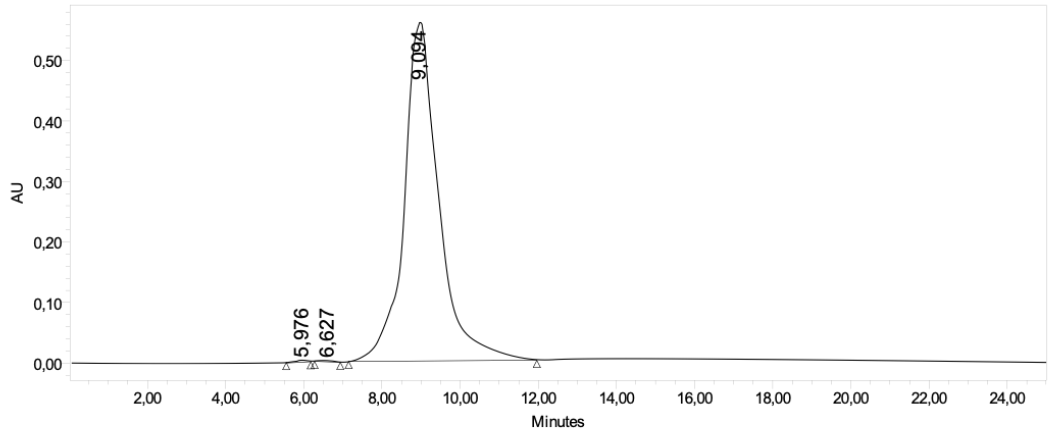

	RT (min)	Area (µV*sec)	% Area	Height (µV)
1	5,976	57365	0,13	2367
2	6,627	27869	0,06	1366
3	9,094	44924077	99,81	560062

SAMPLE INFORMATION			
Sample Name:	50	Acquired By:	Breeze
Sample Type:	Enantiomer B	Sample Set Name:	Halogenated
Vial:	1	Acq. Method:	10%HexiPAISOF25 set
Injection #:	3	Date Acquired:	05/11/2019 12:01:34 CET
Run Time:	25,00 Minutes	Injection Volume:	200,00 ul

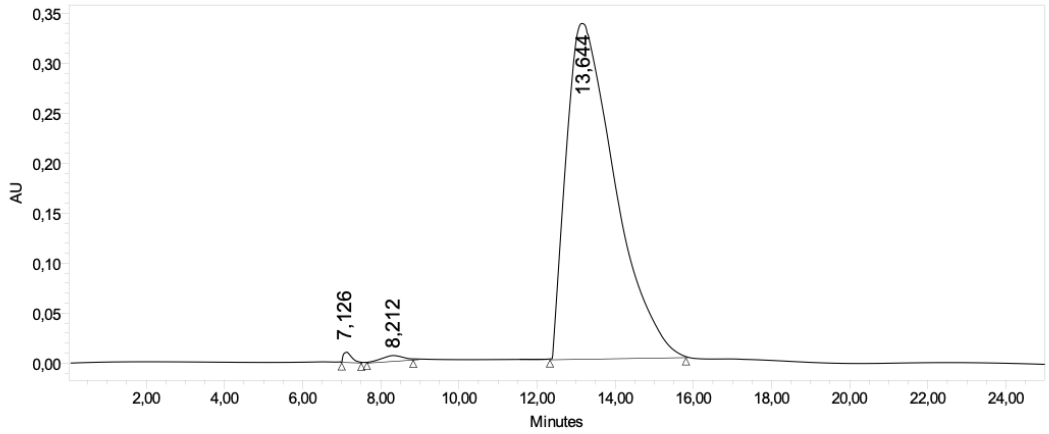

	RT (min)	Area (µV*sec)	% Area	Height (µV)
1	7,126	250627	0,77	8141
2	8,212	550257	1,31	11111
3	13,644	31887052	97,92	335299

SAMPLE INFORMATION			
Sample Name:	58	Acquired By:	Breeze
Sample Type:	Racemate	Sample Set Name:	Halogenated
Vial:	1	Acq. Method:	10%HexiPAISOF10 set
Injection #:	1	Date Acquired:	12/11/2019 10:15:13 CET
Run Time:	40,00 Minutes	Injection Volume:	200,00 ul

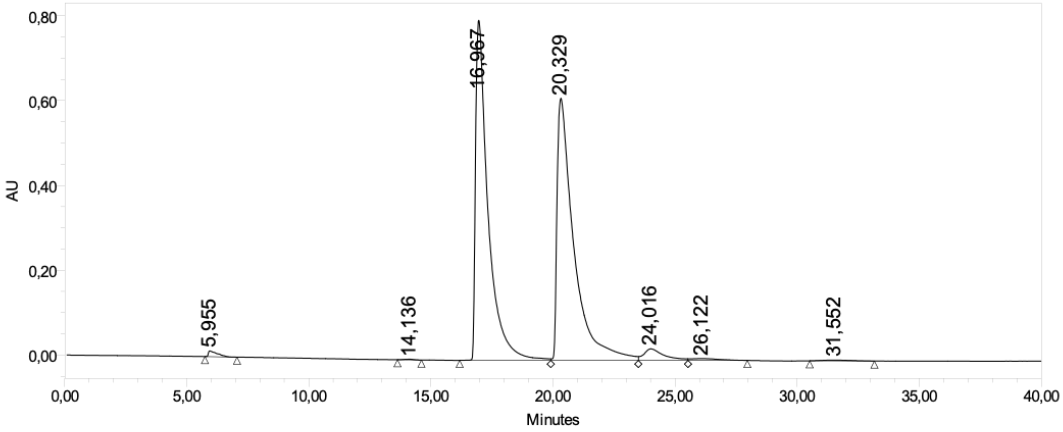

	RT (min)	Area (µV*sec)	% Area	Height (µV)
1	5,955	346793	0,57	13474
2	14,136	43149	0,07	1704
3	16,967	28522694	47,20	801999
4	20,329	29445809	48,73	617995
5	24,016	1563809	2,59	27390
6	26,122	363781	0,60	4388
7	31,552	143889	0,24	1784

SAMPLE INFORMATION

Sample Name:	58	Acquired By:	Breeze
Sample Type:	Enantiomer A	Sample Set Name:	Halogenated
Vial:	1	Acq. Method:	10%HexiPAISOF10 set
Injection #:	2	Date Acquired:	12/11/2019 11:08:15 CET
Run Time:	40,00 Minutes	Injection Volume:	200,00 ul

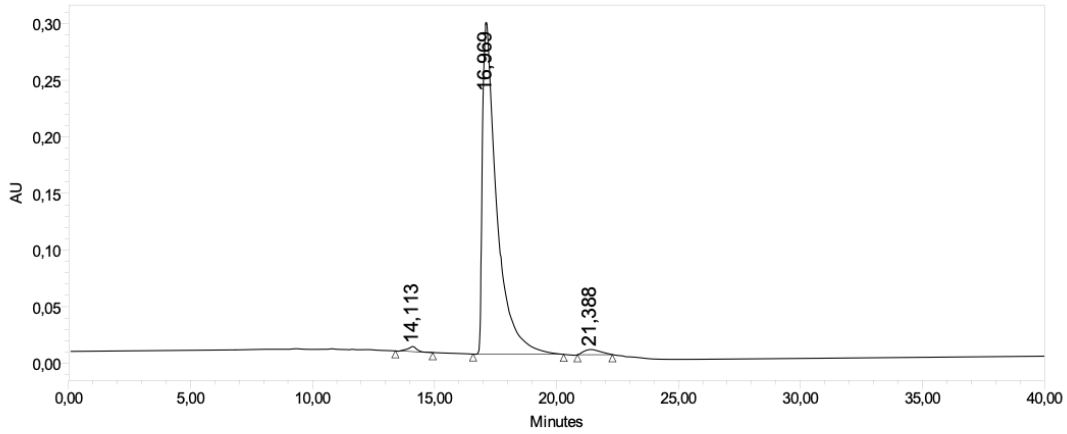

	RT (min)	Area (µV*sec)	% Area	Height (µV)
1	14,113	122523	1,00	4616
2	16,969	11913486	97,24	293326
3	21,388	215723	1,76	4720

SAMPLE INFORMATION			
Sample Name:	58	Acquired By:	Breeze
Sample Type:	Enantiomer B	Sample Set Name:	Halogenated
Vial:	1	Acq. Method:	10%HexiPAISOF10 set
Injection #:	3	Date Acquired:	12/11/2019 12:37:53 CET
Run Time:	40,00 Minutes	Injection Volume:	200,00 ul

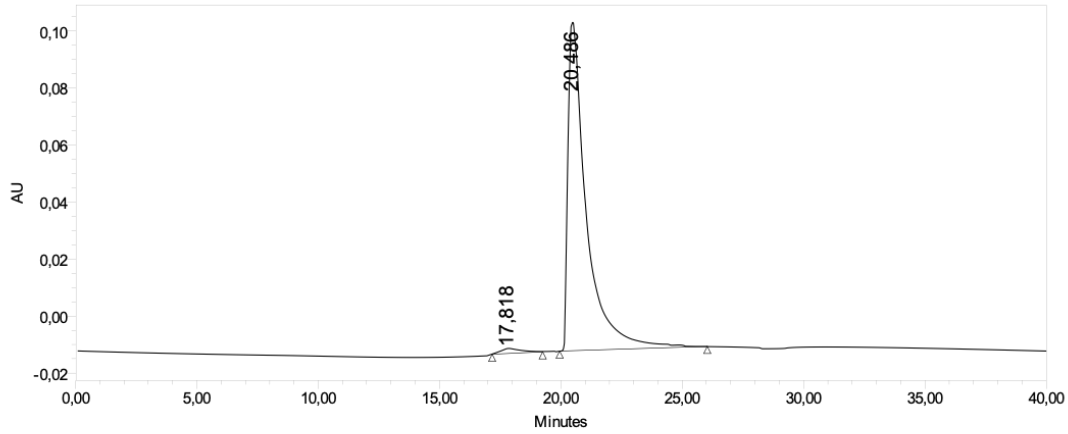

	RT (min)	Area (µV*sec)	% Area	Height (µV)
1	17,818	86535	1,39	1483
2	20,486	6124545	98,61	115233

SAMPLE INFORMATION

Sample Name:	60	Acquired By:	Breeze
Sample Type:	Racemate	Sample Set Name	
Vial:	1	Acq. Method:	20%HexiPAISOF10 set
Injection #:	1	Date Acquired:	22/03/2022 10:31:55 CET
Run Time:	30,00 Minutes	Injection Volume:	250,00 ul

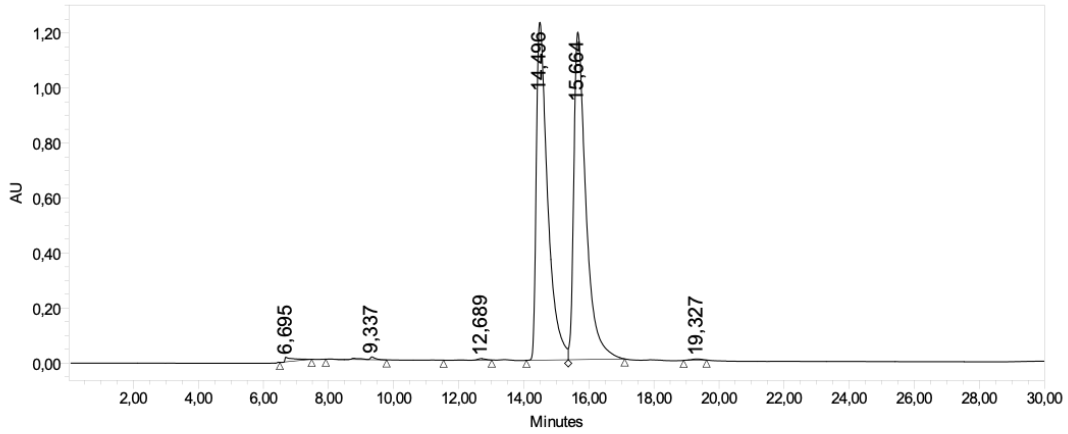

	RT (min)	Area (µV*sec)	% Area	Height (µV)
1	6,695	331828	0,54	17701
2	9,337	221427	0,36	10075
3	12,689	99422	0,16	5023
4	14,496	29629697	48,52	1228531
5	15,664	30685711	50,25	1190205
6	19,327	95227	0,16	4180

SAMPLE INFORMATION			
Sample Name:	60	Acquired By:	Breeze
Sample Type:	Enantiomer A	Sample Set Name	
Vial:	1	Acq. Method:	20%HexiPAISOF10 set
Injection #:	2	Date Acquired:	22/03/2022 11:17:56 CET
Run Time:	30,00 Minutes	Injection Volume:	250,00 ul

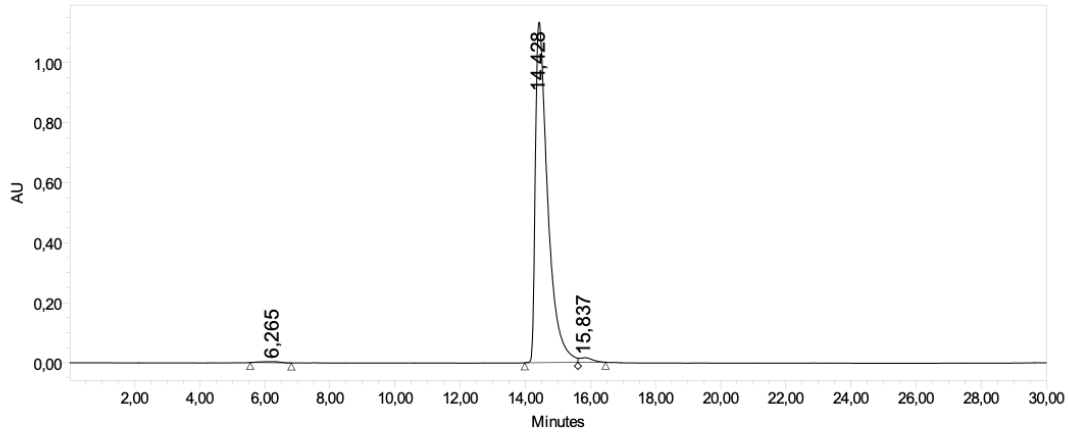

	RT (min)	Area (µV*sec)	% Area	Height (µV)
1	6,265	153541	0,51	3538
2	14,428	29751250	98,05	1135412
3	15,837	438757	1,45	15317

SAMPLE INFORMATION

Sample Name:	60	Acquired By:	Breeze
Sample Type:	Enantiomer B	Sample Set Name	
Vial:	1	Acq. Method:	20%HexiPAISOF10 set
Injection #:	3	Date Acquired:	22/03/2022 11:51:40 CET
Run Time:	30,00 Minutes	Injection Volume:	250,00 ul

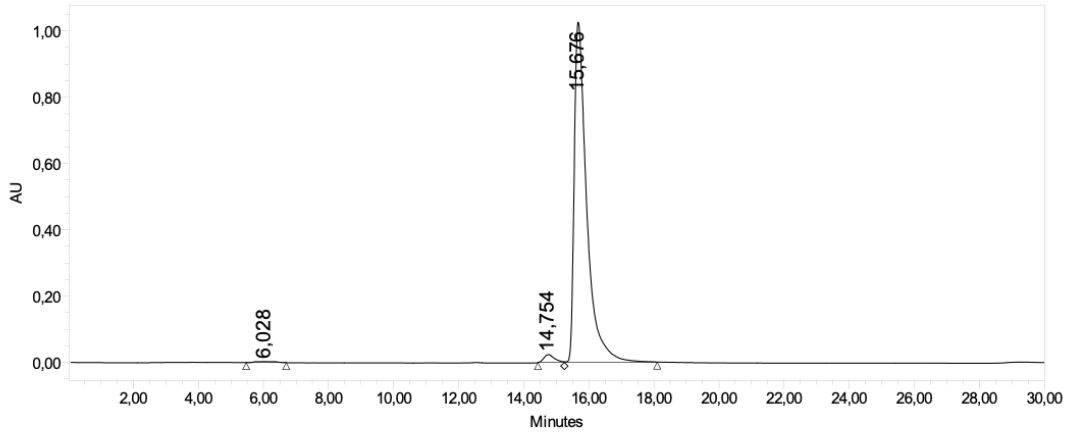

	RT (min)	Area (µV*sec)	% Area	Height (µV)
1	6,028	131923	0,47	3053
2	14,754	552450	1,98	23908
3	15,676	27279141	97,55	1027996

SAMPLE INFORMATION			
Sample Name:	66	Acquired By:	Breeze
Sample Type:	Racemate	Sample Set Name:	Rubén Prieto
Vial:	1	Acq. Method:	10%HexiPAISOF10 set
Injection #:	1	Date Acquired:	12/11/2019 16:12:28 CET
Run Time:	30,00 Minutes	Injection Volume:	200,00 ul

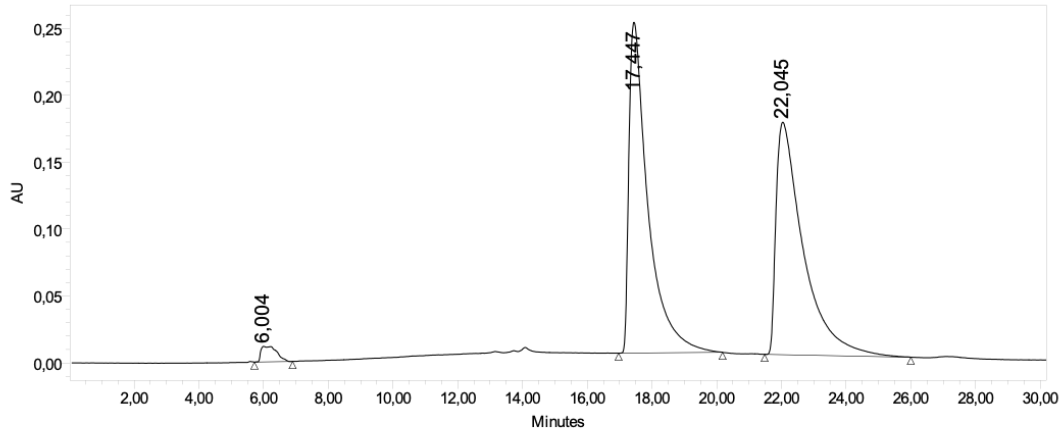

	RT (min)	Area (µV*sec)	% Area	Height (µV)
1	6,004	389275	1,88	11558
2	17,447	10137209	49,05	247407
3	22,045	10142524	49,07	173791

SAMPLE INFORMATION			
Sample Name:	66	Acquired By:	Breeze
Sample Type:	Enantiomer A	Sample Set Name:	Halogenated
Vial:	1	Acq. Method:	10%HexiPAISOF10 set
Injection #:	2	Date Acquired:	12/11/2019 16:43:55 CET
Run Time:	30,00 Minutes	Injection Volume:	200,00 ul

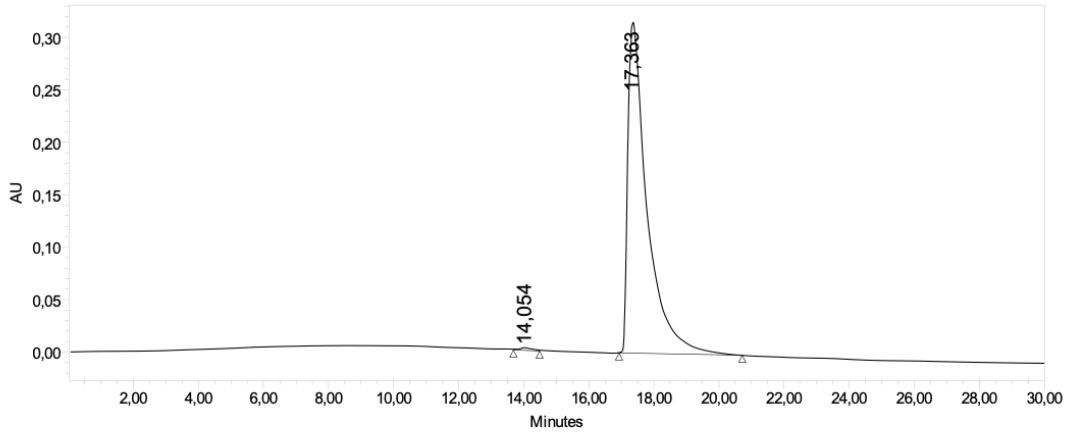

	RT (min)	Area (µV*sec)	% Area	Height (µV)
1	14,054	36505	0,28	2158
2	17,363	13014953	99,72	315685

SAMPLE INFORMATION			
Sample Name:	66	Acquired By:	Breeze
Sample Type:	Enantiomer B	Sample Set Name:	Halogenated
Vial:	1	Acq. Method:	10%HexiPAISOF10 set
Injection #:	3	Date Acquired:	12/11/2019 17:14:39 CET
Run Time:	30,00 Minutes	Injection Volume:	200,00 ul

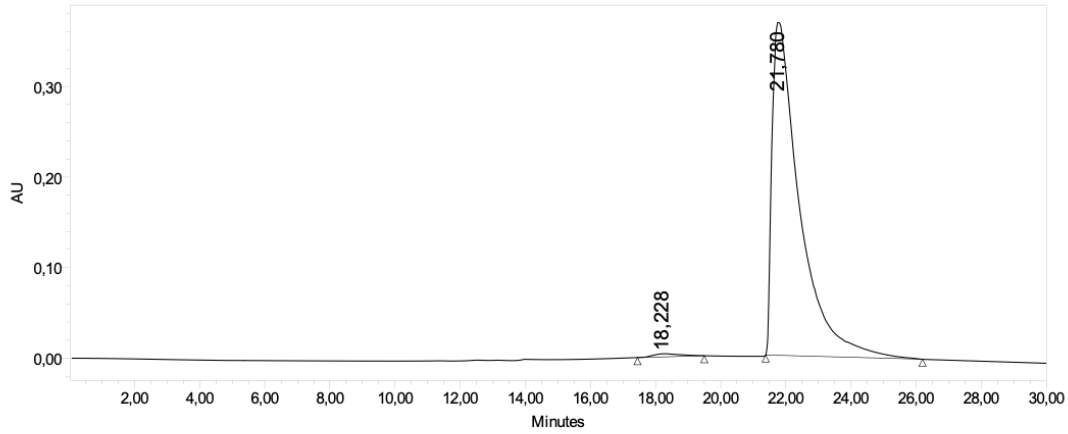

	RT (min)	Area (µV*sec)	% Area	Height (µV)
1	18,228	202867	0,93	3354
2	21,780	21518158	99,07	367510

SAMPLE INFORMATION

Sample Name:	67	Acquired By:	Breeze
Sample Type:	Racemate	Sample Set Name:	Halogenated
Vial:	1	Acq. Method:	20%HexiPAISOF10 set
Injection #:	1	Date Acquired:	13/11/2019 18:11:30 CET
Run Time:	60,00 Minutes	Injection Volume:	200,00 ul

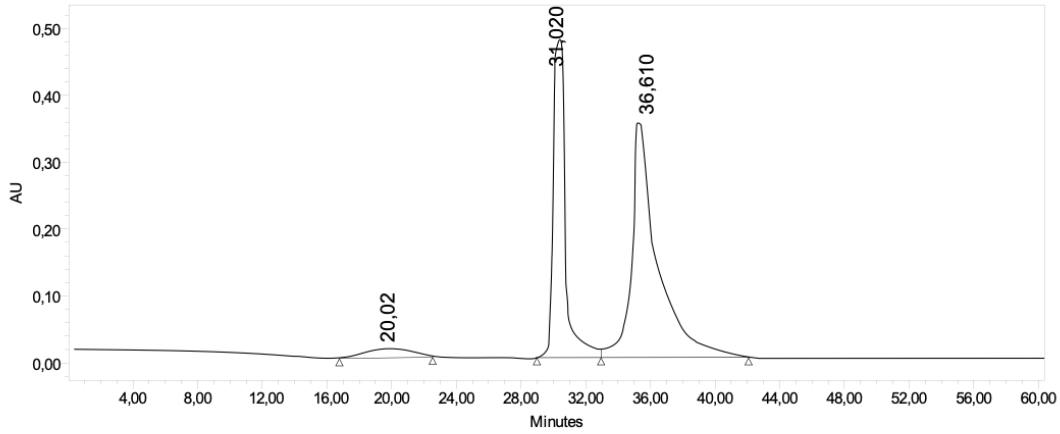

	RT (min)	Area (µV*sec)	% Area	Height (µV)
1	20,02	248921	1,20	23116
2	31,020	20274418	49,35	494814
3	36,610	20285048	49,45	347582

SAMPLE INFORMATION			
Sample Name:	67	Acquired By:	Breeze
Sample Type:	Enantiomer A	Sample Set Name:	Halogenated
Vial:	1	Acq. Method:	20%HexiPAISOF10 set
Injection #:	1	Date Acquired:	13/11/2019 19:15:22 CET
Run Time:	60,00 Minutes	Injection Volume:	200,00 ul

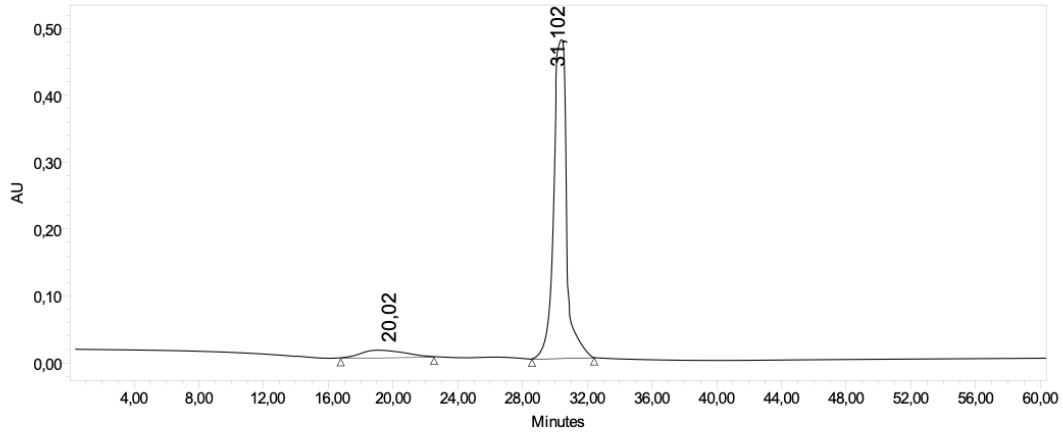

	RT (min)	Area (µV*sec)	% Area	Height (µV)
1	20,020	127111	0,44	1661
2	31,102	27819287	99,56	347811

SAMPLE INFORMATION

Sample Name:	67	Acquired By:	Breeze
Sample Type:	Enantiomer B	Sample Set Name:	Halogenated
Vial:	1	Acq. Method:	20%HexiPAISOF10 set
Injection #:	1	Date Acquired:	13/11/2019 20:11:11 CET
Run Time:	60,00 Minutes	Injection Volume:	200,00 ul

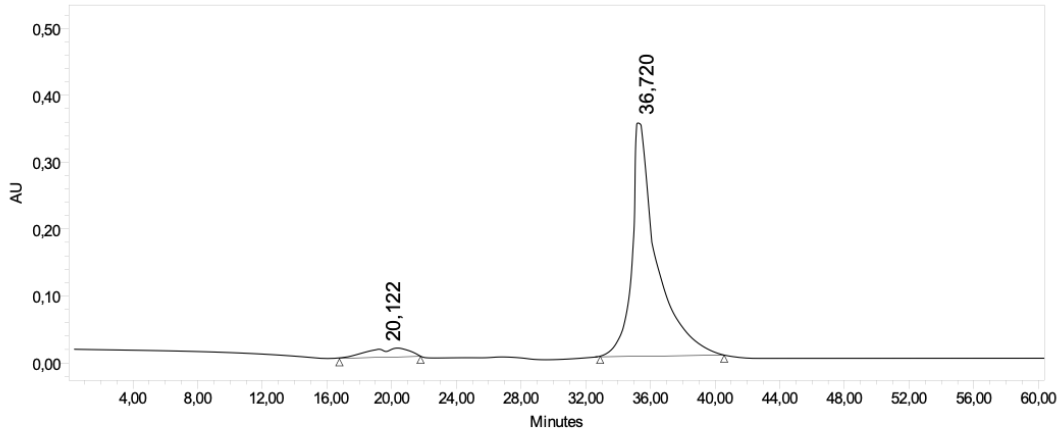

	RT (min)	Area (µV*sec)	% Area	Height (µV)
1	20,122	294666	1,02	3421
2	36,720	28594221	98,98	440192

SAMPLE INFORMATION			
Sample Name:	79	Acquired By:	Breeze
Sample Type:	Racemate	Sample Set Name	
Vial:	2	Acq. Method:	30%DCMiPAISOF10 set
Injection #:	5	Date Acquired:	18/01/2022 16:39:27 CET
Run Time:	12,00 Minutes	Injection Volume:	500,00 ul

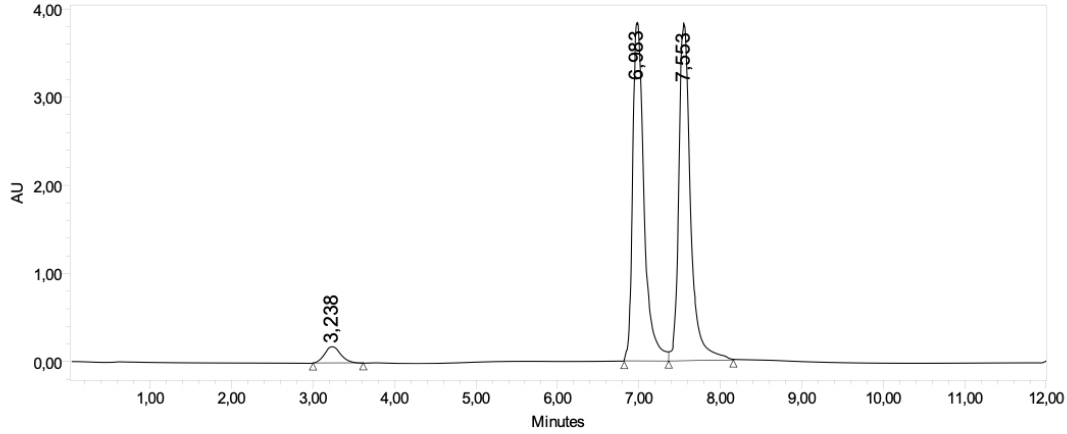

	RT (min)	Area (µV*sec)	% Area	Height (µV)
1	3,238	2470910	3,52	183100
2	6,983	33585027	47,89	3758787
3	7,553	34067111	48,58	3706311

SAMPLE INFORMATION			
Sample Name:	79	Acquired By:	Breeze
Sample Type:	Enantiomer A	Sample Set Name	
Vial:	1	Acq. Method:	30%DCMiPAISOF10 set
Injection #:	1	Date Acquired:	18/01/2022 10:25:33 CET
Run Time:	12,00 Minutes	Injection Volume:	500,00 ul

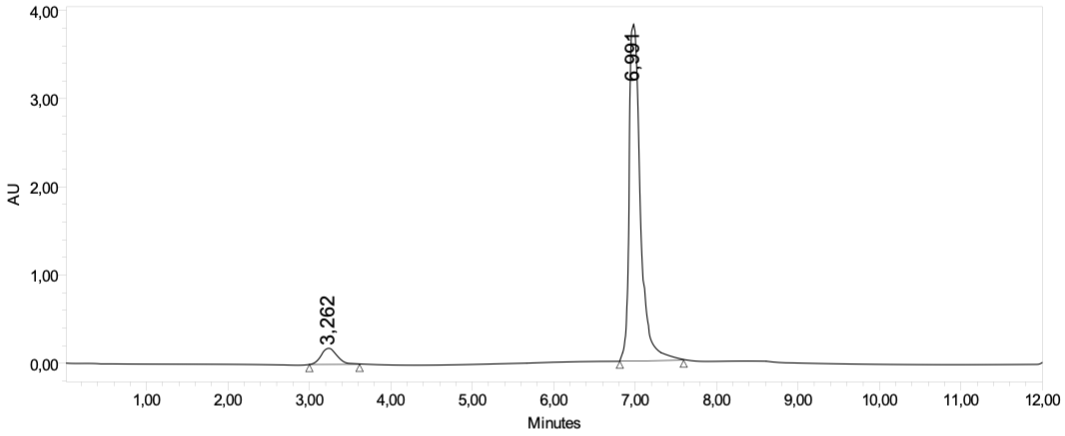

	RT (min)	Area (µV*sec)	% Area	Height (µV)
1	3,262	1254747	3,48	182982
2	6,991	34801190	96,52	3758562

SAMPLE INFORMATION			
Sample Name:	79	Acquired By:	Breeze
Sample Type:	Enantiomer B	Sample Set Name	
Vial:	3	Acq. Method:	30%DCMiPAISOF10 set
Injection #:	3	Date Acquired:	18/01/2022 11:22:21 CET
Run Time:	12,00 Minutes	Injection Volume:	500,00 ul

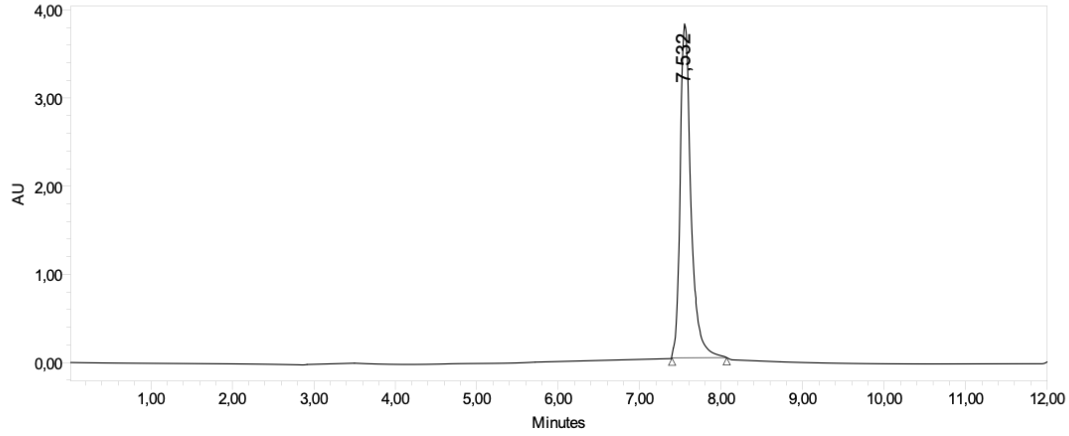

	RT (min)	Area (µV*sec)	% Area	Height (µV)
1	7,532	34801190	100,0	3824892

5.2.3.1 Spectroscopic and analytical data of enantiomers

(±) Isopropyl 4-(furan-2-yl)-2-methyl-1,4-dihydrobenzo[4,5]imidazo[1,2-*a*]pyrimidine-3-carboxylate [ISAM-140].[87] Purified by column chromatography (Hex–AcOEt 4:1 – 1:1). Mp 253 – 255 ºC. ^{1}H NMR (300 MHz, DMSO-d_6), δ (ppm): 10.78 (brs, 1H, NH), 7.67−7.23 (m, 3H, Ar-H), 7.19−6.84 (m, 2H, Ar-H), 6.52 (s, 1H, CH), 6.44 (d, J = 3.3 Hz, 1H, Ar-H), 6.37−6.23 (m, 1H, Ar-H), 4.86 (hept, J = 6.3 Hz, 1H, OC*H*(CH_3)$_2$), 2.44 (s, 3H, CH_3), 1.21 (d, J = 6.2 Hz, 3H, OC*H*(C*H*$_3$)$_2$), 1.05 (d, J = 6.1 Hz, 3H, OC*H*(C*H*$_3$)$_2$). ^{13}C NMR (75 MHz, DMSO-d_6), δ (ppm): 165.0, 153.3, 148.0, 146.0, 143.0, 142.6, 132.0, 122.3, 120.7, 117.2, 110.8, 110.2, 108.2, 94.9, 67.0, 49.7, 22.3, 22.0, 19.1. HRMS (ESI) m/z: calcd for $C_{19}H_{20}N_3O_3$ [M + H]$^+$: 338.1488; found: 338.7927.

Isopropyl (*R*)-4-(furan-2-yl)-2-methyl-1,4-dihydrobenzo[4,5]imidazo[1,2-*a*]pyrimidine-3-carboxylate [(*R*)-ISAM-140]. Chiral separation with a 250 mm x 20 mm Chiralpak® 5µm IE-3 (DAICEL) (isocratic mobile phase Hex–IPA 7:3) to give an enantiomeric excess of >99%. Mp 254 – 256 ºC. ^{1}H NMR (300 MHz, DMSO-d_6), δ (ppm): 10.76 (brs, 1H, NH), 7.41 (d, J = 11.0 Hz, 2H, Ar-H), 7.34 (d, J = 7.7 Hz, 1H, Ar-H), 7.04 (dt, J = 18.2, 7.0 Hz, 2H, Ar-H), 6.52 (s, 1H, CH), 6.44 (d, J = 3.3 Hz, 1H, Ar-H), 6.35 – 6.27 (m, 1H, Ar-H), 4.87 (p, J = 6.3 Hz, 1H, OC*H*(CH_3)$_2$), 2.44 (s, 3H, CH_3), 1.21 (d, J = 6.3 Hz, 3H, OC*H*(C*H*$_3$)$_2$), 1.05 (d, J = 6.4 Hz, 3H, OC*H*(C*H*$_3$)$_2$). ^{13}C NMR (75 MHz, DMSO-d_6), δ (ppm): 165.0, 153.3, 148.0, 146.0, 143.1, 142.6, 132.0, 122.3, 121.0, 117.2, 110.8, 110.2, 108.7, 95.0, 67.0, 49.7, 22.3, 22.1, 19.1. HRMS (APCI) *m/z* calcd for $C_{19}H_{19}N_3O_3$ [M+H]$^+$: 338.1499; found: 338.1501.

Isopropyl (*S*)-4-(furan-2-yl)-2-methyl-1,4-dihydrobenzo[4,5]imidazo[1,2-*a*]pyrimidine-3-carboxylate [(*S*)-ISAM-140]. Chiral separation with a 250 mm x 20 mm Chiralpak® 5µm IE-3 (DAICEL) (isocratic mobile phase Hex–IPA 7:3) to give an enantiomeric excess of >99%. Mp 254 – 256 ºC. ^{1}H NMR (300 MHz, DMSO-d_6), δ (ppm): 10.78 (brs, 1H, NH), 7.42 (d, J = 10.8 Hz, 2H, Ar-H), 7.35 (d, J = 7.8 Hz, 1H, Ar-H), 7.04 (dt, J = 18.2, 7.0 Hz, 2H, Ar-H), 6.52 (s, 1H, CH), 6.44 (d, J = 3.3 Hz, 1H, Ar-H), 6.40 – 6.26 (m, 1H, Ar-H), 4.87 (p, J = 6.3 Hz, 1H, OC*H*(CH_3)$_2$), 2.44 (s, 3H, CH_3), 1.21 (d, J = 6.3 Hz, 3H, OC*H*(C*H*$_3$)$_2$), 1.05 (d, J = 6.4 Hz, 3H, OC*H*(C*H*$_3$)$_2$). ^{13}C NMR (75 MHz, DMSO-d_6), δ (ppm): 165.0, 153.3, 148.0, 146.0, 143.0, 142.6, 132.0, 122.3, 120.7, 117.5, 110.8, 110.3, 108.4, 94.9, 67.0, 49.7, 22.3, 22.2, 19.0. HRMS (APCI) *m/z* calcd for $C_{19}H_{19}N_3O_3$ [M+H]$^+$: 338.1499; found: 338.1501.

(±) Isopropyl 8-fluoro-4-(furan-2-yl)-2-methyl-1,4-dihydrobenzo[4,5]imidazo[1,2-*a*]pyrimidine-3-carboxylate (50). Purified by column chromatography (Hex–AcOEt 3:1 – 1:2). Yield: 19%. Mp: 242 – 243 ºC. ^{1}H NMR (300 MHz, DMSO-d_6), δ (ppm): 10.77 (brs, 1H, NH), 7.44 (s, 1H, Ar-H), 7.34 – 7.28 (m, 2H, Ar-H), 6.93 – 6.86 (m, 1H, Ar-H), 6.53 – 6.49 (m, 1H, Ar-H), 6.35 – 6.32 (m, 1H, Ar-H), 6.20 (s, 1H, CH), 4.88 – 4.84 (m, 1H, OC*H*$(CH_3)_2$), 2.42 (s, 3H, CH_3), 1.20 (d, J = 6.0 Hz, 3H, OCH(C*H*$_3)_2$), 1.04 (d, J = 6.0 Hz, 3H, OCH(C*H*$_3)_2$). ^{13}C NMR (75 MHz, DMSO-d_6), δ (ppm): 166.6, 160.7, 159.0, 153.1, 148.7, 142.8, 142.6, 132.2, 114.2, 113.1, 110.2, 109.5, 102.7, 97.1, 68.3, 54.8, 21.9, 19.2. HRMS (APCI) *m/z*: calcd for $C_{19}H_{19}FN_3O_3$ $[M+H]^+$, 356.1332; found: 356.1343.

Isopropyl (*R*)-8-fluoro-4-(furan-2-yl)-2-methyl-1,4-dihydrobenzo[4,5]imidazo[1,2-a]pyrimidine-3-carboxylate [(*R*)-50]. Chiral separation with a 250 mm x 10 mm Lux® 5 µm Amylose-2 (Phenomenex) (isocratic mobile phase Hex–IPA 9:1) to give an enantiomeric excess of >99%. ^{1}H NMR (300 MHz, $CDCl_3$), δ (ppm): 7.39 (dd, J = 8.8, 4.5 Hz, 1H, Ar-H), 7.35 – 7.26 (m, 2H, Ar-H), 7.19 (dd, J = 8.7, 2.2 Hz, 1H, Ar-H), 7.04 – 6.92 (m, 1H, Ar-H), 6.50 (s, 1H, CH), 6.35 – 6.20 (m, 2H, Ar-H), 5.06 (p, J = 6.3 Hz, 1H, OC*H*$(CH_3)_2$), 2.69 (s, 3H, CH_3), 1.29 (d, J = 6.3 Hz, 3H, OCH(C*H*$_3)_2$), 1.13 (d, J = 6.3 Hz, 3H, OCH(C*H*$_3)_2$).

Isopropyl (*S*)-8-fluoro-4-(furan-2-yl)-2-methyl-1,4-dihydrobenzo[4,5]imidazo[1,2-*a*]pyrimidine-3-carboxylate [(*S*)-50]. Chiral separation with a 250 mm x 10 mm Lux® 5 µm Amylose-2 (Phenomenex) (isocratic mobile phase Hex–IPA 9:1) to give an enantiomeric excess of 97%. ^{1}H NMR (300 MHz, $CDCl_3$), δ (ppm): 7.44 – 7.35 (m, 1H, Ar-H), 7.30 – 7.23 (m, 1H, Ar-H), 7.19 (d, J = 8.4 Hz, 1H, Ar-H), 7.04 – 6.92 (m, 1H, Ar-H), 6.50 (s, 1H, CH), 6.29 (m, 2H, Ar-H), 5.10 – 5.01 (m, 1H, OC*H*$(CH_3)_2$), 2.70 (s, 3H, CH_3), 1.19 – 1.09 (m, 3H, CH_3, OCH(C*H*$_3)_2$), 1.11 (d, J = 1.7 Hz, 3H, OCH(C*H*$_3)_2$).

(±) Isopropyl 8-chloro-4-(furan-2-yl)-2-methyl-1,4-dihydrobenzo[4,5]imidazo[1,2-*a*]pyrimidine-3-carboxylate (58). Purified by column chromatography (Hex–AcOEt 3:1 – 1:1). Yield: 21%. Mp: 252 – 253 ºC. ^{1}H NMR (300 MHz, DMSO-d_6), δ (ppm): 10.90 (brs, 1H, NH), 7.45 – 7.32 (m, 2H, Ar-H), 7.06 – 7.02 (m, 1H, Ar-H), 6.55 (s, 1H, Ar-H), 6.45 (s, 1H, Ar-H), 6.33 (s, 1H, Ar-H), 5.74 (s, 1H, CH), 4.92 – 4.87 (m, 1H, OC*H*$(CH_3)_2$), 2.44 (s, 3H, CH_3), 1.21 (d, J = 6.3 Hz, 3H, OCH(C*H*$_3)_2$), 1.05 (d, J = 6.0 Hz, 3H, OCH(C*H*$_3)_2$). ^{13}C NMR (75 MHz, $CDCl_3$), δ (ppm): 165.0, 152.9, 147.0, 146.9, 142.3, 139.7, 132.3, 126.6, 123.1, 116.9, 110.4, 110.1, 107.9, 96.1, 67.5, 50.1, 22.1, 21.7, 19.2. HRMS (APCI) *m/z* calcd for $C_{19}H_{19}ClN_3O_3$ $[M+H]^+$: 372.1037; found: 372.1042.

Isopropyl (*R*)-8-chloro-4-(furan-2-yl)-2-methyl-1,4-dihydrobenzo[4,5]imidazo[1,2-*a*]pyrimidine-3-carboxylate [(*R*)-58]. Chiral separation with a 250 mm x 20 mm Chiralpak® 5µm IE-3 (DAICEL) (isocratic mobile phase Hex–IPA 9:1) to give an enantiomeric excess of 97%. ^{1}H NMR (300 MHz, DMSO-d_6), δ (ppm): 7.47 – 7.33 (m, 2H, Ar-H), 7.31 – 7.23 (m, 1H, Ar-H), 7.21 – 7.14 (m, 1H, Ar-H), 6.49 (s, 1H, CH), 6.33 – 6.23 (m, 2H, Ar-H), 5.06 (qd, J = 6.5, 5.7 Hz, 1H, OC*H*$(CH_3)_2$), 2.70 (s, 3H, CH_3), 1.32 – 1.26 (m, 3H OCH(C*H*$_3)_2$), 1.13 (d, J = 6.3, 3H, OCH(C*H*$_3)_2$).

Isopropyl (*S*)-*8*-chloro-4-(furan-2-yl)-2-methyl-1,4-dihydrobenzo[4,5]imidazo[1,2-*a*]pyrimidine-3-carboxylate [(*S*)-58]. Chiral separation with a 250 mm x 20 mm Chiralpak® 5µm IE-3 (DAICEL) (isocratic mobile phase Hex–IPA 9:1) to give an enantiomeric excess of 98%. ^{1}H NMR (300 MHz, $CDCl_3$), δ (ppm): 7.57 – 7.44 (m, 2H, Ar-H), 7.42 – 7.32 (m, 2H, Ar-H), 6.55 (s, 1H, Ar-H), 6.39 (s, 1H, Ar-H), 6.33 (s, 1H, Ar-H), 5.12 – 5.02 (m, 1H, OC*H*$(CH_3)_2$), 2.66 (s, 3H, CH_3), 1.33 – 1.20 (m, 3H, OCH(C*H*$_3)_2$), 1.15 (d, J = 6.7 Hz, 3H, OCH(C*H*$_3)_2$).

(±) Isopropyl 8-chloro-4-(furan-3-yl)-2-methyl-1,4-dihydrobenzo[4,5]imidazo[1,2-*a*]pyrimidine-3-carboxylate (60). Purified by column chromatography (Hex–AcOEt 3:1 – 1:1). Yield: 17%. Mp: 256 – 258 ºC. ^{1}H NMR (300 MHz, $CDCl_3$), δ (ppm): 11.95 (brs, 1H, NH), 7.48 (s, 1H, Ar-H), 7.38 (s, 1H, Ar-H), 7.25 (s, 1H, Ar-H), 7.21 – 7.06 (m, 2H, Ar-H), 6.52 (s, 1H, CH), 6.11 (s, 1H, Ar-H), 5.11 – 5.05 (m, 1H, OC*H*$(CH_3)_2$), 2.70 (s, 3H, CH_3), 1.35 (d, J = 6.1 Hz, 3H, OCH(C*H*$_3)_2$), 1.31 (d, J = 6.0 Hz, 3H, OCH(C*H*$_3)_2$). ^{13}C NMR (75 MHz, $CDCl_3$), δ (ppm): 165.3, 147.8, 145.6, 142.3, 141.7, 130.3, 128.2, 126.4, 126.1, 122.7, 121.3, 116.3, 110.2, 99.4, 67.8, 52.1, 21.9, 19.5. HRMS (APCI) *m/z* calcd. for $C_{19}H_{19}ClN_3O_3$ $[M+H]^+$: 372.1109; found: 372.1111.

Isopropyl (*S*)-8-chloro-4-(furan-3-yl)-2-methyl-1,4-dihydrobenzo[4,5]imidazo[1,2-*a*]pyrimidine-3-carboxylate [(*S*)-60]. Chiral separation with a 250 mm x 20 mm Chiralpak® 5µm IE-3 (DAICEL) (isocratic mobile phase Hex–IPA 9:1) to give an enantiomeric excess of 98%. ^{1}H NMR (300 MHz, $CDCl_3$), δ (ppm): 11.90 (brs, 1H, NH), 7.49 (s, 1H, Ar-H), 7.39 (s, 1H, Ar-H), 7.31 (s, 1H, Ar-H), 7.24 – 7.02 (m, 2H, Ar-H), 6.59 (s, 1H, CH), 6.15 (s, 1H, Ar-H), 5.11 – 5.05 (m, 1H, OC*H*$(CH_3)_2$), 2.70 (s, 3H, CH_3), 1.35 (d, J = 6.1 Hz, 3H, OCH(C*H*$_3)_2$), 1.31 (d, J = 6.0 Hz, 3H, OCH(C*H*$_3)_2$).

Isopropyl (*R*)-8-chloro-4-(furan-3-yl)-2-methyl-1,4-dihydrobenzo[4,5]imidazo[1,2-a]pyrimidine-3-carboxylate [(*R*)-60]. Chiral separation with a 250 mm x 20 mm Chiralpak® 5µm IE-3 (DAICEL) (isocratic mobile phase Hex–IPA 9:1) to give an enantiomeric excess of 97%. ^{1}H NMR (300 MHz, $CDCl_3$), δ (ppm): 11.91 (brs, 1H, NH), 7.48 (s, 1H, Ar-H), 7.33 (s, 1H, Ar-H), 7.22 (s, 1H, Ar-H), 7.21 – 7.06 (m, 2H, Ar-H), 6.52 (s, 1H, CH), 6.09 (s, 1H, Ar-H), 5.11 – 5.04 (m, 1H, OC*H*$(CH_3)_2$), 2.69 (s, 3H, CH_3), 1.35 (d, J = 6.1 Hz, 3H, OCH(C*H*$_3)_2$), 1.31 (d, J = 6.0 Hz, 3H, OCH(C*H*$_3)_2$).

(±) Isopropyl 8-bromo-4-(furan-2-yl)-2-methyl-1,4-dihydrobenzo[4,5]imidazo[1,2-*a*]pyrimidine-3-carboxylate (66). Purified by column chromatography (Hex–AcOEt 2:1 – 1:2). Yield: 22%. Mp: 245 – 247 ºC. ^{1}H NMR (300 MHz, $CDCl_3$), δ (ppm): 11.35 (brs, 1H, NH), 7.42 (s, 1H, Ar-H), 7.32 – 7.10 (m, 3H, Ar-H), 6.49 (s, 1H, CH), 6.13 – 6.08 (m, 2H, Ar-H), 5.11 – 4.98 (m, 1H, OC*H*$(CH_3)_2$), 2.69 (s, 3H, CH_3), 1.25 (d, J = 6.0 Hz, 3H, OCH(C*H*$_3)_2$), 1.12 (d, J = 6.1 Hz, 3H, OCH(C*H*$_3)_2$). ^{13}C NMR (75 MHz, $CDCl_3$), δ (ppm): 165.0, 152.8, 147.2, 146.9, 142.3, 140.0, 132.7, 125.9, 117.3, 113.8, 112.9, 110.4, 107.9, 96.1, 67.5, 50.1, 22.1, 21.7, 19.2. HRMS (APCI) *m/z* calcd for $C_{19}H_{19}BrN_3O_3$ $[M+H]^+$: 416,0618; found: 416.0605.

Isopropyl (*R*)-8-bromo-4-(furan-2-yl)-2-methyl-1,4-dihydrobenzo[4,5]imidazo[1,2-*a*]pyrimidine-3-carboxylate [(*R*)-66]. Chiral separation with a 250 mm x 20 mm Chiralpak® 5µm IE-3 (DAICEL) (isocratic mobile phase Hex–IPA 9:1) to give an enantiomeric excess of >99%. ^{1}H NMR (300 MHz, $CDCl_3$), δ (ppm): 11.35 (brs, 1H, NH), 7.41 (s, 1H, Ar-H), 7.33 – 7.11 (m, 3H, Ar-H), 6.50 (s, 1H, CH), 6.13 – 6.08 (m, 2H, Ar-H), 5.11 – 4.98 (m, 1H, OC*H*$(CH_3)_2$), 2.69 (s, 3H, CH_3), 1.25 (d, J = 6.2 Hz, 3H, OCH(C*H*$_3)_2$), 1.12 (d, J = 6.2 Hz, 3H, OCH(C*H*$_3)_2$).

Isopropyl (*S*)-*8*-bromo-4-(furan-2-yl)-2-methyl-1,4-dihydrobenzo[4,5]imidazo[1,2-*a*]pyrimidine-3-carboxylate [(*S*)-66]. Chiral separation with a 250 mm x 20 mm Chiralpak® 5µm IE-3 (DAICEL) (isocratic mobile phase Hex–IPA 9:1) to give an enantiomeric excess of >99%. ^{1}H NMR (300 MHz, $CDCl_3$), δ (ppm): 11.35 (brs, 1H, NH), 7.42 (s, 1H, Ar-H), 7.32 – 7.10 (m, 3H, Ar-H), 6.50 (s, 1H, CH), 6.13 – 6.08 (m, 2H, Ar-H), 5.11 – 4.98 (m, 1H, OC*H*$(CH_3)_2$), 2.69 (s, 3H, CH_3), 1.25 (d, J = 6.2 Hz, 3H, OCH(C*H*$_3)_2$), 1.12 (d, J = 6.0 Hz, 3H, OCH(C*H*$_3)_2$).

(±) Ethyl 8-bromo-4-(furan-3-yl)-2-methyl-1,4-dihydrobenzo[4,5]imidazo[1,2-*a*]pyrimidine-3-carboxylate (67). Purified by column chromatography (Hex–AcOEt 2:1 – 1:2). Yield: 21%. Mp: 228 – 230 ºC. ^{1}H NMR (750 MHz, DMSO-d_6), δ (ppm): 10.9 (s, 1H, NH), 7.53 (d, J = 1.9 Hz, 1H, H-9), 7.45 (dd, J = 1.8, 0.9 Hz, 1H), 7.41 (d, J = 8.4 Hz, 1H, H-6), 7.17 (dd, J = 8.4, 1.9 Hz, 1H, H-7), 6.60 (d, J = 0.8 Hz, 1H, CH), 6.46 (dd, J = 3.3, 0.9 Hz, 1H, Ar-H), 6.33 (dd, J = 3.3, 1.8 Hz, 1H, Ar-H), 4.10 (dq, J = 10.9, 7.1 Hz, 1H, OCH_2CH$_3$), 4.03 (dq, J = 10.9, 7.1 Hz, 1H, OCH_2CH$_3$), 2.45 (d, J = 0.7 Hz, 3H, CH$_3$), 1.16 (t, J = 7.1 Hz, 3H, OCH$_2$CH_3). ^{13}C NMR (126 MHz, CDCl$_3$), δ (ppm): 165.7, 147.4, 145.7, 143.8, 139.8, 131.7, 130.5, 125.4, 124.4, 119.6, 115.9, 110.8, 108.8, 99.2, 60.6, 48.6, 19.8, 14.5. HRMS (APCI) *m/z* calcd for $C_{18}H_{17}BrN_3O_3$ $[M+H]^+$: 402.0375; found: 402.0382.

Ethyl (*S*)-8-bromo-4-(furan-3-yl)-2-methyl-1,4-dihydrobenzo[4,5]imidazo[1,2-*a*]pyrimidine-3-carboxylate [(*S*)-67]. Chiral separation with a 250 mm x 20 mm Chiralpak® 5µm IE-3 (DAICEL) (isocratic mobile phase Hex–IPA 4:1) to give an enantiomeric excess of >99%. ^{1}H NMR (300 MHz, CDCl$_3$), δ (ppm): 11.60 (brs, 1H, NH), 7.62 (s, 1H, Ar-H), 7.36 (s, 1H, Ar-H), 7.29 – 7.09 (m, 2H, Ar-H), 7.06 – 6.98 (m, 1H, Ar-H), 6.50 (s, 1H, CH), 6.15 (s, 1H, Ar-H), 4.26 – 4.08 (m, 2H, OCH_2CH$_3$), 2.62 (s, 3H, CH$_3$), 1.31 (t, J = 7.1 Hz, 3H, OCH$_2$CH_3).

Ethyl (*R*)-8-bromo-4-(furan-3-yl)-2-methyl-1,4-dihydrobenzo[4,5]imidazo[1,2-*a*]pyrimidine-3-carboxylate [(*R*)-67]. Chiral separation with a 250 mm x 20 mm Chiralpak® 5µm IE-3 (DAICEL) (isocratic mobile phase Hex–IPA 4:1) to give an enantiomeric excess of 98%. ^{1}H NMR (300 MHz, CDCl$_3$), δ (ppm): 11.61 (brs, 1H, NH), 7.60 (s, 1H, Ar-H), 7.38 (s, 1H, Ar-H), 7.30 – 7.10 (m, 2H, Ar-H), 7.06 – 7.00 (m, 1H, Ar-H), 6.50 (s, 1H, CH), 6.15 (s, 1H, Ar-H), 4.31 – 4.04 (m, 2H, OCH_2CH$_3$), 2.62 (s, 3H, CH$_3$), 1.31 (t, J = 7.2 Hz, 3H, OCH$_2$CH_3). HRMS (APCI) *m/z* calcd for $C_{18}H_{17}BrN_3O_3$ $[M+H]^+$: 402.0375; found: 402.0402.

(±) Ethyl 8-chloro-2-methyl-4-(oxazol-4-yl)-1,4-dihydrobenzo[4,5]imidazo[1,2-*a*]pyrimidine-3-carboxylate (79). Purified by column chromatography (Hex–AcOEt 1:1). Yield: 11%. Mp: 250 – 252 ºC. ^{1}H NMR (300 MHz, $CDCl_3$), δ (ppm): 7.79 – 7.68 (m, 2H, Ar-H), 7.49 (d, J = 8.1 Hz, 1H, Ar-H), 7.44 – 7.23 (m, 1H, Ar-H), 7.12 (d, J = 8.1 Hz, 1H, Ar-H), 6.57 (s, 1H, CH), 4.24 (q, J = 7.1 Hz, 2H, OC*H*$_2$CH$_3$), 2.72 (s, 3H, CH_3), 1.33 (t, J = 7.1 Hz, 3H, OCH$_2$C*H*$_3$). HRMS (APCI) *m/z*: calcd for $C_{17}H_{15}ClN_4O_3$ $[M+H]^+$: 359.0833; found: 359.0833.

Ethyl (*R*)-8-chloro-2-methyl-4-(oxazol-4-yl)-1,4-dihydrobenzo[4,5]imidazo[1,2-*a*]pyrimidine-3-carboxylate [(*R*)-79]. Chiral separation with a 250 mm x 20 mm Chiralpak® 5µm IE-3 (DAICEL) (isocratic mobile phase DCM–IPA 7:3) to give an enantiomeric excess of >99%. ^{1}H NMR (300 MHz, $CDCl_3$), δ (ppm): 7.80 – 7.68 (m, 2H, Ar-H), 7.48 (d, J = 8.1 Hz, 1H, Ar-H), 7.40 – 7.23 (m, 1H, Ar-H), 7.12 (d, J = 8.1 Hz, 1H, Ar-H), 6.56 (s, 1H, CH), 4.23 (q, J = 7.1 Hz, 2H, OC*H*$_2$CH$_3$), 2.73 (s, 3H, CH_3), 1.32 (t, J = 7.1 Hz, 3H, OCH$_2$C*H*$_3$).

Ethyl (*S*)-8-chloro-2-methyl-4-(oxazol-4-yl)-1,4-dihydrobenzo[4,5]imidazo[1,2-*a*]pyrimidine-3-carboxylate [(*S*)-79]. Chiral separation with a 250 mm x 20 mm Chiralpak® 5µm IE-3 (DAICEL) (isocratic mobile phase DCM–IPA 7:3) to give an enantiomeric excess of >99%. ^{1}H NMR (300 MHz, $CDCl_3$), δ (ppm): 7.80 – 7.71 (m, 2H, Ar-H), 7.48 (d, J = 8.0 Hz, 1H, Ar-H), 7.42 – 7.21 (m, 1H, Ar-H), 7.12 (d, J = 8.0 Hz, 1H, Ar-H), 6.51 (s, 1H, CH), 4.24 (q, J = 7.2 Hz, 2H, OC*H*$_2$CH$_3$), 2.73 (s, 3H, CH_3), 1.35 (t, J = 7.2 Hz, 3H, OCH$_2$C*H*$_3$).

5.2.4 X-ray crystallography of ISAM-140 and of the 67 enantiomers

Crystals were grown by slow evaporation from ethanol [**(*S*)-ISAM-140** and **(*R*)-ISAM-140**] or isopropanol [**(*S*)-67** and **(*R*)-67**] solutions. For the crystal structure determination, the data were collected by applying the omega and phi scans method on a Bruker D8 VENTURE PHOTON III-14 diffractometer using Incoatec multilayer mirror monochromated with Cu-Kα radiation (λ = 1.54178 Å) from a microfocus sealed tube source at 100 K with detector resolution of 7.3910 pixels mm^{-1}. Computing data and reduction were made with the APEX3 v2018.7-2 (BRUKER AXS, 2005). The structure was solved using SHELXT2018/22 and finally refined by full-matrix least-squares based on F2 by SHELXL2018/3.3 An empirical absorption correction was applied using the SADABS2016/2 program. Software used to molecular graphics: ORTEP for Windows. Software used to prepare material for publication: WinGX2018.3 publication routines4 and Mercury.

Detailed crystallographic data for ligands **(*S*)-ISAM-140**, **(*R*)-ISAM-140**, **(*S*)-67** and **(*R*)-67** have been deposited at the Cambridge Crystallographic Data Centre (deposition number CCDC: 1966450, 1966312, 2047365, 2048281 respectively) and are available on request. All non-hydrogen atoms were refined anisotropically, and the hydrogen atom positions were included in the model based on Fourier difference electron density maps. All aromatic CH hydrogen (C-H = 0.95 Å), methine hydrogen (C-H = 1.0 Å) and methylene hydrogen (C-H=0.99 Å) atoms were refined using a riding model with Uiso(H) = 1.2 UeqI. The methyl hydrogen (C-H = 0.98 Å) atoms were refined as a rigid group with torsional freedom [Uiso(H) = 1.5 UeqI] and the hydrogens atom of NH groups (HiN) as a free atom with Uiso(H) = 1.2 UeqI. Details of the experiment are shown in Table 5.1 for **ISAM-140** and Table 5.2 for **67** enantiomers.

Table 5.1. Details of the X-ray experiment of **ISAM-140** enantiomers.

Crystal data	(***R***)-ISAM-140	(***S***)-ISAM-140
CCDC	1966312	1966450
Chemical formula	$C_{19}H_{19}N_3O_3$	$C_{19}H_{19}N_3O_3$
M_r	337.37	337.37
Crystal system	Monoclinic	Monoclinic
Space group	C2	C2
Temperature (K)	100	100
a (Å)	16,4552 (9)	16.4553 (4)
B (Å)	8.0613 (4)	8.0605 (2)
c (Å)	13.5259 (7)	13.5260 (3)
a (°)	90	90
B (°)	112.684 (3)	112.678 (1)
γ (°)	90	90
V (Å^3)	1655.42 (16)	1655.35 (7)
Z	4	4
Radiation type	Cu-Kα	Cu-Kα
μ (mm^{-1})	0.76	0.76
Crystal size (mm)	0.12 × 0.11 × 0.10	0.11 × 0.01 × 0.03
Tmin, Tmax	0.852, 0.929	-
(sinθ/λ)max (Å^{-1})	0.633	0.625
Measured/Independent/ observed [I>2σ(I)] reflection	20568/3488/3(COO)	17353/3370/3346
Rint	0.068	0.076
$R[F^2>2\sigma(F^2)]$,*wR*(*F*2), *S*	0.043, 0.102, 1.10	0.025, 0.069, 1.01
Δ*ρ*max/Δ*ρ*min (eÅ^{-3})	0.19, −0.25	0.16, -0.20
Absolute structure (Flack)	-0.1(2)	-0.02 (4)

Table 5.2. Details of the X-ray experiment of **67** enantiomers.

Crystal data	(***S***)-67	(***R***)-67
CCDC	2047365	2048281
Chemical formula	$2(C_{18}H_{16}BrN_3O_3)\cdot C_3H_8O$	$2(C_{18}H_{16}BrN_3O_3)\cdot C_3H_8O$
M_r	864.59	337.37
Crystal system	Triclinic	Triclinic
Space group	P1	P1
Temperature (K)	100	100
a (Å)	8.1434 (1)	8.1451 (1)
B (Å)	10.0812 (2)	10.0886 (1)
c (Å)	11.7595 (2)	11.7642 (2)
a (°)	99.2705 (9)	99.2342 (6)
B (°)	98.3976 (9)	98.4614 (6)
γ (°)	99.2899 (8)	99.3197 (6)
V (Å^3)	925.51 (3)	926.58 (2)
Z	1	1
Radiation type	Cu-Kα	Cu-Kα
μ (mm^{-1})	3.27	3.27
Crystal size (mm)	0.09 × 0.06 × 0.05	0.20 × 0.14 × 0.06
Tmin, Tmax	0.740, 0.850	0.600, 0.730
Measured/Independent/ observed [I>2σ(I)reflection	42137/7470/6822	67154/7500/7331
Rint	0.058	0.042
$R[F^2>2\sigma(F^2)]$,*wR*(*F*2), *S*	0.041, 0.102, 1.11	0.022, 0.057, 1.04
Δ*ρ*max/Δ*ρ*min (eÅ^{-3})	0.38, −0.57	0.38, -0.31
Absolute structure (Flack)	-0.017 (18)	-0.031 (8)

5.2.5 Free Energy Perturbation data and calculations

Table 5.3. Relative binding free energies ($\Delta\Delta G_{bind}$) obtained from FEP simulations between enantiomer pairs. Data is shown as average ± s.e.m. of 10 independent MD simulations in each case. Values correspond to the bar plot in Figure 3.16.

Eutomer	Distomer	$\Delta\Delta G_{bind}$ ± s.e.m (kcal/mol)	
		Eutomer to Distomer	Distomer to Eutomer
(*S*)-ISAM-140SA	(*R*)-ISAM-140	6.36±0.47	-3.42±0.72
(*S*)-50	(*R*)-50	3.89±0.53	-2.39±0.67
(*S*)-58	(*R*)-58	3.51±0.63	-3.27±0.76
(*R*)-60	(*S*)-60	1.02±0.70	-0.7±0.49
(*S*)-79	(*R*)-79	0.72±0.44	-1.23±0.50

Table 5.4. ΔΔG FEP data for Figure 3.17A-B.

Ligand 1	Ligand 2	Exp. ddG	Pred. ddG	SEM
25	I	-1.021	-0.578	0.505
26	15j	0.764	-0.325	0.485
27	15k	-0.627	-1.716	0.183
28	IV	-0.466	-2.148	0.375
31	VII	-2.1	-0.8	0.16
32	VIII	-1.93	-1.08	0.208
34	58	-1.288	-0.306	0.485
34	II	-1.505	0.372	0.439
35	59	-1.114	-1.691	0.135
35	III	-0.492	1.005	0.183
49	25	1.377	2.062	0.505
49	57	0.144	0.418	0.505
50	26	0.821	0.355	0.485
50	58	0.296	-0.275	0.485
51	27	1.36	0.744	0.183
51	59	-0.38	-2.664	0.183
52	28	0.633	2.292	0.375
52	60	-0.203	-0.252	0.375
54	VI	-0.348	-0.06	0.156
55	31	1.01	0.28	0.16
55	63	0.937	-0.68	0.16
56	32	1.37	0.89	0.208
56	VIII	-0.56	-0.19	0.208
57	I	0.211	1.068	0.505
58	II	-0.216	0.678	0.439
59	III	0.622	2.695	0.183
60	IV	0.37	0.397	0.375
62	54	-0.133	1.05	0.156
62	VI	-0.482	0.99	0.156
63	VII	-2.027	0.16	0.16
73	75	-0.33	-1.12	0.665
74	76	1.542	-1.634	0.322
75	79	-0.646	-0.75	0.665
75	IX	-0.681	0.06	0.434
76	80	-1.644	0.771	0.548
76	X	-0.51	0.785	0.548
77	73	0.659	0.64	0.665
77	79	-0.317	-1.23	0.665
78	74	0.13	1.696	0.322
78	80	0.028	0.834	0.322
79	IX	-0.035	0.81	0.434
80	X	1.134	0.015	0.548

Table 5.5. ΔG FEP data for Figure 3.17C-D.

Ligand	Exp. dG	Pred. dG	SEM
25	-9.7766742	-9.6127997	0.505
26	-10.789619	-10.801816	0.485
27	-9.3605691	-9.0136518	0.183
28	-10.364094	-9.1013982	0.375
31	-8.1624459	-8.4482153	0.16
32	-8.3399159	-8.7834033	0.208
73	-10.020721	-9.6779061	0.665
74	-11.069865	-9.593038	0.322
49	-11.153402	-11.6748	0.71417785
50	**-11.61048**	**-11.156816**	**0**
51	**-10.720956**	**-9.7576518**	**0**
52	-10.99667	-11.393398	0.53033009
54	**-8.4189833**	**-8.1207072**	**0**
55	-9.1723599	-8.7282153	0.22627417
56	**-9.7102747**	**-9.6734033**	**0**
77	**-10.67924**	**-10.317906**	**0**
78	-11.20005	-11.289038	0.45537677
15j	-10.026044	-11.126816	0.68589358
15k	-9.9872445	-10.729652	0.25880108
75	-10.350761	-10.797906	0.94045202
76	**-9.5275918**	**-11.227038**	**0**
57	-11.009195	-11.2588	0.505
58	-11.314252	-11.431816	0.485
59	-11.101058	-12.421652	0.183
60	-11.20005	-11.646398	0.375
62	-8.28581	-9.1707072	0.156
63	-8.2354565	-9.4082153	0.16
79	-10.99667	-11.547906	0.665
80	-11.171622	-10.456038	0.548
I	**-10.797928**	**-10.1908**	**0**
II	-11.530685	-10.753816	0.65336667
III	-10.479431	-9.7266518	0.25880108
IV	**-10.829779**	**-11.249398**	**0**
IX	-11.032137	-10.737906	0.77711035
VI	-8.7673283	-8.1807072	0.156
VII	**-10.262599**	**-9.2482153**	**0**
VIII	-10.270019	-9.8634033	0.208
X	-10.038061	-10.442038	0.548

5.3 SCAFFOLD HOPPING STRATEGIES OF THE 3,4-DIHYDROPYRIMIDIN-2(1*H*)-ONE CHEMOTYPE PROVIDE NOVEL POTENT A_{2B} ADENOSINE RECEPTOR ANTAGONISTS

5.3.1 Synthesis of monocyclic derivatives (81-136)

METHOD C. General procedure for the synthesis of 2-(methyl-, dimethyl-, phenyl-)amino-dihydropyrimidines (Series **V-VII**) and 2-acetamidodihydropyrimidines (Series **VIII**)

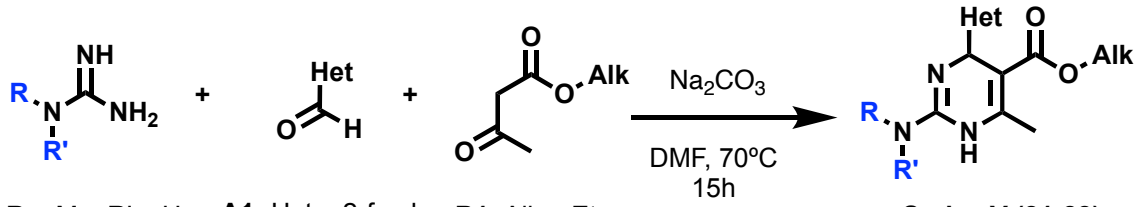

C7: R = Me, R' = H
C8: R = Me, R' = Me
C9: R = Ph, R' = H
C10: R = Ac, R' = H

A1: Het = 2-furyl
A2: Het = 3-furyl
A3: Het = 2-thienyl
A4: Het = 3-thienyl

B1: Alk = Et
B2: Alk = *i*-Pr

Series V (81-88)
Series VI (89-96)
Series VII (97-104)
Series VIII (104-112)

A mixture of guanidine derivative (**C7-10**, 1.5 equiv.), pentagonal carbaldehyde (**A1-4**, 1 equiv.), alkyl acetoacetate (**B1-2**, 1 equiv.) and Na_2CO_3 (1.5 equiv.) in DMF was stirred with orbital stirring at 70 ºC for 15 hours. After completion of the reaction, as indicated by TLC, the solvent was removed in vacuum and the obtained oily residue was purified with flash chromatography at using Hex:AcOEt mixtures as mobile phase.

METHOD D. General procedure for the synthesis of 2-benzamidodihydropyrimidines (Series **IX**) and 2-phenylsulphonamidodihydropyrimidines (Series **X**)

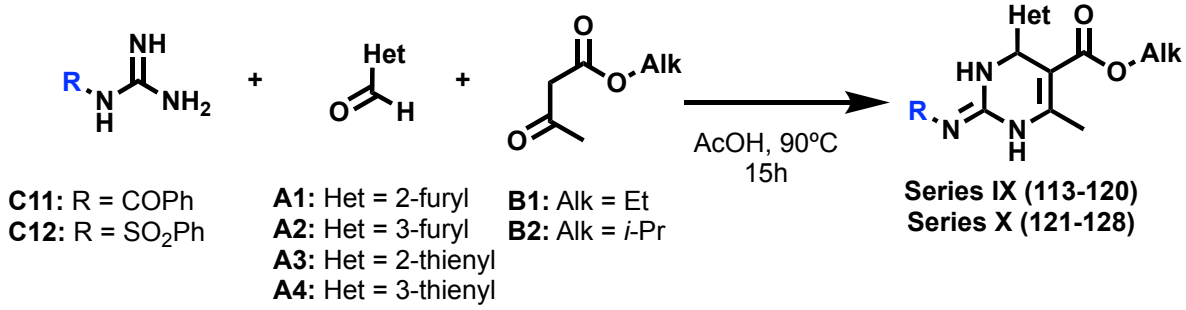

C11: R = COPh
C12: R = SO_2Ph

A1: Het = 2-furyl
A2: Het = 3-furyl
A3: Het = 2-thienyl
A4: Het = 3-thienyl

B1: Alk = Et
B2: Alk = *i*-Pr

Series IX (113-120)
Series X (121-128)

A mixture of guanidine derivative (**C11-12**, 1.5 equiv.), pentagonal carbaldehyde (**A1-4**, 1 equiv.), alkyl acetoacetate (**B1-2**, 1 equiv.) in acetic acid was stirred with orbital stirring at 90 ºC for 15 hours. After completion of the reaction, as indicated by TLC, the reaction mixture was diluted with 10 ml of water and carried to pH 8 with saturated $NaHCO_3$, afterwards was extracted with AcOEt. The organic layer was dried with Na_2SO_4, filtered, and evaporated under vacuum. The obtained oily residue was purified with flash chromatography at using Hex:AcOEt mixtures as mobile phase.

METHOD E. General procedure for the synthesis of 2-((1*H*-benzo[d]imidazol-2-yl)amino)pyrimidines (Series **XI**)

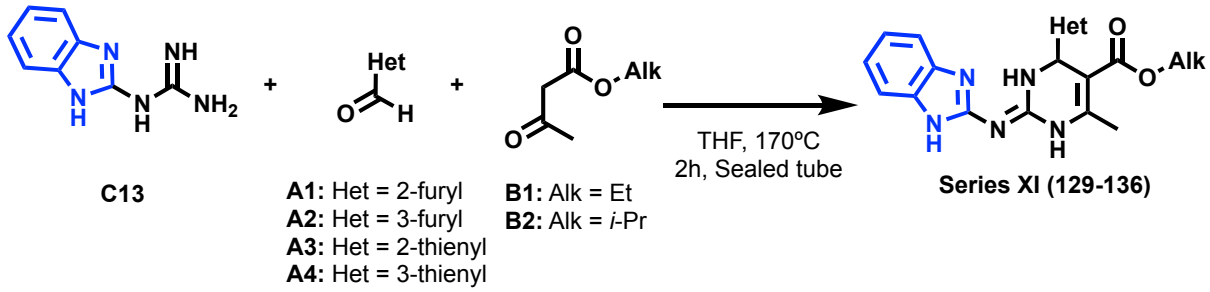

A mixture of 1-(1*H*-benzo[*d*]imidazol-2-yl)guanidine (**C13**, 1 equiv.), pentagonal carbaldehyde (**A1-4**, 1.5 equiv.), alkyl acetoacetate (**B1-2**, 1.5 equiv.), catalyst-free, in THF was stirred in a sealed tube at 170 ºC for 2 hours. After completion of the reaction, as indicated by TLC, the solvent was removed in vacuum and the obtained oily residue was purified with flash chromatography at using DCM:MeOH mixtures as mobile phase.

5.3.2 Synthesis of bicyclic derivatives (137-224 & 233-240)

METHOD F. General procedure for the synthesis of 2-substituted-4,7-dihydro-[1,2,4]triazolo[1,5-*a*]pyrimidines (Series **XII-XVIII**)

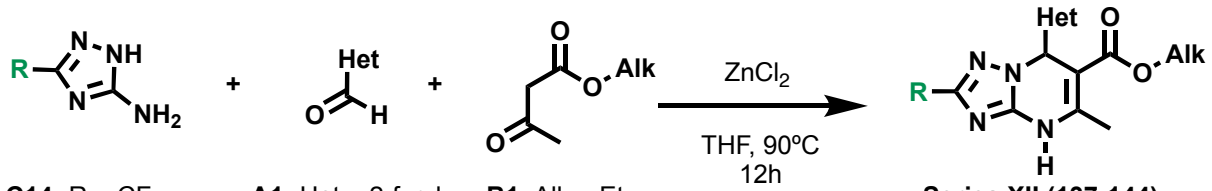

C14: R = CF_3
C15: R = COOMe
C16: R = Ph
C17: R = NMPP
C18: R = SH
C19: R = SMe
C20: R = SBn

A1: Het = 2-furyl
A2: Het = 3-furyl
A3: Het = 2-thienyl
A4: Het = 3-thienyl

B1: Alk = Et
B2: Alk = *i*-Pr

Series XII (137-144)
Series XIII (145-152)
Series XIV (153-160)
Series XV (161-168)
Series XVI (169-176)
Series XVII (177-184)
Series XVIII (185-192)

A mixture of 1*H*-1,2,4-triazol-5-amine-3-substituted derivative (**C14-C20**, 1 equiv.), pentagonal carbaldehyde (**A1-4**, 1.5 equiv.), alkyl acetoacetate (**B1-2**, 1.5 equiv.), and zinc chloride (0.1 equiv.), in THF was stirred with orbital stirring at 90 ºC for 12 hours. After completion of the reaction, as indicated by TLC, the solvent was removed in vacuum and the obtained oily residue was purified with flash chromatography at using Hex:AcOEt mixtures as mobile phase.

METHOD G. General procedure for the synthesis of dihydrotetrazolo[1,5-*a*]pyrimidines (Series **XIX**)

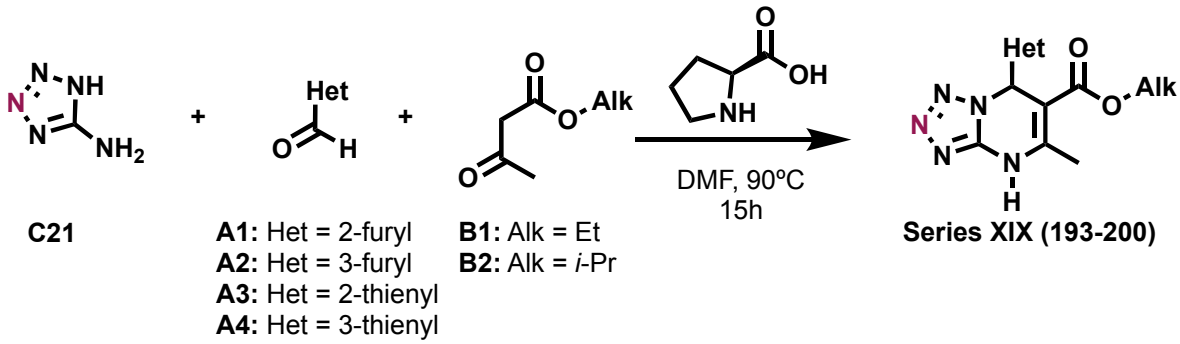

C21

A1: Het = 2-furyl
A2: Het = 3-furyl
A3: Het = 2-thienyl
A4: Het = 3-thienyl

B1: Alk = Et
B2: Alk = *i*-Pr

Series XIX (193-200)

A mixture of 1*H*-tetrazol-5-amine (**C21**, 1 equiv.), pentagonal carbaldehyde (**A1-4**, 1.5 equiv.), alkyl acetoacetate (**B1-2**, 1.5 equiv.), and *L*-proline (0.1 equiv.), in DMF was stirred with orbital stirring at 90 ºC for 15 hours. After completion of the reaction, as indicated by TLC, the solvent was removed in vacuum and the obtained oily residue was purified with flash chromatography at using Hex:AcOEt mixtures as mobile phase.

METHOD H. General procedure for the synthesis of 3-cyano-4,7-dihydropyrazolo[1,5-*a*]pyrimidines (Series **XX**), and 5*H*-thiazolo[3,2-*a*]pyrimidines (Series **XXII**)

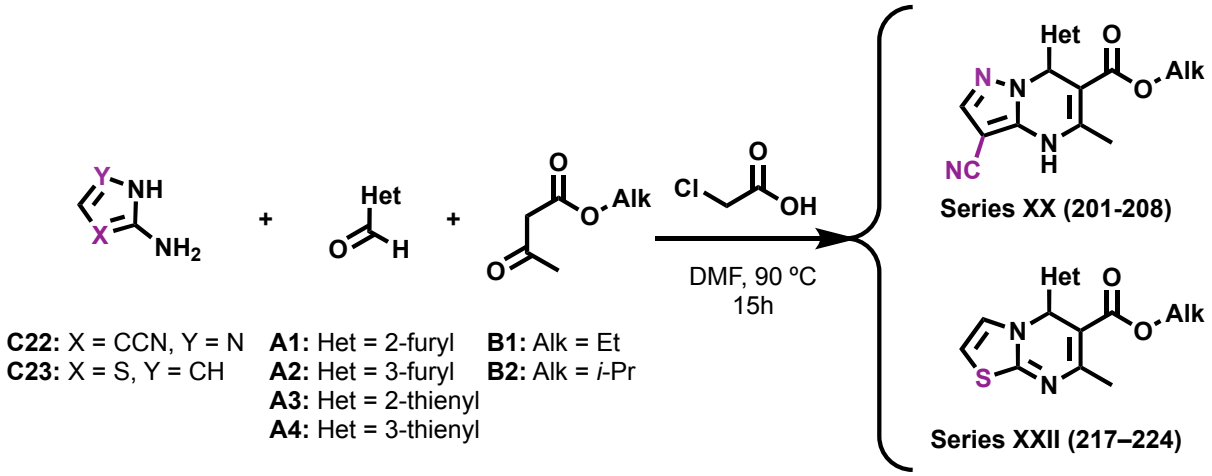

C22: X = CCN, Y = N
C23: X = S, Y = CH

A1: Het = 2-furyl
A2: Het = 3-furyl
A3: Het = 2-thienyl
A4: Het = 3-thienyl

B1: Alk = Et
B2: Alk = *i*-Pr

A mixture of 5-amino-1*H*-pyrazole-4-carbonitrile (**C22**, 1.5 equiv.), or thiazol-2-amine (**C23**, 1.5 equiv.), pentagonal carbaldehyde (**A1-4**, 1 equiv.), alkyl acetoacetate (**B1-2**, 1 equiv.), and chloroacetic acid (0.1 equiv.), in DMF was stirred with orbital stirring at 90 ºC for 15 hours. After completion of the reaction, as indicated by TLC, the solvent was removed in vacuum and the obtained oily residue was purified with flash chromatography at using Hex:AcOEt mixtures as mobile phase.

5.3.3 Synthesis of tricyclic derivatives (209-216 & 225-248)

METHOD I. General procedure for the synthesis of 4,6-dihydropyrimido[1,2-*b*]indazoles (Series **XXI**), 4*H*-benzo[4,5]thiazolo[3,2-*a*]pyrimidines (Series **XXIII**), 7-chloro-4*H*-benzo[4,5]thiazolo[3,2-*a*]pyrimidines (Series **XXIV**), and 8-chloro-4*H*-benzo[4,5]thiazolo[3,2-*a*]pyrimidines (Series **XXV**)

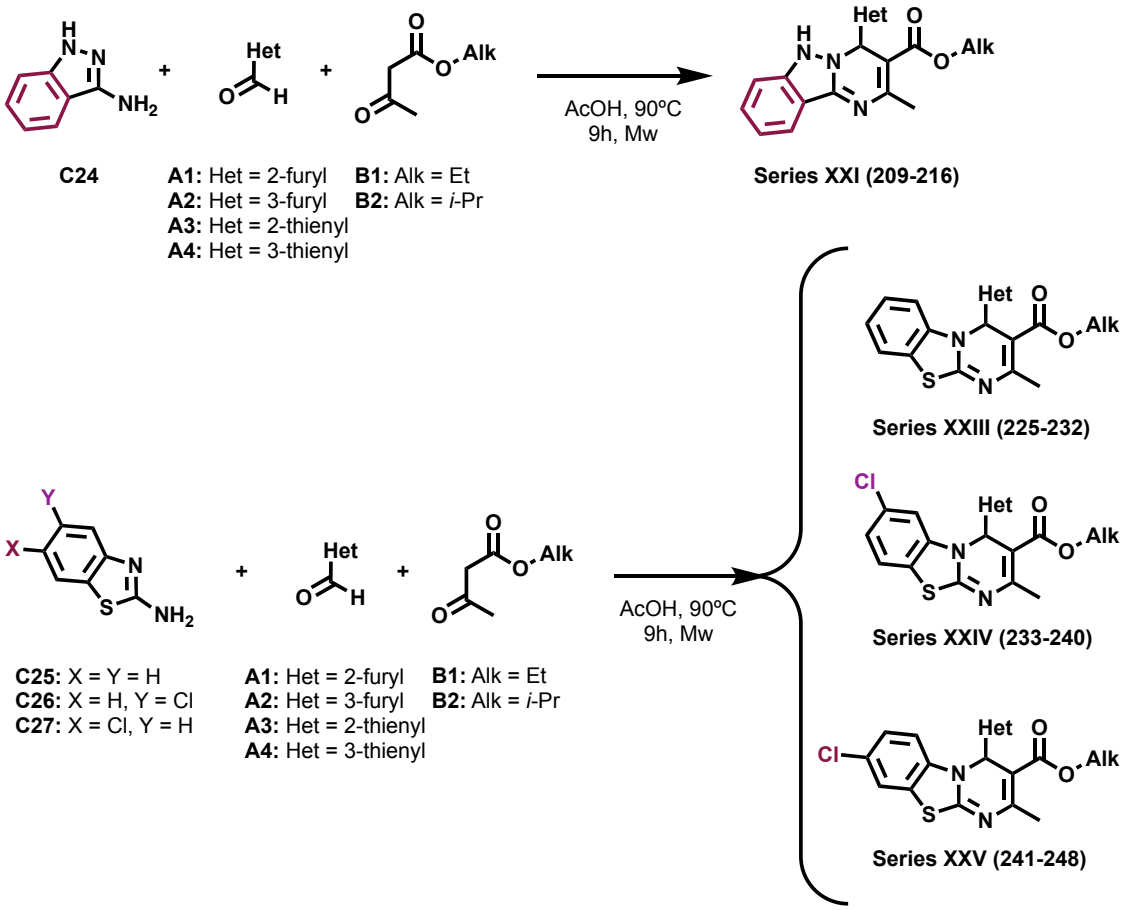

A mixture of 1*H*-indazol-3-amine (**C24**, 1.5 equiv.), benzo[*d*]thiazol-2-amine (**C25**, 1.5 equiv.), 5-chlorobenzo[*d*]thiazol-2-amine (**C26**, 1.5 equiv.), or 6-chlorobenzo[*d*]thiazol-2-amine (**C27**, 1.5 equiv.), pentagonal carbaldehyde (**A1-4**, 1 equiv.), alkyl acetoacetate (**B1-2**, 1 equiv.), in acetic acid was stirred under microwave (Mw) radiation at 90 ºC for 9 hours. After completion of the reaction, as indicated by TLC (benzothiazoles revealing yellow with *p*-anisaldehyde), the reaction mixture was diluted with 10 ml of water and carried to pH 8 with saturated $NaHCO_3$, afterwards was extracted with AcOEt. The organic layer was dried with Na_2SO_4, filtered, and evaporated under vacuum. The obtained oily residue was purified with flash chromatography at using DCM:MeOH mixtures as mobile phase.

5.3.4 Spectroscopic and analytical data for all compounds described

(±) Ethyl 4-(furan-2-yl)-6-methyl-2-(methylamino)-1,4-dihydropyrimidine-5-carboxylate (81). Purified by column chromatography (Hex–AcOEt 5:1 – 2:1). Yield: 37%. Oil at RT. ^{1}H NMR (300 MHz, $CDCl_3$), δ (ppm): 7.30 – 7.27 (m, 1H, ArH), 6.25 (dd, *J* = 3.1, 1.8 Hz, 1H, ArH), 6.07 (d, *J* = 3.2 Hz, 1H, ArH), 5.49 (s, 1H, CH), 5.14 (brs, 2H, NH + N*H*CH_3), 4.17 – 4.02 (m, 2H, OC*H*$_2$$CH_3$), 2.80 (s, 3H, CH_3), 2.36 (s, 3H, NHC*H*$_3$), 1.20 (t, *J* = 7.1 Hz, 3H, OCH_2C*H*$_3$). ^{13}C NMR (75 MHz, $CDCl_3$), δ (ppm): 166.1, 155.4, 153.3, 144.5, 142.0, 110.3, 106.0, 98.1, 61.5, 47.4, 28.3, 27.7, 24.3, 22.4, 20.5, 14.3, 14.1. LRMS (EI) *m/z* calcd. for $C_{13}H_{17}N_3O_3$ $[M]^{+\cdot}$: 263.1 found: 262.8.

(±) Isopropyl 4-(furan-2-yl)-6-methyl-2-(methylamino)-1,4-dihydropyrimidine-5-carboxylate (82). Purified by column chromatography (Hex–AcOEt 5:1 – 2:1). Yield: 45%. Oil at RT. ^{1}H NMR (300 MHz, $CDCl_3$), δ (ppm): 7.27 (s, 1H, ArH), 6.28 – 6.19 (m, 1H, ArH), 6.06 (d, *J* = 2.6 Hz, 1H, ArH), 5.47 (s, 1H, CH), 5.04 – 4.90 (m, 1H, OC*H*$(CH_3)_2$), 4.34 (brs, 2H, NH + N*H*CH_3), 2.78 (s, 3H, CH_3), 2.34 (s, 3H, NHC*H*$_3$), 1.21 (d, *J* = 6.2 Hz, 3H, OCH(C*H*$_3$)$_2$), 1.11 (d, *J* = 6.2 Hz, 3H, OCH(C*H*$_3$)$_2$). ^{13}C NMR (75 MHz, $CDCl_3$), δ (ppm): 165.8, 155.8, 154.0, 153.4, 141.8, 110.3, 105.9, 98.2, 66.9, 47.5, 27.7, 22.1, 21.9, 20.9. LRMS (EI) *m/z* calcd. for $C_{14}H_{19}N_3O_3$ $[M]^{+\cdot}$: 277.1 found: 276.8.

(±) Ethyl 4-(furan-3-yl)-6-methyl-2-(methylamino)-1,4-dihydropyrimidine-5-carboxylate (83). Purified by column chromatography (Hex–AcOEt 5:1 – 2:1). Yield: 31%. Oil at RT. ^{1}H NMR (300 MHz, $CDCl_3$), δ (ppm): 7.35 – 7.27 (m, 2H, ArH), 6.39 – 6.30 (m, 1H, ArH), 5.41 (s, 1H, CH), 4.17 – 4.02 (m, 2H, OC*H*$_2$$CH_3$), 2.80 (s, 3H, CH_3), 2.36 (s, 3H, NHC*H*$_3$), 1.20 (t, *J* = 7.1 Hz, 3H, OCH_2C*H*$_3$). LRMS (EI) *m/z* calcd. for $C_{13}H_{17}N_3O_3$ $[M]^{+\cdot}$: 263.1 found: 262.8.

(±) Isopropyl 4-(furan-3-yl)-6-methyl-2-(methylamino)-1,4-dihydropyrimidine-5-carboxylate (84). Purified by column chromatography (Hex–AcOEt 5:1 – 2:1). Yield: 30%. Mp: 83 – 85 ºC. ^{1}H NMR (300 MHz, $CDCl_3$), δ (ppm): 7.35 – 7.27 (m, 2H, ArH), 6.39 – 6.30 (m, 1H, ArH), 5.41 (s, 1H, CH), 5.07 – 4.93 (m, 1H, OC*H*$(CH_3)_2$), 3.80 (brs, 2H, NH + N*H*CH_3), 2.84 (s, 3H, CH_3), 2.31 (s, 3H, NHC*H*$_3$), 1.24 (d, *J* = 6.3 Hz, 3H, OCH(C*H*$_3)_2$), 1.18 (d, *J* = 6.2 Hz, 3H, OCH(C*H*$_3)_2$). ^{13}C NMR (75 MHz, $CDCl_3$), δ (ppm): 166.3, 154.2, 143.2, 138.7, 129.3, 129.3, 109.0, 100.1, 66.8, 45.9, 27.7, 22.2, 22.0, 20.9. LRMS (EI) *m/z* calcd. for $C_{14}H_{19}N_3O_3$ $[M]^{+\cdot}$: 277.1 found: 276.7.

(±) Ethyl 6-methyl-2-(methylamino)-4-(thiophen-2-yl)-1,4-dihydropyrimidine-5-carboxylate (85). Purified by column chromatography (Hex–AcOEt 5:1 – 2:1). Yield: 39%. Oil at RT. ^{1}H NMR (300 MHz, $CDCl_3$), δ (ppm): 7.13 (dd, *J* = 4.8, 1.4 Hz, 1H, ArH), 6.92 – 6.85 (m, 2H, ArH), 5.69 (s, 1H, CH), 4.90 (brs, 2H, NH + N*H*CH_3), 4.20 – 4.02 (m, 2H, OC*H*$_2$$CH_3$), 2.81 (s, 3H, CH_3), 2.33 (s, 3H, NHC*H*$_3$), 1.22 (t, J = 7.1 Hz, 3H, OCH_2C*H*$_3$). LRMS (EI) *m/z* calcd. for $C_{13}H_{17}N_3O_2S$ $[M]^{+\cdot}$: 279.1 found: 279.0.

(±) Isopropyl 6-methyl-2-(methylamino)-4-(thiophen-2-yl)-1,4-dihydropyrimidine-5-carboxylate (86). Purified by column chromatography (Hex–AcOEt 5:1 – 2:1). Yield: 35%. Mp: 76 – 78 ºC. ^{1}H NMR (300 MHz, $CDCl_3$), δ (ppm): 7.12 (dd, *J* = 4.8, 1.3 Hz, 1H, ArH), 6.93 – 6.85 (m, 2H, ArH), 5.69 (s, 1H, CH), 5.08 – 4.90 (m, 1H, OC*H*$(CH_3)_2$), 2.81 (s, 3H,), 2.33 (s, 3H, NHC*H*$_3$), 1.23 (d, *J* = 6.2 Hz, 3H, OCH(C*H*$_3)_2$), 1.14 (d, *J* = 6.2 Hz, 3H, OCH(C*H*$_3)_2$). LRMS (EI) m/z calcd. for $C_{14}H_{19}N_3O_2S$ $[M]^{+\cdot}$: 293.1 found: 292.9.

(±) Ethyl 6-methyl-2-(methylamino)-4-(thiophen-3-yl)-1,4-dihydropyrimidine-5-carboxylate (87). Purified by column chromatography (Hex–AcOEt 5:1 – 2:1). Yield: 32%. Mp: 105 – 107 ºC. ^{1}H NMR (300 MHz, $CDCl_3$), δ (ppm): 7.20 (dd, *J* = 4.9, 3.0 Hz, 1H, ArH), 7.09 – 7.01 (m, 2H, ArH), 5.50 (s, 1H, CH), 4.75 (brs, 2H, NH + N*H*CH_3), 4.18 – 3.97 (m, 2H, OC*H*$_2$$CH_3$), 2.81 (s, 3H, CH_3), 2.32 (s, 3H, N*H*CH_3), 1.21 (t, *J* = 7.1 Hz, 3H, OCH_2C*H*$_3$). LRMS (EI) m/z calcd. for $C_{13}H_{17}N_3O_2S$ $[M]^{+\cdot}$: 279.1 found: 278.9.

(±) Isopropyl 6-methyl-2-(methylamino)-4-(thiophen-3-yl)-1,4-dihydropyrimidine-5-carboxylate (88). Purified by column chromatography (Hex–AcOEt 5:1 – 2:1). Yield: 29%. Mp: 80 – 82 ºC. ^{1}H NMR (300 MHz, $CDCl_3$), δ (ppm): 7.20 (dd, *J* = 4.8, 3.1 Hz, 1H, ArH), 7.10 – 7.03 (m, 2H, ArH), 5.51 (s, 1H, CH), 5.03 – 4.90 (m, 1H, OC*H*$(CH_3)_2$), 2.82 (s, 3H, CH_3), 2.32 (s, 3H, NHC*H*$_3$), 1.22 (d, *J* = 6.2 Hz, 3H, OCH(C*H*$_3)_2$), 1.12 (d, *J* = 6.2 Hz, 3H, OCH(C*H*$_3)_2$). LRMS (EI) m/z calcd. for $C_{14}H_{19}N_3O_2S$ $[M]^{+\cdot}$: 293.1 found: 292.9.

(±) Ethyl 2-(dimethylamino)-4-(furan-2-yl)-6-methyl-1,4-dihydropyrimidine-5-carboxylate (89). Purified by column chromatography (Hex–AcOEt 6:1 – 3:1). Yield: 40%. Mp: 112 – 114 ºC. ^{1}H NMR (300 MHz, $CDCl_3$), δ (ppm): 7.30 (s, 1H, ArH), 6.28 – 6.21 (m, 1H, ArH), 6.11 – 6.04 (m, 1H, ArH), 5.53 (s, 1H, CH), 4.12 (q, *J* = 7.1 Hz, 2H, OC*H*$_2$CH$_3$), 3.03 (s, 6H, N$(CH_3)_2$), 2.42 (s, 3H, CH_3), 1.21 (t, *J* = 7.1 Hz, 3H, OCH_2C*H*$_3$). ^{13}C NMR (75 MHz, $CDCl_3$), δ (ppm): 166.8, 160.0, 156.3, 153.7, 141.7, 110.2, 105.7, 96.6, 59.2, 47.7, 37.1, 23.5, 14.4. LRMS (EI) *m/z* calcd. for $C_{14}H_{19}N_3O_3$ $[M]^{+\cdot}$: 277.1 found: 276.9.

(±) Isopropyl 2-(dimethylamino)-4-(furan-2-yl)-6-methyl-1,4-dihydropyrimidine-5-carboxylate (90). Purified by column chromatography (Hex–AcOEt 6:1 – 3:1). Yield: 37%. Oil at RT. ^{1}H NMR (300 MHz, $CDCl_3$), δ (ppm): 7.29 (s, 1H, ArH), 6.26 – 6.22 (m, 1H, ArH), 6.06 (d, *J* = 3.0 Hz, 1H, ArH), 5.52 (s, 1H, CH), 5.07 – 4.94 (m, 1H, OC*H*$(CH_3)_2$), 3.02 (s, 6H, N$(CH_3)_2$), 2.40 (s, 3H, CH_3), 1.22 (d, *J* = 6.3 Hz, 3H, OCH(C*H*$_3)_2$), 1.12 (d, *J* = 6.2 Hz, 3H, OCH(C*H*$_3)_2$). ^{13}C NMR (75 MHz, $CDCl_3$), δ (ppm): 166.0, 156.1, 153.3, 144.4, 141.7, 110.3, 105.8, 97.8, 66.5, 47.6, 37.4, 22.6, 22.1, 21.9. LRMS (EI) *m/z* calcd. for $C_{15}H_{21}N_3O_3$ $[M]^{+\cdot}$: 291.2 found: 290.9.

(±) Ethyl 2-(dimethylamino)-4-(furan-2-yl)-6-methyl-1,4-dihydropyrimidine-5-carboxylate (91). Purified by column chromatography (Hex–AcOEt 6:1 – 3:1). Yield: 42%. Oil at RT. ^{1}H NMR (300 MHz, $CDCl_3$), δ (ppm): 7.29 – 7.24 (s, 2H, ArH), 6.33 (s, 1H, ArH), 5.43 (s, 1H, CH), 4.19 – 4.06 (m, 2H, OC*H*$_2$CH$_3$), 3.05 (s, 6H, N$(CH_3)_2$), 2.36 (s, 3H, CH_3), 1.24 (t, *J* = 7.1 Hz, 3H, OCH_2C*H*$_3$). ^{13}C NMR (75 MHz, $CDCl_3$), δ (ppm): 166.8, 157.9, 153.6, 143.1, 138.7, 129.2, 109.0, 99.5, 59.3, 46.0, 37.3, 23.1, 14.4. LRMS (EI) *m/z* calcd. for $C_{14}H_{19}N_3O_3$ $[M]^{+\cdot}$: 277.1 found: 276.9.

(±) Isopropyl 2-(dimethylamino)-4-(furan-3-yl)-6-methyl-1,4-dihydropyrimidine-5-carboxylate (92). Purified by column chromatography (Hex–AcOEt 6:1 – 3:1). Yield: 45%. Mp: 160 – 162 ºC. ^{1}H NMR (300 MHz, $CDCl_3$), δ (ppm): 7.30 -7.24 (m, 2H, ArH), 6.34 (s, 1H, ArH), 5.43 (s, 1H, CH), 5.08 – 4.97 (m, 1H, OC*H*$(CH_3)_2$), 3.05 (s, 6H, N$(CH_3)_2$), 2.36 (s, 3H, CH_3), 1.24 (d, *J* = 6.3 Hz, 3H, OCH(C*H*$_3)_2$), 1.19 (d, *J* = 6.1 Hz, 3H, OCH(C*H*$_3)_2$). ^{13}C NMR (75 MHz, $CDCl_3$), δ (ppm): 166.4, 157.6, 153.7, 143.0, 138.6, 129.2, 109.1, 99.8, 66.4, 45.9, 37.3, 22.9, 22.2, 22.0. LRMS (EI) *m/z* calcd. for $C_{15}H_{21}N_3O_3$ $[M]^{+\cdot}$: 291.2 found: 291.0.

(±) Ethyl 2-(dimethylamino)-6-methyl-4-(thiophen-2-yl)-1,4-dihydropyrimidine-5-carboxylate (93). Purified by column chromatography (Hex–AcOEt 6:1 – 3:1). Yield: 39%. Mp: 134 – 135 ºC. ^{1}H NMR (300 MHz, $CDCl_3$), δ (ppm): 7.11 (dd, *J* = 4.8, 1.3 Hz, 1H, ArH), 6.91 – 6.81 (m, 2H, ArH), 5.73 (s, 1H, CH), 4.19 – 4.06 (m, 2H, OC*H*$_2$CH$_3$), 3.05 (s, 6H, N$(CH_3)_2$), 2.38 (s, 3H, CH_3), 1.23 (t, *J* = 7.1 Hz, 3H, OCH$_2$C*H*$_3$). LRMS (EI) *m/z* calcd. for $C_{14}H_{19}N_3O_2S$ $[M]^{+\cdot}$: 293.1 found: 292.8.

(±) Isopropyl 2-(dimethylamino)-6-methyl-4-(thiophen-2-yl)-1,4-dihydropyrimidine-5-carboxylate (94). Purified by column chromatography (Hex–AcOEt 6:1 – 3:1). Yield: 31%. Mp: 145 – 147 ºC. ^{1}H NMR (300 MHz, $CDCl_3$), δ (ppm): 7.12 (d, *J* = 4.8 Hz, 1H, ArH), 6.91 – 6.84 (m, 2H, ArH), 5.73 (s, 1H, CH), 5.09 – 4.94 (m, 1H, OC*H*$_2$CH$_3$), 3.05 (s, 6H, N$(CH_3)_2$), 2.38 (s, 3H, CH_3), 1.24 (d, *J* = 6.3 Hz, 3H, OCH$_2$C*H*$_3$), 1.16 (d, *J* = 6.2 Hz, 3H). LRMS (EI) *m/z* calcd. for $C_{15}H_{21}N_3O_2S$ $[M]^{+\cdot}$: 307.1 found: 307.1.

(±) Ethyl 2-(dimethylamino)-6-methyl-4-(thiophen-3-yl)-1,4-dihydropyrimidine-5-carboxylate (95). Purified by column chromatography (Hex–AcOEt 6:1 – 3:1). Yield: 36%. Mp: 109 – 110 ºC. ^{1}H NMR (300 MHz, $CDCl_3$), δ (ppm): 7.19 (dd, *J* = 4.8, 2.9 Hz, 1H, ArH), 7.09 – 7.01 (m, 2H, ArH), 5.54 (s, 1H, CH), 4.19 – 4.01 (m, 2H, OC*H*$_2$CH$_3$), 3.04 (s, 6H, N$(CH_3)_2$), 2.36 (s, 3H, CH_3), 1.22 (t, *J* = 7.1 Hz, 3H, OCH$_2$C*H*$_3$). LRMS (EI) *m/z* calcd. for $C_{14}H_{19}N_3O_2S$ $[M]^{+\cdot}$: 293.1 found: 292.8.

(±) Isopropyl 2-(dimethylamino)-6-methyl-4-(thiophen-3-yl)-1,4 dihydropyrimidine-5-carboxylate (96). Purified by column chromatography (Hex–AcOEt 6:1 – 3:1). Yield: 40%. Mp: 157 – 159 ºC. ^{1}H NMR (300 MHz, $CDCl_3$), δ (ppm): 7.19 (dd, *J* = 4.8, 3.2 Hz, 1H, ArH), 7.09 – 7.02 (m, 2H, ArH), 5.55 (s, 1H, CH), 5.07 – 4.92 (m, 1H, OC*H*$(CH_3)_2$), 3.04 (s, 6H, N$(CH_3)_2$), 2.37 (s, 3H, CH_3), 1.23 (d, *J* = 6.2 Hz, 3H, OCH(C*H*$_3)_2$), 1.14 (d, *J* = 6.2 Hz, 3H, OCH(C*H*$_3)_2$). LRMS (EI) *m/z* calcd. for $C_{15}H_{21}N_3O_2S$ $[M]^{+\cdot}$: 307.1 found: 306.9.

(±) Ethyl 4-(furan-2-yl)-6-methyl-2-(phenylamino)-1,4-dihydropyrimidine-5-carboxylate (97). Purified by column chromatography (Hex–AcOEt 4:1 – 2:1). Yield: 48%. Mp: 94 – 96 ºC. ^{1}H NMR (300 MHz, $CDCl_3$), δ (ppm): 7.37 – 7.26 (m, 3H, ArH), 7.06 (t, *J* = 7.4 Hz, 1H, ArH), 6.87 (d, *J* = 7.4 Hz, 2H, ArH), 6.28 (dd, *J* = 3.1, 1.9 Hz, 1H, ArH), 6.09 (d, *J* = 3.2 Hz, 1H, ArH), 5.33 (s, 1H, CH), 4.12 (q, *J* = 7.2 Hz, 2H, OC*H*$_2$CH$_3$), 2.22 (s, 3H, CH_3), 1.20 (t, *J* = 7.1 Hz, 3H, OCH_2C*H*$_3$). LRMS (EI) m/z calcd. for $C_{18}H_{19}N_3O_3$ $[M]^{+\cdot}$: 325.1 found: 324.9.

(±) Isopropyl 4-(furan-2-yl)-6-methyl-2-(phenylamino)-1,4-dihydropyrimidine-5-carboxylate (98). Purified by column chromatography (Hex–AcOEt 4:1 – 2:1). Yield: 45%. Mp: 93 – 94 ºC. ^{1}H NMR (300 MHz, $CDCl_3$), δ (ppm): 7.36 – 7.26 (m, 3H, ArH), 7.06 (t, *J* = 7.4 Hz, 1H, ArH), 6.88 (d, *J* = 7.4 Hz, 2H, ArH), 6.30 – 6.25 (m, 1H, ArH), 6.07 (d, *J* = 3.2 Hz, 1H, ArH), 5.31 (s, 1H, CH), 5.05 – 4.92 (m, 1H, OC*H*$(CH_3)_2$), 2.16 (s, 3H, CH_3), 1.20 (d, *J* = 6.2 Hz, 3H, OCH(C*H*$_3)_2$), 1.12 (d, *J* = 6.2 Hz, 3H, OCH(C*H*$_3)_2$). LRMS (EI) m/z calcd. for $C_{19}H_{21}N_3O_3$ $[M]^{+\cdot}$: 339.2 found: 338.8.

(±) Ethyl 4-(furan-3-yl)-6-methyl-2-(phenylamino)-1,4-dihydropyrimidine-5-carboxylate (99). Purified by column chromatography (Hex–AcOEt 4:1 – 2:1). Yield: 49%. Mp: 176 – 178 ºC. ^{1}H NMR (300 MHz, $CDCl_3$), δ (ppm): 7.36 – 7.23 (m, 4H, ArH), 7.06 (t, *J* = 7.4 Hz, 1H, ArH), 6.92 (d, *J* = 7.3 Hz, 2H, ArH), 6.36 (d, *J* = 0.9 Hz, 1H, ArH), 5.22 (s, 1H, CH), 4.17 – 4.05 (m, 2H, OC*H*$_2$CH$_3$), 2.05 (s, 3H, CH_3), 1.22 (t, *J* = 7.1 Hz, 3H, OCH_2C*H*$_3$). LRMS (EI) m/z calcd. for $C_{18}H_{19}N_3O_3$ $[M]^{+\cdot}$: 325.1 found: 325.1.

(±) Isopropyl 4-(furan-3-yl)-6-methyl-2-(phenylamino)-1,4-dihydropyrimidine-5-carboxylate (100). Purified by column chromatography (Hex–AcOEt 4:1 – 2:1). Yield: 53%. Mp: 154 – 156 ºC. ^{1}H NMR (300 MHz, $CDCl_3$), δ (ppm): 7.35 – 7.23 (m, 4H, ArH), 7.05 (t, *J* = 7.4 Hz, 1H, ArH), 6.91 (d, *J* = 7.3 Hz, 2H, ArH), 6.36 (d, *J* = 0.8 Hz, 1H, ArH), 5.21 (s, 1H, CH), 5.07 – 4.92 (m, 1H, OC*H*$(CH_3)_2$), 2.05 (s, 3H, CH_3), 1.21 (d, *J* = 6.3 Hz, 3H, OCH(C*H*$_3)_2$), 1.17 (d, *J* = 6.2 Hz, 3H, OCH(C*H*$_3)_2$). ^{13}C NMR (75 MHz, $CDCl_3$), δ (ppm): 165.4, 148.0, 147.6, 146.1, 143.3, 138.7, 129.7, 128.6, 123.9, 123.7, 108.7, 100.4, 67.0, 46.0, 22.1, 22.0, 18.8. LRMS (EI) m/z calcd. for $C_{19}H_{21}N_3O_3$ $[M]^{+\cdot}$: 339.2 found: 338.9.

(±) Ethyl 6-methyl-2-(phenylamino)-4-(thiophen-2-yl)-1,4-dihydropyrimidine-5-carboxylate (101). Purified by column chromatography (Hex–AcOEt 4:1 – 2:1). Yield: 39%. Mp: 141 – 143 ºC. ^{1}H NMR (300 MHz, $CDCl_3$), δ (ppm): 7.34 – 7.25 (m, 2H, ArH), 7.17 (dd, *J* = 4.2, 2.0 Hz, 1H, ArH), 7.05 (t, *J* = 7.4 Hz, 1H, ArH), 6.95 – 6.88 (m, 4H, ArH), 5.53 (s, 1H, CH), 4.19 – 4.05 (m, 2H, OC*H*$_2$CH$_3$), 2.11 (s, 3H, CH_3), 1.22 (t, *J* = 7.1 Hz, 3H, OCH_2C*H*$_3$). LRMS (EI) m/z calcd. for $C_{18}H_{19}N_3O_2S$ $[M]^{+\cdot}$: 341.1 found: 341.0.

(±) Isopropyl 6-methyl-2-(phenylamino)-4-(thiophen-2-yl)-1,4-dihydropyrimidine-5-carboxylate (102). Purified by column chromatography (Hex–AcOEt 4:1 – 2:1). Yield: 43%. Mp: 149 – 151 ºC. ^{1}H NMR (300 MHz, $CDCl_3$), δ (ppm): 7.33 – 7.25 (m, 2H, ArH), 7.17 (dd, *J* = 4.2, 2.1 Hz, 1H, ArH), 7.04 (t, *J* = 7.4 Hz, 1H, ArH), 6.96 – 6.88 (m, 4H, ArH), 5.51 (s, 1H, CH), 5.09 – 4.93 (m, 1H, OC*H*$(CH_3)_2$), 2.06 (s, 3H, CH_3), 1.21 (d, *J* = 6.2 Hz, 3H, OCH(C*H*$_3)_2$), 1.15 (d, *J* = 6.2 Hz, 3H, OCH(C*H*$_3)_2$). LRMS (EI) m/z calcd. for $C_{19}H_{21}N_3O_2S$ $[M]^{+\cdot}$: 355.1 found: 354.8.

(±) Ethyl 6-methyl-2-(phenylamino)-4-(thiophen-3-yl)-1,4-dihydropyrimidine-5-carboxylate (103). Purified by column chromatography (Hex–AcOEt 4:1 – 2:1). Yield: 44%. Mp: 169 – 171 ºC. ^{1}H NMR (300 MHz, $CDCl_3$), δ (ppm): 7.33 – 7.21 (m, 3H, ArH), 7.12 – 7.02 (m, 3H, ArH), 6.90 (d, *J* = 7.7 Hz, 2H, ArH), 5.33 (s, 1H, CH), 4.18 – 3.98 (m, 2H, OC*H*$_2$CH$_3$), 2.02 (s, 3H, CH_3), 1.20 (t, *J* = 7.1 Hz, 3H, OCH_2C*H*$_3$). LRMS (EI) m/z calcd. for $C_{18}H_{19}N_3O_2S$ $[M]^{+\cdot}$: 341.1 found: 341.0.

(±) Isopropyl 6-methyl-2-(phenylamino)-4-(thiophen-3-yl)-1,4-dihydropyrimidine-5-carboxylate (104). Purified by column chromatography (Hex–AcOEt 4:1 – 2:1). Yield: 46%. Mp: 158 – 160 ºC. ^{1}H NMR (300 MHz, $CDCl_3$), δ (ppm): 7.33 – 7.22 (m, 3H, ArH), 7.13 – 7.00 (m, 3H, ArH), 6.90 (d, *J* = 7.3 Hz, 2H, ArH), 5.35 (s, 1H, CH), 5.06 – 4.95 (m, 1H, OC*H*$(CH_3)_2$), 2.15 (s, 3H, CH_3), 1.22 (d, *J* = 6.2 Hz, 3H, OCH(C*H*$_3)_2$), 1.15 (d, *J* = 6.2 Hz, 3H, OCH(C*H*$_3)_2$). ^{13}C NMR (75 MHz, $CDCl_3$), δ (ppm): 165.5, 148.0, 147.6, 146.2, 145.4, 129.7, 126.1, 125.9, 123.9, 123.6, 120.7, 100.6, 67.0, 49.7, 22.1, 22.0, 18.9. LRMS (EI) m/z calcd. for $C_{19}H_{21}N_3O_2S$ $[M]^{+\cdot}$: 355.1 found: 354.8.

(±) Ethyl 2-acetamido-4-(furan-2-yl)-6-methyl-1,4-dihydropyrimidine-5-carboxylate (105). Purified by column chromatography (Hex–AcOEt 3:1 – 1:1). Yield: 20%. Mp: 137 – 139 ºC. ^{1}H NMR (300 MHz, $CDCl_3$), δ (ppm): 8.31 (brs, 2H, NH + N*H*$COCH_3$), 7.31 (s, 1H, ArH), 6.27 (dd, *J* = 3.1, 1.8 Hz, 1H, ArH), 6.13 (d, *J* = 3.1 Hz, 1H, ArH), 5.61 (s, 1H, CH), 4.22 – 4.06 (m, 2H, OC*H*$_2CH_3$), 2.38 (s, 3H, NHCOC*H*$_3$), 2.11 (s, 3H, CH_3), 1.21 (t, *J* = 7.1 Hz, 3H, OCH_2C*H*$_3$). LRMS (EI) m/z calcd. for $C_{14}H_{17}N_3O_4$ $[M]^{+\cdot}$: 291.1 found: 290.9.

(±) Isopropyl 2-acetamido-4-(furan-2-yl)-6-methyl-1,4-dihydropyrimidine-5-carboxylate (106). Purified by column chromatography (Hex–AcOEt 3:1 – 1:1). Yield: 23%. Mp: 196 – 198 ºC. ^{1}H NMR (300 MHz, DMSO-*d*$_6$), δ (ppm): 10.31 (brs, 2H, NH + N*H*$COCH_3$), 7.53 (s, 1H, ArH), 6.33 (s, 1H, ArH), 6.09 (d, *J* = 2.9 Hz, 1H, ArH), 5.30 (s, 1H, CH), 4.92 – 4.78 (m, 1H, OC*H*$(CH_3)_2$), 2.24 (s, 3H, NHCOC*H*$_3$), 1.95 (s, 3H, CH_3), 1.15 (d, *J* = 6.2 Hz, 3H, OCH(C*H*$_3)_2$), 1.05 (d, *J* = 6.2 Hz, 3H, OCH(C*H*$_3)_2$). LRMS (EI) *m/z* calcd. for $C_{15}H_{19}N_3O_4$ $[M]^{+\cdot}$: 305.1 found: 304.8.

(±) Ethyl 2-acetamido-4-(furan-3-yl)-6-methyl-1,4-dihydropyrimidine-5-carboxylate (107). Purified by column chromatography (Hex–AcOEt 3:1 – 1:1). Yield: 22%. Oil at RT. ^{1}H NMR (300 MHz, $CDCl_3$), δ (ppm): 7.35 – 7.32 (m, 1H, ArH), 7.31 (s, 1H, ArH), 6.33 (s, 1H, ArH), 5.53 (s, 1H, CH), 4.25 – 4.08 (m, 2H, OC*H*$_2CH_3$), 2.36 (s, 3H, NHCOC*H*$_3$), 2.13 (s, 3H, CH_3), 1.26 (t, *J* = 7.1 Hz, 3H, OCH_2C*H*$_3$). LRMS (EI) *m/z* calcd. for $C_{14}H_{17}N_3O_4$ $[M]^{+\cdot}$: 291.1 found: 290.8.

(±) Isopropyl 2-acetamido-4-(furan-3-yl)-6-methyl-1,4-dihydropyrimidine-5-carboxylate (108). Purified by column chromatography (Hex–AcOEt 3:1 – 1:1). Yield: 21%. Mp: 218 – 220 ºC. ^{1}H NMR (300 MHz, $CDCl_3$), δ (ppm): 9.41 (brs, 2H, NH + N*H*$COCH_3$), 7.31 (s, 1H, ArH), 7.27 (s, 1H, ArH), 6.30 (s, 1H, ArH), 5.49 (s, 1H, CH), 5.11 – 4.95 (m, 1H, OC*H*$(CH_3)_2$), 2.31 (s, 3H, NHCOC*H*$_3$), 2.08 (s, 3H, CH_3), 1.24 (d, *J* = 6.1 Hz, 3H, OCH(C*H*$_3$)$_2$), 1.19 (d, *J* = 6.2 Hz, 3H, OCH(C*H*$_3$)$_2$). ^{13}C NMR (75 MHz, $CDCl_3$), δ (ppm): 179.1, 164.9, 150.5, 144.2, 143.0, 140.3, 130.0, 109.1, 103.8, 68.8, 48.6, 23.3, 22.0, 21.7, 17.7. LRMS (EI) *m/z* calcd. for $C_{15}H_{19}N_3O_4$ $[M]^{+\cdot}$: 305.1 found: 304.8.

(±) Ethyl 2-acetamido-6-methyl-4-(thiophen-2-yl)-1,4-dihydropyrimidine-5-carboxylate (109). Purified by column chromatography (Hex–AcOEt 3:1 – 1:1). Yield: 24%. Oil at RT. ^{1}H NMR (300 MHz, $CDCl_3$), δ (ppm): 8.40 (brs, 2H, NH + N*H*$COCH_3$), 7.17 (d, J = 4.6 Hz, 1H, ArH), 7.02 – 6.81 (m, 2H, ArH), 5.80 (s, 1H, CH), 4.25 – 4.06 (m, 2H, OC*H*$_2$$CH_3$), 2.35 (s, 3H), 2.09 (s, 3H), 1.25 (t, J = 7.1 Hz, 3H, OCH_2C*H*$_3$). LRMS (EI) *m/z* calcd. for $C_{14}H_{17}N_3O_3S$ $[M]^{+\cdot}$: 307.1 found: 306.8.

(±) Isopropyl 2-acetamido-6-methyl-4-(thiophen-2-yl)-1,4-dihydropyrimidine-5-carboxylate (110). Purified by column chromatography (Hex–AcOEt 3:1 – 1:1). Yield: 27%. Mp: 220 – 222 ºC. ^{1}H NMR (300 MHz, $CDCl_3$), δ (ppm): 7.18 (dd, *J* = 4.7, 1.5 Hz, 1H, ArH), 6.98 – 6.83 (m, 2H, ArH), 5.80 (s, 1H, CH), 5.10 – 4.97 (m, 1H, OC*H*$(CH_3)_2$), 2.36 (s, 3H, NHCOC*H*$_3$), 2.11 (s, 3H, CH_3), 1.25 (d, *J* = 6.3 Hz, 3H, OCH(C*H*$_3$)$_2$), 1.16 (d, *J* = 6.3 Hz, 3H, OCH(C*H*$_3$)$_2$). ^{13}C NMR (75 MHz, $CDCl_3$), δ (ppm): 179.7, 164.1, 152.4, 145.7, 144.1, 126.9, 125.3, 124.6, 103.9, 68.2, 48.4, 24.2, 21.9, 21.7, 17.8. LRMS (EI) *m/z* calcd. for $C_{15}H_{19}N_3O_3S$ $[M]^{+\cdot}$: 321.1 found: 320.8.

(±) Ethyl 2-acetamido-6-methyl-4-(thiophen-3-yl)-1,4-dihydropyrimidine-5-carboxylate (111). Purified by column chromatography (Hex–AcOEt 3:1 – 1:1). Yield: 26%. Mp: 215 – 217 ºC. ^{1}H NMR (300 MHz, $CDCl_3$), δ (ppm): 7.25 (s, 1H, ArH), 7.12 (s, 1H, ArH), 7.02 (dd, *J* = 5.0, 1.2 Hz, 1H, ArH), 5.65 (s, 1H, CH), 4.26 – 4.04 (m, 2H, OC*H*$_2$$CH_3$), 2.36 (s, 3H, NHCOC*H*$_3$), 2.14 (s, 3H, CH_3), 1.24 (t, *J* = 7.1 Hz, 3H, OCH_2C*H*$_3$). LRMS (EI) *m/z* calcd. for $C_{14}H_{17}N_3O_3S$ $[M]^{+\cdot}$: 307.1 found: 306.8.

(±) Isopropyl 2-acetamido-6-methyl-4-(thiophen-3-yl)-1,4-dihydropyrimidine-5-carboxylate (112). Purified by column chromatography (Hex–AcOEt 3:1 – 1:1). Yield: 26%. Mp: 224 – 226 ºC. ^{1}H NMR (300 MHz, $CDCl_3$), δ (ppm): 9.20 (brs, 2H, NH + N*H*$COCH_3$), 7.28 – 7.21 (m, 1H, ArH), 7.08 (s, 1H, ArH), 7.03 – 6.98 (m, 1H, ArH, OC*H*$(CH_3)_2$), 5.60 (s, 1H, CH_3), 5.11 – 4.94 (m, 1H, C*H*$(CH_3)_2$), 2.32 (s, 3H, NHCOC*H*$_3$), 2.07 (s, 3H, CH_3), 1.24 (d, J = 6.0 Hz, 3H, OCH(C*H*$_3)_2$), 1.16 (d, J = 6.2 Hz, 3H, OCH(C*H*$_3)_2$). ^{13}C NMR (75 MHz, $CDCl_3$), δ (ppm): 181.5, 164.8, 153.5, 145.6, 144.1, 126.5, 125.9, 125.7, 103.5, 67.8, 49.4, 26.7, 22.1, 21.8, 19.2. LRMS (EI) *m/z* calcd. for $C_{15}H_{19}N_3O_3S$ $[M]^{+\cdot}$: 321.1 found: 321.1.

(±) Ethyl 2-benzamido-4-(furan-2-yl)-6-methyl-1,4-dihydropyrimidine-5-carboxylate (113). Purified by column chromatography (Hex–AcOEt 3:1 – 1:1). Yield: 33%. Oil at RT. ^{1}H NMR (300 MHz, $CDCl_3$), δ (ppm): 10.02 (brs, 2H, NH + N*H*$COCH_3$), 8.13 (d, *J* = 7.3 Hz, 2H, ArH), 7.46 (d, *J* = 7.3Hz, 1H, ArH), 7.38 (d, *J* =7.4 Hz, 2H, ArH), 7.30 (s, 1H, ArH), 6.26 (dd, *J* = 3.0, 1.7 Hz, 1H, ArH), 6.10 (d, *J* = 3.1 Hz, 1H, ArH), 5.54 (s, 1H, CH), 4.17 – 4.05 (m, 2H, OC*H*$_2$$CH_3$), 2.16 (s, 3H, CH_3), 1.19 (t, *J* = 7.1 Hz, 3H, OCH_2C*H*$_3$). ^{13}C NMR (75 MHz, $CDCl_3$), δ (ppm): 177.5, 164.7, 155.1, 153.7, 145.6, 142.7, 136.5, 132.1, 128.1, 127.5, 110.3, 106.7, 100.5, 60.4, 47.3, 18.3, 14.1. HRMS (EI) *m/z* calcd. for $C_{19}H_{19}N_3O_4$ $[M]^{+\cdot}$: 353.1376 found: 353.1389.

(±) Isopropyl 2-benzamido-4-(furan-2-yl)-6-methyl-1,4-dihydropyrimidine-5-carboxylate (114). Purified by column chromatography (Hex–AcOEt 3:1 – 1:1). Yield: 37%. Oil at RT. ^{1}H NMR (300 MHz, $CDCl_3$), δ (ppm): 8.12 (d, *J* = 7.1 Hz, 2H, ArH), 7.47 (d, *J* = 7.1 Hz, 1H, ArH), 7.39 (t, *J* = 7.3 Hz, 2H, ArH), 7.30 (s, 1H, ArH), 6.29 – 6.25 (m, 1H, ArH), 6.12 (d, *J* = 3.2 Hz, 1H, ArH), 5.56 (s, 1H, CH), 5.07 – 4.93 (m, 1H, C*H*$(CH_3)_2$), 2.24 (s, 3H, CH_3), 1.22 (d, *J* = 6.2 Hz, 3H, OCH(C*H*$_3)_2$), 1.11 (d, *J* = 6.2 Hz, 3H, OCH(C*H*$_3)_2$). ^{13}C NMR (75 MHz, $CDCl_3$), δ (ppm): 177.9, 164.2, 155.3, 154.0, 145.3, 142.5, 136.9, 131.9, 128.9, 128.1, 110.3, 106.6, 100.6, 67.8, 47.3, 21.9, 21.6, 18.2. HRMS (EI) *m/z* calcd. for $C_{20}H_{21}N_3O_4$ $[M]^{+\cdot}$: 367.1532 found: 367.1539.

(±) Ethyl 2-benzamido-4-(furan-3-yl)-6-methyl-1,4-dihydropyrimidine-5-carboxylate. (115). Purified by column chromatography (Hex–AcOEt 3:1 – 1:1). Yield: 40%. Oil at RT. ^{1}H NMR (300 MHz, $CDCl_3$), δ (ppm): 10.17 (brs, 2H), 8.13 (d, *J* = 7.6 Hz, 2H, ArH), 7.48 (t, *J* = 7.2 Hz, 1H, ArH), 7.38 (t, *J* = 7.5 Hz, 2H, ArH), 7.34 – 7.21 (m, 2H, ArH), 6.28 (s, 1H, ArH), 5.39 (s, 1H, CH), 4.23 – 4.04 (m, 2H, OCH_2CH_3), 2.09 (s, 3H, CH_3), 1.22 (t, *J* = 7.1 Hz, 3H, OCH_2CH_3). ^{13}C NMR (75 MHz, $CDCl_3$), δ (ppm): 178.40, 164.90, 155.99, 144.81, 143.65, 139.14, 137.29, 131.91, 128.92, 128.17, 127.41, 108.60, 102.66, 60.33, 45.59, 18.09, 14.19. HRMS (EI) *m/z* calcd. for $C_{19}H_{19}N_3O_4$ $[M]^{+\cdot}$: 353.1376 found: 353.1365.

(±) Isopropyl 2-benzamido-4-(furan-3-yl)-6-methyl-1,4-dihydropyrimidine-5-carboxylate (116). Purified by column chromatography (Hex–AcOEt 3:1 – 1:1). Yield: 42%. Oil at RT. ^{1}H NMR (300 MHz, $CDCl_3$), δ (ppm): 10.30 (brs, 2H), 8.13 (d, *J* = 7.3 Hz, 2H, ArH), 7.48 (t, *J* = 7.3 Hz, 1H, ArH), 7.38 (t, *J* = 7.5 Hz, 2H, ArH), 7.34 – 7.21 (m, 2H, ArH), 6.28 (s, 1H, ArH), 5.36 (s, 1H, CH), 5.07 – 4.92 (m, 1H, $CH(CH_3)_2$), 2.07 (s, 3H, CH_3), 1.21 (d, *J* = 6.3 Hz, 3H, $OCH(CH_3)_2$), 1.15 (d, *J* = 6.2 Hz, 3H, $OCH(CH_3)_2$). ^{13}C NMR (75 MHz, $CDCl_3$), δ (ppm): 178.33, 164.38, 155.99, 144.54, 143.60, 139.13, 137.29, 131.92, 128.92, 128.18, 127.47, 108.60, 102.94, 67.83, 45.56, 21.97, 21.74, 17.98. HRMS (EI) *m/z* calcd. for $C_{20}H_{21}N_3O_4$ $[M]^{+\cdot}$: 367.1532 found: 367.1520.

(±) Ethyl 2-benzamido-6-methyl-4-(thiophen-2-yl)-1,4-dihydropyrimidine-5-carboxylate (117). Purified by column chromatography (Hex–AcOEt 3:1 – 1:1). Yield: 38%. Oil at RT. ^{1}H NMR (300 MHz, $CDCl_3$), δ (ppm): 10.35 (brs, 2H), 8.13 (d, *J* = 7.3 Hz, 2H, ArH), 7.48 (t, *J* = 7.2 Hz, 1H, ArH), 7.38 (t, *J* = 7.4 Hz, 2H, ArH), 7.21 – 7.15 (m, 1H, ArH), 6.92 – 6.86 (m, 2H, ArH), 5.69 (s, 1H, CH), 4.20 – 4.03 (m, 2H, OCH_2CH_3), 2.12 (s, 3H, CH_3), 1.21 (t, *J* = 7.1 Hz, 3H, OCH_2CH_3). ^{13}C NMR (75 MHz, $CDCl_3$), δ (ppm): 178.2, 164.8, 155.3, 146.4, 144.8, 137.1, 132.0, 129.0, 128.2, 126.8, 125.3, 124.5, 103.3, 60.4, 49.0, 18.2, 14.1. LRMS (EI) *m/z* calcd. for $C_{19}H_{19}N_3O_3S$ $[M]^{+\cdot}$: 369.1 found: 368.8.

(±) Isopropyl 2-benzamido-6-methyl-4-(thiophen-2-yl)-1,4-dihydropyrimidine-5-carboxylate (118). Purified by column chromatography (Hex–AcOEt 3:1 – 1:1). Yield: 36%. Mp: 101 – 103 ºC. ^{1}H NMR (300 MHz, $CDCl_3$), δ (ppm): 10.16 (brs, 2H), 8.13 (d, *J* = 7.3 Hz, 2H, ArH), 7.48 (t, *J* = 7.2 Hz, 1H, ArH), 7.39 (t, *J* = 7.4 Hz, 2H, ArH), 7.21 – 7.15 (m, 1H, ArH), 6.93 – 6.86 (m, 2H, ArH), 5.68 (s, 1H, CH), 5.05 – 4.95 (m, 1H, C*H*$(CH_3)_2$), 2.17 (s, 3H, CH_3), 1.22 (d, *J* = 6.2 Hz, 3H, OCH(C*H*$_3)_2$), 1.12 (d, *J* = 6.2 Hz, 3H, OCH(C*H*$_3)_2$). LRMS (EI) *m/z* calcd. for $C_{20}H_{21}N_3O_3S$ $[M]^{+\cdot}$: 383.1 found: 382.8.

(±) Ethyl 2-benzamido-6-methyl-4-(thiophen-3-yl)-1,4-dihydropyrimidine-5-carboxylate (119). Purified by column chromatography (Hex–AcOEt 3:1 – 1:1). Yield: 36%. Mp: 178 – 180 ºC. ^{1}H NMR (300 MHz, $CDCl_3$), δ (ppm): 9.89 (brs, 2H), 8.14 (d, *J* = 7.5 Hz, 2H, ArH), 7.49 (t, *J* = 7.1 Hz, 1H, ArH), 7.39 (t, *J* = 7.5 Hz, 2H, ArH), 7.29 – 7.22 (m, 1H, ArH), 7.10 (s, 1H, ArH), 7.03 – 6.97 (m, 1H, ArH), 5.57 (s, 1H, CH), 4.20 – 4.07 (m, 2H, OC*H*$_2$$CH_3$), 2.21 (s, 3H, CH_3), 1.22 (t, *J* = 7.1 Hz, 3H, OCH_2C*H*$_3$). LRMS (EI) *m/z* calcd. for $C_{19}H_{19}N_3O_3S$ $[M]^{+\cdot}$: 369.1 found: 368.8.

(±) Isopropyl 2-benzamido-6-methyl-4-(thiophen-3-yl)-1,4-dihydropyrimidine-5-carboxylate (120). Purified by column chromatography (Hex–AcOEt 3:1 – 1:1). Yield: 39%. Mp: 182 – 184 ºC. ^{1}H NMR (300 MHz, $CDCl_3$), δ (ppm): 10.46 (brs, 2H), 8.14 (d, *J* = 7.3 Hz, 2H, ArH), 7.47 (t, *J* = 7.2 Hz, 1H, ArH), 7.37 (t, *J* = 7.4 Hz, 2H, ArH), 7.22 (dd, *J* = 4.8 Hz, *J* = 2.9 Hz, 1H, ArH), 7.02 (s,1H, ArH), 6.95 (d, *J* = 4.9 Hz, 1H, ArH), 5.45 (s, 1H, CH), 5.03 – 4.89 (m, 1H, C*H*$(CH_3)_2$), 2.05 (s, 3H, CH_3), 1.19 (d, *J* = 6.2 Hz, 3H, OCH(C*H*$_3)_2$), 1.09 (d, *J* = 6.2 Hz, 3H, OCH(C*H*$_3)_2$). LRMS (EI) *m/z* calcd. for $C_{20}H_{21}N_3O_3S$ $[M]^{+\cdot}$: 383.1 found: 382.8.

(±) Ethyl 4-(furan-2-yl)-6-methyl-2-(phenylsulfonamido)-1,4-dihydropyrimidine-5-carboxylate (121). Purified by column chromatography (Hex–AcOEt 3:1 – 1:1). Yield: 17%. Mp: 152 – 154 ºC. ^{1}H NMR (300 MHz, $CDCl_3$), δ (ppm): 8.22 (brs, 1H, NH), 8.03 (brs, 1H, NH), 7.72 (d, *J* = 7.3 Hz, 2H, ArH), 7.52 – 7.43 (m, 1H, ArH), 7.35 (t, *J* = 7.6 Hz, 2H, ArH), 7.26 (s, 1H, CH), 6.26 (dd, *J* = 3.1 Hz, *J* = 1.8 Hz, 1H, ArH), 6.11 (d, *J* = 3.2 Hz, 1H, ArH), 5.58 (d, *J* = 3.4 Hz, 1H, ArH), 4.15 (dd, *J* = 7.1 Hz, *J* = 2.6 Hz, 2H, OC*H*$_2$$CH_3$), 2.40 (s, 3H, CH_3), 1.22 (t, *J* = 7.1 Hz, 3H, OCH_2C*H*$_3$). ^{13}C NMR (75 MHz, $CDCl_3$), δ (ppm): 164.6, 153.2, 151.4, 145.5, 142.7, 142.7, 142.7, 131.8, 128.7, 125.9, 110.4, 106.9, 101.2, 60.6, 47.5, 18.5, 14.2. LRMS (CI) m/z calcd. for $C_{18}H_{20}N_3O_5S$ $[M+H]^{+}$: 389.1 found: 388.9.

(±) Isopropyl 4-(furan-2-yl)-6-methyl-2-(phenylsulfonamido)-1,4-dihydropyrimidine-5-carboxylate (122). Purified by column chromatography (Hex–AcOEt 3:1 – 1:1). Yield: 17%. Mp: 170 – 172 ºC. ^{1}H NMR (300 MHz, $CDCl_3$), δ (ppm): 8.60 (brs, 1H, NH), 8.22 (brs, 1H, NH), 7.68 (d, *J* = 7.5 Hz, 2H, ArH), 7.45 (t, *J* = 7.4 Hz, 1H, ArH), 7.37 – 7.25 (m, 2H, ArH), 7.23 (s, 1H, CH), 6.23 (d, *J* = 1.6 Hz, 1H, ArH), 6.09 (d, *J* = 2.9 Hz, 1H, ArH), 5.58 (d, *J* = 3.2 Hz, 1H, ArH), 5.00 (hept, *J* = 5.9 Hz, 1H, OC*H*$(CH_3)_2$), 2.40 (s, 3H, CH_3), 1.23 (d, *J* = 6.2 Hz, 3H, OCH(C*H*$_3)_2$), 1.14 (d, *J* = 6.2 Hz, 3H, OCH(C*H*$_3)_2$). LRMS (CI) m/z calcd. for $C_{19}H_{22}N_3O_5S$ $[M+H]^+$: 404.1 found: 404.0.

(±) Ethyl 4-(furan-3-yl)-6-methyl-2-(phenylsulfonamido)-1,4-dihydropyrimidine-5-carboxylate (123). Purified by column chromatography (Hex–AcOEt 3:1 – 1:1). Yield: 9%. Mp: 157 – 159 ºC. ^{1}H NMR (300 MHz, $CDCl_3$), δ (ppm): 8.04 (brs, 1H, NH), 7.94 (brs, 1H, NH), 7.78 (d, *J* = 7.6 Hz, 2H, ArH), 7.56 – 7.46 (m, 1H, ArH), 7.40 (t, *J* = 7.7 Hz, 2H, ArH), 7.30 (s, 1H, ArH), 7.20 (s, 1H, ArH), 6.21 (s, 1H, ArH), 5.49 (d, *J* = 3.1 Hz, 1H, ArH), 4.30 – 4.04 (m, 2H, OC*H*$_2$CH$_3$), 2.35 (s, 3H, CH_3), 1.26 (t, *J* = 7.0 Hz, 3H, OCH_2C*H*$_3$). LRMS (CI) m/z calcd. for $C_{18}H_{20}N_3O_5S$ $[M+H]^+$: 390.1 found: 390.2.

(±) Isopropyl 4-(furan-3-yl)-6-methyl-2-(phenylsulfonamido)-1,4-dihydropyrimidine-5-carboxylate (124). Purified by column chromatography (Hex–AcOEt 3:1 – 1:1). Yield: 10%. Mp: 153 – 155 ºC. ^{1}H NMR (300 MHz, $CDCl_3$), δ (ppm): 8.46 (brs, 1H, NH), 8.15 (brs, 1H, NH), 7.73 (d, *J* = 8.0 Hz, 2H, ArH), 7.56 – 7.45 (m, 1H, ArH), 7.36 (t, *J* = 7.7 Hz, 2H, ArH), 7.28 (s, 1H, CH), 7.16 (s, 1H, ArH), 6.20 (s, 1H, ArH), 5.49 (d, *J* = 3.2 Hz, 1H, ArH), 5.20 – 4.89 (m, 1H, OC*H*$(CH_3)_2$), 2.36 (s, 3H, CH_3), 1.24 (d, *J* = 6.0 Hz, 3H, OCH(C*H*$_3)_2$), 1.20 (d, *J* = 6.2 Hz, 3H, OCH(C*H*$_3)_2$). LRMS (CI) m/z calcd. for $C_{19}H_{22}N_3O_5S$ $[M+H]^+$: 404.1 found: 404.0.

(±) Ethyl 6-methyl-2-(phenylsulfonamido)-4-(thiophen-2-yl)-1,4-dihydropyrimidine-5-carboxylate (125). Purified by column chromatography (Hex–AcOEt 3:1 – 1:1). Yield: 45%. Mp: 157 – 159 ºC. ^{1}H NMR (300 MHz, $CDCl_3$), δ (ppm): 8.29 (brs, 1H, ArH), 8.17 (brs, 1H, ArH), 7.74 (d, *J* = 7.9 Hz, 2H, ArH), 7.53 – 7.45 (m, 1H, ArH), 7.41 – 7.31 (m, *J* = 7.7 Hz, 2H, ArH + CH), 7.21 – 7.11 (m, 1H, ArH), 6.87 (d, *J* = 3.3 Hz, 2H, ArH), 5.78 (d, *J* = 3.7 Hz, 1H, ArH), 4.22 – 4.07 (m, 2H, OC*H*$_2$CH$_3$), 2.39 (s, 3H, CH_3), 1.24 (t, *J* = 7.0 Hz, 3H, OCH_2C*H*$_3$). LRMS (CI) m/z calcd. for $C_{18}H_{20}N_3O_4S_2$ $[M+H]^+$: 406.1 found: 406.0.

(±) Isopropyl 6-methyl-2-(phenylsulfonamido)-4-(thiophen-2-yl)-1,4-dihydropyrimidine-5-carboxylate (126). Purified by column chromatography (Hex–AcOEt 3:1 – 1:1). Yield: 3%. Mp: 186 – 188 ºC ^{1}H NMR (300 MHz, $CDCl_3$), δ (ppm): 8.35 (brs, 1H, NH), 8.21 (brs, 1H, NH), 7.73 (d, *J* = 7.6 Hz, 2H, ArH), 7.48 (t, *J* = 7.3 Hz, 1H, ArH), 7.40 – 7.30 (m, *J* = 7.6 Hz, 2H, ArH + CH), 7.22 – 7.12 (m, 1H, ArH), 6.87 (d, *J* = 3.4 Hz, 2H, ArH), 5.77 (d, *J* = 3.1 Hz, 1H, ArH), 5.03 (hept, *J* = 6.6 Hz, 1H, OC*H*$(CH_3)_2$), 2.38 (s, 3H, CH_3), 1.25 (d, *J* = 6.0 Hz, 3H, OCH(C*H*$_3)_2$), 1.16 (d, *J* = 6.2 Hz, 3H, OCH(C*H*$_3)_2$). LRMS (CI) m/z calcd. for $C_{19}H_{22}N_3O_4S_2$ $[M+H]^+$: 420.1 found: 420.2.

(±) Ethyl 6-methyl-2-(phenylsulfonamido)-4-(thiophen-3-yl)-1,4-dihydropyrimidine-5-carboxylate (127). Purified by column chromatography (Hex–AcOEt 3:1 – 1:1). Yield: 19%. Mp: 189 – 191 ºC. ^{1}H NMR (300 MHz, $CDCl_3$), δ (ppm): 8.29 (brs, 1H, NH), 8.17 (brs, 1H, NH), 7.71 (d, *J* = 8.1 Hz, 2H, ArH), 7.55 – 7.44 (m, 1H, ArH), 7.40 – 7.32 (m, 2H, ArH + CH), 7.24 – 7.19 (m, 1H, ArH), 7.02 (s, 1H, ArH), 6.91 (d, *J* = 5.0 Hz, 1H, ArH), 5.61 (d, *J* = 3.7 Hz, 1H, ArH), 4.25 – 4.09 (m, 2H, OC*H*$_2$$CH_3$), 2.37 (s, 3H, CH_3), 1.31 – 1.16 (m, *J* = 7.0 Hz, 3H, OCH_2C*H*$_3$). LRMS (CI) m/z calcd. for $C_{18}H_{20}N_3O_4S_2$ $[M+H]^+$: 406.1 found: 406.0.

(±) Isopropyl 6-methyl-2-(phenylsulfonamido)-4-(thiophen-3-yl)-1,4-dihydropyrimidine-5-carboxylate (128). Purified by column chromatography (Hex–AcOEt 3:1 – 1:1). Yield: 9%. Mp: 201 – 203 ºC. ^{1}H NMR (300 MHz, $CDCl_3$), δ (ppm): 8.09 (brs, 1H, NH), 8.01 (brs, 1H, NH), 7.74 (d, *J* = 7.6 Hz, 2H, ArH), 7.50 (t, J = 7.3 Hz, 1H, ArH), 7.43 – 7.33 (m, 2H, ArH + CH), 7.23 (dd, *J* = 5.1, 3.1 Hz, 1H, ArH), 7.02 (s, 1H, ArH), 6.92 (d, *J* = 4.9 Hz, 1H) , ArH, 5.60 (d, *J* = 3.2 Hz, 1H, ArH), 5.03 (hept, *J* = 6.3 Hz, 1H, OC*H*$(CH_3)_2$), 2.36 (s, 3H, CH_3), 1.24 (d, *J* = 6.2 Hz, 3H, OCH(C*H*$_3)_2$), 1.16 (d, *J* = 6.2 Hz, 3H, OCH(C*H*$_3)_2$). LRMS (CI) m/z calcd. for $C_{19}H_{22}N_3O_4S_2$ $[M+H]^+$: 420.1 found: 420.0.

(±) Ethyl 2-((1*H*-benzo[*d*]imidazol-2-yl)amino)-4-(furan-2-yl)-6-methyl-1,4-dihydropyrimidine-5-carboxylate (129). Purified by column chromatography (DCM–MeOH 99:1 – 95:5). Yield: 25%. Mp: 170-172 ºC. ^{1}H NMR (300 MHz, $CDCl_3$), δ (ppm): 11.64 (brs, 1H, NH), 10.92 (brs, 1H, NH), 8.28 (s, 1H, NH), 7.46 – 7.36 (m, 3H, ArH), 7.19 – 7.09 (m, 2H, ArH), 6.50 (m, 1H, ArH), 6.36 (m, 1H, ArH), 5.79 (m, 1H, ArH), 4.05 (q, *J* = 5.1 Hz, 2H, OC*H*$_2$$CH_3$), 2.27 (s, 3H, CH_3), 1.32 (t, *J* = 5.0 Hz, 3H, OCH_2C*H*$_3$). LRMS (CI) m/z calcd. for $C_{19}H_{20}N_5O_3$ $[M+H]^+$: 365.1 found: 365.1.

(±) Isopropyl 2-((1*H*-benzo[*d*]imidazol-2-yl)amino)-4-(furan-2-yl)-6-methyl-1,4-dihydropyrimidine-5-carboxylate (130). Purified by column chromatography (DCM–MeOH 99:1 – 95:5). Yield: 29%. Mp: 192-194 ºC. ^{1}H NMR (300 MHz, DMSO-d_6), δ (ppm): 11.46 (brs, 1H, NH), 10.81 – 10.32 (brs, 1H, NH), 9.91 (brs, 1H, NH), 7.53 (s, 1H, ArH), 7.38 – 7.12 (m, 2H, ArH), 7.10 – 6.91 (m, 2H, ArH), 6.33 (d, J = 2.7 Hz, 1H, ArH), 6.16 (d, J = 3.2 Hz, 1H, ArH), 5.59 (s, 1H, ArH), 4.97 – 4.78 (m, 1H, OC*H*$(CH_3)_2$), 2.34 (s, 3H, CH_3), 1.19 (d, J = 6.4 Hz, 3H, OCH(C*H*$_3)_2$), 1.09 (d, J = 6.2 Hz, 3H, OCH(C*H*$_3)_2$). LRMS (CI) m/z calcd. for $C_{20}H_{22}N_5O_3$ $[M+H]^+$: 379.2 found: 379.2.

(±) Ethyl 2-((1*H*-benzo[*d*]imidazol-2-yl)amino)-4-(furan-3-yl)-6-methyl-1,4-dihydropyrimidine-5-carboxylate (131). Purified by column chromatography (DCM–MeOH 99:1 – 95:5). Yield: 14%. Mp: 130-132 ºC. ^{1}H NMR (300 MHz, $CDCl_3$), δ (ppm): 7.36 (d, J = 13.3 Hz, 2H, ArH), 7.26 (s, 1H, ArH), 7.23 – 7.16 (m, 1H, ArH), 7.17 (s, 1H, ArH), 7.14 – 7.05 (m, 2H, ArH), 6.38 (s, 1H, ArH), 5.61 (brs, 1H, NH), 4.20 (q, J = 7.1 Hz, 2H, OC*H*$_2$CH$_3$), 2.42 (s, 4H, CH_3 + NH), 1.29 (t, J = 7.2 Hz, 3H, OCH_2C*H*$_3$). LRMS (CI) m/z calcd. for $C_{20}H_{22}N_5O_3$ $[M+H]^+$: 365.1 found: 365.1.

(±) Isopropyl 2-((1*H*-benzo[*d*]imidazol-2-yl)amino)-4-(furan-3-yl)-6-methyl-1,4-dihydropyrimidine-5-carboxylate (132). Purified by column chromatography (DCM–MeOH 99:1 – 95:5). Yield: 12%. Mp: 124-126 ºC. ^{1}H NMR (300 MHz, $CDCl_3$), δ (ppm): 11.27 (brs, 1H, NH), 7.42 – 7.36 (m, 3H, ArH), 7.32 (d, J = 9.3 Hz, 2H, ArH), 7.20 – 7.14 (m, 1H, ArH), 7.11 (brs, 1H, NH), 6.41 – 6.35 (m, 1H, ArH), 5.63 (s, 1H, ArH), 5.09 (p, J = 6.4 Hz, 1H, OC*H*$(CH_3)_2$), 2.43 (brs, 1H, NH), 2.36 (s, 3H, CH_3), 1.26 (dd, J = 12.7, 6.3 Hz, 6H, OCH(C*H*$_3)_2$). LRMS (CI) m/z calcd. for $C_{19}H_{20}N_5O_2S$ $[M+H]^+$: 379.2 found: 379.2.

(±) Ethyl 2-((1*H*-benzo[*d*]imidazol-2-yl)amino)-6-methyl-4-(thiophen-2-yl)-1,4-dihydropyrimidine-5-carboxylate (133). Purified by column chromatography (DCM–MeOH 99:1 – 95:5). Yield: 22%. Mp: 152-154 ºC. ^{1}H NMR (300 MHz, $CDCl_3$), δ (ppm): 12.77 (brs, 1H, NH), 7.49 (s, 1H, ArH), 7.36 – 7.16 (m, 1H, ArH), 7.20 (s, 1H, ArH), 7.16 – 7.08 (m, 2H, ArH), 7.02 (d, J = 3.5 Hz, 1H, ArH), 6.97 – 6.85 (m, 1H, ArH), 6.04 – 5.92 (m, 1H, ArH), 5.77 (brs, 1H, NH), 4.23 (q, J = 7.1 Hz, 2H, OC*H*$_2$CH$_3$), 2.54 (brs, 1H, NH), 2.43 (s, 3H, CH_3), 1.30 (t, J = 7.0 Hz, 3H, OCH_2C*H*$_3$). LRMS (CI) m/z calcd. for $C_{20}H_{22}N_5O_2S$ $[M+H]^+$: 381.1 found: 381.1.

(±) Isopropyl 2-((1*H*-benzo[*d*]imidazol-2-yl)amino)-6-methyl-4-(thiophen-2-yl)-1,4-dihydropyrimidine-5-carboxylate (134). Purified by column chromatography (DCM–MeOH 99:1 – 95:5). Yield: 20%. Mp: 139-141 ºC. ^{1}H NMR (300 MHz, $CDCl_3$), δ (ppm): 10.21 (brs, 1H, NH), 7.50 – 7.44 (m, 2H, ArH), 7.02 – 6.95 (m, 1H, ArH), 6.94 – 6.78 (m, 4H, ArH), 5.97 (s, 1H, ArH), 5.13 – 5.02 (m, 1H, OC*H*$(CH_3)_2$), 2.53 (brs, 1H, NH), 2.37 (brs, 1H, NH), 2.33 (s, 3H, CH_3), 1.28 (d, *J* = 6.2 Hz, 3H, OCH(C*H*$_3)_2$), 1.21 (d, *J* = 6.2 Hz, 3H, OCH(C*H*$_3)_2$). LRMS (CI) m/z calcd. for $C_{19}H_{20}N_5O_2S$ $[M+H]^+$: 395.1 found: 395.1.

(±) Ethyl 2-((1*H*-benzo[*d*]imidazol-2-yl)amino)-6-methyl-4-(thiophen-3-yl)-1,4-dihydropyrimidine-5-carboxylate (135). Purified by column chromatography (DCM–MeOH 99:1 – 95:5). Yield: 12%. Mp: 151-157 ºC. ^{1}H NMR (300 MHz, $CDCl_3$), δ (ppm): 7.58 (s, 1H, ArH), 7.39 (s, 1H, ArH), 7.32 (s, 1H, ArH), 7.14 (s, 1H, ArH), 7.07 (d, *J* = 5.1 Hz, 1H, ArH), 6.96 (t, *J* = 7.5 Hz, 1H, ArH), 6.69 (d, *J* = 7.9 Hz, 1H, ArH), 6.52 (brs, 1H, NH), 5.44 (s, 1H, ArH), 4.16 – 4.07 (m, 2H, OC*H*$_2$$CH_3$), 2.52 (s, 3H, CH_3), 1.29 – 1.15 (m, 4H, OCH_2C*H*$_3$ + NH). LRMS (CI) m/z calcd. for $C_{20}H_{22}N_5O_2S$ $[M+H]^+$: 381.1 found: 381.1.

(±) Isopropyl 2-((1*H*-benzo[*d*]imidazol-2-yl)amino)-6-methyl-4-(thiophen-3-yl)-1,4-dihydropyrimidine-5-carboxylate (136). Purified by column chromatography (DCM–MeOH 99:1 – 95:5). Yield: 10%. Mp: 130-137 ºC. ^{1}H NMR (300 MHz, $CDCl_3$), δ (ppm): 12.62 (brs, 1H, NH), 10.15 (brs, 1H, NH), 7.50 – 7.44 (m, 2H, ArH), 7.26 (s, 1H, ArH), 7.24 – 7.17 (m, 1H, ArH), 7.17 – 7.11 (m, 3H, ArH), 5.80 (brs, 1H, NH), 5.50 (s, 1H, ArH), 5.09 – 5.03 (m, 1H, OC*H*$(CH_3)_2$), 2.28 (s, 3H, CH_3), 1.27 (d, *J* = 6.3 Hz, 3H, OCH(C*H*$_3)_2$), 1.20 (d, *J* = 6.3 Hz, 3H, OCH(C*H*$_3)_2$. LRMS (CI) m/z calcd. for $C_{19}H_{22}N_3O_4S_2$ $[M+H]^+$: 395.1 found: 395.1.

(±) Ethyl 7-(furan-2-yl)-5-methyl-2-(trifluoromethyl)-4,7-dihydro-[1,2,4]triazolo[1,5-*a*]pyrimidine-6-carboxylate (137). Purified by column chromatography (Hex–AcOEt 3:1 – 1:1). Yield: 45%. Mp: 149 – 151 ºC. ^{1}H NMR (300 MHz, $CDCl_3$), δ (ppm): 9.29 (brs, 1H, NH), 7.32 (s, 1H, ArH), 6.57 (s, 1H, CH), 6.39 – 6.27 (m, 2H, ArH), 4.15 (p, *J* = 7.0 Hz, 2H, OC*H*$_2$$CH_3$), 2.56 (s, 3H, CH_3), 1.28 – 1.14 (m, 3H, OCH_2C*H*$_3$). LRMS (CI) m/z calcd. for $C_{14}H_{14}F_3N_4O_3$ $[M+H]^+$: 343.1 found: 343.0.

(±) Isopropyl 7-(furan-2-yl)-5-methyl-2-(trifluoromethyl)-4,7-dihydro-[1,2,4]triazolo[1,5-*a*]pyrimidine-6-carboxylate (138). Purified by column chromatography (Hex–AcOEt 3:1 – 1:1). Yield: 34%. Mp: 171 – 173 ºC. ^{1}H NMR (300 MHz, $CDCl_3$), δ (ppm): 9.69 (brs, 1H, NH), 7.36 – 7.29 (m, 1H, ArH), 6.57 (s, 1H, CH), 6.39 – 6.27 (m, 2H, ArH), 5.08 – 4.94 (m, 1H, C*H*$(CH_3)_2$), 2.55 (s, 3H, CH_3), 1.23 (d, *J* = 6.3 Hz, 3H, OCH(C*H*$_3$)$_2$), 1.08 (d, *J* = 6.3 Hz, 3H, OCH(C*H*$_3$)$_2$). LRMS (CI) m/z calcd. for $C_{15}H_{16}F_3N_4O_3$ $[M+H]^+$: 357.1 found: 357.1.

(±) Ethyl 7-(furan-3-yl)-5-methyl-2-(trifluoromethyl)-4,7-dihydro-[1,2,4]triazolo[1,5-*a*]pyrimidine-6-carboxylate (139). Purified by column chromatography (Hex–AcOEt 3:1 – 1:1). Yield: 55%. Mp: 130 – 132 ºC. ^{1}H NMR (300 MHz, $CDCl_3$), δ (ppm): 9.41 (brs, 1H, NH), 7.40 (s, 1H, ArH), 7.33 (t, *J* = 1.8 Hz, 1H, ArH), 6.51 (s, 1H, ArH), 6.30 (s, 1H, CH), 4.25 – 4.11 (m, 2H, OC*H*$_2$CH$_3$), 2.53 (s, 3H, CH_3), 1.23 (t, *J* = 7.1 Hz, 3H, OCH_2C*H*$_3$). LRMS (CI) m/z calcd. for $C_{14}H_{14}F_3N_4O_3$ $[M+H]^+$: 343.1 found: 343.1.

(±) Isopropyl 7-(furan-3-yl)-5-methyl-2-(trifluoromethyl)-4,7-dihydro-[1,2,4]triazolo[1,5-*a*]pyrimidine-6-carboxylate (140). Purified by column chromatography (Hex–AcOEt 3:1 – 1:1). Yield: 48%. Mp: 165 – 167 ºC. ^{1}H NMR (300 MHz, $CDCl_3$), δ (ppm): 9.18 (brs, 1H, NH), 7.40 (s, 1H, ArH), 7.33 (d, *J* = 1.7 Hz, 1H, ArH), 6.50 (s, 1H, CH), 6.31 (s, 1H, ArH), 5.05 (p, *J* = 6.2 Hz, 1H, OC*H*$(CH_3)_2$), 2.52 (s, 3H, CH_3), 1.25 (d, *J* = 6.2 Hz, 3H, OCH(C*H*$_3$)$_2$), 1.13 (d, *J* = 6.2 Hz, 3H, OCH(C*H*$_3$)$_2$). LRMS (CI) m/z calcd. for $C_{15}H_{16}F_3N_4O_3$ $[M+H]^+$: 357.1 found: 357.0.

(±) Ethyl 5-methyl-7-(thiophen-2-yl)-2-(trifluoromethyl)-4,7-dihydro-[1,2,4]triazolo[1,5-*a*]pyrimidine-6-carboxylate (141). Purified by column chromatography (Hex–AcOEt 3:1 – 1:1). Yield: 33%. Mp: 140 – 143 ºC. ^{1}H NMR (300 MHz, $CDCl_3$), δ (ppm): 9.51 (brs, 1H, NH), 7.29 – 7.19 (m, 1H, ArH), 7.04 (d, *J* = 3.6 Hz, 1H, ArH), 6.98 – 6.89 (m, 1H, ArH), 6.78 (s, 1H, CH), 4.23 – 4.06 (m, 2H, OC*H*$_2$CH$_3$), 2.56 (s, 3H, CH_3), 1.23 – 1.12 (m, 3H, OCH_2C*H*$_3$). LRMS (CI) m/z calcd. for $C_{14}H_{14}F_3N_4O_2S$ $[M+H]^+$: 359.1 found: 359.0.

(±) Isopropyl 5-methyl-7-(thiophen-2-yl)-2-(trifluoromethyl)-4,7-dihydro-[1,2,4]triazolo[1,5-*a*]pyrimidine-6-carboxylate (142). Purified by column chromatography (Hex–AcOEt 3:1 – 1:1). Yield: 53%. Mp: 144 – 146 ºC. ^{1}H NMR (300 MHz, $CDCl_3$), δ (ppm): 9.55 (brs, 1H, NH), 7.29 – 7.20 (m, 1H, ArH), 7.09 – 7.02 (m, 1H, ArH), 6.98 – 6.89 (m, 1H, ArH), 6.76 (s, 1H, CH), 5.01 (p, *J* = 6.2 Hz, 1H, OC*H*$(CH_3)_2$), 2.56 (s, 3H, CH_3), 1.24 (d, *J* = 6.2 Hz, 3H, OCH(C*H*$_3)_2$), 1.03 (d, *J* = 6.2 Hz, 3H, OCH(C*H*$_3)_2$). LRMS (CI) m/z calcd. for $C_{15}H_{16}F_3N_4O_2S$ $[M+H]^+$: 373.1 found: 373.0.

(±) Ethyl 5-methyl-7-(thiophen-3-yl)-2-(trifluoromethyl)-4,7-dihydro-[1,2,4]triazolo[1,5-*a*]pyrimidine-6-carboxylate (143). Purified by column chromatography (Hex–AcOEt 3:1 – 1:1). Yield: 34%. Mp: 175 – 177 ºC. ^{1}H NMR (300 MHz, $CDCl_3$), δ (ppm): 9.41 (brs, 1H, ArH), 7.30 – 7.19 (m, 2H, ArH), 7.01 (dd, *J* = 4.9, 1.5 Hz, 1H, ArH), 6.60 (s, 1H, CH), 4.14 (q, *J* = 7.1 Hz, 2H, OC*H*$_2$CH$_3$), 2.54 (s, 3H, CH_3), 1.18 (t, *J* = 7.1 Hz, 3H, OCH_2C*H*$_3$). LRMS (CI) m/z calcd. for $C_{14}H_{14}F_3N_4O_2S$ $[M+H]^+$: 359.1 found: 359.0.

(±) Isopropyl 5-methyl-7-(thiophen-3-yl)-2-(trifluoromethyl)-4,7-dihydro-[1,2,4]triazolo[1,5-*a*]pyrimidine-6-carboxylate (144). Purified by column chromatography (Hex–AcOEt 3:1 – 1:1). Yield: 39%. Mp: 186 – 188 ºC. ^{1}H NMR (300 MHz, $CDCl_3$), δ (ppm): 9.09 (brs, 1H, NH), 7.29 – 7.21 (m, 2H, ArH), 7.07 – 6.99 (m, 1H, ArH), 6.59 (s, 1H, CH), 5.00 (p, *J* = 6.2 Hz, 1H, OC*H*$(CH_3)_2$), 2.54 (s, 3H, CH_3), 1.23 (d, *J* = 6.2 Hz, 3H, OCH(C*H*$_3)_2$), 1.04 (d, *J* = 6.2 Hz, 3H, OCH(C*H*$_3)_2$). LRMS (CI) m/z calcd. for $C_{15}H_{16}F_3N_4O_2S$ $[M+H]^+$: 373.1 found: 373.0.

(±) 6-Ethyl 2-methyl 7-(furan-2-yl)-5-methyl-4,7-dihydro-[1,2,4]triazolo[1,5-*a*]pyrimidine-2,6-dicarboxylate (145). Purified by column chromatography (Hex–AcOEt 3:1 – 1:1). Yield: 65%. Mp: 186 – 188 ºC. ^{1}H NMR (300 MHz, $CDCl_3$), δ (ppm): 9.98 (brs, 1H, NH), 7.32 – 7.27 (m, 1H, ArH), 6.59 (s, 1H, CH), 6.37 – 6.33 (m, 1H, ArH), 6.31 – 6.25 (m, 1H, ArH), 4.37 – 4.05 (m, 2H, OC*H*$_2$CH$_3$), 3.94 (s, 3H, $COOCH_3$), 2.63 (s, 3H, CH_3), 1.36 – 0.93 (m, 3H, OCH_2C*H*$_3$). ^{13}C NMR (75 MHz, $CDCl_3$), δ (ppm): 165.2, 159.9, 151.8, 151.8, 148.9, 147.3, 142.8, 110.5, 108.4, 96.6, 60.3, 54.0, 52.7, 19.2, 14.1. HRMS (APCI) *m/z* calcd. for $C_{15}H_{17}N_4O_5$ $[M+H]^+$: 333.1193 found: 333.1192.

(±) 6-isopropyl 2-methyl 7-(furan-2-yl)-5-methyl-4,7-dihydro-[1,2,4]triazolo[1,5-a]pyrimidine-2,6-dicarboxylate (146). Purified by column chromatography (Hex–AcOEt 3:1 – 1:1). Yield: 38%. Mp: 232 – 233 ºC. ^{1}H NMR (300 MHz, $CDCl_3$), δ (ppm): 9.85 (brs, 1H, NH), 7.29 (s, 1H, ArH), 6.58 (s, 1H, CH), 6.37 – 6.32 (m, 1H, ArH), 6.32 – 6.26 (m, 1H, ArH), 5.13 – 4.88 (m, 1H, OC*H*$(CH_3)_2$), 3.94 (s, 3H, $COOCH_3$), 2.61 (s, 3H, CH_3), 1.23 (d, J = 6.1 Hz, 3H, OCH(C*H*$_3)_2$), 1.08 (d, *J* = 6.0 Hz, 3H, OCH(C*H*$_3)_2$). ^{13}C NMR (75 MHz, $CDCl_3$), δ (ppm): 164.6, 160.0, 152.0, 151.8, 148.8, 146.9, 142.7, 110.4, 108.4, 96.9, 67.7, 54.1, 52.7, 21.9, 21.6, 19.1. HRMS (APCI) *m/z* calcd. for $C_{16}H_{19}N_4O_5$ $[M+H]^+$: 347.1350 found: 347.1359.

(±) 6-ethyl 2-methyl 7-(furan-3-yl)-5-methyl-4,7-dihydro-[1,2,4]triazolo[1,5-a]pyrimidine-2,6-dicarboxylate (147). Purified by column chromatography (Hex–AcOEt 3:1 – 1:1). Yield: 28%. Mp: 245 – 247 ºC. ^{1}H NMR (300 MHz, $CDCl_3$), δ (ppm): 9.88 (brs, 1H, NH), 7.41 (s, 1H, ArH), 7.30 (d, *J* = 1.6 Hz, 1H, ArH), 6.53 (s, 1H, CH_3), 6.30 (s, 1H, ArH), 4.17 (q, *J* = 7.1 Hz, 2H, OC*H*$_2$$CH_3$), 3.95 (s, 3H, $COOCH_3$), 2.60 (s, 3H, CH_3), 1.23 (t, *J* = 7.1 Hz, 3H, OCH_2C*H*$_3$). ^{13}C NMR (75 MHz, $CDCl_3$), δ (ppm): 165.3, 159.9, 151.7, 148.9, 146.6, 143.5, 140.3, 125.5, 109.0, 98.6, 60.3, 52.7, 52.5, 19.0, 14.1. LRMS (CI) *m/z* calcd. for $C_{15}H_{17}N_4O_5$ $[M+H]^+$: 333.1 found: 333.0.

(±) 6-Isopropyl 2-methyl 7-(furan-3-yl)-5-methyl-4,7-dihydro-[1,2,4]triazolo[1,5-*a*]pyrimidine-2,6-dicarboxylate (148). Purified by column chromatography (Hex–AcOEt 3:1 – 1:1). Yield: 61%. Mp: 272 – 273 ºC. ^{1}H NMR (300 MHz, $CDCl_3$), δ (ppm): 9.86 (brs, 1H, NH), 7.41 (s, 1H, ArH), 7.30 (s, 1H, ArH), 6.52 (s, 1H, ArH), 6.31 (s, 1H, CH), 5.16 – 4.89 (m, 1H, OC*H*$(CH_3)_2$), 3.95 (s, 3H, $COOCH_3$), 2.59 (s, 3H, CH_3), 1.25 (d, *J* = 6.2 Hz, 3H, OCH(C*H*$_3)_2$), 1.14 (d, *J* = 6.3 Hz, 3H, OCH(C*H*$_3)_2$). ^{13}C NMR (75 MHz, $CDCl_3$), δ (ppm): 164.77, 159.91, 151.7, 148.81, 146.17, 143.45, 140.37, 125.48, 109.01, 99.00, 67.86, 52.71, 52.56, 21.99, 21.65, 19.02. HRMS (APCI) *m/z* calcd. for $C_{16}H_{19}N_4O_5$ $[M+H]^+$: 347.1350 found: 347.1352.

(±) 6-ethyl 2-methyl 5-methyl-7-(thiophen-2-yl)-4,7-dihydro-[1,2,4]triazolo[1,5-a]pyrimidine-2,6-dicarboxylate (149). Purified by column chromatography (Hex–AcOEt 3:1 – 1:1). Yield: 23%. Mp: 227 – 229 ºC. ^{1}H NMR (300 MHz, $CDCl_3$), δ (ppm): 9.91 (brs, 1H, NH), 7.21 (dd, *J* = 5.0, 1.2 Hz, 1H, ArH), 7.05 (d, *J* = 2.5 Hz, 1H, ArH), 6.91 (dd, *J* = 5.1, 13.6 Hz, 1H, ArH), 6.80 (s, 1H, CH), 4.24 – 4.08 (m, 2H, OC*H*$_2$CH$_3$), 3.95 (s, 3H, $COOCH_3$), 2.64 (s, 3H, CH_3), 1.18 (t, *J* = 7.1 Hz, 3H, OCH_2CH_3). LRMS (CI) *m/z* calcd. for $C_{15}H_{17}N_4O_4S$ $[M+H]^+$: 349.1 found: 349.0.

(±) 6-isopropyl 2-methyl 5-methyl-7-(thiophen-2-yl)-4,7-dihydro-[1,2,4]triazolo[1,5-a]pyrimidine-2,6-dicarboxylate (150). Purified by column chromatography (Hex–AcOEt 3:1 – 1:1). Yield: 44%. Mp: 209 – 211 ºC. ^{1}H NMR (300 MHz, $CDCl_3$), δ (ppm): 9.47 (brs, 1H, NH), 7.21 (d, J = 4.8 Hz, 1H, ArH), 7.10 – 7.03 (m, 1H, ArH), 6.95 – 6.88 (m, 1H, ArH), 6.78 (s, 1H, CH), 5.25 – 4.84 (m, 1H, OC*H*$(CH_3)_2$), 3.94 (s, 3H, $COOCH_3$), 2.63 (s, 3H, CH_3), 1.23 (d, J = 6.2 Hz, 3H, OCH(C*H*$_3$)$_2$), 1.05 (d, J = 6.0 Hz, 3H, OCH(C*H*$_3$)$_2$). LRMS (CI) *m/z* calcd. for $C_{16}H_{19}N_4O_4S$ $[M+H]^+$: 363.1 found: 363.0.

(±) 6-ethyl 2-methyl 5-methyl-7-(thiophen-3-yl)-4,7-dihydro-[1,2,4]triazolo[1,5-a]pyrimidine-2,6-dicarboxylate (151). Purified by column chromatography (Hex–AcOEt 3:1 – 1:1). Yield: 33%. Mp: 257 – 259 ºC. ^{1}H NMR (300 MHz, $CDCl_3$), δ (ppm): 9.92 (brs, 1H, NH), 7.26 – 7.14 (m, 2H, ArH), 7.02 (dd, *J* = 4.8, 1.6 Hz, 1H, ArH), 6.62 (s, 1H, CH), 4.25 – 4.05 (m, 2H, OC*H*$_2$CH$_3$), 3.94 (s, 3H, $COOCH_3$), 2.61 (s, 3H, CH_3), 1.18 (t, J = 7.1 Hz, 3H, OCH_2CH_3). LRMS (CI) *m/z* calcd. for $C_{15}H_{17}N_4O_4S$ $[M+H]^+$: 349.1 found: 349.0.

(±) 6-isopropyl 2-methyl 5-methyl-7-(thiophen-3-yl)-4,7-dihydro-[1,2,4]triazolo[1,5-a]pyrimidine-2,6-dicarboxylate (152). Purified by column chromatography (Hex–AcOEt 3:1 – 1:1). Yield: 28%. Mp: 266 – 268 ºC. ^{1}H NMR (300 MHz, $CDCl_3$), δ (ppm): 9.69 (brs, 1H, NH), 7.29 – 7.17 (m, 2H, ArH), 7.03 (d, *J* = 4.4 Hz, 1H, ArH), 6.61 (s, 1H, CH), 5.08 – 4.89 (m, 1H, OC*H*$(CH_3)_2$), 3.93 (s, 3H, $COOCH_3$), 2.60 (s, 3H, CH_3), 1.22 (d, *J* = 6.2 Hz, 3H, OCH(C*H*$_3$)$_2$), 1.05 (d, *J* = 6.3 Hz, 3H, OCH(C*H*$_3$)$_2$). LRMS (CI) *m/z* calcd. for $C_{16}H_{19}N_4O_4S$ $[M+H]^+$: 363.1 found: 363.0.

(±) Ethyl 7-(furan-2-yl)-5-methyl-2-phenyl-4,7-dihydro-[1,2,4]triazolo[1,5-*a*]pyrimidine-6-carboxylate (153). Purified by column chromatography (Hex–AcOEt 3:1 – 1:1). Yield: 29%. Mp: 199 – 201 ºC. ^{1}H NMR (300 MHz, $CDCl_3$), δ (ppm): 9.68 (brs, 1H, NH), 8.04 – 7.93 (m, 2H, ArH), 7.48 – 7.35 (m, 3H, ArH), 7.31 (s, 1H, ArH), 6.59 (s, 1H, CH), 6.38 – 6.25 (m, 2H, ArH), 4.24 – 4.01 (m, 2H, OCH_2CH_3), 2.31 (s, 3H, CH_3), 1.19 (t, *J* = 7.1 Hz, 3H, OCH_2CH_3). ^{13}C NMR (75 MHz, $CDCl_3$), δ (ppm): 165.4, 159.9, 152.8, 148.5, 146.8, 142.5, 130.3, 129.6, 128.5, 126.6, 110.4, 107.9, 96.5, 60.1, 53.5, 19.3, 14.1. LRMS (CI) *m/z* calcd. for $C_{19}H_{19}N_4O_3$ $[M+H]^+$: 351.1 found: 351.0.

(±) Isopropyl 7-(furan-2-yl)-5-methyl-2-phenyl-4,7-dihydro-[1,2,4]triazolo[1,5-*a*]pyrimidine-6-carboxylate (154). Purified by column chromatography (Hex–AcOEt 3:1 – 1:1). Yield: 32%. Mp: 197 – 199 ºC. ^{1}H NMR (300 MHz, $CDCl_3$), δ (ppm): 8.85 (brs, 1H, NH), 8.04 – 7.95 (m, 2H, ArH), 7.47 – 7.34 (m, 3H, ArH), 7.34 – 7.28 (m, 1H, ArH), 6.58 (s, 1H, CH), 6.37 – 6.26 (m, 2H, ArH), 5.00 (hept, *J* = 6.2 Hz, 1H, $OCH(CH_3)_2$), 2.38 (s, 3H, CH_3), 1.23 (d, *J* = 6.2 Hz, 3H, $OCH(CH_3)_2$), 1.08 (d, *J* = 6.3 Hz, 3H, $OCH(CH_3)_2$). ^{13}C NMR (75 MHz, $CDCl_3$), δ (ppm): 164.8, 159.8, 152.8, 148.3, 146.3, 142.4, 130.2, 129.6, 128.5, 126.5, 110.3, 107.9, 96.8, 67.4, 53.5, 21.9, 21.6, 19.2. LRMS (CI) *m/z* calcd. for $C_{20}H_{21}N_4O_3$ $[M+H]^+$: 365.2 found: 365.1.

(±) Ethyl 7-(furan-3-yl)-5-methyl-2-phenyl-4,7-dihydro-[1,2,4]triazolo[1,5-*a*]pyrimidine-6-carboxylate (155). Purified by column chromatography (Hex–AcOEt 3:1 – 1:1). Yield: 29%. Mp: 186 – 188 ºC. ^{1}H NMR (300 MHz, $CDCl_3$), δ (ppm): 9.62 (brs, 1H, NH), 8.04 – 7.94 (m, 2H, ArH), 7.49 – 7.36 (m, 4H, ArH), 7.36 – 7.28 (m, 1H, ArH), 6.54 (s, 1H, CH), 6.33 (d, *J* = 2.0 Hz, 1H, ArH), 4.17 (q, *J* = 7.1 Hz, 2H, OCH_2CH_3), 2.27 (s, 3H, CH_3), 1.24 (t, *J* = 7.1 Hz, 3H, OCH_2CH_3). ^{13}C NMR (75 MHz, $CDCl_3$), δ (ppm): 165.6, 159.9, 148.5, 146.0, 143.2, 139.9, 130.3, 129.65, 128.5, 126.5, 126.2, 109.2, 98.5, 60.2, 52.0, 19.3, 14.2. LRMS (CI) *m/z* calcd. for $C_{19}H_{19}N_4O_3$ $[M+H]^+$: 351.1 found: 351.0.

(±) Isopropyl 7-(furan-3-yl)-5-methyl-2-phenyl-4,7-dihydro-[1,2,4]triazolo[1,5-*a*]pyrimidine-6-carboxylate (156). Purified by column chromatography (Hex–AcOEt 3:1 – 1:1). Yield: 32%. Mp: 169 – 171 ºC. ^{1}H NMR (300 MHz, $CDCl_3$), δ (ppm): 8.61 (brs, 1H, NH), 8.04 – 7.95 (m, 2H, ArH), 7.47 – 7.36 (m, 3H, ArH), 7.31 (s, 2H, ArH), 6.52 (s, 1H, CH), 6.33 (s, 1H, ArH), 5.05 (hept, J = 6.7 Hz, 1H, OC*H*$(CH_3)_2$), 2.35 (s, 3H, CH_3), 1.26 (d, J = 5.9 Hz, 3H, OCH(C*H*$_3)_2$), 1.16 (d, J = 6.1 Hz, 3H, OCH(C*H*$_3)_2$). ^{13}C NMR (75 MHz, $CDCl_3$), δ (ppm): 165.1, 159.9, 148.6, 145.8, 143.2, 140.1, 130.4, 129.6, 128.6, 126.5, 126.2, 109.2, 98.8, 67.6, 52.0, 22.1, 21.7, 19.2. LRMS (CI) *m/z* calcd. for $C_{20}H_{21}N_4O_3$ $[M+H]^+$: 365.2 found: 365.1.

(±) Ethyl 5-methyl-2-phenyl-7-(thiophen-2-yl)-4,7-dihydro-[1,2,4]triazolo[1,5-*a*]pyrimidine-6-carboxylate (157). Purified by column chromatography (Hex–AcOEt 3:1 – 1:1). Yield: 41%. Mp: 183 – 185 ºC. ^{1}H NMR (300 MHz, $CDCl_3$), δ (ppm): 8.74 (brs, 1H, NH), 7.99 (dd, J = 7.6, 2.1 Hz, 2H, ArH), 7.47 – 7.35 (m, 3H, ArH), 7.20 (dd, J = 5.1, 1.3 Hz, 1H, ArH), 7.07 – 6.98 (m, 1H, ArH), 6.91 (dd, J = 5.1, 3.6 Hz, 1H, ArH), 6.80 (s, 1H, CH), 4.15 (q, J = 7.1 Hz, 2H, OC*H*$_2$CH$_3$), 2.40 (s, 3H, CH_3), 1.20 (t, J = 7.1 Hz, 3H, OCH$_2$C*H*$_3$). LRMS (CI) *m/z* calcd. for $C_{19}H_{19}N_4O_2S$ $[M+H]^+$: 367.1 found: 367.0.

(±) Isopropyl 5-methyl-2-phenyl-7-(thiophen-2-yl)-4,7-dihydro-[1,2,4]triazolo[1,5-*a*]pyrimidine-6-carboxylate (158). Purified by column chromatography (Hex–AcOEt 3:1 – 1:1). Yield: 38%. Mp: 149 – 151 ºC. ^{1}H NMR (300 MHz, $CDCl_3$), δ (ppm): 8.74 (brs, 1H, NH), 8.12 – 8.01 (m, 2H, ArH), 7.42 – 7.32 (m, 3H, ArH), 7.26 – 7.18 (m, 1H, ArH), 7.07 – 6.98 (m, 1H, ArH), 6.99 – 6.82 (m, 1H, ArH), 6.72 (s, 1H, CH), 5.05 (hept, J = 6.1 Hz, 1H, OC*H*$(CH_3)_2$), 2.34 (s, 3H, CH_3), 1.27 (d, J = 6.0 Hz, 3H, OCH(C*H*$_3)_2$), 1.15 (d, J = 6.1 Hz, 3H, OCH(C*H*$_3)_2$). LRMS (CI) *m/z* calcd. for $C_{20}H_{21}N_4O_2S$ $[M+H]^+$: 381.1 found: 381.0.

(±) Ethyl 5-methyl-2-phenyl-7-(thiophen-3-yl)-4,7-dihydro-[1,2,4]triazolo[1,5-*a*]pyrimidine-6-carboxylate (159). Purified by column chromatography (Hex–AcOEt 3:1 – 1:1). Yield: 44%. Mp: 213 – 215 ºC. ^{1}H NMR (300 MHz, $CDCl_3$), δ (ppm): 9.62 (brs, 1H, NH), 8.05 – 7.95 (m, 2H, ArH), 7.50 – 7.37 (m, 3H, ArH), 7.31 – 7.20 (m, 2H, ArH), 7.11 – 7.02 (m, 1H, ArH), 6.65 (s, 1H, CH), 4.15 (q, J = 7.1 Hz, 2H, OC*H*$_2$CH$_3$), 2.31 (s, 3H, CH_3), 1.21 (t, J = 7.1 Hz, 3H, OCH$_2$C*H*$_3$). LRMS (CI) *m/z* calcd. for $C_{19}H_{19}N_4O_2S$ $[M+H]^+$: 367.1 found: 367.0.

(±) Isopropyl 5-methyl-2-phenyl-7-(thiophen-3-yl)-4,7-dihydro-[1,2,4]triazolo[1,5-*a*]pyrimidine-6-carboxylate (160). Purified by column chromatography (Hex–AcOEt 3:1 – 1:1). Yield: 43%. Mp: 195 – 197 ºC. ^{1}H NMR (300 MHz, $CDCl_3$), δ (ppm): 9.31 (brs, 1H, NH), 8.02 – 7.93 (m, 2H, ArH), 7.44 – 7.36 (m, 2H, ArH), 7.29 – 7.18 (m, 3H, ArH), 7.10 – 7.02 (m, 1H, ArH), 6.62 (s, 1H, CH), 5.00 (hept, *J* = 6.2 Hz, 1H, C*H*$(CH_3)_2$), 2.31 (s, 3H, CH_3), 1.23 (d, *J* = 6.2 Hz, 3H, CH(C*H*$_3$)$_2$), 1.06 (d, *J* = 6.2 Hz, 3H, CH(C*H*$_3$)$_2$). LRMS (CI) *m/z* calcd. for $C_{20}H_{21}N_4O_2S$ $[M+H]^+$: 381.1 found: 381.0.

(±) Ethyl 7-(furan-2-yl)-5-methyl-2-(4-methylpiperazin-1-yl)-4,7-dihydro-[1,2,4]triazolo[1,5-*a*]pyrimidine-6-carboxylate (161). Purified by column chromatography (Hex–AcOEt 2:1 – 1:2). Yield: 28%. Oil at RT. ^{1}H NMR (300 MHz, $CDCl_3$), δ (ppm): 8.50 (brs, 1H, NH), 7.27 (d, *J* = 6.7 Hz, 1H, ArH), 6.33 (s, 1H, CH), 6.31 – 6.21 (m, 2H, ArH), 4.10 (m, 2H, OC*H*$_2$CH$_3$), 3.39 (t, *J* = 5.0 Hz, 4H, Pp), 2.65 – 2.42 (m, 7H, Pp + CH_3), 2.33 (s, 3H, NCH_3), 1.17 (t, *J* = 7.1 Hz, 3H, OCH_2C*H*$_3$). LRMS (CI) *m/z* calcd. for $C_{18}H_{25}N_6O_3$ $[M+H]^+$: 373.2 found: 373.1.

(±) Isopropyl 7-(furan-2-yl)-5-methyl-2-(4-methylpiperazin-1-yl)-4,7-dihydro-[1,2,4]triazolo[1,5-*a*]pyrimidine-6-carboxylate (162). Purified by column chromatography (Hex–AcOEt 2:1 – 1:2). Yield: 32%. Oil at RT. ^{1}H NMR (300 MHz, $CDCl_3$), δ (ppm): 7.95 (brs, 1H, NH), 7.29 (s, 1H, ArH), 6.33 (s, 1H, ArH), 6.31 – 6.21 (m, 1H, ArH), 5.30 (s, 1H, CH), 4.98 (hept, *J* = 6.2 Hz, 1H, OC*H*$(CH_3)_2$), 3.43 – 3.33 (m, 4H, Pp), 2.53 – 2.43 (m, 7H, Pp + CH_3), 2.32 (s, 3H, CH_3), 1.21 (d, *J* = 6.2 Hz, 3H, OCH(C*H*$_3$)$_2$), 1.06 (d, *J* = 6.2 Hz, 3H, OCH(C*H*$_3$)$_2$). ^{13}C NMR (75 MHz, $CDCl_3$), δ (ppm): 158.9, 146.9, 146.4, 145.8, 142.0, 113.1, 110.3, 107.5, 70.2, 54.3, 53.9, 45.8, 45.2, 21.7, 21.6, 19.1. LRMS (CI) *m/z* calcd. for $C_{19}H_{27}N_6O_3$ $[M+H]^+$: 387.2 found: 387.1.

(±) Ethyl 7-(furan-3-yl)-5-methyl-2-(4-methylpiperazin-1-yl)-4,7-dihydro-[1,2,4]triazolo[1,5-*a*]pyrimidine-6-carboxylate (163). Purified by column chromatography (Hex–AcOEt 2:1 – 1:2). Yield: 31%. Oil at RT. ^{1}H NMR (300 MHz, $CDCl_3$), δ (ppm): 9.78 (brs, 1H, NH), 7.43 – 7.19 (m, 2H, ArH), 6.33 – 6.13 (m, 2H, ArH), 4.11 (q, *J* = 7.1 Hz, 2H, OC*H*$_2$CH$_3$), 3.51 – 3.22 (m, 4H, Pp), 2.72 – 2.18 (m, 10H, Pp + CH_3 + NCH_3), 1.19 (t, *J* = 7.0 Hz, 3H, OCH_2C*H*$_3$). LRMS (CI) *m/z* calcd. for $C_{18}H_{25}N_6O_3$ $[M+H]^+$: 373.2 found: 373.2.

(±) Isopropyl 7-(furan-3-yl)-5-methyl-2-(4-methylpiperazin-1-yl)-4,7-dihydro-[1,2,4]triazolo[1,5-*a*]pyrimidine-6-carboxylate (164). Purified by column chromatography (Hex–AcOEt 2:1 – 1:2). Yield: 25%. Oil at RT. ^{1}H NMR (300 MHz, $CDCl_3$), δ (ppm): 8.56 (brs, 1H, NH), 7.45 – 7.16 (m, 2H, ArH), 6.40 – 6.20 (m, 2H, ArH + CH), 5.14 – 4.92 (m, 1H, OC*H*$(CH_3)_2$), 3.49 – 3.31 (m, 4H, Pp), 2.56 – 2.26 (m, 10H, Pp + CH_3 + NCH_3), 1.23 (d, *J* = 6.3 Hz, 3H, OCH(C*H*$_3)_2$), 1.14 (d, *J* = 6.2 Hz, 3H, OCH(C*H*$_3)_2$). ^{13}C NMR (75 MHz, $CDCl_3$), δ (ppm): 166.5, 165.3, 147.9, 147.0, 143.1, 142.9, 126.3, 110.0, 109.2, 67.4, 54.2, 51.1, 45.3, 45.0, 23.2, 21.6, 21.4. LRMS (CI) *m/z* calcd. for $C_{19}H_{27}N_6O_3$ $[M+H]^+$: 387.2 found: 387.0.

(±) Ethyl 5-methyl-2-(4-methylpiperazin-1-yl)-7-(thiophen-2-yl)-4,7-dihydro-[1,2,4]triazolo[1,5-*a*]pyrimidine-6-carboxylate (165). Purified by column chromatography (Hex–AcOEt 2:1 – 1:2). Yield: 27%. Oil at RT. ^{1}H NMR (300 MHz, $CDCl_3$), δ (ppm): 9.47 – 9.24 (brs, 1H, NH), 7.17 (dd, *J* = 5.0, 1.3 Hz, 1H, ArH), 7.00 – 6.84 (m, 2H, ArH), 6.55 (s, 1H, CH), 4.12 (q, *J* = 7.1 Hz, 2H, OC*H*$_2$CH$_3$), 3.36 (t, *J* = 5.0 Hz, 4H, Pp), 2.58 – 2.37 (m, 7H, Pp + CH_3), 2.30 (s, 3H, NCH_3), 1.18 (t, *J* = 7.1 Hz, 3H, OCH_2C*H*$_3$). LRMS (CI) *m/z* calcd. for $C_{18}H_{25}N_6O_2S$ $[M+H]^+$: 389.2 found: 389.1.

(±) Isopropyl 5-methyl-2-(4-methylpiperazin-1-yl)-7-(thiophen-2-yl)-4,7-dihydro-[1,2,4]triazolo[1,5-*a*]pyrimidine-6-carboxylate (166). Purified by column chromatography (Hex–AcOEt 2:1 – 1:2). Yield: 34%. Oil at RT. ^{1}H NMR (300 MHz, $CDCl_3$), δ (ppm): 9.80 (brs, 1H, NH), 7.19 (dd, *J* = 5.0 Hz, *J* = 1.3 Hz, 1H, ArH), 6.97 (dd, *J* = 3.7 Hz, *J* = 1.3 Hz, 1H, ArH), 6.90 (dd, *J* = 5.0, 3.5 Hz, 1H), 6.55 (s, 1H, CH), 5.00 (hept, *J* = 6.2 Hz, 1H, OC*H*$(CH_3)_2$), 3.38 (t, *J* = 4.9 Hz, 4H, Pp), 2.57 – 2.38 (m, 7H, Pp + CH_3), 2.33 (s, 3H, NCH_3), 1.22 (d, *J* = 6.2 Hz, 3H, OCH(C*H*$_3)_2$), 1.05 (d, *J* = 6.2 Hz, 3H, OCH(C*H*$_3)_2$). LRMS (CI) *m/z* calcd. for $C_{19}H_{27}N_6O_2S$ $[M+H]^+$: 403.2 found: 403.1.

(±) Ethyl 5-methyl-2-(4-methylpiperazin-1-yl)-7-(thiophen-3-yl)-4,7-dihydro-[1,2,4]triazolo[1,5-*a*]pyrimidine-6-carboxylate (167). Purified by column chromatography (Hex–AcOEt 2:1 – 1:2). Yield: 30%. Oil at RT. ^{1}H NMR (300 MHz, $CDCl_3$), δ (ppm): 9.14 (brs, 1H, NH), 7.37 – 7.08 (m, 2H, ArH), 6.95 (dd, *J* = 4.9, 1.4 Hz, 1H, ArH), 6.38 (s, 1H, CH), 5.08 (hept, *J* = 6.0 Hz, 1H, OC*H*$(CH_3)_2$), 3.38 (t, *J* = 4.9 Hz, 4H, Pp), 2.58 – 2.36 (m, 7H, Pp + CH_3), 2.29 (s, 3H, NCH_3), 1.19 (d, *J* = 6.0 Hz, 3H, OCH(C*H*$_3)_2$), 1.01 (d, *J* = 6.0 Hz, 3H, OCH(C*H*$_3)_2$). LRMS (CI) *m/z* calcd. for $C_{18}H_{25}N_6O_2S$ $[M+H]^+$: 389.2 found: 389.1.

(±) Isopropyl 5-methyl-2-(4-methylpiperazin-1-yl)-7-(thiophen-3-yl)-4,7-dihydro-[1,2,4]triazolo[1,5-*a*]pyrimidine-6-carboxylate (168). Purified by column chromatography (Hex–AcOEt 2:1 – 1:2). Yield: 29%. Oil at RT. ^{1}H NMR (300 MHz, $CDCl_3$), δ (ppm): 9.02 (brs, 1H, NH), 7.37 – 7.08 (m, 2H, ArH), 6.95 (dd, *J* = 4.9, 1.4 Hz, 1H, ArH), 6.40 (s, 1H, CH), 5.08 (hept, *J* = 6.2 Hz, 1H, OC*H*$(CH_3)_2$), 3.36 (t, *J* = 5.1 Hz, 4H, Pp), 2.58 – 2.38 (m, 7H, Pp + CH_3), 2.31 (s, 3H, NCH_3), 1.23 (d, *J* = 6.3 Hz, 3H, OCH(C*H*$_3)_2$), 1.03 (d, *J* = 6.2 Hz, 3H, OCH(C*H*$_3)_2$). LRMS (CI) *m/z* calcd. for $C_{19}H_{27}N_6O_2S$ $[M+H]^+$: 403.2 found: 403.1.

(±) Ethyl 7-(furan-2-yl)-2-mercapto-5-methyl-4,7-dihydro-[1,2,4]triazolo[1,5-*a*]pyrimidine-6-carboxylate (169). Purified by column chromatography (Hex–AcOEt 2:1 – 1:2). Yield: 42%. Mp: 248 – 250 ºC. ^{1}H NMR (300 MHz, $CDCl_3$), δ (ppm): 11.97 (brs, 1H, SH), 9.66 (brs, 1H, NH), 7.26 (s, 1H, ArH), 6.50 (s, 1H, ArH), 6.44 (s, 1H, CH), 6.30 (s, 1H, ArH), 4.23 – 4.11 (m, 2H, OC*H*$_2$$CH_3$), 2.53 (s, 3H, CH_3), 1.26 (t, *J* = 6.9 Hz, 3H, OC*H*$_2$$CH_3$). LRMS (CI) *m/z* calcd. for $C_{13}H_{15}N_4O_3S$ $[M+H]^+$: 307.1 found: 307.2.

(±) Isopropyl 7-(furan-2-yl)-2-mercapto-5-methyl-4,7-dihydro-[1,2,4]triazolo[1,5-*a*]pyrimidine-6-carboxylate (170). Purified by column chromatography (Hex–AcOEt 2:1 – 1:2). Yield: 43%. Mp: 255 – 257 ºC. ^{1}H NMR (300 MHz, $CDCl_3$), δ (ppm): 7.50 (d, *J* = 5.8 Hz, 1H, NH), 7.29 (m, 1H, ArH), 6.86 – 6.60 (m, 1H, ArH), 6.55 – 6.42 (m, 1H, ArH), 5.20 – 5.00 (m, 1H), 2.45 (s, 3H), 1.35 (d, *J* = 6.3 Hz, 3H), 1.28 (d, *J* = 6.3 Hz, 3H). LRMS (CI) *m/z* calcd. for $C_{14}H_{17}N_4O_3S$ $[M+H]^+$: 321.1 found: 321.0.

(±) Ethyl 7-(furan-3-yl)-2-mercapto-5-methyl-4,7-dihydro-[1,2,4]triazolo[1,5-*a*]pyrimidine-6-carboxylate (171). Purified by column chromatography (Hex–AcOEt 2:1 – 1:2). Yield: 39%. Mp: 257 – 259 ºC. ^{1}H NMR (300 MHz, $CDCl_3$), δ (ppm): 13.29 (brs, 1H, SH), 10.79 (brs, 1H, NH), 7.58 (s, 1H, ArH), 7.52 (d, *J* = 2.0 Hz, 1H, ArH), 6.38 (s, 1H, CH), 6.09 (s, 1H, ArH), 4.07 (q, *J* = 7.1 Hz, 2H, OC*H*$_2$$CH_3$), 2.48 (s, 3H, CH_3), 1.15 (t, *J* = 7.3 Hz, 3H, OCH_2C*H*$_3$). LRMS (CI) *m/z* calcd. for $C_{13}H_{15}N_4O_3S$ $[M+H]^+$: 307.1 found: 307.1.

(±) Isopropyl 7-(furan-3-yl)-2-mercapto-5-methyl-4,7-dihydro-[1,2,4]triazolo[1,5-*a*]pyrimidine-6-carboxylate (172). Purified by column chromatography (Hex–AcOEt 2:1 – 1:2). Yield: 47%. Mp: 259 – 261 ºC. ^{1}H NMR (300 MHz, $CDCl_3$), δ (ppm): 12.25 (brs, 1H, SH), 9.78 (brs, 1H, NH), 7.57 (s, 1H, ArH), 7.32 (m, 1H, ArH), 6.42 (s, 1H, CH), 6.34 (s, 1H, ArH), 5.09 – 4.97 (m, 1H, OC*H*$(CH_3)_2$), 2.52 (s, 3H, CH_3), 1.27 (d, *J* = 6.6 Hz, 3H, OCH(C*H*$_3)_2$), 1.16 (d, *J* = 6.1 Hz, 3H, OCH(C*H*$_3)_2$). LRMS (CI) *m/z* calcd. for $C_{14}H_{17}N_4O_3S$ $[M+H]^+$: 321.1 found: 321.1.

(±) Ethyl 2-mercapto-5-methyl-7-(thiophen-2-yl)-4,7-dihydro-[1,2,4]triazolo[1,5-*a*]pyrimidine-6-carboxylate (173). Purified by column chromatography (Hex–AcOEt 2:1 – 1:2). Yield: 52%. Mp: 271 – 273 ºC. ^{1}H NMR (300 MHz, $CDCl_3$), δ (ppm): 13.35 (brs, 1H, SH), 10.95 (brs, 1H, NH), 7.38 (d, *J* = 5.2 Hz, 1H, ArH), 7.07 (d, *J* = 3.5 Hz, 1H, ArH), 6.96 – 6.86 (m, 1H, ArH), 6.38 (s, 1H, CH), 4.07 (q, *J* = 7.2 Hz, 2H, OC*H*$_2$CH$_3$), 2.39 (s, 3H, CH_3), 1.11 (t, *J* = 7.1 Hz, 3H, OCH_2C*H*$_3$). LRMS (CI) *m/z* calcd. for $C_{13}H_{15}N_4O_2S_2$ $[M+H]^+$: 323.1 found: 323.0.

(±) Isopropyl 2-mercapto-5-methyl-7-(thiophen-2-yl)-4,7-dihydro-[1,2,4]triazolo[1,5-*a*]pyrimidine-6-carboxylate (174). Yield: 48%. Mp: 248 – 250 ºC. ^{1}H NMR (300 MHz, DMSO-d_6), δ (ppm): 13.34 (brs, 1H, SH), 10.90 (brs, 1H, NH), 7.38 (dd, *J* = 5.1, 1.3 Hz, 1H, ArH), 7.11 – 7.03 (m, 1H, ArH), 6.91 (dd, *J* = 5.1, 3.5 Hz, 1H, ArH), 6.36 (s, 1H, CH), 4.88 (hept, *J* = 6.2 Hz, 1H, OC*H*$(CH_3)_2$), 2.39 (s, 3H, CH_3), 1.19 (d, *J* = 6.2 Hz, 3H, OCH(C*H*$_3)_2$), 1.05 (d, *J* = 6.2 Hz, 3H, OCH(C*H*$_3)_2$). LRMS (CI) *m/z* calcd. for $C_{14}H_{17}N_4O_2S_2$ $[M+H]^+$: 337.1 found: 337.0.

(±) Ethyl 2-mercapto-5-methyl-7-(thiophen-3-yl)-4,7-dihydro-[1,2,4]triazolo[1,5-*a*]pyrimidine-6-carboxylate (175). Purified by column chromatography (Hex–AcOEt 2:1 – 1:2). Yield: 33%. Mp: 271 – 273 ºC ^{1}H NMR (300 MHz, DMSO-d_6), δ (ppm): 13.31 (brs, 1H, SH), 10.83 (brs, 1H, NH), 7.46 – 7.37 (m, 1H, ArH), 7.37 – 7.29 (m, 1H, ArH), 7.07 – 6.98 (m, 1H, ArH), 6.19 (s, 1H, CH), 4.14 – 3.96 (m, 2H, OC*H*$_2$CH$_3$), 2.37 (s, 3H, CH_3), 1.10 (t, *J* = 7.1 Hz, 3H, OCH_2CH_3). LRMS (CI) *m/z* calcd. for $C_{13}H_{15}N_4O_2S_2$ $[M+H]^+$: 323.1 found: 323.0.

(±) Isopropyl 2-mercapto-5-methyl-7-(thiophen-3-yl)-4,7-dihydro-[1,2,4]triazolo[1,5-*a*]pyrimidine-6-carboxylate (176). Purified by column chromatography (Hex–AcOEt 2:1 – 1:2). Yield: 29%. Mp: 239 – 241 ºC. ^{1}H NMR (300 MHz, DMSO-d_6), δ (ppm): 12.83 (brs, 1H, SH), 10.22 (brs, 1H, NH), 7.50 – 7.32 (m, 1H, ArH), 7.33 – 7.22 (m, 1H, ArH), 7.12 – 6.95 (m, 1H, ArH), 6.10 (s, 1H, CH), 4.99 (hept, J = 6.1 Hz, 1H, OC*H*$(CH_3)_2$), 2.42 (s, 3H, CH_3), 1.20 (d, J = 6.1 Hz, 3H, OCH(C*H*$_3)_2$), 1.07 (d, J = 6.1 Hz, 3H, OCH(C*H*$_3)_2$). LRMS (CI) *m/z* calcd. for $C_{14}H_{17}N_4O_2S_2$ $[M+H]^+$: 337.1 found: 336.1.

(±) Ethyl- 7-(furan-2-yl)-5-methyl-2-(methylthio)-4,7-dihydro-[1,2,4]triazolo[1,5-*a*]pyrimidine-6-carboxylate (177). Purified by column chromatography (Hex–AcOEt 2:1 – 1:2). Yield: 41%. Mp: 209 – 211 ºC. ^{1}H NMR (300 MHz, $CDCl_3$), δ (ppm): 10.97 (brs, 1H, NH), 7.34 – 7.25 (m, 1H, ArH), 6.47 (s, 1H, CH), 6.28 (s, 2H, ArH), 4.12 (p, J = 8.0, 3.8 Hz, 2H, OC*H*$_2$CH$_3$), 2.63 (s, 3H, SCH_3), 2.53 (s, 3H, CH_3), 1.19 (t, J = 7.1 Hz, 3H, OCH_2C*H*$_3$).^{13}C NMR (75 MHz, $CDCl_3$), δ (ppm): 165. 5, 159.2, 152.8, 148.7, 147.1, 142.4, 110.3, 107.7, 96.4, 60.1, 53.4, 19.3, 14.4, 14.1. HRMS (APCI) *m/z* calcd. for $C_{14}H_{17}N_4O_3S$ $[M+H]^+$: 321.1016 found: 321.1018.

(±) Isopropyl 7-(furan-2-yl)-5-methyl-2-(methylthio)-4,7-dihydro-[1,2,4]triazolo[1,5-*a*]pyrimidine-6-carboxylate (178). Purified by column chromatography (Hex–AcOEt 2:1 – 1:2). Yield: 32%. Mp: 218 – 220 ºC. ^{1}H NMR (300 MHz, $CDCl_3$), δ (ppm): 10.66 (brs, 1H, NH), 7.34 – 7.25 (m, 1H, ArH), 6.46 (s, 1H, CH), 6.32 – 6.24 (m, 2H, ArH), 4.99 (p, J = 6.2 Hz, 1H, OC*H*$(CH_3)_2$), 2.62 (s, 3H, SCH_3), 2.53 (s, 3H, CH_3), 1.22 (d, J = 6.2 Hz, 3H, OCH(C*H*$_3)_2$), 1.06 (d, J = 6.2 Hz, 3H, OCH(C*H*$_3)_2$). ^{13}C NMR (75 MHz, $CDCl_3$), δ (ppm): 164.9, 159.2, 153.0, 148.6, 146.8, 142.3, 110.3, 107.7, 96.6, 67.4, 53.4, 22.0, 21.6, 20.0, 14.4. HRMS (APCI) *m/z* calcd. for $C_{15}H_{19}N_4O_3S$ $[M+H]^+$: 335.1117 found: 335.1176.

(±) Ethyl 7-(furan-3-yl)-5-methyl-2-(methylthio)-4,7-dihydro-[1,2,4]triazolo[1,5-a]pyrimidine-6-carboxylate (179). Purified by column chromatography (Hex–AcOEt 2:1 – 1:2). Yield: 22%. Mp: 221 – 223 ºC. ^{1}H NMR (300 MHz, $CDCl_3$), δ (ppm): 10.58 (brs, 1H, NH), 7.36 (s, 1H, ArH), 7.30 (s, 1H, ArH), 6.42 (s, 1H, CH), 6.28 (s, 1H, ArH), 4.16 (q, J = 7.1 Hz, 2H, OC*H*$_2$CH$_3$), 2.59 (s, 3H, sCH_3), 2.54 (s, 3H, CH_3), 1.24 (t, J = 7.1 Hz, 3H, OCH_2C*H*$_3$). LRMS (CI) *m/z* calcd. for $C_{14}H_{17}N_4O_3S$ $[M+H]^+$: 321.1 found: 321.1.

(±) Isopropyl- 7-(furan-3-yl)-5-methyl-2-(methylthio)-4,7-dihydro- [1,2,4]triazolo[1,5-*a*]pyrimidine-6-carboxylate (180). Purified by column chromatography (Hex–AcOEt 2:1 – 1:2). Yield: 30%. Mp: 224 – 225 ºC. ^{1}H NMR (300 MHz, $CDCl_3$), δ (ppm): 10.92 (brs, 1H, NH), 7.36 (s, 1H, ArH), 7.30 (s, 1H, ArH), 6.41 (s, 1H, CH), 6.29 (s, 1H, ArH), 5.03 (hept, *J* = 6.2 Hz, 1H, OC*H*$(CH_3)_2$), 2.60 (s, 3H, SCH_3), 2.54 (s, 3H, CH_3), 1.24 (d, *J* = 6.2 Hz, 3H, OCH(C*H*$_3)_2$), 1.14 (d, *J* = 6.3 Hz, 3H, OCH(C*H*$_3)_2$).^{13}C NMR (75 MHz, $CDCl_3$), δ (ppm): 165.1, 159.0, 148.7, 146.2, 143.1, 140.0, 126.1, 109.2, 98.6, 67.6, 51.8, 22.1, 21.7, 19.2, 14.4. HRMS (APCI) *m/z* calcd. for $C_{15}H_{19}N_4O_3S$ $[M+H]^+$: 335.1172 found: 335.1173.

(±) Ethyl 5-methyl-2-(methylthio)-7-(thiophen-2-yl)-4,7-dihydro-[1,2,4]triazolo[1,5-a]pyrimidine-6-carboxylate (181). Purified by column chromatography (Hex–AcOEt 2:1 – 1:2). Yield: 24%. Mp: 233 – 235 ºC. ^{1}H NMR (300 MHz, $CDCl_3$), δ (ppm): 10.77 (brs, 1H, NH), 7.29 – 7.16 (m, 1H, ArH), 7.03 – 6.86 (m, 2H, ArH), 6.68 (s, 1H, CH), 4.13 (q, *J* = 7.1 Hz, 2H, OC*H*$_2$CH$_3$), 2.63 (s, 3H, SCH_3), 2.54 (d, *J* = 1.5 Hz, 3H, CH_3), 1.20 (t, *J* = 7.1 Hz, 3H, OCH_2C*H*$_3$). LRMS (CI) *m/z* calcd. for $C_{14}H_{17}N_4O_2S_2$ $[M+H]^+$: 337.1 found: 336.1.

(±) Isopropyl 5-methyl-2-(methylthio)-7-(thiophen-2-yl)-4,7-dihydro-[1,2,4]triazolo[1,5-a]pyrimidine-6-carboxylate (182). Purified by column chromatography (Hex–AcOEt 2:1 – 1:2). Yield: 22%. Mp: 237 – 239 ºC. ^{1}H NMR (300 MHz, $CDCl_3$), δ (ppm): 10.63 (brs, 1H, NH), 7.20 (d, *J* = 5.1 Hz, 1H, ArH), 6.99 (d, *J* = 3.4 Hz, 1H, ArH), 6.91 (dd, *J* = 5.1, 3.5 Hz, 1H, ArH), 6.66 (s, 1H, CH), 5.01 (p, *J* = 6.2 Hz, 1H, OC*H*$(CH_3)_2$), 2.62 (s, 3H, SCH_3), 2.54 (s, 3H, CH_3), 1.23 (d, *J* = 6.3 Hz, 3H, OCH(C*H*$_3)_2$), 1.04 (d, *J* = 6.2 Hz, 3H, OCH(C*H*$_3)_2$).MS (CI) *m/z* calcd. for $C_{15}H_{19}N_4O_2S_2$ $[M+H]^+$: 351.1 found: 351.0.

(±) Ethyl 5-methyl-2-(methylthio)-7-(thiophen-3-yl)-4,7-dihydro-[1,2,4]triazolo[1,5-a]pyrimidine-6-carboxylate (183). Purified by column chromatography (Hex–AcOEt 2:1 – 1:2). Yield: 26%. Mp: 234 – 236 ºC. ^{1}H NMR (300 MHz, $CDCl_3$), δ (ppm): 10.70 (s, 1H, NH), 7.29 – 7.14 (m, 2H, ArH), 6.99 (s, 1H, CH), 6.51 (s, 1H, ArH), 4.19 – 4.06 (m, 2H, OC*H*$_2$CH$_3$), 2.61 (s, 3H, SCH_3), 2.52 (s, 3H, CH_3), 1.19 (t, *J* = 7.1 Hz, 3H, OCH_2C*H*$_3$). LRMS (CI) *m/z* calcd. for $C_{14}H_{17}N_4O_2S_2$ $[M+H]^+$: 337.1 found: 337.0.

(±) Isopropyl 5-methyl-2-(methylthio)-7-(thiophen-3-yl)-4,7-dihydro-[1,2,4]triazolo[1,5-a]pyrimidine-6-carboxylate (184). Purified by column chromatography (Hex–AcOEt 2:1 – 1:2). Yield: 33%. 224 – 226 ºC. ^{1}H NMR (300 MHz, $CDCl_3$), δ (ppm): 10.58 (s, 1H, NH), 7.29 – 7.15 (m, 2H, ArH), 7.00 (dd, *J* = 4.8, 1.5 Hz, 1H, ArH), 6.50 (s, 1H, CH), 5.00 (p, *J* = 6.2 Hz, 1H, OC*H*$(CH_3)_2$), 2.60 (s, 3H, SCH_3), 2.53 (s, 3H, CH_3), 1.22 (d, *J* = 6.3 Hz, 3H, OCH(C*H*$_3)_2$), 1.05 (d, *J* = 6.3 Hz, 3H, OCH(C*H*$_3)_2$). LRMS (CI) *m/z* calcd. for $C_{15}H_{19}N_4O_2S_2$ $[M+H]^+$: 351.1 found: 351.0.

(±) Ethyl 2-(benzylthio)-7-(furan-2-yl)-5-methyl-4,7-dihydro-[1,2,4]triazolo[1,5-*a*]pyrimidine-6-carboxylate (185). Purified by column chromatography (Hex–AcOEt 3:1 – 1:1). Yield: 43%. Mp: 205 – 207 ºC. ^{1}H NMR (300 MHz, $CDCl_3$), δ (ppm): 9.83 (brs, 1H, NH), 7.34 – 7.17 (m, 6H, ArH), 6.46 (s, 1H, CH), 6.34 – 6.25 (m, 2H, ArH), 4.44 – 3.92 (m, 4H, SC*H*$_2C_6H_5$ + OC*H*$_2CH_3$), 2.55 (s, 3H, CH_3), 1.29 – 1.13 (m, 3H, OCH_2C*H*$_3$). LRMS (CI) *m/z* calcd. for $C_{20}H_{21}N_4O_3S$ $[M+H]^+$: 397.1 found: 397.0.

(±) Isopropyl 2-(benzylthio)-7-(furan-2-yl)-5-methyl-4,7-dihydro-[1,2,4]triazolo[1,5-*a*]pyrimidine-6-carboxylate (186). Purified by column chromatography (Hex–AcOEt 3:1 – 1:1). Yield: 48%. Mp: 210 – 212 ºC. ^{1}H NMR (300 MHz, $CDCl_3$), δ (ppm): 10.17 (brs, 1H, NH), 7.46 – 7.15 (m, 6H, ArH), 6.45 (s, 1H, CH), 6.35 – 6.23 (m, 2H, ArH), 4.99 (hept, *J* = 6.3 Hz, 1H, OC*H*$(CH_3)_2$), 4.32 (d, *J* = 13.0 Hz, 1H, C*H*$_2C_6H_5$), 4.20 (d, *J* = 13.0 Hz, 1H, C*H*$_2C_6H_5$), 2.56 (s, 3H, CH_3), 1.23 (d, *J* = 6.2 Hz, 3H, OCH(C*H*$_3)_2$), 1.06 (d, *J* = 6.2 Hz, 3H, OCH(C*H*$_3)_2$). ^{13}C NMR (75 MHz, $CDCl_3$), δ (ppm): 164.9, 157.7, 153.0, 148.5, 146.8, 142.3, 137.2, 129.0, 128.5, 127.3, 110.4, 107.8, 96.5, 67.4, 53.5, 36.4, 22.0, 21.6, 19.3. LRMS (CI) *m/z* calcd. for $C_{21}H_{23}N_4O_3S$ $[M+H]^+$: 411.1 found: 411.0.

(±) Ethyl 2-(benzylthio)-7-(furan-3-yl)-5-methyl-4,7-dihydro-[1,2,4]triazolo[1,5-*a*]pyrimidine-6-carboxylate (187). Purified by column chromatography (Hex–AcOEt 3:1 – 1:1). Yield: 44%. Mp: 225 – 227 ºC. ^{1}H NMR (300 MHz, $CDCl_3$), δ (ppm): 9.95 (brs, 1H, NH), 7.29 – 7.20 (m, 7H, ArH), 6.40 (s, 1H, ArH), 6.23 (s, 1H, CH), 4.37 – 4.12 (m, 4H, SC*H*$_2C_6H_5$ + OC*H*$_2CH_3$), 2.53 (s, 3H, CH_3), 1.29 – 1.17 (m, 3H, OCH_2C*H*$_3$). LRMS (CI) *m/z* calcd. for $C_{20}H_{21}N_4O_3S$ $[M+H]^+$: 397.1 found: 397.0.

(±) Isopropyl 2-(benzylthio)-7-(furan-3-yl)-5-methyl-4,7-dihydro-[1,2,4]triazolo[1,5-*a*]pyrimidine-6-carboxylate (188). Purified by column chromatography (Hex–AcOEt 3:1 – 1:1). Yield: 41%. Mp: 195 – 197 ºC. ^{1}H NMR (300 MHz, $CDCl_3$), δ (ppm): 10.28 (brs, 1H, NH), 7.35 – 7.18 (m, 7H, ArH), 6.39 (s, 1H, CH), 6.25 (s, 1H, ArH), 5.04 (p, *J* = 6.2 Hz, 1H, OC*H*$(CH_3)_2$), 4.31 (d, *J* = 13.1 Hz, 1H, SC*H*$_2C_6H_5$), 4.21 (d, *J* = 13.1 Hz, 1H, C*H*$_2C_6H_5$), 2.53 (s, 3H, CH_3), 1.25 (d, *J* = 6.2 Hz, 3H, OCH(C*H*$_3)_2$), 1.14 (d, *J* = 6.2 Hz, 3H, OCH(C*H*$_3)_2$). ^{13}C NMR (75 MHz, $CDCl_3$), δ (ppm): 165.1, 148.5, 146.0, 143.1, 140.3, 140.0, 137.1, 128.9, 128.4, 127.4, 126.1, 109.2, 98.5, 67.6, 51.9, 36.4, 22.1, 21.7, 19.3. LRMS (CI) *m/z* calcd. for $C_{21}H_{23}N_4O_3S$ $[M+H]^+$: 411.1 found: 411.0.

(±) Ethyl 2-(benzylthio)-5-methyl-7-(thiophen-2-yl)-4,7-dihydro-[1,2,4]triazolo[1,5-*a*]pyrimidine-6-carboxylate (189). Purified by column chromatography (Hex–AcOEt 3:1 – 1:1). Yield: 33%. Mp: 195 – 197 ºC. ^{1}H NMR (300 MHz, $CDCl_3$), δ (ppm): 10.13 (s, 1H, NH), 7.43 – 7.11 (m, 5H, ArH), 7.00 – 6.87 (m, 3H, ArH), 6.66 (s, 1H, CH), 4.45 – 4.04 (m, 4H, SC*H*$_2C_6H_5$ + OC*H*$_2CH_3$), 2.56 (s, 3H, CH_3), 1.18 (t, *J* = 7.1 Hz, 3H, OCH_2CH_3).MS (CI) *m/z* calcd. for $C_{20}H_{21}N_4O_2S_2$ $[M+H]^+$: 413.1 found: 413.0.

(±) Isopropyl 2-(benzylthio)-5-methyl-7-(thiophen-2-yl)-4,7-dihydro-[1,2,4]triazolo[1,5-*a*]pyrimidine-6-carboxylate (190). Purified by column chromatography (Hex–AcOEt 3:1 – 1:1). Yield: 38%. Mp: 174 – 176 ºC. ^{1}H NMR (300 MHz, $CDCl_3$), δ (ppm): 10.40 (brs, 1H, NH), 7.34 – 7.17 (m, 6H, ArH), 7.02 – 6.87 (m, 2H, ArH), 6.65 (s, 1H, CH), 5.00 (hept, *J* = 6.2 Hz, 1H, OC*H*$(CH_3)_2$), 4.32 (d, *J* = 13.1 Hz, 1H, C*H*$_2C_6H_5$), 4.20 (d, *J* = 13.2 Hz, 1H, SC*H*$_2C_6H_5$), 2.57 (s, 3H, CH_3), 1.23 (d, *J* = 6.3 Hz, 3H, CH(C*H*$_3)_2$), 1.04 (d, *J* = 6.2 Hz, 3H, CH(C*H*$_3)_2$). LRMS (CI) *m/z* calcd. for $C_{21}H_{23}N_4O_2S_2$ $[M+H]^+$: 427.1 found: 427.0.

(±) Ethyl 2-(benzylthio)-5-methyl-7-(thiophen-3-yl)-4,7-dihydro-[1,2,4]triazolo[1,5-*a*]pyrimidine-6-carboxylate (191). Purified by column chromatography (Hex–AcOEt 3:1 – 1:1). Yield: 33%. Mp: 205 – 207 ºC ^{1}H NMR (300 MHz, $CDCl_3$), δ (ppm): 10.34 (brs, 1H, NH), 7.32 – 7.17 (m, 6H, ArH), 7.14 (d, *J* = 3.2 Hz, 1H, ArH), 7.01 – 6.92 (m, 1H, ArH), 6.50 (s, 1H, CH), 4.37 – 3.94 (m, 4H, SC*H*$_2C_6H_5$ + OC*H*$_2CH_3$), 2.55 (s, 3H, CH_3), 1.18 (t, *J* = 7.1 Hz, 3H, OCH_2CH_3). LRMS (CI) *m/z* calcd. for $C_{20}H_{21}N_4O_2S_2$ $[M+H]^+$: 413.1 found: 413.0.

(±) Isopropyl 2-(benzylthio)-5-methyl-7-(thiophen-3-yl)-4,7-dihydro-[1,2,4]triazolo[1,5-*a*]pyrimidine-6-carboxylate (192). Purified by column chromatography (Hex–AcOEt 3:1 – 1:1). Yield: 36%. Mp: 185 – 187 ºC ^{1}H NMR (300 MHz, $CDCl_3$), δ (ppm): 10.44 (s, 1H, NH), 7.31 – 7.18 (m, 6H, ArH), 7.15 (dd, *J* = 2.9, 1.3 Hz, 1H, ArH), 6.98 (dd, *J* = 5.0, 1.4 Hz, 1H, ArH), 6.48 (s, 1H, CH), 5.00 (p, *J* = 6.2 Hz, 1H, OC*H*$(CH_3)_2$), 4.31 (d, *J* = 13.1 Hz, 1H, SC*H*$_2C_6H_5$), 4.17 (d, *J* = 13.2 Hz, 1H, SC*H*$_2C_6H_5$), 2.55 (s, 3H, CH_3), 1.23 (d, *J* = 6.2 Hz, 3H, OCH(C*H*$_3)_2$), 1.04 (d, *J* = 6.2 Hz, 3H, OCH(C*H*$_3)_2$). LRMS (CI) *m/z* calcd. for $C_{21}H_{23}N_4O_2S_2$ $[M+H]^+$: 427.1 found: 427.0.

(±) Ethyl 7-(furan-2-yl)-5-methyl-4,7-dihydrotetrazolo[1,5-a]pyrimidine-6-carboxylate (193). Purified by column chromatography (Hex–AcOEt 1:1 – 1:3). Yield: 25%. Mp: 242 – 244 ºC. ^{1}H NMR (300 MHz, $CDCl_3$), δ (ppm): 11.08 (brs, 1H, NH), 7.31 (s, 1H, ArH), 6.85 (s, 1H, CH), 6.37 (s, 1H, ArH), 6.31 (s, 1H, ArH), 4.37 – 3.95 (m, 2H, OC*H*$_2CH_3$), 2.68 (s, 3H, CH_3), 1.21 (t, *J* = 7.0 Hz, 3H, OCH_2C*H*$_3$). ^{13}C NMR (75 MHz, DMSO-*d*$_6$), δ (ppm): 164.87, 152.36, 149.07, 147.78, 143.78, 111.22, 108.79, 95.63, 60.17, 52.56, 18.89, 14.38. LRMS (CI) *m/z* calcd. for $C_{12}H_{14}N_5O_3$ $[M+H]^+$: 276.1 found: 276.0.

(±) Isopropyl 7-(furan-2-yl)-5-methyl-4,7-dihydrotetrazolo[1,5-a]pyrimidine-6-carboxylate (194). Purified by column chromatography (Hex–AcOEt 1:1 – 1:3). Yield: 52%. Mp: 204 - 206 ºC. ^{1}H NMR (300 MHz, $CDCl_3$), δ (ppm): 11.31 (brs, 1H, NH), 7.31 (s, 1H, ArH), 6.83 (s, 1H, CH), 6.36 (s, 1H, ArH), 6.33 – 6.28 (m, 1H, ArH), 5.03 (hept, *J* = 6.3 Hz, 1H, OC*H*$(CH_3)_2$), 2.67 (s, 3H, CH_3), 1.25 (d, *J* = 6.2 Hz, 3H, OCH(C*H*$_3)_2$), 1.08 (d, *J* = 6.2 Hz, 3H, OCH(C*H*$_3)_2$). ^{13}C NMR (75 MHz, $CDCl_3$), δ (ppm): 164.2, 151.3, 148.9, 146.8, 143.1, 110.6, 108.7, 96.7, 68.1, 52.9, 22.0, 21.6, 19.4. LRMS (CI) *m/z* calcd. for $C_{13}H_{16}N_5O_3$ $[M+H]^+$: 290.1 found: 290.2.

(±) Ethyl 7-(furan-3-yl)-5-methyl-4,7-dihydrotetrazolo[1,5-a]pyrimidine-6-carboxylate (195). Purified by column chromatography (Hex–AcOEt 1:1 – 1:3). Yield: 66%. Mp: 196 - 198 ºC. ^{1}H NMR (300 MHz, $CDCl_3$), δ (ppm): 10.96 (brs, 1H, NH), 7.41 (s, 1H, ArH), 7.33 (s, 1H, ArH), 6.79 (s, 1H, CH), 6.30 (s, 1H, ArH), 4.27 – 4.07 (m, 2H, OC*H*$_2CH_3$), 2.65 (s, 3H, CH_3), 1.24 (t, *J* = 7.1 Hz, 3H, OCH_2C*H*$_3$). LRMS (CI) *m/z* calcd. for $C_{12}H_{14}N_5O_3$ $[M+H]^+$: 276.1 found: 276.0.

(±) Isopropyl 7-(furan-3-yl)-5-methyl-4,7-dihydrotetrazolo[1,5-a]pyrimidine-6-carboxylate (196). Purified by column chromatography (Hex–AcOEt 1:1 – 1:3). Yield: 61%. Mp: 218 – 220 ºC. ^{1}H NMR (300 MHz, $CDCl_3$), δ (ppm): 10.69 (brs, 1H, NH), 7.42 (m, 1H, ArH), 7.33 (d, *J* = 1.6 Hz, 1H, ArH), 6.77 (s, 1H, CH_3), 6.32 (s, 1H, ArH), 5.16 – 4.94 (m, 1H, OC*H*$(CH_3)_2$), 2.64 (s, 3H, CH_3), 1.26 (d, *J* = 6.2 Hz, 3H, OCH(C*H*$_3)_2$), 1.14 (d, *J* = 6.2 Hz, 3H, OCH(C*H*$_3)_2$). ^{13}C NMR (75 MHz, $CDCl_3$), δ (ppm): 164.36, 148.99, 145.97, 143.80, 140.47, 125.11, 108.87, 98.76, 68.21, 51.47, 21.98, 21.59, 19.36. LRMS (CI) *m/z* calcd. for $C_{13}H_{16}N_5O_3$ $[M+H]^+$: 290.1 found: 290.0.

(±) Ethyl 5-methyl-7-(thiophen-2-yl)-4,7-dihydrotetrazolo[1,5-*a*]pyrimidine-6-carboxylate (197). Purified by column chromatography (Hex–AcOEt 1:1 – 1:3). Yield: 68%. Mp: 189 – 191 ºC. ^{1}H NMR (300 MHz, $CDCl_3$), δ (ppm): 10.93 (brs, 1H, NH), 7.24 – 7.22 (m, 1H, ArH), 7.06 (s, 2H, ArH + CH), 6.98 – 6.90 (m, 1H, ArH), 4.27 – 4.08 (m, 2H, OC*H*$_2$CH$_3$), 2.69 (s, 3H, CH_3), 1.18 (t, *J* = 7.1 Hz, 3H, OCH_2C*H*$_3$). LRMS (CI) *m/z* calcd. for $C_{12}H_{14}N_5O_2S$ $[M+H]^+$: 292.1 found: 292.0.

(±) Isopropyl 5-methyl-7-(thiophen-2-yl)-4,7-dihydrotetrazolo[1,5-*a*]pyrimidine-6-carboxylate (198). Purified by column chromatography (Hex–AcOEt 1:1 – 1:3). Yield: 61%. Mp: 226 – 228 ºC. ^{1}H NMR (300 MHz, $CDCl_3$), δ (ppm): 10.86 (brs, 1H, NH), 7.24 (s, 1H, ArH), 7.09 (dd, *J* = 3.7, 1.5 Hz 1H, ArH), 7.04 (s, 1H, CH), 6.94 (dd, *J* = 5.1, 3.6 Hz, 1H, ArH), 5.14 – 4.86 (m, 1H, OC*H*$(CH_3)_2$), 2.69 (s, 3H, CH_3), 1.24 (d, *J* = 6.2 Hz, 3H, OCH(C*H*$_3)_2$), 1.03 (d, *J* = 6.2 Hz, 3H, OCH(C*H*$_3)_2$). LRMS (CI) *m/z* calcd. for $C_{13}H_{16}N_5O_2S$ $[M+H]^+$: 306.1 found: 306.0.

(±) Ethyl 5-methyl-7-(thiophen-3-yl)-4,7-dihydrotetrazolo[1,5-*a*]pyrimidine-6-carboxylate (199). Purified by column chromatography (Hex–AcOEt 1:1 – 1:3). Yield: 63%. Mp: 210 – 212 ºC. ^{1}H NMR (300 MHz, $CDCl_3$), δ (ppm): 10.93 (brs, 1H, NH), 7.26 (s, 2H, ArH), 7.05 – 6.98 (m, 1H, ArH), 6.88 (s, 1H, CH), 4.29 – 4.02 (m, 2H, OC*H*$_2$CH$_3$), 2.67 (s, 3H, CH_3), 1.18 (t, *J* = 7.0 Hz, 3H, OCH_2C*H*$_3$). LRMS (CI) *m/z* calcd. for $C_{12}H_{14}N_5O_2S$ $[M+H]^+$: 292.1 found: 292.0.

(±) Isopropyl 5-methyl-7-(thiophen-3-yl)-4,7-dihydrotetrazolo[1,5-*a*]pyrimidine-6-carboxylate (200): Purified by column chromatography (Hex–AcOEt 1:1 – 1:3). Yield: 63%. Mp: 220 – 224 ºC. ^{1}H NMR (300 MHz, $CDCl_3$), δ (ppm): 10.78 (brs, 1H, NH), 7.26 (s, 2H, ArH), 7.07 – 7.02 (m, 1H, ArH), 6.86 (s, 1H, CH), 5.13 – 4.82 (m, 1H, OC*H*$(CH_3)_2$), 2.67 (s, 3H, CH_3), 1.24 (d, *J* = 6.2 Hz, 3H, OCH(C*H*$_3)_2$), 1.03 (d, *J* = 6.2 Hz, 3H, OCH(C*H*$_3)_2$). LRMS (CI) *m/z* calcd. for $C_{13}H_{16}N_5O_2S$ $[M+H]^+$: 306.1 found: 306.0.

(±) Ethyl 3-cyano-7-(furan-2-yl)-5-methyl-4,7-dihydropyrazolo[1,5-a]pyrimidine-6-carboxylate (201). Purified by column chromatography (Hex–AcOEt 1:1 – 1:3). Yield: 35%. Mp: 227 – 228 ºC. ^{1}H NMR (300 MHz, DMSO-*d*$_6$), δ (ppm): 10.96 (brs, 1H, NH), 7.86 (s, 1H, ArH), 7.50 (s, 1H, CH), 6.43- 6.23 (m, 3H, ArH), 4.15 - 3.87 (m, 2H, OC*H*$_2$CH$_3$), 2.41 (s, 3H, CH_3), 1.09 (t, *J* = 6.6 Hz, 3H, OCH_2C*H*$_3$); ^{13}C NMR (75 MHz, DMSO-*d*$_6$), δ (ppm): 165.2, 153.4, 146.6, 143.3, 142.9, 141.7, 113.7, 111.0, 108.0, 95.8, 74.0, 60.0, 53.4, 18.4, 14.4. HRMS (APCI) *m/z* calcd. for $C_{15}H_{15}N_4O_3$ $[M+H]^+$: 299.1139 found: 299.1137.

(±) Isopropyl 3-cyano-7-(furan-2-yl)-5-methyl-4,7-dihydropyrazolo[1,5-a]pyrimidine-6-carboxylate (202). Purified by column chromatography (Hex–AcOEt 1:1 – 1:3). Yield: 44%. Mp: 224 – 226 ºC. ^{1}H NMR (300 MHz, DMSO-*d*$_6$), δ (ppm): 10.93 (brs, 1H, NH), 7.86 (s, 1H, ArH), 7.51 (s, 1H, ArH), 6.37 – 6.33 (m, 1H, ArH), 6.30 (s, 2H, CH), 4.98 – 4.66 (m, 1H, OC*H*$(CH_3)_2$), 2.41 (s, 3H, CH_3), 1.17 (d, *J* = 6.2 Hz, 3H, OCH(C*H*$_3)_2$), 0.99 (d, *J* = 6.2 Hz, 3H, OCH(C*H*$_3)_2$). ^{13}C NMR (75 MHz, $CDCl_3$), δ (ppm): 164.7, 152.8, 145.2, 142.5, 142.2, 141.9, 113.4, 110.4, 107.9, 97.0, 73.6, 67.7, 53.6, 22.0, 21.6, 18.5. LRMS (CI) *m/z* calcd. for $C_{16}H_{17}N_4O_3$ $[M+H]^+$: 313.1 found: 313.0.

(±) Ethyl 3-cyano-7-(furan-3-yl)-5-methyl-4,7-dihydropyrazolo[1,5-a]pyrimidine-6-carboxylate (203). Purified by column chromatography (Hex–AcOEt 1:1 – 1:3). Yield: 64%. Mp: 200 – 202 ºC. ^{1}H NMR (300 MHz, DMSO-*d*$_6$), δ (ppm): 10.85 (brs, 1H, NH), 7.92 – 7.83 (m, 1H, ArH), 7.51 (s, 2H, ArH), 6.23 (s, 1H, ArH), 6.20 (s, 1H, CH), 4.12 – 3.97 (m, 2H, OC*H*$_2$CH$_3$), 2.39 (s, 3H, CH_3), 1.14 (t, *J* = 7.0 Hz, 3H, OCH_2C*H*$_3$). LRMS (CI) *m/z* calcd. for $C_{15}H_{15}N_4O_3$ $[M+H]^+$: 299.1 found: 299.0.

(±) Isopropyl 3-cyano-7-(furan-3-yl)-5-methyl-4,7-dihydropyrazolo[1,5-a]pyrimidine-6-carboxylate (204). Purified by column chromatography (Hex–AcOEt 1:1 – 1:3). Yield: 33%. Mp: 180 – 183 ºC. ^{1}H NMR (300 MHz, DMSO-*d*$_6$), δ (ppm): 10.82 (brs, 1H, NH), 7.86 (s, 1H, ArH), 7.51 (s, 2H, ArH), 6.21 (s, 2H, ArH + CH), 5.01 - 4.78 (m, 1H, OC*H*(CH$_3$)$_2$), 2.39 (s, 3H, CH$_3$), 1.18 (d, *J* = 6.4 Hz, 3H, OCH(C*H*$_3$)$_2$), 1.06 (d, *J* = 6.3 Hz, 3H, OCH(C*H*$_3$)$_2$). ^{13}C NMR (75 MHz, DMSO-*d*$_6$), δ (ppm): 164.6, 145.9, 144.1, 142.8, 141.7, 140.4, 126.9, 113.9, 109.5, 97.8, 73.8, 67.3, 51.8, 22.2, 21.9, 18.3. HRMS (APCI) *m/z* calcd. for $C_{16}H_{17}N_4O_3$ 313.1295 found: 313.1293.

(±) Ethyl 3-cyano-5-methyl-7-(thiophen-2-yl)-4,7-dihydropyrazolo[1,5-a]pyrimidine-6-carboxylate (205). Purified by column chromatography (Hex–AcOEt 1:1 – 1:3). Yield: 12%. Mp: 194 – 196 ºC. ^{1}H NMR (300 MHz, DMSO-*d*$_6$), δ (ppm): 11.02 (brs, 1H, NH), 7.91 (s, 1H, ArH), 7.45 – 7.38 (m, *J* = 4.8, 1.5 Hz, 1H, ArH), 6.97 – 6.87 (m, 2H, ArH), 6.54 (s, 1H, CH), 4.16 – 3.95 (m, 2H, OC*H*$_2$CH$_3$), 2.44 (s, 3H, CH$_3$), 1.12 (t, *J* = 7.1 Hz, 3H, OCH$_2$C*H*$_3$). LRMS (CI) *m/z* calcd. for $C_{15}H_{15}N_4O_2S$ $[M+H]^+$: 315.1 found: 315.0.

(±) Isopropyl 3-cyano-5-methyl-7-(thiophen-2-yl)-4,7-dihydropyrazolo[1,5-a]pyrimidine-6-carboxylate (206). Purified by column chromatography (Hex–AcOEt 1:1 – 1:3). Yield: 13%. Mp: 201 – 203 ºC. ^{1}H NMR (300 MHz, DMSO-*d*$_6$), δ (ppm): 10.98 (brs, 1H, NH), 7.89 (s, 1H, ArH), 7.40 (d, *J* = 4.3 Hz, 1H, ArH), 6.89 (s, 2H, ArH), 6.50 (s, 1H, CH), 4.95 – 4.76 (m, 1H, OC*H*(CH$_3$)$_2$), 2.42 (s, 3H, CH$_3$), 1.17 (d, *J* = 6.2 Hz, 3H, OCH(C*H*$_3$)$_2$), 0.99 (d, *J* = 6.2 Hz, 3H, OCH(C*H*$_3$)$_2$). LRMS (CI) *m/z* calcd. for $C_{16}H_{17}N_4O_2S$ $[M+H]^+$: 329.1 found: 329.0.

(±) Ethyl 3-cyano-5-methyl-7-(thiophen-3-yl)-4,7-dihydropyrazolo[1,5-a]pyrimidine-6-carboxylate (207). Purified by column chromatography (Hex–AcOEt 1:1 – 1:3). Yield: 49%. Mp: 217 – 219 ºC. ^{1}H NMR (300 MHz, DMSO-*d*$_6$), δ (ppm): 10.88 (brs, 1H, NH), 7.86 (s, 1H, ArH), 7.45 – 7.37 (m, 1H, ArH), 7.26 (s, 1H, ArH), 6.84 (d, *J* = 4.9 Hz, 1H, ArH), 6.33 (s, 1H, CH), 4.12 – 3.94 (m, 2H, OC*H*$_2$CH$_3$), 2.40 (s, 3H, CH$_3$), 1.10 (t, *J* = 6.9 Hz, 3H, OCH$_2$C*H*$_3$). LRMS (CI) *m/z* calcd. for $C_{15}H_{15}N_4O_2S$ $[M+H]^+$: 315.1 found: 315.1.

(±) Isopropyl 3-cyano-5-methyl-7-(thiophen-3-yl)-4,7-dihydropyrazolo[1,5-a]pyrimidine-6-carboxylate (208). Purified by column chromatography (Hex–AcOEt 1:1 – 1:3). Yield: 53%. Mp: 221 – 223 ºC. ^{1}H NMR (300 MHz, DMSO-d_6), δ (ppm): 10.85 (brs, 1H, NH), 7.85 (s, 1H, ArH), 7.41 (s, 1H, ArH), 7.27 (s, 1H, ArH), 6.86 (d, J = 4.9 Hz, 1H, ArH), 6.31 (s, 1H, CH), 4.94 – 4.75 (m, 1H, OC*H*$(CH_3)_2$), 2.40 (s, 3H, CH_3), 1.17 (d, J = 6.3 Hz, 3H, OCH(C*H*$_3)_2$), 0.98 (d, J = 6.1 Hz, 3H, OCH(C*H*$_3)_2$). LRMS (CI) *m/z* calcd. for $C_{16}H_{17}N_4O_2S$ $[M+H]^+$: 329.1 found: 329.0.

(±) Ethyl 4-(furan-2-yl)-2-methyl-4,6-dihydropyrimido[1,2-*b*]indazole-3-carboxylate (209). Purified by column chromatography (Hex–AcOEt 3:1 – 1:1). Yield: 39%. Mp: 233 – 236 ºC. ^{1}H NMR (300 MHz, DMSO-d_6), δ (ppm): 10.79 (s, 1H, NH), 7.74 (dd, J = 8.4, 1.2 Hz, 1H, ArH), 7.45 (p, J = 1.0 Hz, 1H, ArH), 7.35 (dd, J = 8.8, 1.1 Hz, 1H, ArH), 7.24 – 7.10 (m, 1H, ArH), 6.89 (dd, J = 8.4, 6.4 Hz, 1H, ArH), 6.59 (s, 1H, CH), 6.37 – 6.23 (m, 2H, ArH), 4.14 – 3.93 (m, 2H, OC*H*$_2$CH$_3$), 2.51 (s, 3H, CH_3), 1.12 (t, J = 7.1 Hz, 3H, OCH_2C*H*$_3$). LRMS (CI) m/z calcd. for $C_{18}H_{18}N_3O_3$ $[M+H]^+$: 324.1 found: 324.0.

(±) Isopropyl 4-(furan-2-yl)-2-methyl-4,6-dihydropyrimido[1,2-*b*]indazole-3-carboxylate (210). Purified by column chromatography (Hex–AcOEt 3:1 – 1:1). Yield: 27%. Mp: 235 – 237 ºC. ^{1}H NMR (300 MHz, DMSO-d_6), δ (ppm): 10.78 (s, 1H, NH), 7.76 (d, J = 8.4 Hz, 1H, ArH), 7.48 (s, 1H, ArH), 7.37 (d, J = 8.9 Hz, 1H, ArH), 7.19 (t, J = 7.8 Hz, 1H, ArH), 6.91 (t, J = 7.8 Hz, 1H, ArH), 6.60 (d, J = 3.0 Hz, 1H, CH), 6.32 (dd, J = 12.3, 3.2 Hz, 2H, ArH), 4.95 – 4.81 (m, 1H, OC*H*$(CH_3)_2$), 2.53 (s, 3H, CH_3), 1.22 (dd, J = 6.4, 2.9 Hz, 3H, OCH(C*H*$_3)_2$), 1.05 (dd, J = 6.4, 2.8 Hz, 3H, OCH(C*H*$_3)_2$). ^{13}C NMR (75 MHz, $CDCl_3$), δ (ppm): 169.9, 159.5, 152.7, 151.2, 147.5, 135.6, 131.9, 125.1, 124.2, 121.6, 115.6, 112.2, 98.3, 71.5, 59.2, 27.0, 26.7, 23.8. LRMS (CI) m/z calcd. for $C_{19}H_{20}N_3O_3$ $[M+H]^+$: 338.1 found: 338.0.

(±) Ethyl 4-(furan-3-yl)-2-methyl-4,6-dihydropyrimido[1,2-b]indazole-3-carboxylate (211). Purified by column chromatography (Hex–AcOEt 3:1 – 1:1). Yield: 28%. Mp: 221 – 223 ºC. ^{1}H NMR (300 MHz, DMSO-d_6), δ (ppm): 10.69 (s, 1H, NH), 7.73 (dd, J = 8.4, 1.2 Hz, 1H, ArH), 7.51 (s, 1H, ArH), 7.46 (t, J = 1.7 Hz, 1H, ArH), 7.36 (d, J = 8.8 Hz, 1H, ArH), 7.23 – 7.09 (m, 1H, ArH), 6.89 (dd, J = 8.5, 6.5 Hz, 1H, ArH), 6.51 (s, 1H, CH), 6.18 (d, J = 1.8 Hz, 1H, ArH), 4.08 (qd, J = 7.1, 2.2 Hz, 2H, OC*H*$_2$CH$_3$), 2.49 (s, 3H, CH_3), 1.17 (t, J = 7.1 Hz, 3H, OCH_2C*H*$_3$). LRMS (CI) m/z calcd. for $C_{18}H_{18}N_3O_3$ $[M+H]^+$: 324.1 found: 324.1.

(±) Isopropyl 4-(furan-3-yl)-2-methyl-4,6-dihydropyrimido[1,2-b]indazole-3-carboxylate (212). Purified by column chromatography (Hex–AcOEt 3:1 – 1:1). Yield: 35%. Mp: 219 – 221 ºC ^{1}H NMR (300 MHz, DMSO-*d*$_6$), δ (ppm): 10.66 (s, 1H, NH), 7.78 – 7.68 (m, 1H, ArH), 7.54 – 7.42 (m, 2H, ArH), 7.35 (dd, *J* = 8.8, 0.9 Hz, 1H, ArH), 7.22 – 7.11 (m, 1H, ArH), 6.94 – 6.83 (m, 1H, ArH), 6.49 (s, 1H, CH), 6.19 (s, 1H, ArH), 4.91 (p, *J* = 6.2 Hz, 1H, OC*H*(CH$_3$)$_2$), 2.48 (s, 3H, 22), 1.21 (d, *J* = 6.2 Hz, 3H, OCH(C*H*$_3$)$_2$), 1.09 (d, *J* = 6.2 Hz, 3H, OCH(C*H*$_3$)$_2$). LRMS (CI) m/z calcd. for $C_{19}H_{20}N_3O_3$ $[M+H]^+$: 338.1 found: 338.0.

(±) Ethyl 2-methyl-4-(thiophen-2-yl)-4,6-dihydropyrimido[1,2-b]indazole-3-carboxylate (213). Purified by column chromatography (Hex–AcOEt 3:1 – 1:1). Yield: 30%. Mp: 226 – 228 ºC. ^{1}H NMR (300 MHz, DMSO-*d*$_6$), δ (ppm): 10.84 (s, 1H, NH), 7.80 – 7.65 (m, 1H, ArH), 7.43 – 7.28 (m, 2H, ArH), 7.24 – 7.10 (m, 1H, ArH), 6.97 – 6.81 (m, 3H, ArH + CH), 6.80 (s, 1H, ArH), 4.16 – 3.98 (m, 2H, OC*H*$_2$CH$_3$), 2.52 (s, 3H, CH$_3$), 1.13 (t, *J* = 7.1 Hz, 3H, OCH$_2$C*H*$_3$). LRMS (CI) m/z calcd. for $C_{18}H_{18}N_3O_2S$ $[M+H]^+$: 340.1 found: 340.0.

(±) Isopropyl 2-methyl-4-(thiophen-2-yl)-4,6-dihydropyrimido[1,2-b]indazole-3-carboxylate (214). Purified by column chromatography (Hex–AcOEt 3:1 – 1:1). Yield: 15%. Mp: 225 – 227 ºC. ^{1}H NMR (300 MHz, DMSO-*d*$_6$), δ (ppm): 10.81 (s, 1H, NH), 7.74 (d, *J* = 8.4 Hz, 1H, ArH), 7.41 – 7.30 (m, 2H, ArH), 7.23 – 7.11 (m, 1H, ArH), 6.95 – 6.83 (m, 3H, ArH), 6.78 (s, 1H, CH), 4.89 (p, *J* = 6.1 Hz, 1H, OC*H*(CH$_3$)$_2$), 2.52 (s, 3H, CH$_3$), 1.24 – 1.16 (m, 3H, OCH(C*H*$_3$)$_2$), 1.03 (d, *J* = 6.2 Hz, 3H, OCH(C*H*$_3$)$_2$). LRMS (CI) m/z calcd. for $C_{19}H_{20}N_3O_2S$ $[M+H]^+$: 354.1 found: 354.1.

(±) Ethyl 2-methyl-4-(thiophen-3-yl)-4,6-dihydropyrimido[1,2-*b*]indazole-3-carboxylate (215). Purified by column chromatography (Hex–AcOEt 3:1 – 1:1). Yield: 27%. Mp: 250 – 252 ºC. ^{1}H NMR (300 MHz, DMSO-*d*$_6$), δ (ppm): 10.71 (s, 1H, NH), 7.74 (d, *J* = 8.4 Hz, 1H, ArH), 7.39 – 7.31 (m, 1H, ArH), 7.29 (s, 1H, ArH), 7.27 – 7.21 (m, 1H, ArH), 7.21 – 7.10 (m, 1H, ArH), 6.94 – 6.80 (m, 2H, ArH), 6.61 (s, 1H, CH), 4.18 – 3.91 (m, 2H, OC*H*$_2$CH$_3$), 2.48 (s, 3H, CH$_3$), 1.13 (t, *J* = 7.0 Hz, 3H, OCH$_2$C*H*$_3$). LRMS (CI) m/z calcd. for $C_{18}H_{18}N_3O_2S$ $[M+H]^+$: 340.1 found: 340.1.

(±) Isopropyl 2-methyl-4-(thiophen-3-yl)-4,6-dihydropyrimido[1,2-b]indazole-3-carboxylate (216). Purified by column chromatography (Hex–AcOEt 3:1 – 1:1). Yield: 28%. Mp: 216 – 218 ºC ^{1}H NMR (300 MHz, DMSO-d_6), δ (ppm): 10.69 (s, 1H, NH), 7.74 (d, J = 8.3 Hz, 1H, ArH), 7.39 – 7.29 (m, 2H, ArH), 7.29 – 7.22 (m, 1H, ArH), 7.21 – 7.10 (m, 1H, ArH), 6.94 – 6.82 (m, 2H, ArH), 6.60 (s, 1H, CH), 4.87 (p, J = 6.2 Hz, 1H, OCH(CH$_3$)$_2$), 2.49 (s, 3H, CH$_3$), 1.20 (d, J = 6.2 Hz, 3H, OCH(CH_3)$_2$), 1.03 (d, J = 6.2 Hz, 3H, OCH(CH_3)$_2$). LRMS (CI) m/z calcd. for $C_{19}H_{20}N_3O_2S$ $[M+H]^+$: 354.1 found: 354.1.

(±) Ethyl 5-(furan-2-yl)-7-methyl-5H-thiazolo[3,2-a]pyrimidine-6-carboxylate (217). Yield: 30%. Mp: 140 – 142 ºC ^{1}H NMR (300 MHz, $CDCl_3$), δ (ppm): 7.37 – 7.30 (m, 1H, ArH), 6.85 (d, J = 4.8 Hz, 1H, CH), 6.48 – 6.14 (m, 4H, ArH), 4.13 (p, J = 6.9 Hz, 2H, OCH_2CH$_3$), 2.48 (s, 3H, CH$_3$), 1.19 (t, J = 7.1 Hz, 3H, OCH$_2$CH_3). LRMS (CI) m/z calcd. for $C_{14}H_{15}N_2O_3S$ $[M+H]^+$: 291.1 found: 291.1.

(±) Isopropyl 5-(furan-2-yl)-7-methyl-5H-thiazolo[3,2-a]pyrimidine-6-carboxylate (218). Purified by column chromatography (Hex–AcOEt 3:1 – 1:1). Yield: 37%. Mp: 141 – 143 ºC. ^{1}H NMR (300 MHz, $CDCl_3$), δ (ppm): 7.33 (dd, J = 1.8, 0.9 Hz, 1H, ArH), 6.80 (d, J = 4.7 Hz, 1H, ArH), 6.35 – 6.18 (m, 4H, ArH), 5.00 (p, J = 6.3 Hz, 1H, OCH(CH$_3$)$_2$), 2.46 (s, 3H, CH$_3$), 1.28 – 1.18 (m, 3H, OCH(CH_3)$_2$), 1.07 (d, J = 6.2 Hz, 3H, OCH(CH_3)$_2$). LRMS (CI) m/z calcd. for $C_{15}H_{17}N_2O_3S$ $[M+H]^+$: 305.1 found: 305.0.

(±) Ethyl 5-(furan-3-yl)-7-methyl-5H-thiazolo[3,2-a]pyrimidine-6-carboxylate (219). Purified by column chromatography (Hex–AcOEt 3:1 – 1:1). Yield: 33%. Oil at RT. ^{1}H NMR (300 MHz, $CDCl_3$), δ (ppm): 7.36 – 7.28 (m, 2H, ArH), 6.68 (s, 1H, ArH), 6.39 (s, 1H, CH), 6.27 (d, J = 16.4 Hz, 2H, ArH), 4.16 (q, J = 3.7 Hz, 2H, OCH_2CH$_3$), 2.42 (s, 3H, CH$_3$), 1.26 (t, J = 7.1 Hz, 3H, OCH$_2$CH_3). LRMS (CI) m/z calcd. for $C_{14}H_{15}N_2O_3S$ $[M+H]^+$: 291.1 found: 291.1.

(±) Isopropyl 5-(furan-3-yl)-7-methyl-5H-thiazolo[3,2-a]pyrimidine-6-carboxylate (220). Purified by column chromatography (Hex–AcOEt 3:1 – 1:1). Yield: 36%. Oil at RT. ^{1}H NMR (300 MHz, $CDCl_3$), δ (ppm): 7.37 (s, 1H, ArH), 7.34 – 7.23 (m, 2H, ArH), 6.64 (d, J = 4.7 Hz, 1H, ArH), 6.36 – 6.28 (m, 1H, ArH), 6.21 (s, 1H, CH), 5.04 (p, J = 6.2 Hz, 1H, OCH(CH$_3$)$_2$), 2.39 (s, 3H, CH$_3$), 1.22 (s, 3H, OCH(CH_3)$_2$), 1.19 (d, J = 6.2 Hz, 3H, OCH(CH_3)$_2$). LRMS (CI) m/z calcd. for $C_{15}H_{17}N_2O_3S$ $[M+H]^+$: 305.1 found: 305.1.

(±) Ethyl 7-methyl-5-(thiophen-2-yl)-5*H*-thiazolo[3,2-*a*]pyrimidine-6-carboxylate (221). Purified by column chromatography (Hex–AcOEt 3:1 – 1:1). Yield: 40%. Mp: 144 – 146 ºC. ^{1}H NMR (300 MHz, $CDCl_3$), δ (ppm): 7.24 – 7.12 (m, 1H, ArH), 7.01 – 6.81 (m, 2H, ArH), 6.77 – 6.64 (m, 1H, ArH), 6.47 (s, 1H, CH), 6.39 – 6.23 (m, 1H, ArH), 4.25 – 3.97 (m, 2H, OCH_2CH_3), 2.57 – 2.31 (m, 3H, CH_3), 1.38 – 1.06 (m, 3H, OCH_2CH_3). LRMS (CI) m/z calcd. for $C_{14}H_{15}N_2O_2S_2$ $[M+H]^+$: 307.0 found: 307.0.

(±) Isopropyl 7-methyl-5-(thiophen-2-yl)-5*H*-thiazolo[3,2-*a*]pyrimidine-6-carboxylate (222). Purified by column chromatography (Hex–AcOEt 3:1 – 1:1). Yield: 42%. Mp: 127 – 129 ºC. ^{1}H NMR (300 MHz, $CDCl_3$), δ (ppm): 7.23 (d, J = 16.0 Hz, 1H, ArH), 6.97 – 6.86 (m, 2H, ArH), 6.73 (d, J = 4.8 Hz, 1H, 18), 6.47 (s, 1H, CH), 6.33 (d, J = 4.8 Hz, 1H, ArH), 5.01 (p, J = 6.2 Hz, 1H, ArH), 2.44 (s, 3H, CH_3), 1.24 (d, J = 6.3 Hz, 3H, $OCH(CH_3)_2$), 1.10 (d, J = 6.2 Hz, 3H, $OCH(CH_3)_2$). LRMS (CI) m/z calcd. for $C_{15}H_{17}N_2O_2S_2$ $[M+H]^+$: 321.1 found: 321.0.

(±) Ethyl 7-methyl-5-(thiophen-3-yl)-5*H*-thiazolo[3,2-*a*]pyrimidine-6-carboxylate (223). Purified by column chromatography (Hex–AcOEt 3:1 – 1:1). Yield: 35%. Mp: 123 – 125 ºC. ^{1}H NMR (300 MHz, $CDCl_3$), δ (ppm): 7.30 – 7.19 (m, 1H, ArH), 7.15 (s, 1H, ArH), 7.06 – 6.97 (m, 1H, ArH), 6.63 (s, 1H, CH), 6.31 (d, J = 7.2 Hz, 2H, ArH), 4.12 (q, J = 7.1 Hz, 2H, OCH_2CH_3), 2.41 (s, 3H, CH_3), 1.23 (t, J = 7.1 Hz, 3H, OCH_2CH_3). LRMS (CI) m/z calcd. for $C_{14}H_{15}N_2O_2S_2$ $[M+H]^+$: 307.0 found: 307.1.

(±) Isopropyl 7-methyl-5-(thiophen-3-yl)-5*H*-thiazolo[3,2-*a*]pyrimidine-6-carboxylate (224). Purified by column chromatography (Hex–AcOEt 3:1 – 1:1). Yield: 33%. Mp: 129 – 131 ºC. ^{1}H NMR (300 MHz, $CDCl_3$), δ (ppm): 7.28 – 7.20 (m, 1H, ArH), 7.19 – 7.11 (m, 1H, ArH), 7.07 – 6.92 (m, 1H, ArH), 6.64 (s, 1H, CH), 6.32 (d, J = 4.9 Hz, 2H, Ar-H), 4.99 (q, J = 6.2 Hz, 1H, $OCH(CH_3)_2$), 2.41 (s, 3H, CH_3), 1.24 (d, J = 6.3 Hz, 3H, $OCH(CH_3)_2$), 1.12 (d, J = 6.2 Hz, 3H, $OCH(CH_3)_2$). LRMS (CI) m/z calcd. for $C_{15}H_{17}N_2O_2S_2$ $[M+H]^+$: 321.1 found: 321.1.

(±) Ethyl 4-(furan-2-yl)-2-methyl-4H-benzo[4,5]thiazolo[3,2-a]pyrimidine-3-carboxylate (225). Purified by column chromatography (Hex–AcOEt 3:1 – 1:1). Yield: 22%. Mp: 128 – 129 ºC. ^{1}H NMR (300 MHz, $CDCl_3$), δ (ppm): 7.46 (dd, J = 7.6, 1.1 Hz, 1H, ArH), 7.46 – 7.30 (m, 2H, ArH), 7.30 – 7.12 (m, 2H, ArH), 6.52 (s, 1H, CH), 6.33 – 6.18 (m, 2H, ArH), 4.19 (q, J = 7.1 Hz, 2H, OCH_2CH_3), 2.50 (s, 3H, CH_3), 1.26 (t, J = 7.1 Hz, 3H, OCH_2CH_3). HRMS (APCI) m/z calcd. for $C_{18}H_{17}N_2O_3S$ $[M+H]^{+\cdot}$: 341.0882 found: 341.0892.

(±) Isopropyl 4-(furan-2-yl)-2-methyl-4H-benzo[4,5]thiazolo[3,2-a]pyrimidine-3-carboxylate (226). Purified by column chromatography (Hex–AcOEt 3:1 – 1:1). Yield: 15%. Mp: 122 – 124 ºC. ^{1}H NMR (300 MHz, $CDCl_3$), δ (ppm): 7.46 – 7.29 (m, 3H, ArH), 7.26 – 7.12 (m, 2H, ArH), 6.48 (s, 1H, CH), 6.30 – 6.16 (m, 2H, ArH), 5.12 – 4.96 (m, 1H, OC*H*$(CH_3)_2$), 2.48 (s, 3H, CH_3), 1.27 (d, *J* = 6.2 Hz, 3H, OCH(C*H*$_3)_2$), 1.15 (d, *J* = 6.2 Hz, 3H, OCH(C*H*$_3)_2$). ^{13}C NMR (75 MHz, $CDCl_3$), δ (ppm): 165.8, 162.7, 155.8, 153.5, 142.2, 138.0, 126.5, 124.0, 123.7, 122.1, 111.7, 110.4, 108.6, 99.9, 67.3, 50.5, 23.4, 22.1, 21.9. HRMS (EI) m/z calcd. for $C_{19}H_{18}N_2O_3S$ $[M]^{+\cdot}$: 354.1038 found: 354.1035.

(±) Ethyl 4-(furan-3-yl)-2-methyl-4*H*-benzo[4,5]thiazolo[3,2-*a*]pyrimidine-3-carboxylate (227). Purified by column chromatography (Hex–AcOEt 3:1 – 1:1). Yield: 25%. Mp: 116 – 117 ºC. ^{1}H NMR (300 MHz, $CDCl_3$), δ (ppm): 7.47 (dd, *J* = 8.2, 1.2 Hz, 1H, ArH), 7.41 – 7.06 (m, 5H, ArH), 6.45 (s, 1H, CH), 6.28 (dd, *J* = 1.9, 0.9 Hz, 1H, ArH), 4.22 (q, *J* = 7.1 Hz, 2H, OC*H*$_2$CH$_3$), 2.44 (s, 3H, CH_3), 1.32 (t, *J* = 7.1 Hz, 3H, OCH_2C*H*$_3$). ^{13}C NMR (75 MHz, $CDCl_3$), δ (ppm): 166.4, 163.2, 155.6, 143.5, 139.5, 137.8, 126.6, 125.3, 124.0, 123.8, 122.3, 111.3, 108.9, 101.7, 60.1, 49.1, 23.6, 14.4. LRMS (CI) m/z calcd. for $C_{18}H_{17}N_2O_3S$ $[M+H]^+$: 341.1 found: 341.0.

(±) Isopropyl 4-(furan-3-yl)-2-methyl-4H-benzo[4,5]thiazolo[3,2-a]pyrimidine-3-carboxylate (228). Purified by column chromatography (Hex–AcOEt 3:1 – 1:1). Yield: 20%. Mp: 113 – 115 ºC. ^{1}H NMR (300 MHz, $CDCl_3$), δ (ppm): 7.46 (d, *J* = 7.7 Hz, 1H, ArH), 7.37 – 7.11 (m, 5H, ArH), 6.43 (s, 1H, CH), 6.27 (s, 1H, ArH), 5.17 – 5.00 (m, 1H, OC*H*$(CH_3)_2$), 2.42 (s, 3H, CH_3), 1.30 (d, *J* = 6.3 Hz, 3H, OCH(C*H*$_3)_2$), 1.27 (d, *J* = 6.3 Hz, 3H, OCH(C*H*$_3)_2$). ^{13}C NMR (75 MHz, $CDCl_3$), δ (ppm): 165.9, 163.1, 154.8, 143.4, 139.5, 137.7, 126.7, 125.2, 124.1, 123.9, 122.3, 111.3, 108.9, 102.1, 67.6, 49.1, 23.3, 22.1, 22.0. HRMS (EI) m/z calcd. for $C_{19}H_{18}N_2O_3S$ $[M]^{+\cdot}$: 354.1038 found: 354.1049.

(±) Ethyl 2-methyl-4-(thiophen-2-yl)-4*H*-benzo[4,5]thiazolo[3,2-*a*]pyrimidine-3-carboxylate (229). Purified by column chromatography (Hex–AcOEt 3:1 – 1:1). Yield: 22%. Oil at RT. ^{1}H NMR (300 MHz, $CDCl_3$), δ (ppm): 7.47 (d, *J* = 7.8 Hz, 1H, ArH), 7.40 – 7.09 (m, 4H, ArH), 6.96 (d, *J* = 3.6 Hz, 1H, ArH), 6.83 (dd, *J* = 5.1 Hz, *J* = 3.5 Hz, 1H, ArH), 6.73 (s, 1H, CH), 4.22 (q, *J* = 7.1 Hz, 2H, OCH_2CH_3), 2.47 (s, 3H, CH_3), 1.31 (t, *J* = 7.1 Hz, 3H, OCH_2CH_3). ^{13}C NMR (75 MHz, $CDCl_3$), δ (ppm): 166.3, 162.9, 155.4, 143.7, 137.7, 126.6, 126.5, 125.6, 125.5, 124.1, 123.9, 122.3, 111.6, 102.6, 60.2, 52.2, 23.5, 14.4. LRMS (CI) m/z calcd. for $C_{18}H_{17}N_2O_2S_2$ $[M+H]^+$: 357.1 found: 357.1.

(±) Isopropyl 2-methyl-4-(thiophen-2-yl)-4*H*-benzo[4,5]thiazolo[3,2-*a*]pyrimidine-3-carboxylate (230). Purified by column chromatography (Hex–AcOEt 3:1 – 1:1). Yield: 29%. Mp: 172 – 173 ºC. ^{1}H NMR (300 MHz, $CDCl_3$), δ (ppm): 7.51 (d, *J* = 7.8 Hz, 1H, ArH), 7.38 – 7.10 (m, 4H, ArH), 6.92 (d, *J* = 3.6 Hz, 1H, ArH), 6.83 (dd, *J* = 5.2, 3.4 Hz, 1H, ArH), 6.74 (s, 1H, CH), 4.88 (m, 1H, $OCH(CH_3)_2$), 2.41 (s, 3H, CH_3), 1.23 (d, *J* = 6.3 Hz, 3H, $OCH(CH_3)_2$), 1.16 (d, *J* = 6.2 Hz, 3H, $OCH(CH_3)_2$). ^{13}C NMR (75 MHz, $CDCl_3$), δ (ppm): 165.8, 162.7, 155.2, 143.8, 137.7, 126.6, 126.5, 125.6, 125.5, 124.1, 123.9, 122.3, 111.5, 102.9, 67.6, 52.2, 23.5, 22.2, 22.0. LRMS (CI) m/z calcd. for $C_{19}H_{19}N_2O_2S_2$ $[M+H]^+$: 371.1 found: 371.1.

(±) Ethyl 2-methyl-4-(thiophen-3-yl)-4*H*-benzo[4,5]thiazolo[3,2-*a*]pyrimidine-3-carboxylate (231). Purified by column chromatography (Hex–AcOEt 3:1 – 1:1). Yield: 16%. Mp: 167 – 169 ºC. ^{1}H NMR (300 MHz, $CDCl_3$), δ (ppm): 7.44 (dd, *J* = 8.1, 1.2 Hz, 1H, ArH), 7.36 – 6.91 (m, 6H, ArH), 6.55 (s, 1H, CH), 4.20 (q, *J* = 7.2 Hz, 2H, OCH_2CH_3), 2.43 (s, 3H, CH_3), 1.30 (t, *J* = 7.1 Hz, 3H, OCH_2CH_3). ^{13}C NMR (75 MHz, $CDCl_3$), δ (ppm): 166.5, 163.2, 155.1, 141.7, 137.9, 126.7, 126.4, 126.1, 124.0, 123.8, 122.5, 122.2, 111.5, 102.5, 60.1, 52.8, 23.6, 14.4. LRMS (CI) m/z calcd. for $C_{18}H_{17}N_2O_2S_2$ $[M+H]^+$: 357.1 found: 357.1.

(±) Isopropyl 2-methyl-4-(thiophen-3-yl)-4*H*-benzo[4,5]thiazolo[3,2-*a*]pyrimidine-3-carboxylate (232). Purified by column chromatography (Hex–AcOEt 3:1 – 1:1). Yield: 18%. Mp: 182 – 184 ºC. ^{1}H NMR (300 MHz, $CDCl_3$), δ (ppm): 7.49 – 7.43 (m, 1H, ArH), 7.29 (dd, *J* = 8.0, 1.4 Hz, 1H, Ar-H), 7.21 – 7.12 (m, 4H, ArH), 7.04 (dd, *J* = 5.0, 1.3 Hz, 1H, ArH), 6.55 (s, 1H, CH), 5.15 – 5.02 (m, 1H, OC*H*$(CH_3)_2$), 2.44 (s, 3H, CH_3), 1.30 (d, J = 6.2 Hz, 3H, OCH(C*H*$_3)_2$), 1.25 (d, J = 6.2 Hz, 3H, OCH(C*H*$_3)_2$). ^{13}C NMR (75 MHz, $CDCl_3$), δ (ppm): 166.0, 163.0, 154.6, 141.7, 137.9, 126.6, 126.3, 126.2, 123.9, 123.8, 122.5, 122.2, 111.4, 102.8, 67.5, 52.8, 23.5, 22.2, 22.0. HRMS (CI) m/z calcd. for $C_{19}H_{19}N_2O_2S_2$ $[M+H]^{+\cdot}$: 370.0810 found: 370.0812.

(±) Ethyl 7-chloro-4-(furan-2-yl)-2-methyl-4*H*-benzo[4,5]thiazolo[3,2-*a*]pyrimidine-3-carboxylate (233). Purified by column chromatography (Hex–AcOEt 3:1 – 1:1). Yield: 22%. Mp: 181 – 183 ºC. ^{1}H NMR (300 MHz, $CDCl_3$), δ (ppm): 7.40 – 7.32 (m, 2H, ArH), 7.31 – 7.25 (m, 1H, ArH), 7.17 (s, 1H, ArH), 6.44 (s, 1H, CH), 6.35 – 6.23 (m, 2H, ArH), 4.33 – 4.08 (m, 2H, OC*H*$_2$CH$_3$), 2.49 (s, 3H, CH_3), 1.26 (t, *J* = 7.1 Hz, 3H, OCH$_2$C*H*$_3$). LRMS (CI) m/z calcd. for $C_{18}H_{16}ClN_2O_3S$ $[M+H]^{+\cdot}$: 375.0 found: 375.1.

(±) Isopropyl 7-chloro-4-(furan-2-yl)-2-methyl-4*H*-benzo[4,5]thiazolo[3,2-*a*]pyrimidine-3-carboxylate (234). Purified by column chromatography (Hex–AcOEt 3:1 – 1:1). Yield: 25%. Mp: 154 – 156 ºC. ^{1}H NMR (300 MHz, $CDCl_3$), δ (ppm): 7.40 – 7.36 (m, 1H, ArH), 7.34 (s, 1H, ArH), 7.30 (dd, *J* = 1.8, 0.9 Hz, 1H, ArH), 7.17 (dd, *J* = 8.3, 1.9 Hz, 1H, ArH), 6.43 (s, 1H, CH), 6.32 – 6.22 (m, 2H, ArH), 5.15 – 4.98 (m, 1H, OC*H*$(CH_3)_2$), 2.50 (s, 3H, CH_3), 1.30 (d, *J* = 6.2 Hz, 3H, OCH(C*H*$_3)_2$), 1.18 (d, *J* = 6.2 Hz, 3H, OCH(C*H*$_3)_2$). ^{13}C NMR (75 MHz, CDCl3), δ (ppm): ^{13}C NMR (75 MHz, cdcl$_3$), δ 165.5, 162.5, 155.6, 153.1, 142.5, 139.1, 132.8, 124.2, 122.8, 122.1, 112.0, 110.6, 108.9, 100.4, 67.5, 50.6, 23.4, 22.1, 21.8. LRMS (CI) m/z calcd. for $C_{19}H_{18}ClN_2O_3S$ $[M+H]^{+\cdot}$: 389.0 found: 389.1.

(±) Ethyl 7-chloro-4-(furan-3-yl)-2-methyl-4*H*-benzo[4,5]thiazolo[3,2-*a*]pyrimidine-3-carboxylate (235). Purified by column chromatography (Hex–AcOEt 3:1 – 1:1). Yield: 35%. Mp: 170 – 172 ºC. ^{1}H NMR (300 MHz, $CDCl_3$), δ (ppm): 7.41 – 7.35 (m, 2H, ArH), 7.28 (dd, *J* = 3.3, 1.4 Hz, 1H, ArH), 7.18 (dd, *J* = 1.9, 0.8 Hz, 1H, ArH), 7.16 – 7.12 (m, 1H, ArH), 6.39 (s, 1H, CH), 6.30 (dd, *J* = 1.9, 1.0 Hz, 1H, ArH), 4.40 – 4.05 (m, 2H, OC*H*$_2$CH$_3$), 2.44 (s, 3H, CH_3), 1.34 (t, *J* = 7.1, 0.8 Hz, 3H, OCH_2CH_3). ^{13}C NMR (75 MHz, CDCl3), δ (ppm): 166.2, 162.5, 155.2, 143.7, 139.6, 138.9, 132.9, 124.8, 124.2, 123.0, 122.2, 111.6, 108.8, 102.4, 60.3, 49.3, 23.4, 14.4. LRMS (CI) m/z calcd. for $C_{18}H_{16}ClN_2O_3S$ $[M+H]^{+\cdot}$: 375.0 found: 375.1.

(±) Isopropyl 7-chloro-4-(furan-3-yl)-2-methyl-4*H*-benzo[4,5]thiazolo[3,2-*a*]pyrimidine-3-carboxylate (236). Purified by column chromatography (Hex–AcOEt 3:1 – 1:1). Yield: 19%. Mp: 140 – 142 ºC. ^{1}H NMR (300 MHz, $CDCl_3$), δ (ppm): 7.38 (dd, *J* = 2.8, 1.4 Hz, 1H, ArH), 7.35 (s, 1H, ArH), 7.30 – 7.26 (m, 1H, ArH), 7.16 (d, *J* = 1.9 Hz, 1H, ArH), 7.14 – 7.10 (m, 1H, ArH), 6.36 (s, 1H, CH), 6.30 (d, *J* = 2.0 Hz, 1H, ArH), 5.22 – 5.01 (m, 1H, OC*H*$(CH_3)_2$), 2.43 (s, 3H, CH_3), 1.32 (d, *J* = 6.5 Hz, 3H, $OCH(CH_3)_2$), 1.29 (d, *J* = 6.1 Hz, 3H, $OCH(CH_3)_2$). LRMS (CI) m/z calcd. for $C_{19}H_{18}ClN_2O_3S$ $[M+H]^{+\cdot}$: 389.1 found: 390.0.

(±) Ethyl 7-chloro-2-methyl-4-(thiophen-2-yl)-4*H*-benzo[4,5]thiazolo[3,2-*a*]pyrimidine-3-carboxylate (237). Purified by column chromatography (Hex–AcOEt 3:1 – 1:1). Yield: 17%. Mp: 156 – 158 ºC. ^{1}H NMR (300 MHz, $CDCl_3$), δ (ppm): 7.37 (d, *J* = 8.4 Hz, 1H, ArH), 7.24 (d, *J* = 8.1 Hz, 1H, ArH), 7.15 (dd, *J* = 8.6, 2.9 Hz, 2H, ArH), 6.97 (d, *J* = 3.7 Hz, 1H, ArH), 6.92 – 6.80 (m, 1H, ArH), 6.63 (d, *J* = 6.6 Hz, 1H, CH), 4.29 – 4.14 (m, 2H, OC*H*$_2$CH$_3$), 2.46 (s, 3H, CH_3), 1.31 (t, *J* = 7.1 Hz, 3H, OCH_2CH_3). LRMS (CI) m/z calcd. for $C_{18}H_{16}ClN_2O_2S_2$ $[M+H]^{+\cdot}$: 391.0 found: 391.1.

(±) Isopropyl 7-chloro-2-methyl-4-(thiophen-2-yl)-4*H*-benzo[4,5]thiazolo[3,2-*a*]pyrimidine-3-carboxylate (238). Purified by column chromatography (Hex–AcOEt 3:1 – 1:1). Yield: 32%. Mp: 163 – 165 ºC. ^{1}H NMR (300 MHz, $CDCl_3$), δ (ppm): 7.36 (d, *J* = 8.3 Hz, 1H, ArH), 7.22 (s, 1H, ArH), 7.20 – 7.10 (m, 2H, ArH), 6.96 (s, 1H, ArH), 6.90 – 6.81 (m, 1H, ArH), 6.62 (s, 1H, CH), 5.15 – 5.02 (m, 1H, OC*H*$(CH_3)_2$), 2.45 (s, 3H, CH_3), 1.31 (d, *J* = 6.2 Hz, 3H, $OCH(CH_3)_2$), 1.24 (d, *J* = 6.2 Hz, 3H, $OCH(CH_3)_2$). LRMS (CI) m/z calcd. for $C_{19}H_{18}ClN_2O_2S_2$ $[M+H]^{+\cdot}$: 405.0 found: 405.0.

(±) Ethyl 7-chloro-2-methyl-4-(thiophen-3-yl)-4*H*-benzo[4,5]thiazolo[3,2-*a*]pyrimidine-3-carboxylate (239). Purified by column chromatography (Hex–AcOEt 3:1 – 1:1). Yield: 33%. Mp: 180 – 182 ºC. ^{1}H NMR (300 MHz, $CDCl_3$), δ (ppm): 7.38 (dd, *J* = 8.0, 0.7 Hz, 1H, ArH), 7.25 – 7.20 (m, 2H, ArH), 7.17 (d, *J* = 1.9 Hz, 1H, ArH), 7.13 (d, *J* = 1.6 Hz, 1H, ArH), 7.05 (dd, *J* = 4.8, 1.6 Hz, 1H, ArH), 6.50 (s, 1H, CH), 4.40 – 4.06 (m, 2H, OC*H*$_2$CH$_3$), 2.45 (s, 3H, CH_3), 1.34 (t, *J* = 7.1 Hz, 3H, OCH_2CH_3). LRMS (CI) m/z calcd. for $C_{18}H_{16}ClN_2O_2S_2$ $[M+H]^{+\cdot}$: 390.0 found: 390.1.

(±) Isopropyl 7-chloro-2-methyl-4-(thiophen-3-yl)-4*H*-benzo[4,5]thiazolo[3,2-*a*]pyrimidine-3-carboxylate (240). Purified by column chromatography (Hex–AcOEt 3:1 – 1:1). Yield: 37%. Mp: 170 – 172 ºC. ^{1}H NMR (300 MHz, $CDCl_3$), δ (ppm): 7.40 – 7.34 (m, 1H, ArH), 7.25 – 7.20 (m, 2H, ArH), 7.15 (d, *J* = 9.6 Hz, 2H, ArH), 7.05 (dd, *J* = 4.8, 1.7 Hz, 1H, ArH), 6.47 (s, 1H, CH), 5.19 – 5.05 (m, 1H, OC*H*$(CH_3)_2$), 2.45 (s, 3H, CH_3), 1.33 (d, *J* = 6.3 Hz, 3H, $OCH(CH_3)_2$), 1.27 (d, *J* = 6.2 Hz, 3H, $OCH(CH_3)_2$). LRMS (CI) m/z calcd. for $C_{19}H_{18}ClN_2O_2S_2$ $[M+H]^{+\cdot}$: 405.1 found: 405.0.

(±) Ethyl 8-chloro-4-(furan-2-yl)-2-methyl-4*H*-benzo[4,5]thiazolo[3,2-*a*]pyrimidine-3-carboxylate (241). Purified by column chromatography (Hex–AcOEt 3:1 – 1:1). Yield: 22%. Mp: 143 – 145 ºC. ^{1}H NMR (300 MHz, $CDCl_3$), δ (ppm): 7.43 (s, 1H, ArH), 7.30 (s, 2H, Ar-H), 7.28 – 7.22 (m, 1H, Ar-H), 6.46 (s, 1H, ArH), 6.32 – 6.19 (m, 2H, ArH + CH), 4.18 (q, *J* = 6.9 Hz, 2H, OC*H*$_2$CH$_3$), 2.49 (s, 3H, CH_3), 1.25 (t, *J* = 7.1 Hz, 3H, OCH_2CH_3). LRMS (CI) m/z calcd. for $C_{18}H_{16}ClN_2O_3S$ $[M+H]^{+\cdot}$: 375.0 found: 375.1.

(±) Isopropyl 8-chloro-4-(furan-2-yl)-2-methyl-4*H*-benzo[4,5]thiazolo[3,2-*a*]pyrimidine-3-carboxylate (242). Purified by column chromatography (Hex–AcOEt 3:1 – 1:1). Yield: 29%. Oil at RT. ^{1}H NMR (300 MHz, $CDCl_3$), δ (ppm): 7.46 (t, *J* = 1.3 Hz, 1H, ArH), 7.33 (d, *J* = 1.2 Hz, 2H, ArH), 7.28 (d, *J* = 1.5 Hz, 1H, ArH), 6.47 (s, 1H, ArH), 6.37 – 6.15 (m, 2H, ArH + CH), 5.08 (p, *J* = 6.2 Hz, 1H, OC*H*$(CH_3)_2$), 2.51 (s, 3H, CH_3), 1.30 (d, *J* = 6.3 Hz, 3H, $OCH(CH_3)_2$), 1.18 (d, *J* = 6.2 Hz, 3H, $OCH(CH_3)_2$). LRMS (CI) m/z calcd. for $C_{19}H_{18}ClN_2O_3S$ $[M+H]^{+\cdot}$: 381.1 found: 389.1.

(±) Ethyl 8-chloro-4-(furan-3-yl)-2-methyl-4*H*-benzo[4,5]thiazolo[3,2-*a*]pyrimidine-3-carboxylate (243). Purified by column chromatography (Hex–AcOEt 3:1 – 1:1). Yield: 37%. Mp: 131 – 133 ºC. ^{1}H NMR (300 MHz, $CDCl_3$), δ (ppm): 7.48 (d, *J* = 2.0 Hz, 1H, ArH), 7.38 (t, *J* = 1.2 Hz, 1H, ArH), 7.33 – 7.25 (m, 2H, ArH), 7.09 (d, *J* = 8.7 Hz, 1H, ArH), 6.43 (s, 1H, CH), 6.28 (d, *J* = 1.9, 0.9 Hz, 1H, ArH), 4.31 – 4.15 (m, 2H, OC*H*$_2$CH$_3$), 2.46 (s, 3H), 1.34 (t, *J* = 7.1 Hz, 3H). LRMS (CI) m/z calcd. for $C_{18}H_{16}ClN_2O_3S$ $[M+H]^{+\cdot}$: 375.0 found: 375.1.

(±) Isopropyl 8-chloro-4-(furan-3-yl)-2-methyl-4*H*-benzo[4,5]thiazolo[3,2-*a*]pyrimidine-3-carboxylate (244). Purified by column chromatography (Hex–AcOEt 3:1 – 1:1). Yield: 34%. Oil at RT. ^{1}H NMR (300 MHz, $CDCl_3$), δ (ppm): 7.44 (d, *J* = 2.0 Hz, 1H, ArH), 7.35 (s, 1H, ArH), 7.29 – 7.23 (m, 2H, ArH), 7.05 (d, *J* = 8.6 Hz, 1H, ArH), 6.38 (s, 1H, CH), 6.27 (d, *J* = 1.7 Hz, 1H, ArH), 5.10 (p, *J* = 6.2 Hz, 1H, OC*H*(CH$_3$)$_2$), 2.42 (s, 3H, CH$_3$), 1.30 (d, *J* = 6.2 Hz, 3H, OCH(C*H*$_3$)$_2$), 1.27 (d, *J* = 6.3 Hz, 3H, OCH(C*H*$_3$)$_2$). LRMS (CI) m/z calcd. for $C_{19}H_{18}ClN_2O_3S$ $[M+H]^{+\cdot}$: 389.1 found: 389.0.

(±) Ethyl 8-chloro-2-methyl-4-(thiophen-2-yl)-4*H*-benzo[4,5]thiazolo[3,2-*a*]pyrimidine-3-carboxylate (245). Purified by column chromatography (Hex–AcOEt 3:1 – 1:1). Yield: 35%. Mp: 139 – 141 ºC. ^{1}H NMR (300 MHz, $CDCl_3$), δ (ppm): 7.46 (s, 1H, ArH), 7.31 – 7.23 (m, 1H, ArH), 7.21 – 7.12 (m, 2H, ArH), 6.95 (d, *J* = 3.5 Hz, 1H, ArH), 6.85 (t, *J* = 5.0, 3.5, 1.3 Hz, 1H, ArH), 6.69 (s, 1H, CH), 4.31 – 4.16 (m, 2H, OC*H*$_2$CH$_3$), 2.47 (s, 3H, CH$_3$), 1.31 (t, *J* = 7.1, 1.2 Hz, 3H, OCH$_2$C*H*$_3$). LRMS (CI) m/z calcd. for $C_{18}H_{16}ClN_2O_2S_2$ $[M+H]^{+\cdot}$: 391.0 found: 391.0.

(±) Isopropyl 8-chloro-2-methyl-4-(thiophen-2-yl)-4*H*-benzo[4,5]thiazolo[3,2-*a*]pyrimidine-3-carboxylate (246). Purified by column chromatography (Hex–AcOEt 3:1 – 1:1). Yield: 28%. Mp: 105 – 107 ºC. ^{1}H NMR (300 MHz, $CDCl_3$), δ (ppm): 7.47 (s, 1H, ArH), 7.29 (d, *J* = 7.6, 4.8 Hz, 1H, ArH), 7.24 – 7.13 (m, 2H, ArH), 6.98 (d, *J* = 3.7 Hz, 1H, ArH), 6.91 – 6.83 (m, 1H, ArH), 6.69 (s, 1H, CH), 5.21 – 5.04 (m, 1H, OC*H*(CH$_3$)$_2$), 2.49 (s, 3H, CH$_3$), 1.32 (dd, *J* = 6.4, 2.1 Hz, 3H, OCH(C*H*$_3$)$_2$), 1.26 (dd, *J* = 6.3, 1.9 Hz, 3H, OCH(C*H*$_3$)$_2$. LRMS (CI) m/z calcd. for $C_{19}H_{18}ClN_2O_2S_2$ $[M+H]^{+\cdot}$: 405.0 found: 405.0.

(±) Ethyl 8-chloro-2-methyl-4-(thiophen-3-yl)-4*H*-benzo[4,5]thiazolo[3,2-*a*]pyrimidine-3-carboxylate (247). Purified by column chromatography (Hex–AcOEt 3:1 – 1:1). Yield: 27%. Mp: 142 – 145 ºC. ^{1}H NMR (300 MHz, $CDCl_3$), δ (ppm): 7.46 (d, *J* = 2.0 Hz, 1H, ArH), 7.33 – 7.14 (m, 3H, ArH), 7.13 – 6.97 (m, 2H, ArH), 6.54 (s, 1H, CH), 4.38 – 4.11 (m, 2H, OC*H*$_2$CH$_3$), 2.46 (s, 3H, 16), 1.33 (td, *J* = 7.1, 1.6 Hz, 3H, OCH$_2$C*H*$_3$). LRMS (CI) m/z calcd. for $C_{18}H_{16}ClN_2O_2S_2$ $[M+H]^{+\cdot}$: 391.0 found: 391.0.

(±) Isopropyl 8-chloro-2-methyl-4-(thiophen-3-yl)-4*H*-benzo[4,5]thiazolo[3,2-*a*]pyrimidine-3-carboxylate (248). Purified by column chromatography (Hex–AcOEt 3:1 – 1:1). Yield: 31%. Mp: 149 – 151 ºC. ^{1}H NMR (300 MHz, $CDCl_3$), δ (ppm): 7.45 (d, *J* = 2.1 Hz, 1H, ArH), 7.29 – 7.20 (m, 1H, ArH), 7.24 – 7.14 (m, 2H, ArH), 7.11 – 6.97 (m, 2H, ArH), 6.51 (s, 1H, CH), 5.08 (p, *J* = 6.3 Hz, 1H, OC*H*(CH$_3$)$_2$), 2.44 (s, 3H, CH$_3$), 1.30 (d, *J* = 6.3 Hz, 3H, OCH(C*H*$_3$)$_2$), 1.24 (d, *J* = 6.2 Hz, 3H, OCH(C*H*$_3$)$_2$). LRMS (CI) m/z calcd. for $C_{19}H_{18}ClN_2O_2S_2$ $[M+H]^{+\cdot}$: 405.0 found: 405.0.

5.3.5 Chiral HPLC separation of enantiomers and characterization of 226, 228, and 243

The chiral resolution was performed using a Water Breeze™ 2 (binary pump: 1525, detector UV/Visible 2489, 7725i Manual Injector Kit 1500 Series) using a 250 mm x 20 mm Chiralpak® 5µm IE-3 (DAICEL). All the separations were performed at 25 ºC with *Hex*/*i*-propanol mixture in different percentages as mobile phase (*see spectroscopic and analytical data*). The enantiomers **(*R*)-226** (0.5 mg, t_R = 14.37 min), **(*S*)-226** (0.5 mg, t_R = 17.12 min), **(*S*)-228** (0.5 mg, t_R = 16.92 min)], **(*R*)-228** (0.5 mg, t_R = 22.02 min), **(*S*)-243** (0.5 mg, t_R = 16.95 min), and **(*R*)-243** (0.5 mg, t_R = 23.71 min) were isolated, their stereochemical purity analyzed by chiral HPLC (e.e.: >99% for each enantiomer, reports showed below, chromatogram at 254 nM) and then characterized by ^{1}H NMR and circular dichroism (CD).

CD spectra were recorded on a Jasco-815 system equipped with a Peltier-type thermostatic accessory (CDF-426S, Jasco). Measurements were carried out at 20 °C using a 1 mm quartz cell in a volume of 600 μL. Compounds (0.5 mg) were dissolved in MeOH (1.0 mL) and then diluted 10-fold in MeOH. The instrument settings were bandwidth, 1.0 nm; data pitch, 1.0 nm; speed, 500 nm/min; accumulation, 10; wavelengths, 400−190 nm.

SAMPLE INFORMATION			
Sample Name:	226	Acquired By:	Breeze
Sample Type:	Racemate	Sample Set Name	
Vial:	1	Acq. Method:	40%HexiPAISOF10 set
Injection #:	1	Date Acquired:	29/01/2021 9:00:57 CET
Run Time:	60,00 Minutes	Injection Volume:	500,00 ul

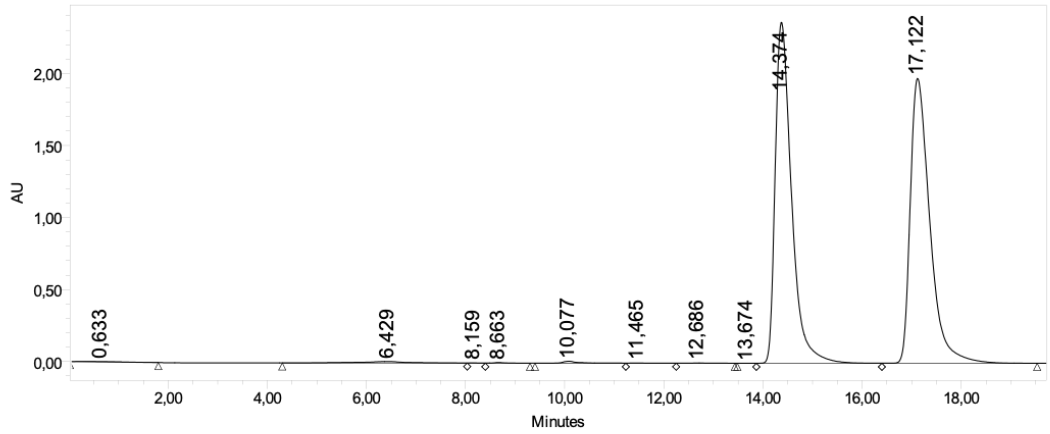

	RT (min)	Area (µV*sec)	% Area	Height (µV)
1	0,633	132563	0,12	2331
2	6,429	725049	0,66	10224
3	8,159	19258	0,02	1408
4	8,663	61148	0,06	3838
5	10,077	296738	0,27	13469
6	11,465	31609	0,03	913
7	12,686	38982	0,04	1204
8	13,674	1516	0,00	111
9	14,374	54112054	49,46	2370399
10	17,122	53988655	49,35	1978419

SAMPLE INFORMATION			
Sample Name:	226	Acquired By:	Breeze
Sample Type:	Enantiomer A	Sample Set Name	
Vial:	1	Acq. Method:	40%HexiPAISOF10 set
Injection #:	60,00	Date Acquired:	29/01/2021 9:23:02 CET
Run Time:	Minutes	Injection Volume:	500,00 ul

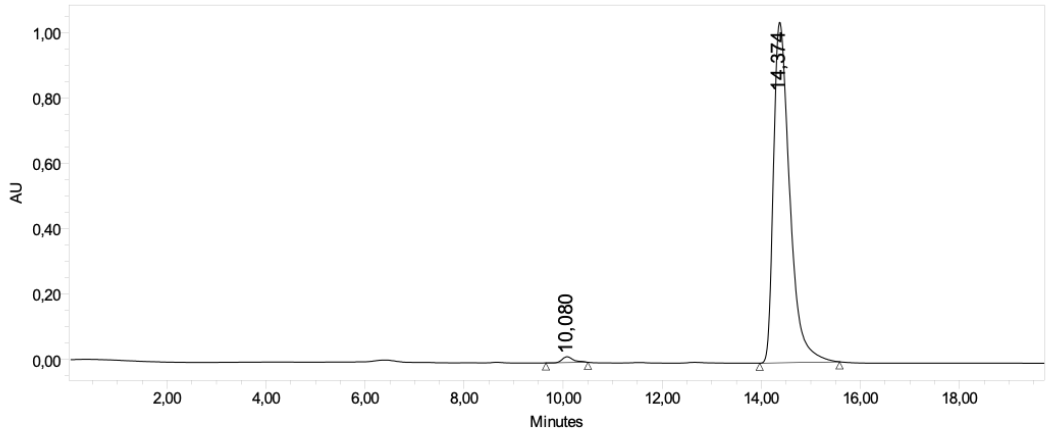

	RT (min)	Area (µV*sec)	% Area	Height (µV)
1	10,080	283385	1,18	17953
2	14,374	23642004	98,82	1042660

SAMPLE INFORMATION			
Sample Name:	226	Acquired By:	Breeze
Sample Type:	Enantiomer B	Sample Set Name	
Vial:	1	Acq. Method:	40%HexiPAISOF10 set
Injection #:	1	Date Acquired:	29/01/2021 10:05:10 CET
Run Time:	60,00 Minutes	Injection Volume:	500,00 ul

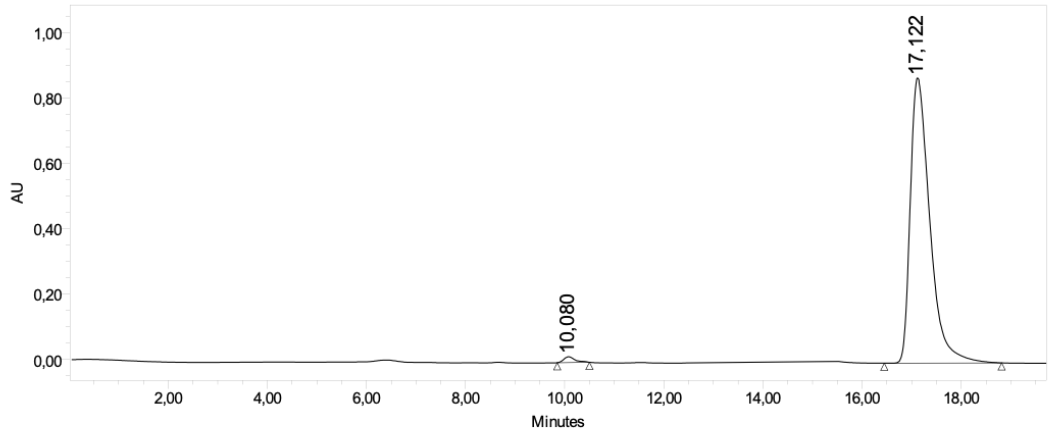

	RT (min)	Area (µV*sec)	% Area	Height (µV)
1	10,080	277591	1,15	17798
2	17,122	23795664	98,85	871744

SAMPLE INFORMATION

Sample Name:	228	Acquired By:	Breeze
Sample Type:	Racemate	Sample Set Name	
Vial:	1	Acq. Method:	30%HexiPAISOF10 set
Injection #:	1	Date Acquired:	20/04/2022 14:00:05 CET
Run Time:	30,00 Minutes	Injection Volume:	250,00 ul

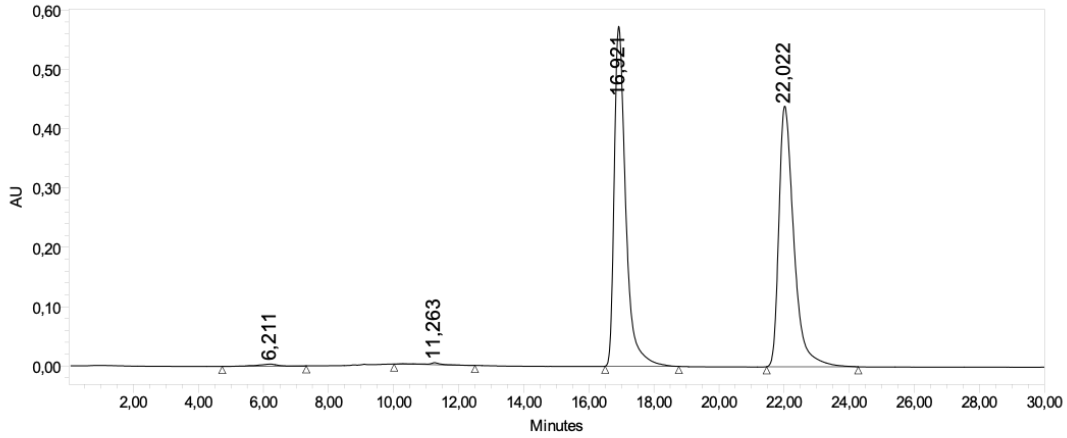

	RT (min)	Area (µV*sec)	% Area	Height (µV)
1	6,211	143297	0,51	3305
2	11,263	119927	0,42	3431
3	16,921	14013156	49,50	573739
4	22,022	14031887	49,57	439702

SAMPLE INFORMATION			
Sample Name:	228	Acquired By:	Breeze
Sample Type:	Enantiomer A	Sample Set Name	
Vial:	1	Acq. Method:	30%HexiPAISOF10 set
Injection #:	1	Date Acquired:	21/04/2022 8:29:42 CET
Run Time:	30,00 Minutes	Injection Volume:	250,00 ul

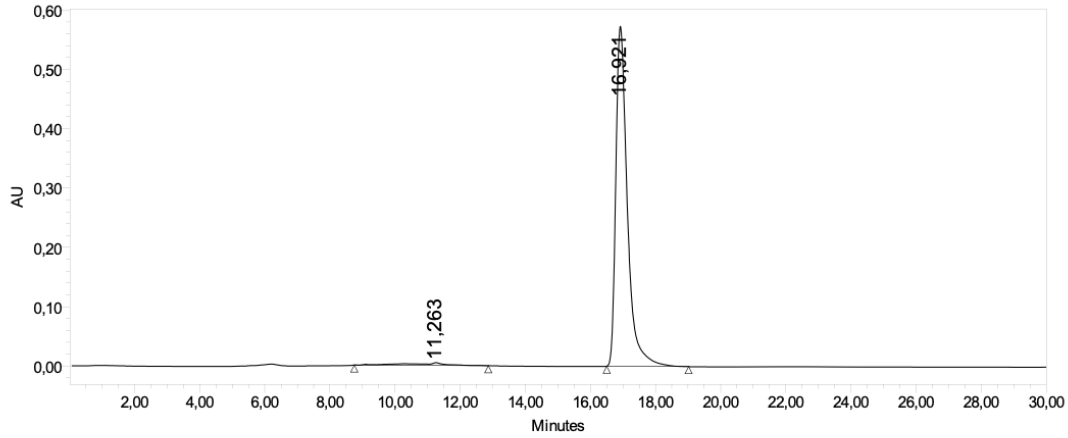

	RT (min)	Area (µV*sec)	% Area	Height (µV)
1	11,263	382109	2,65	4635
2	16,921	14033441	97,35	573790

SAMPLE INFORMATION

Sample Name:	228	Acquired By:	Breeze
Sample Type:	Enantiomer B	Sample Set Name	
Vial:	1	Acq. Method:	30%HexiPAISOF10 set
Injection #:	1	Date Acquired:	21/04/2022 11:22:42 CET
Run Time:	30,00 Minutes	Injection Volume:	250,00 ul

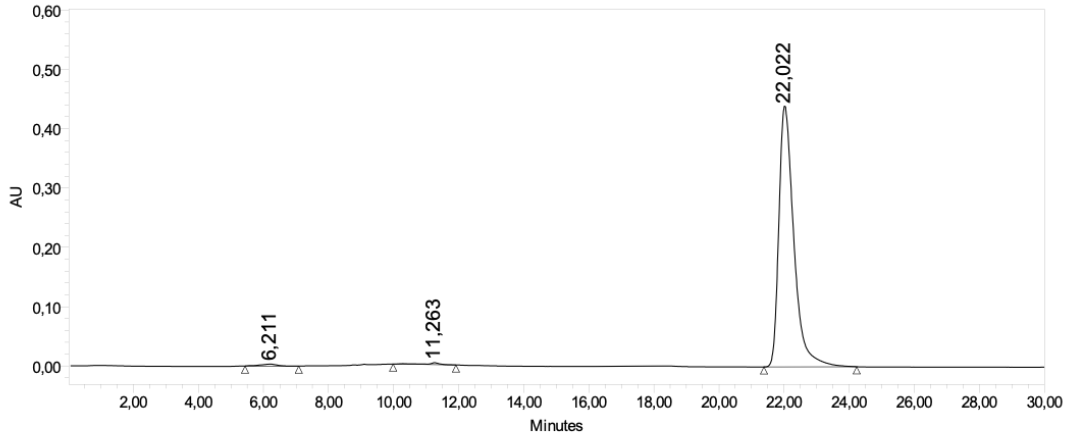

	RT (min)	Area (µV*sec)	% Area	Height (µV)
1	6,211	105773	0,74	2990
2	11,263	102783	0,72	3257
3	22,022	14059764	98,54	440021

SAMPLE INFORMATION			
Sample Name:	243	Acquired By:	Breeze
Sample Type:	Racemate	Sample Set Name	
Vial:	1	Acq. Method:	30%HexiPAISOF10 set
Injection #:	1	Date Acquired:	21/04/2022 8:05:10 CET
Run Time:	30,00 Minutes	Injection Volume:	250,00 ul

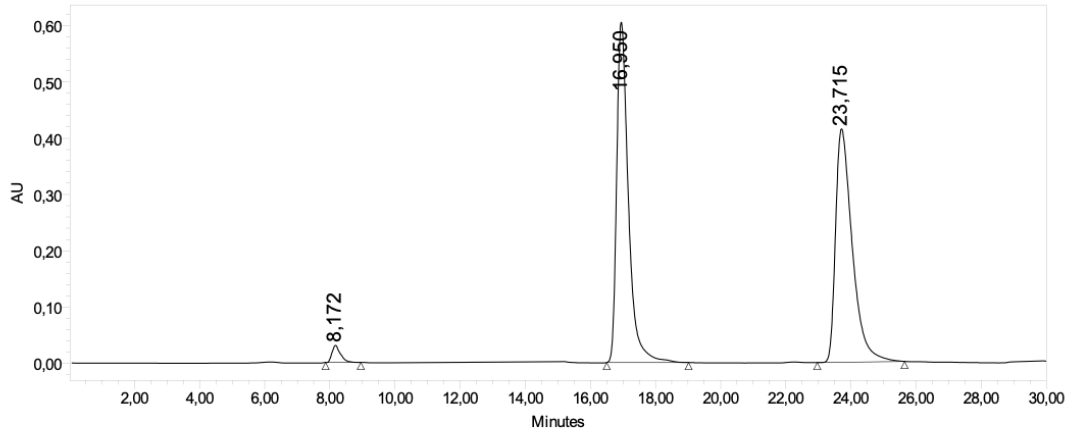

	RT (min)	Area (µV*sec)	% Area	Height (µV)
1	8,172	547834	1,80	30610
2	16,950	15078543	49,58	605657
3	23,715	14785137	48,62	415127

SAMPLE INFORMATION			
Sample Name:	243	Acquired By:	Breeze
Sample Type:	Enantiomer A	Sample Set Name	
Vial:	1	Acq. Method:	30%HexiPAISOF10 set
Injection #:	1	Date Acquired:	20/04/2022 16:05:05 CET
Run Time:	30,00 Minutes	Injection Volume:	250,00 ul

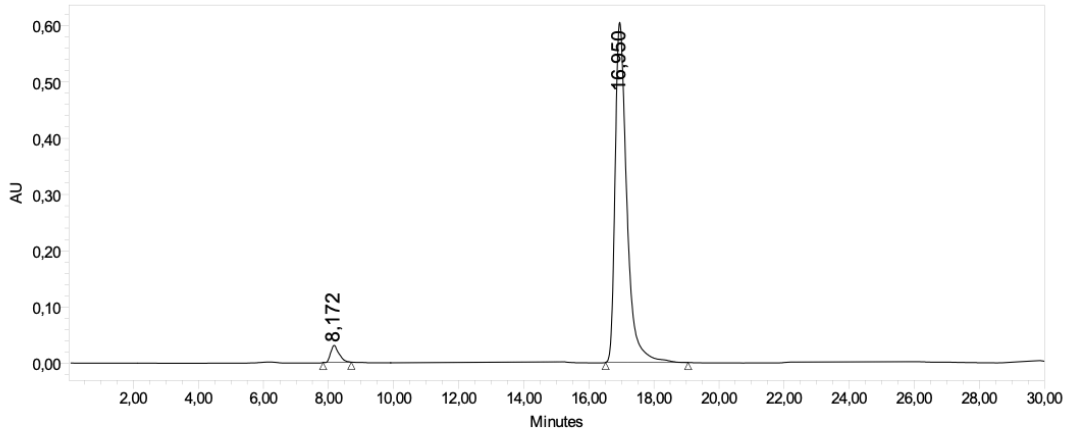

	RT (min)	Area (µV*sec)	% Area	Height (µV)
1	8,172	528568	3,39	30383
2	16,950	15062314	96,61	605442

SAMPLE INFORMATION			
Sample Name:	243	Acquired By:	Breeze
Sample Type:	Enantiomer B	Sample Set Name	
Vial:	1	Acq. Method:	30%HexiPAISOF10 set
Injection #:	1	Date Acquired:	21/04/2022 11:42:21 CET
Run Time:	30,00 Minutes	Injection Volume:	250,00 ul

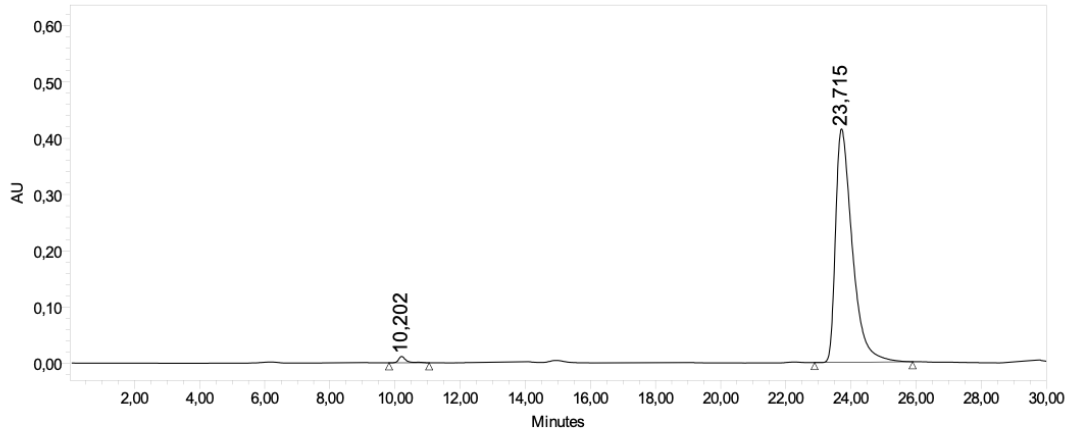

	RT (min)	Area (µV*sec)	% Area	Height (µV)
1	10,202	175950	1,17	11199
2	23,715	14834598	98,83	415276

5.3.5.2 Spectroscopic and analytical data of enantiomers

(±) Isopropyl 4-(furan-2-yl)-2-methyl-4H-benzo[4,5]thiazolo[3,2-a]pyrimidine-3-carboxylate (226). Purified by column chromatography (Hex–AcOEt 3:1 – 1:1). Yield: 15%. Mp: 122 – 124 ºC. ^{1}H NMR (300 MHz, $CDCl_3$), δ (ppm): 7.46 – 7.29 (m, 3H, ArH), 7.26 – 7.12 (m, 2H, ArH), 6.48 (s, 1H, CH), 6.30 – 6.16 (m, 2H, ArH), 5.12 – 4.96 (m, 1H, OC*H*(CH_3)$_2$), 2.48 (s, 3H, CH_3), 1.27 (d, *J* = 6.2 Hz, 3H, OCH(C*H*$_3$)$_2$), 1.15 (d, *J* = 6.2 Hz, 3H, OCH(C*H*$_3$)$_2$). ^{13}C NMR (75 MHz, $CDCl_3$), δ (ppm): 165.8, 162.7, 155.8, 153.5, 142.2, 138.0, 126.5, 124.0, 123.7, 122.1, 111.7, 110.4, 108.6, 99.9, 67.3, 50.5, 23.4, 22.1, 21.9. HRMS (EI) m/z calcd. for $C_{19}H_{18}N_2O_3S$ $[M]^{+\cdot}$: 354.1038 found: 354.1035.

Isopropyl (*R*)-4-(furan-2-yl)-2-methyl-4H-benzo[4,5]thiazolo[3,2-a]pyrimidine-3-carboxylate [(*R*)-226]. Chiral separation with a 250 mm x 20 mm Chiralpak® 5µm IE-3 (DAICEL) (isocratic mobile phase Hex–IPA 6:4) to give an enantiomeric excess of >99%. ^{1}H NMR (300 MHz, $CDCl_3$), δ (ppm): 7.46 – 7.29 (m, 3H, ArH), 7.26 – 7.10 (m, 2H, ArH), 6.48 (s, 1H, CH), 6.32 – 6.16 (m, 2H, ArH), 5.12 – 4.97 (m, 1H, OC*H*(CH_3)$_2$), 2.48 (s, 3H, CH_3), 1.27 (d, *J* = 6.2 Hz, 3H, OCH(C*H*$_3$)$_2$), 1.15 (d, *J* = 6.2 Hz, 3H, OCH(C*H*$_3$)$_2$). HRMS (APCI) m/z calcd. for $C_{19}H_{19}N_2O_3S$ $[M+H]^{+\cdot}$: 355.1038 found: 355.1026.

Isopropyl (*S*)-4-(furan-2-yl)-2-methyl-4H-benzo[4,5]thiazolo[3,2-a]pyrimidine-3-carboxylate [(*S*)-226]. Chiral separation with a 250 mm x 20 mm Chiralpak® 5µm IE-3 (DAICEL) (isocratic mobile phase Hex–IPA 6:4) to give an enantiomeric excess of >99%. ^{1}H NMR (300 MHz, $CDCl_3$), δ (ppm): 7.46 – 7.29 (m, 3H, ArH), 7.27 – 7.10 (m, 2H, ArH), 6.48 (s, 1H, CH), 6.32 – 6.16 (m, 2H, ArH), 5.10 – 4.96 (m, 1H, OC*H*(CH_3)$_2$), 2.48 (s, 3H, CH_3), 1.27 (d, *J* = 6.2 Hz, 3H, OCH(C*H*$_3$)$_2$), 1.15 (d, *J* = 6.2 Hz, 3H, OCH(C*H*$_3$)$_2$). HRMS (APCI) m/z calcd. for $C_{19}H_{19}N_2O_3S$ $[M+H]^{+\cdot}$: 355.1038 found: 355.1024.

(±) Isopropyl 4-(furan-3-yl)-2-methyl-4H-benzo[4,5]thiazolo[3,2-a]pyrimidine-3-carboxylate (228). Purified by column chromatography (Hex–AcOEt 3:1 – 1:1). Yield: 20%. Mp: 113 – 115 ºC. ^{1}H NMR (300 MHz, $CDCl_3$), δ (ppm): 7.46 (d, *J* = 7.7 Hz, 1H, ArH), 7.37 – 7.11 (m, 5H, ArH), 6.43 (s, 1H, CH), 6.27 (s, 1H, ArH), 5.17 – 5.00 (m, 1H, OC*H*$(CH_3)_2$), 2.42 (s, 3H, CH_3), 1.30 (d, *J* = 6.3 Hz, 3H, OCH(C*H*$_3)_2$), 1.27 (d, *J* = 6.3 Hz, 3H, OCH(C*H*$_3)_2$). ^{13}C NMR (75 MHz, $CDCl_3$), δ (ppm): 165.9, 163.1, 154.8, 143.4, 139.5, 137.7, 126.7, 125.2, 124.1, 123.9, 122.3, 111.3, 108.9, 102.1, 67.6, 49.1, 23.3, 22.1, 22.0. HRMS (EI) m/z calcd. for $C_{19}H_{18}N_2O_3S$ $[M]^{+\cdot}$: 354.1038 found: 354.1049.

Isopropyl (*S*)-4-(furan-3-yl)-2-methyl-4H-benzo[4,5]thiazolo[3,2-a]pyrimidine-3-carboxylate [(*S*)-228]. Chiral separation with a 250 mm x 20 mm Chiralpak® 5µm IE-3 (DAICEL) (isocratic mobile phase Hex–IPA 7:3) to give an enantiomeric excess of >99%. ^{1}H NMR (300 MHz, $CDCl_3$), δ (ppm): 7.46 (d, *J* = 7.7 Hz, 1H, ArH), 7.39 – 7.10 (m, 5H, ArH), 6.43 (s, 1H, CH), 6.27 (s, 1H, ArH), 5.17 – 5.00 (m, 1H, OC*H*$(CH_3)_2$), 2.42 (s, 3H, CH_3), 1.30 (d, *J* = 6.3 Hz, 3H, OCH(C*H*$_3)_2$), 1.27 (d, *J* = 6.3 Hz, 3H, OCH(C*H*$_3)_2$). HRMS (APCI) m/z calcd. for $C_{19}H_{19}N_2O_3S$ $[M+H]^{+\cdot}$: 355.1038 found: 355.1039.

Isopropyl (*R*)-4-(furan-3-yl)-2-methyl-4H-benzo[4,5]thiazolo[3,2-a]pyrimidine-3-carboxylate [(*R*)-228]. Chiral separation with a 250 mm x 20 mm Chiralpak® 5µm IE-3 (DAICEL) (isocratic mobile phase Hex–IPA 7:3) to give an enantiomeric excess of >99%. ^{1}H NMR (300 MHz, $CDCl_3$), δ (ppm): 7.46 (d, *J* = 7.7 Hz, 1H, ArH), 7.39 – 7.10 (m, 5H, ArH), 6.43 (s, 1H, CH), 6.27 (s, 1H, ArH), 5.17 – 5.00 (m, 1H, OC*H*$(CH_3)_2$), 2.42 (s, 3H, CH_3), 1.30 (d, *J* = 6.3 Hz, 3H, OCH(C*H*$_3)_2$), 1.27 (d, *J* = 6.3 Hz, 3H, OCH(C*H*$_3)_2$). HRMS (APCI) m/z calcd. for $C_{19}H_{19}N_2O_3S$ $[M+H]^{+\cdot}$: 355.1038 found: 355.1038.

(±) Ethyl 8-chloro-4-(furan-3-yl)-2-methyl-4*H*-benzo[4,5]thiazolo[3,2-*a*]pyrimidine-3-carboxylate (243). Purified by column chromatography (Hex–AcOEt 3:1 – 1:1). Yield: 37%. Mp: 131 – 133 ºC. ^{1}H NMR (300 MHz, $CDCl_3$), δ (ppm): 7.48 (d, *J* = 2.0 Hz, 1H, ArH), 7.38 (t, *J* = 1.2 Hz, 1H, ArH), 7.33 – 7.25 (m, 2H, ArH), 7.09 (d, *J* = 8.7 Hz, 1H, ArH), 6.43 (s, 1H, CH), 6.28 (d, *J* = 1.9, 0.9 Hz, 1H, ArH), 4.31 – 4.15 (m, 2H, OC*H*$_2$CH$_3$), 2.46 (s, 3H), 1.34 (t, *J* = 7.1 Hz, 3H). LRMS (CI) m/z calcd. for $C_{18}H_{16}ClN_2O_3S$ $[M+H]^{+\cdot}$: 375.0 found: 375.1.

Ethyl (*S*)-*8*-chloro-4-(furan-3-yl)-2-methyl-4*H*-benzo[4,5]thiazolo[3,2-*a*]pyrimidine-3-carboxylate [(*S*)-243]. Chiral separation with a 250 mm x 20 mm Chiralpak® 5µm IE-3 (DAICEL) (isocratic mobile phase Hex–IPA 7:3) to give an enantiomeric excess of >99%. ^{1}H NMR (300 MHz, $CDCl_3$), δ (ppm): 7.48 (d, *J* = 2.0 Hz, 1H, ArH), 7.38 (t, *J* = 1.2 Hz, 1H, ArH), 7.33 – 7.25 (m, 2H, ArH), 7.09 (d, *J* = 8.7 Hz, 1H, ArH), 6.43 (s, 1H, CH), 6.28 (d, *J* = 1.9, 0.9 Hz, 1H, ArH), 4.31 – 4.15 (m, 2H, OC*H*$_2$CH$_3$), 2.46 (s, 3H), 1.34 (t, *J* = 7.1 Hz, 3H). LRMS (CI) m/z calcd. for $C_{18}H_{16}ClN_2O_3S$ $[M+H]^{+\cdot}$: 375.0 found: 375.1.

Ethyl (*R*)-*8*-chloro-4-(furan-3-yl)-2-methyl-4*H*-benzo[4,5]thiazolo[3,2-*a*]pyrimidine-3-carboxylate [(*R*)-243]. Chiral separation with a 250 mm x 20 mm Chiralpak® 5µm IE-3 (DAICEL) (isocratic mobile phase Hex–IPA 7:3) to give an enantiomeric excess of >99%. ^{1}H NMR (300 MHz, $CDCl_3$), δ (ppm): 7.48 (d, *J* = 2.0 Hz, 1H, ArH), 7.38 (t, *J* = 1.2 Hz, 1H, ArH), 7.33 – 7.25 (m, 2H, ArH), 7.09 (d, *J* = 8.7 Hz, 1H, ArH), 6.43 (s, 1H, CH), 6.28 (d, *J* = 1.9, 0.9 Hz, 1H, ArH), 4.31 – 4.15 (m, 2H, OC*H*$_2$CH$_3$), 2.46 (s, 3H), 1.34 (t, *J* = 7.1 Hz, 3H). LRMS (CI) m/z calcd. for $C_{18}H_{16}ClN_2O_3S$ $[M+H]^{+\cdot}$: 375.0 found: 375.1.

5.4 *N*-SUBSTITUTION OF A_{2B}AR ANTAGONISTS WITH PYRIMIDINONE CHEMOTYPE

5.4.1 Synthesis of mono-, bi-, and tricyclic Biginelli derivatives for alkylation (D1-D4)

METHOD J. General procedure for the synthesis of 2-oxo-1,2,3,4-tetrahydropyrimidines (**D1-14**)

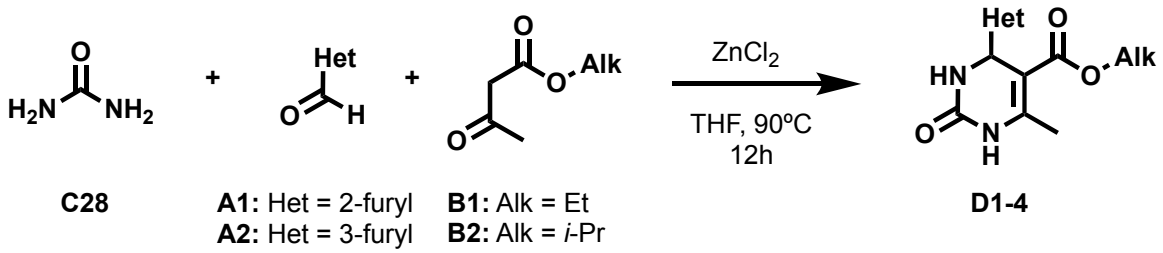

C28 **A1:** Het = 2-furyl **A2:** Het = 3-furyl **B1:** Alk = Et **B2:** Alk = *i*-Pr **D1-4**

A mixture of urea (**C28**, 1 equiv.), pentagonal carbaldehyde (**A1-2**, 1.5 equiv.), alkyl acetoacetate (**B1-2**, 1.5 equiv.) and $ZnCl_2$ (0.1 equiv.) in THF was stirred at 90 ºC for 12 hours. After completion of the reaction, as indicated by TLC (revealing green with *p*-anisaldehyde), the solvent was removed in vacuum and the obtained oily residue was purified with flash chromatography at using DCM:MeOH mixtures as mobile phase.

METHOD K. General procedure for the synthesis of 1,4-dihydrobenzo[4,5]imidazo[1,2-*a*]pyrimidines (**D5-8**)

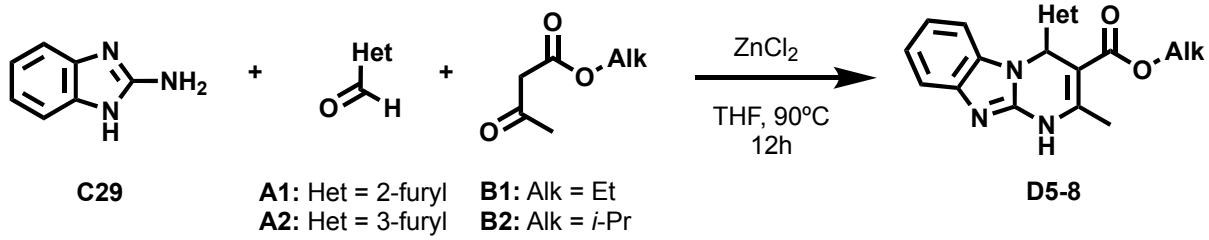

C29 **A1:** Het = 2-furyl **A2:** Het = 3-furyl **B1:** Alk = Et **B2:** Alk = *i*-Pr **D5-8**

A mixture of 1*H*-benzo[*d*]imidazol-2-amine (**C29**, 1.5 equiv.), pentagonal carbaldehyde (**A1-2**, 1 equiv.), alkyl acetoacetate (**B1-2**, 1 equiv.) and $ZnCl_2$ (0.1 equiv.) in THF was stirred at 90 ºC for 12 hours. After completion of the reaction, as indicated by TLC (revealing green with *p*-anisaldehyde), the solvent was removed in vacuum and the obtained oily residue was purified with flash chromatography at using DCM:MeOH mixtures as mobile phase.

5.4.2 Synthesis of alkylated and benzylated derivatives (249-310)

METHOD L. General procedure for the synthesis of N^1-alkyl and N^1-benzyl 2-oxo-1,2,3,4-tetrahydropyrimidines (Series **XXVI**)

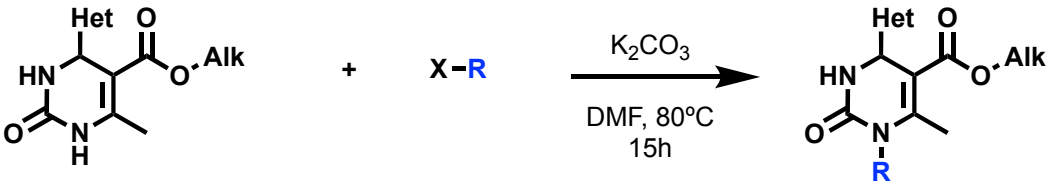

D1: Het = 2-furyl, Alk = Et
D2: Het = 2-furyl, Alk = *i*-Pr
D3: Het = 3-furyl, Alk = Et
D4: Het = 3-furyl, Alk = *i*-Pr

E1: R = *n*-Pr
E2: R = Bn
E3: R = 2-F-Bn

Series XXVI (249-260)

A mixture of the appropriate 2-oxo-1,2,3,4-tetrahydropyrimidine (**D1-4**, 1 equiv.), alkyl or benzyl halide (**E1-3**, 3 equiv.), and potassium carbonate (4 equiv.) in DMF was stirred at 80 ºC for 15 hours. After completion of the reaction, as indicated by TLC (revealing green with *p*-anisaldehyde), the solvent was removed in vacuum and the obtained oily residue was purified with flash chromatography at using DCM:AcOEt mixtures as mobile phase.

METHOD M. General procedure for the synthesis of N^1-alkyl, N^1-benzyl, N^{10}-alkyl, and N^{10}-benzyl 1,4-dihydrobenzo[4,5]imidazo[1,2-*a*]pyrimidines (Series **XXVII-XXVIII**)

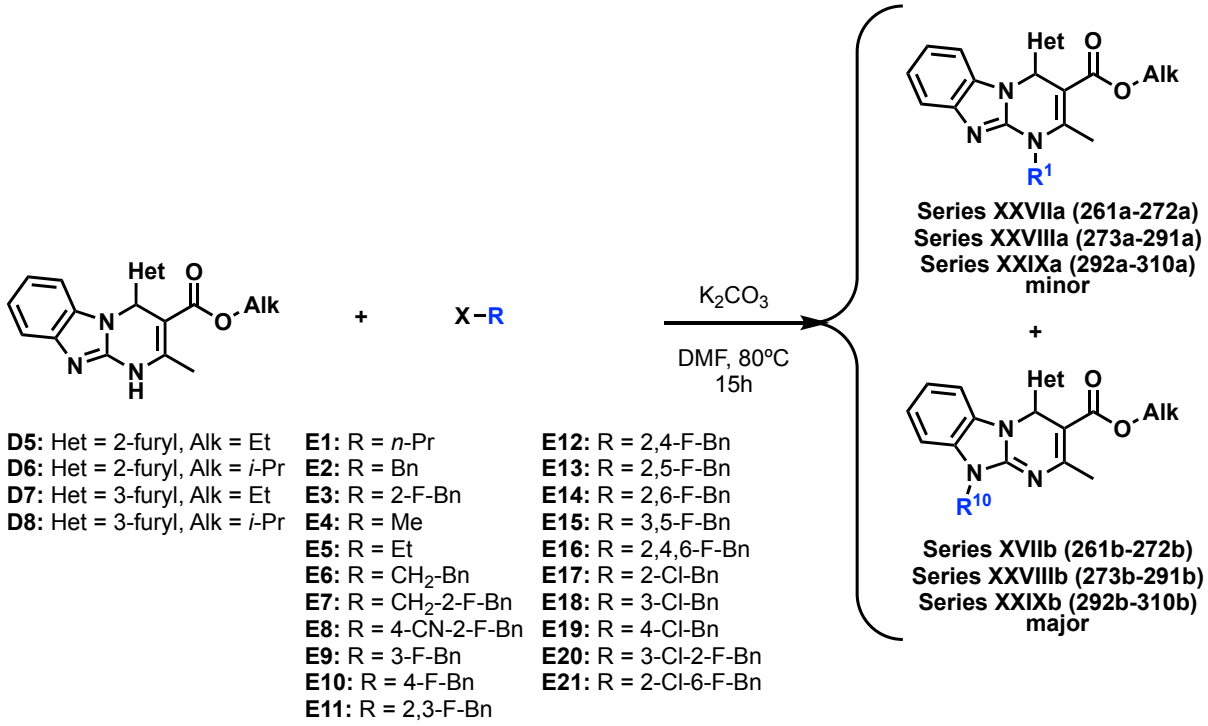

D5: Het = 2-furyl, Alk = Et
D6: Het = 2-furyl, Alk = *i*-Pr
D7: Het = 3-furyl, Alk = Et
D8: Het = 3-furyl, Alk = *i*-Pr

E1: R = *n*-Pr
E2: R = Bn
E3: R = 2-F-Bn
E4: R = Me
E5: R = Et
E6: R = CH_2-Bn
E7: R = CH_2-2-F-Bn
E8: R = 4-CN-2-F-Bn
E9: R = 3-F-Bn
E10: R = 4-F-Bn
E11: R = 2,3-F-Bn

E12: R = 2,4-F-Bn
E13: R = 2,5-F-Bn
E14: R = 2,6-F-Bn
E15: R = 3,5-F-Bn
E16: R = 2,4,6-F-Bn
E17: R = 2-Cl-Bn
E18: R = 3-Cl-Bn
E19: R = 4-Cl-Bn
E20: R = 3-Cl-2-F-Bn
E21: R = 2-Cl-6-F-Bn

A mixture of the appropriate 1,4-dihydrobenzo[4,5]imidazo[1,2-*a*]pyrimidine (**D5-D8**, 1 equiv.), alkyl or benzyl halide (**E1-21**, 3 equiv.), and potassium carbonate (4 equiv.) in DMF was stirred at 80 ºC for 15 hours. After completion of the reaction, as indicated by TLC (revealing green with *p*-anisaldehyde), the solvent was removed in vacuum and the obtained oily residue was purified with flash chromatography at using DCM:AcOEt mixtures as mobile phase.

5.4.3 Spectroscopic and analytical data for all compounds described

(±) Ethyl 4-(furan-2-yl)-6-methyl-2-oxo-1,2,3,4-tetrahydropyrimidine-5-carboxylate (D1).[140] Purified by column chromatography (DCM–MeOH 99:1 – 97:3). Yield: 80%. Mp: 210 – 212 ºC (ethanol). ^{1}H NMR (300 MHz, DMSO-d_6), δ (ppm): 9.25 (s, 1H, NH), 7.74 (d, J = 3.1 Hz, 1H, Ar-H), 7.54 (d, J = 1.6 Hz, 1H, Ar-H), 6.34 (dd, J = 3.1, 1.9 Hz, 1H, Ar-H), 6.08 (d, J = 3.1 Hz, 1H, NH), 5.19 (d, J = 3.3 Hz, 1H, CH), 4.02 (q, J = 7.1 Hz, 2H, OCH_2CH$_3$), 2.22 (s, 3H, CH$_3$), 1.12 (t, J = 7.1 Hz, 3H, OCH$_2$CH_3). ^{13}C NMR (75 MHz, DMSO-d_6), δ (ppm): 165.2, 156.0, 152.7, 149.5, 142.3, 110.5, 105.5, 96.9, 59.4, 47.8, 17.9, 14.3. Elem. Anal. calculated for $C_{12}H_{14}N_2O_4$, C, 57.59; H, 5.64; N, 11.19; found C, 57.63; H, 5.70; N, 11.22.

(±) Ethyl 4-(furan-2-yl)-6-methyl-2-oxo-1-propyl-1,2,3,4-tetrahydropyrimidine-5-carboxylate (249). Purified by column chromatography (DCM–AcOEt 99:1 – 98:2). Yield: 49%. Mp: 223 – 225 ºC. ^{1}H NMR (300 MHz, $CDCl_3$), δ (ppm): 7.32 – 7.23 (m, 1H, Ar-H), 6.25 (dd, J = 3.3, 1.8 Hz, 1H, Ar-H), 6.11 – 6.03 (m, 1H, Ar-H), 5.72 – 5.62 (m, 1H, NH), 5.41 (d, J = 3.2 Hz, 1H, CH), 4.15 (qd, J = 7.1, 1.1 Hz, 2H, OCH_2CH$_3$), 3.92 (ddd, J = 14.3, 9.3, 6.2 Hz, 1H, CH_2CH$_2$CH$_3$), 3.50 (ddd, J = 14.6, 9.2, 5.6 Hz, 1H, CH_2CH$_2$CH$_3$), 2.53 (s, 3H, CH$_3$), 1.72 – 1.40 (m, 2H, CH$_2$CH_2CH$_3$), 1.29 – 1.16 (m, 3H, OCH$_2$CH_3), 0.89 (t, J = 7.4 Hz, 3H, CH$_2$CH$_2$CH_3). LRMS (CI) m/z calcd. for $C_{15}H_{21}N_2O_4$ $[M+H]^+$: 293.1 found: 293.0.

(±) Ethyl 1-benzyl-4-(furan-2-yl)-6-methyl-2-oxo-1,2,3,4-tetrahydropyrimidine-5-carboxylate (250). Purified by column chromatography (DCM–AcOEt 99:1 – 98:2). Yield: 48%. Mp: 240 – 242 ºC. ^{1}H NMR (300 MHz, $CDCl_3$), δ (ppm): 7.38 – 7.15 (m, 6H, Ar-H), 6.30 (dd, J = 3.1, 1.8 Hz, 1H, Ar-H), 6.11 (d, J = 3.2 Hz, 1H, NH), 5.70 (d, J = 1.8 Hz, 1H, Ar-H), 5.51 (d, J = 3.0 Hz, 1H, CH), 5.32 (d, J = 16.8 Hz, 1H, CH_2C$_6$H$_5$), 4.83 (d, J = 16.7 Hz, 1H, CH_2C$_6$H$_5$), 4.23 – 4.05 (m, 2H, OCH_2CH$_3$), 2.46 (s, 3H, CH$_3$), 1.23 (t, J = 7.1 Hz, 3H, OCH$_2$CH_3).^{13}C NMR (75 MHz, $CDCl_3$), δ (ppm): 165.6, 154.8, 154.3, 150.4, 142.3, 137.9, 128.6, 127.1, 126.3, 110.2, 106.0, 102.4, 60.3, 47.9, 46.0, 16.4, 14.2. LRMS (CI) m/z calcd. for $C_{19}H_{21}N_2O_4$ $[M+H]^+$: 341.1 found: 341.1.

(±) Ethyl 1-(2-fluorobenzyl)-4-(furan-2-yl)-6-methyl-2-oxo-1,2,3,4-tetrahydropyrimidine-5-carboxylate (251). Purified by column chromatography (DCM–AcOEt 99:1 – 98:2). Yield: 44%. Mp: 250 – 252 ºC. ^{1}H NMR (300 MHz, $CDCl_3$), δ (ppm): 7.32 – 6.95 (m, 5H), 6.26 (dd, *J* = 3.0, 1.8 Hz, 1H), 6.13 – 5.97 (m, 2H), 5.48 (d, *J* = 3.1 Hz, 1H), 5.24 (d, *J* = 17.2 Hz, 1H), 4.92 (d, *J* = 17.1 Hz, 1H), 4.13 (q, *J* = 7.2 Hz, 2H), 2.43 (s, 3H), 1.21 (t, *J* = 7.1 Hz, 3H). LRMS (CI) m/z calcd. for $C_{19}H_{19}FN_2O_4$ $[M+H]^+$: 359.1 found: 359.0.

(±) Isopropyl 4-(furan-2-yl)-6-methyl-2-oxo-1,2,3,4-tetrahydropyrimidine-5-carboxylate (D2).[140] Purified by column chromatography (DCM–MeOH 99:1 – 97:3). Yield: 80%. Mp: 204 – 205 ºC (ethanol). ^{1}H NMR (300 MHz, $CDCl_3$), δ (ppm): 8.12 (s, 1H, NH), 7.31 (*d*, *J* = 1.8 Hz, 1H, Ar-H), 6.26 (dd, *J* = 3.2, 1.8 Hz, 1H, Ar-H), 6.10 (d, *J* = 3.2 Hz, 1H, NH), 5.94 (s, 1H, Ar-H), 5.46 (d, *J* = 2.9 Hz, 1H, CH), 5.04 – 4.96 (m, 1H, OC*H*$(CH_3)_2$), 2.34 (s, 3H, CH_3), 1.23 (d, *J* = 6.2 Hz, 3H, OCH(C*H*$_3)_2$), 1.12 (d, *J* = 6.2 Hz, 3H, OCH(C*H*$_3)_2$). ^{13}C NMR (75 MHz, DMSO-*d*$_6$), δ (ppm): 164.7, 156.2, 152.5, 149.2, 142.2, 110.4, 105.4, 97.1, 66.5, 47.9, 21.9, 21.7, 17.8. Elem. Anal. calculated for $C_{13}H_{16}N_2O_4$, C, 59.08; H, 6.10; N, 10.60; found C, 58.11; H, 6.07; N, 10.62.

(±) Isopropyl 4-(furan-2-yl)-6-methyl-2-oxo-1-propyl-1,2,3,4-tetrahydropyrimidine-5-carboxylate (252). Purified by column chromatography (DCM–AcOEt 99:1 – 98:2). Yield: 45%. Mp: 224 – 225 ºC. ^{1}H NMR (300 MHz, $CDCl_3$), δ (ppm): 7.28 (dt, *J* = 2.8, 1.3 Hz, 1H, Ar-H), 6.25 (dd, *J* = 3.3, 1.8 Hz, 1H, Ar-H), 6.07 (d, *J* = 3.2 Hz, 1H, Ar-H), 6.01 (brs, 1H, NH), 5.42 (d, *J* = 3.2 Hz, 1H, CH), 5.16 – 4.90 (m, 1H, OC*H*$(CH_3)_2$), 3.92 (ddd, *J* = 15.4, 9.2, 6.2 Hz, 1H, C*H*$_2CH_2CH_3$), 3.50 (ddd, *J* = 14.6, 9.2, 5.6 Hz, 1H, C*H*$_2CH_2CH_3$),2.52 (s, 3H, CH_3), 1.74 – 1.42 (m, 2H, CH_2C*H*$_2CH_3$), 1.25 (dd, *J* = 6.4, 2.6 Hz, 3H, OCH(C*H*$_3)_2$), 1.14 (dd, *J* = 6.4, 2.6 Hz, 3H, OCH(C*H*$_3)_2$), 0.89 (t, *J* = 7.6 Hz, 3H, CH_2CH_2C*H*$_3$). ^{13}C NMR (75 MHz, $CDCl_3$), δ (ppm): 165.3, 155.1, 154.3, 149.9, 142.1, 110.1, 105.6, 102.5, 67.5, 47.7, 44.1, 23.0, 22.0, 21.7, 16.0, 11.0. LRMS (CI) m/z calcd. for $C_{16}H_{23}N_2O_4$ $[M+H]^+$: 307.2 found: 307.2.

(±) Isopropyl 1-benzyl-4-(furan-2-yl)-6-methyl-2-oxo-1,2,3,4-tetrahydropyrimidine-5-carboxylate (253). Purified by column chromatography (DCM–AcOEt 99:1 – 98:2). Yield: 52%. Mp: 229 – 231 ºC. ^{1}H NMR (300 MHz, $CDCl_3$), δ (ppm): 7.43 – 7.12 (m, 6H, Ar-H), 6.29 (dd, *J* = 3.3, 1.8 Hz, 1H, Ar-H), 6.16 (d, *J* = 3.3 Hz, 1H, CH), 6.10 (dd, *J* = 3.2, 0.9 Hz, 1H, Ar-H), 5.50 (d, *J* = 3.0 Hz, 1H, NH), 5.31 (d, *J* = 16.7 Hz, 1H, C*H*$_2$C$_6$H$_5$), 5.13 – 4.94 (m, *J* = 6.2 Hz, 1H, OC*H*(CH$_3$)$_2$), 4.82 (d, *J* = 16.7 Hz, 1H, C*H*$_2$C$_6$H$_5$), 2.44 (s, 3H, CH$_3$), 1.25 (d, *J* = 6.3 Hz, 3H, OCH(C*H*$_3$)$_2$), 1.14 (d, *J* = 6.2 Hz, 3H, OCH(C*H*$_3$)$_2$). ^{13}C NMR (75 MHz, $CDCl_3$), δ (ppm): 165.1, 154.9, 154.5, 150.1, 142.2, 137.9, 128.7, 127.1, 126.3, 110.2, 106.0, 102.7, 67.7, 47.9, 45.9, 22.0, 21.7, 16.3. LRMS (CI) m/z calcd. for $C_{20}H_{23}N_2O_4$ $[M+H]^+$: 355.2 found: 355.2.

(±) Isopropyl 1-(2-fluorobenzyl)-4-(furan-2-yl)-6-methyl-2-oxo-1,2,3,4-tetrahydropyrimidine-5-carboxylate (254). Purified by column chromatography (DCM–AcOEt 99:1 – 98:2). Yield: 51%. Mp: 233 – 234 ºC. ^{1}H NMR (300 MHz, $CDCl_3$), δ (ppm): 7.40 – 6.89 (m, 5H, Ar-H), 6.57 (d, *J* = 3.4 Hz, 1H, NH), 6.26 (dd, *J* = 3.3, 1.8 Hz, 1H, Ar-H), 6.13 – 6.04 (m, 1H, Ar-H), 5.48 (d, *J* = 3.3 Hz, 1H, CH), 5.24 (d, *J* = 17.2 Hz, 1H, C*H*$_2$C$_6$H$_4$F), 5.01 (dt, *J* = 12.5, 6.2 Hz, 1H, OC*H*(CH$_3$)$_2$), 4.91 (d, *J* = 17.2 Hz, 1H, C*H*$_2$C$_6$H$_4$F), 2.42 (s, 3H, CH$_3$), 1.23 (d, *J* = 6.3 Hz, 3H, OCH(C*H*$_3$)$_2$), 1.12 (d, *J* = 6.3 Hz, 3H, OCH(C*H*$_3$)$_2$). ^{13}C NMR (75 MHz, $CDCl_3$), δ (ppm) 165.1, 162.7, 159.8 (d, *J* = 245.5 Hz, Ar-CF), 154.7 (d, *J* = 16.9 Hz, Ar-C), 149.7, 142.2, 128.7 (d, *J* = 8.1 Hz, Ar-C), 128.1 (d, *J* = 3.9 Hz, Ar-C), 125.0 (d, *J* = 13.9 Hz, Ar-C), 124.3 (d, *J* = 3.6 Hz, Ar-C), 115.2 (d, *J* = 21.2 Hz, Ar-C), 110.2, 105.9, 102.9, 67.7, 47.7, 39.6 (d, *J* = 5.6 Hz, *C*H$_2$C$_6$H$_4$F), 22.0, 21.7, 15.9. LRMS (CI) m/z calcd. for $C_{20}H_{22}FN_2O_4$ $[M+H]^+$: 373.1 found: 373.1.

(±) Ethyl 4-(furan-3-yl)-6-methyl-2-oxo-1,2,3,4-tetrahydropyrimidine-5-carboxylate (D3).[140] Purified by column chromatography (DCM–MeOH 99:1 – 97:3). Yield: 82%. Mp: 202 – 204 ºC (ethanol). ^{1}H NMR (300 MHz, DMSO-*d*$_6$), δ (ppm): 9.15 (s, 1H, NH), 7.63 (s, 1H, NH), 7.54 (d, *J* = 1.6 Hz, 1H, Ar-H), 7.36 (d, *J* = 0.7 Hz, 1H, Ar-H), 6.32 (dd, *J* = 1.6, 0.7 Hz, 1H, Ar-H), 5.08 (s, 1H, CH), 4.05 (q, *J* = 7.1 Hz, 2H, OC*H*$_2$CH$_3$), 2.19 (s, 3H, CH$_3$), 1.16 (t, *J* = 7.1 Hz, 3H, OCH$_2$C*H*$_3$). ^{13}C NMR (75 MHz, DMSO-*d*$_6$), δ (ppm): 164.8, 155.3, 145.9, 142.0, 136.8, 128.7, 128.3, 125.8, 109.6, 59.9, 21.7, 11.4. Elem. Anal. calculated for $C_{12}H_{14}N_2O_4$, C, 57.59; H, 5.64; N, 11.19; found C, 57.61; H, 5.68; N, 11.20.

(±) Ethyl 4-(furan-3-yl)-6-methyl-2-oxo-1-propyl-1,2,3,4-tetrahydropyrimidine-5-carboxylate (255). Purified by column chromatography (DCM–AcOEt 99:1 – 98:2). Yield: 62%. Mp: 217 – 219 ºC. ^{1}H NMR (300 MHz, $CDCl_3$), δ (ppm): 7.31 (s, 1H, Ar-H), 7.26 (s, 1H, Ar-H), 6.40 – 6.32 (m, 1H, NH), 6.29 (s, 1H, Ar-H), 5.34 (d, *J* = 2.7 Hz, 1H, CH), 4.18 (q, *J* = 7.1 Hz, 2H, OCH_2CH_3), 3.89 (ddd, *J* = 15.2, 9.5, 6.1 Hz, 1H, $CH_2CH_2CH_3$), 3.48 (ddd, *J* = 14.7, 9.5, 5.7 Hz, 1H, $CH_2CH_2CH_3$), 2.48 (s, 3H, CH_3), 1.70 – 1.41 (m, 2H, $CH_2CH_2CH_3$), 1.27 (t, *J* = 6.8 Hz, 3H, OCH_2CH_3), 0.86 (t, *J* = 7.4 Hz, 3H, $CH_2CH_2CH_3$). ^{13}C NMR (75 MHz, $CDCl_3$), δ (ppm): 166.0, 154.7, 149.2, 143.4, 138.8, 128.2, 108.7, 104.5, 60.2, 45.9, 44.1, 23.1, 16.0, 14.3, 11.2. LRMS (CI) m/z calcd. for $C_{15}H_{21}N_2O_4$ $[M+H]^+$: 293.1 found: 293.1.

(±) Ethyl 1-benzyl-4-(furan-3-yl)-6-methyl-2-oxo-1,2,3,4-tetrahydropyrimidine-5-carboxylate (256). Purified by column chromatography (DCM–AcOEt 99:1 – 98:2). Yield: 61%. Mp: 229 – 230 ºC. ^{1}H NMR (300 MHz, $CDCl_3$), δ (ppm) 7.44 – 7.14 (m, 6H, Ar-H + NH), 7.14 – 7.00 (m, 2H, Ar-H), 6.29 (d, *J* = 2.1 Hz, 1H, Ar-H), 5.42 (d, *J* = 3.5 Hz, 1H, CH), 5.23 (d, *J* = 16.5 Hz, 1H, $CH_2C_6H_5$), 4.82 (d, *J* = 16.7 Hz, 1H, $CH_2C_6H_5$), 4.17 (q, *J* = 7.2 Hz, 2H, OCH_2CH_3), 2.40 (s, 3H, CH_3), 1.25 (t, *J* = 7.0 Hz, 3H, OCH_2CH_3). ^{13}C NMR (75 MHz, $CDCl_3$), δ (ppm): 165.9, 155.5, 149.4, 143.4, 139.1, 137.9, 128.7, 128.7, 127.2, 126.2, 109.0, 104.9, 60.3, 45.9, 45.8, 16.3, 14.3. LRMS (CI) m/z calcd. for $C_{19}H_{21}N_2O_4$ $[M+H]^+$: 341.1 found: 341.1.

(±) Ethyl 1-(2-fluorobenzyl)-4-(furan-3-yl)-6-methyl-2-oxo-1,2,3,4-tetrahydropyrimidine-5-carboxylate (257). Purified by column chromatography (DCM–AcOEt 99:1 – 98:2). Yield: 59%. Mp: 239 – 240 ºC. ^{1}H NMR (300 MHz, $CDCl_3$), δ (ppm): 7.30 (s, 2H, Ar-H), 7.20 (s, 2H, Ar-H), 7.07 – 6.86 (m, 3H, Ar-H), 6.26 (s, 1H, Ar-H), 5.40 (s, 1H, CH), 5.18 (d, *J* = 16.4 Hz, 1H, $CH_2C_6H_4F$), 4.90 (d, *J* = 16.2 Hz, 1H, $CH_2C_6H_4F$), 4.16 (q, *J* = 7.0 Hz, 2H, OCH_2CH_3), 2.39 (s, 3H, CH_3), 1.24 (t, *J* = 7.1 Hz, 3H, OCH_2CH_3). ^{13}C NMR (75 MHz, $CDCl_3$), δ (ppm): 165.8, 159.8 (d, *J* = 245.6 Hz, Ar-CF), 155.5, 149.2, 143.4, 139.1, 128.8 (d, *J* = 7.8 Hz, Ar-C), 128.1 (d, *J* = 7.3 Hz, Ar-C), 124.9 (d, *J* = 14.1 Hz, Ar-C), 124.3 (d, *J* = 3.2 Hz, Ar-C), 115.3 (d, *J* = 21.1 Hz, Ar-C), 108.9, 105.0, 60.4, 45.8, 39.7 (d, *J* = 4.4 Hz, $CH_2C_6H_4F$), 15.9, 14.2. LRMS (CI) m/z calcd. for $C_{19}H_{20}FN_2O_4$ $[M+H]^+$: 359.1 found: 359.2.

(±) Isopropyl 4-(furan-3-yl)-6-methyl-2-oxo-1,2,3,4-tetrahydropyrimidine-5-carboxylate (D4).[140] Purified by column chromatography (DCM–MeOH 99:1 – 97:3). Yield: 80%. Mp: 197 – 201 ºC (ethanol). ^{1}H NMR (300 MHz, DMSO-d_6), δ (ppm): 9.12 (s, 1H, NH), 7.62 (s, 1H, NH), 7.54 (d, J = 1.7 Hz, 1H, Ar-H), 7.35 (d, J = 0.8 Hz, 1H, Ar-H), 6.31 (dd, J = 1.6, 0.7 Hz, 1H, Ar-H), 5.07 (d, J = 3.4 Hz, 1H, CH), 4.91 – 4.87 (m, 1H, OC*H*$(CH_3)_2$), 2.19 (s, 3H, CH_3), 1.18 (d, J = 6.2 Hz, 3H, OCH(C*H*$_3)_2$), 1.12 (d, J = 6.2 Hz, 3H, OCH(C*H*$_3)_2$). HRMS (EI) m/z calcd. for $C_{13}H_{16}N_2O_4$: 264.1110, found: 264.1105.

(±) Isopropyl 4-(furan-3-yl)-6-methyl-2-oxo-1-propyl-1,2,3,4-tetrahydropyrimidine-5-carboxylate (258). Purified by column chromatography (DCM–AcOEt 99:1 – 98:2). Yield: 49%. Mp: 242 – 244 ºC. ^{1}H NMR (300 MHz, $CDCl_3$), δ (ppm): 7.34 – 7.25 (m, 1H, Ar-H), 6.26 (dt, J = 3.3, 2.1 Hz, 1H, Ar-H), 6.08 (d, J = 3.2 Hz, 1H, Ar-H), 5.68 (d, J = 3.4 Hz, 1H, NH), 5.41 (d, J = 3.3 Hz, 1H, CH), 5.03 (dtt, J = 12.5, 9.0, 4.9 Hz, 1H, OC*H*$(CH_3)_2$), 3.92 (ddd, J = 15.6, 9.3, 6.2 Hz, 1H, C*H*$_2CH_2CH_3$), 3.51 (ddd, J = 14.6, 9.1, 5.6 Hz, 1H, C*H*$_2CH_2CH_3$), 2.54 (d, J = 2.4 Hz, 3H, CH_3), 1.71 – 1.46 (m, 2H, CH_2C*H*$_2CH_3$), 1.26 (dd, J = 6.3, 2.8 Hz, 3H, OCH(C*H*$_3)_2$, 1.15 (dd, J = 6.2, 2.6 Hz, 3H, OCH(C*H*$_3)_2$), 0.96 – 0.84 (m, 3H, CH_2CH_2C*H*$_3$). LRMS (CI) m/z calcd. for $C_{16}H_{23}N_2O_4$ $[M+H]^+$: 307.2 found: 307.2.

(±) Isopropyl 1-benzyl-4-(furan-3-yl)-6-methyl-2-oxo-1,2,3,4-tetrahydropyrimidine-5-carboxylate (259). Purified by column chromatography (DCM–AcOEt 99:1 – 98:2). Yield: 49%. Mp: 250 – 251 ºC. ^{1}H NMR (300 MHz, $CDCl_3$), δ (ppm): 7.37 – 7.16 (m, 6H, Ar-H), 6.30 (dd, J = 3.2, 1.8 Hz, 1H, CH), 6.11 (d, J = 3.2 Hz, 1H, NH), 5.69 (d, J = 2.9 Hz, 1H, Ar-H), 5.50 (d, J = 3.2 Hz, 1H, Ar-H), 5.31 (d, J = 16.7 Hz, 1H, C*H*$_2C_6H_5$), 5.03 (hept, J = 6.3 Hz, 1H, OC*H*$(CH_3)_2$), 4.83 (d, J = 16.7 Hz, 1H, C*H*$_2C_6H_5$), 2.45 (s, 3H, CH_3), 1.26 (d, J = 6.3 Hz, 3H, OCH(C*H*$_3)_2$), 1.14 (d, J = 6.3 Hz, 3H, OCH(C*H*$_3)_2$). LRMS (CI) m/z calcd. for $C_{20}H_{23}N_2O_4$ $[M+H]^+$: 355.2 found: 355.2.

(±) Isopropyl 1-(2-fluorobenzyl)-4-(furan-3-yl)-6-methyl-2-oxo-1,2,3,4-tetrahydropyrimidine-5-carboxylate (260). Purified by column chromatography (DCM–AcOEt 99:1 – 98:2). Yield: 36%. Mp: 242 – 244 ºC. ^{1}H NMR (300 MHz, $CDCl_3$), δ (ppm): 7.38 – 6.90 (m, 6H, Ar-H), 6.29 – 6.23 (m, 1H, NH), 6.09 (s, 1H, Ar-H), 5.51 – 5.44 (m, 1H, CH), 5.35 – 5.14 (m, 1H, C*H*$_2C_6H_4F$), 5.13 – 4.84 (m, 2H, C*H*$_2C_6H_4F$ + OC*H*$(CH_3)_2$), 2.43 (d, J = 2.7 Hz, 3H, CH_3), 1.28 – 1.19 (m, 3H, OCH(C*H*$_3)_2$), 1.12 (d, J = 6.2 Hz, 3H, OCH(C*H*$_3)_2$). LRMS (CI) m/z calcd. for $C_{20}H_{22}FN_2O_4$ $[M+H]^+$: 373.1 found: 373.2.

(±) Ethyl 4-(furan-2-yl)-2-methyl-1,4-dihydrobenzo[4,5]imidazo[1,2-*a*]pyrimidine-3-carboxylate (D5). Purified by column chromatography (dichloromethane–MeOH 9:1). Yield: 55%. Mp: 174 – 176 ºC. ^{1}H NMR (300 MHz, DMSO-*d*$_6$), δ (ppm): 10.80 (brs, 1H, NH), 7.60−7.21 (m, 3H, Ar-H), 7.18−6.87 (m, 2H, Ar-H), 6.55 (s, 1H, CH), 6.43 (d, *J* = 3.2 Hz, 1H, Ar-H), 6.30 (dd, *J* = 3.2, 1.8 Hz, 1H, Ar-H), 4.33−3.76 (m, 2H, OC*H*$_2$CH$_3$), 2.44 (s, 3H, CH$_3$), 1.14 (t, *J* = 7.1 Hz, 3H, OCH$_2$C*H*$_3$). ^{13}C NMR (75 MHz, DMSO-*d*$_6$), δ (ppm): 165.5, 153.4, 148.1, 146.1, 142.9, 132.1, 122.3, 120.7, 117.3, 110.8, 110.1, 108.0, 95.0, 59.7, 49.7, 19.0, 14.6. HRMS (ESI) m/z calcd. for $C_{18}H_{18}N_3O_3$ $[M+H]^+$: 324.3582 found: 324.1343.

(±) Ethyl 4-(furan-2-yl)-2-methyl-1-propyl-1,4-dihydrobenzo[4,5]imidazo[1,2-*a*]pyrimidine-3-carboxylate (261a). Purified by column chromatography (DCM–AcOEt 99:1 – 98:2). Yield: 22%. Oil at RT. ^{1}H NMR (300 MHz, $CDCl_3$), δ (ppm): 7.54 (t, *J* = 10.1 Hz, 1H, Ar-H), 7.43 – 7.31 (m, 1H, Ar-H), 7.29 – 7.06 (m, 3H, Ar-H), 6.54 (s, 1H, CH), 6.19 (dq, *J* = 5.5, 2.4 Hz, 2H, Ar-H), 4.45 – 4.24 (m, 1H, C*H*$_2$CH$_2$CH$_3$), 4.26 – 4.08 (m, 2H, OC*H*$_2$CH$_3$), 4.01 (ddd, *J* = 14.7, 9.3, 5.7 Hz, 1H, C*H*$_2$CH$_2$CH$_3$), 2.70 (s, 3H, CH$_3$), 1.99 – 1.59 (m, 2H, CH$_2$C*H*$_2$CH$_3$), 1.25 (t, *J* = 7.1 Hz, 3H, CH$_2$CH$_2$C*H*$_3$), 1.03 (d, *J* = 7.4 Hz, 3H, OCH$_2$C*H*$_3$). ^{13}C NMR (75 MHz, $CDCl_3$), δ (ppm): 166.1, 153.2, 148.9, 142.1, 142.0, 122.3, 120.9, 117.5, 110.2, 109.2, 107.2, 98.0, 60.2, 49.4, 49.2, 46.8, 22.5, 21.9, 15.8, 14.3, 10.9. LRMS (CI) m/z calcd. for $C_{21}H_{24}N_3O_3$ $[M+H]^+$: 366.2 found: 366.2.

(±) Ethyl 4-(furan-2-yl)-2-methyl-10-propyl-4,10-dihydrobenzo[4,5]imidazo[1,2-*a*]pyrimidine-3-carboxylate (261b). Purified by column chromatography (DCM–AcOEt 99:1 – 98:2). Yield: 28%. Oil at RT. ^{1}H NMR (300 MHz, $CDCl_3$), δ (ppm): 7.45 – 6.80 (m, 5H, Ar-H), 6.49 (s, 1H, CH), 6.20 (d, *J* = 5.3 Hz, 2H, Ar-H), 4.22 – 3.90 (m, 4H, C*H*$_2$CH$_2$CH$_3$ + OC*H*$_2$CH$_3$), 2.53 (s, 3H, CH$_3$), 1.82 (hept, *J* = 7.7 Hz, 2H, CH$_2$C*H*$_2$CH$_3$), 1.21 (dd, *J* = 13.6, 6.9 Hz, 3H, CH$_2$CH$_2$C*H*$_3$), 0.96 (q, *J* = 6.3 Hz, 3H, OCH$_2$C*H*$_3$). LRMS (CI) m/z calcd. for $C_{21}H_{24}N_3O_3$ $[M+H]^+$: 366.2 found: 366.2.

(±) Ethyl 1-benzyl-4-(furan-2-yl)-2-methyl-1,4-dihydrobenzo[4,5]imidazo[1,2-*a*]pyrimidine-3-carboxylate (262a). Purified by column chromatography (DCM–AcOEt 99:1 – 98:2). Yield: 22%. Oil at RT. ^{1}H NMR (300 MHz, $CDCl_3$), δ (ppm): 7.55 (dd, *J* = 7.2, 1.6 Hz, 1H, Ar-H), 7.46 – 6.96 (m, 9H, Ar-H), 6.62 (s, 1H, CH), 6.27 – 6.19 (m, 2H, Ar-H), 5.76 (d, *J* = 16.8 Hz, 1H, C*H*$_2$C$_6$H$_5$), 5.31 (d, *J* = 14.5 Hz, 1H, C*H*$_2$C$_6$H$_5$), 4.29 – 4.06 (m, 2H, OC*H*$_2$CH$_3$), 2.59 (s, 3H, CH_3), 1.25 (t, *J* = 7.1 Hz, 3H, OCH$_2$C*H*$_3$). ^{13}C NMR (75 MHz, $CDCl_3$), δ 165.9, 153.0, 149.0, 147.8, 142.2, 142.0, 137.1, 132.9, 128.8, 127.5, 126.2, 122.5, 121.1, 117.7, 110.3, 109.4, 107.5, 98.4, 60.3, 49.4, 48.7, 16.2, 14.3. LRMS (CI) m/z calcd. for $C_{25}H_{24}N_3O_3$ $[M+H]^+$: 414.2 found: 414.2.

(±) Ethyl 10-benzyl-4-(furan-2-yl)-2-methyl-4,10-dihydrobenzo[4,5]imidazo[1,2-*a*]pyrimidine-3-carboxylate (262b). Purified by column chromatography (DCM–AcOEt 99:1 – 98:2). Yield: 28%. Oil at RT. ^{1}H NMR (300 MHz, $CDCl_3$), δ (ppm): 7.39 – 7.23 (m, 7H, Ar-H), 7.07 (dt, *J* = 17.7, 7.5 Hz, 2H, Ar-H), 6.92 (d, *J* = 7.7 Hz, 1H, Ar-H), 6.56 (s, 1H, CH), 6.32 – 6.19 (m, 2H, Ar-H), 5.43 – 5.11 (m, 2H, C*H*$_2$C$_6$H$_5$), 4.29 – 4.05 (m, 2H, OC*H*$_2$CH$_3$), 2.60 (s, 3H, CH_3), 1.32 – 1.18 (m, 3H, OCH$_2$C*H*$_3$). LRMS (CI) m/z calcd. for $C_{25}H_{24}N_3O_3$ $[M+H]^+$: 414.2 found: 414.2.

(±) Ethyl 1-(2-fluorobenzyl)-4-(furan-2-yl)-2-methyl-1,4-dihydrobenzo[4,5]imidazo[1,2-*a*]pyrimidine-3-carboxylate (263a). Purified by column chromatography (DCM–AcOEt 99:1 – 98:2). Yield: 28%. Oil at RT. ^{1}H NMR (300 MHz, $CDCl_3$), δ (ppm): 7.58 (d, *J* = 7.4 Hz, 1H, Ar-H), 7.46 – 7.37 (m, 1H, Ar-H), 7.36 – 7.01 (m, 7H, Ar-H), 6.63 (s, 1H, CH), 6.25 (d, *J* = 1.3 Hz, 2H, Ar-H), 5.77 (d, *J* = 17.3 Hz, 1H, C*H*$_2$C$_6$H$_4$F), 5.44 (d, *J* = 17.3 Hz, 1H, C*H*$_2$C$_6$H$_4$F), 4.32 – 4.09 (m, 2H, OC*H*$_2$CH$_3$), 2.62 (s, 3H, CH_3), 1.27 (t, *J* = 7.1 Hz, 3H, OCH$_2$C*H*$_3$). LRMS (CI) m/z calcd. for $C_{25}H_{23}FN_3O_3$ $[M+H]^+$: 432.2 found: 432.2.

(±) Ethyl 10-(2-fluorobenzyl)-4-(furan-2-yl)-2-methyl-4,10-dihydrobenzo[4,5]imidazo[1,2-*a*]pyrimidine-3-carboxylate (263b). Purified by column chromatography (DCM–AcOEt 99:1 – 98:2). Yield: 28%. Oil at RT. ^{1}H NMR (300 MHz, $CDCl_3$), δ (ppm): 7.41 – 7.21 (m, 6H, Ar-H), 7.15 – 7.03 (m, 3H, Ar-H), 6.57 (s, 1H, CH), 6.27 (d, *J* = 11.3 Hz, 2H, Ar-H), 5.39 – 5.29 (m, 2H, C*H*$_2$C$_6$H$_4$F), 4.18 (dd, *J* = 11.2, 7.0 Hz, 2H, OC*H*$_2$CH$_3$), 2.61 (s, 3H, 20), 1.25 (t, *J* = 7.2 Hz, 3H, 27). LRMS (CI) m/z calcd. for $C_{25}H_{23}FN_3O_3$ $[M+H]^+$: 432.2 found: 432.2.

(±) Isopropyl 4-(Furan-2-yl)-2-methyl-1,4-dihydrobenzo[4,5]imidazo[1,2-a]pyrimidine-3-carboxylate (D6). Purified by column chromatography (dichloromethane−MeOH 9:1). Yield: 61%. Mp: 253 − 255 °C. ^{1}H NMR (300 MHz, DMSO-*d*$_6$), δ (ppm): 10.78 (brs, 1H, NH), 7.67−7.23 (m, 3H, Ar-H), 7.19−6.84 (m, 2H, Ar-H), 6.52 (s, 1H, CH), 6.44 (d, *J* = 3.3 Hz, 1H, Ar-H), 6.37−6.23 (m, 1H, Ar-H), 4.86 (hept, *J* = 6.3 Hz, 1H, OC*H*(CH$_3$)$_2$), 2.44 (s, 3H, CH$_3$), 1.21 (d, *J* = 6.2 Hz, 3H, OC*H*(C*H*$_3$)$_2$), 1.05 (d, *J* = 6.1 Hz, 3H, OC*H*(C*H*$_3$)$_2$). ^{13}C NMR (75 MHz, DMSO-*d*$_6$), δ (ppm): 165.0, 153.3, 148.0, 146.0, 143.0, 142.6, 132.0, 122.3, 120.7, 117.2, 110.8, 110.2, 108.2, 94.9, 67.0, 49.7, 22.3, 22.0, 19.1. HRMS (ESI) m/z: calcd for $C_{19}H_{20}N_3O_3$ $[M + H]^+$, 338.1488; found, 338.7927.

(±) Isopropyl 4-(furan-2-yl)-2-methyl-1-propyl-1,4-dihydrobenzo[4,5]imidazo[1,2-a]pyrimidine-3-carboxylate (264a). Purified by column chromatography (DCM–AcOEt 99:1 – 98:2). Yield: 21%. Mp: 172 – 173 ºC. ^{1}H NMR (300 MHz, $CDCl_3$), δ (ppm): 7.60 – 7.51 (m, 1H, Ar-H), 7.38 (d, *J* = 8.0 Hz, 1H, Ar-H), 7.29 – 7.06 (m, 3H, Ar-H), 6.52 (s, 1H, CH), 6.18 (m, 2H, Ar-H), 5.05 (hept, *J* = 6.3 Hz, 1H, OC*H*(CH$_3$)$_2$), 4.33 (ddd, *J* = 15.1, 9.4, 5.9 Hz, 1H, C*H*$_2$CH$_2$CH$_3$), 4.01 (ddd, *J* = 14.8, 9.4, 5.7 Hz, 1H, C*H*$_2$CH$_2$CH$_3$), 2.70 (s, 3H, CH$_3$), 2.01 – 1.63 (m, 2H, CH$_2$C*H*$_2$CH$_3$), 1.29 (d, *J* = 6.3 Hz, 3H, OCH(C*H*$_3$)$_2$), 1.13 (d, *J* = 6.3 Hz, 3H, OCH(C*H*$_3$)$_2$), 1.02 (t, *J* = 7.4 Hz, 3H, CH$_2$CH$_2$C*H*$_3$). LRMS (CI) m/z calcd. for $C_{22}H_{26}N_3O_3$ $[M+H]^+$: 380.5 found: 380.2.

(±) Isopropyl 4-(furan-2-yl)-2-methyl-10-propyl-4,10-dihydrobenzo[4,5]imidazo[1,2-a]pyrimidine-3-carboxylate (264b). Purified by column chromatography (DCM–AcOEt 99:1 – 98:2). Yield: 24%. Oil at RT. ^{1}H NMR (300 MHz, $CDCl_3$), δ (ppm): 7.40 – 7.31 (m, 1H, Ar-H), 7.24 (d, *J* = 10.0 Hz, 1H, Ar-H), 7.21 – 7.10 (m, 2H, Ar-H), 7.15 – 7.04 (m, 1H, Ar-H), 6.49 (s, 1H, CH), 6.22 (s, 2H, Ar-H), 5.02 (p, *J* = 6.2 Hz, 1H, OC*H*(CH$_3$)$_2$), 4.15 – 3.93 (m, 2H, C*H*$_2$CH$_2$CH$_3$), 2.55 (s, 3H, CH$_3$), 1.93 – 1.74 (m, 2H, CH$_2$C*H*$_2$CH$_3$), 1.25 (d, *J* = 6.2 Hz, 3H, OCH(C*H*$_3$)$_2$), 1.09 (d, *J* = 6.2 Hz, 3H, CH(C*H*$_3$)$_2$), 0.97 (t, *J* = 7.3 Hz, 3H, CH$_2$CH$_2$C*H*$_3$). LRMS (CI) m/z calcd. for $C_{22}H_{26}N_3O_3$ $[M+H]^+$: 380.5 found: 380.2.

(±) Isopropyl 1-benzyl-4-(furan-2-yl)-2-methyl-1,4-dihydrobenzo[4,5]imidazo[1,2-a]pyrimidine-3-carboxylate (265a). Purified by column chromatography (DCM–AcOEt 99:1 – 98:2). Yield: 22%. Mp: 188 – 184 ºC. ^{1}H NMR (300 MHz, $CDCl_3$), δ (ppm): 7.57 (d, *J* = 7.8 Hz, 1H, Ar-H), 7.46 – 7.40 (m, 1H, Ar-H), 7.40 – 7.32 (m, 1H, Ar-H), 7.32 (s, 2H, Ar-H), 7.32 (s, 1H, Ar-H), 7.32 – 7.21 (m, 2H, Ar-H), 7.24 – 7.10 (m, 1H, Ar-H), 7.14 (s, 1H, Ar-H), 6.60 (s, 1H, Ar-H), 6.27 – 6.22 (m, 2H, CH), 5.77 (d, *J* = 16.9 Hz, 1H, C*H*$_2$C$_6$H$_5$), 5.33 (d, *J* = 16.9 Hz, 1H, C*H*$_2$C$_6$H$_5$), 5.05 (hept, *J* = 6.3 Hz, 1H, OC*H*(CH$_3$)$_2$), 2.61 (s, 3H, CH$_3$), 1.30 (d, *J* = 6.2 Hz, 3H, OCH(C*H*$_3$)$_2$), 1.14 (d, *J* = 6.2 Hz, 3H, OCH(C*H*$_3$)$_2$). ^{13}C NMR (75 MHz, $CDCl_3$), δ (ppm): 165.4, 153.1, 148.7, 147.7, 142.2, 141.8, 137.1, 132.9, 128.9, 127.5, 126.2, 122.5, 121.1, 117.7, 110.3, 109.5, 107.6, 98.7, 67.7, 49.5, 48.7, 22.1, 21.7, 16.1. LRMS (CI) m/z calcd. for $C_{26}H_{26}N_3O_3$ $[M+H]^+$: 428.2 found: 428.2.

(±) Isopropyl 10-benzyl-4-(furan-2-yl)-2-methyl-4,10-dihydrobenzo[4,5]imidazo[1,2-a]pyrimidine-3-carboxylate (265b). Purified by column chromatography (DCM–AcOEt 99:1 – 98:2). Yield: 22%. Oil at RT. ^{1}H NMR (300 MHz, $CDCl_3$), δ (ppm): 7.38 – 7.21 (m, 7H, Ar-H), 7.16 – 6.97 (m, 2H, Ar-H), 6.92 (d, *J* = 7.6 Hz, 1H, Ar-H), 6.52 (s, 1H, CH), 6.29 – 6.19 (m, 2H, Ar-H), 5.52 – 5.12 (m, 2H, C*H*$_2$-C$_6$H$_5$), 5.04 (p, *J* = 6.2 Hz, 1H, OC*H*(CH$_3$)$_2$), 2.57 (s, 3H, CH$_3$), 1.25 (d, *J* = 6.2 Hz, 3H, OCH(C*H*$_3$)$_2$), 1.11 (d, *J* = 6.2 Hz, 3H, OCH(C*H*$_3$)$_2$). ^{13}C NMR (75 MHz, $CDCl_3$), δ (ppm): 166.3, 160.1, 154.9, 148.8, 141.8, 135.6, 130.8, 129.3, 128.8, 127.9, 127.6, 122.9, 122.3, 110.4, 109.8, 109.1, 107.7, 95.8, 66.5, 50.4, 45.4, 24.8, 22.3, 22.0. LRMS (CI) m/z calcd. for $C_{26}H_{26}N_3O_3$ $[M+H]^+$: 428.2 found: 428.2.

(±) Isopropyl 1-(2-fluorobenzyl)-4-(furan-2-yl)-2-methyl-1,4-dihydrobenzo[4,5]-imidazo-[1,2-a]pyrimidine-3-carboxylate (266a). Purified by column chromatography (DCM–AcOEt 99:1 – 98:2). Yield 27%. Mp: 182 – 183 ºC. ^{1}H NMR (300 MHz, $CDCl_3$), δ (ppm): 7.72 – 7.51 (m, 1H, Ar-H), 7.52 (dd, *J* = 7.3, 2.0 Hz, 1H, Ar-H), 7.41 – 7.00 (m, 7H, Ar-H), 6.61 (s, 1H, CH), 6.31 (d, *J* = 1.7 Hz, 2H, Ar-H), 5.82 (d, *J* = 17.4 Hz, 1H, C*H*$_2$C$_6$H$_4$F), 5.52 (d, *J* = 17.4 Hz, 1H, C*H*$_2$C$_6$H$_4$F), 5.13 (hept, *J* = 6.3 Hz, 1H, OC*H*(CH$_3$)$_2$), 2.64 (s, 3H, CH$_3$), 1.31 (d, *J* = 6.2 Hz, 3H, OCH(C*H*$_3$)$_2$), 1.21 (d, *J* = 6.26 Hz, 3H, OCH(C*H*$_3$)$_2$). ^{13}C NMR (75 MHz, $CDCl_3$), δ (ppm): 165.4, 160.5 (d, *J* = 246.3 Hz, Ar-CF), 153.0, 148.3, 147.5, 142.2, 141.8, 132.9, 129.1 (d, *J* = 8.1 Hz, Ar-C), 127.8 (d, *J* = 3.6 Hz, Ar-C), 124.6 (d, *J* = 3.6 Hz, Ar-C), 124.3 (d, *J* = 13.7 Hz, Ar-C), 122.6, 121.2, 117.7, 115.5 (d, *J* = 21.1 Hz, Ar-C), 110.3, 109.5, 107.6, 98.9, 67.8, 49.5, 42.5 (d, *J* = 5.6 Hz, *C*H$_2$C$_6$H$_4$F), 22.1, 21.7, 15.8. HRMS (APCI) *m/z* calcd. for $C_{26}H_{25}FN_3O_3$ $[M+H]^+$: 446.1874; found: 446.1876.

(±) Isopropyl 10-(2-fluorobenzyl)-4-(furan-2-yl)-2-methyl-1,4-dihydrobenzo[4,5]-imidazo[1,2-a]pyrimidine-3-carboxylate (266b). Purified by column chromatography (DCM–AcOEt 99:1 – 98:2). Yield: 38%. Mp: 166 – 167 ºC. ^{1}H NMR (300 MHz, $CDCl_3$), δ (ppm): 7.42 – 7.21 (m, 4H, Ar-H), 7.12 (m, 5H, Ar-H), 6.61 (s, 1H, CH), 6.43 – 6.21 (m, 2H, Ar-H), 5.52 – 5.31 (m, 2H, C*H*$_2$C$_6$H$_4$F), 5.12 (hept, *J* = 6.4 Hz, 1H, OC*H*(CH$_3$)$_2$), 2.61 (s, 3H, CH$_3$), 1.3 (d, *J* = 6.3 Hz, 3H, OCH(C*H*$_3$)$_2$), 1.21 (d, *J* = 6.3 Hz, 3H, OCH(C*H*$_3$)$_2$). ^{13}C NMR (75 MHz, $CDCl_3$), δ (ppm): 166.3, 160.5 (d, *J* = 246.3 Hz, Ar-CF), 160.2, 154.9, 148.9, 141.8, 130.6, 130.1 (d, *J* = 3.7 Hz, Ar-C), 129.7 (d, *J* = 8.2 Hz, Ar-C), 129.2, 124.6 (d, *J* = 3.6 Hz, Ar-C), 122.7 (d, *J* = 42.7 Hz, Ar-C), 115.5 (d, *J* = 21.5 Hz, Ar-C), 110.4, 109.7, 108.8 (d, *J* = 2.8 Hz, Ar-C), 107.7, 95.9, 66.4, 50.4, 38.5 (d, *J* = 5.3 Hz, *C*H$_2$C$_6$H$_4$F), 24.9, 22.3, 22.0. HRMS (APCI) *m/z* calcd. for $C_{26}H_{25}FN_3O_3$ $[M+H]^+$: 446.1874; found: 446.1877.

(±) Ethyl 4-(Furan-3-yl)-2-methyl-1,4-dihydrobenzo[4,5]imidazo[1,2-a]pyrimidine-3-carboxylate (D7). Purified by column chromatography (Hex−AcOEt 7:3). Yield: 72%. Mp: 270 − 271 °C. ^{1}H NMR (300 MHz, DMSO-*d*$_6$), δ (ppm): 10.70 (brs, 1H, NH), 7.68 (s, 1H, Ar-H), 7.53−7.21 (m, 3H, Ar-H), 7.02 (dt, *J* = 19.3, 7.4 Hz, 2H, Ar-H), 6.44 (s, 1H, CH), 6.16 (d, *J* = 2.3 Hz, 1H, Ar-H), 4.33−3.76 (m, 2H, OC*H*$_2$CH$_3$), 2.40 (s, 3H, CH$_3$), 1.17 (t, *J* = 7.1 Hz, 3H, OCH$_2$C*H*$_3$). ^{13}C NMR (75 MHz, DMSO-*d*$_6$), δ (ppm): 165.6, 147.4, 146.3, 144.1, 142.8, 140.5, 131.9, 126.2, 122.2, 120.6, 117.2, 110.1, 109.2, 97.1, 59.8, 47.7, 19.0, 14.6. HRMS (ESI) m/z: calcd for $C_{18}H_{18}N_3O_3$ $[M + H]^+$, 324.3582; found, 324.9974.

(±) Ethyl 4-(furan-3-yl)-2-methyl-1-propyl-1,4-dihydrobenzo[4,5]imidazo[1,2-a]pyrimidine-3-carboxylate (267a). Purified by column chromatography (DCM–AcOEt 99:1 – 98:2). Yield: 29%. Mp: 96 – 98 ºC. ^{1}H NMR (300 MHz, $CDCl_3$), δ (ppm): 7.68 – 7.51 (m, 1H, Ar-H), 7.37 – 7.00 (m, 5H, Ar-H), 6.49 (s, 1H, Ar-H), 6.07 (s, 1H, CH), 4.49 – 4.15 (m, 3H, OC*H*$_2$CH$_3$ + C*H*$_2$CH$_2$CH$_3$), 4.07 – 3.89 (m, 1H, C*H*$_2$CH$_2$CH$_3$), 2.65 (s, 3H, CH$_3$), 2.00 – 1.65 (m, 2H, CH$_2$C*H*$_2$CH$_3$), 1.33 (t, *J* = 7.9 Hz, 3H, OCH$_2$C*H*$_3$), 1.02 (t, *J* = 7.4 Hz, 3H, CH$_2$CH$_2$C*H*$_3$). LRMS (CI) m/z calcd. for $C_{21}H_{24}N_3O_3$ $[M+H]^+$: 366.2 found: 366.2.

(±) Ethyl 4-(furan-3-yl)-2-methyl-10-propyl-4,10-dihydrobenzo[4,5]imidazo[1,2-a]pyrimidine-3-carboxylate (267b). Purified by column chromatography (DCM–AcOEt 99:1 – 98:2). Yield: 31%. Oil at RT. ^{1}H NMR (300 MHz, $CDCl_3$), δ (ppm): 7.40 (s, 1H, Ar-H), 7.34 – 7.08 (m, 5H, Ar-H), 6.51 (s, 1H, Ar-H), 6.26 (s, 1H, CH), 4.35 – 4.01 (m, 4H, OCH_2CH_3 + $CH_2CH_2CH_3$), 2.21 (s, 3H, CH_3), 2.03 – 1.76 (m, 2H, $CH_2CH_2CH_3$), 1.34 (t, J = 7.2 Hz, 3H, OCH_2CH_3), 1.03 (t, J = 7.5 Hz, 3H, $CH_2CH_2CH_3$). LRMS (CI) m/z calcd. for $C_{21}H_{24}N_3O_3$ $[M+H]^+$: 366.2 found: 366.2.

(±) Ethyl 1-benzyl-4-(furan-3-yl)-2-methyl-1,4-dihydrobenzo[4,5]imidazo[1,2-a]pyrimidine-3-carboxylate (268a). Purified by column chromatography (DCM–AcOEt 99:1 – 98:2). Yield: 32%. Mp: 97 – 98 ºC. ^{1}H NMR (300 MHz, $CDCl_3$), δ (ppm): 7.57 (d, J = 7.7 Hz, 1H, Ar-H), 7.45 – 6.88 (m, 10H, Ar-H), 6.57 (s, 1H, Ar-H), 6.09 (d, J = 1.8 Hz, 1H, CH), 5.65 (d, J = 16.8 Hz, 1H, $CH_2C_6H_5$), 5.33 (d, J = 16.7 Hz, 1H, $CH_2C_6H_5$), 4.23 (q, J = 7.1 Hz, 2H, OCH_2CH_3), 2.56 (s, 3H, CH_3), 1.57 – 1.11 (m, 3H, OCH_2CH_3). ^{13}C NMR (75 MHz, $CDCl_3$), δ (ppm): 166.1, 148.0, 143.4, 142.0, 139.5, 137.1, 132.7, 128.9, 128.6, 127.6, 127.0, 126.3, 125.8, 122.5, 121.2, 117.8, 109.2, 108.8, 60.5, 48.7, 47.7, 16.3, 14.4. LRMS (CI) m/z calcd. for $C_{25}H_{24}N_3O_3$ $[M+H]^+$: 414.2 found: 414.2.

(±) Ethyl 10-benzyl-4-(furan-3-yl)-2-methyl-4,10-dihydrobenzo[4,5]imidazo[1,2-a]pyrimidine-3-carboxylate (268b). Purified by column chromatography (DCM–AcOEt 99:1 – 98:2). Yield: 29%. Oil at RT. ^{1}H NMR (300 MHz, $CDCl_3$), δ (ppm): 7.81 – 6.76 (m, 11H, Ar-H), 6.50 (s, 1H, CH), 6.25 (s, 1H, CH), 5.32 (s, 2H, $CH_2C_6H_5$), 4.48 – 3.86 (m, 2H, OCH_2CH_3), 2.53 (s, 3H, CH_3), 1.30 (t, J = 7.1 Hz, 3H, OCH_2CH_3). LRMS (CI) m/z calcd. for $C_{25}H_{24}N_3O_3$ $[M+H]^+$: 414.2 found: 414.2.

(±) Ethyl 1-(2-fluorobenzyl)-4-(furan-3-yl)-2-methyl-1,4-dihydrobenzo[4,5]imidazo[1,2-a]pyrimidine-3-carboxylate (269a). Purified by column chromatography (DCM–AcOEt 99:1 – 98:2). Yield: 37%. Mp: 111 – 113 ºC. ^{1}H NMR (300 MHz, $CDCl_3$), δ (ppm): 7.66 – 7.49 (m, 1H, Ar-H), 7.37 – 6.92 (m, 9H, Ar-H), 6.57 (s, 1H, Ar-H), 6.10 (s, 1H, CH), 5.66 (d, *J* = 17.2 Hz, 1H, C*H*$_2$C$_6$H$_4$F), 5.44 (d, *J* = 17.1 Hz, 1H, C*H*$_2$C$_6$H$_4$F), 4.25 (q, *J* = 7.1 Hz, 2H, OC*H*$_2$CH$_3$), 2.56 (s, 3H, CH_3), 1.34 (t, *J* = 7.1 Hz, 3H, OCH$_2$C*H*$_3$). ^{13}C NMR (75 MHz, $CDCl_3$), δ (ppm): 166.0, 160.0 (d, *J* = 246.0 Hz, Ar-CF), 147.9, 147.7, 143.4, 141.9, 139.5, 132.6, 129.3 (d, *J* = 8.2 Hz, Ar-C), 128.0 (d, *J* = 3.8 Hz, Ar-C), 125.7, 124.6 (d, *J* = 3.7 Hz, Ar-C), 124.3, 124.1, 122.6, 121.2, 117.8, 115.6 (d, *J* = 21.3 Hz, Ar-C), 109.2, 108.7, 60.5, 47.7 (CH), 42.6 (d, *J* = 5.4 Hz, *C*H$_2$C$_6$H$_4$F), 15.9, 14.4. HRMS (APCI) m/z calcd. for $C_{25}H_{23}FN_3O_3$ $[M+H]^+$: 432.1645 found: 432.1632.

(±) Ethyl 10-(2-fluorobenzyl)-4-(furan-3-yl)-2-methyl-4,10-dihydrobenzo[4,5]imidazo[1,2-a]pyrimidine-3-carboxylate (269b). Purified by column chromatography (DCM–AcOEt 99:1 – 98:2). Yield: 18%. Oil at RT. ^{1}H NMR (300 MHz, $CDCl_3$), δ (ppm): 7.51 – 7.21 (m, 4H, Ar-H), 7.21 – 6.98 (m, 6H, Ar-H), 6.53 (s, 1H, CH), 6.29 (s, 1H, Ar-H), 5.60 – 5.26 (m, 2H, C*H*$_2$C$_6$H$_4$F), 4.47 – 4.04 (m, 2H, OC*H*$_2$CH$_3$), 2.57 (s, 3H, CH_3), 1.34 (t, *J* = 7.1 Hz, 3H, OCH$_2$C*H*$_3$). LRMS (CI) m/z calcd. for $C_{25}H_{23}FN_3O_3$ $[M+H]^+$: 432.2 found: 432.2.

(±) Isopropyl 4-(Furan-3-yl)-2-methyl-1,4-dihydrobenzo[4,5]imidazo[1,2-a]pyrimidine-3-carboxylate (D8). Purified by column chromatography (Hex−AcOEt 7:3). Yield: 71%. Mp: 269 − 270 °C. ^{1}H NMR (300 MHz, DMSO-*d*$_6$), δ (ppm): 10.68 (brs, 1H, NH), 7.71 (s, 1H, Ar-H), 7.53−7.18 (m, 3H, Ar-H), 7.01 (dddd, *J* = 16.7, 9.1, 7.4, 4.5 Hz, 2H, Ar-H), 6.41 (d, *J* = 2.6 Hz, 1H, CH), 6.27−6.00 (m, 1H, Ar-H), 4.88 (p, *J* = 6.2 Hz, 1H, OC*H*(CH$_3$)$_2$), 2.40 (s, 3H, CH_3), 1.21 (d, *J* = 6.2 Hz, 3H, OCH(C*H*$_3$)$_2$), 1.08 (d, *J* = 6.6 Hz, 3H OCH(C*H*$_3$)$_2$). ^{13}C NMR (75 MHz, DMSO-*d*$_6$), δ (ppm): 165.1, 147.1, 146.3, 144.1, 142.8, 140.7, 132.0, 126.2, 122.2, 120.5, 117.2, 110.2, 109.3, 97.3 67.0, 47.7, 22.3, 22.0, 19.0. HRMS (ESI) m/z: calcd for $C_{19}H_{20}N_3O_3$ [M + H]+, 338.3812; found, 338.4765.

(±) Isopropyl 4-(furan-3-yl)-2-methyl-1-propyl-1,4-dihydrobenzo[4,5]imidazo[1,2-*a*]pyrimidine-3-carboxylate (270a). Purified by column chromatography (DCM–AcOEt 99:1 – 98:2). Yield: 22%. Mp: 96 – 98 ºC. ^{1}H NMR (300 MHz, $CDCl_3$), δ (ppm): 7.57 (dt, *J* = 7.9, 0.9 Hz, 1H, Ar-H), 7.25 – 7.02 (m, 5H, Ar-H), 6.47 (s, 1H, CH), 6.09 (dd, *J* = 1.8, 0.9 Hz, 1H, Ar-H), 5.11 (hept, *J* = 6.3 Hz, 1H, OC*H*$(CH_3)_2$), 4.31 (ddd, *J* = 15.2, 9.8, 5.8 Hz, 1H, C*H*$_2$$CH_2CH_3$), 3.98 (ddd, *J* = 14.9, 9.7, 5.6 Hz, 1H, C*H*$_2$$CH_2CH_3$), 2.64 (s, 3H, CH_3), 1.95 – 1.65 (m, 2H, CH_2C*H*$_2$$CH_3$), 1.32 (d, *J* = 6.3 Hz, 3H, OCH(C*H*$_3$)$_2$), 1.26 (d, *J* = 6.2 Hz, 3H, OCH(C*H*$_3$)$_2$), 1.01 (t, *J* = 7.4 Hz, 3H, CH_2CH_2C*H*$_3$). ^{13}C NMR (75 MHz, $CDCl_3$), δ 165.7, 147.6, 143.4, 143.3, 142.2, 139.3, 132.4, 125.9, 122.3, 120.8, 117.6, 109.0, 108.7, 100.8, 67.8, 47.4, 46.7, 22.6, 22.2, 21.9, 15.8, 11.0. LRMS (CI) m/z calcd. for $C_{22}H_{26}N_3O_3$ $[M+H]^+$: 380.2 found: 380.2.

(±) Isopropyl 4-(furan-3-yl)-2-methyl-10-propyl-4,10-dihydrobenzo[4,5]imidazo[1,2-*a*]pyrimidine-3-carboxylate (270b). Purified by column chromatography (DCM–AcOEt 99:1 – 98:2). Yield: 31%. Oil at RT. ^{1}H NMR (300 MHz, $CDCl_3$), δ (ppm): 7.34 (t, *J* = 1.2 Hz, 1H, Ar-H), 7.25 – 7.02 (m, 5H, Ar-H), 6.44 (s, 1H, Ar-H), 6.23 (dd, *J* = 1.9, 0.9 Hz, 1H, CH), 5.07 (hept, *J* = 6.2 Hz, 1H, OC*H*$(CH_3)_2$), 4.09 – 3.98 (m, 2H, C*H*$_2$$CH_2CH_3$), 2.49 (s, 3H, CH_3), 1.84 (hept, *J* = 7.4 Hz, 2H, CH_2C*H*$_2$$CH_3$), 1.28 (d, *J* = 6.3 Hz, 3H, OCH(C*H*$_3$)$_2$), 1.21 (d, *J* = 6.2 Hz, 3H, OCH(C*H*$_3$)$_2$), 0.97 (t, *J* = 7.4 Hz, 3H, CH_2CH_2C*H*$_3$). LRMS (CI) m/z calcd. for $C_{22}H_{26}N_3O_3$ $[M+H]^+$: 380.2 found: 380.2.

(±) Isopropyl 1-benzyl-4-(furan-3-yl)-2-methyl-1,4-dihydrobenzo[4,5]imidazo[1,2-*a*]pyrimidine-3-carboxylate (271a). Purified by column chromatography (DCM–AcOEt 99:1 – 98:2). Yield: 31%. Mp: 102 – 104 ºC. ^{1}H NMR (300 MHz, $CDCl_3$), δ (ppm): 7.56 (d, *J* = 7.7 Hz, 1H, Ar-H), 7.45 – 7.04 (m, 10H, Ar-H), 6.53 (d, *J* = 3.8 Hz, 1H, CH), 6.14 – 6.07 (m, 1H, Ar-H), 5.66 (d, *J* = 16.8 Hz, 1H, C*H*$_2$$C_6H_5$), 5.33 (d, *J* = 17.8 Hz, 1H, C*H*$_2$$C_6H_5$), 5.10 (p, *J* = 6.2 Hz, 1H, OC*H*$(CH_3)_2$), 2.55 (s, 3H, CH_3), 1.31 (d, *J* = 6.2 Hz, 3H, OCH(C*H*$_3$)$_2$), 1.25 (d, *J* = 6.4 Hz, 3H, OCH(C*H*$_3$)$_2$). LRMS (CI) m/z calcd. for $C_{26}H_{26}N_3O_3$ $[M+H]^+$: 428.2 found: 428.2.

(±) Isopropyl 1-benzyl-4-(furan-3-yl)-2-methyl-1,4-dihydrobenzo[4,5]imidazo[1,2-*a*]pyrimidine-3-carboxylate (271b). Purified by column chromatography (DCM–AcOEt 99:1 – 98:2). Yield: 39%. Oil at RT. ^{1}H NMR (300 MHz, $CDCl_3$), δ (ppm): 7.41 – 7.19 (m, 7H, Ar-H), 7.17 – 6.98 (m, 3H, Ar-H), 6.97 – 6.88 (m, 1H, Ar-H), 6.48 (s, 1H, CH), 6.30 – 6.24 (m, 1H, Ar-H), 5.37 – 5.19 (m, 2H, C*H*$_2$C$_6$H$_5$), 5.09 (hept, *J* = 6.1 Hz, 1H, OC*H*(CH$_3$)$_2$), 2.51 (s, 3H, CH$_3$), 1.30 (d, *J* = 6.3 Hz, 3H, OCH(C*H*$_3$)$_2$), 1.23 (d, *J* = 6.2 Hz, 3H, OCH(C*H*$_3$)$_2$). LRMS (CI) m/z calcd. for $C_{26}H_{26}N_3O_3$ $[M+H]^+$: 428.2 found: 428.2.

(±) Isopropyl 1-(2-fluorobenzyl)-4-(furan-3-yl)-2-methyl-1,4-dihydrobenzo[4,5]imidazo[1,2-*a*]pyrimidine-3-carboxylate (272a). Purified by column chromatography (DCM–AcOEt 99:1 – 98:2). Yield: 39%. Mp: 105 – 107 ºC. ^{1}H NMR (300 MHz, $CDCl_3$), δ (ppm): 7.59 (dd, *J* = 7.6, 1.3 Hz, 1H, Ar-H), 7.39 – 6.97 (m, 9H, Ar-H), 6.57 (s, 1H, CH), 6.14 (dd, *J* = 1.9, 0.9 Hz, 1H, Ar-H), 5.68 (d, *J* = 17.1 Hz, 1H, C*H*$_2$C$_6$H$_4$F), 5.44 (d, *J* = 17.1 Hz, 1H, C*H*$_2$C$_6$H$_4$F), 5.14 (hept, *J* = 6.3 Hz, 1H, OC*H*(CH$_3$)$_2$), 2.57 (s, 3H, CH$_3$), 1.34 (d, *J* = 6.2 Hz, 3H, OC*H*(C*H*$_3$)$_2$), 1.28 (d, *J* = 6.3 Hz, 3H, OC*H*(C*H*$_3$)$_2$). LRMS (CI) m/z calcd. for $C_{26}H_{25}FN_3O_3$ $[M+H]^+$: 446.2 found: 446.1.

(±) Isopropyl 10-(2-fluorobenzyl)-4-(furan-3-yl)-2-methyl-4,10-dihydrobenzo[4,5]imidazo[1,2-*a*]pyrimidine-3-carboxylate (272b). Purified by column chromatography (DCM–AcOEt 99:1 – 98:2). Yield: 46%. Oil at RT. ^{1}H NMR (300 MHz, $CDCl_3$), δ (ppm): 7.56 – 7.19 (m, 3H, Ar-H), 7.10 (t, *J* = 9.2 Hz, 6H, Ar-H), 6.49 (s, 1H, CH), 6.27 (dd, *J* = 1.9, 0.9 Hz, 1H, Ar-H), 5.35 (d, *J* = 19.5 Hz, 3H, CH + C*H*$_2$C$_6$H$_4$F), 5.11 (p, *J* = 6.2 Hz, 1H, OC*H*(CH$_3$)$_2$), 2.55 (s, 3H, CH$_3$), 1.32 (d, *J* = 6.3 Hz, 3H, OCH(C*H*$_3$)$_2$), 1.26 (d, *J* = 6.2 Hz, 3H, OCH(C*H*$_3$)$_2$). LRMS (CI) m/z calcd. for $C_{26}H_{25}FN_3O_3$ $[M+H]^+$: 446.2 found: 446.2.

(±) Isopropyl 4-(furan-2-yl)-1,2-dimethyl-1,4-dihydrobenzo[4,5]imidazo[1,2-a]pyrimidine-3-carboxylate (273a). Purified by column chromatography (DCM–AcOEt 99:1 – 98:2). Yield: 33%. Mp: 130 – 131 ºC. ^{1}H NMR (300 MHz, $CDCl_3$), δ (ppm): 7.59 – 7.50 (m, 1H, Ar-H), 7.42 – 7.33 (m, 1H, Ar-H), 7.27 – 6.92 (m, 3H, Ar-H), 6.53 (s, 1H, CH), 6.23 – 6.14 (m, 2H, Ar-H), 5.05 (hept, *J* = 6.3 Hz, 1H, OC*H*(CH$_3$)$_2$), 3.66 (s, 3H, NCH$_3$), 2.69 (s, 3H, CH$_3$), 1.28 (m, 3H, OCH(C*H*$_3$)$_2$), 1.12 (d, *J* = 6.2 Hz, 3H, OCH(C*H*$_3$)$_2$). LRMS (CI) m/z calcd. for $C_{20}H_{22}N_3O_3$ $[M+H]^+$: 352.2 found: 352.2.

(±) Isopropyl 4-(furan-2-yl)-2,10-dimethyl-4,10-dihydrobenzo[4,5]imidazo[1,2-*a*]pyrimidine-3-carboxylate (273b). Purified by column chromatography (DCM–AcOEt 99:1 – 98:2). Yield: 38%. Oil at RT. ^{1}H NMR (300 MHz, $CDCl_3$), δ (ppm): 7.36 (dd, *J* = 7.2, 1.8 Hz, 1H, Ar-H), 7.28 – 7.22 (m, 1H, Ar-H), 7.22 – 7.10 (m, 2H, Ar-H), 7.07 (dd, *J* = 7.2, 1.9 Hz, 1H, Ar-H), 6.49 (s, 1H, CH), 6.25 – 6.18 (m, 2H, Ar-H), 5.02 (p, *J* = 6.2 Hz, 1H, OC*H*$(CH_3)_2$), 3.60 (s, 3H, NCH_3), 2.57 (s, 3H, CH_3), 1.26 (d, *J* = 6.2 Hz, 3H, OCH(C*H*$_3)_2$), 1.08 (d, *J* = 6.2 Hz, 3H, OCH(C*H*$_3)_2$). LRMS (CI) m/z calcd. for $C_{20}H_{22}N_3O_3$ $[M+H]^+$: 352.2 found: 352.2.

(±) Isopropyl 1-ethyl-4-(furan-2-yl)-2-methyl-1,4-dihydrobenzo[4,5]imidazo[1,2-*a*]pyrimidine-3-carboxylate (274a). Purified by column chromatography (DCM–AcOEt 99:1 – 98:2). Yield: 22%. Mp: 120 – 122 ºC. ^{1}H NMR (300 MHz, $CDCl_3$), δ (ppm): 7.56 (d, *J* = 7.8 Hz, 1H, Ar-H), 7.37 (d, *J* = 7.7 Hz, 1H, Ar-H), 7.22 – 7.06 (m, 3H, Ar-H), 6.51 (s, 1H, CH), 6.23 – 6.14 (m, 2H, Ar-H), 5.04 (p, *J* = 6.2 Hz, 1H, OC*H*$(CH_3)_2$), 4.26 (dq, *J* = 18.4, 7.4 Hz, 2H, C*H*$_2CH_3$), 2.71 (s, 3H, CH_3), 1.40 (t, *J* = 7.0 Hz, 3H, CH_2C*H*$_3$), 1.29 (d, *J* = 6.3 Hz, 3H, OCH(C*H*$_3)_2$), 1.12 (d, *J* = 6.3 Hz, 3H, OCH(C*H*$_3)_2$). LRMS (CI) m/z calcd. for $C_{21}H_{24}N_3O_3$ $[M+H]^+$: 366.2 found: 366.1.

(±) Isopropyl 10-ethyl-4-(furan-2-yl)-2-methyl-4,10-dihydrobenzo[4,5]imidazo[1,2-*a*]pyrimidine-3-carboxylate (274b). Purified by column chromatography (DCM–AcOEt 99:1 – 98:2). Yield: 31%. Oil at RT. ^{1}H NMR (300 MHz, $CDCl_3$), δ (ppm): 7.58 (d, *J* = 7.8 Hz, 1H, Ar-H), 7.38 (d, *J* = 7.7 Hz, 1H, Ar-H), 7.23 – 7.08 (m, 3H, Ar-H), 6.51 (s, 1H, CH), 6.19 (dt, *J* = 6.3, 3.1 Hz, 2H, Ar-H), 5.05 (p, *J* = 6.3 Hz, 1H, OC*H*$(CH_3)_2$), 4.28 (dp, *J* = 26.5, 7.4 Hz, 2H, C*H*$_2CH_3$), 2.71 (s, 3H, CH_3), 1.41 (t, *J* = 7.0 Hz, 3H, CH_2C*H*$_3$), 1.29 (d, *J* = 6.2 Hz, 3H, OCH(C*H*$_3)_2$), 1.13 (d, *J* = 6.3 Hz, 3H, OCH(C*H*$_3)_2$). LRMS (CI) m/z calcd. for $C_{21}H_{24}N_3O_3$ $[M+H]^+$: 366.2 found: 366.1.

(±) Isopropyl 4-(furan-2-yl)-2-methyl-1-(prop-2-yn-1-yl)-1,4-dihydrobenzo[4,5]imidazo[1,2-*a*]pyrimidine-3-carboxylate (275a). Purified by column chromatography (DCM–AcOEt 99:1 – 98:3). Yield: 38%. Mp: 114 – 115 ºC. ^{1}H NMR (300 MHz, $CDCl_3$), δ (ppm): 7.58 (d, *J* = 7.8 Hz, 1H, Ar-H), 7.39 (d, *J* = 7.6 Hz, 1H, Ar-H), 7.24 – 7.14 (m, 2H, Ar-H), 7.13 (t, *J* = 7.4 Hz, 1H, Ar-H), 6.52 (s, 1H, CH), 6.22 – 6.18 (m, 2H, Ar-H), 5.13 – 4.79 (m, 3H, C*H*$_2$CCH + OC*H*$(CH_3)_2$), 2.84 (s, 3H, CH_3), 2.35 (s, 1H, CH_2CCH), 1.29 (d, *J* = 6.2 Hz, 3H, OCH(C*H*$_3)_2$), 1.13 (d, *J* = 6.1 Hz, 3H, OCH(C*H*$_3)_2$). ^{13}C NMR (75 MHz, $CDCl_3$), δ (ppm): 165.6, 153.4, 147.7, 146.8, 142.4, 142.2, 133.2, 122.8, 121.5, 118.2, 110.6, 109.8, 107.8, 99.8, 78.8, 73.3, 68.1, 49.7, 35.6, 22.4, 22.0, 16.0. LRMS (CI) m/z calcd. for $C_{22}H_{22}N_3O_3$ $[M+H]^+$: 376.2 found: 376.2.

(±) Isopropyl 4-(furan-2-yl)-2-methyl-10-(prop-2-yn-1-yl)-1,4-dihydrobenzo[4,5]imidazo[1,2-a]pyrimidine-3-carboxylate (275b). Purified by column chromatography (DCM–AcOEt 99:1 – 98:3). Yield: 42%. Oil at RT. ^{1}H NMR (300 MHz, $CDCl_3$), δ (ppm): 7.61 (d, *J* = 7.8 Hz, 1H, Ar-H), 7.42 (d, *J* = 7.6 Hz, 1H, Ar-H), 7.20 – 7.14 (m, 2H, Ar-H), 7.11 – 7.03 (m, 1H, Ar-H), 6.52 (s, 1H, CH), 6.20 – 6.16 (m, 2H, Ar-H), 5.16 – 4.75 (m, 3H, C*H*$_2$CCH + OC*H*$(CH_3)_2$), 2.83 (s, 3H, CH_3), 2.35 (s, 1H, CH_2CCH), 1.28 (d, *J* = 6.2 Hz, 3H, OCH(C*H*$_3)_2$), 1.12 (d, *J* = 6.2 Hz, 3H, OCH(C*H*$_3)_2$). LRMS (CI) m/z calcd. for $C_{22}H_{22}N_3O_3$ $[M+H]^+$: 376.2 found: 376.2.

(±) Isopropyl 4-(furan-2-yl)-2-methyl-1-phenethyl-4,10-dihydrobenzo[4,5]imidazo[1,2-*a*]pyrimidine-3-carboxylate (276a). Purified by column chromatography (DCM–AcOEt 99:1 – 98:3). Yield: 27%. Oil at RT. ^{1}H NMR (300 MHz, $CDCl_3$), δ (ppm): 7.73 (d, *J* = 8.2 Hz, 1H, Ar-H), 7.48 – 7.41 (m, 1H, Ar-H), 7.38 – 7.11 (m, 8H, Ar-H), 6.56 (s, 1H, Ar-H), 6.36 – 6.18 (m, 2H, Ar-H + CH), 5.05 (p, *J* = 6.2 Hz, 1H, C*H*$(CH_3)_2$), 4.73 – 4.40 (m, 1H, C*H*$_2CH_2C_6H_5$), 4.39 – 4.20 (m, 1H, C*H*$_2CH_2C_6H_5$), 3.27 – 2.99 (m, 2H, CH_2C*H*$_2C_6H_5$), 2.52 (s, 3H, CH_3), 1.29 (d, *J* = 6.3 Hz, 3H, OCH(C*H*$_3)_2$), 1.13 (d, *J* = 6.2 Hz, 3H, OCH(C*H*$_3)_2$). LRMS (CI) m/z calcd. for $C_{27}H_{28}N_3O_3$ $[M+H]^+$: 442.4 found: 442.2.

(±) Isopropyl 4-(furan-2-yl)-2-methyl-10-phenethyl-4,10-dihydrobenzo[4,5]imidazo[1,2-*a*]pyrimidine-3-carboxylate (276b). Purified by column chromatography (DCM–AcOEt 99:1 – 98:3). Yield: 33%. Oil at RT. ^{1}H NMR (300 MHz, $CDCl_3$), δ (ppm): 7.39 – 7.28 (m, 1H, Ar-H), 7.28 – 7.10 (m, 6H, Ar-H), 7.16 – 7.01 (m, 2H, Ar-H), 6.94 – 6.82 (m, 1H, Ar-H), 6.49 (s, 1H, CH), 6.22 (s, 2H, Ar-H), 5.04 (hept, J = 6.3 Hz, 1H, OC*H*$(CH_3)_2$), 4.39 – 4.20 (m, 2H, C*H*$_2$CH$_2$C$_6$H$_5$), 3.21 – 2.99 (m, 2H, CH$_2$C*H*$_2$C$_6$H$_5$), 2.57 (s, 3H, CH_3), 1.27 (d, J = 6.2 Hz, 3H, OCH(C*H*$_3$)$_2$), 1.11 (d, J = 6.2 Hz, 3H, OCH(C*H*$_3$)$_2$). LRMS (CI) m/z calcd. for $C_{27}H_{28}N_3O_3$ $[M+H]^+$: 442.4 found: 442.2.

(±) Isopropyl 1-(2-fluorophenethyl)-4-(furan-2-yl)-2-methyl-1,4-dihydrobenzo[4,5]imidazo[1,2-*a*]pyrimidine-3-carboxylate (277a). Purified by column chromatography (DCM–AcOEt 99:1 – 98:3). Yield: 18%. Mp: 158 – 160 ºC. ^{1}H NMR (300 MHz, $CDCl_3$), δ (ppm): 7.64 – 7.55 (m, 1H, Ar-H), 7.46 – 7.37 (m, 1H, Ar-H), 7.35 – 7.00 (m, 7H, Ar-H), 6.53 (s, 1H, CH), 6.22 (dd, J = 3.1, 1.1 Hz, 1H, Ar-H), 6.16 (dd, J = 3.2, 1.1 Hz, 1H, Ar-H), 5.03 (p, J = 6.3 Hz, 1H, OC*H*$(CH_3)_2$), 4.60 – 4.46 (m, 1H, C*H*$_2$CH$_2$C$_6$H$_4$F), 4.38 – 4.22 (m, 1H, C*H*$_2$CH$_2$C$_6$H$_4$F), 3.30 – 3.04 (m, 2H, CH$_2$C*H*$_2$C$_6$H$_4$F), 2.60 (s, 3H, CH_3), 1.28 (d, J = 6.2 Hz, 3H, OCH(C*H*$_3$)$_2$), 1.11 (d, J = 6.2 Hz, 3H, OCH(C*H*$_3$)$_2$). LRMS (CI) m/z calcd. for $C_{27}H_{27}FN_3O_3$ $[M+H]^+$: 459.2 found: 459.2.

(±) Isopropyl 10-(2-fluorophenethyl)-4-(furan-2-yl)-2-methyl-4,10-dihydrobenzo[4,5]imidazo[1,2-*a*]pyrimidine-3-carboxylate (277b). Purified by column chromatography (DCM–AcOEt 99:1 – 98:3). Yield: 29%. Oil at RT. ^{1}H NMR (300 MHz, $CDCl_3$), δ (ppm): 7.36 – 7.27 (m, 1H, Ar-H), 7.27 – 7.23 (m, 1H, Ar-H), 7.23 – 6.89 (m, 7H, Ar-H), 6.48 (s, 1H, CH), 6.22 (d, J = 1.3 Hz, 2H, Ar-H), 5.03 (p, J = 6.2 Hz, 1H, OC*H*$(CH_3)_2$), 4.28 (td, J = 7.2, 4.4 Hz, 2H, C*H*$_2$CH$_2$C$_6$H$_4$F), 3.13 (t, J = 7.4 Hz, 2H, CH$_2$C*H*$_2$C$_6$H$_4$F), 2.54 (s, 3H, CH_3), 1.27 (d, J = 6.2 Hz, 3H, OCH(C*H*$_3$)$_2$), 1.10 (d, J = 6.2 Hz, 3H, OCH(C*H*$_3$)$_2$). LRMS (CI) m/z calcd. for $C_{27}H_{27}FN_3O_3$ $[M+H]^+$: 459.2 found: 459.2.

(±) Isopropyl 1-(4-cyano-2-fluorobenzyl)-4-(furan-2-yl)-2-methyl-1,4-dihydrobenzo[4,5]imidazo[1,2-*a*]pyrimidine-3-carboxylate (278a). Purified by column chromatography (DCM–AcOEt 99:1 – 98:3). Yield: 22%. Oil at RT. ^{1}H NMR (300 MHz, $CDCl_3$), δ (ppm): 7.62 (t, *J* = 7.5 Hz, 1H, Ar-H), 7.54 – 7.07 (m, 7H, Ar-H), 6.59 (s, 1H, CH), 6.30 – 6.19 (m, 2H, Ar-H), 5.70 (d, *J* = 18.0 Hz, 1H, OC*H*$_2$C$_6$H$_3$FCN), 5.43 (d, *J* = 18.0 Hz, 1H, OC*H*$_2$C$_6$H$_3$FCN), 5.05 (hept, *J* = 6.3 Hz, 1H, OC*H*(CH$_3$)$_2$), 2.56 (s, 3H, CH$_3$), 1.30 (d, *J* = 6.2 Hz, 3H, OCH(C*H*$_3$)$_2$), 1.15 (d, *J* = 6.2 Hz, 3H, OCH(C*H*$_3$)$_2$). LRMS (CI) m/z calcd. for $C_{27}H_{24}FN_4O_3$ $[M+H]^+$: 471.2 found: 471.2.

(±) Isopropyl 10-(4-cyano-2-fluorobenzyl)-4-(furan-2-yl)-2-methyl-4,10-dihydrobenzo[4,5]imidazo[1,2-*a*]pyrimidine-3-carboxylate (278b). Purified by column chromatography (DCM–AcOEt 99:1 – 98:3). Yield: 22%. Oil at RT. ^{1}H NMR (300 MHz, $CDCl_3$), δ (ppm): 7.49 – 7.30 (m, 4H, Ar-H), 7.30 – 7.20 (m, 1H, Ar-H), 7.20 – 7.02 (m, 2H, Ar-H), 7.02 – 6.89 (m, 1H, Ar-H), 6.51 (s, 1H, CH), 6.33 – 6.18 (m, 2H, Ar-H), 5.34 (s, 2H, C*H*$_2$C$_6$H$_3$FCN), 5.16 – 4.90 (m, 1H, O*CH*(CH$_3$)$_2$), 2.53 (d, *J* = 1.3 Hz, 3H, CH$_3$), 1.32 (d, *J* = 6.3 Hz, 3H, OCH(C*H*$_3$)$_2$), 1.10 (d, *J* = 6.2 Hz, 3H, OCH(C*H*$_3$)$_2$). LRMS (CI) m/z calcd. for $C_{27}H_{24}FN_4O_3$ $[M+H]^+$: 471.2 found: 471.2.

(±) Isopropyl 1-(3-fluorobenzyl)-4-(furan-2-yl)-2-methyl-1,4-dihydrobenzo[4,5]imidazo[1,2-*a*]pyrimidine-3-carboxylate (279a). Purified by column chromatography (DCM–AcOEt 99:1 – 98:3). Yield: 22%. Oil at RT. ^{1}H NMR (300 MHz, $CDCl_3$), δ (ppm): 7.54 (d, *J* = 7.6 Hz, 1H, Ar-H), 7.39 (d, *J* = 7.6 Hz, 1H, Ar-H), 7.36 – 7.22 (m, 2H, Ar-H), 7.25 – 7.03 (m, 4H, Ar-H), 6.95 (t, *J* = 8.6 Hz, 1H, Ar-H), 6.59 (s, 1H, CH), 6.31 – 6.20 (m, 2H, CH + Ar-H), 5.77 (d, *J* = 17.1 Hz, 1H, C*H*$_2$C$_6$H$_5$), 5.28 (d, *J* = 17.2 Hz, 1H, C*H*$_2$C$_6$H$_5$), 5.12 – 4.98 (m, 1H, OC*H*(CH$_3$)$_2$), 2.58 (s, 3H, CH$_3$), 1.30 (d, *J* = 6.2 Hz, 3H, OCH(C*H*$_3$)$_2$), 1.15 (d, *J* = 6.3 Hz, 3H, OCH(C*H*$_3$)$_2$). LRMS (CI) m/z calcd. for $C_{26}H_{25}FN_3O_3$ $[M+H]^+$: 446.2 found: 446.2.

(±) Isopropyl 10-(3-fluorobenzyl)-4-(furan-2-yl)-2-methyl-4,10-dihydrobenzo[4,5]imidazo[1,2-*a*]pyrimidine-3-carboxylate (279b). Purified by column chromatography (DCM–AcOEt 99:1 – 98:3). Yield: 27%. Oil at RT. ^{1}H NMR (300 MHz, $CDCl_3$), δ (ppm): 7.38 – 7.22 (m, 3H, Ar-H), 7.09 (p, *J* = 7.9 Hz, 3H, Ar-H), 7.04 – 6.86 (m, 3H, Ar-H), 6.53 (s, 1H, CH), 6.30 – 6.19 (m, 2H, Ar-H), 5.26 (q, *J* = 15.9 Hz, 2H, C*H*$_2$C$_6$H$_4$F), 5.04 (p, *J* = 6.2 Hz, 1H, OC*H*(CH$_3$)$_2$), 2.56 (s, 3H, CH$_3$), 1.27 (d, *J* = 6.2 Hz, 3H, OCH(C*H*$_3$)$_2$), 1.11 (d, *J* = 6.2 Hz, 3H, OCH(C*H*$_3$)$_2$). LRMS (CI) m/z calcd. for $C_{26}H_{25}FN_3O_3$ $[M+H]^+$: 446.2 found: 446.2.

(±) Isopropyl 1-(4-fluorobenzyl)-4-(furan-2-yl)-2-methyl-1,4-dihydrobenzo[4,5]imidazo[1,2-*a*]pyrimidine-3-carboxylate (280a). Purified by column chromatography (DCM–AcOEt 99:1 – 98:3). Yield: 28%. Mp: 153 – 155 ºC. ^{1}H NMR (300 MHz, $CDCl_3$), δ (ppm): 7.55 (d, *J* = 7.6 Hz, 1H, Ar-H), 7.40 (d, *J* = 7.5 Hz, 1H, Ar-H), 7.29 – 7.12 (m, 4H, Ar-H), 7.01 (t, *J* = 8.6 Hz, 3H, Ar-H), 6.58 (s, 1H, CH), 6.26 – 6.18 (m, 2H, Ar-H), 5.70 (d, *J* = 16.8 Hz, 1H, C*H*$_2$C$_6$H$_4$F), 5.28 (d, *J* = 15.8 Hz, 1H, C*H*$_2$C$_6$H$_4$F), 5.11 – 4.99 (m, 1H, OC*H*(CH$_3$)$_2$), 2.59 (s, 3H, CH$_3$), 1.29 (d, *J* = 6.3 Hz, 3H, OCH(C*H*$_3$)$_2$), 1.13 (d, *J* = 6.3 Hz, 3H, OCH(C*H*$_3$)$_2$). LRMS (CI) m/z calcd. for $C_{26}H_{25}FN_3O_3$ $[M+H]^+$: 446.2 found: 446.2.

(±) Isopropyl 10-(4-fluorobenzyl)-4-(furan-2-yl)-2-methyl-4,10-dihydrobenzo[4,5]imidazo[1,2-*a*]pyrimidine-3-carboxylate (280b). Purified by column chromatography (DCM–AcOEt 99:1 – 98:3). Yield: 33%. Oil at RT. ^{1}H NMR (300 MHz, $CDCl_3$), δ (ppm): 7.38 – 7.21 (m, 5H, Ar-H), 7.15 – 6.87 (m, 4H, Ar-H), 6.52 (s, 1H, CH), 6.29 – 6.19 (m, 2H, Ar-H), 5.41 – 5.12 (m, 2H, C*H*$_2$C$_6$H$_4$F), 5.03 (p, *J* = 6.2 Hz, 1H, OC*H*(CH$_3$)$_2$), 2.56 (s, 3H, CH$_3$), 1.28 (d, *J* = 6.2 Hz, 3H, OCH(C*H*$_3$)$_2$), 1.11 (d, *J* = 6.2 Hz, 3H, OCH(C*H*$_3$)$_2$). LRMS (CI) m/z calcd. for $C_{26}H_{25}FN_3O_3$ $[M+H]^+$: 446.2 found: 446.2.

(±) Isopropyl 1-(2,3-difluorobenzyl)-4-(furan-2-yl)-2-methyl-1,4-dihydrobenzo[4,5]imidazo[1,2-*a*]pyrimidine-3-carboxylate (281a). Purified by column chromatography (DCM–AcOEt 99:1 – 98:3). Yield: 33%. Oil at RT. ^{1}H NMR (300 MHz, $CDCl_3$), δ (ppm): 7.54 (d, *J* = 6.9 Hz, 1H, Ar-H), 7.40 (d, *J* = 7.0 Hz, 1H, Ar-H), 7.29 – 7.07 (m, 4H, Ar-H), 7.12 – 7.00 (m, 1H, Ar-H), 7.05 – 6.91 (m, 1H, Ar-H), 6.59 (s, 1H, CH), 6.27 – 6.19 (m, 2H, Ar-H), 5.72 (d, *J* = 17.4 Hz, 1H, C*H*$_2$C$_6$H$_3$F$_2$), 5.43 (d, *J* = 17.4 Hz, 1H, C*H*$_2$C$_6$H$_3$F$_2$), 5.05 (hept, *J* = 6.2 Hz, 1H, OC*H*(CH$_3$)$_2$), 2.59 (s, 3H, CH$_3$), 1.30 (d, *J* = 6.2 Hz, 3H, OCH(C*H*$_3$)$_2$), 1.14 (d, *J* = 6.2 Hz, 3H, OCH(C*H*$_3$)$_2$). LRMS (CI) m/z calcd. for $C_{26}H_{24}F_2N_3O_3$ $[M+H]^+$: 464.2 found: 464.2.

(±) Isopropyl 10-(2,3-difluorobenzyl)-4-(furan-2-yl)-2-methyl-4,10-dihydrobenzo[4,5]imidazo[1,2-*a*]pyrimidine-3-carboxylate (281b). Purified by column chromatography (DCM–AcOEt 99:1 – 98:3). Yield: 42%. Oil at RT. ^{1}H NMR (300 MHz, $CDCl_3$), δ (ppm): 7.38 – 7.28 (m, 1H, Ar-H), 7.28 – 7.21 (m, 2H, Ar-H), 7.20 – 6.90 (m, 5H, Ar-H), 6.51 (s, 1H, CH), 6.29 – 6.18 (m, 2H, Ar-H), 5.44 – 5.25 (m, 2H, C*H*$_2$C$_6$H$_3$F$_2$), 5.03 (hept, *J* = 6.2 Hz, 1H, OC*H*(CH$_3$)$_2$), 2.56 (s, 3H, CH$_3$), 1.26 (d, *J* = 6.2 Hz, 3H, OCH(C*H*$_3$)$_2$), 1.11 (d, *J* = 6.2 Hz, 3H, OCH(C*H*$_3$)$_2$). LRMS (CI) m/z calcd. for $C_{26}H_{24}F_2N_3O_3$ $[M+H]^+$: 464.2 found: 464.2.

(±) Isopropyl 1-(2,4-difluorobenzyl)-4-(furan-2-yl)-2-methyl-1,4-dihydrobenzo[4,5]imidazo[1,2-*a*]pyrimidine-3-carboxylate (282a). Purified by column chromatography (DCM–AcOEt 99:1 – 98:3). Yield: 32%. Mp: 140 – 142 ºC. ^{1}H NMR (300 MHz, $CDCl_3$), δ (ppm): 7.56 – 7.47 (m, 1H, 13), 7.44 – 7.11 (m, 4H, Ar-H), 6.91 – 6.70 (m, 3H, Ar-H), 6.60 – 6.54 (m, 1H, CH), 6.23 (d, *J* = 1.4 Hz, 2H, Ar-H), 5.62 (d, *J* = 17.2 Hz, 1H, C*H*$_2$C$_6$H$_3$F$_2$), 5.32 (d, *J* = 17.2 Hz, 1H, C*H*$_2$C$_6$H$_3$F$_2$), 5.05 (p, *J* = 6.3 Hz, 1H, OC*H*(CH$_3$)$_2$), 2.58 (s, 3H, CH$_3$), 1.30 (d, *J* = 6.2 Hz, 3H, OCH(C*H*$_3$)$_2$), 1.14 (d, *J* = 6.2 Hz, 3H, OCH(C*H*$_3$)$_2$). LRMS (CI) m/z calcd. for $C_{26}H_{24}F_2N_3O_3$ $[M+H]^+$: 464.2 found: 464.2.

(±) Isopropyl 10-(2,4-difluorobenzyl)-4-(furan-2-yl)-2-methyl-4,10-dihydrobenzo[4,5]imidazo[1,2-*a*]pyrimidine-3-carboxylate (282b). Purified by column chromatography (DCM–AcOEt 99:1 – 98:3). Yield: 41%. Oil at RT. ^{1}H NMR (300 MHz, $CDCl_3$), δ (ppm): 7.47 – 7.29 (m, 2H, Ar-H), 7.29 – 7.20 (m, 1H, Ar-H), 7.19 – 7.03 (m, 2H, Ar-H), 7.08 – 6.96 (m, 1H, Ar-H), 6.92 – 6.73 (m, 2H, Ar-H), 6.51 (s, 1H, CH), 6.28 – 6.18 (m, 2H, Ar-H), 5.37 – 5.17 (m, 2H, C*H*$_2$C$_6$H$_3$F$_2$), 5.03 (hept, *J* = 6.1 Hz, 1H, OC*H*(CH$_3$)$_2$), 2.56 (s, 3H, CH$_3$), 1.26 (d, *J* = 6.2 Hz, 3H, OCH(C*H*$_3$)$_2$), 1.11 (d, *J* = 6.2 Hz, 3H, OCH(C*H*$_3$)$_2$). LRMS (CI) m/z calcd. for $C_{26}H_{24}F_2N_3O_3$ $[M+H]^+$: 464.2 found: 464.2.

(±) Isopropyl 1-(2,5-difluorobenzyl)-4-(furan-2-yl)-2-methyl-1,4-dihydrobenzo[4,5]imidazo[1,2-*a*]pyrimidine-3-carboxylate (283a). Purified by column chromatography (DCM–AcOEt 99:1 – 98:3). Yield: 26%. Mp: 103 – 105 ºC. ^{1}H NMR (300 MHz, $CDCl_3$), δ (ppm): 7.60 – 7.47 (m, 1H, Ar-H), 7.37 (dd, *J* = 7.9, 1.5 Hz, 1H, Ar-H), 7.28 – 6.82 (m, 6H, Ar-H), 6.58 (s, 1H, CH), 6.30 (dd, *J* = 3.3, 0.8 Hz, 1H, Ar-H), 6.24 (dd, *J* = 3.3, 1.8 Hz, 1H, Ar-H), 5.73 (d, *J* = 17.7 Hz, 1H, C*H*$_2$C$_6$H$_3$F$_2$), 5.31 (d, *J* = 17.6 Hz, 1H, C*H*$_2$C$_6$H$_3$F$_2$), 5.06 (p, *J* = 6.3 Hz, 1H, OC*H*(CH$_3$)$_2$), 2.63 – 2.52 (m, 3H, CH$_3$), 1.31 (d, *J* = 6.2 Hz, 3H, OCH(C*H*$_3$)$_2$), 1.17 (d, *J* = 6.2 Hz, 3H, OCH(C*H*$_3$)$_2$). LRMS (CI) m/z calcd. for $C_{26}H_{24}F_2N_3O_3$ $[M+H]^+$: 464.2 found: 464.2.

(±) Isopropyl 10-(2,5-difluorobenzyl)-4-(furan-2-yl)-2-methyl-4,10-dihydrobenzo[4,5]imidazo[1,2-*a*]pyrimidine-3-carboxylate (283b). Purified by column chromatography (DCM–AcOEt 99:1 – 98:3). Yield: 32%. Oil at RT. ^{1}H NMR (300 MHz, $CDCl_3$), δ (ppm): 7.37 – 7.28 (m, 1H, Ar-H), 7.28 – 7.20 (m, 1H, Ar-H), 7.19 – 6.85 (m, 6H, Ar-H), 6.51 (s, 1H, CH), 6.30 – 6.18 (m, 2H, Ar-H), 5.38 – 5.20 (m, 2H, C*H*$_2$C$_6$H$_3$F$_2$), 5.04 (p, *J* = 6.2 Hz, 1H, OC*H*(CH$_3$)$_2$), 2.56 (s, 3H, CH$_3$), 1.27 (d, *J* = 6.2 Hz, 3H, OCH(C*H*$_3$)$_2$), 1.12 (d, *J* = 6.2 Hz, 3H, OCH(C*H*$_3$)$_2$). LRMS (CI) m/z calcd. for $C_{26}H_{24}F_2N_3O_3$ $[M+H]^+$: 464.2 found: 464.2.

(±) Isopropyl 1-(2,6-difluorobenzyl)-4-(furan-2-yl)-2-methyl-1,4-dihydrobenzo[4,5]imidazo[1,2-*a*]pyrimidine-3-carboxylate (284a). Purified by column chromatography (DCM–AcOEt 99:1 – 98:3). Yield: 22%. Mp: 126 – 128 ºC. ^{1}H NMR (300 MHz, $CDCl_3$), δ (ppm): 7.65 – 7.49 (m, 1H, Ar-H), 7.48 – 7.37 (m, 1H, Ar-H), 7.34 – 7.07 (m, 5H, Ar-H), 6.87 (t, *J* = 8.2 Hz, 1H, Ar-H), 6.54 (s, 1H, CH), 6.19 (dd, *J* = 3.3, 1.8 Hz, 1H, Ar-H), 6.14 – 6.07 (m, 1H, Ar-H), 5.95 (d, *J* = 16.5 Hz, 1H, C*H*$_2$C$_6$H$_3$F$_2$), 5.38 – 5.25 (m, 1H, C*H*$_2$C$_6$H$_3$F$_2$), 5.02 (p, *J* = 6.2 Hz, 1H, OC*H*(CH$_3$)$_2$), 2.64 (s, 3H, CH$_3$), 1.27 (d, *J* = 6.2 Hz, 3H, OCH(C*H*$_3$)$_2$), 1.08 (d, *J* = 6.2 Hz, 3H, OCH(C*H*$_3$)$_2$). HRMS (CI) m/z calcd. for $C_{26}H_{24}F_2N_3O_3$ $[M+H]^+$: 464.1707 found: 464.1716.

(±) Isopropyl 10-(2,6-difluorobenzyl)-4-(furan-2-yl)-2-methyl-4,10-dihydrobenzo[4,5]imidazo[1,2-*a*]pyrimidine-3-carboxylate (284b). Purified by column chromatography (DCM–AcOEt 99:1 – 98:3). Yield: 22%. Oil at RT. ^{1}H NMR (300 MHz, $CDCl_3$), δ (ppm): 7.41 – 7.20 (m, 3H, Ar-H), 7.17 – 6.94 (m, 3H, Ar-H), 6.88 (t, *J* = 7.9 Hz, 2H, Ar-H), 6.49 (s, 1H, CH), 6.29 – 6.13 (m, 2H, Ar-H), 5.50 – 5.24 (m, 2H, C*H*$_2$C$_6$H$_3$F$_2$), 5.11 – 4.91 (m, 1H, OC*H*(CH$_3$)$_2$), 2.57 (s, 3H, CH$_3$), 1.26 (d, *J* = 6.2 Hz, 3H, OCH(C*H*$_3$)$_2$), 1.09 (d, *J* = 6.2 Hz, 3H, OCH(C*H*$_3$)$_2$). LRMS (CI) m/z calcd. for $C_{26}H_{24}F_2N_3O_3$ $[M+H]^+$: 464.2 found: 464.2.

(±) Isopropyl 1-(3,5-difluorobenzyl)-4-(furan-2-yl)-2-methyl-1,4-dihydrobenzo[4,5]imidazo[1,2-*a*]pyrimidine-3-carboxylate (285a). Purified by column chromatography (DCM–AcOEt 99:1 – 98:3). Yield: 16%. Mp: 126 – 128 ºC. ^{1}H NMR (500 MHz, $CDCl_3$), δ (ppm): 7.55 (d, *J* = 8.0 Hz, 1H, Ar-H), 7.41 – 7.36 (m, 1H, Ar-H), 7.27 (s, 1H, Ar-H), 7.25 – 7.13 (m, 2H, Ar-H), 6.97 – 6.89 (m, 2H, Ar-H), 6.77 – 6.69 (m, 1H, Ar-H), 6.60 (s, 1H, CH), 6.32 (dd, *J* = 3.3, 0.8 Hz, 1H, Ar-H), 6.29 – 6.24 (m, 1H, Ar-H), 5.82 (d, *J* = 17.4 Hz, 1H, C*H*$_2$C$_6$H$_3$F$_2$), 5.24 (d, *J* = 17.5 Hz, 1H, C*H*$_2$C$_6$H$_3$F$_2$), 5.07 (p, *J* = 6.2 Hz, 1H, OC*H*(CH$_3$)$_2$), 2.59 (s, 3H, CH$_3$), 1.32 (d, *J* = 6.2 Hz, 3H, OCH(C*H*$_3$)$_2$), 1.18 (d, *J* = 6.2 Hz, 3H, OCH(C*H*$_3$)$_2$). LRMS (CI) m/z calcd. for $C_{26}H_{24}F_2N_3O_3$ $[M+H]^+$: 464.2 found: 464.2.

(±) Isopropyl 10-(3,5-difluorobenzyl)-4-(furan-2-yl)-2-methyl-4,10-dihydrobenzo[4,5]imidazo[1,2-*a*]pyrimidine-3-carboxylate (285b). Purified by column chromatography (DCM–AcOEt 99:1 – 98:3). Yield: 18%. Oil at RT. ^{1}H NMR (500 MHz, $CDCl_3$), δ (ppm): 7.38 – 7.33 (m, 1H, Ar-H), 7.26 (dd, *J* = 1.8, 0.9 Hz, 1H, Ar-H), 7.15 (td, *J* = 7.7, 1.2 Hz, 1H, Ar-H), 7.14 – 7.07 (m, 2H, Ar-H), 6.94 – 6.88 (m, 1H, Ar-H), 6.88 – 6.80 (m, 2H, Ar-H), 6.77 – 6.67 (m, 1H, Ar-H), 6.54 (s, 1H, CH), 6.31 – 6.22 (m, 2H, Ar-H), 5.34 – 5.18 (m, 1H, C*H*$_2$C$_6$H$_3$F$_2$), 5.06 (p, *J* = 6.2 Hz, 1H, OC*H*(CH$_3$)$_2$), 2.56 (s, 3H, CH$_3$), 1.29 (d, *J* = 6.2 Hz, 3H, OCH(C*H*$_3$)$_2$), 1.14 (d, *J* = 6.2 Hz, 3H, OCH(C*H*$_3$)$_2$). LRMS (CI) m/z calcd. for $C_{26}H_{24}F_2N_3O_3$ $[M+H]^+$: 464.2 found: 464.2.

(±) Isopropyl 4-(furan-2-yl)-2-methyl-1-(2,4,6-trifluorobenzyl)-1,4-dihydrobenzo[4,5]imidazo[1,2-*a*]pyrimidine-3-carboxylate (286a). Purified by column chromatography (DCM–AcOEt 99:1 – 98:3). Yield: 38%. Oil at RT. ^{1}H NMR (300 MHz, $CDCl_3$), δ (ppm): 7.54 (m, 1H, Ar-H), 7.43 (dd, *J* = 7.0, 2.0 Hz, 1H, Ar-H), 7.29 – 7.16 (m, 2H, Ar-H), 7.22 – 7.13 (m, 1H, Ar-H), 6.53 (d, *J* = 2.5 Hz, 1H, CH), 6.44 (s, 2H, Ar-H), 6.20 (dd, *J* = 3.4, 1.9 Hz, 1H, Ar-H), 6.11 (d, *J* = 3.2 Hz, 1H, Ar-H), 5.81 (d, *J* = 16.3 Hz, 1H, C*H*$_2$C$_6$H$_2$F$_3$), 5.31 (d, *J* = 16.9 Hz, 1H, C*H*$_2$C$_6$H$_2$F$_3$), 5.12 – 4.94 (m, 1H, OC*H*(CH$_3$)$_2$), 2.64 (d, *J* = 2.2 Hz, 3H, CH$_3$), 1.30 (d, *J* = 6.2 Hz, 3H, OCH(C*H*$_3$)$_2$), 1.11 (d, *J* = 6.2 Hz, 3H, OCH(C*H*$_3$)$_2$). LRMS (CI) m/z calcd. for $C_{26}H_{23}F_3N_3O_3$ $[M+H]^+$: 481.2 found: 481.2.

(±) Isopropyl 4-(furan-2-yl)-2-methyl-10-(2,4,6-trifluorobenzyl)-4,10-dihydrobenzo[4,5]imidazo[1,2-*a*]pyrimidine-3-carboxylate (286b). Purified by column chromatography (DCM–AcOEt 99:1 – 98:3). Yield: 42%. Oil at RT. ^{1}H NMR (300 MHz, $CDCl_3$), δ (ppm): 7.52 (d, *J* = 7.2 Hz, 1H, Ar-H), 7.40 – 7.27 (m, 1H, Ar-H), 7.27 – 7.19 (m, 1H, Ar-H), 7.19 – 6.93 (m, 3H, Ar-H), 6.74 – 6.57 (m, 2H, Ar-H), 6.48 (s, 1H, CH), 6.27 – 6.16 (m, 1H, Ar-H), 5.45 – 5.16 (m, 2H, OC*H*$_2$C$_6$H$_2$F$_3$), 5.10 – 4.95 (m, 1H, OC*H*(CH$_3$)$_2$), 2.56 (s, 3H, CH$_3$), 1.26 (d, *J* = 6.3 Hz, 3H, OCH(C*H*$_3$)$_2$), 1.10 (d, *J* = 6.3 Hz, 3H, OCH(C*H*$_3$)$_2$). LRMS (CI) m/z calcd. for $C_{26}H_{23}F_3N_3O_3$ $[M+H]^+$: 481.2 found: 481.2.

(±) Isopropyl 1-(2-chlorobenzyl)-4-(furan-2-yl)-2-methyl-1,4-dihydrobenzo[4,5]imidazo[1,2-*a*]pyrimidine-3-carboxylate (287a). Purified by column chromatography (DCM–AcOEt 99:1 – 98:3). Yield: 22%. Mp: 128 – 130 ºC. ^{1}H NMR (300 MHz, $CDCl_3$), δ (ppm): 7.60 – 7.48 (m, 1H, Ar-H), 7.48 – 7.35 (m, 2H, Ar-H), 7.29 – 7.05 (m, 6H, Ar-H), 6.68 – 6.55 (m, 1H, CH), 6.36 – 6.18 (m, 2H, Ar-H), 5.72 (d, *J* = 17.8 Hz, 1H, C*H*$_2$C$_6$H$_4$Cl), 5.45 (d, *J* = 17.8 Hz, 1H, C*H*$_2$C$_6$H$_4$Cl), 5.05 (hept, *J* = 6.2 Hz, 1H, OC*H*(CH$_3$)$_2$), 2.54 (s, 3H, CH_3), 1.30 (d, *J* = 6.3 Hz, 3H, OCH(C*H*$_3$)$_2$), 1.14 (d, *J* = 6.2 Hz, 3H, OCH(C*H*$_3$)$_2$). LRMS (CI) m/z calcd. for $C_{26}H_{25}ClN_3O_3$ $[M+H]^+$: 462.1 found: 462.2.

(±) Isopropyl 10-(2-chlorobenzyl)-4-(furan-2-yl)-2-methyl-4,10-dihydrobenzo[4,5]imidazo[1,2-*a*]pyrimidine-3-carboxylate (287b). Purified by column chromatography (DCM–AcOEt 99:1 – 98:3). Yield: 28%. Oil at RT. ^{1}H NMR (300 MHz, $CDCl_3$), δ (ppm): 7.49 – 7.30 (m, 2H, Ar-H), 7.30 – 6.95 (m, 6H, Ar-H), 6.90 (d, *J* = 7.7 Hz, 1H, Ar-H), 6.54 (s, 1H, CH), 6.33 – 6.19 (m, 2H, Ar-H), 5.40 (s, 2H, C*H*$_2$C$_6$H$_4$Cl), 5.04 (p, *J* = 6.2 Hz, 1H, OC*H*(CH$_3$)$_2$), 2.53 (s, 3H, CH_3), 1.27 (d, *J* = 6.3 Hz, 3H, OCH(C*H*$_3$)$_2$), 1.11 (d, *J* = 6.2 Hz, 3H, OCH(C*H*$_3$)$_2$). LRMS (CI) m/z calcd. for $C_{26}H_{25}ClN_3O_3$ $[M+H]^+$: 462.1 found: 462.2.

(±) Isopropyl 1-(3-chlorobenzyl)-4-(furan-2-yl)-2-methyl-1,4-dihydrobenzo[4,5]imidazo[1,2-*a*]pyrimidine-3-carboxylate (288a). Purified by column chromatography (DCM–AcOEt 99:1 – 98:3). Yield: 21%. Oil at RT. ^{1}H NMR (300 MHz, $CDCl_3$), δ (ppm): 7.52 (d, *J* = 7.1 Hz, 1H, Ar-H), 7.46 – 7.06 (m, 8H, Ar-H), 6.57 (s, 1H, CH), 6.38 – 6.13 (m, 2H, Ar-H), 5.75 (d, *J* = 17.2 Hz, 1H, C*H*$_2$C$_6$H$_4$Cl), 5.16 (d, *J* = 17.2 Hz, 1H, C*H*$_2$C$_6$H$_4$Cl), 5.05 (p, *J* = 6.2 Hz, 1H, OC*H*(CH$_3$)$_2$), 2.56 (s, 3H, CH_3), 1.30 (d, *J* = 6.2 Hz, 3H, OCH(C*H*$_3$)$_2$), 1.15 (d, *J* = 6.2 Hz, 3H, OCH(C*H*$_3$)$_2$). LRMS (CI) m/z calcd. for $C_{26}H_{25}ClN_3O_3$ $[M+H]^+$: 462.1 found: 462.2.

(±) Isopropyl 10-(3-chlorobenzyl)-4-(furan-2-yl)-2-methyl-4,10-dihydrobenzo[4,5]imidazo[1,2-*a*]pyrimidine-3-carboxylate (288b). Purified by column chromatography (DCM–AcOEt 99:1 – 98:3). Yield: 33%. Oil at RT. ^{1}H NMR (300 MHz, $CDCl_3$), δ (ppm): 7.37 – 7.01 (m, 8H, Ar-H), 6.89 (dt, *J* = 7.1, 1.4 Hz, 1H, Ar-H), 6.52 (s, 1H, CH), 6.37 – 6.18 (m, 2H, Ar-H), 5.35 – 5.11 (m, 2H, OC*H*$_2$C$_6$H$_4$Cl), 5.11 – 4.95 (m, 1H, OC*H*(CH$_3$)$_2$), 2.55 (d, *J* = 1.1 Hz, 3H, CH$_3$), 1.27 (dd, *J* = 6.3, 1.2 Hz, 3H, OCH(C*H*$_3$)$_2$), 1.12 (dd, *J* = 6.2, 1.2 Hz, 3H, OCH(C*H*$_3$)$_2$). LRMS (CI) m/z calcd. for $C_{26}H_{25}ClN_3O_3$ $[M+H]^+$: 462.1 found: 462.2.

(±) Isopropyl 1-(4-chlorobenzyl)-4-(furan-2-yl)-2-methyl-1,4-dihydrobenzo[4,5]imidazo[1,2-*a*]pyrimidine-3-carboxylate (289a). Purified by column chromatography (DCM–AcOEt 99:1 – 98:3). Yield: 37%. Mp: 172 – 174 ºC. ^{1}H NMR (300 MHz, $CDCl_3$), δ (ppm): 7.60 – 7.49 (m, 1H, Ar-H), 7.47 – 7.34 (m, 1H, Ar-H), 7.35 – 7.04 (m, 7H, Ar-H), 6.58 (s, 1H, CH), 6.34 – 6.18 (m, 2H, Ar-H), 5.69 (d, *J* = 16.8 Hz, 1H, C*H*$_2$C$_6$H$_4$Cl), 5.27 (d, *J* = 14.7 Hz, 1H, C*H*$_2$C$_6$H$_4$Cl), 5.16 – 4.90 (m, 1H, OC*H*(CH$_3$)$_2$), 2.57 (s, 3H, CH$_3$), 1.29 (dd, *J* = 6.2, 1.3 Hz, 3H, OCH(C*H*$_3$)$_2$), 1.13 (dd, *J* = 6.2, 1.3 Hz, 3H, OCH(C*H*$_3$)$_2$). LRMS (CI) m/z calcd. for $C_{26}H_{25}ClN_3O_3$ $[M+H]^+$: 462.1 found: 462.2.

(±) Isopropyl 10-(4-chlorobenzyl)-4-(furan-2-yl)-2-methyl-4,10-dihydrobenzo[4,5]imidazo[1,2-*a*]pyrimidine-3-carboxylate (289b). Purified by column chromatography (DCM–AcOEt 99:1 – 98:3). Yield: 44%. Oil at RT. ^{1}H NMR (300 MHz, $CDCl_3$), δ (ppm): 7.50 – 7.20 (m, 6H, Ar-H), 7.20 – 6.99 (m, 2H, Ar-H), 6.89 (d, *J* = 7.6 Hz, 1H, Ar-H), 6.52 (s, 1H, CH), 6.32 – 6.17 (m, 2H, Ar-H), 5.38 – 5.11 (m, 2H, C*H*$_2$C$_6$H$_4$Cl), 5.03 (p, *J* = 6.2 Hz, 1H, OC*H*(CH$_3$)$_2$), 2.55 (s, 3H, CH$_3$), 1.26 (d, *J* = 6.3 Hz, 3H, OCH(C*H*$_3$)$_2$), 1.11 (d, *J* = 6.2 Hz, 3H, OCH(C*H*$_3$)$_2$). LRMS (CI) m/z calcd. for $C_{26}H_{25}ClN_3O_3$ $[M+H]^+$: 462.1 found: 462.2.

(±) Isopropyl 1-(3-chloro-2-fluorobenzyl)-4-(furan-2-yl)-2-methyl-1,4-dihydrobenzo[4,5]imidazo[1,2-*a*]pyrimidine-3-carboxylate (290a). Purified by column chromatography (DCM–AcOEt 99:1 – 98:3). Yield: 32%. Mp: 102 – 104 ºC. ^{1}H NMR (300 MHz, $CDCl_3$), δ (ppm): 7.61 – 7.45 (m, 1H, Ar-H), 7.45 – 7.35 (m, 1H, Ar-H), 7.35 – 7.08 (m, 4H, Ar-H), 7.08 – 6.86 (m, 2H, Ar-H), 6.58 (s, 1H, CH), 6.35 – 6.13 (m, 2H, Ar-H), 5.65 (d, *J* = 17.5 Hz, 1H, C*H*$_2$C$_6$H$_3$ClF), 5.36 (d, *J* = 17.5 Hz, 1H, C*H*$_2$C$_6$H$_3$ClF), 5.05 (hept, *J* = 6.2 Hz, 1H, OC*H*(CH$_3$)$_2$), 2.57 (s, 3H, CH$_3$), 1.30 (d, *J* = 6.2 Hz, 3H, OCH(C*H*$_3$)$_2$), 1.15 (d, *J* = 6.2 Hz, 3H, OCH(C*H*$_3$)$_2$). LRMS (CI) m/z calcd. for $C_{26}H_{24}ClFN_3O_3$ $[M+H]^+$: 480.1 found: 480.1.

(±) Isopropyl 10-(3-chloro-2-fluorobenzyl)-4-(furan-2-yl)-2-methyl-4,10-dihydrobenzo[4,5]imidazo[1,2-*a*]pyrimidine-3-carboxylate (290b). Purified by column chromatography (DCM–AcOEt 99:1 – 98:3). Yield: 42%. Oil at RT. ^{1}H NMR (300 MHz, $CDCl_3$), δ (ppm): 7.61 – 6.83 (m, 8H, Ar-H), 6.51 (s, 1H, CH), 6.33 – 6.18 (m, 2H, Ar-H), 5.41 – 5.23 (m, 2H, C*H*$_2$C$_6$H$_3$ClF), 5.04 (hept, *J* = 6.2 Hz, 1H, OC*H*(CH$_3$)$_2$), 2.56 (s, 3H, CH$_3$), 1.27 (d, *J* = 6.2 Hz, 3H, OCH(C*H*$_3$)$_2$), 1.11 (d, *J* = 6.2 Hz, 3H, OCH(C*H*$_3$)$_2$). LRMS (CI) m/z calcd. for $C_{26}H_{24}ClFN_3O_3$ $[M+H]^+$: 480.1 found: 480.1.

(±) Isopropyl 1-(2-chloro-6-fluorobenzyl)-4-(furan-2-yl)-2-methyl-1,4-dihydrobenzo[4,5]imidazo[1,2-*a*]pyrimidine-3-carboxylate (291a). Purified by column chromatography (DCM–AcOEt 99:1 – 98:3). Yield: 37%. Oil at RT. ^{1}H NMR (300 MHz, $CDCl_3$), δ (ppm): 7.68 – 7.36 (m, 3H, Ar-H), 7.34 – 6.78 (m, 5H, Ar-H), 6.55 (s, 1H, CH), 6.28 – 6.09 (m, 2H, Ar-H), 5.99 (d, *J* = 16.6 Hz, 1H, C*H*$_2$C$_6$H$_3$ClF), 5.40 (d, *J* = 16.6 Hz, 1H, C*H*$_2$C$_6$H$_3$ClF), 5.14 – 4.90 (m, 1H, OC*H*(CH$_3$)$_2$), 2.58 (s, 3H, CH$_3$), 1.27 (d, *J* = 6.2 Hz, 3H, OCH(C*H*$_3$)$_2$), 1.07 (d, *J* = 6.2 Hz, 3H, OCH(C*H*$_3$)$_2$). LRMS (CI) m/z calcd. for $C_{26}H_{24}ClFN_3O_3$ $[M+H]^+$: 480.1 found: 480.1.

(±) Isopropyl 10-(2-chloro-6-fluorobenzyl)-4-(furan-2-yl)-2-methyl-4,10-dihydrobenzo[4,5]imidazo[1,2-*a*]pyrimidine-3-carboxylate (291b). Purified by column chromatography (DCM–AcOEt 99:1 – 98:3). Yield: 44%. Oil at RT. ^{1}H NMR (300 MHz, $CDCl_3$), δ (ppm): 7.44 – 7.13 (m, 4H, Ar-H), 7.13 – 6.90 (m, 3H, Ar-H), 6.89 – 6.78 (m, 1H, Ar-H), 6.50 (s, 1H, CH), 6.29 – 6.17 (m, 2H, Ar-H), 5.59 – 5.36 (m, 2H, C*H*$_2$C$_6$H$_3$ClF), 5.13 – 4.95 (m, 1H, OC*H*(CH$_3$)$_2$), 2.57 (s, 3H, CH$_3$), 1.26 (d, *J* = 6.2 Hz, 3H, OCH(C*H*$_3$)$_2$), 1.10 (d, *J* = 6.2 Hz, 3H, OCH(C*H*$_3$)$_2$). LRMS (CI) m/z calcd. for $C_{26}H_{24}ClFN_3O_3$ $[M+H]^+$: 480.1 found: 480.1.

(±) Ethyl 4-(furan-3-yl)-1,2-dimethyl-1,4-dihydrobenzo[4,5]imidazo[1,2-a]pyrimidine-3-carboxylate (292a). Purified by column chromatography (DCM–AcOEt 99:1 – 98:2). Yield: 33%. Mp: 130 – 132 ºC. ^{1}H NMR (300 MHz, $CDCl_3$), δ (ppm): 7.61 – 7.52 (m, 1H, Ar-H), 7.33 – 7.05 (m, 5H, Ar-H), 6.50 (s, 1H, CH), 6.13 – 6.06 (m, 1H, Ar-H), 4.24 (q, *J* = 7.1 Hz, 2H, OCH_2CH_3), 3.66 (d, *J* = 0.9 Hz, 3H, NCH_3), 2.64 (s, 3H, CH_3), 1.33 (td, *J* = 7.1, 0.9 Hz, 3H, OCH_2CH_3). LRMS (CI) m/z calcd. for $C_{19}H_{20}N_3O_3$ $[M+H]^+$: 338.1 found: 338.1.

(±) Ethyl 4-(furan-3-yl)-2,10-dimethyl-4,10-dihydrobenzo[4,5]imidazo[1,2-*a*]pyrimidine-3-carboxylate (292b). Purified by column chromatography (DCM–AcOEt 99:1 – 98:2). Yield: 38%. Mp: 62 – 64 ºC. ^{1}H NMR (300 MHz, $CDCl_3$), δ (ppm): 7.36 (s, 1H, Ar-H), 7.24 – 7.02 (m, 5H, Ar-H), 6.47 (s, 1H, CH), 6.24 (s, 1H, Ar-H), 4.18 (dd, *J* = 7.1, 4.6 Hz, 2H, OCH_2CH_3), 3.61 (s, 3H, NCH_3), 2.51 (s, 3H, CH_3), 1.29 (t, *J* = 7.1 Hz, 3H, OCH_2CH_3). LRMS (CI) m/z calcd. for $C_{19}H_{20}N_3O_3$ $[M+H]^+$: 338.1 found: 338.1.

(±) Ethyl 1-ethyl-4-(furan-3-yl)-2-methyl-1,4-dihydrobenzo[4,5]imidazo[1,2-*a*]pyrimidine-3-carboxylate (293a). Purified by column chromatography (DCM–AcOEt 99:1 – 98:2). Yield: 22%. Mp: 106 – 108 ºC. ^{1}H NMR (300 MHz, $CDCl_3$), δ (ppm): 7.58 (dd, *J* = 7.4, 1.7 Hz, 1H, Ar-H), 7.23 – 7.05 (m, 5H, Ar-H), 6.48 (s, 1H, CH), 6.07 (dd, *J* = 1.9, 0.9 Hz, 1H, Ar-H), 4.30 – 4.21 (m, 4H, OCH_2CH_3 + NCH_2CH_3), 2.66 (s, 3H, CH_3), 1.41 (t, *J* = 7.0 Hz, 3H, NCH_2CH_3), 1.33 (t, *J* = 7.1 Hz, 3H, OCH_2CH_3). LRMS (CI) m/z calcd. for $C_{20}H_{22}N_3O_3$ $[M+H]^+$: 352.2 found: 352.1.

(±) Ethyl 10-ethyl-4-(furan-3-yl)-2-methyl-4,10-dihydrobenzo[4,5]imidazo[1,2-*a*]pyrimidine-3-carboxylate (293b). Purified by column chromatography (DCM–AcOEt 99:1 – 98:2). Yield: 31%. Oil at RT. ^{1}H NMR (300 MHz, $CDCl_3$), δ (ppm): 7.35 (s, 1H, Ar-H), 7.24 – 7.08 (m, 5H, Ar-H), 6.46 (s, 1H, CH), 6.22 (d, *J* = 1.9 Hz, 1H, Ar-H), 4.22 – 4.14 (m, 4H, OCH_2CH_3 + NCH_2CH_3), 2.51 (s, CH_3), 1.40 (t, *J* = 7.2 Hz, 3H, NCH_2CH_3), 1.29 (t, *J* = 7.1 Hz, 3H, OCH_2CH_3). LRMS (CI) m/z calcd. for $C_{20}H_{22}N_3O_3$ $[M+H]^+$: 352.2 found: 352.1.

(±) Ethyl 4-(furan-3-yl)-2-methyl-1-(prop-2-yn-1-yl)-1,4-dihydrobenzo[4,5]imidazo[1,2-*a*]pyrimidine-3-carboxylate (294a). Purified by column chromatography (DCM–AcOEt 99:1 – 98:3). Yield: 38%. Mp: 112 – 114 ºC. ^{1}H NMR (300 MHz, $CDCl_3$), δ (ppm): 7.60 (d, *J* = 7.4 Hz, 1H, Ar-H), 7.31 (s, 1H, Ar-H), 7.24 – 7.07 (m, 4H, Ar-H), 6.48 (s, 1H, CH), 6.13 (s, 1H, Ar-H), 5.08 (dd, *J* = 18.2, 2.3 Hz, 1H, C*H*$_2$CCH), 4.93 (dd, *J* = 16.9, 1.2 Hz, 1H, C*H*$_2$CCH), 4.25 (q, *J* = 7.1 Hz, 2H, OC*H*$_2$CH$_3$), 2.78 (s, 3H, CH_3), 2.36 (s, 1H, CH_2CCH), 1.33 (t, *J* = 7.1 Hz, 3H, OCH_2CH_3). LRMS (CI) m/z calcd. for $C_{21}H_{20}N_3O_3$ $[M+H]^+$: 362.1 found: 362.1.

(±) Ethyl 4-(furan-3-yl)-2-methyl-10-(prop-2-yn-1-yl)-1,4-dihydrobenzo[4,5]imidazo[1,2-a]pyrimidine-3-carboxylate (294b). Purified by column chromatography (DCM–AcOEt 99:1 – 98:3). Yield: 42%. Oil at RT. ^{1}H NMR (300 MHz, $CDCl_3$), δ (ppm): 7.36 (s, 1H, Ar-H), 7.32 – 6.99 (m, 5H, Ar-H), 6.46 (s, 1H, CH), 6.24 (s, 1H, Ar-H), 4.90 (s, 2H, C*H*$_2$CCH), 4.18 (dd, *J* = 7.1, 4.7 Hz, 2H, OC*H*$_2$CH$_3$), 2.49 (s, 3H, CH_3), 2.37 (d, *J* = 18.1 Hz, 1H, CH_2CCH), 1.36 – 1.23 (m, 3H, OCH_2CH_3). LRMS (CI) m/z calcd. for $C_{21}H_{20}N_3O_3$ $[M+H]^+$: 362.1 found: 362.1.

(±) Ethyl 4-(furan-3-yl)-2-methyl-1-phenethyl-1,4-dihydrobenzo[4,5]imidazo[1,2-*a*]pyrimidine-3-carboxylate (295a). Purified by column chromatography (DCM–AcOEt 99:1 – 98:3). Yield: 27%. Mp: 113 – 115 ºC. ^{1}H NMR (300 MHz, $CDCl_3$), δ (ppm): 7.62 (d, *J* = 7.7 Hz, 1H, Ar-H), 7.42 – 7.02 (m, 10H, Ar-H), 6.50 (s, 1H, CH), 6.05 (dd, *J* = 1.9, 0.9 Hz, 1H, Ar-H), 4.58 (ddd, *J* = 14.7, 9.1, 5.8 Hz, 1H, C*H*$_2$CH$_2$C$_6$H$_5$), 4.34 – 4.17 (m, 3H, C*H*$_2$CH$_2$C$_6$H$_5$ + OC*H*$_2$CH$_3$), 3.29 – 2.96 (m, 2H, CH$_2$C*H*$_2$C$_6$H$_5$), 2.52 (s, 3H, CH_3), 1.33 (t, *J* = 7.1 Hz, 3H, OCH_2CH_3). LRMS (CI) m/z calcd. for $C_{26}H_{26}N_3O_3$ $[M+H]^+$: 428.2 found: 428.2.

(±) Ethyl 4-(furan-3-yl)-2-methyl-10-phenethyl-4,10-dihydrobenzo[4,5]imidazo[1,2-*a*]pyrimidine-3-carboxylate (295b). Purified by column chromatography (DCM–AcOEt 99:1 – 98:3). Yield: 33%. Oil at RT. ^{1}H NMR (300 MHz, $CDCl_3$), δ (ppm): 7.34 – 7.15 (m, 7H, Ar-H), 7.13 – 7.03 (m, 3H, Ar-H), 6.96 – 6.88 (m, 1H, Ar-H), 6.45 (s, 1H, CH), 6.18 (t, *J* = 1.2 Hz, 1H, Ar-H), 4.30 (t, *J* = 7.8 Hz, 2H, C*H*$_2$CH$_2$C$_6$H$_5$), 4.18 (qt, *J* = 7.1, 3.7 Hz, 2H, OC*H*$_2$CH$_3$), 3.17 – 3.03 (m, 2H, CH$_2$C*H*$_2$C$_6$H$_5$), 2.49 (s, 3H, CH_3), 1.30 (t, *J* = 7.1 Hz, 3H, OCH_2CH_3). LRMS (CI) m/z calcd. for $C_{26}H_{26}N_3O_3$ $[M+H]^+$: 428.2 found: 428.2.

(±) Ethyl 1-(2-fluorophenethyl)-4-(furan-3-yl)-2-methyl-1,4-dihydrobenzo[4,5]imidazo[1,2-*a*]pyrimidine-3-carboxylate (296a). Purified by column chromatography (DCM–AcOEt 99:1 – 98:3). Yield: 18%. Oil at RT. ^{1}H NMR (300 MHz, $CDCl_3$), δ (ppm): 7.62 (s, 1H, Ar-H), 7.31 – 7.00 (m, 9H, Ar-H), 6.50 (s, 1H, CH), 6.07 (s, 1H, Ar-H), 4.62 – 4.46 (m, 1H, C*H*$_2$CH$_2$C$_6$H$_4$F), 4.29 – 4.11 (m, 3H, OC*H*$_2$CH$_3$ + C*H*$_2$CH$_2$C$_6$H$_4$F), 3.30 – 3.02 (m, 2H, CH$_2$C*H*$_2$C$_6$H$_4$F), 2.57 (s, 3H, CH$_3$), 1.32 (t, *J* = 7.1 Hz, 3H, OCH$_2$C*H*$_3$). LRMS (CI) m/z calcd. for $C_{26}H_{25}FN_3O_3$ $[M+H]^+$: 446.2 found: 446.2.

(±) Ethyl 10-(2-fluorophenethyl)-4-(furan-3-yl)-2-methyl-4,10-dihydrobenzo[4,5]imidazo[1,2-*a*]pyrimidine-3-carboxylate (296b). Purified by column chromatography (DCM–AcOEt 99:1 – 98:3). Yield: 29%. Oil at RT. ^{1}H NMR (300 MHz, $CDCl_3$), δ (ppm): 7.32 (s, 1H, Ar-H), 7.24 – 6.90 (m, 9H, Ar-H), 6.44 (s, 1H, CH), 6.20 (dd, *J* = 1.8, 0.9 Hz, 1H, Ar-H), 4.31 (t, *J* = 7.2 Hz, 2H, C*H*$_2$CH$_2$C$_6$H$_4$F), 4.18 (qt, *J* = 7.7, 3.9 Hz, 2H, OC*H*$_2$CH$_3$), 3.16 (t, *J* = 7.2 Hz, 2H, CH$_2$C*H*$_2$C$_6$H$_4$F), 2.48 (s, 3H, CH$_3$), 1.29 (t, *J* = 7.1 Hz, 3H, OCH$_2$C*H*$_3$). LRMS (CI) m/z calcd. for $C_{26}H_{25}FN_3O_3$ $[M+H]^+$: 446.2 found: 446.2.

(±) Ethyl 1-(4-cyano-2-fluorobenzyl)-4-(furan-3-yl)-2-methyl-1,4-dihydrobenzo[4,5]imidazo[1,2-*a*]pyrimidine-3-carboxylate (297a). Purified by column chromatography (DCM–AcOEt 99:1 – 98:3). Yield: 22%. Mp: 80 – 82 ºC. ^{1}H NMR (300 MHz, $CDCl_3$), δ (ppm): 7.63 – 7.11 (m, 9H, Ar-H), 6.58 (s, 1H, CH), 6.07 (s, 1H, Ar-H), 5.69 – 5.42 (m, 2H, C*H*$_2$C$_6$H$_3$FCN), 4.26 (q, *J* = 7.0 Hz, 2H, OC*H*$_2$CH$_3$), 2.52 (s, 3H, CH$_3$), 1.34 (t, *J* = 7.1 Hz, 3H, OCH$_2$C*H*$_3$). LRMS (CI) m/z calcd. for $C_{26}H_{22}FN_4O_3$ $[M+H]^+$: 457.2 found: 457.2.

(±) Ethyl 10-(4-cyano-2-fluorobenzyl)-4-(furan-3-yl)-2-methyl-4,10-dihydrobenzo[4,5]imidazo[1,2-*a*]pyrimidine-3-carboxylate (297b). Purified by column chromatography (DCM–AcOEt 99:1 – 98:3). Yield: 22%. Oil at RT. ^{1}H NMR (300 MHz, $CDCl_3$), δ (ppm): 7.42 – 7.33 (m, 4H, Ar-H), 7.28 – 7.19 (m, 2H, Ar-H), 7.19 – 7.08 (m, 2H, Ar-H), 7.03 – 6.93 (m, 1H, Ar-H), 6.48 (s, 1H, CH), 6.26 – 6.19 (m, 1H, Ar-H), 5.36 (s, 2H, C*H*$_2$C$_6$H$_3$FCN), 4.26 – 4.06 (m, 2H, OC*H*$_2$CH$_3$), 2.48 (s, 3H, CH$_3$), 1.34 – 1.24 (m, 3H, OCH$_2$C*H*$_3$). LRMS (CI) m/z calcd. for $C_{26}H_{22}FN_4O_3$ $[M+H]^+$: 457.2 found: 457.2.

(±) Ethyl 1-(3-fluorobenzyl)-4-(furan-3-yl)-2-methyl-1,4-dihydrobenzo[4,5]imidazo[1,2-*a*]pyrimidine-3-carboxylate (298a). Purified by column chromatography (DCM–AcOEt 99:1 – 98:3). Yield: 22%. Mp: 119 – 121 ºC. ^{1}H NMR (300 MHz, $CDCl_3$), δ (ppm): 7.57 (d, *J* = 7.7 Hz, 1H, Ar-H), 7.25 (d, *J* = 7.0 Hz, 6H, Ar-H), 7.22 – 6.85 (m, 3H, Ar-H), 6.57 (s, 1H, CH), 6.08 (s, 1H, Ar-H), 5.60 (d, *J* = 16.9 Hz, 1H, C*H*$_2$C$_6$H$_4$F), 5.37 (d, *J* = 17.1 Hz, 1H, C*H*$_2$C$_6$H$_4$F), 4.24 (q, *J* = 7.1 Hz, 2H, OC*H*$_2$CH$_3$), 2.54 (s, 3H, CH_3), 1.33 (t, *J* = 7.1 Hz, 3H, OCH$_2$C*H*$_3$). LRMS (CI) m/z calcd. for $C_{25}H_{23}FN_4O_3$ $[M+H]^+$: 432.2 found: 432.2.

(±) Ethyl 10-(3-fluorobenzyl)-4-(furan-3-yl)-2-methyl-4,10-dihydrobenzo[4,5]imidazo[1,2-*a*]pyrimidine-3-carboxylate (298b). Purified by column chromatography (DCM–AcOEt 99:1 – 98:3). Yield: 27%. Oil at RT. ^{1}H NMR (300 MHz, $CDCl_3$), δ (ppm): 7.72 – 6.79 (m, 10H, Ar-H), 6.49 (s, 1H, CH), 6.25 (s, 1H, Ar-H), 5.27 (s, 2H, CH$_2$C$_6$H$_4$F), 4.21 (s, 2H, OC*H*$_2$CH$_3$), 2.51 (s, 3H, CH_3), 1.30 (t, *J* = 7.1 Hz, 3H, OCH$_2$C*H*$_3$). LRMS (CI) m/z calcd. for $C_{25}H_{23}FN_4O_3$ $[M+H]^+$: 432.2 found: 432.2.

(±) Ethyl 1-(4-fluorobenzyl)-4-(furan-3-yl)-2-methyl-1,4-dihydrobenzo[4,5]imidazo[1,2-*a*]pyrimidine-3-carboxylate (299a). Purified by column chromatography (DCM–AcOEt 99:1 – 98:3). Yield: 28%. Mp: 122 – 124 ºC. ^{1}H NMR (300 MHz, $CDCl_3$), δ (ppm): 7.57 (d, *J* = 7.8 Hz, 1H, Ar-H), 7.30 – 7.08 (m, 7H, Ar-H), 7.00 (t, *J* = 8.6 Hz, 2H, Ar-H), 6.56 (s, 1H, CH), 6.06 (s, 1H, Ar-H), 5.59 (d, *J* = 16.6 Hz, 1H, CH$_2$C$_6$H$_4$F), 5.33 (d, *J* = 16.6 Hz, 1H, CH$_2$C$_6$H$_4$F), 4.25 (q, *J* = 7.1 Hz, 2H, OC*H*$_2$CH$_3$), 2.56 (s, 3H, CH_3), 1.33 (t, *J* = 7.1 Hz, 3H, OCH$_2$C*H*$_3$). ^{13}C NMR (75 MHz, $CDCl_3$), δ (ppm): 166.0, 162.2 (d, *J* = 246.2 Hz, Ar-CF), 147.9, 147.6, 143.4, 142.1, 139.5, 132.8 (d, *J* = 3.3 Hz, Ar-CF), 132.7, 128.1 (d, *J* = 8.2 Hz, Ar-C), 125.8, 122.5, 121.2, 117.9, 115.8 (d, *J* = 21.7 Hz, Ar-CF), 109.2, 108.9, 108.7, 60.4, 48.0, 47.7, 16.2, 14.3. LRMS (CI) m/z calcd. for $C_{25}H_{23}FN_3O_3$ $[M+H]^+$: 432.2 found: 432.2.

(±) Ethyl 10-(4-fluorobenzyl)-4-(furan-3-yl)-2-methyl-4,10-dihydrobenzo[4,5]imidazo[1,2-*a*]pyrimidine-3-carboxylate (299b). Purified by column chromatography (DCM–AcOEt 99:1 – 98:3). Yield: 33%. Oil at RT. ^{1}H NMR (300 MHz, $CDCl_3$), δ (ppm): 7.37 (s, 1H, Ar-H), 7.32 (dd, *J* = 8.7, 5.3 Hz, 2H, Ar-H), 7.23 (t, *J* = 1.6 Hz, 1H, Ar-H), 7.19 – 6.88 (m, 6H, Ar-H), 6.49 (s, 1H, CH), 6.28 – 6.21 (m, 1H, Ar-H), 5.25 (d, *J* = 3.7 Hz, 2H, OC*H*$_2$CH$_3$), 4.31 – 4.07 (m, 2H, C*H*$_2$C$_6$H$_4$F), 2.52 (s, 3H, CH_3), 1.31 (t, *J* = 7.1 Hz, 3H, OCH$_2$C*H*$_3$). ^{13}C NMR (75 MHz, $CDCl_3$), δ (ppm): 166.9, 162.4 (d, *J* = 246.8 Hz, Ar-CF), 159.7, 143.2, 143.1, 139.4, 139.2, 131.48 (d, *J* = 3.3 Hz, Ar-CF), 129.4, 129.3, 126.3, 122.7, 122.3, 115.8 (d, *J* = 21.6 Hz, Ar-C), 109.4, 109.1, 108.9, 108.7, 59.5, 48.6, 44.6, 24.8, 14.5. LRMS (CI) m/z calcd. for $C_{25}H_{23}FN_{33}$ $[M+H]^+$: 432.2 found: 432.2.

(±) Ethyl 1-(2,3-difluorobenzyl)-4-(furan-3-yl)-2-methyl-1,4-dihydrobenzo[4,5]imidazo[1,2-*a*]pyrimidine-3-carboxylate (300a). Purified by column chromatography (DCM–AcOEt 99:1 – 98:3). Yield: 33%. Oil at RT. ^{1}H NMR (300 MHz, $CDCl_3$), δ (ppm): 7.56 (d, *J* = 7.8 Hz, 1H, Ar-H), 7.29 – 7.02 (m, 6H, Ar-H), 7.02 – 6.86 (m, 2H, Ar-H), 6.56 (s, 1H, CH), 6.09 (s, 1H, Ar-H), 5.64 (d, *J* = 17.3 Hz, 1H, C*H*$_2$C$_6$H$_3$F$_2$), 5.46 (d, *J* = 17.2 Hz, 1H, C*H*$_2$C$_6$H$_3$F$_2$), 4.25 (q, *J* = 7.2 Hz, 2H, OC*H*$_2$CH$_3$), 2.54 (s, 3H, CH_3), 1.33 (t, *J* = 7.1 Hz, 3H, OC*H*$_2$CH$_3$). LRMS (CI) m/z calcd. for $C_{25}H_{22}F_2N_3O_3$ $[M+H]^+$: 450.1 found: 450.1.

(±) Ethyl 10-(2,3-difluorobenzyl)-4-(furan-3-yl)-2-methyl-4,10-dihydrobenzo[4,5]imidazo[1,2-*a*]pyrimidine-3-carboxylate (300b). Purified by column chromatography (DCM–AcOEt 99:1 – 98:3). Yield: 42%. Oil at RT. ^{1}H NMR (300 MHz, $CDCl_3$), δ (ppm): 7.37 (s, 1H, Ar-H), 7.22 (s, 1H, Ar-H), 7.19 – 6.94 (m, 6H, Ar-H), 6.48 (s, 1H, CH), 6.24 (s, 1H, Ar-H), 5.35 (s, 2H, C*H*$_2$C$_6$H$_3$F$_2$), 4.19 (dd, *J* = 7.0, 3.5 Hz, 3H, OC*H*$_2$CH$_3$), 2.51 (s, 3H, CH_3), 1.30 (t, *J* = 7.1 Hz, 3H, OCH$_2$C*H*$_3$). LRMS (CI) m/z calcd. for $C_{25}H_{22}F_2N_3O_3$ $[M+H]^+$: 450.1 found: 450.1.

(±) Ethyl 1-(2,4-difluorobenzyl)-4-(furan-3-yl)-2-methyl-1,4-dihydrobenzo[4,5]imidazo[1,2-*a*]pyrimidine-3-carboxylate (301a). Purified by column chromatography (DCM–AcOEt 99:1 – 98:3). Yield: 32%. Mp: 99 – 101 ºC. ^{1}H NMR (300 MHz, $CDCl_3$), δ (ppm): 7.57 (dt, *J* = 8.0, 0.9 Hz, 1H, Ar-H), 7.35 – 7.05 (m, 6H, Ar-H), 6.92 – 6.72 (m, 2H, Ar-H), 6.56 (s, 1H, CH), 6.07 (dd, *J* = 1.9, 1.0 Hz, 1H, Ar-H), 5.58 (d, *J* = 16.9 Hz, 1H, C*H*$_2$C$_6$H$_3$F$_2$), 5.39 (d, *J* = 16.9 Hz, 1H, C*H*$_2$C$_6$H$_3$F$_2$), 4.25 (qd, *J* = 7.1, 0.8 Hz, 2H, OC*H*$_2$CH$_3$), 2.56 (s, 3H, CH$_3$), 1.34 (t, *J* = 7.1 Hz, 3H, OCH$_2$C*H*$_3$). LRMS (CI) m/z calcd. for $C_{25}H_{22}F_2N_3O_3$ $[M+H]^+$: 450.1 found: 450.1.

(±) Ethyl 10-(2,4-difluorobenzyl)-4-(furan-3-yl)-2-methyl-4,10-dihydrobenzo[4,5]imidazo[1,2-*a*]pyrimidine-3-carboxylate (301b). Purified by column chromatography (DCM–AcOEt 99:1 – 98:3). Yield: 41%. Oil at RT. ^{1}H NMR (300 MHz, $CDCl_3$), δ (ppm): 7.46 – 7.32 (m, 2H, Ar-H), 7.30 – 7.18 (m, 1H, Ar-H), 7.17 – 6.99 (m, 4H, Ar-H), 6.91 – 6.76 (m, 2H, Ar-H), 6.48 (s, 1H, CH), 6.23 (dd, *J* = 1.9, 0.9 Hz, 1H, Ar-H), 5.29 (s, 2H, C*H*$_2$C$_6$H$_3$F$_2$), 4.21 – 4.06 (m, 2H, OC*H*$_2$CH$_3$), 2.52 (s, 3H, CH$_3$), 1.30 (t, *J* = 7.1 Hz, 3H, OCH$_2$C*H*$_3$). LRMS (CI) m/z calcd. for $C_{25}H_{22}F_2N_3O_3$ $[M+H]^+$: 450.1 found: 450.1.

(±) Ethyl 1-(2,5-difluorobenzyl)-4-(furan-3-yl)-2-methyl-1,4-dihydrobenzo[4,5]imidazo[1,2-*a*]pyrimidine-3-carboxylate (302a). Purified by column chromatography (DCM–AcOEt 99:1 – 98:3). Yield: 26%. Mp: 105 – 107 ºC. ^{1}H NMR (300 MHz, $CDCl_3$), δ (ppm): 7.56 (d, *J* = 7.8 Hz, 1H, Ar-H), 7.30 – 6.80 (m, 8H, Ar-H), 6.57 (s, 1H, CH), 6.09 (s, 1H, Ar-H), 5.56 (d, *J* = 17.4 Hz, 1H, C*H*$_2$C$_6$H$_3$F$_2$), 5.41 (d, *J* = 17.1 Hz, 1H, C*H*$_2$C$_6$H$_3$F$_2$), 4.25 (q, *J* = 7.0 Hz, 2H, OC*H*$_2$CH$_3$), 2.54 (s, 3H, CH$_3$), 1.33 (t, *J* = 7.1 Hz, 3H, OCH$_2$C*H*$_3$). LRMS (CI) m/z calcd. for $C_{25}H_{22}F_2N_3O_3$ $[M+H]^+$: 450.1 found: 450.1.

(±) Ethyl 10-(2,5-difluorobenzyl)-4-(furan-3-yl)-2-methyl-4,10-dihydrobenzo[4,5]imidazo[1,2-*a*]pyrimidine-3-carboxylate (302b). Purified by column chromatography (DCM–AcOEt 99:1 – 98:3). Yield: 32%. Oil at RT. ^{1}H NMR (300 MHz, $CDCl_3$), δ (ppm): 7.38 (s, 1H, Ar-H), 7.34 – 7.19 (m, 1H, Ar-H), 7.14 – 6.84 (m, 7H, Ar-H), 6.48 (s, 1H, CH), 6.25 (d, *J* = 1.8 Hz, 1H, Ar-H), 5.29 (d, *J* = 3.2 Hz, 2H, C*H*$_2$C$_6$H$_3$F$_2$), 4.19 (qt, *J* = 7.2, 3.7 Hz, 2H, OC*H*$_2$CH$_3$), 2.52 (s, 3H, CH$_3$), 1.30 (t, *J* = 7.1 Hz, 3H, OCH$_2$C*H*$_3$). LRMS (CI) m/z calcd. for $C_{25}H_{22}F_2N_3O_3$ $[M+H]^+$: 450.1 found: 450.1.

(±) Ethyl 1-(2,6-difluorobenzyl)-4-(furan-3-yl)-2-methyl-1,4-dihydrobenzo[4,5]imidazo[1,2-*a*]pyrimidine-3-carboxylate (303a). Purified by column chromatography (DCM–AcOEt 99:1 – 98:3). Yield: 22%. Mp: 132 – 133 ºC. ^{1}H NMR (300 MHz, $CDCl_3$), δ (ppm): 7.58 (d, *J* = 8.0 Hz, 1H, Ar-H), 7.32 – 7.05 (m, 6H, Ar-H), 6.89 (t, *J* = 8.2 Hz, 2H, Ar-H), 6.52 (s, 1H, Ar-H), 6.13 (d, *J* = 1.4 Hz, 1H, Ar-H), 6.04 (d, *J* = 16.5 Hz, 1H, C*H*$_2$C$_6$H$_3$F$_2$), 5.24 (d, *J* = 16.4 Hz, 1H, C*H*$_2$C$_6$H$_3$F$_2$), 4.28 – 4.15 (m, 2H, OC*H*$_2$CH$_3$), 2.58 (s, 3H, CH_3), 1.31 (t, *J* = 7.1 Hz, 3H, OCH$_2$C*H*$_3$). LRMS (CI) m/z calcd. for $C_{25}H_{22}F_2N_3O_3$ $[M+H]^+$: 450.1 found: 450.1.

(±) Ethyl 10-(2,6-difluorobenzyl)-4-(furan-3-yl)-2-methyl-4,10-dihydrobenzo[4,5]imidazo[1,2-*a*]pyrimidine-3-carboxylate (303b). Purified by column chromatography (DCM–AcOEt 99:1 – 98:3). Yield: 22%. Oil at RT. ^{1}H NMR (300 MHz, $CDCl_3$), δ (ppm): 7.40 – 7.15 (m, 3H, Ar-H), 7.12 – 6.80 (m, 6H, Ar-H), 6.46 (s, 1H, CH), 6.25 (d, *J* = 1.8 Hz, 1H, Ar-H), 5.72 – 5.17 (m, 2H, C*H*$_2$C$_6$H$_3$F$_2$), 4.18 (qt, *J* = 7.6, 3.8 Hz, 2H, OC*H*$_2$CH$_3$), 2.51 (s, 3H, CH_3), 1.30 (t, *J* = 7.1 Hz, 3H, OCH$_2$C*H*$_3$). LRMS (CI) m/z calcd. for $C_{25}H_{22}F_2N_3O_3$ $[M+H]^+$: 450.1 found: 450.1.

(±) Ethyl 1-(3,5-difluorobenzyl)-4-(furan-3-yl)-2-methyl-1,4-dihydrobenzo[4,5]imidazo[1,2-*a*]pyrimidine-3-carboxylate (304a). Purified by column chromatography (DCM–AcOEt 99:1 – 98:3). Yield: 16%. Mp: 131 – 133 ºC. ^{1}H NMR (500 MHz, $CDCl_3$), δ (ppm): 7.56 (dt, *J* = 7.8, 1.0 Hz, 1H, Ar-H), 7.29 – 7.08 (m, 5H, Ar-H), 6.82 – 6.64 (m, 3H, Ar-H), 6.57 (s, 1H, CH), 6.09 (dd, *J* = 1.9, 1.0 Hz, 1H, Ar-H), 5.53 (d, *J* = 17.3 Hz, 1H, C*H*$_2$C$_6$H$_3$F$_2$), 5.36 (d, *J* = 17.1 Hz, 1H, C*H*$_2$C$_6$H$_3$F$_2$), 4.25 (q, *J* = 7.1 Hz, 2H, OC*H*$_2$CH$_3$), 2.55 – 2.49 (m, 3H, CH_3), 1.33 (t, *J* = 7.1 Hz, 3H, OCH$_2$C*H*$_3$). LRMS (CI) m/z calcd. for $C_{25}H_{22}F_2N_3O_3$ $[M+H]^+$: 450.1 found: 450.1.

(±) Ethyl 10-(3,5-difluorobenzyl)-4-(furan-3-yl)-2-methyl-4,10-dihydrobenzo[4,5]imidazo[1,2-*a*]pyrimidine-3-carboxylate (304b). Purified by column chromatography (DCM–AcOEt 99:1 – 98:3). Yield: 18%. Oil at RT. ^{1}H NMR (500 MHz, $CDCl_3$), δ (ppm): 7.39 (s, 1H, Ar-H), 7.31 – 7.18 (m, 1H, Ar-H), 7.18 – 7.02 (m, 3H, Ar-H), 6.92 (d, *J* = 6.7 Hz, 1H, Ar-H), 6.83 (d, *J* = 6.5 Hz, 2H, Ar-H), 6.73 (dd, *J* = 9.8, 7.6 Hz, 1H, Ar-H), 6.49 (s, 1H, CH), 6.25 (s, 1H, Ar-H), 5.25 (s, 2H, C*H*$_2$C$_6$H$_3$F$_2$), 4.26 – 4.05 (m, 2H, OC*H*$_2$CH$_3$), 2.50 (s, 3H, CH_3), 1.30 (t, *J* = 7.1 Hz, 3H, OCH$_2$C*H*$_3$). LRMS (CI) m/z calcd. for $C_{25}H_{22}F_2N_3O_3$ $[M+H]^+$: 450.1 found: 450.1.

(±) Ethyl 4-(furan-3-yl)-2-methyl-1-(2,4,6-trifluorobenzyl)-1,4-dihydrobenzo[4,5]imidazo[1,2-*a*]pyrimidine-3-carboxylate (305a). Purified by column chromatography (DCM–AcOEt 99:1 – 98:3). Yield: 38%. Mp: 129 – 131 ºC. ^{1}H NMR (300 MHz, $CDCl_3$), δ (ppm): 7.57 (d, *J* = 7.9 Hz, 1H, Ar-H), 7.29 – 7.05 (m, 5H, Ar-H), 6.67 (t, *J* = 8.4 Hz, 2H, Ar-H), 6.51 (s, 1H, CH), 6.09 (s, 1H, Ar-H), 5.96 (d, *J* = 16.4 Hz, 1H, C*H*$_2$C$_6$H$_2$F$_3$), 5.18 (d, *J* = 16.4 Hz, 1H, C*H*$_2$C$_6$H$_2$F$_3$), 4.23 (q, *J* = 7.4 Hz, 2H, OC*H*$_2$CH$_3$), 2.58 (s, 3H, CH_3), 1.32 (t, *J* = 7.1 Hz, 3H, OCH$_2$C*H*$_3$). LRMS (CI) m/z calcd. for $C_{25}H_{21}F_3N_3O_3$ $[M+H]^+$: 468.1 found: 468.2.

(±) Ethyl 4-(furan-3-yl)-2-methyl-10-(2,4,6-trifluorobenzyl)-4,10-dihydrobenzo[4,5]imidazo[1,2-*a*]pyrimidine-3-carboxylate (305b). Purified by column chromatography (DCM–AcOEt 99:1 – 98:3). Yield: 42%. Mp: 62 – 64 ºC. ^{1}H NMR (300 MHz, $CDCl_3$), δ (ppm): 7.35 (s, 1H, Ar-H), 7.26 (s, 1H, Ar-H), 7.14 – 6.94 (m, 4H, Ar-H), 6.68 (t, *J* = 8.3 Hz, 2H, Ar-H), 6.45 (s, 1H, CH), 6.23 (s, 1H, Ar-H), 5.59 – 5.10 (m, 2H, C*H*$_2$C$_6$H$_2$F$_3$), 4.26 – 4.08 (m, 2H, OC*H*$_2$CH$_3$), 2.50 (s, 3H, CH_3), 1.30 (t, *J* = 7.1 Hz, 3H, OCH$_2$C*H*$_3$). LRMS (CI) m/z calcd. for $C_{25}H_{21}F_3N_3O_3$ $[M+H]^+$: 468.1 found: 468.2.

(±) Ethyl 1-(2-chlorobenzyl)-4-(furan-3-yl)-2-methyl-1,4-dihydrobenzo[4,5]imidazo[1,2-*a*]pyrimidine-3-carboxylate (306a). Purified by column chromatography (DCM–AcOEt 99:1 – 98:3). Yield: 22%. Mp: 131 – 133 ºC. ^{1}H NMR (300 MHz, $CDCl_3$), δ (ppm): 7.55 (d, *J* = 7.7 Hz, 1H, Ar-H), 7.40 (d, *J* = 8.1 Hz, 1H, Ar-H), 7.34 – 7.09 (m, 8H, Ar-H), 6.60 (s, 1H, CH), 6.15 (s, 1H, Ar-H), 5.61 (d, *J* = 17.7 Hz, 1H, C*H*$_2$C$_6$H$_4$Cl), 5.48 (d, *J* = 17.7 Hz, 1H, C*H*$_2$C$_6$H$_4$Cl), 4.25 (q, *J* = 7.1 Hz, 2H, OC*H*$_2$CH$_3$), 2.48 (s, 3H, CH_3), 1.33 (t, *J* = 7.0 Hz, 3H, OCH$_2$C*H*$_3$). LRMS (CI) m/z calcd. for $C_{25}H_{23}ClN_3O_3$ $[M+H]^+$: 448.1 found: 448.1.

(±) Ethyl 10-(2-chlorobenzyl)-4-(furan-3-yl)-2-methyl-4,10-dihydrobenzo[4,5]imidazo[1,2-*a*]pyrimidine-3-carboxylate (306b). Purified by column chromatography (DCM–AcOEt 99:1 – 98:3). Yield: 28%. Oil at RT. ^{1}H NMR (300 MHz, $CDCl_3$), δ (ppm): 7.46 – 7.36 (m, 2H, Ar-H), 7.29 – 6.97 (m, 7H, Ar-H), 6.91 (d, *J* = 7.1 Hz, 1H, Ar-H), 6.51 (s, 1H, CH), 6.27 (d, *J* = 1.9 Hz, 1H, Ar-H), 5.51 – 5.26 (m, 2H, C*H*$_2$C$_6$H$_4$Cl), 4.28 – 4.05 (m, 2H, OC*H*$_2$CH$_3$), 2.49 (s, 3H, CH_3), 1.28 (dt, *J* = 13.9, 7.1 Hz, 3H, OCH$_2$C*H*$_3$). LRMS (CI) m/z calcd. for $C_{25}H_{23}ClN_3O_3$ $[M+H]^+$: 448.1 found: 448.1.

(±) Ethyl 1-(3-chlorobenzyl)-4-(furan-3-yl)-2-methyl-1,4-dihydrobenzo[4,5]imidazo[1,2-*a*]pyrimidine-3-carboxylate (307a). Purified by column chromatography (DCM–AcOEt 99:1 – 98:3). Yield: 21%. Mp: 111 – 113 ºC. ^{1}H NMR (300 MHz, $CDCl_3$), δ (ppm): 7.56 (d, *J* = 7.9 Hz, 1H, Ar-H), 7.30 – 7.08 (m, 9H, Ar-H), 6.57 (s, 1H, CH), 6.09 (s, 1H, Ar-H), 5.60 (d, *J* = 16.8 Hz, 1H, C*H*$_2$C$_6$H$_4$Cl), 5.33 (d, *J* = 16.9 Hz, 1H, C*H*$_2$C$_6$H$_4$Cl), 4.24 (q, *J* = 7.1 Hz, 2H, OC*H*$_2$CH$_3$), 2.53 (s, 3H, CH_3), 1.33 (t, *J* = 7.1 Hz, 3H, OCH$_2$C*H*$_3$). LRMS (CI) m/z calcd. for $C_{25}H_{23}ClN_3O_3$ $[M+H]^+$: 448.1 found: 448.1.

(±) Ethyl 10-(3-chlorobenzyl)-4-(furan-3-yl)-2-methyl-4,10-dihydrobenzo[4,5]imidazo[1,2-*a*]pyrimidine-3-carboxylate (307b). Purified by column chromatography (DCM–AcOEt 99:1 – 98:3). Yield: 33%. Oil at RT. ^{1}H NMR (300 MHz, $CDCl_3$), δ (ppm): 7.38 (s, 1H, Ar-H), 7.34 – 7.02 (m, 8H, Ar-H), 6.96 – 6.88 (m, 1H, Ar-H), 6.49 (s, 1H, CH), 6.25 (d, *J* = 1.8 Hz, 1H, Ar-H), 5.25 (d, *J* = 3.7 Hz, 2H, C*H*$_2$C$_6$H$_4$Cl), 4.19 (qq, *J* = 7.2, 3.8 Hz, 2H, OC*H*$_2$CH$_3$), 2.50 (s, 3H, CH_3), 1.35 – 1.23 (m, 3H, OCH$_2$C*H*$_3$). LRMS (CI) m/z calcd. for $C_{25}H_{23}ClN_3O_3$ $[M+H]^+$: 448.1 found: 448.1.

(±) Ethyl 1-(4-chlorobenzyl)-4-(furan-3-yl)-2-methyl-1,4-dihydrobenzo[4,5]imidazo[1,2-*a*]pyrimidine-3-carboxylate (308a). Purified by column chromatography (DCM–AcOEt 99:1 – 98:3). Yield: 37%. Mp: 162 – 164 ºC. ^{1}H NMR (300 MHz, $CDCl_3$), δ (ppm): 7.56 (d, *J* = 7.8 Hz, 1H, Ar-H), 7.33 – 7.07 (m, 9H, Ar-H), 6.55 (s, 1H, CH), 6.06 (s, 1H, Ar-H), 5.56 (d, *J* = 16.9 Hz, 1H, C*H*$_2$C$_6$H$_4$Cl), 5.32 (d, *J* = 16.9 Hz, 1H, C*H*$_2$C$_6$H$_4$Cl), 4.24 (q, *J* = 7.2 Hz, 2H, OC*H*$_2$CH$_3$), 2.53 (s, 3H, CH_3), 1.32 (td, *J* = 7.1, 1.5 Hz, 3H, OCH$_2$C*H*$_3$). LRMS (CI) m/z calcd. for $C_{25}H_{23}ClN_3O_3$ $[M+H]^+$: 448.1 found: 448.1.

(±) Ethyl 10-(4-chlorobenzyl)-4-(furan-3-yl)-2-methyl-4,10-dihydrobenzo[4,5]imidazo[1,2-*a*]pyrimidine-3-carboxylate (308b). Purified by column chromatography (DCM–AcOEt 99:1 – 98:3). Yield: 44%. Oil at RT. ^{1}H NMR (300 MHz, $CDCl_3$), δ (ppm): 7.37 (s, 1H, Ar-H), 7.34 – 7.19 (m, 5H, Ar-H), 7.14 – 7.01 (m, 3H, Ar-H), 6.92 (s, 1H, Ar-H), 6.48 (s, 1H, CH), 6.24 (s, 1H, Ar-H), 5.33 – 5.15 (m, 2H, C*H*$_2$C$_6$H$_4$Cl), 4.17 (ddd, *J* = 19.4, 11.0, 5.4 Hz, 2H, OC*H*$_2$CH$_3$), 2.50 (s, 3H, CH_3), 1.33 – 1.20 (m, 3H, OCH$_2$C*H*$_3$). LRMS (CI) m/z calcd. for $C_{25}H_{23}ClN_3O_3$ $[M+H]^+$: 448.1 found: 448.1.

(±) Ethyl 1-(3-chloro-2-fluorobenzyl)-4-(furan-3-yl)-2-methyl-1,4-dihydrobenzo[4,5]imidazo[1,2-*a*]pyrimidine-3-carboxylate (309a). Purified by column chromatography (DCM–AcOEt 99:1 – 98:3). Yield: 32%. Mp: 159 – 161 ºC. ^{1}H NMR (300 MHz, $CDCl_3$), δ (ppm): 7.56 (d, *J* = 7.8 Hz, 1H, Ar-H), 7.43 – 6.86 (m, 8H, Ar-H), 6.56 (s, 1H, CH), 6.08 (s, 1H, Ar-H), 5.62 (d, *J* = 17.5 Hz, 1H, C*H*$_2$C$_6$H$_4$FCl), 5.45 (d, *J* = 17.4 Hz, 1H, C*H*$_2$C$_6$H$_4$FCl), 4.25 (d, *J* = 7.1 Hz, 2H, OC*H*$_2$CH$_3$), 2.54 (s, 3H, CH_3), 1.38 – 1.20 (m, 3H, OCH$_2$C*H*$_3$). LRMS (CI) m/z calcd. for $C_{25}H_{22}ClFN_3O_3$ $[M+H]^+$: 466.1 found: 466.1.

(±) Ethyl 10-(3-chloro-2-fluorobenzyl)-4-(furan-3-yl)-2-methyl-4,10-dihydrobenzo[4,5]imidazo[1,2-*a*]pyrimidine-3-carboxylate (309b). Purified by column chromatography (DCM–AcOEt 99:1 – 98:3). Yield: 42%. Oil at RT. ^{1}H NMR (300 MHz, $CDCl_3$), δ (ppm): 7.39 – 7.16 (m, 4H, Ar-H), 7.11 (d, *J* = 2.9 Hz, 3H, Ar-H), 7.03 (d, *J* = 8.3 Hz, 2H, Ar-H), 6.48 (s, 1H, CH), 6.23 (s, 1H, Ar-H), 5.35 (s, 2H, C*H*$_2$C$_6$H$_3$FCl), 4.24 – 4.05 (m, 2H, OC*H*$_2$CH$_3$), 2.50 (s, 3H, CH_3), 1.26 (dt, *J* = 19.9, 7.3 Hz, 3H, OCH$_2$C*H*$_3$). LRMS (CI) m/z calcd. for $C_{25}H_{22}ClFN_3O_3$ $[M+H]^+$: 466.1 found: 466.1.

(±) Ethyl 1-(2-chloro-6-fluorobenzyl)-4-(furan-3-yl)-2-methyl-1,4-dihydrobenzo[4,5]imidazo[1,2-*a*]pyrimidine-3-carboxylate (310a). Purified by column chromatography (DCM–AcOEt 99:1 – 98:3). Yield: 37%. Mp: 144 – 146 ºC. ^{1}H NMR (300 MHz, $CDCl_3$), δ (ppm): 7.58 (d, *J* = 7.9 Hz, 1H, Ar-H), 7.26 (d, *J* = 2.0 Hz, 6H, Ar-H), 7.13 (q, *J* = 8.9 Hz, 1H, Ar-H), 6.97 (s, 1H, Ar-H), 6.54 (s, 1H, CH), 6.20 (s, 1H, Ar-H), 6.07 (d, *J* = 16.7 Hz, 1H, C*H*$_2$C$_6$H$_4$FCl), 5.37 (d, *J* = 16.4 Hz, 1H, C*H*$_2$C$_6$H$_4$FCl), 4.25 – 4.15 (m, 2H, O*CH*$_2$CH$_3$), 2.54 (s, 3H, CH_3), 1.30 (t, *J* = 7.2 Hz, 3H, OCH$_2$C*H*$_3$). LRMS (CI) m/z calcd. for $C_{25}H_{22}ClFN_3O_3$ $[M+H]^+$: 466.1 found: 466.1.

(±) Ethyl 10-(2-chloro-6-fluorobenzyl)-4-(furan-3-yl)-2-methyl-4,10-dihydrobenzo[4,5]imidazo[1,2-*a*]pyrimidine-3-carboxylate (310b). Purified by column chromatography (DCM–AcOEt 99:1 – 98:3). Yield: 44%. Oil at RT. ^{1}H NMR (300 MHz, $CDCl_3$), δ (ppm): 7.35 (s, 1H, Ar-H), 7.32 – 7.18 (m, 3H, Ar-H), 7.10 – 6.97 (m, 4H, Ar-H), 6.85 (d, *J* = 7.7 Hz, 1H, Ar-H), 6.47 (s, 1H, CH), 6.25 (s, 1H, Ar-H), 5.64 – 5.37 (m, 2H, C*H*$_2$C$_6$H$_3$FCl), 4.24 – 4.14 (m, 2H, OC*H*$_2$CH$_3$), 2.51 (s, 3H, CH_3), 1.36 – 1.24 (m, 3H, OCH$_2$C*H*$_3$). LRMS (CI) m/z calcd. for $C_{25}H_{22}ClFN_3O_3$ $[M+H]^+$: 466.1 found: 466.1.

5.4.4 Chiral HPLC separation of enantiomers and characterization of 257, 266a, 269a, and 284a

The chiral resolution was performed using a Water Breeze™ 2 (binary pump: 1525, detector UV/Visible 2489, 7725i Manual Injector Kit 1500 Series) using a 250 mm x 20 mm Chiralpak® 5µm IE-3 (DAICEL). All the separations were performed at 25 ºC with *Hex*/*i*-propanol mixture in different percentages as mobile phase (*see spectroscopic and analytical data*). The enantiomers **(*S*)-257** (2.0 mg, t_R = 11.91 min), **(*R*)-257** (2.0 mg, t_R = 15.30 min), **(*R*)-266** (1.0 mg, t_R = 22.96 min), **(*S*)-266a** (1.0 mg, t_R = 36.90 min), **(*S*)-269a** (1.0 mg, t_R = 16.41 min), **(*R*)-269a** (0.5 mg, t_R = 27.76 min), **(*R*)-284a** (1.0 mg, t_R = 17.14 min)], **(*S*)-284a** (1.0 mg, t_R = 21.38 min), were isolated, their stereochemical purity analyzed by chiral HPLC (e.e.: >99% for each enantiomer, reports showed below, chromatogram at 254 nM) and then characterized by ^{1}H NMR and circular dichroism (CD).

CD spectra were recorded on a Jasco-815 system equipped with a Peltier-type thermostatic accessory (CDF-426S, Jasco). Measurements were carried out at 20 °C using a 1 mm quartz cell in a volume of 600 μL. Compounds (0.5 mg) were dissolved in MeOH (1.0 mL) and then diluted 10-fold in MeOH. The instrument settings were bandwidth, 1.0 nm; data pitch, 1.0 nm; speed, 500 nm/min; accumulation, 10; wavelengths, 400−190 nm.

SAMPLE INFORMATION

Sample Name:	253	Acquired By:	Breeze
Sample Type:	Racemate	Sample Set Name	
Vial:	1	Acq. Method:	50%HexiPAISOF10 set
Injection #:	1	Date Acquired:	07/05/2022 15:53:52 CET
Run Time:	40,00 Minutes	Injection Volume:	500,00 ul

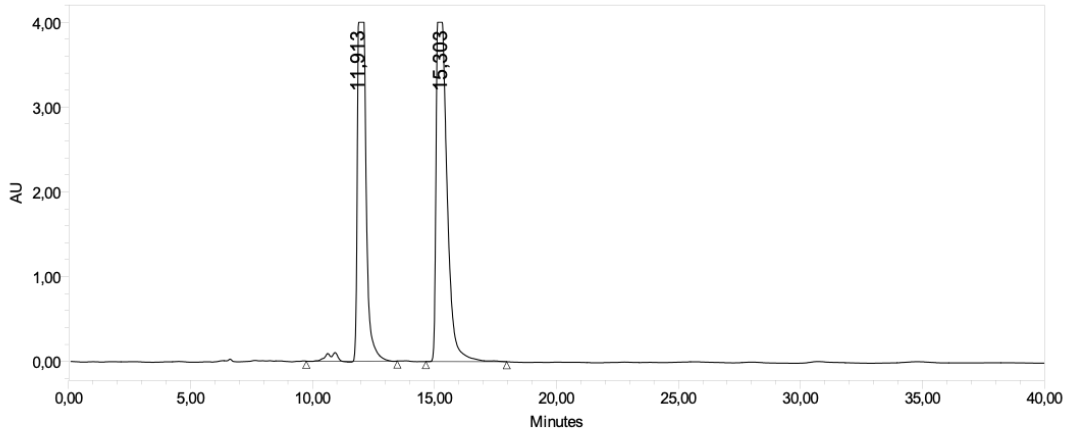

	RT (min)	Area (µV*sec)	% Area	Height (µV)
1	11,913	103348946	45,08	4078997
2	15,303	125924791	54,92	4017500

SAMPLE INFORMATION			
Sample Name:	257	Acquired By:	Breeze
Sample Type:	Enantiomer A	Sample Set Name	
Vial:	1	Acq. Method:	50%HexiPAISOF10 set
Injection #:	1	Date Acquired:	07/05/2022 18:52:51 CET
Run Time:	40,00 Minutes	Injection Volume:	500,00 ul

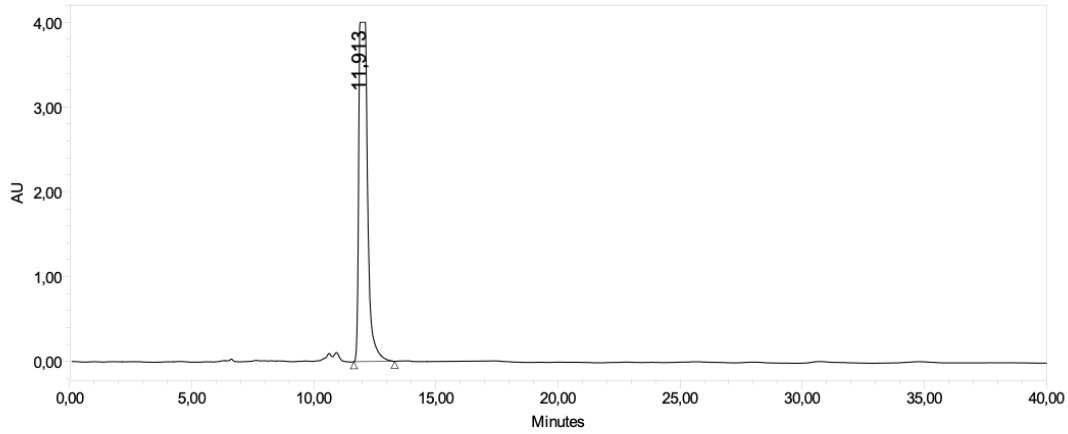

	RT (min)	Area (µV*sec)	% Area	Height (µV)
1	11,913	100548292	100,00	4085371

SAMPLE INFORMATION			
Sample Name:	257	Acquired By:	Breeze
Sample Type:	Enantiomer B	Sample Set Name	
Vial:	1	Acq. Method:	50%HexiPAISOF10 set
Injection #:	1	Date Acquired:	08/05/2022 19:52:51 CET
Run Time:	40,00 Minutes	Injection Volume:	500,00 ul

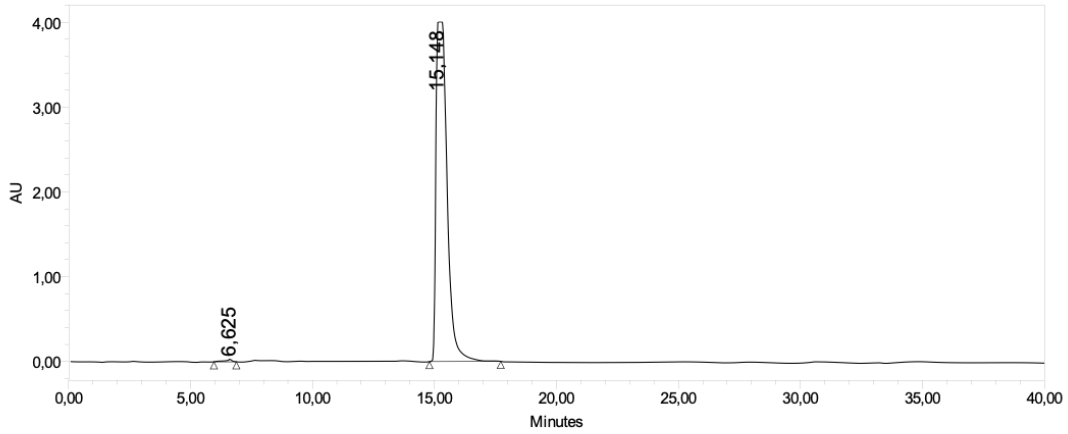

	RT (min)	Area (µV*sec)	% Area	Height (µV)
1	6,625	610059	0,48	32008
2	15,148	125385099	99,52	4055931

SAMPLE INFORMATION			
Sample Name:	266a	Acquired By:	Breeze
Sample Type:	Racemate	Sample Set Name	
Vial:	1	Acq. Method:	20%HexiPAISOF10 set
Injection #:	1	Date Acquired:	03/07/2019 9:57:46 CEST
Run Time:	53,33 Minutes	Injection Volume:	200,00 ul

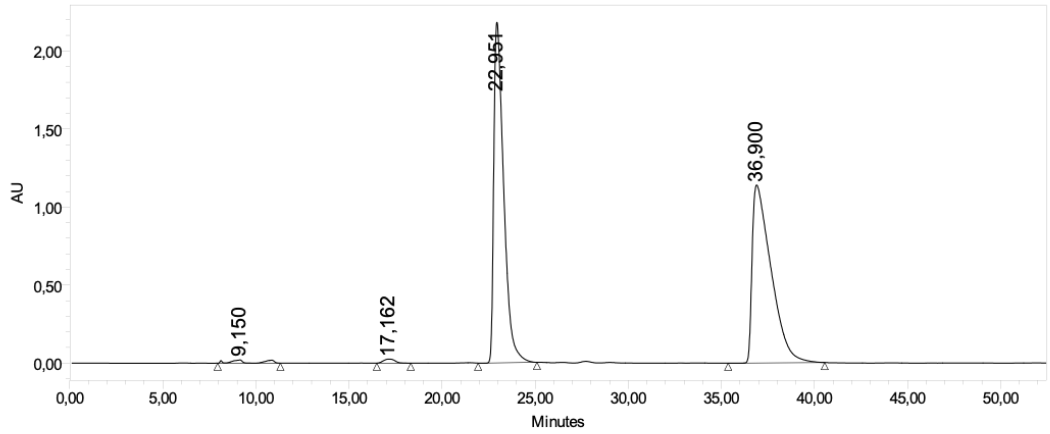

Channel: 2487Channel 1; Channel Desc.: ; Processing Method: 2

	RT (min)	Area (µV*sec)	% Area	Height (µV)
1	9,150	1531163	0,94	20966
2	17,162	1087925	0,67	25517
3	22,951	80354677	49,26	2182937
4	36,900	80155042	49,14	1140367

SAMPLE INFORMATION			
Sample Name:	266a	Acquired By:	Breeze
Sample Type:	Enantiomer A	Sample Set Name	
Vial:	1	Acq. Method:	20%HexiPAISOF10 set
Injection #:	1	Date Acquired:	04/07/2019 16:10:02 CEST
Run Time:	53,33 Minutes	Injection Volume:	200,00 ul

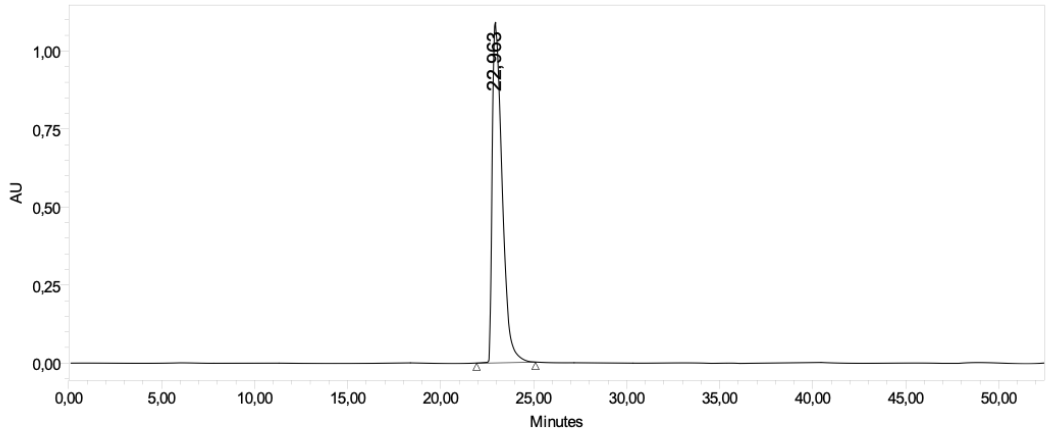

	RT (min)	Area (µV*sec)	% Area	Height (µV)
1	22,963	36524853	100,00	2182937

SAMPLE INFORMATION			
Sample Name:	266a	Acquired By:	Breeze
Sample Type:	Enantiomer B	Sample Set Name	
Vial:	1	Acq. Method:	20%HexiPAISOF10 set
Injection #:	1	Date Acquired:	04/07/2019 19:02:23 CEST
Run Time:	53,33 Minutes	Injection Volume:	200,00 ul

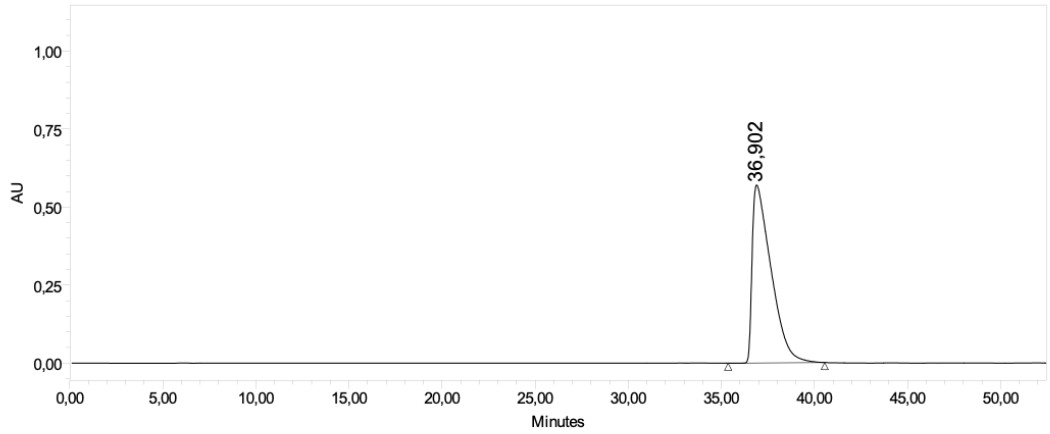

	RT (min)	Area (µV*sec)	% Area	Height (µV)
4	36,902	40077055	100,00	570183

SAMPLE INFORMATION

Sample Name:	269a	Acquired By:	Breeze
Sample Type:	Racemate	Sample Set Name	
Vial:	1	Acq. Method:	50%HexiPAISOF10 set
Injection #:	1	Date Acquired:	03/05/2022 14:37:00 CET
Run Time:	40,00 Minutes	Injection Volume:	300,00 ul

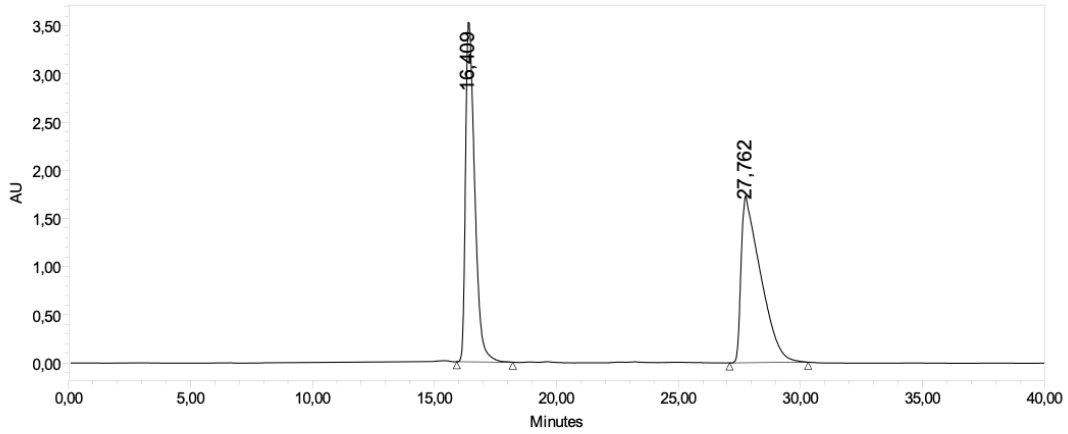

	RT (min)	Area (µV*sec)	% Area	Height (µV)
1	16,409	92310576	49,09	3530214
2	27,762	95727075	50,91	1659654

SAMPLE INFORMATION			
Sample Name:	269a	Acquired By:	Breeze
Sample Type:	Enantiomer A	Sample Set Name	
Vial:	1	Acq. Method:	50%HexiPAISOF10 set
Injection #:	1	Date Acquired:	04/05/2022 09:22:00 CET
Run Time:	40,00 Minutes	Injection Volume:	300,00 ul

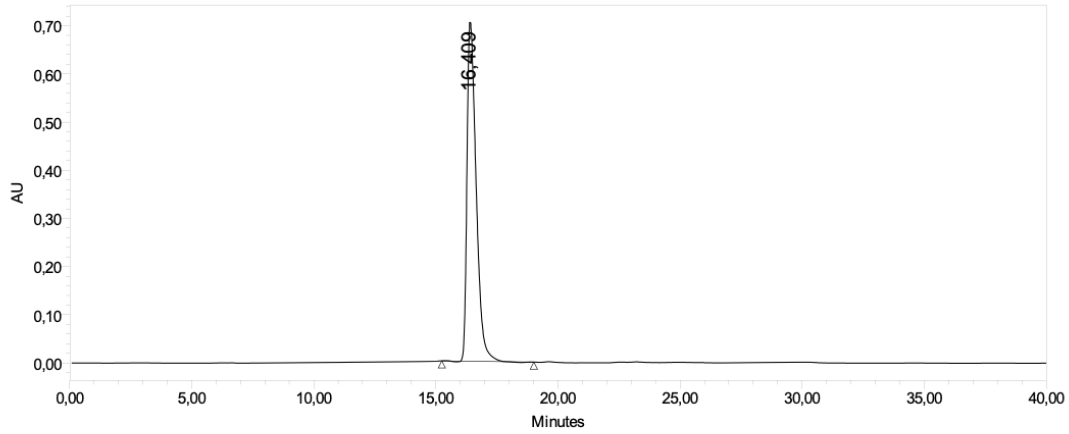

	RT (min)	Area (µV*sec)	% Area	Height (µV)
1	16,409	92020785	100,00	3523853

SAMPLE INFORMATION

Sample Name:	269a	Acquired By:	Breeze
Sample Type:	Enantiomer B	Sample Set Name	
Vial:	1	Acq. Method:	50%HexiPAISOF10 set
Injection #:	1	Date Acquired:	04/05/2022 11:00:01 CET
Run Time:	40,00 Minutes	Injection Volume:	300,00 ul

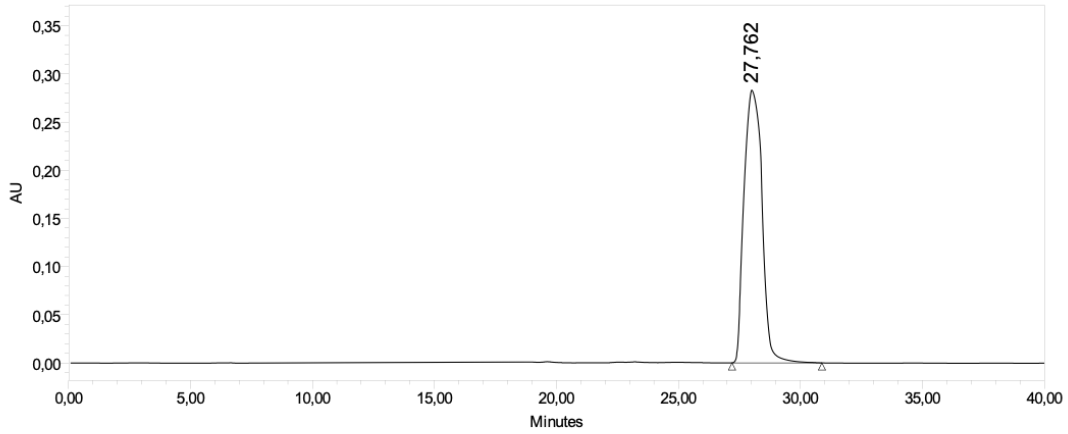

	RT (min)	Area (µV*sec)	% Area	Height (µV)
1	27,762	24112552	100,00	415101

SAMPLE INFORMATION			
Sample Name:	284a	Acquired By:	Breeze
Sample Type:	Racemate	Sample Set Name	
Vial:	1	Acq. Method:	50%HexiPAISOF10 set
Injection #:	1	Date Acquired:	25/04/2022 16:00:56 CET
Run Time:	30,00 Minutes	Injection Volume:	500,00 ul

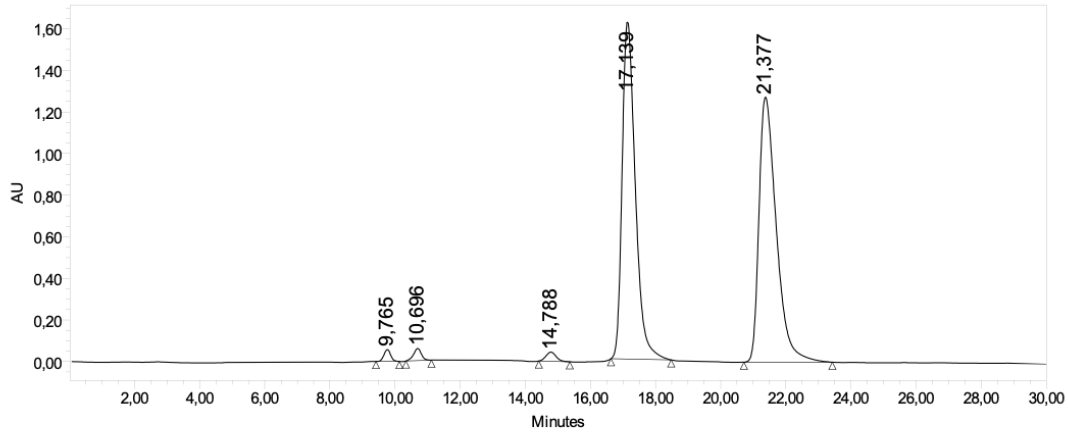

	RT (min)	Area (µV*sec)	% Area	Height (µV)
1	9,765	821391	0,86	57065
2	10,696	980228	1,03	58414
3	14,788	964608	1,01	44401
4	17,139	45603910	47,83	1620199
5	21,377	46982794	49,27	1274165

SAMPLE INFORMATION			
Sample Name:	284a	Acquired By:	Breeze
Sample Type:	Enantiomer A	Sample Set Name	
Vial:	1	Acq. Method:	50%HexiPAISOF10 set
Injection #:	1	Date Acquired:	25/04/2022 18:10:21 CET
Run Time:	30,00 Minutes	Injection Volume:	250,00 ul

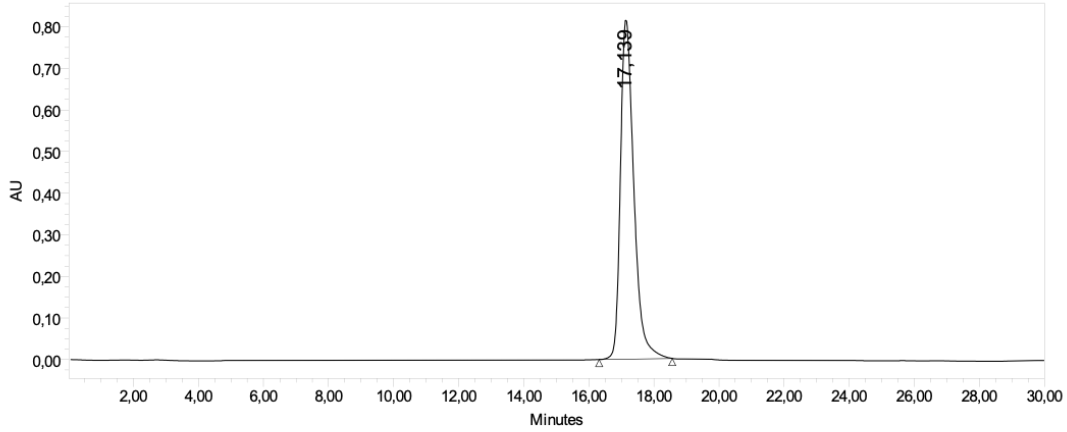

	RT (min)	Area (µV*sec)	% Area	Height (µV)
1	17,139	46542895	100,00	1630273

SAMPLE INFORMATION			
Sample Name:	284a	Acquired By:	Breeze
Sample Type:	Enantiomer B	Sample Set Name	
Vial:	1	Acq. Method:	50%HexiPAISOF10 set
Injection #:	1	Date Acquired:	25/04/2022 17:32:20 CET
Run Time:	30,00 Minutes	Injection Volume:	250,00 ul

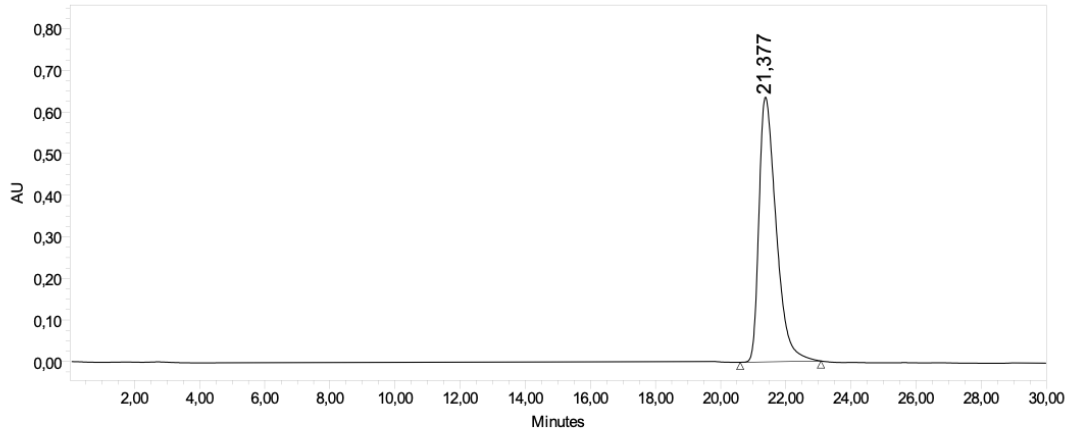

	RT (min)	Area (µV*sec)	% Area	Height (µV)
1	21,377	23269624	100,00	636354

5.4.4.1 Spectroscopic and analytical data of enantiomers

(±) Ethyl 1-(2-fluorobenzyl)-4-(furan-3-yl)-6-methyl-2-oxo-1,2,3,4-tetrahydropyrimidine-5-carboxylate (257). Purified by column chromatography (DCM–AcOEt 99:1 – 98:2). Yield: 59%. Mp: 239 – 240 ºC. ^{1}H NMR (300 MHz, $CDCl_3$), δ (ppm): 7.30 (s, 2H, Ar-H), 7.20 (s, 2H, Ar-H), 7.07 – 6.86 (m, 3H, Ar-H), 6.26 (s, 1H, Ar-H), 5.40 (s, 1H, CH), 5.18 (d, *J* = 16.4 Hz, 1H, C*H*$_2$C$_6$H$_4$F), 4.90 (d, *J* = 16.2 Hz, 1H, C*H*$_2$C$_6$H$_4$F), 4.16 (q, *J* = 7.0 Hz, 2H, OC*H*$_2$CH$_3$), 2.39 (s, 3H, CH_3), 1.24 (t, *J* = 7.1 Hz, 3H, OCH$_2$C*H*$_3$). ^{13}C NMR (75 MHz, $CDCl_3$), δ (ppm): 165.8, 159.8 (d, *J* = 245.6 Hz, Ar-CF), 155.5, 149.2, 143.4, 139.1, 128.8 (d, *J* = 7.8 Hz, Ar-C), 128.1 (d, *J* = 7.3 Hz, Ar-C), 124.9 (d, *J* = 14.1 Hz, Ar-C), 124.3 (d, *J* = 3.2 Hz, Ar-C), 115.3 (d, *J* = 21.1 Hz, Ar-C), 108.9, 105.0, 60.4, 45.8, 39.7 (d, *J* = 4.4 Hz, *C*H$_2$C$_6$H$_4$F), 15.9, 14.2. LRMS (CI) m/z calcd. for $C_{19}H_{20}FN_2O_4$ $[M+H]^+$: 359.1 found: 359.2.

Ethyl (*S*)-1-(2-fluorobenzyl)-4-(furan-3-yl)-6-methyl-2-oxo-1,2,3,4-tetrahydropyrimidine-5-carboxylate [(*S*)-257]. Chiral separation with a 250 mm x 20 mm Chiralpak® 5µm IE-3 (DAICEL) (isocratic mobile phase Hex–IPA 1:1) to give an enantiomeric excess of >99%. ^{1}H NMR (300 MHz, $CDCl_3$), δ (ppm): 7.30 (s, 2H, Ar-H), 7.20 (s, 2H, Ar-H), 7.05 – 6.74 (m, 3H, Ar-H), 6.27 (s, 1H, Ar-H), 5.41 (s, 1H, CH), 5.17 (d, *J* = 16.3 Hz, 1H, C*H*$_2$C$_6$H$_4$F), 4.90 (d, *J* = 16.2 Hz, 1H, C*H*$_2$C$_6$H$_4$F), 4.16 (q, *J* = 7.0 Hz, 2H, OC*H*$_2$CH$_3$), 2.39 (s, 3H, CH_3), 1.24 (t, *J* = 7.1 Hz, 3H, OCH$_2$C*H*$_3$). LRMS (CI) m/z calcd. for $C_{19}H_{20}FN_2O_4$ $[M+H]^+$: 359.1 found: 359.2.

Ethyl (*R*)-1-(2-fluorobenzyl)-4-(furan-3-yl)-6-methyl-2-oxo-1,2,3,4-tetrahydropyrimidine-5-carboxylate [(*R*)-257]. Chiral separation with a 250 mm x 20 mm Chiralpak® 5µm IE-3 (DAICEL) (isocratic mobile phase Hex–IPA 1:1) to give an enantiomeric excess of >99%. ^{1}H NMR (300 MHz, $CDCl_3$), δ (ppm): 7.31 (s, 2H, Ar-H), 7.22 (s, 2H, Ar-H), 7.13 – 6.81 (m, 3H, Ar-H), 6.26 (s, 1H, Ar-H), 5.46 (s, 1H, CH), 5.18 (d, *J* = 16.4 Hz, 1H, C*H*$_2$C$_6$H$_4$F), 4.90 (d, *J* = 16.3 Hz, 1H, C*H*$_2$C$_6$H$_4$F), 4.16 (q, *J* = 7.0 Hz, 2H, OC*H*$_2$CH$_3$), 2.41 (s, 3H, CH_3), 1.23 (t, *J* = 7.0 Hz, 3H, OCH$_2$C*H*$_3$). LRMS (CI) m/z calcd. for $C_{19}H_{20}FN_2O_4$ $[M+H]^+$: 359.1 found: 359.2.

(±) Isopropyl 1-(2-fluorobenzyl)-4-(furan-2-yl)-2-methyl-1,4-dihydrobenzo[4,5]-imidazo-[1,2-a]pyrimidine-3-carboxylate (266a). Purified by column chromatography (DCM–AcOEt 99:1 – 98:2). Yield 27%. Mp: 182 – 183 ºC. ^{1}H NMR (300 MHz, $CDCl_3$), δ (ppm): 7.72 – 7.51 (m, 1H, Ar-H), 7.52 (dd, *J* = 7.3, 2.0 Hz, 1H, Ar-H), 7.41 – 7.00 (m, 7H, Ar-H), 6.61 (s, 1H, CH), 6.31 (d, *J* = 1.7 Hz, 2H, Ar-H), 5.82 (d, *J* = 17.4 Hz, 1H, C*H*$_2$C$_6$H$_4$F), 5.52 (d, *J* = 17.4 Hz, 1H, C*H*$_2$C$_6$H$_4$F), 5.13 (hept, *J* = 6.3 Hz, 1H, OC*H*(CH$_3$)$_2$), 2.64 (s, 3H, CH$_3$), 1.31 (d, *J* = 6.2 Hz, 3H, OCH(C*H*$_3$)$_2$), 1.21 (d, *J* = 6.26 Hz, 3H, OCH(C*H*$_3$)$_2$). ^{13}C NMR (75 MHz, $CDCl_3$), δ (ppm): 165.4, 160.5 (d, *J* = 246.3 Hz, Ar-CF), 153.0, 148.3, 147.5, 142.2, 141.8, 132.9, 129.1 (d, *J* = 8.1 Hz, Ar-C), 127.8 (d, *J* = 3.6 Hz, Ar-C), 124.6 (d, *J* = 3.6 Hz, Ar-C), 124.3 (d, *J* = 13.7 Hz, Ar-C), 122.6, 121.2, 117.7, 115.5 (d, *J* = 21.1 Hz, Ar-C), 110.3, 109.5, 107.6, 98.9, 67.8, 49.5, 42.5 (d, *J* = 5.6 Hz, *C*H$_2$C$_6$H$_4$F), 22.1, 21.7, 15.8. HRMS (APCI) *m/z* calcd. for $C_{26}H_{25}FN_3O_3$ $[M+H]^+$: 446.1874; found: 446.1876.

Isopropyl (*R*)-1-(2-fluorobenzyl)-4-(furan-2-yl)-2-methyl-1,4-dihydrobenzo[4,5]-imidazo-[1,2-a]pyrimidine-3-carboxylate [(*R*)-266a]. Chiral separation with a 250 mm x 20 mm Chiralpak® 5µm IE-3 (DAICEL) (isocratic mobile phase Hex–IPA 4:1) to give an enantiomeric excess of >99%. Mp: 182 – 183 ºC. ^{1}H NMR (300 MHz, $CDCl_3$), δ (ppm): 7.71 – 7.52 (m, 1H, Ar-H), 7.52 (dd, *J* = 7.27, 2.03 Hz, 1H, Ar-H), 7.41 – 7.02 (m, 7H, Ar-H), 6.61 (s, 1H, CH), 6.33 (d, *J* = 1.6 Hz, 2H, Ar-H), 5.82 (d, *J* = 17.4 Hz, 1H, C*H*$_2$C$_6$H$_4$F), 5.51 (d, *J* = 17.4 Hz, 1H, C*H*$_2$C$_6$H$_4$F), 5.12 (hept, *J* = 6.4 Hz, 1H, OC*H*(CH$_3$)$_2$), 2.61 (s, 3H, CH$_3$), 1.33 (d, *J* = 6.3 Hz, 3H, OCH(C*H*$_3$)$_2$), 1.22 (d, *J* = 6.3 Hz, 3H, OCH(C*H*$_3$)$_2$). HRMS (APCI) *m/z* calcd. for $C_{26}H_{25}FN_3O_3$ $[M+H]^+$: 446.1874; found: 446.1872.

Isopropyl (*S*)-1-(2-fluorobenzyl)-4-(furan-2-yl)-2-methyl-1,4-dihydrobenzo[4,5]-imidazo-[1,2-a]pyrimidine-3-carboxylate [(*S*)-266a)]. Chiral separation with a 250 mm x 20 mm Chiralpak® 5µm IE-3 (DAICEL) (isocratic mobile phase Hex–IPA 4:1) to give an enantiomeric excess of >99%. Mp: 182 – 183 ºC. ^{1}H NMR (300 MHz, $CDCl_3$), δ (ppm): 7.72 – 7.49 (m, 1H, Ar-H), 7.49 (dd, *J* = 7.2, 2.0 Hz, 1H, Ar-H), 7.41 – 7.05 (m, 7H, Ar-H), 6.62 (s, 1H, CH), 6.32 (d, *J* = 1.7 Hz, 2H, Ar-H), 5.81 (d, *J* = 17.4 Hz, 1H, C*H*$_2$C$_6$H$_4$F), 5.52 (d, *J* = 17.4 Hz, 1H, C*H*$_2$C$_6$H$_4$F), 5.13 (hept, *J* = 6.3 Hz, 1H, OC*H*(CH$_3$)$_2$), 2.63 (s, 3H, CH$_3$), 1.33 (d, *J* = 6.3 Hz, 3H, OCH(C*H*$_3$)$_2$), 1.22 (d, *J* = 6.3 Hz, 3H, OCH(C*H*$_3$)$_2$). HRMS (APCI) *m/z* calcd. for $C_{26}H_{25}FN_3O_3$ $[M+H]^+$: 446.1874; found: 446.1874.

(±) Ethyl 1-(2-fluorobenzyl)-4-(furan-3-yl)-2-methyl-1,4-dihydrobenzo[4,5]imidazo[1,2-a]pyrimidine-3-carboxylate (269a). Purified by column chromatography (DCM–AcOEt 99:1 – 98:2). Yield: 37%. Mp: 111 – 113 ºC. ^{1}H NMR (300 MHz, $CDCl_3$), δ (ppm): 7.66 – 7.49 (m, 1H, Ar-H), 7.37 – 6.92 (m, 9H, Ar-H), 6.57 (s, 1H, Ar-H), 6.10 (s, 1H, CH), 5.66 (d, *J* = 17.2 Hz, 1H, C*H*$_2$C$_6$H$_4$F), 5.44 (d, *J* = 17.1 Hz, 1H, C*H*$_2$C$_6$H$_4$F), 4.25 (q, *J* = 7.1 Hz, 2H, OC*H*$_2$CH$_3$), 2.56 (s, 3H, CH_3), 1.34 (t, *J* = 7.1 Hz, 3H, OCH$_2$C*H*$_3$). ^{13}C NMR (75 MHz, $CDCl_3$), δ (ppm): 166.0, 160.0 (d, *J* = 246.0 Hz, Ar-CF), 147.9, 147.7, 143.4, 141.9, 139.5, 132.6, 129.3 (d, *J* = 8.2 Hz, Ar-C), 128.0 (d, *J* = 3.8 Hz, Ar-C), 125.7, 124.6 (d, *J* = 3.7 Hz, Ar-C), 124.3, 124.1, 122.6, 121.2, 117.8, 115.6 (d, *J* = 21.3 Hz, Ar-C), 109.2, 108.7, 60.5, 47.7 (CH), 42.6 (d, *J* = 5.4 Hz, *C*H$_2$C$_6$H$_4$F), 15.9, 14.4. HRMS (APCI) m/z calcd. for $C_{25}H_{23}FN_3O_3$ $[M+H]^+$: 432.1645 found: 432.1632.

Ethyl (*S*)-1-(2-fluorobenzyl)-4-(furan-3-yl)-2-methyl-1,4-dihydrobenzo[4,5]imidazo[1,2-a]pyrimidine-3-carboxylate [(*S*)-269a]. Chiral separation with a 250 mm x 20 mm Chiralpak® 5µm IE-3 (DAICEL) (isocratic mobile phase Hex–IPA 1:1) to give an enantiomeric excess of >99%. ^{1}H NMR (300 MHz, $CDCl_3$), δ (ppm): 7.72 – 6.92 (m, 10H, Ar-H), 6.55 (s, 1H, Ar-H), 6.09 (s, 1H, CH), 5.66 (d, *J* = 17.2 Hz, 1H, C*H*$_2$C$_6$H$_4$F), 5.44 (d, *J* = 17.1 Hz, 1H, C*H*$_2$C$_6$H$_4$F), 4.25 (q, *J* = 7.1 Hz, 2H, OC*H*$_2$CH$_3$), 2.56 (s, 3H, CH_3), 1.34 (t, *J* = 7.1 Hz, 3H, OCH$_2$C*H*$_3$). HRMS (APCI) m/z calcd. for $C_{25}H_{23}FN_3O_3$ $[M+H]^+$: 432.1645 found: 432.1631.

Ethyl (*R*)-1-(2-fluorobenzyl)-4-(furan-3-yl)-2-methyl-1,4-dihydrobenzo[4,5]imidazo[1,2-a]pyrimidine-3-carboxylate [(*R*)-269a]. Chiral separation with a 250 mm x 20 mm Chiralpak® 5µm IE-3 (DAICEL) (isocratic mobile phase Hex–IPA 1:1) to give an enantiomeric excess of >99%. ^{1}H NMR (300 MHz, $CDCl_3$), δ (ppm): 7.71 – 6.91 (m, 10H, Ar-H), 6.55 (s, 1H, Ar-H), 6.14 (s, 1H, CH), 5.67 (d, *J* = 17.1 Hz, 1H, C*H*$_2$C$_6$H$_4$F), 5.44 (d, *J* = 17.2 Hz, 1H, C*H*$_2$C$_6$H$_4$F), 4.25 (q, *J* = 7.1 Hz, 2H, OC*H*$_2$CH$_3$), 2.56 (s, 3H, CH_3), 1.34 (t, *J* = 7.1 Hz, 3H, OCH$_2$C*H*$_3$). HRMS (APCI) m/z calcd. for $C_{25}H_{23}FN_3O_3$ $[M+H]^+$: 432.1645 found: 432.1631.

(±) Isopropyl 1-(2,6-difluorobenzyl)-4-(furan-2-yl)-2-methyl-1,4-dihydrobenzo[4,5]imidazo[1,2-*a*]pyrimidine-3-carboxylate (284a). Purified by column chromatography (DCM–AcOEt 99:1 – 98:3). Yield: 22%. Mp: 126 – 128 ºC. ^{1}H NMR (300 MHz, $CDCl_3$), δ (ppm): 7.65 – 7.49 (m, 1H, Ar-H), 7.48 – 7.37 (m, 1H, Ar-H), 7.34 – 7.07 (m, 5H, Ar-H), 6.87 (t, *J* = 8.2 Hz, 1H, Ar-H), 6.54 (s, 1H, CH), 6.19 (dd, *J* = 3.3, 1.8 Hz, 1H, Ar-H), 6.14 – 6.07 (m, 1H, Ar-H), 5.95 (d, *J* = 16.5 Hz, 1H, C*H*$_2$C$_6$H$_3$F$_2$), 5.38 – 5.25 (m, 1H, C*H*$_2$C$_6$H$_3$F$_2$), 5.02 (p, *J* = 6.2 Hz, 1H, OC*H*(CH$_3$)$_2$), 2.64 (s, 3H, CH$_3$), 1.27 (d, *J* = 6.2 Hz, 3H, OCH(C*H*$_3$)$_2$), 1.08 (d, *J* = 6.2 Hz, 3H, OCH(C*H*$_3$)$_2$). HRMS (CI) m/z calcd. for $C_{26}H_{24}F_2N_3O_3$ $[M+H]^+$: 464.1707 found: 464.1716.

Isopropyl (*R*)-1-(2,6-difluorobenzyl)-4-(furan-2-yl)-2-methyl-1,4-dihydrobenzo[4,5]imidazo[1,2-*a*]pyrimidine-3-carboxylate [(*R*)-284a]. Chiral separation with a 250 mm x 20 mm Chiralpak® 5µm IE-3 (DAICEL) (isocratic mobile phase Hex–IPA 1:1) to give an enantiomeric excess of >99. ^{1}H NMR (300 MHz, $CDCl_3$), δ (ppm): 7.65 – 7.45 (m, 1H, Ar-H), 7.41 – 7.07 (m, 6H, Ar-H), 6.87 (t, *J* = 8.2 Hz, 1H, Ar-H), 6.54 (s, 1H, CH), 6.19 (dd, *J* = 3.3, 1.8 Hz, 1H, Ar-H), 6.14 – 6.07 (m, 1H, Ar-H), 5.95 (d, *J* = 16.7 Hz, 1H, C*H*$_2$C$_6$H$_3$F$_2$), 5.38 – 5.25 (m, 1H, C*H*$_2$C$_6$H$_3$F$_2$), 5.01 (p, *J* = 6.3 Hz, 1H, OC*H*(CH$_3$)$_2$), 2.64 (s, 3H, CH$_3$), 1.27 (d, *J* = 6.3 Hz, 3H, OCH(C*H*$_3$)$_2$), 1.08 (d, *J* = 6.3 Hz, 3H, OCH(C*H*$_3$)$_2$). HRMS (CI) m/z calcd. for $C_{26}H_{24}F_2N_3O_3$ $[M+H]^+$: 464.1707 found: 464.1712.

Isopropyl (*S*)-1-(2,6-difluorobenzyl)-4-(furan-2-yl)-2-methyl-1,4-dihydrobenzo[4,5]imidazo[1,2-*a*]pyrimidine-3-carboxylate [(*S*)-284a]. Chiral separation with a 250 mm x 20 mm Chiralpak® 5µm IE-3 (DAICEL) (isocratic mobile phase Hex–IPA 1:1) to give an enantiomeric excess of >99%. ^{1}H NMR (300 MHz, $CDCl_3$), δ (ppm): 7.65 – 7.45 (m, 1H, Ar-H), 7.41 – 7.07 (m, 6H, Ar-H), 6.87 (t, *J* = 8.2 Hz, 1H, Ar-H), 6.56 (s, 1H, CH), 6.19 (dd, *J* = 3.3, 1.8 Hz, 1H, Ar-H), 6.14 – 6.07 (m, 1H, Ar-H), 5.95 (d, *J* = 16.6 Hz, 1H, C*H*$_2$C$_6$H$_3$F$_2$), 5.38 – 5.25 (m, 1H, C*H*$_2$C$_6$H$_3$F$_2$), 5.01 (p, *J* = 6.3 Hz, 1H, OC*H*(CH$_3$)$_2$), 2.64 (s, 3H, CH$_3$), 1.26 (d, *J* = 6.2 Hz, 3H, OCH(C*H*$_3$)$_2$), 1.09 (d, *J* = 6.3 Hz, 3H, OCH(C*H*$_3$)$_2$). HRMS (CI) m/z calcd. for $C_{26}H_{24}F_2N_3O_3$ $[M+H]^+$: 464.1707 found: 464.1712.

5.5 OPTIMIZATION AND PRE-CLINICAL VALIDATION OF $A_{2B}AR$ ANTAGONISTS AS DRUGS FOR CANCER (IMMUNO)THERAPY.

5.5.1 *In vitro* and *ex vivo* validation of antiproliferative effects

The proliferation assays in breast cancer and osteosarcoma were conducted by the research group of Prof. Andreas Lundqvist (Karolinska Institute, Sweden). The proliferation assays (and all related ones) in colorectal cancer and glioblastoma were performed in the ONCOMET group (Santiago Health Research Institute) under the supervision of Dr. Miguel Abal and Dr. Jorge Barbazán.

5.5.1.1 Cell culture

HCT116, U87 and U251 cell lines were purchased from the American Type Culture Collection (ATCC) and cultured in DMEM GlutaMAX (ThermoFisher Scientific), supplemented with 10% Fetal Bovine Serum (FBS) (ThermoFisher Scientific) and 1% Penicillin Streptomycin (PS). GlutaMAX supplement (2 mM) was added for HCT116 culture. Cell cultures were regularly tested for the presence of mycoplasma. Human colorectal Cancer Associated Fibroblasts (CAFs) primary cultures were obtained and immortalized as described in bibliography,[226,227] and maintained in DMEM GlutaMAX, 10% FBS, 1% Insulin Transferrin Selenium (ITS) (ThermoFisher Scientific).

Fresh tumor tissue from "cancer type" resections were digested and processed into single cell suspension using gentleMACS tumor dissociation kit (Miltenyi Biotec). Tumor cells were then isolated by negative selection using a tumor cell isolation kit (Miltenyi Biotec). Adherent cells were passaged at least five times before being used for experiments. All cell lines were maintained in RPMI 1640 or DMEM GlutaMAX media (Thermo Fisher Scientific) supplemented with 10% HyClone Fetal Bovine Serum (FBS) (GE Healthcare) and 1% Penicillin Streptomycin (PS) (Life Technologies). A tumor cell line and TIL culture from a breast cancer specimen was established as previously described.[228] Human osteosarcoma cell line U2OS (ATCC) was used in comparison to patient-derived sarcoma cell lines for relative adenosine production and ADO ectonucleotidase expression by flow cytometry.

5.5.1.2 Cell viability assay (AlamarBlue)

To test the effect of $A_{2B}AR$ (and dual $A_{2A}AR/A_{2B}AR$) antagonism on the proliferation, different cell lines were seeded on a 96-well in complete medium at the indicated densities (Table 5.6) and incubated overnight to allow attachment. Cells were then incubated for 24h or

48h with solutions containing **ISAM-MM42**, **ISAM-J1881** or **ISAM-H143** at 2.5, 5 and 10 μM in complete medium. For three-dose assays, cells were incubated for 72 hours with a dose applied every 24 hours. Controls with the equivalent amount of DMSO, used as the solvent for the indicated antagonists, were as well performed. After incubation, the number of viable cells was determined by using AlamarBlue (10%, ThermoFisher Scientific) following manufacturer's recommendations, measuring fluorescence at 590 nm. Proliferation rates for each condition were represented as % proliferation respect to the appropriate DMSO controls.

Table 5.6. Experimental conditions for AlamarBlue assay for the different cell lines

Cell line	Cells/well	Single dose	Multiple dose	Culture medium
HCT116	5,000	*Treatment:* 2.5, 5 and 10 μM *Incubation times:* 24/48h	*Treatment:* 3 doses, one each 24h of 2.5, 5 and 10 μM *Incubation times:* 24h until last dose	DMEM
*h*CAFs	5,000	*Treatment:* 2.5, 5 and 10 μM *Incubation times:* 24/48h	*Treatment:* 3 doses, one each 24h of 2.5, 5 and 10 μM *Incubation times:* 24h until last dose	DMEM supplemented with 1% ITS
Human Primary colorectal	20,000	*Treatment:* 10 μM *Incubation time:* 48h	-	DMEM
CT26	5,000	*Treatment:* 2.5, 5 and 10 μM *Incubation times:* 24/48h	-	DMEM
*m*CAFs	2,000	*Treatment:* 2.5, 5 and 10 μM *Incubation times:* 24/48h	-	DMEM supplemented with 1% ITS
U87	2,000	*Treatment:* 100, 30, 10, 3, 1, and 0.3 μM *Incubation times:* 48h	-	DMEM
U251	2,000	*Treatment:* 100, 30, 10, 3, 1, and 0.3 μM *Incubation times:* 48h	-	DMEM

5.5.1.3 Cell viability assay (Cell-Titer Glo)

From breast cancer single cell suspension, $3x10^3$ cells were seeded and cultured in an ultra-low attachment 384-well plate (Corning) with DMEM-F12 media (Thermo Fisher Scientific) containing 20% FBS and 1% PS. Treatment with A_{2B}AR antagonist at various concentrations were stated in the result section. After four days, Cell-Titer Glo reagent (Promega) was used to measure cell viability in accordance with the manufacturer's instructions and luminescence was measured in an EnSpire Multilabel Reader (PerkinElmer).

5.5.1.4 ADORA gene expression analysis

To assess the gene expression of ADORA2A and ADORA2B genes, RNA was first extracted from cell cultures of HCT116, *h*CAFs, CT26, *m*CAFs, U87 and U251 cell lines using the RNAeasy Mini kit (Qiagen), following manufacturer's protocol. After RNA quantification (Nanodrop, ThermoFisher Scientific), cDNA was synthesized using the M-muLV reverse transcriptase kit (Roche) as indicated by the manufacturer and used for downstream gene expression analysis using the following TaqMan probes (ThermoFisher Scientific): human ADORA2A (Hs00169123_m1) human ADORA2B (Hs00386497_m1) mouse Adora2A (Mm00802075_m1) mouse Adora2B (Mm00839292_m1). The expression of GAPDH was used as a control to normalize results across samples (human GAPDH: Hs999999905_m1; mouse Gapdh: Mm99999915_g1). 60 ng of total cDNA were loaded per well, and qPCR was run following standard recommended conditions on a QuantStudio 3 qPCR system (Applied Biosystems).

GPCR expression was calculated with the Equation 5.3, where GoI refers to the gene of interest. ΔCq values were calculated by substracting raw Cq values for each cancer cell line to the Cq value obtained for GADPH. The final obtained values were then transformed to a Log_2 scale for visualization purposes, calculating the fold change between two different cell lines with the Equation 5.4

Equation 5.3. Absolute gene expression calculation. $\Delta Cq = mean(GoI) - mean(GADPH)$.

$$Absolute\ gene\ expression\ (AGE) = 40 - \Delta Cq$$

Equation 5.4. Fold change calculation. $\Delta\Delta Cq = \Delta Cq_1 - \Delta Cq_2$ ($1\ and\ 2\ are\ two\ different\ genes$)

$$Fold\ change = 2^{-\Delta\Delta Cq}$$

5.5.1.5 Confocal imaging

Images were acquired on an inverted confocal microscope (Leica SP8) using laser lanes 405, 488, 561 and 533nm, an HC-PL-APO CS2 40x/1.30 oil immersion objective, and non-descanned HyD detectors. For each experiment and stage position a Zstack was acquired with a Zstep of 1 µm. For data visualization, a representative Z position was selected for each image stack.

5.5.1.6 EdU incorporation assays and Cleaved Caspase 3 immunostaining

After the specified treatment times, cancer cells/CAFs were incubated for 30 min with a 10 μM EdU solution in a complete medium. Cells were then fixed, and EdU incorporation was revealed as recommended, using the Click-iT EdU Alexa Fluor 647 Imaging kit (ThermoFisher Scientific). The same sample was then used to assess apoptosis using cleaved caspase 3 as a marker. For this, samples were blocked with 3% BSA (w/v) in PBS (v/v) solution for 1h at RT. Primary antibody were prepared in a 0.05% Tx100/PBS (v/v) solution and incubated overnight in humidified chambers at RT. Cells were then washed 3 times with PBS and incubated with secondary antibodies and DAPI, for 1h at RT, washed 3 times in PBS and mounted using AquaPolyMount (Polysciences). Antibodies references and dilutions are listed in Table 5.7.

Table 5.7. Antibodies references and dilutions

Antibody	Distributor	Catalog Nº	Dilution
CC3 (Rabbit Monoclonal)	Cell Signalling	9661	1:200
Secondary: Anti Rabbit Alexa Fluor 568	ThermoFisher	A11011	1:200
DAPI	ThermoFisher	D1306	1:200

5.5.1.7 Image analysis

For EdU and Cleave Caspase 3 stainings, 10-15 random images were taken per condition. The total number of cells was determined based on the DAPI channel and quantified automatically using an Image J (Fiji) v2.3.0/1.53f homemade macro. The total number of cells positive for EdU and Cleaved Caspase 3 was quantified manually and plotted as % to the total number of cells per analyzed field.

5.5.2 *In vitro* and *ex vivo* evaluation of immunostimulatory effects

The preliminary evaluation of immunostimulatory effects was conducted by the research group of Professor Iria Gómez-Touriño (University of Santiago de Compostela, Spain). The remaining assays were conducted by the research group of Prof. Andreas Lundqvist (Karolinska Institute, Sweden).

5.5.2.1 Preliminary evaluation of the immunostimulatory effect

Peripheral blood mononuclear cells (PBMCs) were isolated from a healthy donor, stained with CFSE (Abcam) following the manufacturer's protocol, and cultured in duplicates

in U-bottom 96-well plates at a density of $1.5x10^5$ cells/well in RPMI 1640 medium (Gibco) supplemented with 10% AB Human Serum (Sigma-Aldrich) and 1% Penicillin-Streptomycin (Gibco). PBMCs were stimulated with ImmunoCult™ Human CD3/CD28 T Cell Activator (STEMCELL Technologies) and 50 U/mL Interleukin 2 (Gibco). Adenosine was then added at a final concentration of 0.1mM and compounds **50** and **58** at 15µM. DMSO was used as vehicle control. PBMCs were kept in culture with the different treatments for 3 days in an incubator at 37°C and 5% CO_2. After the culture period, cells were washed twice with DPBS (Gibco) and CFSE fluorescence measured in a BD Accuri flow cytometer. The data was analyzed using FlowJo software (BD): the percentage of $CFSE^+$ cells, and their median fluorescence intensity (MFI) was quantified for each treatment condition, and a ratio against the stimulated condition without adenosine was calculated for each treatment. Positive values indicate increases in the variable compared to the stimulated control, while negative values indicate decreases in the measured variable.

5.5.2.2 Expansion of tumor infiltrating lymphocytes

Digested tumor resections were cultured in suspension with 5% human serum in AIM-V (Thermo Fisher Scientific) or X-VIVO20 (Lonza) media supplemented with 3000 IU/mL of IL-15 (Novartis). After seven days, irradiated PBMCs (100Gy) pooled from at least three healthy donors were added as feeder cells at 200:1 ratio with addition of anti-CD3 functional grade antibody and 500 IU/mL of IL-15. After an additional ten days of culture, TILs were harvested and analyzed for purity using flow cytometry and maintained with 500IU/mL of IL-15.

5.5.2.3 Proliferation assay with exogenous adenosine

Freshly isolated PBMCs and NK cells were stained with 5 μM FITC-conjugated carboxyfluorescein succinimidyl ester (CFSE) (BioLegend) in phosphate-buffered saline (PBS) (Life Technologies) at room temperature for five minutes. CSFE stained cells were washed with flow cytometer buffer thrice. CSFE-labelled healthy PBMCs and NK cells were cultured in 96-well plates with X-VIVO20 and 1% PS for three and six days respectively. Healthy PBMCs were incubated with Human T-activator CD3/CD28 beads at 1:4 ratio (Thermo Fisher Scientific) and IL-2 (Novartis) at 100 IU/mL. Healthy donor NK cells were incubated with 1000 IU/mL IL-2 only. $2x10^5$ PBMCs and $5x10^4$ NK cells were counted for treatment with ADO (Sigma-Aldrich) and 12 µM of A_{2B}AR antagonist at the same day.

5.5.2.4 Proliferation assay with CD73-expressing patient-derived sarcoma spheroid

A malignant peripheral nerve sheath tumor (MPNST) patient-derived sarcoma cell line was used to grow spheroid by seeding $1x10^4$ cells per well in a 96-well ultra-low attachment plate (Thermo Fisher Scientific) with DMEM-F12 media containing 20% FBS and 1% PS for five days. $1x10^5$ CSFE-labelled healthy PBMCs, ratio of 10:1, were added to the CD73 expressing, adenosine-producing spheroid at day five. Similar to the proliferation assay with exogenous ADO, CD3/CD28 beads at 1:4 ratio and IL-2 at 100IU/mL were added. A_{2B}AR antagonism treatment at 12 μM was added at the same day.

5.5.2.5 Spheroid infiltration in autologous TILs

Spheroids were prepared using patient-derived sarcoma cell lines. $1x10^4$ cells were seeded per well in 96-well ultra-low attachment plate with DMEM-F12 media containing 20% FBS and 1% PS for five days. $3x10^4$ CSFE-labelled autologous expanded TILs, at Effector: Target ratio of 3:1, were added to the spheroid at day five with A_{2B}AR antagonism treatment at 12 μM. After three days, spheroid was removed and split into two groups – IN and OUT. IN indicates TILs infiltrated into the sphere, while OUT indicates TILs that did not infiltrate into the sphere. Spheroids were washed with PBS at least twice. GentleMACS tumor dissociation kit (Miltenyi Biotec) was used to digest the spheroids for FC analysis.

5.5.2.6 Real-time imaging

Brightfield and phase contrast images under 4X objective were acquired every six hours on IncuCyte S3 system (Essen BioScience). For breast cancer patient-derived spheroid culture, $1x10^4$ cells per well were seeded with A_{2B}AR antagonist at 12 μM treatment for six days real time imaging. For spheroid infiltration, after the addition of CSFE-labelled autologous expanded TILs and treatment with A_{2B}AR antagonist at 12 μM, green fluorescence images were acquired for three days. All spheroid invasion analysis was performed using top hat segmentation with IncuCyte software.

5.5.2.7 IFNγ and Perforin cytokine production assay

Experimental setup was adopted from a previous study whereby AR antagonist was added to pre-treat cells before exogenous adenosine treatment for intracellular and cytokine staining.[187] In brief, PBMCs were treated with 12 μM of A_{2B}AR antagonists for 90 minutes before the addition of 50 μM of adenosine for 2 hours. Cells were harvested after 2 days of CD3/CD28 bead stimulation before treatment with PMA/ionomycin (Sigma Aldrich) and golgi-

inhibitors (BD biosciences). After 3 hours of subsequent incubation, intracellular staining was performed for IFNγ and Perforin (Table 5.8).

5.5.2.8 Flow cytometry and statistical analysis

Cell surface was stained with mouse monoclonal anti-human antibodies against CD3, CD4, CD8, CD45RA, CD56 and CD19, listed in Table 5.8. Cell surface antibodies and live/dead (L/D) marker were incubated with samples at 4°C for 20 minutes after washing twice with flow cytometry buffer containing 5% FBS in PBS. For spheroid infiltrated TIL phenotyping, digested IN and OUT spheroids were stained with cell surface marker and analyzed on NovoCyte (ACEA Bioscience) with the use of FlowJo software (Tree Star) by gating single cell based on forward and side scatters.

Table 5.8. List of cell surface antibodies used in flow cytometry. A) $A_{2A}AR$ & $A_{2B}AR$ expression profiling, B) CFSE Proliferation and Annexin V viability assay, C) ADO ectonucleotidase expression, D) Spheroid infiltrated TIL phenotyping E) Extracellular ADO uptake assay. F) IFNy and Perforin cytokine

Antigen	Conjugate	Distributor	Catalog N°	A	B	C	D	E	F
CD3 (T cell)	PerCP/Cy5.5	BioLengend	30429	✓			✓		
	PE-CF594	BD Bioscience	562280		✓			✓	✓
CD4 (Th cell)	Pacific Blue	BD Bioscience	558116	✓	✓		✓	✓	✓
CD8 (CTL)	PE/Cy7	eBioscience	25-0088-42	✓	✓		✓	✓	✓
CD45RA (Naïve T cell)	Brilliant Violet 650	BioLegend	304136	✓	✓				
CD27 (Central memory marker)	Brilliant Violet 605	BioLegend	302830	✓	✓				
CD56 (NK cell)	APC/Cy7	BioLegend	318331	✓					
	Brilliant Violet 570	BD Horizon	564058		✓		✓		
CD19 (B cell)	Brilliant Violet 570	BioLegend	302235	✓					
CD45 (Leukocyte)	Brilliant Violet 650	BioLegend	304044			✓			
CD73	APC/Cy7	BioLegend	344022			✓			
CD39	PE/Cy7	BioLegend	328211			✓			
CD11a	PE	BioLegend	301208				✓		
CD49a	APC/Fire 750	BioLegend	328317				✓		
CD69	Brilliant Violet 785	BioLegend	310931				✓		✓
CD103	APC	BioLegend	350215				✓		
IFNy	eFluor450	eBioscience	48-7319-42						✓
Perforin	PE	BioLegend	308106						✓
Live/Dead marker	Aqua	Thermo Fisher	L34966	✓		✓	✓		
	Near-IR	Thermo Fisher	L10119		✓			✓	✓

5.5.2.9 Statistical analysis

Experimental replicates are presented as mean ± standard deviation (SD) and median in box plot stated in the figure legend of the result section. Statistical analysis was performed using Prism 9 (GraphPad, Dotmatics) and stated in figure legends.

6 REFERENCES

(1) Global Cancer Observatory https://gco.iarc.fr/.

(2) Thompson, E. A.; Powell, J. D. Inhibition of the Adenosine Pathway to Potentiate Cancer Immunotherapy: Potential for Combinatorial Approaches. *Annu. Rev. Med.* **2021**, *72*, 331–348.

(3) Malik, D.; Mahendiratta, S.; Kaur, H.; Medhi, B. Futuristic Approach to Cancer Treatment. *Gene* **2021**, *805*, 145906.

(4) Hanahan, D.; Weinberg, R. A. The Hallmarks of Cancer. *Cell* **2000**, *100*, 57–70.

(5) Hanahan, D.; Weinberg, R. A. Hallmarks of Cancer: The next Generation. *Cell* **2011**, *144*, 646–674.

(6) Hanahan, D. Hallmarks of Cancer: New Dimensions. *Cancer Discov.* **2022**, *12*, 31–46.

(7) Witsch, E.; Sela, M.; Yarden, Y. Roles for Growth Factors in Cancer Progression. *Physiology* **2010**, *25*, 85–101.

(8) Cooper, G. M. Tumor Suppressor Genes. **2000**.

(9) Shay, J. W. Role of Telomeres and Telomerase in Aging and Cancer. *Cancer Discov.* **2016**, *6*, 584–593.

(10) Smith-Sonneborn, J. Telomerase Biology Associations Offer Keys to Cancer and Aging Therapeutics. *Curr. Aging Sci.* **2019**, *13*, 11–21.

(11) Bergers, G.; Benjamin, L. E. Tumorigenesis and the Angiogenic Switch. *Nat. Rev. Cancer* **2003**, *3*, 401–410.

(12) Talmadge, J. E.; Fidler, I. J. AACR Centennial Series: The Biology of Cancer Metastasis: Historical Perspective. *Cancer Res.* **2010**, *70*, 5649–5669.

(13) Vijayan, D.; Young, A.; Teng, M. W. L.; Smyth, M. J. Targeting Immunosuppressive Adenosine in Cancer. *Nat. Rev. Cancer* **2017**, *17*, 709–724.

(14) Gao, Z.-G.; Jacobson, K. A. Molecular Sciences A 2B Adenosine Receptor and Cancer. *Int. J. Mol. Sci.* **2019**, *1*, 1–18.

(15) Kalinski, P. *Tumor Immune Microenvironment in Cancer Progression and Cancer Therapy*; 2017; p 264.

(16) Junttila, M. R.; de Sauvage, F. J. Influence of Tumour Micro-Environment Heterogeneity on Therapeutic Response. *Nature* **2013**, *501*, 346–354.

(17) Kroeger, D. R.; Milne, K.; Nelson, B. H. Tumor-Infiltrating Plasma Cells Are Associated with Tertiary Lymphoid Structures, Cytolytic T-Cell Responses, and Superior Prognosis in Ovarian Cancer. *Clin. Cancer Res.* **2016**, *22*, 3005–3015.

(18) Kumari, S.; Advani, D.; Sharma, S.; Ambasta, R. K.; Kumar, P. Combinatorial Therapy in Tumor Microenvironment: Where Do We Stand? *Biochim. Biophys. Acta BBA - Rev. Cancer* **2021**, *1876*, 188585–188585.

(19) Faget, D. V.; Ren, Q.; Stewart, S. A. Unmasking Senescence: Context-Dependent Effects of SASP in Cancer. *Nat. Rev. Cancer* **2019**, *19*, 439–453.

(20) Ruhland, M. K.; Loza, A. J.; Capietto, A.-H.; Luo, X.; Knolhoff, B. L.; Flanagan, K. C.; Belt, B. A.; Alspach, E.; Leahy, K.; Luo, J.; Schaffer, A.; Edwards, J. R.; Longmore, G.; Faccio, R.; DeNardo, D. G.; Stewart, S. A. Stromal Senescence Establishes an Immunosuppressive Microenvironment That Drives Tumorigenesis. *Nat. Commun.* **2016**, *7*, 11762–11762.

(21) Antonioli, L.; Blandizzi, C.; Pacher, P.; Haskó, G. Immunity, Inflammation and Cancer: A Leading Role for Adenosine. *Nat. Rev. Cancer* **2013**, *13*, 842–857.

(22) Kimiz-Gebologlu, I.; Gulce-Iz, S.; Biray-Avci, C. Monoclonal Antibodies in Cancer Immunotherapy. *Mol. Biol. Rep.* **2018**, *45*, 2935–2940.

(23) FDA-Approved Drugs https://www.accessdata.fda.gov/scripts/cder/daf/.

(24) Download medicine data | European Medicines Agency https://www.ema.europa.eu/en/medicines/download-medicine-data.

(25) Maj, T.; Wang, W.; Crespo, J.; Zhang, H.; Wang, W.; Wei, S.; Zhao, L.; Vatan, L.; Shao, I.; Szeliga, W. Oxidative Stress Controls Regulatory T Cell Apoptosis and Suppressor Activity and PD-L1-Blockade Resistance in Tumor. *Nat. Immunol.* **2017**, *18*, 1332–1332.

(26) Hayashi, H.; Nakagawa, K. Combination Therapy with PD-1 or PD-L1 Inhibitors for Cancer. *Int. J. Clin. Oncol.* **2020**, *25*, 818–830.

(27) Yu, F.; Zhu, C.; Xie, Q.; Wang, Y. Adenosine A2A Receptor Antagonists for Cancer Immunotherapy. *J. Med. Chem.* **2020**, *63*, 12196–12212.

(28) Borodovsky, A.; Barbon, C. M.; Wang, Y.; Ye, M.; Prickett, L.; Chandra, D.; Shaw, J.; Deng, N.; Sachsenmeier, K.; Clarke, J. D.; Linghu, B.; Brown, G. A.; Brown, J.;

Congreve, M.; Cheng, R. K.; Dore, A. S.; Hurrell, E.; Shao, W.; Woessner, R.; Reimer, C.; Drew, L.; Fawell, S.; Schuller, A. G.; Mele, D. A. Small Molecule AZD4635 Inhibitor of A2AR Signaling Rescues Immune Cell Function Including CD103+ Dendritic Cells Enhancing Anti-Tumor Immunity. *J. Immunother. Cancer* **2020**, *8*, 1–17.

(29) Allard, B.; Longhi, M. S.; Robson, S. C.; Stagg, J. The Ectonucleotidases CD39 and CD73: Novel Checkpoint Inhibitor Targets. *Immunol. Rev.* **2017**, *276*, 121–144.

(30) Di Virgilio, F.; Adinolfi, E. Extracellular Purines, Purinergic Receptors and Tumor Growth. *Oncogene* **2017**, *36*, 293–303.

(31) Allard, D.; Allard, B.; Stagg, J. On the Mechanism of Anti-CD39 Immune Checkpoint Therapy. *J. Immunother. Cancer* **2020**, *8*, 1–11.

(32) Sepúlveda, C.; Palomo, I.; Fuentes, E. Role of Adenosine A2b Receptor Overexpression in Tumor Progression. *Life Sci.* **2016**, *166*, 92–99.

(33) Borea, P. A.; Gessi, S.; Merighi, S.; Vincenzi, F.; Varani, K. Pathological Overproduction: The Bad Side of Adenosine. *Br. J. Pharmacol.* **2017**, *174*, 1945–1960.

(34) Kumar, V. Adenosine as an Endogenous Immunoregulator in Cancer Pathogenesis: Where to Go? *Purinergic Signal* **2013**, *9*, 145–165.

(35) Ohta, A.; Gorelik, E.; Prasad, S. J.; Ronchese, F.; Lukashev, D.; Wong, M. K.; Huang, X.; Caldwell, S.; Liu, K.; Smith, P.; Chen, J. F.; Jackson, E. K.; Apasov, S.; Abrams, S.; Sitkovsky, M. A2A Adenosine Receptor Protects Tumors from Antitumor T Cells. *Proc Natl Acad Sci U A* **2006**, *103*, 13132–13137.

(36) Borea, P. A.; Gessi, S.; Merighi, S.; Vincenzi, F.; Varani, K. Pharmacology of Adenosine Receptors: The State of the Art. *Physiol. Rev.* **2018**, *98*, 1591–1625.

(37) Shi, L.; Yang, L.; Wu, Z.; Xu, W.; Song, J.; Guan, W. Adenosine Signaling: Next Checkpoint for Gastric Cancer Immunotherapy? *Int Immunopharmacol* **2018**, *63*, 58–65.

(38) Whiteside, T. L. Targeting Adenosine in Cancer Immunotherapy: A Review of Recent Progress. *Expert Rev. Anticancer Ther.* **2017**, *17*, 527–535.

(39) Allard, B.; Beavis, P. A.; Darcy, P. K.; Stagg, J. Immunosuppressive Activities of Adenosine in Cancer. *Curr. Opin. Pharmacol.* **2016**, *29*, 7–16.

(40) Horenstein, A. L.; Chillemi, A.; Zaccarello, G.; Bruzzone, S.; Quarona, V.; Zito, A.; Serra, S.; Malavasi, F. A CD38/CD203a/CD73 Ectoenzymatic Pathway Independent of

CD39 Drives a Novel Adenosinergic Loop in Human T Lymphocytes. *Oncoimmunology* **2013**, *2*, e26246–e26246.

(41) Antonioli, L.; Fornai, M.; Blandizzi, C.; Pacher, P.; Haskó, G. Adenosine Signaling and the Immune System: When a Lot Could Be Too Much. *Immunol. Lett.* **2019**, *205*, 9–15.

(42) Ohta, A.; Sitkovsky, M. Role of G-Protein-Coupled Adenosine Receptors in Downregulation of Inflammation and Protection from Tissue Damage. *Nature* **2001**, *414*, 916–920.

(43) Hinz, S.; Navarro, G.; Borroto-Escuela, D.; Seibt, B. F.; Ammon, Y.-C.; de Filippo, E.; Danish, A.; Lacher, S. K.; Červinková, B.; Rafehi, M.; Fuxe, K.; Schiedel, A. C.; Franco, R.; Müller, C. E. Adenosine A2A Receptor Ligand Recognition and Signaling Is Blocked by A2B Receptors. *Oncotarget* **2018**, *9*, 13593–13611.

(44) Cekic, C.; Linden, J. Adenosine A2A Receptors Intrinsically Regulate CD8+ T Cells in the Tumor Microenvironment. *Cancer Res.* **2014**, *74*, 7239–7249.

(45) Kjaergaard, J.; Hatfield, S.; Jones, G.; Ohta, A.; Sitkovsky, M. A 2A Adenosine Receptor Gene Deletion or Synthetic A 2A Antagonist Liberate Tumor-Reactive CD8 + T Cells from Tumor-Induced Immunosuppression. *J. Immunol.* **2018**, *201*, 782–791.

(46) Ohta, A. A.; Kini, R.; Ohta, A. A.; Subramanian, M.; Madasu, M.; Sitkovsky, M. The Development and Immunosuppressive Functions of CD4+ CD25+ FoxP3+ Regulatory T Cells Are under Influence of the Adenosine-A2A Adenosine Receptor Pathway. *Front. Immunol.* **2012**, *3*, 1–12.

(47) Panther, E.; Corinti, S.; Idzko, M.; Herouy, Y.; Napp, M.; La Sala, A.; Girolomoni, G.; Norgauer, J. Adenosine Affects Expression of Membrane Molecules, Cytokine and Chemokine Release, and the T-Cell Stimulatory Capacity of Human Dendritic Cells. *Blood* **2003**, *101*, 3985–3990.

(48) Sitkovsky, M. V. Lessons from the A2A Adenosine Receptor Antagonist– Enabled Tumor Regression and Survival in Patients with Treatment-Refractory Renal Cell Cancer. *Cancer Discov.* **2020**, *10*, 16–19.

(49) Congreve, M.; Brown, G. A.; Borodovsky, A.; Lamb, M. L. Targeting Adenosine A 2A Receptor Antagonism for Treatment of Cancer. *Expert Opin. Drug Discov.* **2018**, *13*, 997–1003.

(50) Fredholm, B. B.; IJzerman, A. P.; Jacobson, K. A.; Linden, J.; Müller, C. E. International Union of Basic and Clinical Pharmacology. LXXXI. Nomenclature and Classification of Adenosine Receptors - An Update. *Pharmacol. Rev.* **2011**, *63*, 1–34.

(51) Chen, S.; Akdemir, I.; Fan, J.; Linden, J.; Zhang, B.; Cekic, C. The Expression of Adenosine A2B Receptor on Antigen Presenting Cells Suppresses CD8+ T Cell Responses and Promotes Tumor Growth. *Cancer Immunol. Res.* **2020**, canimm.0833.2019-canimm.0833.2019.

(52) Corona, S. P.; Sobhani, N.; Generali, D. Adenosine A2B Receptor: Novel Anti-Cancer Therapeutic Implications. *J. Cancer Metastasis Treat.* **2017**, *3*, 206–206.

(53) Leone, R. D.; Emens, L. A. Targeting Adenosine for Cancer Immunotherapy. *J. Immunother. Cancer* **2018**, *6*, 1–9.

(54) Piedra-Quintero, Z. L.; Wilson, Z.; Nava, P.; Guerau-de-Arellano, M. CD38: An Immunomodulatory Molecule in Inflammation and Autoimmunity. *Front. Immunol.* **2020**, *11*, 3111–3111.

(55) Jacob, F.; Pérez Novo, C.; Bachert, C.; Van Crombruggen, K. Purinergic Signaling in Inflammatory Cells: P2 Receptor Expression, Functional Effects, and Modulation of Inflammatory Responses. *Purinergic Signal.* **2013**, *9*, 285–306.

(56) Panjehpour, M.; Karami-Tehrani, F. Adenosine Modulates Cell Growth in the Human Breast Cancer Cells via Adenosine Receptors. *Oncol. Res.* **2007**, *16*, 575–585.

(57) Bahreyni, A.; Samani, S. S.; Rahmani, F.; Behnam-Rassouli, R.; Khazaei, M.; Ryzhikov, M.; Parizadeh, M. R.; Avan, A.; Hassanian, S. M. Role of Adenosine Signaling in the Pathogenesis of Breast Cancer. *J. Cell. Physiol.* **2018**, *233*, 1836–1843.

(58) Schneider, E.; Rissiek, A.; Winzer, R.; Puig, B.; Rissiek, B.; Haag, F.; Mittrücker, H. W.; Magnus, T.; Tolosa, E. Generation and Function of Non-Cell-Bound Cd73 in Inflammation. *Front. Immunol.* **2019**, *10*.

(59) Ludwig, N.; Azambuja, J. H.; Rao, A.; Gillespie, D. G.; Jackson, E. K.; Whiteside, T. L. Adenosine Receptors Regulate Exosome Production. *Purinergic Signal.* **2020**, *16*, 231–240.

(60) Clayton, A.; Al-Taei, S.; Webber, J.; Mason, M. D.; Tabi, Z. Cancer Exosomes Express CD39 and CD73, Which Suppress T Cells through Adenosine Production. *J. Immunol.* **2011**, *187*, 676–683.

(61) Bahreyni, A.; Khazaei, M.; Rajabian, M.; Ryzhikov, M.; Avan, A.; Hassanian, S. M. Therapeutic Potency of Pharmacological Adenosine Receptor Agonist/Antagonist in Angiogenesis, Current Status and Perspectives. *J. Pharm. Pharmacol.* **2018**, *70*, 191–196.

(62) Antonioli, L.; Pacher, P.; Vizi, E. S.; Haskó, G. CD39 and CD73 in Immunity and Inflammation. *Trends Mol. Med.* **2013**, *19*, 355–367.

(63) Jacobson, K. A.; Tosh, D. K.; Jain, S.; Gao, Z. G. Historical and Current Adenosine Receptor Agonists in Preclinical and Clinical Development. *Front. Cell. Neurosci.* **2019**, *13*, 1–17.

(64) Jin, K.; Mao, C.; Chen, L.; Wang, L.; Liu, Y.; Yuan, J. Review Adenosinergic Pathway: A Hope in the Immunotherapy of Glioblastoma. *Cancers* **2021**, *13*, 1–21.

(65) Gorain, B.; Choudhury, H.; Yee, G. S.; Bhattamisra, S. K. Adenosine Receptors as Novel Targets for the Treatment of Various Cancers. *Curr. Pharm. Des.* **2019**, *25*, 2828–2841.

(66) Gao, Z. G.; Jacobson, K. A. A2B Adenosine Receptor and Cancer. *Int. J. Mol. Sci.* **2019**, *20*, 1–18.

(67) Barletta, K. E.; Ley, K.; Mehrad, B. Regulation of Neutrophil Function by Adenosine. *Arterioscler. Thromb. Vasc. Biol.* **2012**, *32*, 856–864.

(68) Aherne, C. M.; Collins, C. B.; Masterson, J. C.; Tizzano, M.; Boyle, T. A.; Westrich, J. A.; Parnes, J. A.; Furuta, G. T.; Rivera-Nieves, J.; Eltzschig, H. K. Neuronal Guidance Molecule Netrin-1 Attenuates Inflammatory Cell Trafficking during Acute Experimental Colitis. *Gut* **2012**, *61*, 695–705.

(69) Garcia-Garcia, L.; Olle, L.; Martin, M.; Roca-Ferrer, J.; Muñoz-Cano, R. Adenosine Signaling in Mast Cells and Allergic Diseases. *Int. J. Mol. Sci.* **2021**, *22*, 5203–5203.

(70) Ferrari, D.; Vuerich, M.; Casciano, F.; Longhi, M. S.; Melloni, E.; Secchiero, P.; Zech, A.; Robson, S. C.; Müller, T.; Idzko, M. Eosinophils and Purinergic Signaling in Health and Disease. *Front. Immunol.* **2020**, *11*.

(71) Allard, B.; Allard, D.; Buisseret, L.; Stagg, J. The Adenosine Pathway in Immuno-Oncology. *Nat. Rev. Clin. Oncol.* **2020**, *17*, 611–629.

(72) Sorrentino, C.; Miele, L.; Porta, A.; Pinto, A.; Morello, S. Myeloid-Derived Suppressor Cells Contribute to A2B Adenosine Receptor-Induced VEGF Production and Angiogenesis in a Mouse Melanoma Model. *Oncotarget* **2015**, *6*, 27478–27489.

(73) Ryzhov, S. V.; Pickup, M. W.; Chytil, A.; Gorska, A. E.; Zhang, Q.; Owens, P.; Feoktistov, I.; Moses, H. L.; Novitskiy, S. V. Role of TGF-β Signaling in Generation of CD39+/CD73+ Myeloid Cells in Tumors. *J. Immunol.* **2014**, *193*, 3155 LP – 3164.

(74) Fleming, V.; Hu, X.; Weber, R.; Nagibin, V.; Groth, C.; Altevogt, P.; Utikal, J.; Umansky, V. Targeting Myeloid-Derived Suppressor Cells to Bypass Tumor-Induced Immunosuppression. *Front. Immunol.* **2018**, *9*.

(75) Morello, S.; Pinto, A.; Blandizzi, C.; Antonioli, L. Myeloid Cells in the Tumor Microenvironment: Role of Adenosine. *OncoImmunology* **2016**, *5*, 1–8.

(76) Haskó, G.; Csóka, B.; Németh, Z. H.; Vizi, E. S.; Pacher, P. A2B Adenosine Receptors in Immunity and Inflammation. *Trends Immunol.* **2009**, *30*, 263–270.

(77) Sek, K.; Mølck, C.; Stewart, G. D.; Kats, L.; Darcy, P. K.; Beavis, P. A. Targeting Adenosine Receptor Signaling in Cancer Immunotherapy. *Int. J. Mol. Sci.* **2018**, *19*.

(78) Allard, B.; Pommey, S.; Smyth, M.; Stagg, J. Targeting CD73 Enhances the Antitumor Activity of Anti-PD-1 and Anti-CTLA-4 MAbs. *Clin. Cancer Res. Off. J. Am. Assoc. Cancer Res.* **2013**, *19*.

(79) Cheng, R. K. Y.; Segala, E.; Robertson, N.; Deflorian, F.; Doré, A. S.; Errey, J. C.; Fiez-Vandal, C.; Marshall, F. H.; Cooke, R. M. Structures of Human A1 and A2A Adenosine Receptors with Xanthines Reveal Determinants of Selectivity. *Structure* **2017**, *25*, 1275–1285.

(80) Glukhova, A.; Thal, D. M.; Nguyen, A. T.; Vecchio, E. A.; Jörg, M.; Scammells, P. J.; May, L. T.; Sexton, P. M.; Christopoulos, A. Structure of the Adenosine A1 Receptor Reveals the Basis for Subtype Selectivity. *Cell* **2017**, *168*, 867-877.e13.

(81) Sun, B.; Bachhawat, P.; Chu, M. L. H.; Wood, M.; Ceska, T.; Sands, Z. A.; Mercier, J.; Lebon, F.; Kobilka, T. S.; Kobilka, B. K. Crystal Structure of the Adenosine A2A Receptor Bound to an Antagonist Reveals a Potential Allosteric Pocket. *Proc. Natl. Acad. Sci. U. S. A.* **2017**, *114*, 2066–2071.

(82) Jaakola, V. P.; Griffith, M. T.; Hanson, M. A.; Cherezov, V.; Chien, E. Y. T.; Lane, J. R.; Ijzerman, A. P.; Stevens, R. C.; Ellen, Y. T.; Lane, J. R.; Ijzerman, A. P.; Stevens, R. C. The 2.6 Angstrom Crystal Structure of a Human A2A Adenosine Receptor Bound to an Antagonist. *Science* **2008**, *322*, 1211–1217.

(83) Xu, F.; Wu, H.; Katritch, V.; Han, G. W.; Jacobson, K. A.; Gao, Z.-G.; Cherezov, V.; Stevens, R. C. Structure of an Agonist-Bound Human A2A Adenosine Receptor. *Science* **2011**, *332*, 322–327.

(84) Chen, Y.; Zhang, J.; Weng, Y.; Xu, Y.; Lu, W.; Liu, W.; Liu, M.; Hua, T.; Song, G. Cryo-EM Structure of the Human Adenosine A2B Receptor–Gs Signaling Complex. *Sci. Adv. 8*, eadd3709.

(85) Liu, W.; Chun, E.; Thompson, A. A.; Chubukov, P.; Xu, F.; Katritch, V.; Han, G. W.; Roth, C. B.; Heitman, L. H.; IJzerman, A. P.; Cherezov, V.; Stevens, R. C. Structural Basis for Allosteric Regulation of GPCRs by Sodium Ions. *Science* **2012**, *337*, 232–236.

(86) Val, C.; Rodriguez-Garcia, C.; Prieto-Díaz, R.; Crespo, A.; Azuaje, J.; Carbajales, C.; Majellaro, M.; Diaz-Holguin, A.; Brea, J.; Loza, M.; Gioé-Gallo, C.; Contino, M.; Stefanachi, A.; García-Mera, X.; Estévez, J.; Gutiérrez-de-Terán, H.; Sotelo, E. Optimization of 2-Amino-4,6-Diarylpyrimidine-5-Carbonitriles as Potent and Selective A1 Antagonists. *J. Med. Chem. 65*, 2091–2106.

(87) El Maatougui, A.; Azuaje, J.; González-Gómez, M.; Miguez, G.; Crespo, A.; Carbajales, C.; Escalante, L.; García-Mera, X.; Gutiérrez-De-Terán, H.; Sotelo, E. Discovery of Potent and Highly Selective A2B Adenosine Receptor Antagonist Chemotypes. *J. Med. Chem.* **2016**, *59*, 1967–1983.

(88) Baltos, J. A.; Paoletta, S.; Nguyen, A. T. N.; Gregory, K. J.; Tosh, D. K.; Christopoulos, A.; Jacobson, K. A.; May, L. T. Structure-Activity Analysis of Biased Agonism at the Human Adenosine A3 Receptor. *Mol. Pharmacol.* **2016**, *90*, 12–22.

(89) Ciruela, F.; Ferré, S.; Casadó, V.; Cortés, A.; Cunha, R. A.; Lluis, C.; Franco, R. Heterodimeric Adenosine Receptors: A Device to Regulate Neurotransmitter Release. *Cell. Mol. Life Sci.* **2006**, *63*, 2427–2431.

(90) Fuxe, K.; Ferré, S.; Canals, M.; Torvinen, M.; Terasmaa, A.; Marcellino, D.; Goldberg, S. R.; Staines, W.; Jacobsen, K. X.; Lluis, C.; Woods, A. s.; Agnati, L. F.; Franco, R. Adenosine A2A and Dopamine D2 Heteromeric Receptor Complexes and Their Function. *J. Mol. Neurosci.* **2005**, *26*, 209–220.

(91) Pinna, A. Adenosine A2A Receptor Antagonists in Parkinson's Disease: Progress in Clinical Trials from the Newly Approved Istradefylline to Drugs in Early Development and Those Already Discontinued. *CNS Drugs* **2014**, *28*, 455–474.

(92) Müller, C. E.; Jacobson, K. A. Recent Developments in Adenosine Receptor Ligands and Their Potential as Novel Drugs. *Biochim. Biophys. Acta - Biomembr.* **2011**, *1808*, 1290–1308.

(93) Müller, C. E.; Baqi, Y.; Hinz, S.; Namasivayam, V. Medicinal Chemistry of A2B Adenosine Receptors. *Receptors* **2018**, *34*, 137–168.

(94) Jacobson, K. A.; IJzerman, A. P.; Müller, C. E. Medicinal Chemistry of P2 and Adenosine Receptors: Common Scaffolds Adapted for Multiple Targets. *Biochem. Pharmacol.* **2021**, *187*.

(95) Deb, P. K.; Deka, S.; Borah, P.; Abed, S. N.; Klotz, K.-N. Medicinal Chemistry and Therapeutic Potential of Agonists, Antagonists and Allosteric Modulators of A1 Adenosine Receptor: Current Status and Perspectives. *Curr. Pharm. Des.* **2019**, *25*, 2697–2715.

(96) Jacobson, K. A.; Klutz, A. M.; Tosh, D. K.; Ivanov, A. A.; Preti, D.; Baraldi, P. G. *Medicinal Chemistry of the A3 Adenosine Receptor: Agonists, Antagonists, and Receptor Engineering*; Handbook of Experimental Pharmacology; 2009; Vol. 193, p 159.

(97) Abdel-Hamid, M.; Novotny, L.; Hamza, H. Stability Study of Selected Adenosine Nucleosides Using LC and LC/MS Analyses. *J. Pharm. Biomed. Anal.* **2000**, *22*, 745–755.

(98) Tang, J.; Zou, Y.; Li, L.; Lu, F.; Xu, H.; Ren, P.; Bai, F.; Niedermann, G.; Zhu, X. BAY 60-6583 Enhances the Antitumor Function of Chimeric Antigen Receptor-Modified T Cells Independent of the Adenosine A2b Receptor. *Front. Pharmacol.* **2021**, *12*, 1–12.

(99) Daly, J. W.; Padgett, W. L.; Secunda, S. I.; Thompson, R. D.; Olsson, R. A. Structure-Activity Relationships for 2-Substituted Adenosines at A1 and A2 Adenosine Receptors. *Pharmacology* **1993**, *46*, 91–100.

(100) Kuno, A.; Critz, S. D.; Cui, L.; Solodushko, V.; Yang, X.-M.; Krahn, T.; Albrecht, B.; Philipp, S.; Cohen, M. V.; Downey, J. M. Protein Kinase C Protects Preconditioned Rabbit Hearts by Increasing Sensitivity of Adenosine A2b-Dependent Signaling during Early Reperfusion. *J. Mol. Cell. Cardiol.* **2007**, *43*, 262–271.

(101) Melman, A.; Gao, Z.-G.; Kumar, D.; Wan, T. C.; Gizewski, E.; Auchampach, J. A.; Jacobson, K. A. Design of (N)-Methanocarba Adenosine 5′-Uronamides as Species-

Independent A3 Receptor-Selective Agonists. *Bioorg. Med. Chem. Lett.* **2008**, *18*, 2813–2819.

(102) Gao, Y.; Phillis, J. W. CGS 15943, An Adenosine A2 Receptor Antagonist, Reduces Cerebral Ischemic Injury in the Mongolian Gerbil. *Life Sci.* **1994**, *55*, PL61–PL65.

(103) Klotz, K.-N. Adenosine Receptors and Their Ligands. *Naunyn. Schmiedebergs Arch. Pharmacol.* **2000**, *362*, 382–391.

(104) Williams, M.; Francis, J.; Ghai, G.; Braunwalder, A.; Psychoyos, S.; Stone, G. A.; Cash, W. D. Biochemical Characterization of the Triazoloquinazoline CGS 15943A, a Novel, Nonxanthine Adenosine Antagonist. *J. Pharmacol. Exp. Ther.* **1987**, *241*, 415–415.

(105) Martinson, E. A.; Johnson, R. A.; Wells, J. N. Potent Adenosine Receptor Antagonists That Are Selective for the A1 Receptor Subtype. *Mol. Pharmacol.* **1987**, *31*, 247–252.

(106) Weyler, S.; Fülle, F.; Diekmann, M.; Schumacher, B.; Hinz, S.; Klotz, K.-N. N.; Müller, C. E. Improving Potency, Selectivity, and Water Solubility of Adenosine A 1 Receptor Antagonists: Xanthines Modified at Position 3 and Related Pyrimido[1,2,3-Cd]Purinediones. *ChemMedChem* **2006**, *1*, 891–902.

(107) Jacobson, K. A.; Gallo-Rodriguez, C.; Melman, N.; Fischer, B.; Maillard, M.; van Bergen, A.; van Galen, P. J. M.; Karton, Y. Structure-Activity Relationships of 8-Styrylxanthines as A2-Selective Adenosine Antagonists. *J. Med. Chem.* **1993**, *36*, 1333–1342.

(108) Borrmann, T.; Hinz, S.; Bertarelli, D. C. G.; Li, W.; Florin, N. C.; Scheiff, A. B.; Müller, C. E. 1-Alkyl-8-(Piperazine-1-Sulfonyl)Phenylxanthines: Development and Characterization of Adenosine A2B Receptor Antagonists and a New Radioligand with Subnanomolar Affinity and Subtype Specificity. *J. Med. Chem.* **2009**, *52*, 3994–4006.

(109) Müller, C. E.; Diekmann, M.; Thorand, M.; Ozola, V. [3H]8-Ethyl-4-Methyl-2-Phenyl-(8R)-4,5,7,8-Tetrahydro-1H-Imidazo [2,1-i]-Purin-5-One ([3H]PSB-11), a Novel High-Affinity Antagonist Radioligand for Human A3 Adenosine Receptors. *Bioorg. Med. Chem. Lett.* **2002**, *12*, 501–503.

(110) Shimada, J.; Suzuki, F.; Nonaka, H.; Ishii, A. 8-Polycycloalkyl-1,3-Dipropylxanthines as Potent and Selective Antagonists for A1-Adenosine Receptors. *J. Med. Chem.* **1992**, *35*, 924–930.

(111) Kiesman, W. F.; Zhao, J.; Conlon, P. R.; Dowling, J. E.; Petter, R. C.; Lutterodt, F.; Jin, X.; Smits, G.; Fure, M.; Jayaraj, A.; Kim, J.; Sullivan, G.; Linden, J. Potent and Orally

Bioavailable 8-Bicyclo[2.2.2]Octylxanthines as Adenosine A1 Receptor Antagonists. *J. Med. Chem.* **2006**, *49*, 7119–7131.

(112) Cacciari, B.; Spalluto, G.; Federico, S. A2A Adenosine Receptor Antagonists as Therapeutic Candidates: Are They Still an Interesting Challenge? *Mini-Rev. Med. Chem.* **2018**, *18*, 1168–1174.

(113) P.C Churchill; K. XAC, a Functionalized Congener of 1,3-Dialkylxanthine, Antagonizes A1 Adenosine Receptor-Mediated Inhibition of Renin Secretion In Vitro. *Bone* **2008**, *23*, 1–7.

(114) Ji, X.; Kim, Y. C.; Ahern, D. G.; Linden, J.; Jacobson, K. A. [3H]MRS 1754, a Selective Antagonist Radioligand for A(2B) Adenosine Receptors. *Biochem. Pharmacol.* **2001**, *61*, 657–663.

(115) Cagnina, R. E.; Ramos, S. I.; Marshall, M. A.; Wang, G.; Frazier, C. R.; Linden, J. Adenosine A2B Receptors Are Highly Expressed on Murine Type II Alveolar Epithelial Cells. *Am. J. Physiol. Lung Cell. Mol. Physiol.* **2009**, *297*, L467–L474.

(116) Baraldi, P. G.; Aghazadeh Tabrizi, M.; Preti, D.; Bovero, A.; Fruttarolo, F.; Romagnoli, R.; Moorman, A. R.; Gessi, S.; Merighi, S.; Varani, K.; Andrea Borea, P. [3H]-MRE 2029-F20, a Selective Antagonist Radioligand for the Human A2B Adenosine Receptors. *Bioorg. Med. Chem. Lett.* **2004**, *14*, 3607–3610.

(117) Nieto, M. I.; Balo, M. C.; Brea, J.; Caamaño, O.; Fernández, F.; García-Mera, X.; López, C.; Loza, M. I.; Rodríguez-Borges, J. E.; Vidal, B. Synthesis and Pharmacological Evaluation of Novel Substituted 9-Deazaxanthines as A2B Receptor Antagonists. *Eur. J. Med. Chem.* **2010**, *45*, 2884–2892.

(118) Carotti, A.; Stefanachi, A.; Raviña, E.; Sotelo, E.; Loza, M. I.; Cadavid, M. I.; Centeno, N. B.; Nicolotti, O. 8-Substituted-9-Deazaxanthines as Adenosine Receptor Ligands: Design, Synthesis and Structure-Affinity Relationships at A2B. *Eur. J. Med. Chem.* **2004**, *39*, 879–887.

(119) Stefanachi, A.; Nicolotti, O.; Leonetti, F.; Cellamare, S.; Campagna, F.; Loza, M. I.; Brea, J. M.; Mazza, F.; Gavuzzo, E.; Carotti, A. 1,3-Dialkyl-8-(Hetero)Aryl-9-OH-9-Deazaxanthines as Potent A2B Adenosine Receptor Antagonists: Design, Synthesis, Structure–Affinity and Structure–Selectivity Relationships. *Bioorg. Med. Chem.* **2008**, *16*, 9780–9789.

(120) Yan, L.; Müller, C. E. Preparation, Properties, Reactions, and Adenosine Receptor Affinities of Sulfophenylxanthine Nitrophenyl Esters: Toward the Development of Sulfonic Acid Prodrugs with Peroral Bioavailability. *J. Med. Chem.* **2004**, *47*, 1031–1043.

(121) Jiang, J.; Seel, C. J.; Temirak, A.; Namasivayam, V.; Arridu, A.; Schabikowski, J.; Baqi, Y.; Hinz, S.; Hockemeyer, J.; Müller, C. E. A2B Adenosine Receptor Antagonists with Picomolar Potency. *J. Med. Chem.* **2019**, *62*, 4032–4055.

(122) Kim, Y.-C.; Ji, X.; Jacobson, K. A. Derivatives of the Triazoloquinazoline Adenosine Antagonist (CGS15943) Are Selective for the Human A3 Receptor Subtype. *J. Med. Chem.* **1996**, *39*, 4142–4148.

(123) Abdelrahman, A.; Yerande, S. G.; Namasivayam, V.; Klapschinski, T. A.; Alnouri, M. W.; El-Tayeb, A.; Müller, C. E. Substituted 4-Phenylthiazoles: Development of Potent and Selective A1, A3 and Dual A1/A3 Adenosine Receptor Antagonists. *Eur. J. Med. Chem.* **2020**, *186*, 111879–111879.

(124) Kim, Y. C.; Ji, X. D.; Melman, N.; Linden, J.; Jacobson, K. A. Anilide Derivatives of an 8-Phenylxanthine Carboxylic Congener Are Highly Potent and Selective Antagonists at Human A(2B) Adenosine Receptors. *J. Med. Chem.* **2000**, *43*, 1165–1172.

(125) Ukena, D.; Padgett, W. L.; Hong, O.; Daly, J. W.; Daly, D. T.; Olsson, R. A. N 6-Substituted 9-Methyladenines: A New Class of Adenosine Receptor Antagonists. *FEBS Lett.* **1987**, *215*, 203–208.

(126) Kalk, P.; Eggert, B.; Relle, K.; Godes, M.; Heiden, S.; Sharkovska, Y.; Fischer, Y.; Ziegler, D.; Bielenberg, G.-W.; Hocher, B. The Adenosine A1 Receptor Antagonist SLV320 Reduces Myocardial Fibrosis in Rats with 5/6 Nephrectomy without Affecting Blood Pressure. *Br. J. Pharmacol.* **2007**, *151*, 1025–1032.

(127) Jiang, J.-L.; Li, A.-H.; Jang, S.-Y.; Chang, L.; Melman, N.; Moro, S.; Ji, X.-D.; Lobkovsky, E. B.; Clardy, J. C.; Jacobson, K. A. Chiral Resolution and Stereospecificity of 6-Phenyl-4-Phenylethynyl- 1,4-Dihydropyridines as Selective A3 Adenosine Receptor Antagonists. *J. Med. Chem.* **1999**, *42*, 3055–3065.

(128) van Veldhoven, J. P. D.; Chang, L. C. W.; von Frijtag Drabbe Künzel, J. K.; Mulder-Krieger, T.; Struensee-Link, R.; Beukers, M. W.; Brussee, J.; IJzerman, A. P. A New

Generation of Adenosine Receptor Antagonists: From Di- to Trisubstituted Aminopyrimidines. *Bioorg. Med. Chem.* **2008**, *16*, 2741–2752.

(129) Miranda-Pastoriza, D.; Bernardez, R.; Azuaje, J.; Prieto-Díaz, R.; Majellaro, M.; Tamhankar, A.; Koenekoop, L.; González, A.; Gioé-Gallo, C.; Mallo-Abreu, A.; Brea, J.; Loza, M.; García-Rey, A.; García-Mera, X.; Gutiérrez-de-Terán, H.; Sotelo, E. Exploring Non-Orthosteric Interactions with a Series of Potent and Selective A3 Antagonists. *ACS Med. Chem. Lett. 0*, null-null.

(130) Azuaje, J.; Jespers, W.; Yaziji, V.; Mallo, A.; Majellaro, M.; Caamaño, O.; Loza, M. I.; Cadavid, M. I.; Brea, J.; Åqvist, J.; Sotelo, E.; Gutiérrez-De-Terán, H. Effect of Nitrogen Atom Substitution in A3 Adenosine Receptor Binding: N-(4,6-Diarylpyridin-2-Yl)Acetamides as Potent and Selective Antagonists. *J. Med. Chem.* **2017**, *60*, 7502–7511.

(131) Yaziji, V.; Rodríguez, D.; Gutiérrez-de-Terán, H.; Coelho, A.; Caamaño, O.; García-Mera, X.; Brea, J.; Loza, M. I.; Cadavid, M. I.; Sotelo, E. Pyrimidine Derivatives as Potent and Selective A3 Adenosine Receptor Antagonists. *J. Med. Chem.* **2011**, *54*, 457–471.

(132) Asano, T.; Noda, Y.; Tanaka, K.-I.; Yamakawa, N.; Wada, M.; Mashimo, T.; Fukunishi, Y.; Mizushima, T.; Takenaga, M. A2B Adenosine Receptor Inhibition by the Dihydropyridine Calcium Channel Blocker Nifedipine Involves Colonic Fluid Secretion. *Sci. Rep.* **2020**, *10*, 3555–3555.

(133) Chang, L. C. W.; Spanjersberg, R. F.; Von Frijtag Drabbe Künzel, J. K.; Mulder-Krieger, T.; Van Den Hout, G.; Beukers, M. W.; Brussee, J.; IJzerman, A. P. 2,4,6-Trisubstituted Pyrimidines as a New Class of Selective Adenosine A1 Receptor Antagonists. *J. Med. Chem.* **2004**, *47*, 6529–6540.

(134) Scheiff, A. B.; Yerande, S. G.; El-Tayeb, A.; Li, W.; Inamdar, G. S.; Vasu, K. K.; Sudarsanam, V.; Müller, C. E. 2-Amino-5-Benzoyl-4-Phenylthiazoles: Development of Potent and Selective Adenosine A1 Receptor Antagonists. *Bioorg. Med. Chem.* **2010**, *18*, 2195–2203.

(135) Piersanti, G.; Bartoccini, F.; Lucarini, S.; Cabri, W.; Stasi, M. A.; Riccioni, T.; Borsini, F.; Tarzia, G.; Minetti, P. Synthesis and Biological Evaluation of Metabolites of 2-n-Butyl-9-Methyl-8-[1,2,3]Triazol-2-Yl-9H-Purin-6-Ylamine (ST1535), A Potent

Antagonist of the A2A Adenosine Receptor for the Treatment of Parkinson's Disease. *J. Med. Chem.* **2013**, *56*, 5456–5463.

(136) Doyle, S. E.; Breslin, F. J.; Rieger, J. M.; Beauglehole, A.; Lynch, W. J. Time and Sex-Dependent Effects of an Adenosine A2A/A1 Receptor Antagonist on Motivation to Self-Administer Cocaine in Rats. *Pharmacol. Biochem. Behav.* **2012**, *102*, 257–263.

(137) Beauglehole, A.; Rieger, J. M.; Thompson, R. D. Preparation of Adenines as Selective Antagonists of A2A Adenosine Receptors for Treating Parkinson's and Other Diseases. *World Intellect. Prop. Organ.* **2005**, No. WO2005097140.

(138) Vidal, B.; Nueda, A.; Esteve, C.; Domenech, T.; Benito, S.; Reinoso, R. F.; Pont, M.; Calbet, M.; López, R.; Cadavid, M. I.; Loza, M. I.; Cárdenas, Á.; Godessart, N.; Beleta, J.; Warrellow, G.; Ryder, H. Discovery and Characterization of 4'-(2-Furyl)-N-Pyridin-3-Yl-4,5'-Bipyrimidin-2'-Amine (LAS38096), a Potent, Selective, and Efficacious A2B Adenosine Receptor Antagonist. *J. Med. Chem.* **2007**, *50*, 2732–2736.

(139) Jiang, J.; van Rhee, A. M.; Chang, L.; Patchornik, A.; Ji, X.; Evans, P.; Melman, N.; Jacobson, K. A. Structure-Activity Relationships of 4-(Phenylethynyl)-6-Phenyl-1,4-Dihydropyridines as Highly Selective A3 Adenosine Receptor Antagonists. *J. Med. Chem.* **1997**, *40*, 2596–2608.

(140) Crespo, A.; El Maatougui, A.; Biagini, P.; Azuaje, J.; Coelho, A.; Brea, J.; Loza, M. I.; Cadavid, M. I.; García-Mera, X.; Gutiérrez-De-Terán, H.; Sotelo, E. Discovery of 3,4-Dihydropyrimidin-2(1H)-Ones as a Novel Class of Potent and Selective A2B Adenosine Receptor Antagonists. *ACS Med. Chem. Lett.* **2013**, *4*, 1031–1036.

(141) Majellaro, M.; Jespers, W.; Crespo, A.; Nunez, M.; Novio, S.; Azuaje, J.; Prieto-Díaz, R.; Gioe, C.; Alispahic, B.; Brea, J.; Loza, M.; Freire-Garabal, M.; Garcia-Santiago, C.; Rodriguez-Garcia, C.; García-Mera, X.; Caamaño, O.; Masaguer, C. F.; Sardina, F. J.; Stefanachi, A.; El Maatougui, A.; Mallo-Abreu, A.; Åqvist, J.; Gutiérrez-de-Terán, H.; Sotelo, E. 3,4-Dihydropyrimidin-2(1H)-Ones as Antagonists of the Human A2B Adenosine Receptor: Optimization, Structure–Activity Relationship Studies, and Enantiospecific Recognition. *J. Med. Chem.* **2021**, *64*, 458–480.

(142) Carbajales, C.; Azuaje, J.; Oliveira, A.; Loza, M. I.; Brea, J.; Cadavid, M. I.; Masaguer, C. F.; García-Mera, X.; Gutiérrez-De-Terán, H.; Sotelo, E. Enantiospecific Recognition at the A2B Adenosine Receptor by Alkyl 2-Cyanoimino-4-Substituted-6-Methyl-1,2,3,4-Tetrahydropyrimidine-5-Carboxylates. *J. Med. Chem.* **2017**, *60*, 3372–3382.

(143) Mallo-Abreu, A.; Majellaro, M.; Jespers, W.; Azuaje, J.; Caamaño, O.; García-Mera, X.; Brea, J. M.; Loza, M. I.; Gutiérrez-De-Terán, H.; Sotelo, E. Trifluorinated Pyrimidine-Based A2B Antagonists: Optimization and Evidence of Stereospecific Recognition. *J. Med. Chem.* **2019**, *62*, 9315–9330.

(144) Mallo-Abreu, A.; Prieto-Díaz, R.; Jespers, W.; Azuaje, J.; Majellaro, M.; Velando, C.; García-Mera, X.; Caamaño, O.; Brea, J.; Loza, M. I.; Gutiérrez-De-Terán, H.; Sotelo, E. Nitrogen-Walk Approach to Explore Bioisosteric Replacements in a Series of Potent A2B Adenosine Receptor Antagonists. *J. Med. Chem.* **2020**, *63*, 7721–7739.

(145) Kappe, C. O. Biologically Active Dihydropyrimidones of the Biginelli-Type - A Literature Survey. *Eur. J. Med. Chem.* **2000**, *35*, 1043–1052.

(146) Gilead Exercises Options to Three Arcus Biosciences Clinical-Stage Programs and Adds Research Collaboration.

(147) Gilead Goes All in on Its Arcus Alliance, Paying $725M Cash for Rights to a Slate of Cancer Drugs. And There's No Room for Failure – Endpoints News.

(148) Galezowski, M.; Wegrzyn, P.; Bobowska, A.; Commandeur, C.; Dziedzic, K.; Nowogrodzki, M.; Obara, A.; Szeremeta-Spisak, J.; Dzielak, A.; Lozinska, I.; Dudek, M.; Janiga, A.; Reus, J.; Wronowski, M.; Swirski, M.; Radzimierski, A.; Ziembik, M.; Mierzwicka, J.; Wojcik-Jaszczynska, K.; Gocek, E.; Grycuk, K.; Golas, A.; Pierzchala, O.; Zachmann, J.; Nowak, M. Abstract 3770: Characterization of Novel Dual A 2A /A 2B Adenosine Receptor Antagonists for Cancer Immunotherapy; Boston, 2018; pp 3770–3770.

(149) Dziedzic, K.; Węgrzyn, P.; Gałęzowski, M.; Bońkowska, M.; Grycuk, K.; Satała, G.; Wiatrowska, K.; Wiklik, K.; Brzózka, K.; Nowak, M. Release of Adenosine-Induced Immunosuppression: Comprehensive Characterization of Dual A2A/A2B Receptor Antagonist. *Int. Immunopharmacol.* **2021**, *96*, 107645–107645.

(150) Zaynagetdinov, R.; Schiemann, K.; Nallaparaju, K.; Belousova, N.; Matevossian, A.; Chen, Z.; Kradjian, G.; Pandya, M.; Dawra, N.; Krauel, E.-M.; Petrova, E.; Poeschke, O.; Fischer, D.; Lecomte, M.; Blaukat, A.; Huck, B.; Moisan, J. Abstract 3499: M1069 as Dual A2A/A2B Adenosine Receptor Antagonist Counteracts Immune-Suppressive Mechanisms of Adenosine and Reduces Tumor Growth in Vivo. *Cancer Res.* **2022**, *82*, 3499–3499.

(151) First in Human Study of M1069 in Advanced Solid Tumors - Full Text View - ClinicalTrials.Gov.

(152) Powderly, J. D.; de Souza, P. L.; Gutierrez, R.; Horvath, L.; Seitz, L.; Ashok, D.; Park, A.; Walters, M. J.; Karakunnel, J. J.; Berry, W.; Rieger, A.; Garofalo, A.; Lai, D. W.; Chaudhry, A. AB928, a Novel Dual Adenosine Receptor Antagonist, Combined with Chemotherapy or AB122 (Anti-PD-1) in Patients (Pts) with Advanced Tumors: Preliminary Results from Ongoing Phase I Studies. *J. Clin. Oncol.* **2019**, *37*, 2604–2604.

(153) Fredholm, B. B. Adenosine - A Physiological or Pathophysiological Agent? *J. Mol. Med.* **2014**, *92*, 201–206.

(154) Huang, Z. L.; Zhang, Z.; Qu, W. M. *Roles of Adenosine and Its Receptors in Sleep-Wake Regulation*, 1st ed.; International Review of Neurobiology; Elsevier Inc., 2014; Vol. 119, p 371.

(155) Pasquini, S.; Contri, C.; Borea, P. A.; Vincenzi, F.; Varani, K. Adenosine and Inflammation: Here, There and Everywhere. *Int. J. Mol. Sci.* **2021**, *22*, 1–24.

(156) Fredholm, B. B. Adenosine, an Endogenous Distress Signal, Modulates Tissue Damage and Repair. *Cell Death Differ.* **2007**, *14*, 1315–1323.

(157) Wilson, C. N.; S. Jamal, M. Adenosine Receptors in Health and Disease. In *Handbook of Experimental Pharmacology*; Springer: Berlin, 2009; Vol. 193, pp 41–75.

(158) Aherne, C. M.; Kewley, E. M.; Eltzschig, H. K. The Resurgence of A2B Adenosine Receptor Signaling. *Biochim. Biophys. Acta - Biomembr.* **2011**, *1808*, 1329–1339.

(159) Vecchio, E. A.; White, P. J.; May, L. T. The Adenosine A2B G Protein-Coupled Receptor: Recent Advances and Therapeutic Implications. *Pharmacol. Ther.* **2019**, *198*, 20–33.

(160) Jain, S.; Jacobson, K. A. Purinergic Signaling in Diabetes and Metabolism. *Biochem. Pharmacol.* **2021**, *187*, 114393–114404.

(161) Abo-Salem, O. M.; Hayallah, A. M.; Bilkei-Gorzo, A.; Filipek, B.; Zimmer, A.; Müller, C. E. Antinociceptive Effects of Novel A2B Adenosine Receptor Antagonists. *J. Pharmacol. Exp. Ther.* **2004**, *308*, 358–366.

(162) Popoli, P.; Pepponi, R. Potential Therapeutic Relevance of Adenosine A 2B and A 2A Receptors in the Central Nervous System. *CNS Neurol. Disord.-Drug Targets* **2012**, *11*, 664–674.

(163) Franco, R.; Cordomí, A.; Llinas del Torrent, C.; Lillo, A.; Serrano-Marín, J.; Navarro, G.; Pardo, L. Structure and Function of Adenosine Receptor Heteromers. *Cell. Mol. Life Sci.* **2021**, *78*, 3957–3968.

(164) Franco, R.; Rivas-Santisteban, R.; Navarro, G.; Reyes-Resina, I. Adenosine Receptor Antagonists to Combat Cancer and to Boost Anti-Cancer Chemotherapy and Immunotherapy. *Cells* **2021**, *10*, 2831–2844.

(165) Wang, X.; Jespers, W.; Prieto-Díaz, R.; Majellaro, M.; IJzerman, A. P.; van Westen, G. J. P. P.; Sotelo, E.; Heitman, L. H.; Gutiérrez-de-Terán, H. Identification of V6.51L as a Selectivity Hotspot in Stereoselective A2B Adenosine Receptor Antagonist Recognition. *Sci. Rep.* **2021**, *11*, 1–10.

(166) RDKit https://www.rdkit.org.

(167) Fernández-Dueñas, V.; Gómez-Soler, M.; Jacobson, K. A.; Kumar, S. T.; Fuxe, K.; Borroto-Escuela, D. O.; Ciruela, F. Molecular Determinants of A2AR–D2R Allosterism: Role of the Intracellular Loop 3 of the D2R. *J. Neurochem.* **2012**, *123*, 373–384.

(168) Xu, Y.; Xie, X.; Duan, Y.; Wang, L.; Cheng, Z.; Cheng, J. A Review of Impedance Measurements of Whole Cells. *Biosens. Bioelectron.* **2016**, *77*, 824–836.

(169) Linden, J.; Thai, T.; Figler, H.; Jin, X.; Robeva, A. S. Characterization of Human A_{2B} Adenosine Receptors: Radioligand Binding, Western Blotting, and Coupling to $G_q$in Human Embryonic Kidney 293 Cells and HMC-1 Mast Cells. *Mol. Pharmacol.* **1999**, *56*, 705.

(170) Kenakin, T. Quantifying Biological Activity in Chemical Terms: A Pharmacology Primer To Describe Drug Effect. *ACS Chem. Biol.* **2009**, *4*, 249–260.

(171) Atwood, B. K.; Lopez, J.; Wager-Miller, J.; Mackie, K.; Straiker, A. Expression of G Protein-Coupled Receptors and Related Proteins in HEK293, AtT20, BV2, and N18 Cell Lines as Revealed by Microarray Analysis. *BMC Genomics* **2011**, *12*, 14–28.

(172) ClinicalTrials.gov https://is.gd/tZZvst (accessed 2022 -09 -15).

(173) Krenn, W.; Verdino, P.; Uray, G.; Faber, K.; Kappe, A. C. O. Determination of Absolute Configuration in 4-Aryl-3,4-Dihydro-2(1H)-Pyrimidones by High Performance Liquid Chromatography and CD Spectroscopy 1. *Chirality* **1999**, *11*, 659–662.

(174) Crespo, A.; El Maatougui, A.; Azuaje, J.; Escalante, L.; Majellaro, M.; Loza, M. I.; Brea, J.; Cadavid, M. I.; Gutiérrez-de-Terán, H.; Sotelo, E. Exploring the Influence of

the Substituent at Position 4 in a Series of 3,4-Dihydropyrimidin-2(1H)-One A2B Adenosine Receptor Antagonists. *Chem. Heterocycl. Compd.* **2017**, *53*, 316–321.

(175) Guengerich, F. P.; Waterman, M. R.; Egli, M. Recent Structural Insights into Cytochrome P450 Function. *Trends Pharmacol. Sci.* **2016**, *37*, 625–640.

(176) McDonnell, A. M.; Dang, C. H. Basic Review of the Cytochrome P450 System. *J. Adv. Pract. Oncol.* **2013**, *4*, 263–268.

(177) Zhou, Y.; Wang, J.; Gu, Z.; Wang, S.; Zhu, W.; Aceña, J. L.; Soloshonok, V. A.; Izawa, K.; Liu, H. Next Generation of Fluorine-Containing Pharmaceuticals, Compounds Currently in Phase II–III Clinical Trials of Major Pharmaceutical Companies: New Structural Trends and Therapeutic Areas. *Chem. Rev.* **2016**, *116*, 422–518.

(178) Shah, P.; Westwell, A. D. The Role of Fluorine in Medicinal Chemistry. *J. Enzyme Inhib. Med. Chem.* **2007**, *22*, 527–540.

(179) Jespers, W.; Verdon, G.; Azuaje, J.; Majellaro, M.; Keränen, H.; García-Mera, X.; Congreve, M.; Deflorian, F.; de Graaf, C.; Zhukov, A.; Doré, A. S.; Mason, J. S.; Åqvist, J.; Cooke, R. M.; Sotelo, E.; Gutiérrez-de-Terán, H. X-Ray Crystallography and Free Energy Calculations Reveal the Binding Mechanism of A2A Adenosine Receptor Antagonists. *Angew. Chem. Int. Ed.* **2020**, *59*, 16536–16543.

(180) Yaziji, V.; Rodríguez, D.; Coelho, A.; García-Mera, X.; El Maatougui, A.; Brea, J.; Loza, M. I.; Cadavid, M. I.; Gutiérrez-De-Terán, H.; Sotelo, E. Selective and Potent Adenosine A3 Receptor Antagonists by Methoxyaryl Substitution on the N-(2,6-Diarylpyrimidin-4-Yl)Acetamide Scaffold. *Eur. J. Med. Chem.* **2013**, *59*, 235–242.

(181) Ramsay, R. R.; Popovic-Nikolic, M. R.; Nikolic, K.; Uliassi, E.; Bolognesi, M. L. A Perspective on Multi-Target Drug Discovery and Design for Complex Diseases. *Clin. Transl. Med.* **2018**, *7*, 3–3.

(182) Raghavendra, N. M.; Pingili, D.; Kadasi, S.; Mettu, A.; Prasad, S. V. U. M. Dual or Multi-Targeting Inhibitors: The next Generation Anticancer Agents. *Eur. J. Med. Chem.* **2018**, *143*, 1277–1300.

(183) Hann, M. M. Molecular Obesity, Potency and Other Addictions in Drug Discovery. *MedChemComm* **2011**, *2*, 349–355.

(184) Barbazán, J.; Majellaro, M.; Martínez, A. L.; Brea, J. M.; Sotelo, E.; Abal, M. Identification of A2BAR as a Potential Target in Colorectal Cancer Using Novel Fluorescent GPCR Ligands. *Biomed. Pharmacother.* **2022**, *153*, 113408–113408.

(185) Yi, Y.; Zhou, Y.; Chu, X.; Zheng, X.; Fei, D.; Lei, J.; Qi, H.; Dai, Y. Blockade of Adenosine A2b Receptor Reduces Tumor Growth and Migration in Renal Cell Carcinoma. *J. Cancer* **2020**, *11*, 421–431.

(186) Ferretti, M.; Fabbiano, C.; Bari, M. D.; Conte, C.; Castigli, E.; Sciaccaluga, M.; Ponti, D.; Ruggieri, P.; Raco, A.; Ricordy, R.; Calogero, A.; Tata, A. M. M2 Receptor Activation Inhibits Cell Cycle Progression and Survival in Human Glioblastoma Cells. *J. Cell. Mol. Med.* **2013**, *17*, 552–566.

(187) Mastelic-Gavillet, B.; Navarro Rodrigo, B.; Décombaz, L.; Wang, H.; Ercolano, G.; Ahmed, R.; Lozano, L. E.; Ianaro, A.; Derré, L.; Valerio, M.; Tawadros, T.; Jichlinski, P.; Nguyen-Ngoc, T.; Speiser, D. E.; Verdeil, G.; Gestermann, N.; Dormond, O.; Kandalaft, L.; Coukos, G.; Jandus, C.; Ménétrier-Caux, C.; Caux, C.; Ho, P. C.; Romero, P.; Harari, A.; Vigano, S. Adenosine Mediates Functional and Metabolic Suppression of Peripheral and Tumor-Infiltrating CD8+ T Cells. *J. Immunother. Cancer* **2019**, *7*, 1–16.

(188) Saze, Z.; Schuler, P. J.; Hong, C.-S.; Cheng, D.; Jackson, E. K.; Whiteside, T. L. Adenosine Production by Human B Cells and B Cell–Mediated Suppression of Activated T Cells. *Blood* **2013**, *122*, 9–18.

(189) Zhi, X.; Chen, S.; Zhou, P.; Shao, Z.; Wang, L.; Ou, Z.; Yin, L. RNA Interference of Ecto-5'-Nucleotidase (CD73) Inhibits Human Breast Cancer Cell Growth and Invasion. *Clin Exp Metastasis* **2007**, *24*, 439–448.

(190) Rusakiewicz, S.; Semeraro, M.; Sarabi, M.; Desbois, M.; Locher, C.; Mendez, R.; Vimond, N.; Concha, A.; Garrido, F.; Isambert, N.; Chaigneau, L.; Le Brun-Ly, V.; Dubreuil, P.; Cremer, I.; Caignard, A.; Poirier-Colame, V.; Chaba, K.; Flament, C.; Halama, N.; Jaĝer, D.; Eggermont, A.; Bonvalot, S.; Commo, F.; Terrier, P.; Opolon, P.; Emile, J. F.; Coindre, J. M.; Kroemer, G.; Chaput, N.; Le Cesne, A.; Blay, J. Y.; Zitvogel, L. Immune in Filtrates Are Prognostic Factors in Localized Gastrointestinal Stromal Tumors. *Cancer Res.* **2013**, *73*, 3499–3510.

(191) Fujii, H.; Arakawa, A.; Utsumi, D.; Sumiyoshi, S.; Yamamoto, Y.; Kitoh, A.; Ono, M.; Matsumura, Y.; Kato, M.; Konishi, K.; Shiga, T.; Sano, S.; Sakaguchi, S.; Miyagawa-Hayashino, A.; Takahashi, K.; Uezato, H.; Miyachi, Y.; Tanioka, M. CD8(+) Tumor-Infiltrating Lymphocytes at Primary Sites as a Possible Prognostic Factor of Cutaneous Angiosarcoma. *Int J Cancer* **2014**, *134*, 2393–2402.

(192) Balch, C. M.; Riley, L. B.; Bae, Y. J.; Salmeron, M. A.; Platsoucas, C. D.; von Eschenbach, A.; Itoh, K. Patterns of Human Tumor-Infiltrating Lymphocytes in 120 Human Cancers. *Arch Surg* **1990**, *125*, 200–205.

(193) Morandi, F.; Morandi, B.; Horenstein, A. L.; Chillemi, A.; Quarona, V.; Zaccarello, G.; Carrega, P.; Ferlazzo, G.; Mingari, M. C.; Moretta, L.; Pistoia, V.; Malavasi, F. A Non-Canonical Adenosinergic Pathway Led by CD38 in Human Melanoma Cells Induces Suppression of T Cell Proliferation. *Oncotarget* **2015**, *6*, 25602–25618.

(194) Bray, L. J.; Hutmacher, D. W.; Bock, N. Addressing Patient Specificity in the Engineering of Tumor Models. *Front Bioeng Biotechnol* **2019**, *7*, 217–217.

(195) Liao, W.; Wang, J.; Xu, J.; You, F.; Pan, M.; Xu, X.; Weng, J.; Han, X.; Li, S.; Li, Y.; Liang, K.; Peng, Q.; Gao, Y. High-Throughput Three-Dimensional Spheroid Tumor Model Using a Novel Stamp-like Tool. *J. Tissue Eng.* **2019**, *10*, 2041731419889184–2041731419889184.

(196) Duhen, T.; Duhen, R.; Montler, R.; Moses, J.; Moudgil, T.; de Miranda, N. F.; Goodall, C. P.; Blair, T. C.; Fox, B. A.; McDermott, J. E.; Chang, S. C.; Grunkemeier, G.; Leidner, R.; Bell, R. B.; Weinberg, A. D. Co-Expression of CD39 and CD103 Identifies Tumor-Reactive CD8 T Cells in Human Solid Tumors. *Nat Commun* **2018**, *9*, 2724–2724.

(197) Cheuk, S.; Schlums, H.; Gallais Serezal, I.; Martini, E.; Chiang, S. C.; Marquardt, N.; Gibbs, A.; Detlofsson, E.; Introini, A.; Forkel, M.; Hoog, C.; Tjernlund, A.; Michaelsson, J.; Folkersen, L.; Mjosberg, J.; Blomqvist, L.; Ehrstrom, M.; Stahle, M.; Bryceson, Y. T.; Eidsmo, L. CD49a Expression Defines Tissue-Resident CD8(+) T Cells Poised for Cytotoxic Function in Human Skin. *Immunity* **2017**, *46*, 287–300.

(198) Longo, P. A.; Kavran, J. M.; Kim, M.-S.; Leahy, D. J. Chapter Eighteen - Transient Mammalian Cell Transfection with Polyethylenimine (PEI). In *Methods in Enzymology*; Lorsch, J., Ed.; Academic Press, 2013; Vol. 529, pp 227–240.

(199) Taura, J.; Fernández-Dueñas, V.; Ciruela, F. Determination of GPCR-Mediated CAMP Accumulation in Rat Striatal Synaptosomes. In *Receptor and Ion Channel Detection in the Brain: Methods and Protocols*; Luján, R., Ciruela, F., Eds.; Springer New York: New York, NY, 2016; pp 455–463.

(200) Leff, P.; Dougall, I. G. Further Concerns over Cheng-Prusoff Analysis. *Trends Pharmacol. Sci.* **1993**, *14*, 110–112.

(201) Solly, K.; Wang, X.; Xu, X.; Strulovici, B.; Zheng, W. Application of Real-Time Cell Electronic Sensing (RT-CES) Technology to Cell-Based Assays. *ASSAY Drug Dev. Technol.* **2004**, *2*, 363–372.

(202) Stallaert, W.; Dorn, J. F.; van der Westhuizen, E.; Audet, M.; Bouvier, M. Impedance Responses Reveal B2-Adrenergic Receptor Signaling Pluridimensionality and Allow Classification of Ligands with Distinct Signaling Profiles. *PLOS ONE* **2012**, *7*, e29420.

(203) Hillger, J. M.; Schoop, J.; Boomsma, D. I.; Eline Slagboom, P.; IJzerman, A. P.; Heitman, L. H. Whole-Cell Biosensor for Label-Free Detection of GPCR-Mediated Drug Responses in Personal Cell Lines. *Biosens. Bioelectron.* **2015**, *74*, 233–242.

(204) Núñez, F.; Taura, J.; Camacho, J.; López-Cano, M.; Fernández-Dueñas, V.; Castro, N.; Castro, J.; Ciruela, F. PBF509, an Adenosine A2A Receptor Antagonist With Efficacy in Rodent Models of Movement Disorders. *Front. Pharmacol.* **2018**, *9*, 1–10.

(205) Motulsky, H. J.; Brown, R. E. Detecting Outliers When Fitting Data with Nonlinear Regression – a New Method Based on Robust Nonlinear Regression and the False Discovery Rate. *BMC Bioinformatics* **2006**, *7*, 123–123.

(206) Šícho, M.; Stork, C.; Mazzolari, A.; de Bruyn Kops, C.; Pedretti, A.; Testa, B.; Vistoli, G.; Svozil, D.; Kirchmair, J. FAME 3: Predicting the Sites of Metabolism in Synthetic Compounds and Natural Products for Phase 1 and Phase 2 Metabolic Enzymes. *J. Chem. Inf. Model.* **2019**, *59*, 3400–3412.

(207) Rydberg, P.; Gloriam, D. E.; Olsen, L. The SMARTCyp Cytochrome P450 Metabolism Prediction Server. *Bioinformatics* **2010**, *26*, 2988–2989.

(208) Lu, C.; Wu, C.; Ghoreishi, D.; Chen, W.; Wang, L.; Damm, W.; Ross, G. A.; Dahlgren, M. K.; Russell, E.; Von Bargen, C. D.; Abel, R.; Friesner, R. A.; Harder, E. D. OPLS4: Improving Force Field Accuracy on Challenging Regimes of Chemical Space. *J. Chem. Theory Comput.* **2021**, *17*, 4291–4300.

(209) Marelius, J.; Kolmodin, K.; Feierberg, I.; Åqvist, J. Q: A Molecular Dynamics Program for Free Energy Calculations and Empirical Valence Bond Simulations in Biomolecular Systems. *J. Mol. Graph. Model.* **1998**, *16*, 213–225.

(210) Jespers, W.; Esguerra, M.; Åqvist, J.; Gutiérrez-De-Terán, H. Qligfep: An Automated Workflow for Small Molecule Free Energy Calculations in Q. *J. Cheminformatics* **2019**, *11*, 1–16.

(211) Lee, F. S.; Warshel, A. A Local Reaction Field Method for Fast Evaluation of Long-Range Electrostatic Interactions in Molecular Simulations. *J. Chem. Phys.* **1992**, *97*, 3100–3107.

(212) King, G.; Warshel, A. A Surface Constrained All-Atom Solvent Model for Effective Simulations of Polar Solutions. *J. Chem. Phys.* **1989**, *91*, 3647–3661.

(213) Robertson, M. J.; Tirado-Rives, J.; Jorgensen, W. L. Improved Peptide and Protein Torsional Energetics with the OPLS-AA Force Field. *J. Chem. Theory Comput.* **2015**, *11*, 3499–3509.

(214) Banks, J. L.; Beard, H. S.; Cao, Y.; Cho, A. E.; Damm, W.; Farid, R.; Felts, A. K.; Halgren, T. A.; Mainz, D. T.; Maple, J. R.; Murphy, R.; Philipp, D. M.; Repasky, M. P.; Zhang, L. Y.; Berne, B. J.; Friesner, R. A.; Gallicchio, E.; Levy, R. M. Integrated Modeling Program, Applied Chemical Theory (IMPACT). *J. Comput. Chem.* **2005**, *26*, 1752–1780.

(215) Ryckaert, J.-P. J. P.; Ciccotti, G.; Berendsen, H. J. C. H. Numerical Integration of the Cartesian Equations of Motion of a System with Constraints: Molecular Dynamics of n-Alkanes. *J. Comput. Phys.* **1977**, *23*, 327–341.

(216) Bennett, C. H. Efficient Estimation of Free Energy Differences from Monte Carlo Data. *J. Comput. Phys.* **1976**, *22*, 245–268.

(217) Wang, L.; Deng, Y.; Knight, J. L.; Wu, Y.; Kim, B.; Sherman, W.; Shelley, J. C.; Lin, T.; Abel, R. Modeling Local Structural Rearrangements Using FEP/REST: Application to Relative Binding Affinity Predictions of CDK2 Inhibitors. *J. Chem. Theory Comput.* **2013**, *9*, 1282–1293.

(218) Hagberg, A. A.; Schult, D. A.; Swart, P. J. Exploring Network Structure, Dynamics, and Function Using NetworkX. *7th Python Sci. Conf. SciPy 2008* **2008**, 11–15.

(219) Wang, L.; Wu, Y.; Deng, Y.; Kim, B.; Pierce, L.; Krilov, G.; Lupyan, D.; Robinson, S.; Dahlgren, M. K.; Greenwood, J.; Romero, D. L.; Masse, C.; Knight, J. L.; Steinbrecher, T.; Beuming, T.; Damm, W.; Harder, E.; Sherman, W.; Brewer, M.; Wester, R.; Murcko, M.; Frye, L.; Farid, R.; Lin, T.; Mobley, D. L.; Jorgensen, W. L.; Berne, B. J.; Friesner, R. A.; Abel, R. Accurate and Reliable Prediction of Relative Ligand Binding Potency in Prospective Drug Discovery by Way of a Modern Free-Energy Calculation Protocol and Force Field. *J. Am. Chem. Soc.* **2015**, *137*, 2695–2703.

(220) Sastre, S.; Casasnovas, R.; Muñoz, F.; Frau, J. Isodesmic Reaction for Accurate Theoretical PKa Calculations of Amino Acids and Peptides. *Phys. Chem. Chem. Phys.* **2016**, *18*, 11202–11212.

(221) Ho, J.; Coote, M. L. PKa Calculation of Some Biologically Important Carbon Acids - An Assessment of Contemporary Theoretical Procedures. *J. Chem. Theory Comput.* **2009**, *5*, 295–306.

(222) Casasnovas, R.; Ortega-Castro, J.; Frau, J.; Donoso, J.; Muñoz, F. Theoretical PKa Calculations with Continuum Model Solvents, Alternative Protocols to Thermodynamic Cycles. *Int. J. Quantum Chem.* **2014**, *114*, 1350–1363.

(223) Ho, J.; Coote, M. L. A Universal Approach for Continuum Solvent PKa Calculations: Are We There Yet? *Theor. Chem. Acc.* **2010**, *125*, 3–21.

(224) Marenich, A. V.; Cramer, C. J.; Truhlar, D. G. Universal Solvation Model Based on Solute Electron Density and on a Continuum Model of the Solvent Defined by the Bulk Dielectric Constant and Atomic Surface Tensions. *J. Phys. Chem. B* **2009**, *113*, 6378–6396.

(225) Frisch, M. ea; Trucks, G.; Schlegel, H. B.; Scuseria, G.; Robb, M.; Cheeseman, J.; Scalmani, G.; Barone, V.; Petersson, G.; Nakatsuji, H. Gaussian 16, Revision C.01. **2016**.

(226) Glentis, A.; Oertle, P.; Mariani, P.; Chikina, A.; El Marjou, F.; Attieh, Y.; Zaccarini, F.; Lae, M.; Loew, D.; Dingli, F.; Sirven, P.; Schoumacher, M.; Gurchenkov, B. G.; Plodinec, M.; Vignjevic, D. M. Cancer-Associated Fibroblasts Induce Metalloprotease-Independent Cancer Cell Invasion of the Basement Membrane. *Nat. Commun.* **2017**, *8*, 924–924.

(227) Barbazan, J.; Pérez-González, C.; Gómez-González, M.; Dedenon, M.; Richon, S.; Latorre, E.; Serra, M.; Mariani, P.; Descroix, S.; Sens, P.; Trepat, X.; Vignjevic, D. M. Cancer-Associated Fibroblasts Actively Compress Cancer Cells and Modulate Mechanotransduction. *bioRxiv* **2021**, 2021.04.05.438443-2021.04.05.438443.

(228) Yang, Y.; Neo, S. Y.; Chen, Z.; Cui, W.; Chen, Y.; Guo, M.; Wang, Y.; Xu, H.; Kurzay, A.; Alici, E.; Holmgren, L.; Haglund, F.; Wang, K.; Lundqvist, A. Thioredoxin Activity Confers Resistance against Oxidative Stress in Tumor-Infiltrating NK Cells. *J. Clin. Invest.* **2020**, *130*, 5508–5522.

(229) Daina, A.; Michielin, O.; Zoete, V. SwissADME: A Free Web Tool to Evaluate Pharmacokinetics, Drug-Likeness and Medicinal Chemistry Friendliness of Small Molecules. *Sci. Rep.* **2017**, *7*, 42717.

(230) Daina, A.; Zoete, V. A BOILED-Egg To Predict Gastrointestinal Absorption and Brain Penetration of Small Molecules. *ChemMedChem* **2016**, *11*, 1117–1121.

(231) Wager, T. T.; Hou, X.; Verhoest, P. R.; Villalobos, A. Moving beyond Rules: The Development of a Central Nervous System Multiparameter Optimization (CNS MPO) Approach To Enable Alignment of Druglike Properties. *ACS Chem. Neurosci.* **2010**, *1*, 435–449.

(232) Wager, T. T.; Hou, X.; Verhoest, P. R.; Villalobos, A. Central Nervous System Multiparameter Optimization Desirability: Application in Drug Discovery. *ACS Chem. Neurosci.* **2016**, *7*, 767–775.

(233) Schultes, S.; de Graaf, C.; Haaksma, E. E. J.; de Esch, I. J. P.; Leurs, R.; Krämer, O. Ligand Efficiency as a Guide in Fragment Hit Selection and Optimization. *Fragm. Based Drug Discov.* **2010**, *7*, e157–e162.

7 SUPPLEMENTARY RESULTS

7.1 *IN SILICO* STUDY OF THE PHYSICOCHEMICAL PROPERTIES OF THE MOLECULES OBTAINED

We present a preliminary *in silico* study on the pharmacokinetic properties of these new compounds, highlighting how these properties can impact their efficacy and safety as cancer immunotherapeutic agents. Overall, the findings presented in this chapter underscore the importance of our work in the context of cancer immunotherapy and provide a strong foundation for the continued exploration of these novel drug candidates.

ADMET (Absorption, Distribution, Metabolism, Excretion and Toxicity) profiling plays a crucial role in drug design beyond just affinity and selectivity, providing essential information about how a drug is absorbed, distributed, metabolized, eliminated, and, ultimately, the basis to understand toxicity. Understanding and optimizing these pharmacokinetic properties is vital for developing safe and effective drugs. By considering ADME factors during the drug design process, researchers can predict and optimize a compound's pharmacokinetic properties, leading to improved efficacy, reduced toxicity, and better patient outcomes. Incorporating ADMET profiling early in drug development enables the identification and selection of promising candidates and helps prioritize resources towards compounds with favorable pharmacokinetic profiles for further development. Although it does not replace experimental validation, *in silico* evaluation of ADMET profile can offer valuable insights for the design of new compounds or the selection of the most suitable ones for further *in vitro* and *in vivo* biological validation.

For the *in silico* evaluation of absorption and distribution of the compounds obtained in this thesis, a set of physicochemical descriptors is proposed. These properties include molecular weight (Mw), lipophilicity (LogP and logD at pH 7.4), topological polar surface area (TPSA), the number of hydrogen bond donors (HBD), pKa, and the number of heavy atoms (HAC). These properties have been calculated using both the SwissADME simulator and Chemaxon software.[229] In order to facilitate the understanding of the calculated values and their effect on the absorption and distribution profile, two validated graphical representations have been used. The first one is the Brain Or IntestinaL EstimateD permeation method, also known as

BOILED-Egg, which correlates lipophilicity (WlogP) with TPSA (Figure 7.1A). In 2016, Antoine Daina and Vincent Zoete proposed this intuitively remarkable model for simultaneously estimating the access across the blood-brain barrier and gastrointestinal absorption of molecules by considering only these two physicochemical descriptors.[230] The representation is entirely intuitive, depicting two regions: the white (molecules that are absorbed in the gastrointestinal tract) and the yolk (molecules capable of crossing the BBB). The second representation, slightly more advanced, is the CNS Multiparameter Optimization (MPO) algorithm developed by Wager and a team of researchers at Pfizer.[231,232] This algorithm utilizes six common physicochemical descriptors (molecular weight (MW), logP, logD at pH 7.4, TPSA, the number of H-bond donors (HBD), and the pKa of the most basic center of the molecule). Their study revealed that both existing CNS drugs on the market and potential candidates demonstrated high MPO scores, known as desirability scores, of 4 or above on a scale from 0 to 6 (Figure 7.1B).[232] Since its publication, the CNS MPO Score has gained wide acceptance as an algorithm within the CNS-focused medicinal chemistry community.

Ligand efficiency has been calculated for following the Equation 7.1. The term "Heavy Atom Count" (HAC) refers to the number of atoms in a molecule that are not hydrogen atoms. The value of the gas constant (R) is 0.001987 kcal·mol^{-1}·K^{-1}, and the temperature (T) is 298 K. In summary, smaller compounds with higher affinity tend to exhibit higher values of LE (ligand efficiency). Values above 0.30 are recommended, with the average for marketed drugs being 0.44.[233] As Figure 7.1C illustrates that the model monocycles show the highest ligand efficiency (LE) values, followed by bicyclic and tricyclic compounds. This thesis has incorporated different substitution profiles and bioisosterism strategies. As a result, certain compounds have experienced a minor reduction in LE values (0.3), while others have maintained it due to a significant increase in affinity. It is worth noting that the majority of compounds in this study surpass the recommended LE value, which is a remarkable achievement considering the substantial increase in metabolic stability and the development of dual-target drugs.

$$LE = \frac{\Delta G}{HAC} = \frac{-RTln(K_i)}{HAC}$$

Equation 7.1. Calculation of ligand efficiency (LE).

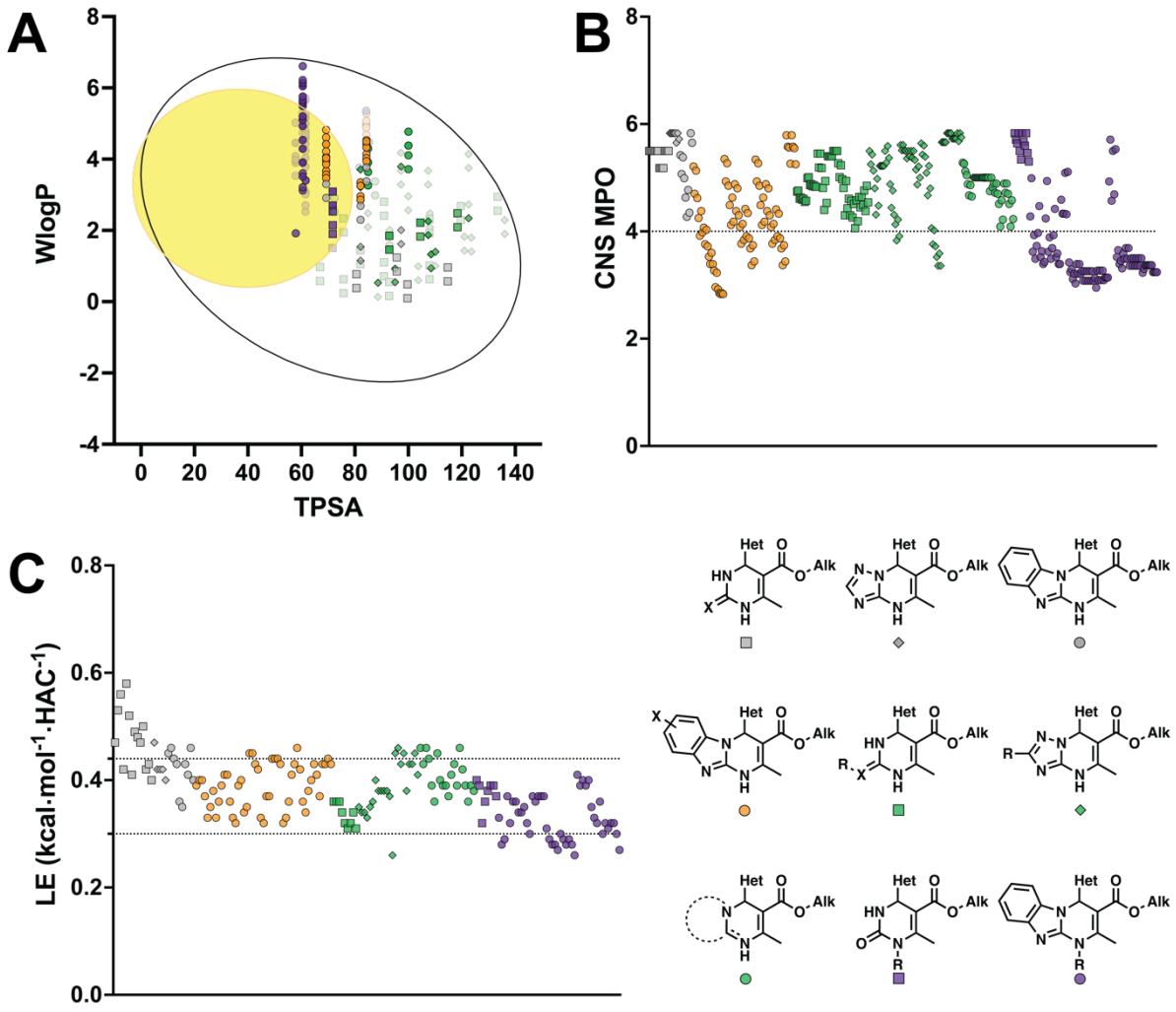

Figure 7.1. A) *Brain Or IntestinaL EstimateD permeation* method (BOILED-Egg) representation for all ligands obtained in this thesis. The white region is the physicochemical space of molecules with highest probability of being absorbed by the gastrointestinal tract, and the yellow region (yolk) is the physicochemical space of molecules with highest probability to permeate to the brain. Yolk and white areas are not mutually exclusive. B) CNS Multiparameter Optimization calculated for all ligands obtained in this thesis. The CNS Multiparameter Optimization (MPO) algorithm was employed to evaluate all the ligands obtained in this thesis. Ligands exhibiting values above four on the CNS MPO scale are deemed to have a high probability of crossing the blood-brain barrier (BBB). C) Ligand Efficiency (LE) calculation for the active ligands (K_i $hA_{2B}AR$ < 1000 nM) obtained in this thesis (Recommended ≥ 0.30, average of accepted drugs = 0.44).

8 APPENDICES

APPENDIX 1. PHD PUBLICATION LIST AND AUTHOR CONTRIBUTION

The results of **Chapter I** have been published in:

Exploring the Effect of Halogenation in a Series of Potent and Selective A_{2B} Adenosine Receptor Antagonists. Prieto-Díaz, R.;[1,2,3] González-Gómez, M.;[1,2] Fojo-Carballo, H.;[1,2] Azuaje, J.;[1,2] El Maatougui, A.;[1,2] Majellaro, M.;[1,2] Loza, M. I.;[4,5] Brea, J.;[4,5]* Fernández-Dueñas, V.;[6,7] Paleo, M. R.;[1,2] Díaz-Holguín, A.;[3] Garcia-Pinel, B.;[4,8] Mallo-Abreu, A.;[1,2] Estévez, J. C.;[1,2] Andújar-Arias, A.;[1,2] García-Mera, X.;[2] Gomez-Tourino, I.;[4,8] Ciruela, F.;[6,7] Salas, C. O.;[9] Gutiérrez-de-Terán, H.;[3]* Sotelo, E.[1,2]*. *J. Med. Chem.* **2023**, *66*, 890–912.

[1]Center for Research in Biological Chemistry and Molecular Materials (CIQUS), University of Santiago de Compostela, 15782 Santiago de Compostela, Spain. [2]Department of Organic Chemistry, Faculty of Pharmacy, University of Santiago de Compostela, 15782 Santiago de Compostela, Spain. [3]Department of Cell and Molecular Biology, Uppsala University, Biomedical Center, 75124 Uppsala, Sweden. [4]Center for Research in Metabolic Diseases (CIMUS). University of Santiago de Compostela, 15782 Santiago de Compostela, Spain. [5]Department of Pharmacology, Pharmacy and Pharmaceutical Technology, Faculty of Pharmacy, University of Santiago de Compostela, 15782 Santiago de Compostela, Spain. [6]Pharmacology Unit, Department of Pathology and Experimental Therapeutics, Faculty of Medicine and Health Sciences, Institute of Neuroscience, University of Barcelona, 08907 L'Hospitalet de Llobregat, Spain. [7]Neuropharmacology and Pain Group, Neuroscience Program, Institut d'Investigació Biomèdica de Bellvitge, IDIBELL, 08907 L'Hospitalet de Llobregat, Spain. [8]Department of Biochemistry and Molecular Biology. Faculty of Pharmacy, University of Santiago de Compostela, 15782 Santiago de Compostela, Spain. [9]Department of Organic Chemistry, Faculty of Chemistry and Pharmacy, Pontificia Universidad Católica de Chile, Vicuña Mackenna 4860, Macul, Santiago 7820436, Chile.

Impact factor: 8.039 (N° 3/63 (D1) in the category of Medicinal Chemistry (JCR 2021)). ISSN: 0022-2623.

Contribution

Research conceptualization, synthesis, purification and structural characterization, separation and characterization of enantiomers, docking and molecular dynamics (FEP) studies, data analysis and manuscript writing.

The results of **Chapter IV** have been published in:

A_{2B} Adenosine Receptor Antagonists Rescue Lymphocyte Activity in Adenosine-Producing Patient-Derived Cancer Models. Tay A. H. M.;[1,2#] Prieto-Díaz, R.;[3,#] Neo, S.;[1] Tong, L.;[1] Chen, X.;[1] Carannante, V.;[4] Önfelt, B.;[4,5] Hartman, J.;[1] Haglund, F.;[1] Majellaro, M.;[3] Azuaje, J.;[2] Garcia-Mera, X.;[2] Brea, J. M.;[6] Loza, M. I.;[6] Jespers, W.;[7] Gutierrez-De-Teran, H.;[7] Sotelo, E.;[3] Lundqvist, A. *J Immunother Cancer* **2022**, *10*, 4592–4592.

[#]Authors contributed equally. [1]Department of Oncology-Pathology, Karolinska Institute, Stockholm SE-17177, Sweden. [2]School of Biological Sciences, Nanyang Technological University, Singapore. [3]Center for Research in Biological Chemistry and Molecular Materials (CiQUS), University of Santiago de Compostela, Santiago de Compostela ES-15782, Spain. [4]Department of Microbiology, Tumor and Cell Biology, Science for Life Laboratory, Karolinska Institutet, Stockholm, Sweden. [5]Department of Applied Physics, Science for Life Laboratory, KTH Royal Institute of Technology, Stockholm SE-11419, Sweden. [6]Center for Research in Molecular Medicine and Chronic Diseases (CiMUS), University of Santiago de Compostela, Santiago de Compostela ES-15782, Spain. [7]Department of Cell and Molecular Biology, Uppsala University, Uppsala SE-75124, Sweden.

Impact factor: 8.039 (N° 3/63 (D1) in the category of Medicinal Chemistry (JCR 2021). ISSN: 2051-1426.

Contribution

Synthesis, purification and characterization of ligands, data analysis and manuscript writing.

APPENDIX 2. PUBLISHER'S PERMISSION FOR USE OF THE PUBLICATIONS

J. Med. Chem. **2023**

This article is an open access publication and may be used for authors in their own thesis in accordance with American Chemical Society (Creative Commons 4.0 License). Readers of this Thesis are kindly reminded to seek additional permissions related to this publication from ACS. The article is available online: https://pubs.acs.org/doi/10.1021/acs.jmedchem.2c01768

J Immunother Cancer **2022**

This article is an open access publication and may be used for authors in their own thesis in accordance with British Medical Journal Publishing Group (Creative Commons 4.0 License). The article is available online: https://jitc.bmj.com/content/10/5/e004592

APPENDIX 3. PERMISSION TO PUBLISH IMAGES AND FIGURES

Rubén Prieto Díaz, the doctoral candidate, affirms that all the other images, schemes, and figures shown in this Doctoral Thesis have been personally elaborated.

Santiago de Compostela, July 17, 2023

APPENDIX 4. CONFLICT OF INTEREST

Rubén Prieto Díaz, the doctoral candidate, affirms that there is no conflict of interest associated with his Doctoral Thesis.

Santiago de Compostela, July 17, 2023

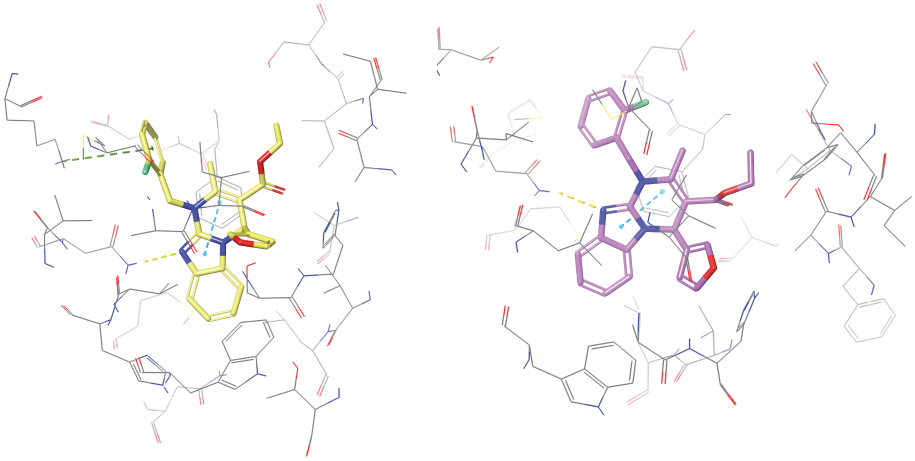

This doctoral thesis focuses on the study of purinergic signaling in cancer, specifically targeting adenosine receptors. The main objective is the development of potent and selective non-xanthine-based antagonists for adenosine A_{2B} receptors, with potential applications in cancer-targeted therapies. Molecular design strategies, synthesis, biological evaluation, structure-activity relationships, enantiospecific recognition and molecular modeling are explored. To the end, a rational method for dual A_{2A}/A_{2B} antagonists were obtained. The optimization and preclinical validation of new ligands for cancer (immuno)therapy are investigated, revealing promising data in terms of pharmacokinetics and pharmacodynamics.